ANTIMALARIAL BENZIMIDAZOLES AND RELATED STRUCTURES INCORPORATING AN INTRAMOLECULAR HYDROGEN BONDING MOTIF: MEDICINAL CHEMISTRY AND MECHANISTIC STUDIES

Henrietta Dede Attram

Supervisor:

Prof. Kelly Chibale

Department of Chemistry, University of Cape Town

Thesis Presented for the Degree of

DOCTOR OF PHILOSOPHY

In the Department of Chemistry

UNIVERSITY OF CAPE TOWN

June 2021

DECLARATION

I, **Henrietta Dede Attram**, hereby:

(a) grant the University of Cape Town license to reproduce this thesis, in whole or in part, for the purpose of research;

(b) declare that this thesis is my original work, both in concept and execution, with my supervisor's appropriate supervision. Where input from others have been included, acknowledgements have been made;

(c) declare that this thesis or part of it has not been presented nor is intended to be submitted to any other University for the award of a degree.

Signature: Signed by candidate **Date:** 28th June 2021

DEDICATION

To

My family and Frank Nana Yaw Abekah for always encouraging me to go the extra mile on every adventure, especially on this Ph.D. journey.

ACKNOWLEDGEMENTS

This Ph.D. thesis is the out-turn of the endeavour and support of various individuals to whom I am immensely grateful. First and foremost, I would like to express my deepest gratitude to my supervisor Professor Kelly Chibale for funding and an exemplary mentorship. The opportunity to pursue my Ph.D. under your supervision is a rare privilege that helped me unravel my potential and for which I would always beholden.

To Elaine Rutherfoord-Jones, Saroja Naicker, Ayesha Banderker, Deirdre van Rooyen, Deidre Brooks and the entire administrative team, thank you for the exceptional administrative roles you played in making this dream a reality.

I want to thank the UCT Department of Medicine, Division of Clinical Pharmacology, Dr. Sergio Wittlin of the Swiss Tropical and Public Health Institute and Professor Lyn-Marie Birkholtz of the University of Pretoria for carrying out the various pharmacological assays. Many thanks to Pete Roberts for executing my NMR spectroscopy experiments and Dr. Hong Su for acquiring the crystallographic data for this thesis work. I also appreciate the efforts of Constance Mawunyo Korkor for conducting fluorescence live-cell imaging and heme fractionation experiments. Furthermore, Radwan Alnajjar is also acknowledged for performing the DFT calculations reported in this work.

My sincere thanks to the University of Cape Town, South African Medical Research Council, and South African Research Chairs initiative of the Department of Science and Technology administered through the South African National Research Foundation for the generous financial support that made this work possible.

Special thanks to Dr. Richard Amewu of the Chemistry Department, University of Ghana, for the recommendation that made my Ph.D. candidature possible with my supervisor. I can never thank you enough. I am also grateful to Prof. Dorcas Osei-Safo for the mentorship, prayers and advice during my undergraduate studies that have brought me this far.

To all members, both past and present of the KC research group and H3D, who played various roles in moulding my research experience, I thank you for the friendship, constructive criticism and feedback.

Finally, I am grateful to God for my family and the ever-loving Ghanaian caucus in Cape Town for the support provided through encouragement, care, love and prayers. May God richly bless you all.

PUBLICATIONS AND CONFERENCES

Publications

- Attram, H. D.; Wittlin, S.; Chibale, K. Incorporation of an Intramolecular Hydrogen Bonding Motif in the Side Chain of Antimalarial Benzimidazoles. *Medchemcomm* **2019**, *10* (3), 450–455. https://doi.org/10.1039/C8MD00608C.

- Dziwornu, G. A.; Attram, H. D.; Gachuhi, S.; Chibale, K. Chemotherapy for Human Schistosomiasis: How Far Have We Come? What's New? Where Do We Go from Here? *RSC Med. Chem.* **2020**, *11* (4), 455–490. https://doi.org/10.1039/D0MD00062K.

Conferences

- **Gordon Research Seminar** (Biology of host-parasite interactions) Newport, Rhode Island, USA. June 09-June 10, 2018.
- **Gordon Research Conferences** (Biology of host-parasite interactions) Newport, Rhode Island, USA. June 10-June 15, 2018.
- **4th Southern Africa Malaria Research Conference 2018**, Johannesburg, South Africa. July 30- August 1, 2018.
- **Western Cape Young Chemists' Symposium 2019,** Cape Town, South Africa. May 17, 2019.
- **68th American Society of Tropical Medicine and Hygiene Annual Meeting,** Maryland, USA. November 20-24, 2019.

ABSTRACT

Malaria, an infectious disease caused by *Plasmodium* parasites, continues to take an enormous toll on human health, particularly in tropical regions. According to the World Health Organization (WHO), progress against malaria eradication has stalled, specifically in the African region. Global efforts to curb the disease are being undermined by the gaps in access to vital tools. In 2019, about 229 million cases were recorded compared to the 228 million cases recorded in 2018. This is an annual estimate that has not changed significantly over the last four (4) years. Also, children under the age of five (5) years account for most malaria deaths worldwide. Chemotherapy represents one of the most effective control measures to mitigate the malaria burden, with the WHO presently recommending the use of artemisinin combination therapies (ACTs) to treat uncomplicated malaria. However, there is compelling evidence from Southeast Asia and recently in Rwanda (Africa) describing the emergence and spread of ACT resistance, characterized by reduced clearance rates of *P. falciparum* parasites. In some countries, resistance to partner drugs such as amodiaquine has been observed. These developments highlight the need to expand the antimalarial drug arsenal by exploring and developing new compound classes, preferably with a combination of novel modes of action, multistage activity, good safety profile, efficacy at low doses and reduced tendency to the development of resistance.

In this study, two classes of compounds, benzimidazoles and imidazopyridines, incorporating an intramolecular hydrogen bonding (IMHB) motif, were explored for their antimalarial potential. These two chemotypes were selected on account of their privileged nature due to their capacity to interact with various biological systems, leading to a wide variety of biological activities, including antimalarial activity. Structural modifications around the benzimidazole scaffold resulted in the classification of these analogues into 1*H*-benzimidazoles and *N*-benzyl benzimidazoles (astemizole-based). In this regard, 33 benzimidazole analogues were synthesized, fully characterized and evaluated *in vitro* for their antiplasmodium activity against both the drug-sensitive NF54 and the multidrug-resistant K1 strains of the *Plasmodium* parasite. As a result, the 1*H*-benzimidazole analogues manifested sub-micromolar potencies against the chloroquine-sensitive NF54 strain of *P. falciparum*, with IC_{50} values between 0.079 µM and 0.968 µM. The most potent analogue within this series was compound **1.3** (Figure 1) with an IC_{50} of 0.079 µM against the chloroquine-sensitive strain and 0.335 µM against the multidrug-resistant (K1) strain. The resistance index of compound **1.3** (RI = 4) suggests the possibility of cross-resistance with drugs like chloroquine.

The *N*-benzyl benzimidazole (astemizole-based) also displayed sub-micromolar activity against the chloroquine-sensitive strain of the parasite, with compound **2.3** (Figure 1) displaying the highest potency (IC_{50} *Pf*NF54 = 0.029 µM and IC_{50} *Pf*K1 = 0.117 µM) within the series. Generally, the benzimidazole analogues exhibited poor activity against the sexual gametocyte stage of the *Plasmodium* parasite in comparison to the asexual blood stage. However, compound **1.3** displayed sub-micromolar potency (IC_{50} = 0.382 µM) against early-stage gametocytes. Furthermore, selected potent analogues showed low cytotoxicity (SI = 39-1500) when tested *in vitro* against the Chinese Hamster Ovary cells. The *N*-benzyl benzimidazole analogues, designed based on the known antihistamine drug astemizole, were tested against the hERG (human ether-a-go-go-related)-encoded potassium ion channel. These analogues expressed >40% inhibition against the hERG ion channel at the highest test concentration with potencies between 0.96 and 13.24 µM. Regardless, these compounds showed an improved cardiotoxicity risk relative to verapamil, a potent hERG channel inhibitor (IC_{50} = 0.58 µM), and the control drug used in the experiment. In addition, the five (5) selected potent analogues displayed low microsomal metabolic stability in mouse, rat and human liver microsomes. This impeded the advancement of these potent analogues to *in vivo* efficacy studies. Meanwhile, metabolite identification studies provided insight into the metabolic hotspots, which can be addressed in future optimization campaigns to address this liability.

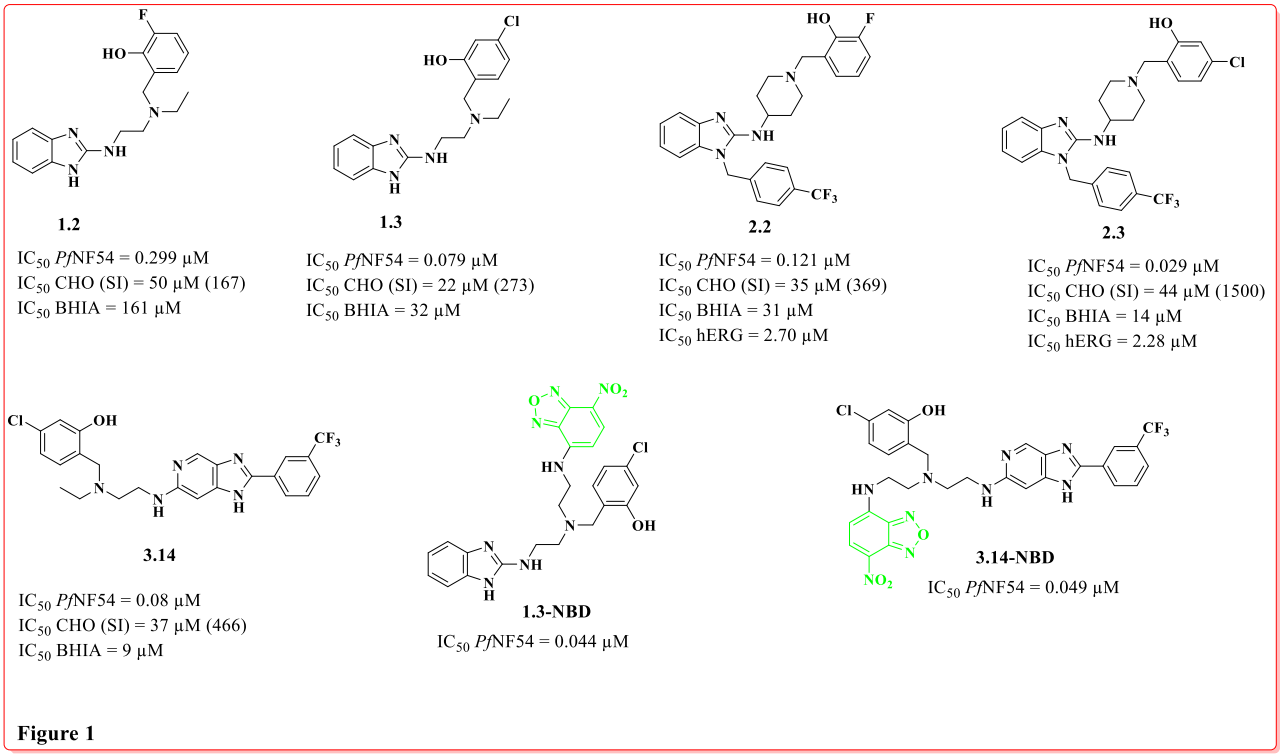

Figure 1

On the other hand, the imidazopyridine analogues were designed using the 1*H*-benzimidazole frontrunner analogue **1.3** as a guide. A structure-activity relationship (SAR) plan was pursued to produce diverse analogues due to modifications around the core scaffold. The SAR was explored with aromatic and aliphatic groups. As a result, 19 structural variants were synthesized and evaluated *in vitro* for their antiplasmodium activity against both the drug-sensitive NF54 and the multidrug-resistant K1 strains of the *Plasmodium* parasite. 13 of these analogues showed potencies of <1 μM with compound **3.14** (IC_{50} = 0.08 μM) displaying the highest potency within the series. Subsequently, most of the active analogues showed a favourable cytotoxicity profile against CHO cells, with compound **3.14** being the least cytotoxic (SI = 466). Like the benzimidazoles, selected potent imidazopyridine analogues exhibited low microsomal metabolic stability in mouse, rat and human liver microsomes, posing a hurdle to the progression of these compounds to *in vivo* proof of concept studies.

Aqueous solubility studies and physicochemical profiling of all the target compounds were carried out. The solubility results obtained were correlated with physicochemical parameters such as cLogP, melting points, TLC retardation factors and HPLC retention times to establish a solubility-property relationship across both classes of compounds. The correlation assessment revealed that different factors simultaneously affect the solubility of compounds across a series; hence, it may be crucial to assess these factors based on individual cases rather than an entire class of compounds. Also, the physicochemical assessment showed that both the benzimidazoles and the imidazopyridines complied with Lipinski's RO5 and Veber's rule. Single crystal X-ray structure analysis, IR spectroscopy, and DFT calculations were used to ascertain the presence of IMHB in the target compounds. Representative analogues **1.2** and **2.2** were used for these studies.

In an effort to elucidate the mechanism of action, novel fluorescent analogues [**1.3-NBD** (IC_{50} *Pf*NF54 = 0.044 μM) and **3.14-NBD** (IC_{50} *Pf*NF54 = 0.049 μM)] of the frontrunner compounds **1.3** and **3.14** were synthesized and pharmacologically validated as suitable probes for fluorescence live-cell imaging. The extrinsic fluorophore 7-nitrobenz-2-oxa-1,3-diazole (NBD) was employed due to the absence of intrinsic fluorescence properties in both compounds. Live-cell microscopy showed localization of both fluorescent analogues in all the studied organelles except the nucleus. While this suggests that the nucleus may not be a site of action for antiplasmodium activity, incorrect localization due to the NBD tag cannot be excluded. Based on the results from the live-cell imaging where both fluorescent probes accumulated in acidic organelles like the digestive vacuole and the neutral lipid bodies that

have been implicated in hemozoin formation, it was hypothesized that the parent compounds **1.3** and **3.14** could be inhibiting the formation of hemozoin. Docking studies employed to investigate this hypothesis predicted intermolecular interactions between the parent compounds and the heme/hemozoin surfaces to inhibit hemozoin formation. The heme fractionation studies of compound **1.3** showed a dose-dependent increase in heme levels with a subsequent decrease in hemozoin levels at increasing compound concentrations. In essence, these observations support hemozoin inhibition as a mechanism of action of compound **1.3** while pointing to other targets within the parasite based on widespread association with other organelles. However, compound **3.14** showed no significant change in heme levels, but a decrease in hemozoin levels with increasing compound concentration was observed. This indicates that compound **3.14** is not a hemozoin inhibitor but could be targeting different digestive vacuole processes.

LIST OF ABBREVIATIONS

ACTs	Artemisinin Combination Therapies
ADME	Absorption, Distribution, Metabolism and Excretion
ADMET	Absorption, Distribution, Metabolism, Excretion and Toxicity
API	Active Pharmaceutical Ingredient
AR	Analytical Reagent
ATR	Attenuated Total Reflectance
BCS	Biopharmaceutics Classification System
BHIA	Beta-Hematin Inhibition Activity
$CDCl_3$	Chloroform (deuterated)
CHO	Chinese Hamster Ovary (cells)
CQ	Chloroquine
CYP450	Cytochrome P-450
DCM	Dichloromethane
DDT	Dichlorodiphenyltrichloroethane
DFT	Density Functional Theory
DHAP	Dihydroartemisinin-Piperaquine
DHFR	Dihydrofolate Reductase
DHPS	Dihydropteroate Synthase
DMPK	Drug Metabolism and Pharmacokinetics
DMSO	Dimethyl Sulfoxide
DNDi	Drugs for Neglected Diseases Initiative
DOT	Directly Observed Therapy
DV	Digestive Vacuole
ECG	Electrocardiogram
ER	Endoplasmic Reticulum
G6PD	Glucose-6-Phosphate Dehydrogenase
GDP	Gross Domestic Product
GI	Gastrointestinal
GSK	GlaxoSmithKline
HBA	Hydrogen Bond Acceptor
HBD	Hydrogen Bond Donor
hERG	Human Ether-a-go-go Related Gene

HLM	Human Liver Microsomes
HPLC-MS	High-Pressure Liquid Chromatography-Mass Spectrometry
HTS	High Throughput Screening
IC_{50}	50% Inhibitory Concentration
IMHB	Intramolecular Hydrogen Bonding
iPS	Induced Pluripotent Stem
IPTp	Intermittent Preventive Treatment in pregnancy
IR	Infrared
IRS	Indoor Residual Spraying
ITNs	Insecticide-Treated Nets
LC-MS	Liquid Chromatography – Mass Spectrometry
LDH	Lactate Dehydrogenase
LLINs	Long-Lasting Insecticidal Nets
Log P	Lipophilicity
malERA	Malaria Eradication Research Agenda
MDA	Mass Drug Administration
MeOD	Methanol (deuterated)
MLEM	Model List of Essential Medicines
MLM	Mouse Liver Microsomes
MMV	Medicines for Malaria Venture
MoA	Mechanism of Action
MW	Molecular Weight
NBD	7-nitrobenz-2-oxa-1,3-diazole
NMR	Nuclear Magnetic Resonance
NP-40	Nonidet P-40
PBS	Phosphate-Buffered Saline
PD	Pharmacodynamics
Pd/C	Palladium on Carbon
***Pf*PI4K**	*Plasmodium falciparum* Phosphatidylinositol 4-Kinase
PK	Pharmacokinetics
PMB	*Para*-methoxybenzyl
RB	Rotatable Bond
RBM	Roll Back Malaria

R_f	Retardation Factor
RI	Resistance Index
RLM	Rat Liver Microsomes
RMSD	Root Mean Square Deviation
RO5	Rule of Five
SAR	Structure-Activity Relationship
SD	Standard Deviation
SERCaP	Single Encounter Radical Cure and Prophylaxis
SI	Selectivity Index
SP	Sulfadoxine-Pyrimethamine
TCPs	Target Candidate Profiles
TdP	Torsades de Pointes
TFA	Trifluoroacetic Acid
TLC	Thin Layer Chromatography
TPPs	Target Product Profiles
tPSA	Topological Polar Surface Area
t_R	Retention Time
UPR	Upfolded Protein Response
WHO	World Health Organization
XIC	Extracted Ion Chromatogram
XRD	X-Ray Diffraction

TABLE OF CONTENTS

LIST OF FIGURES

LIST OF SCHEMES

LIST OF TABLES

CHAPTER 1

INTRODUCTION AND LITERATURE REVIEW

1.1 Chapter Overview

This chapter provides a background on malaria as a disease in the context of its history, epidemiology, control, and preventive strategies. Together with antimalarials in the drug development pipeline, the status and challenges of malaria treatment options are discussed, taking into account the malaria eradication agenda with accompanying newly defined target candidate profiles (TCPs) and target product profiles (TPPs) for the next generation of antimalarials. Following is a discussion on some drug discovery methods to identify hits and leads for further development. Physicochemical parameters critical in drug development and strategies to modify these parameters towards improving their aptness for development are also outlined. Furthermore, the need to profile drug candidates against drug off-targets, such as the human ether-a-go-go-related gene (hERG) potassium ion channel, is presented. The concept of intramolecular hydrogen bonding (IMHB) and its importance in medicinal chemistry is highlighted, along with the various experimental descriptors by which IMHB in molecules could be ascertained. A literature synopsis of various pharmacological properties of benzimidazole and imidazopyridine chemotypes explored in this thesis research is also summarized. Finally, the chapter concludes with the justification of the research study, the research question, and the study's specific aim and objectives.

1.2 Malaria: Introduction and History

Malaria, of all diseases, is perhaps the one with the most subtle interplay with human history. Genetic variations in humans, such as thalassaemia, glucose-6-phosphate dehydrogenase deficiency, and sickle-cell traits, owe their prevalence to malaria.[1] Centuries after the Romans initially proposed the idea, it was believed that malaria was caused by "bad air" rising from swamplands.[2] Major advances in medicine and dedicated efforts of individual scientists helped shift the understanding of the disease from the ancient mythology-based approach to a precise scientific insight.[2]

In the blood of infected patients, malaria parasites were first discovered by Charles Louis Alphonse Laveran, a French Army surgeon. An Italian neurophysiologist, Camillo Golgi, later described the different species of malaria parasite based on the recurrence of attacks they

caused and the number of parasites released when the red blood cells in which they lodge ruptured. In 1898-1899, Giovanni Batista Grassi and co-workers showed that the female *Anopheles* mosquito was responsible for transmitting malaria from one human to another.[2,3]

Given the ruinous effects of malaria, the origins of the *Plasmodium* parasites infecting humans have long been a subject of interest. One long-lasting hypothesis suggested that humans and chimpanzees each acquired *P. falciparum*-like infections from their common ancestor and that these parasites co-evolved with their relevant host species for millions of years.[4] On the contrary, *P. vivax* was believed to have resulted from cross-species transmission of a parasite from a macaque in Southeast Asia.[5–7] However, both theories have been refuted recently following the characterization of additional *Plasmodium* parasites from African apes. It is presently clear that *P. falciparum* infection is relatively new to humans but originated from a gorilla, likely within the past 10,000 years.[8,9] Similarly, *P. vivax* did not emerge from Asia but represents a bottleneck lineage that escaped out of Africa.[10]

1.3 Epidemiology of Malaria

In humans, malaria is currently caused by five *Plasmodium* parasites: *P. falciparum*, *P. vivax*, *P. malariae*, *P. ovale* and *P. knowlesi. P. vivax* prevails mainly in South America, while *P. malariae* may occur in all malaria-endemic areas, although its prevalence is generally low. *P. ovale* and *P. falciparum* are distributed primarily in the tropics, particularly in Africa, with *falciparum* infections being the leading cause of mortalities worldwide.[11] *P. knowlesi* infection occurs only in some forested regions of Southeast Asia.[11]

Malaria transmission is more prevalent in places where the mosquito lifespan is longer. This gives the parasite enough time to complete its development inside the mosquito. The long life expectancy of the African vector species is why nearly 90% of the world's malaria cases are in Africa.[12] Climatic conditions such as rainfall patterns, temperature and humidity may influence the number and survival of mosquitoes. In most places, the transmission is seasonal, with a crest throughout and immediately after the rainy season. Malaria epidemics can arise when climate and other conditions support transmission in areas where individuals have little or no immunity to malaria. They can also occur when individuals with low immunity move into regions with high malaria transmission, to find work or as refugees.[12]

According to the World Malaria Report 2020, about 229 million malaria cases and 409 000 deaths were recorded in 2019. The WHO African Region continues to carry an unreasonably

high share (94%) of the global malaria burden. Consistently, children below five years are the most vulnerable group affected by the disease, and in 2019, they accounted for 67% (274 000) of all malaria deaths worldwide.[13]

Complications that arise from malaria are the cause of morbidity and mortality. Common non-specific manifestations include general body weakness, headache, fever, nausea and other gastrointestinal symptoms. Due to their effects on red blood cells, which often lead to haemolysis, anaemia is a common consequence. Prolonged or untreated malaria leads to compromised functioning of vital organs such as the spleen, liver, lungs, kidney, or even the brain, causing cerebral malaria.[14]

Direct and indirect economic losses occur in the setting of malaria. Households use a range of preventive measures such as mosquito coils, aerosol sprays, bed nets and mosquito repellents to differing degrees in different areas, which increases the cost of living. Indirect economic loss involves the opportunity cost of time foregone by the sick individual due to illness and the opportunity cost of healthy household members' time spent treating or attending to the ill person or accompanying them for treatment. Huge sums of money are expended on treatment and prevention programs besides the loss of working hours that lead to a reduction in the GDPs of affected countries.[15]

1.3.1 Malaria Parasite Life Cycle

Malaria is transmitted and spread from one person to another through the bite of the female *Anopheles* mosquito. There are about 400 distinctive species of *Anopheles* mosquitoes, but only 30 are vectors of significant importance.[16] During a blood meal, an infected mosquito injects sporozoites, which travel through the bloodstream to lodge in the liver (Figure 1.1). Further development occurs in the hepatocytes, producing merozoites, which infect the red blood cells upon release from the liver. The erythrocytic phase of malaria infection is then initiated.[17] The asexual division continues in the red blood cells, which burst to release more merozoites to infect other red blood cells. Some of the merozoites in the red blood cells develop into gametocytes, which are taken up by a mosquito during feeding. The gametocytes mature in the vector's gut as male (microgametocytes) and female (macrogametocytes) gametes and eventually fuse to form a zygote. The zygotes transform into motile ookinetes, which later develop into oocysts within the mid-gut of the mosquito. Upon further division of the oocysts, sporozoites are produced, which concentrate in the vector's salivary glands and are deposited

in the bloodstream of the next human host during a blood meal.[17] The most common mode of malaria transmission is from the anthropoid vector to the human host. Other ways of transmission include congenital malaria, which is transmitted from mother-to-child during pregnancy or at birth,[18] human blood transfusion[19] or even organ transplantation.[20]

In infections caused by *P. vivax* and *P. ovale*, there is a distinct dormant hepatic stage of the parasite called hypnozoites. These 'sleeping forms' may prevail for weeks, months, or years before getting reactivated to initiate the erythrocytic stage of infection.[21]

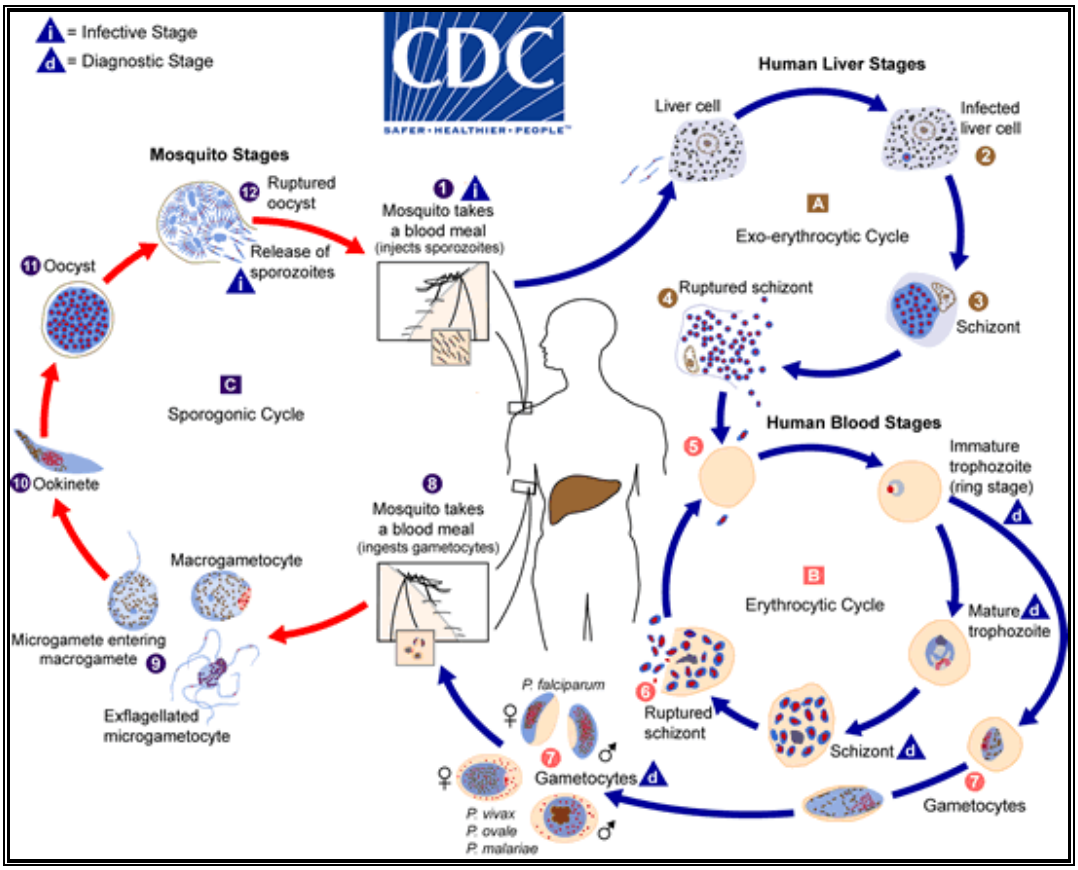

Figure 1.1: Malaria parasite life cycle.[22]

1.4 Malaria Control, Prevention and Treatment

Malaria is a complex disease to control primarily due to the vector and parasites' profoundly versatile nature. Whereas successful tools have been and will proceed to be developed to combat malaria, over time, the parasites and mosquitoes will evolve to evade those tools if used in confinement or used ineffectually. To achieve sustainable control over malaria, healthcare experts will require a combination of new approaches and tools. Research could play an essential role in the development of those next-generation strategies.

1.4.1 Vector Management and Control

Vector control can be achieved by making contact with the human host and mosquito impossible or merely killing the mosquitoes. Early vector control strategies included the screening of houses, mosquito nets, the drainage or filling of swamps and other water bodies used by mosquitoes for breeding, and the application of oil or Paris green to breeding places.[23] The revelation of the insecticidal properties of dichlorodiphenyltrichloroethane (DDT) in the 1940s[24] and the subsequent discovery of other insecticides shifted the focus of malaria vector control to the deployment of insecticides to attack both the larval and adult stages of mosquito vectors.[23]

The core vector control interventions applicable for all populations at risk of malaria in most epidemiological and ecological settings are the deployment of insecticide-treated mosquito nets (ITNs) that are prequalified by WHO, which in many settings are the long-lasting insecticidal nets (LLINs) and indoor residual spraying (IRS) with a product prequalified by WHO. Since 2000, 78% of the malaria clinical cases averted through interventions have been due to insecticidal vector control, namely through the widespread scale-up of ITNs and IRS.[25]

The resistance of malaria vectors to insecticides currently used in ITNs and IRS threatens malaria prevention efforts. Resistance to the four commonly used insecticide classes-pyrethroids, organochlorines, carbamates and organophosphates are reported across all WHO malaria regions.[26] Insecticide resistance is undoubtedly a significant challenge to the control of malaria vectors worldwide. This limits the tools available to achieve the goal of controlling and eliminating the disease. It is of utmost importance that novel insecticides and new control tools be designed to help manage and mitigate the impact of insecticide resistance.[26]

1.4.2 Chemoprophylaxis and Chemoprevention

Chemoprophylaxis refers to the use of antimalarial drugs to prevent the development of malaria in travellers to endemic areas. Although malaria chemoprophylaxis usually refers to all malaria species, there is a distinction between *P. falciparum* malaria prophylaxis and prophylaxis of the relapsing malaria species; thus, the choice of chemoprophylaxis also varies. It must be noted that no antimalarial prophylactic regimen gives complete protection, but good chemoprophylaxis (compliance to recommended drug regimen) significantly reduces the risk of the fatal disease.[27,28]

Malaria chemoprophylaxis comes in two phases- primary and terminal prophylaxis. Primary prophylaxis requires the use of antimalarial drugs at a recommended dosage, 2-20 days before departure to endemic areas and continued for the duration of stay and then 1-4 weeks after return. Primary prophylaxis may be causal or suppressive. Causal prophylaxis prevents infection in the liver by inhibiting the pre-erythrocytic schizogony. Primaquine and proguanil are effective as causal prophylactic drugs. Suppressive prophylaxis entails the use of blood schizonticides to suppress the blood forms of the malaria parasite and thus protect against clinical illness.[29]

On the other hand, terminal prophylaxis is the administration of primaquine for two weeks after returning from a malarious zone to tackle the hypnozoites of *P. vivax* and *P. ovale* that can cause relapses.[29]

Malaria chemoprevention is the sporadic administration of full treatment courses of an antimalarial medicine to children and pregnant women during the malaria season in highly seasonal transmission regions. The objective is to prevent malarial illness by maintaining therapeutic antimalarial drug concentrations in the blood throughout the highest malarial risk. Sulfadoxine-pyrimethamine (SP) as an intermittent preventive treatment for malaria in pregnancy (IPTp) has shown the ability to reduce maternal anaemia, low birth weight and perinatal mortality in sub-Saharan Africa.[25]

1.4.3 Vaccination

Several research projects for the discovery of malaria vaccines are ongoing. The only vaccine to have completed Phase 3 testing is RTS, S, which has been in development since 1987 by GlaxoSmithKline (GSK) and is designed to stop the *Plasmodium falciparum* malaria parasite from entering the liver, preventing the subsequent deadly blood stages.[30] During clinical trials, RTS, S reduced clinical incidence by 39% and severe malaria by 31.5% among children aged 5–17 months who completed all four doses. Following a positive scientific opinion of the European Medicines Authority under Article 58 in July 2015, the WHO recommended that RTS, S be implemented on a pilot scale in some parts of about three to five sub-Saharan African countries.[31] The integration of the RTS, S vaccine into the national immunization programmes of Malawi, Ghana and Kenya over the next five years is, therefore, an exciting moment for public health. Various other pre-erythrocytic vaccines are in trials, but none have shown the potential of RTS, S. Researchers are working on improving the efficacy of the vaccine to get it

to be more than 50% effective by employing prime boost technology, adjuvants and antigen optimization.[30] Recently, another promising vaccine, R21/Matrix-M has been reported to be 77% effective against the disease. In a randomized controlled trial, the low-dose, circumsporozoite, protein-based vaccine was safe with high-level efficacy over 12 months when administered to 450 children aged 5-17 months in Burkina Faso. A larger trial in children aged 5 months – 3 years will be performed across four African countries to confirm the findings.[32,33]

1.4.4 Mass Drug Administration Programme

Mass drug administration (MDA) refers to providing a therapeutic dose of an effective antimalarial drug to the entire target population, regardless of infection status or symptoms.[34] MDA has re-emerged as a recommended tool by the WHO to accelerate transmission interruption in areas approaching elimination. As rapid diagnostic tools are being used, they are not sensitive enough to detect the last parasite. Consequently, they leave large parts of the asymptomatic reservoir undetected.[35] Community erratic controlled trials of MDA with the long-acting antimalarial dihydroartemisinin-piperaquine (DHAP) and other interventions have shown this technique prudent and effective at significantly reducing malaria prevalence and incidence in pre-elimination settings.[36–38] This strategy is further exemplified by a recent trial in a low transmission area in Zambia. Two rounds of MDA-DHAP on top of a standard of care of improved access to case management, vector control and surveillance were evaluated. *Plasmodium falciparum* parasite prevalence in children under five years of age under the MDA programme remarkably reduced from 7.7% at baseline during peak transmission to <1% during the following year's peak season 3-months post-MDA. This represents an 87% larger decrease compared to the standard of care. These findings have influenced the Zambia National Malaria Elimination Centre to add MDA-DHAP to its package of interventions in areas targeting subnational elimination.[34]

1.5 Malaria Chemotherapy

Chemotherapy remains, undoubtedly, the mainstay of malaria control and has evolved since the first antimalarial drug, quinine. This drug was isolated from the bark of a high altitude tree called *Cinchona officinalis*, native to South America. It was the earliest remedy for malaria, with its use dating back to the 17th century.[39] Resistance was first reported in the 1980s[40] and

is no longer employed as front-line therapy for malaria. Nonetheless, quinine is on the WHO's Model List of Essential Medicines (MLEM) to treat acute malaria cases where artemisinins are not accessible. The MLEM consists of the drugs that are considered to be efficacious and safe to meet the most important needs in a health system.[41]

Chloroquine (CQ), a 4-aminoquinoline, was used to treat all forms of malaria during the 1940s. CQ (Figure 1.2) was clinically used for malaria treatment until resistant parasites emerged and spread. This brought about a discontinued use of CQ in many countries.[42–45] Chloroquine is on the MLEM to treat *P. vivax* in regions where resistance has not evolved.[41] Other quinoline agents such as pamaquine were employed as an antimalarial before the discovery of chloroquine. Mepacrine was predominantly used as a prophylactic, sold under the trade name Atabrine during the Second World War. It is no longer used today due to the high chance of undesirable side effects such as toxic psychosis.[46] Subsequent research led to discovering the prophylactic primaquine, an 8-aminoquinoline, with remarkable activity against *P. vivax* and *P. ovale* malaria.[47]

During the 1970s, mefloquine (Figure 1.2) was developed by the United States Army[48] and is still being used today. It was initially introduced to treat chloroquine-resistant malaria and used both as a curative and a prophylactic drug. Resistance against mefloquine was first reported in 1986.[49] It is thought that the structurally related quinoline drugs exhibit their antimalarial activity by the accumulation of ferriprotoporphyrin IX, a toxic metabolite resulting from the interference of hemoglobin metabolism in the parasite.[50] In those parts of the world where parasite sensitivity to the quinoline drugs has declined and where few alternatives are available, cure rates have been improved when the drug is combined with the antibiotics tetracycline or clindamycin.[51]

Simultaneously during World War II, drug development focused on pyrimidine derivatives based upon their presence in nucleic acids and their metabolism by protein systems effectively blocked by antimalarial sulphonamides. Research in this direction resulted in the development of the antifolate antimalarial agents.[52] Antifolate antimalarials are subdivided into two classes: inhibitors of dihydropteroate synthase (DHPS) and inhibitors of dihydrofolate reductase (DHFR). Synergy is achieved when DHPS and DHFR inhibitors are used in combination in the treatment of malaria.[52]

Proguanil (Figure 1.2) was the primary detailed antimalarial antifolate agent, and studies demonstrated that it is a prodrug that metabolizes to its triazine form chlorcycloguanil, an

inhibitor of the parasite DHFR.[53] Further studies on proguanil showed that chlorination of the phenyl ring and the increase in the linker between the phenyl ring and the diaminopyrimidine ring increase the potency of this class of antifolates.[52] As a result, chlorproguanil and clociguanil were discovered.[52] Chlorproguanil was used in combination with dapsone, a sulphonamide, for the treatment of uncomplicated malaria, but haemolysis in glucose-6-phosphate dehydrogenase (G6PD)-deficient patients led to its withdrawal from clinical use.[54] Pyrimethamine, a 2,4-diaminopyrimidine, with structural similarities to proguanil, has been the most widely used antimalarial antifolate agent. It is utilized in combination with other antimalarial drugs, and to a lesser extent, it has been used in monotherapy.[55–57]

The increased exposure of non-immune persons to resistant strains rekindled interest in sulphonamides and sulfones as antimalarials. These sulpha drugs are known to inhibit the enzyme dihydropteroate synthase (DHPS) that catalyzes the first step in the pathway that involves the synthesis of dihydrofolate from para-aminobenzoic acid.[52] In the past, attempts were made to use these sulpha drugs as monotherapy but were abandoned because of their low efficacy and unacceptable toxicity.[58] The scrutiny in this class of antifolates was encouraged when it was demonstrated that they synergized with DHFR inhibitors, thus explaining their use as components in antifolate combinations. As exemplified, the sulfadoxine-pyrimethamine combination is the preferred option for preventing malaria among pregnant women and as an intermittent preventive therapy. Similarly, trimethoprim-sulfamethoxazole with the trade name co-trimoxazole has been widely used in the treatment of childhood fevers, bacterial infections and traveller's diarrhoea.[50,59–61]

The introduction of artemisinin-derived drugs in the 21st century has perhaps revived hopes of conquering malaria. Tu Youyou first isolated artemisinin from the plant *Artemisia annua*, a herb commonly used in Chinese traditional medicine.[62] The evidence of the antimalarial properties of artemisinin existed as far back as the 1970s. It was still not widely used until early 2000, when the WHO approved it as a drug of choice for uncomplicated malaria.[63,64] Artemisinins are efficacious against all multi-drug resistant forms of *P. falciparum*. The most common semi-synthetic derivatives of artemisinin are artesunate, artemether and arteether. These are prodrugs that are transformed to the active metabolite, dihydroartemisinin.[65]

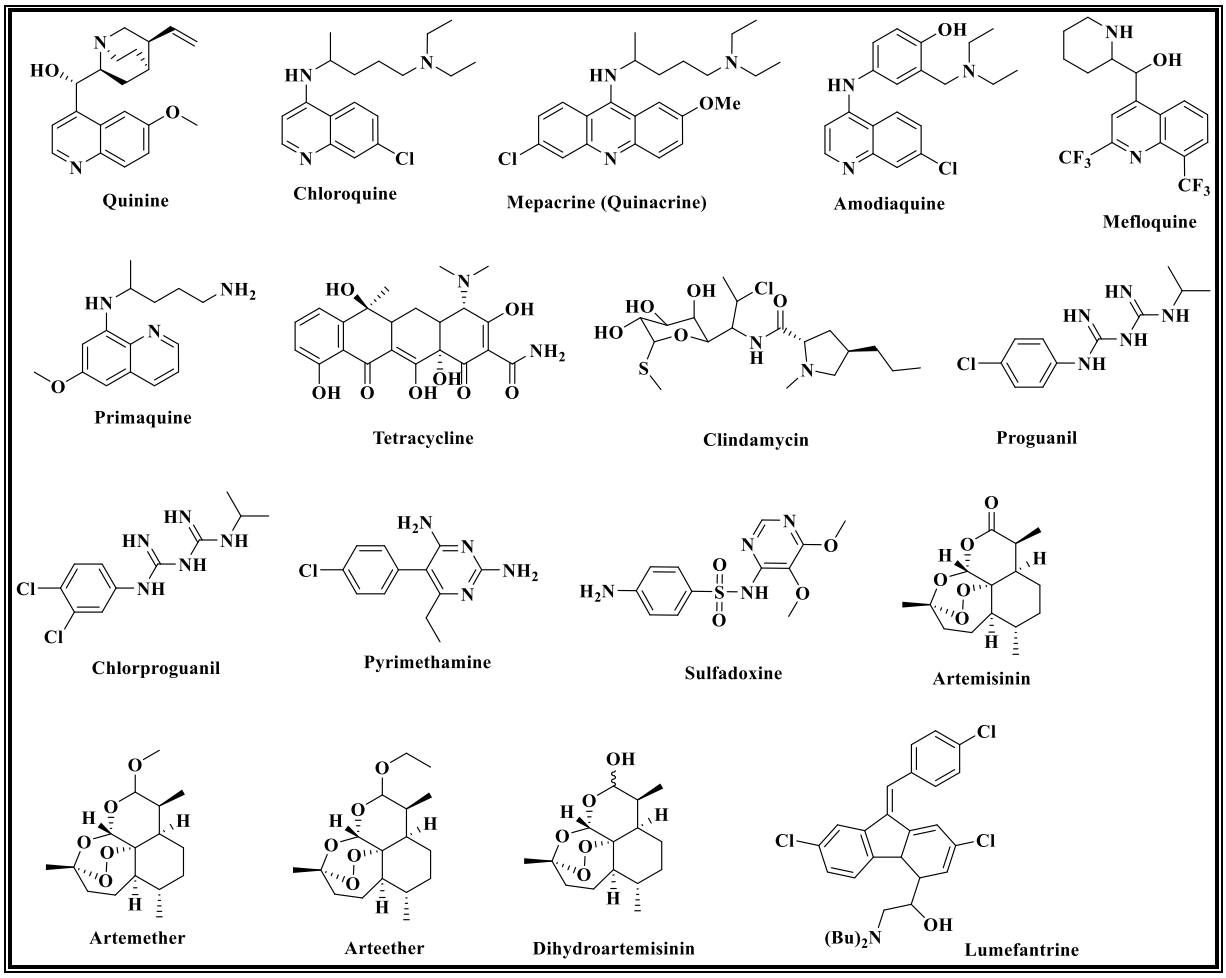

Figure 1.2: Chemical structures of some past and current antimalarial drugs.

The mechanism of action (MoA) of artemisinin and its derivatives is thought to be due to the endoperoxide groups. When the parasite is located inside red blood cells, it consumes hemoglobin within its digestive vacuole by the hemoglobin degradation enzymes.[51] The process releases ferrous ions, which catalyze the cleavage of the peroxy moiety to form oxygen or carbon-free radicals. These free radical intermediates disrupt the biomembrane and inhibit the cysteine protease of the vacuoles.[51] Evidence of other possible mechanisms of action has been found. A computational approach to determine the MoA based on previous studies has identified haem and *Pf*ATP6 (Ca^{2+} transporter) as potential targets.[66] In more recent years, artemisinin was shown to be related to the up-regulation of the unfolded protein response (UPR) pathways, which may be connected to decreased parasite development.[67] In another study, artemisinin has also been shown to be a potent inhibitor of *P. falciparum* phosphatidylinositol-3-kinase (*Pf*P13K).[68]

The ascendancy of the artemisinins is their ability to rapidly clear blood parasites to below detectable levels. Due to their short elimination half-lives (typically 2-5 hours), they do not encourage selection pressure for the development of resistance.[68] Unfortunately, reports of resistance to artemisinin-based drugs have emerged, especially in Southeast Asian countries like Cambodia, Thailand and Vietnam.[69] Recent reports also suggest the emergence of resistance to these drugs in some parts of Africa (Rwanda).[70,71] To curb resistance and achieve high efficacy, artemisinins are used in combination with other antimalarial drugs like mefloquine, amodiaquine, lumefantrine, sulfadoxine-pyrimethamine (SP) and piperaquine. The drugs used in combination with the artemisinins are recommended to act via a different mechanism. They should also have a slower *in vivo* elimination to achieve synergy, reduce the chances of developing resistance, and minimize side effects.[45,72–74]

1.5.1 Challenges in malaria chemotherapy

Over the decades, several actions and strategies have been employed for the control and eradication of malaria. However, challenges still abound, with the emergence and spread of drug-resistant parasites being the most daunting threat to the continuity of current therapies.[75–78] Interactions among people from malaria-endemic and non-endemic regions also hamper malaria eradication efforts as transmission remains an undeniable fact.[79,80] Most of the current drugs act principally at only one of the *Plasmodium* life cycle stages (Figure 1.3), mainly the erythrocytic stage associated with malaria's clinical symptoms. Drugs capable of targeting all the life cycle stages of the plasmodium parasite are needed if malaria eradication is to be attained. Also, newer medications that act by novel mechanisms and can interrupt the parasite life at multiple stages are urgently needed.[81] Furthermore, the current portfolio of antimalarials, both in clinical use and development, has several other shortfalls that warrant the search for better alternatives. For instance, primaquine, which is the sole clinical agent against the hepatic forms of *P. vivax*, causes fatal haemolysis among patients who lack glucose-6-phosphate dehydrogenase (G6PD), an enzyme involved in regulating cellular oxidative stress.[47,82] Similarly, amodiaquine is associated with hepatotoxicity and agranulocytosis, thought to result from its metabolism to the quinone imine and reactive aldehyde metabolites, respectively.[83–86] Neurological backlash has also been ascribed to the use of mefloquine amongst some patients.[87–89]

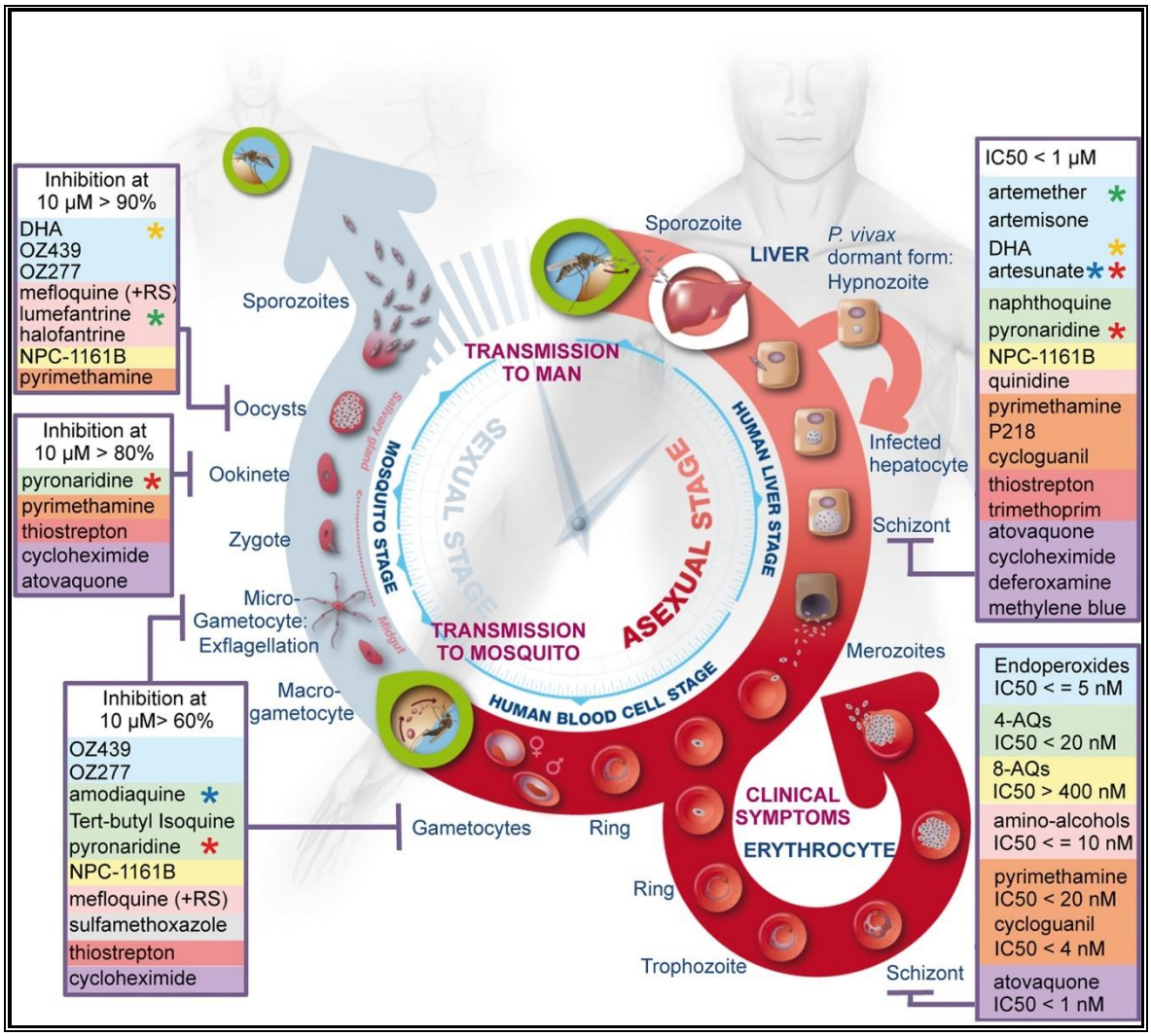

Figure 1.3: The activities of some current antimalarial drugs on the life cycle stages of *Plasmodium*.[90]

1.6 Current Antimalarials in Clinical Development

In an effort to reduce the global malaria burden, new product development partnerships such as Medicines for Malaria Venture (MMV) and the Drugs for Neglected Diseases Initiative (DNDi) were created. These partnerships have harnessed the expertise of the pharmaceutical industry and malaria academics, with financial support from funding organizations like the Bill and Melinda Gates Foundation. Consequently, the recent decade has seen a spring up of partnerships and collaborations featuring academic institutions, pharmaceutical companies and non-governmental organizations geared towards drug discovery for neglected tropical diseases.[50,91,92]

The model of malaria control and elimination has been expanded to encompass a goal of global eradication. The Malaria Eradication Research Agenda (malERA) was developed to address knowledge gaps and modern tools needed to eradicate malaria globally. MalERA was initiated after the rectification of malaria elimination as a long-standing intent during the Malaria Forum summoned by the Bill and Melinda Gates Foundation in October 2007. This was subsequently supported by the WHO, the Roll Back Malaria (RBM) Partnership and many other organizations and institutions.[93] Given this initiative, a proposal was published for the types of molecules [target candidate profiles (TCP)] and medicines [target product profiles (TPP)] required, setting clear goals for new therapies.[94] The 'candidate' in TCP refers to a single molecule usually in conventional regulatory preclinical safety assessment or human volunteer studies. The 'product' in TPP, on the other hand, refers to a final product, which may contain two or more active candidates and, importantly, the appropriate formulation.[95] In public healthcare, the publication and feedback for TCPs and TPPs is a critical part of their refinement. Because drug development takes over a decade to complete, TCPs and TPPs are living documents; thus, they need to be streamlined to reflect changes in patient needs and the clinical landscape, new safety findings and technical progress.[95] Table 1.1 below gives an overview of newly defined TPPs and TCPs.

Table 1.1: Overview of newly defined TPPs and TCPs.[95]

Profile	**Intended Use**
TPP-1	Case management; treatment of acute uncomplicated malaria in children or adults. Uses a combination of two or more molecules with TCP-1 activity, plus TCP-5 for reducing transmission and TCP-3 for relapse prevention, when such molecules become available. For severe malaria, a parenteral formulation of a single fast-acting TCP-1 would be appropriate.
TPP-2	Chemoprotection: given to subjects migrating into areas of high endemicity or during epidemics. Uses a combination of TCP-4 activity, potentially with TCP-1 support for emerging infections.
TCP-1	Molecules that clear asexual blood-stage parasitaemia
TCP-3	Molecules with activity against hypnozoites (mainly *P. vivax*)
TCP-4	Molecules with activity against hepatic schizonts
TCP-5	Molecules that block transmission (targeting parasite gametocytes)

TCP-6	Molecules that block transmission by targeting the insect vector (endectocides)

For eradication to be effective, drug therapy must annihilate the human reservoir of infection, and this is an objective best achieved by Single Encounter Radical Cure and Prophylaxis (SERCaP).[93] Such a single-dose treatment would be efficient against malaria-resistant strains, cure clinical malaria, stop transmission and prevent relapses. In addition, SERCaP represents the ideal treatment because it could promote compliance since it could easily be administered as directly observed therapy (DOT).[94] Ideally, a SERCaP medicine would be universally well-tolerated in vulnerable populations and those with co-infection and thus be suitable for MDA programmes. Also, an ideal treatment should offer prophylaxis for a minimum of one month post-treatment. It is paramount to emphasize that this may not be achievable; thus, compromises will undeniably have to be made.[94,95]

These eradication strategies have resulted in current approaches in designing new antimalarial compounds with chemical structures (Figure 1.3) different from the 'traditional' chemical scaffolds of existing antimalarial agents. Novel chemotherapeutic agents have emerged over the past few years with promising potential as future antimalarials. Table 1.2, adapted from the MMV's portfolio, shows antimalarial compounds, including those supported by MMV at different phases of clinical development. After pre-clinical evaluation, the clinical development of a drug candidate consists of three phases. During phase I, the safety, tolerability and dosing in healthy adult volunteers are determined. The drug candidate then progresses to phase II, where it is tested in a limited number of patients for proof-of-concept and further safety evaluation. Phase III clinical trials involve many patients in endemic countries and aim to compare efficacy with the standard of care. This phase also reconfirms safety before the product is finally licensed.

Table 1.2: Summary of antimalarial drug candidates at different phases of development.[α]

Translational		**Product Development**	
Preclinical	**Human volunteers**	**Patient exploratory**	**Patient confirmatory**
MMV371 Janssen	**M5717** Merck KGaA	**Ganaplacide/Lumefantrine** Novartis	**Dihydroartemisinin-**

			piperaquine dispersable Alfasigma
MMV183 (TropIQ)	**ZY19489** Zydus Cadilla	**Cipargamin** Novartis	**Artemether-lumefantrine <5kg** Novartis
MMV646 (Jacobus)	**Atoguanil** Ipca	**Ferroquine** (Sanofi)	**Sulfadoxine-pyrimethamine** Swipha/Biogaran
INE963 Novartis	**MMV533** Sanofi		**Sulfadoxine-pyrimethamine** Enzor Pharmaceutical
GSK701 GSK			

[α]Adapted from MMV's summary of the global portfolio of antimalarial candidates in clinical development (last updated February 2021).[96]

MMV646 (JPC-3210) is a trifluoromethyl pyridine analogue that resulted from a comprehensive structure-activity relationship studies of the 2-aminomethylphenol class of compounds.[97] It is an erythrocytic schizonticide with *in vitro* potency against multidrug-resistant cell lines of *P.falciparum*, low cytotoxicity, *in vivo* efficacy against murine malaria.[97] It showed a favourable preclinical pharmacokinetics, including a long plasma elimination half-life of 4.5 days in mice and 11.8 days in monkeys. MMV646 displayed a high oral bioavailability (86%) and a linear single-oral-dose pharmacokinetics across the dose range of 5 to 40 mg/kg of body weight in mice.[98] The mechanism of action of MMV646 is currently unknown. Its potency against multiple drug-resistant strains underpins the hypothesis that its MoA is different from currently used antimalarials.[99] It is in the final stages of preclinical development prior to testing in humans.

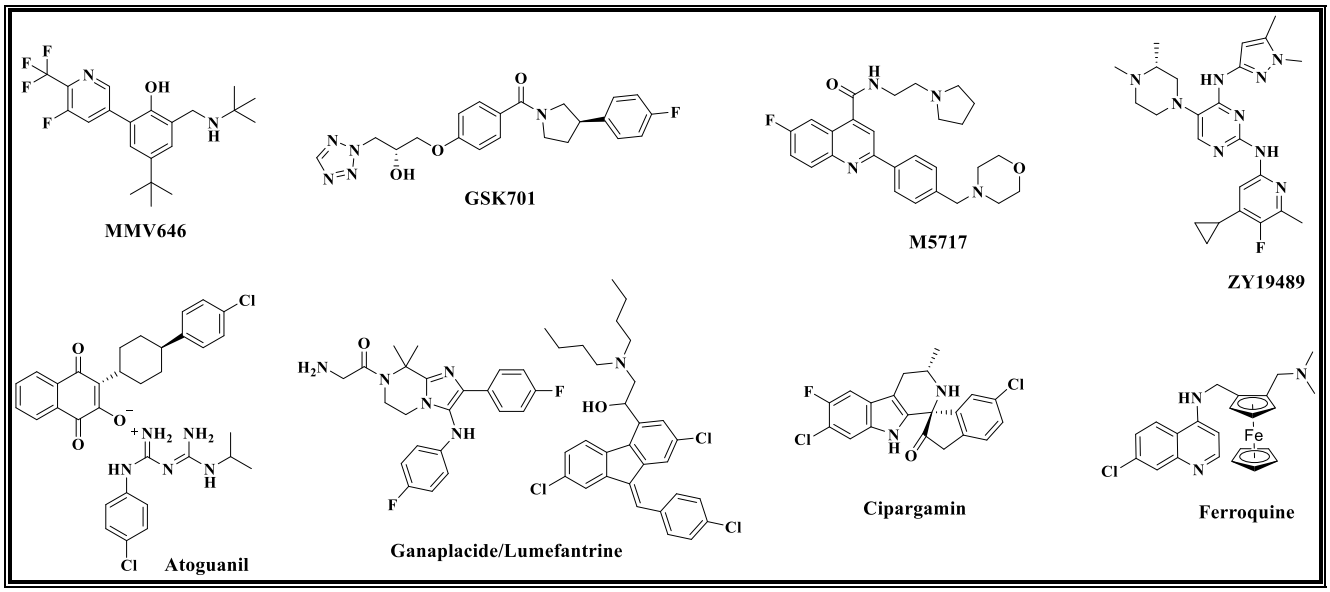

Figure 1.4: Chemical structures of some new antimalarial clinical candidates.

GSK701 (MMV1582367) is a new antimalarial in preclinical trials discovered by GlaxoSmithKline with support from the Wellcome Trust.[96] It is potent and active against resistant strains of *P.falciparum*, fast killing both *in vitro* and *in vivo* with a low single dose prediction (250 mg). GSK701 is reported to have a novel mechanism of action that is distinct from already existing antimalarials.[96]

M5717, shown to have potency against multiple stages of the Plasmodium parasite through a novel mechanism of action was developed by a team led by the Drug Discovery Unit (DDU) in Dundee in 2015.[100,101] This compound showed almost equal potency against several drug-resistant strains(3D7, K1, W2, 7G8, TM89C2A, D6 ana V1/S) and similar potencies across multiple life cycle stages (liver schizonts, gametocytes and ookinetes).[100] When evaluated *in vivo* in a *P.berghei* mouse model for a single dose efficacy, it showed > 99% reduction in parasitemia at doses of 4 x 30 mg/kg p.o and an ED_{90} of 0.1-0.3 mg/kg.[101] M5717 could be used as a long-duration partner in combination therapy with a fast-acting compound due to its ability to clear blood-stage parasites via a novel mechanism of action (*Pfe*EF2 inhibition).[94] It is presently in Phase I clinical trials.

ZY19489 (MMV253)is a novel triaminopyrimidine discovered by AstraZeneca in 2015 via a phenotypic high-throughput screen and further medicinal chemistry optimizations.[102] It showed good *in vitro* potency and *in vivo* efficacy when administered orally in a *P. falciparum* SCID mouse model. *Plasmodium* parasites were cleared below the detection limit after 4 days of

daily treatment with a 20 mg/kg dose, and a maximum kill rate was observed at 40 mg/kg.[102] No spontaneous reduction in potency was observed when the compound was screened against various resistant mutant strains with different resistance mechanisms due to its novel mechanism of action (*Pf*ATP4 inhibition).[102] ZY19489 has the potential to be a single-dose cure for P. falciparum and P. vivax malaria due to its rapid parasites killing activity across all the intraerythrocytic stages, long half-life, low resistance potential and novel mechanism of action. It has recently completed phase I clinical trials in healthy volunteers and would be evaluated in multiple ascending dose (MAD) phase I and phase I combination studies.[103]

Atoguanil is a co-formulated prophylactic antimalarial with the active ingredients atovaquone and proguanil. It was jointly developed by Ipca laboratories and MMV. Atoguanil's mechanism of action is through the interference with two pathways involved in the biosynthesis of pyrimidines required for nucleic acid replication. The presence of atovaquone also makes atoguanil a *P. falciparum* mitochondrial electron transporter inhibitor and is presently in phase I clinical study.[96]

Ganaplacide/Lumefantrine is an antimalarial combination therapy of Ganaplacide (an imidazolopiperazine), also known as KAF156 and lumefantrine (a synthetic amino alcohol fluorene derivative). Ganaplacide was identified by Novartis via a high-throughput screen and medicinal chemistry optimization program.[104,105] It has a prophylactic potential and has shown transmission-blocking activity in a Standard Membrane Feeding Assay.[106] Lumefantrine is a slow-acting antimalarial mostly used in combination therapies. Ganaplacide/Lumefantrine is reported to affect the parasite's internal protein secretory pathway, but the target is unknown. Decreased susceptibility to ganaplacide is associated with mutations in three *P.falciparum* genes, namely, CARL (cyclic amine resistance locus), UDP-galactose and Acetyl-CoA transporters.[96]

Cipargamin, also known as **KAE609,** is a synthetic antimalarial belonging to the spiroindolone class. It possesses both the potency (average IC_{50} of 550 pM against asexual blood-stage *P. falciparum*) and favourable pharmacokinetics (elimination half-life of approximately 24 hours in humans) required for a single-dose cure.[107,108] This feature could help slow the onset of parasite resistance, which is not shared by existing, approved antimalarial drugs. **Cipargamin** is also unique in its ability to block transmission to mosquitoes and is a parasite P-type ATPase4 inhibitor.[109,110] It is currently in phase II clinical trials to treat acute, uncomplicated malaria due to *P. falciparum* mono-infection.

Ferroquine is a member of the 4-aminoquinoline family, discovered by Sanofi-Aventis that has shown promising efficacy and safety profile both as monotherapy and in combination with artesunate.[111] It retains activity against chloroquine- and piperaquine-resistant parasites *in vitro* and has a long elimination half-life of 16 days.[111] The basic centres of the 4-aminoquinoline core enable the accumulation of ferroquine in the acidic environment of the digestive vacuole. This prevents hemozoin formation, causing a build-up of toxic heme and consequently leads to the death of the parasite.[112] In addition, the ferrocene core generates toxic free radicals, which provide an additional mechanism of action.[113] Following the termination of the artefenomel-ferroquine combination, the rights of ferroquine have been transferred to MMV for further investigation in a new Phase II combination study.[103]

1.7 Approaches to Drug Discovery and Development

1.7.1 Phenotypic Whole-Cell Screening and Target-based Strategies

The overall goal of all drug discovery efforts is to develop efficacious and safe therapeutics to treat diseases effectively. Phenotypic-based screening strategies were the foundation of pharmaceutical drug discovery well before molecular target-based drug discovery became popular.[114] The principal application of cell-based phenotypic assays is to screen large compound libraries to identify chemical matter starting points for drug discovery projects. Usually, a characteristic associated with the disease is exploited, and compounds are then tested to identify active hit compounds that enhance the disease phenotype.[114] Primary hits identified from phenotypic screens may have different targets, and lead compounds can further be developed from these hits with or without the knowledge of the target. However, identification of the target could facilitate structure-activity relationship (SAR) studies. Phenotypic screening enables the discovery of lead compounds for many rare diseases understudied or lacking effective drug therapy. Furthermore, recent rapid advances in various technologies for cell-based phenotypic screening, including induced pluripotent stem (iPS) cell technologies[115] and gene-editing tools such as CRISPR-Cas[116], have enabled the development of novel cell-based disease models that promise to more realistically recapitulate human disease biology.

The molecular target-based approach for drug discovery, on the other hand, generally begins with target identification relevant to a disease of interest. Through basic research, molecular targets are often discovered with studies involving animal disease models and clinical observations of patient phenotypes.[114,117,118] Assay development is initiated once a suitable

target has been identified and validated, followed by high throughput screening (HTS) of chemical libraries to identify inhibitors or antagonists against the target. The most active compounds are then confirmed and validated in orthogonal assays that are more physiologically related to the target. Chemical optimization to characterize the SAR of the lead series and augment favourable absorption, distribution, metabolism and excretion (ADME) is then carried out. Pharmacokinetic/pharmacodynamic (PK/PD) properties of the compounds are also assessed.[114,118] For about three decades now, molecular target-based screening has become the dominant approach in early drug discovery, albeit with its limitations.[119] Recent analysis has revealed that high attrition rates in Phase II and Phase III clinical trials are mainly due to a lack of drug efficacy and other factors.[120,121] Amidst factors such as the weak correlation of animal models with human diseases and genetic variation of patient populations, invalidated targets for a disease is a notable factor for many failed drug candidates. The number of validated druggable targets currently available for drug development is apparently more limited than previously perceived.[122,123]

Overall, both phenotypic screening- and target-based approaches to drug discovery have limitations. Thus, rather than viewing both approaches as opposing alternatives in novel drug discovery, they should be seen as complementary approaches that can increase the chances of discovering and developing drugs with novel efficacious molecular mechanisms of action. The trend toward 'empirical drug discovery' [124,125] recognizes the complementarity with target-based campaigns. As unveiled using phenotypic screening, the biological relevance alleviates the danger of possible failure in the development pipeline.[119]

1.7.2 Drug Repurposing, Repositioning and Rescue

De novo drug discovery is a time-consuming, laborious, costly and high-risk process, often with low returns regarding the number of drugs that finally make it to the market. This has served as a source of inspiration for other alternatives with chances of shortening the time and reducing financial investments, especially in neglected tropical diseases. Drug repurposing is an effective strategy in finding new indications for existing drugs.[126,127] Even though the terms drug repurposing and drug repositioning are often used interchangeably, drug repurposing refers to cases where an existing drug, approved by a regulatory agency in one disease area, is found to be active against another disease. In contrast, drug repositioning refers to cases where a drug active in one disease is used as a template for chemical modification to generate

derivatives optimized for another disease. An extension of this concept is drug rescue, where new uses are found for drugs that have failed for one disease indication, either pre-or post-approval or abandoned in development.[126] One of the advantages of these approaches is that in many cases, they have already proven to be adequately safe in preclinical models and, at least, at early-stage trials in humans, hence being less likely to fail from a safety perspective in subsequent efficacy trials. Regarding approved drugs, they have successfully passed clinical trials and regulatory scrutiny and undergone post-marketing surveillance.[128] While new uses for drugs (such as bupropion, thalidomide, sildenafil and aspirin) have sometimes been found fortuitously, some strategies exist to identify drugs that can be used for other indications. These strategies include similarities in cell biology and drug targets, computational approaches and exploitation of genome information.[129,130]

1.8 Physicochemical Properties in Drug Discovery and Development

Physicochemical properties propel a drug's metabolism, efficacy and safety by controlling binding affinities for macromolecules. Studies have shown that physicochemical properties such as molecular weight, lipophilicity, polarity, ionization, and hydrogen bonding influence a compound's overall properties and, consequently, have a bearing on solubility and permeability. Drugs must be sufficiently soluble and permeable to reach the site of action and be capable of being successfully formulated.[131–134]

1.8.1 Solubility

Solubility, the phenomenon of dissolution of a solute in a solvent to give a homogenous system, is one of the descriptive parameters to achieve the desired concentration of a drug in systemic circulation for a desired pharmacological response.[135] Solubility has a crucial role in the success of *in vitro* absorption, distribution, metabolism, excretion and toxicity (ADMET) as well as bioassays. Compounds with poor aqueous solubility often lead to artificially weak potency and low high-throughput screening hit rates. The low solubility of compounds in assays can lead to the misinterpretation of data as good selectivity and mistakenly identifying inferior compounds for further advancement. In this regard, information on solubility during the early stages of drug discovery is beneficial to guide compound selection, help decision-making and provide an early alert for potential issues in ADMET.[136] Insoluble compounds also contribute to poor oral absorption and poor oral bioavailability. Apart from solubility-limited

absorption, oral absorption can also be dissolution-rate-limited. Thus, if compounds have a slow dissolution rate, they might miss the absorption window in the small intestine and have a reduced fraction absorbed. Solubility data can be used to simulate *in vivo* pharmacokinetics, which could aid prediction for efficacious doses, especially solubility in intestinal fluids.[136,137]

Information on the solubility of an active pharmaceutical ingredient (API) is pivotal in predicting human oral pharmacokinetics and designing dose regimens in clinical trials. Poorly soluble drugs are associated with wavering absorption and inconsistent exposures during testing. The variability in the pharmacokinetics of a drug candidate can hinder its development and may require further investigations to meet the criteria set by drug regulatory authorities. Overall, this negatively impacts the costs and time taken in developing a drug.[136]

1.8.2 Lipophilicity and permeability

For a drug development program to be successful, it requires the optimization of specific and potent recognition by its pharmacodynamic targets and efficient delivery to these target sites. Lead compounds require not only good solubility but also the right lipophilicity. Lipophilicity (Log P) is a measure of the partitioning of a compound in a hydrophobic solvent (octanol) and a hydrophilic solvent (water) at equilibrium. Although solubility is necessary for compound dissolution, lipophilicity allows it to cross the phospholipid membranes. Lipophilicity affects the ADMET characteristics of drugs, contributes to their permeability through membranes, impacts their pharmacokinetics, and affects their pharmacodynamic and toxicological profile.[138,139] Compounds with high lipophilicity are mostly associated with high affinity for biomolecules such as proteins, resulting in high plasma protein binding, which affects the concentration of unbound drug in the plasma. This consequently impacts pharmacokinetic parameters such as clearance and volume of distribution, which are crucial for determining *in vivo* efficacy.[138] The ability of a compound to bind to any target is, in part, a function of its lipophilicity, and this contribution is higher for more lipophilic compounds. These effects result in unspecific binding of compounds to most, if not all targets. Hence, more lipophilic compounds are more promiscuous in binding and give rise to off-target pharmacological responses, resulting in high toxicity.[132,140]

Drug molecules encounter several different membrane barriers such as gastrointestinal (GI) epithelial cells, blood capillary wall, hepatocyte membrane, blood-brain barrier and the target cell membrane. The speed at which drug molecules cross these membrane barriers is a measure

of their permeability. The primary route for permeability is passive diffusion driven by a concentration gradient.[141] Even though lower molecular weight molecules travel faster across membranes, the right balance of polarity is required for association with the phospholipid bilayers made up of inner hydrophobic and outer hydrophilic layers. Lipophilicity is necessary for the interaction of compounds with the inner hydrophobic layers, while polar groups aid with the interactions associated with the hydrophilic surfaces, most importantly for oral drugs. Altogether, solubility, permeability and metabolic stability are key factors that determine the ultimate drug concentration in systemic circulation, thus the bioavailability.[138,142]

1.8.3 Biopharmaceutical Classification System

The Biopharmaceutics Classification System (BCS) is a guide for predicting the intestinal drug absorption provided by the U.S. Food and Drug Administration. This system confines the prediction using the parameters, solubility and intestinal permeability. The solubility parameter is based on the highest dose strength of an abrupt liberated product. When the highest dose strength of a drug is soluble in 250 mL or lower of aqueous media over the pH range of 1 to 7.5 at 37 °C, that drug is considered highly soluble. The intestinal permeability parameter is based on a comparison to the intravenous injection. A drug is considered highly permeable when the extent of absorption in humans is 90% or more of an administered dose.[143,144] Based on the BCS, drugs are classified into four categories based on their solubility and intestinal permeability. These categories are:

- Class I- High solubility, high permeability
- Class II- Low solubility, high permeability
- Class III- High solubility, low permeability
- Class IV- low solubility, low permeability

The BCS concept has been used for formulation design from the early to the clinical stages of drug development. Drug molecules in the BCS class I category are defined as highly soluble and highly permeable. There is no rate-limiting step for oral absorption, and formulation for this class of drugs is designed to ensure rapid dissolution in the gastrointestinal tract. The bioavailability of BCS class II drugs is rate-limited by their dissolution due to low solubility; thus, a small increase in dissolution rate sometimes results in a substantial increase in bioavailability. Enhancing the dissolution rate of this class of drugs is thought to be the critical factor for improving their bioavailability. BCS class III drugs have a bioavailability that is rate-

limited by the membrane permeability in the gastrointestinal tract. These drugs require modification of their polarity by introducing lipophilic groups as in prodrugs to enhance permeability. BCS class IV is the least favourable category comprising drugs with low solubility and low permeability, making *in vitro* to *in vivo* correlation almost impossible. This usually results in high costs of drug development and formulation design for these types of drugs.[145–147]

1.8.4 Strategies to Improve Physicochemical Characteristics

Characterization of hits and leads in drug discovery is often based on inadequate physicochemical properties that require optimization. One of the key properties that is mostly focused on is solubility, and several approaches have been developed to address this issue. These approaches include physical modification, chemical or structural modification and supramolecular derivatization. Formulation strategies are also employed as the last resort in later stages of development.[135,136,144] Physical modifications such as particle size reduction is a strategy that improves solubility by expanding the surface area to volume ratio to allow greater interaction with the solvent, which causes an increase in solubility. Other physical methods include modifying the crystal habit like polymorphs, drug dispersion in carriers like eutectic mixtures, solid dispersions and cryogenic techniques.[135,148,149]

Structural modification can also improve solubility by disrupting molecular planarity and symmetry to reduce crystal packing or by introducing water solubilizing groups at positions on the core scaffold in such a manner that does not negatively impact other properties. A typical example is the introduction of alkoxy amines to the core pharmacophore, which successfully led to the discovery of amlodipine (a calcium channel blocker),[150] tamoxifen (an oestrogen receptor modulator)[151] and farnesoid X receptor (FXR) agonists[152] with a significant increase in solubility compared to the original leads. The case of the FXR agonist is illustrated in Figure 1.5. The lead compound **FXR-450** displayed low solubility (0.014 mg/mL) and poor bioavailability (21%) when administered orally by employing the standard suspension formulation (2% Tween 80 with 0.5% methylcellulose). The introduction of a basic amine led to the identification of candidate **B**, which demonstrated an approximately 18-fold solubility as a free base and 423-fold as a hydrochloride salt. The oral bioavailability was consequently increased to 53%.[152] Molecules that contain ionizable groups, either cationic or anionic, lend themselves to the formation of salts with improved biopharmaceutical properties compared to

the parent molecule. Appropriate salt forms enhance the dissolution rate as well as the oral absorption.[136,144]

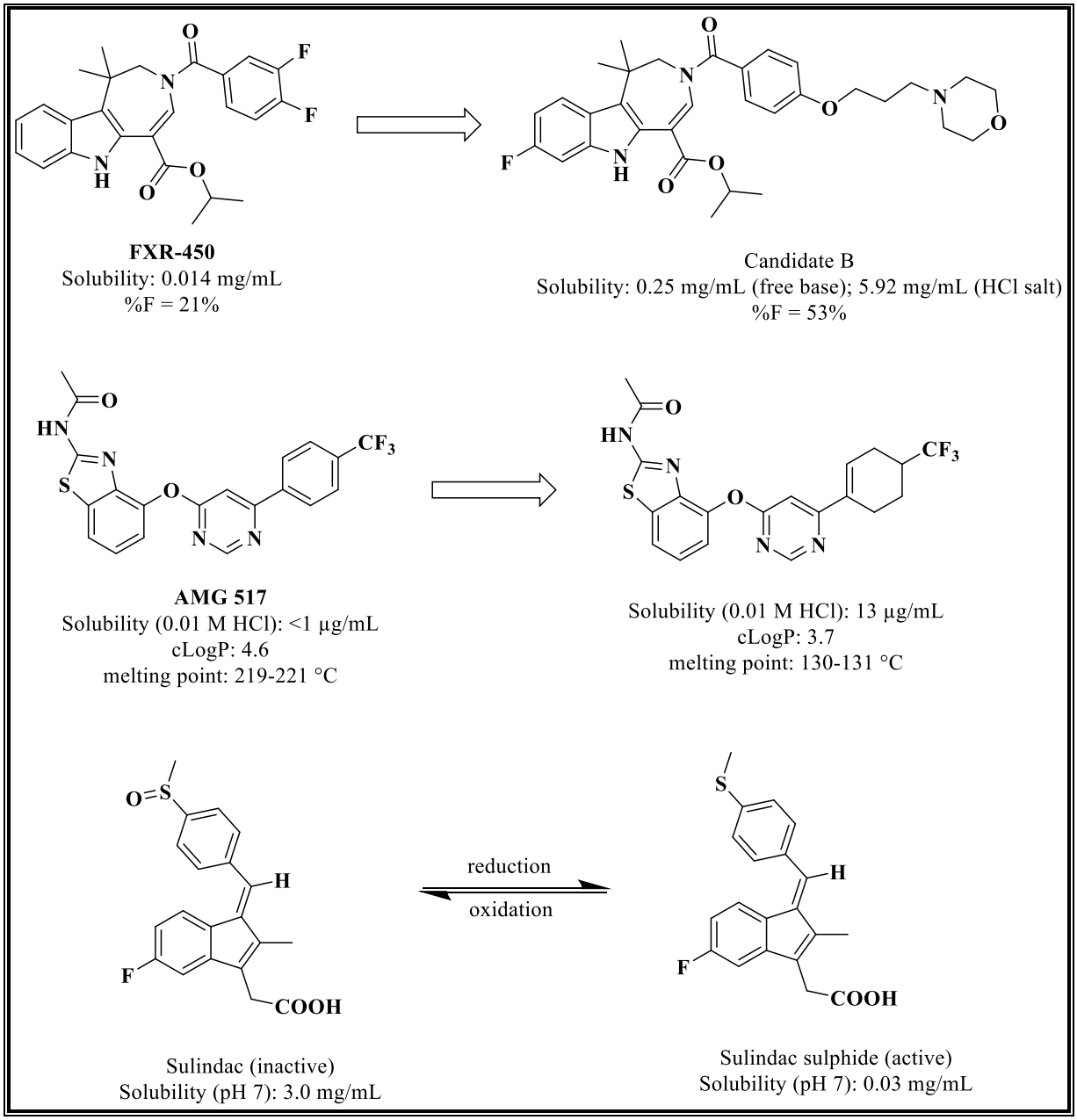

Figure 1.5: Chemical modification approaches to improve solubility.

The reduction of aromaticity, a feature associated with lipophilicity, is another strategy in optimizing solubility. This involves the replacement of phenyl rings with other heteroaromatic rings with hydrogen bonding capability. Cyclic saturated systems have also been used to disrupt molecular planarity and discourage pi-pi stacking that usually results in high energy forms with low melting points and decreased solvation energy.[144] The vanilloid receptor 1

(TRPV1) antagonist **AMG 517** (Figure 1.5) is a classic example of this approach. The thermodynamic aqueous solubility of **AMG 517** was reported as <1 µg/mL in phosphate-buffered saline (PBS) but the introduction of saturation into the 4-(trifluoromethyl)phenyl ring improved solubility by 13-fold even though potency was compromised.[153]

Prodrugs are compounds that are not biologically active but have to be transformed into active products by chemical or enzymatic reactions.[154–156] Prodrug approaches can be applied to improve the solubility of poorly soluble drugs. This enhances oral absorption and enables safe and effective intravenous formulations.[156] An example of a prodrug is sulindac (a bioprecursor prodrug), which bears a sulfoxide group that undergoes metabolism through reduction to the active sulphide (Figure 1.5).[155] The polar nature of the sulfoxide group increases its interaction with solvent than the reduced sulphide; hence, at pH 7, the sulfoxide prodrug demonstrates a 100-fold higher solubility (3.0 mg/mL) than its sulphide analogue (0.03 mg/mL).[157] Other prodrugs designed to improve water solubility involve adding an ionizable moiety to the parent molecule.[155] However, in considering a prodrug strategy, it is crucial to consider the potential toxicity liability caused by the release of the prodrug-solubilizing adjunct from the prodrug.

1.9 Cardiotoxicity in Chemotherapy

Cardiotoxicity represents the most recurring adverse drug reaction and cause of withdrawal for marketed drugs.[158] It has been noted that safety liabilities related to cardiotoxicity account for 45% of the total post-approval drug withdrawal from the market compared to hepatotoxicity.[159] The most common form of cardiovascular toxicity related to marketed drugs is the prolongation of the QT interval, which is associated with polymorphic ventricular tachycardia or torsade de pointes, which can be fatal. Examples of drugs that have been withdrawn from the market due to this form of toxicity include terfenadine, astemizole, grepafloxacin, terodiline, droperidol, lidoflazine, sertindole, levomethadyl and cisapride (Figure 1.6).[160] To avoid delivering drug candidates with high cardiotoxicity risk, it is paramount that the pharmaceutical industry develops effective methods of identifying and characterizing such risks during the early stages of drug development.

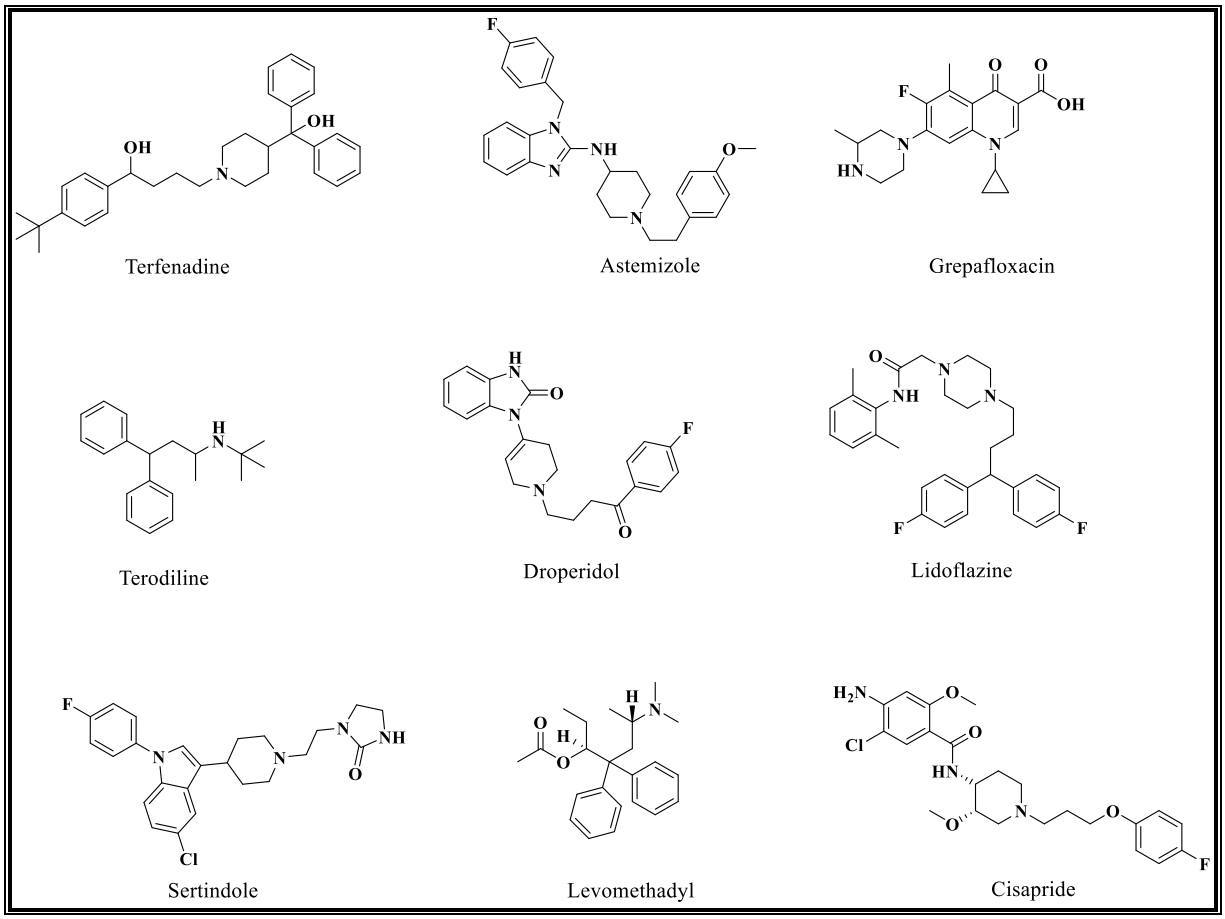

Figure 1.6: Examples of drugs withdrawn from the market due to cardiotoxicity.

1.9.1 Underlying Mechanisms of Cardiotoxicity: Inhibition of the human *ether-a-go-go*-related gene (hERG) K^+ Channel

The repolarization phase of myocytes is primarily driven by the outward movement of potassium ions (K^+) at the cellular level. A variety of potassium channel subtypes are present in the heart. The two most important potassium currents that participate in ventricular repolarisation are the subtypes of the delayed rectifier current, I_{Kr} (rapid) and I_{Ks} (slow).[161] More often than not, drugs that prolong the action potential and delay ventricular repolarization do so through blockade of either of these outward potassium currents, predominantly the rapid delayed rectifying potassium current, I_{Kr}. Clinically, blockade of the I_{Kr} current manifests as a prolonged QT interval and the appearance of other T or U wave abnormalities on the surface electrocardiogram (ECG).[161] Prolongation of the QT interval leads to a rare, life-threatening form of cardiac arrhythmia known as torsades de pointes (TdP), which has been the leading safety reason for the withdrawal of drugs from clinical use.[162] A generic but non-clinical strategy to assess and reduce the risk of QT interval prolongation, usually in the context of drug

discovery, is the assessment of the compound's potency at the human *ether-a-go-go*-related gene (hERG), which encodes the pore-forming α subunits of the channel carrying rapid delayed rectifying potassium current (I_{Kr}).[162] Apart from the direct inhibition of the hERG channel, other mechanisms can account for a drug's ability to prolong the QT interval. Consequently, additional non-clinical data can be generated from a variety of *in vitro* and *in vivo* assays together with the hERG assays to refine the integrated risk assessment.[162]

1.9.2 Strategies to Counter hERG Activity

An extensive literature survey conducted by Jamieson and colleagues establishes various concepts based on case studies of the successful strategies to mitigate hERG liabilities.[163] The challenge in mitigating hERG lies in balancing its affinity without altering the preferred pharmacological effect since both hERG blockers and non-blockers share a narrow SAR that hinders pharmacomodulation.[164] The optimization strategies described by Jamieson *et al*. were categorized based on similarities in the chemical modification approach employed. These strategies, which will be discussed in detail, include discrete structural modifications, the formation of zwitterions, control of lipophilicity (log P) and attenuation of pKa.[163] However, it should be noted that applying any of these strategies in isolation is not a panacea for mitigating hERG inhibition.

Mutagenesis studies combined with homology modelling of the hERG channel suggest that the major determinants of hERG-drug interaction are π-stacking and hydrophobic interactions between aromatic residues lining the large cavity of the channel and aromatic moieties appropriately positioned in a drug molecule.[165,166] The binding mode of cisapride as a representative example is illustrated in Figure 1.7. Subtle or extensive modification of such molecular features in a drug molecule could disrupt the presumed interactions and affinity for the hERG channel. Structural modifications, however, are not restricted to distal aryl rings but also include introducing constraints in the molecule and varying the stereochemistry where necessary.[163]

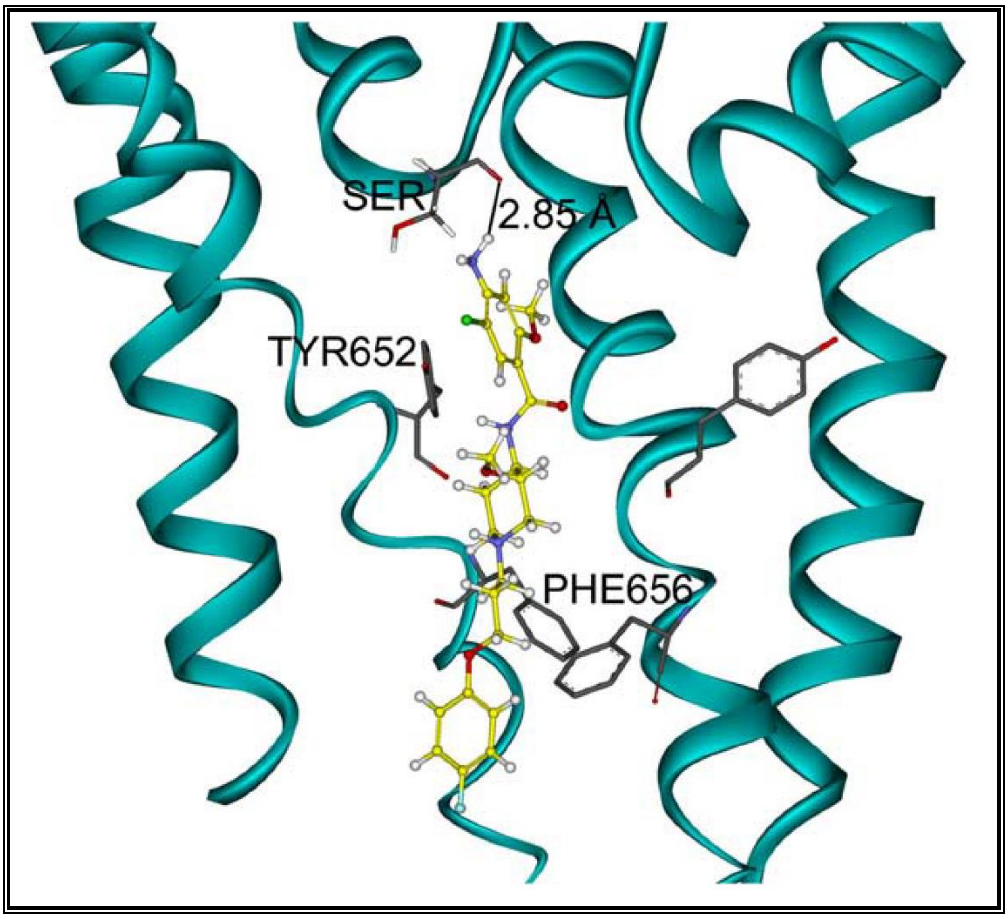

Figure 1.7: Cisapride docked into the partially open state of the hERG channel.[167]

Blum et al. demonstrated the application of subtle structural changes in a series of Y5 antagonists' aryl-1H-imidazole compounds that displayed a high affinity for the hERG channel. The introduction of *gem*-dimethyl moiety between the hydroxyl and amide groups resulted in compound **1,** with about 14-fold less potency against the hERG channel (Figure 1.8). Also, the modification did not alter lipophilicity or basicity.[168] In a CCR5 program, Kim and co-workers adopted a strategy of modifying a distal aryl ring in a 1,3,4-trisubstituted pyrrolidine series by incorporating a trifluoromethyl group in compound **2,** which resulted in compound **3** (Figure 1.8) with significantly reduced activity at the hERG channel.[169]

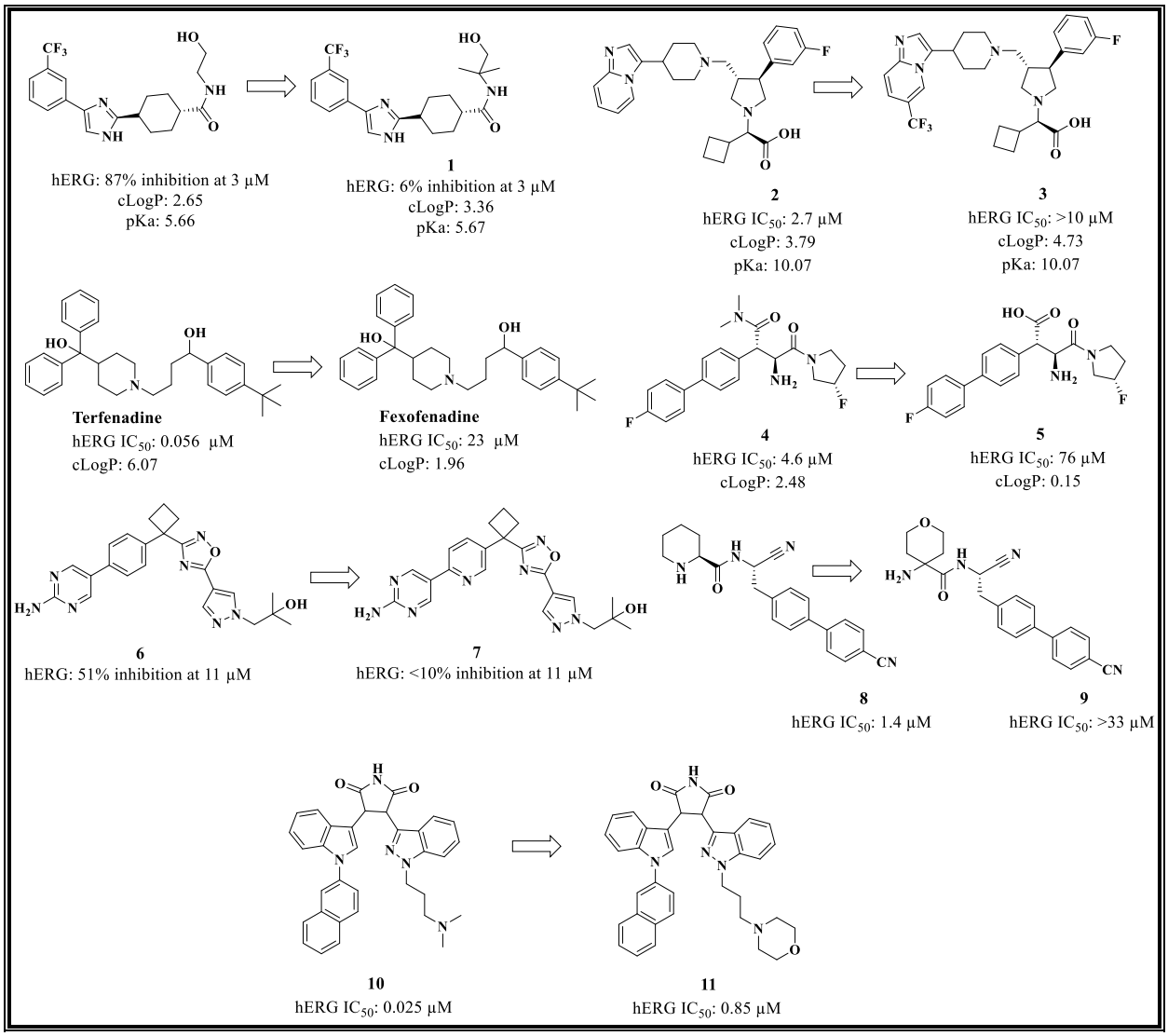

Figure 1.8: Chemical modification approaches to mitigate hERG activity.

Zwitterionic formation is another approach to mitigating hERG inhibition. Zwitterionic species physically limit the membrane permeability by preventing a drug molecule's access to the proposed transmembrane binding site, thus reducing potential interaction with hERG.[163] A classic example of this approach is the story of terfenadine, a second-generation antihistamine launched in 1982. Post-marketing surveillance implicated terfenadine in several TdP-related cases, which led to its withdrawal from the market. In addition, prolongation of the QT interval was reported when terfenadine was administered concurrently with food or drugs that inhibit cytochrome P450 3A4 (CYP3A4) enzyme resulting in elevated plasma concentrations of the drug.[170] Nonetheless, it was discovered that the carboxylate metabolite (Figure 1.8), which was later marketed as fexofenadine, was responsible for the therapeutic efficacy of terfenadine.

Additionally, fexofenadine exhibits significantly reduced hERG affinity (IC_{50} = 23 μM) and has no effect on the QT interval.[171] Its reduced hERG affinity could be ascribed to the reduced cell membrane permeability; hence, its limited access to the channel's intracellular lumen is thought to be critical for hERG blockade.[163] In a similar approach, researchers from Merck reported that incorporating an acid moiety or its related bioisostere into an amine-containing pharmacophore to embellish a zwitterionic system resulted in minimized hERG activity.[172–174] In their work on biaryl-β-methylphenylalanine DPPIV (dipeptidyl peptidase IV) inhibitors, the carboxylic acid-containing derivative **5** was 16-fold less potent on the hERG channel in comparison to the parent carboxamide **4** (Figure 1.8).[173] Unfortunately, the zwitterion approach has shortcomings of suboptimal oral bioavailability attributed to poor oral bioavailability.[173,174]

Evidence revealing the existence of a lipophilic ligand-binding site in the hERG ion channel has help rationalize that compounds with higher lipophilicity tend to be at higher risk of hERG inhibition.[165,175] A general strategy to decrease hERG affinity has then consisted of reducing the lipophilicity of potential hERG ligands.[176] A recent study by Bartolozzi *et al*. investigated an oxadiazole series as potent 5-lipoxygenase-activating protein inhibitors.[177] In their work, the phenyl core in compound **6** was modified by adding heteroatoms to reduce lipophilicity since the series occupied the hydrophobic pocket in the protein. It was demonstrated that, in general, pyridyl derivatives, as exemplified in compound **7** (Figure 1.8), exhibited lower hERG inhibition in comparison to the phenyl analogues.[177] Furber and co-workers also disclosed the discovery of piperidinecarboxamide acetonitrile series as dipeptidyl peptidase I inhibitors, which unfortunately was flawed with high affinity towards the hERG channel.[178] Lipophilicity was reduced when an oxygen atom was introduced in the form of a pyran ring as in compound **9**, thereby decreasing hERG affinity by 30-fold compared to the lead compound **8** (Figure 1.8).[178]

Attenuation of pKa for drug candidates that contain basic nitrogens is a unique approach in addressing hERG liabilities. Ligands with a basic nitrogen moiety are likely to be protonated at physiological pH, leading to hERG blockade.[163] The ligand-binding affinity for such basic amine-containing compounds is attributed to the π-cation interactions between the amine's protonated nitrogen and the aromatic residues within the cavity of the hERG channel.[165,166] Lowering the pKa of a basic nitrogen would, therefore, reduce the proportion of molecules in the protonated form at physiological pH and subsequently disrupt any putative π-cation interactions with the hERG channel. Comparably, incorporating alkoxy/hydroxyl groups at the β-position relative to the amine may shield the protonatable centre, thereby destabilizing any

π-cation interactions and reducing affinity for hERG.[179] An indolylindazoylmaleimide series of highly potent and selective protein kinase C-β (PKC-β) inhibitors reported by Johnson & Johnson showed very potent activity against the hERG channel.[180] The most potent compound **10** in the series (IC_{50} = 5 nM) displayed high hERG activity (K_i = 25 nM). It caused a dose-dependent increase in the QTc interval by 7%, 11% and 15% at 1, 3 and 10 mg/kg, respectively, when administered intravenously to anesthetized pigs. The SAR in this series suggests that the basic amino group is critical for PKC-β activity and significant for hERG affinity. Impressively, when the more basic dimethylamino moiety in the most potent compound **10** was replaced with a less basic morpholino moiety as in compound **11**, the hERG activity was significantly reduced (K_i = 850 nM) while conserving activity at PKC-β (IC_{50} = 18 nM).[180]

1.10 The Concept of Intramolecular Hydrogen Bonding (IMHB) in Medicinal Chemistry

A hydrogen bond is defined as a non-covalent bond between a donor pair D-H (in which the hydrogen atom H is bound to a more electronegative atom D) and a neighbouring electronegative acceptor A.[181] A hydrogen bond is formed when the covalent bond length between atoms D and H (d_{DH}), the non-covalent bond length between atoms H and A (d_{HA}) and the angle between the two bonds are encompassed in well-defined numerical ranges. In drug discovery, the hydrogen bond donor pair is usually an amino (-NH) or a hydroxyl (-OH) group, while the electronegative atom with a partial negative charge includes groups such as a carbonyl or a tertiary amine.[182]

An intramolecular hydrogen bond (IMHB) may exist when both the hydrogen bond acceptor (HBA) and the hydrogen bond donor (HBD) are in close proximity on the same molecule hence, allowing the formation of a pseudo ring. Practically, an IMHB does not differ from any other hydrogen bond, except that the simultaneous presence of HBD and HBA groups within the same molecule inflicts additional hydrogen bond formation restrictions. For instance, if the molecule is flexible, it allows the positioning of the HBD and HBA to be energetically favourable. The bond lengths and the bond angles fall within the prescribed ranges for the formation of a hydrogen bond. On the other hand, if the molecule is rigid, the HBD and HBA must be correctly oriented if an IMHB is to be formed.[182] It is noteworthy that an equilibrium, described by a thermodynamic constant (K_{IMHB}), exists between closed conformations in which an IMHB is formed and open conformations in which the polar groups are exposed to solvents (Figure 1.9).[182,183] The presence of IMHB has been shown to significantly alter molecular

properties due to the formation of various conformers that consequently influence solubility, permeability, pharmacokinetic and pharmacodynamic processes, and protein binding affinity.[184–186]

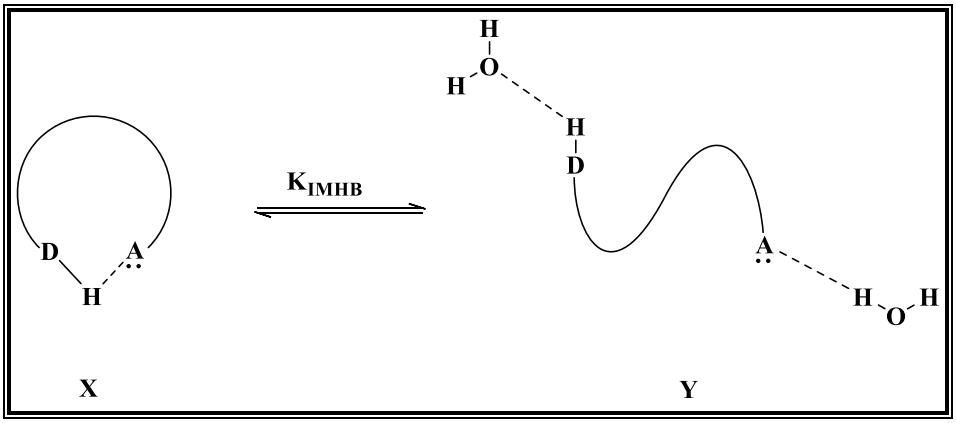

Figure 1.9: Thermodynamic equilibrium between closed (IMHB) and open conformations.

A hydrogen bond is strong enough to restrict the rotation of fragments by forming the most commonly 5−8-membered rings. More importantly, IMHBs are weak enough to allow these fragments to come apart and lose their orientational specificity in high dielectric media such as water (Figure 1.9). The chameleon-like nature of an IMHB becomes evident when one realizes that an IMHB is unlikely to form in water. The polar groups may serve to increase solubility by easily forming intermolecular hydrogen bonds with water. On the other hand, compounds that can participate in IMHB eliminate water more readily when entering a low dielectric environment like a hydrophobic phospholipid bilayer. In that regard, IMHB results in lipophilic, less polar molecular conformations, which are expected to have higher passive membrane permeability.[187] Simply put, a decrease in polarity is sometimes achieved through the formation of IMHBs, where the HBD and HBA atoms are effectively shielded from water, thereby reducing the energetic penalty of desolvation required in moving from an aqueous environment through a phospholipid bilayer.[188]

A significant focus lies in increasing potency and the ADMET profile of drug candidates during the optimization phase of drug discovery, and IMHB strategies may be applied to achieve these goals. For instance, a pseudo ring due to a static IMHB could replace a heterocycle and improve potency.[189,190] Similarly, the introduction of an IMHB that forms a pseudo-nine-atom ring in a peptidic molecule was used by Yang and co-workers to obtain a best-in-class inhibitor (**MAI-400**) against the interaction of adenomatous polyposis coli (APC) with Rho guanine-nucleotide-exchange factor 4 (Asef).[191] The binding affinity of **MAI-400** for APC is thought

to be enhanced by the intramolecular hydrogen bond between the L185 backbone carbonyl oxygen and the S184 side-chain hydroxy group that was demonstrated by the crystal structure (Figure 1.10) of **MAI-400** in complex with APC.[191]

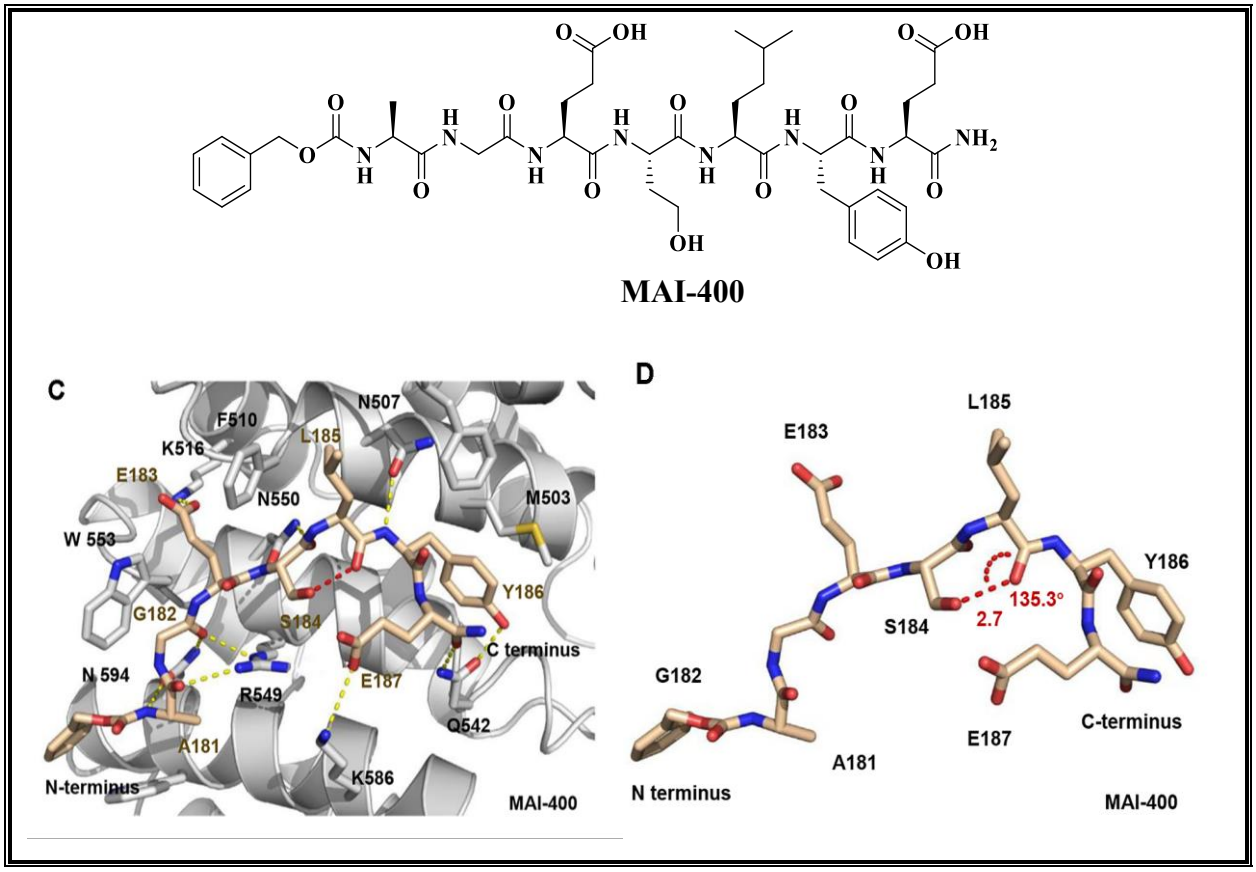

Figure 1.10: (C) Binding interactions between MA1-400 and APC. (D) IMHB in the crystal structure of MAI-400.[191]

1.10.1 Methods to Assess the Propensity of Compounds to Form IMHBs

Unfortunately, one cannot merely examine a given two-dimensional structure and immediately describe the presence of one or more IMHBs and determine their strength. This is mainly because the thermodynamic equilibrium of closed versus open conformations depends on various intricate factors such as geometry, type of solvent etc., acting simultaneously.[192] Successful implementation of IMHB considerations in drug discovery programs requires experimental tools that assess compounds' propensity to form IMHBs. Molecular modelling could suggest structural modifications to transform a lead molecule, which cannot form IMHB, into an optimized lead with some propensity to form IMHB. However, the new molecule should be experimentally investigated for its effective capacity to form IMHBs once it is synthesized.[193] The most common tools used to investigate IMHBs are spectroscopy (NMR,

infrared and Raman), diffraction (X-ray and neutron), calorimetry and theoretical methods such as the density functional theory.[194]

Abraham and co-workers described the most convenient strategy for the use of NMR in quantitative assessments of IMHB. Briefly, ^{1}H NMR chemical shifts are measured in the solvents dimethyl sulfoxide and deuterochloroform. The difference in the chemical shifts of an OH or NH group in these two solvents $\Delta\delta = \delta(DMSO) - \delta(CDCl_3)$ is then converted into the hydrogen bond acidity, A, of the group using the equation $A= 0.0065 + 0.133\Delta\delta$. The NMR A value, A_{NMR}, can be used as a quantitative assessment of intramolecular hydrogen bonding. For hydroxy compounds, if $A > 0.5$, then the OH group is not part of an intramolecular hydrogen bond. If $A < 0.1$, then the OH group forms part of an intramolecular hydrogen bond. For NH compounds, if $A > 0.16$, the NH group is not part of an intramolecular hydrogen bond, and if $A < 0.05$, the NH group is part of an intramolecular hydrogen bond.[195] Whaley et al. extended the application of this NMR method to determine A_{NMR} values for OH groups in some hydroxyflavones (Figure 1.11).[196] The values of the differences in chemical shifts $\Delta\delta$ for the OH groups are outlined in Table 1.3, together with the A_{NMR} values calculated. In the case of 5-hydroxyflavone, a strong IMHB is observed, which involves the formation of a six-membered intramolecular ring between the 5-hydroxy group and the flavone carbonyl group. A relatively weaker IMHB is observed with the five-membered intramolecular ring formed between the 3-hydroxy and carbonyl groups.[196]

Table 1.3: Chemical shifts and A_{NMR} values for hydroxyflavones

Compound	δ		$\Delta\delta$	A_{NMR}	Presence/absence of IMHB
	DMSO	$CDCl_3$			
3-hydroxyflavone	9.62	7.00	2.62	0.35	Present (weak)
5-hydroxyflavone	12.67	12.56	0.11	0.02	Present (strong)
6-hydroxyflavone	9.96	5.44	4.51	0.61	Absent
7-hydroxyflavone	10.83	5.81	5.02	0.67	Absent

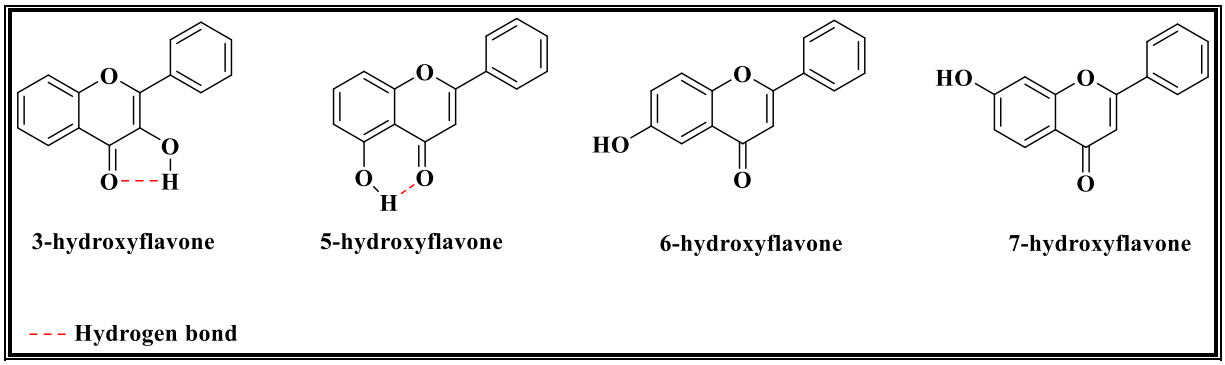

Figure 1.11: Chemical structures of hydroxyflavones assessed by NMR for IMHB.

Infrared spectroscopy (IR) could also provide insight into IMHB's existence since the formation of an IMHB causes a shift to lower wavenumbers in the IR stretching vibration band of the proton-donor (D–H) bond. The shift may be treated as a measure of the hydrogen bond strength since it correlates with other typical measurements such as hydrogen bond energy and the proton-acceptor (H-A) distance. Assignment of an intramolecular hydrogen bond by IR spectroscopy, therefore, is more explicit in a non-hydrogen-bonding solvent or very weak hydrogen-bonding solvent such as chloroform, with dilute conditions to reduce the potential for dimer formation of the solute and also for solutes with only a limited number of amide NH groups to minimize band overlap.[193] Karas and co-workers employed IR measurements to investigate the effect of alkyl substituents on the IMHB strength of different 1,3-disubstituted acyclic alcohols (Figure1.12).[197] In their study, both free OH stretching ($\nu^{\text{Free}}{}_{\text{OH}}$) and OH stretching involved in intramolecular hydrogen bonding ($\nu^{\text{IMHB}}{}_{\text{OH}}$) were observed for all the compounds. The free OH stretching frequency appeared at around 3630 cm^{-1} while frequencies involved in IMHB were observed at 3561, 3552, 3543, 3539, 3527, 3550, 3539, 3547 and 3527 cm^{-1} for compounds **12-20**, respectively. The difference between both frequencies ($\Delta\nu = \nu^{\text{Free}}{}_{\text{OH}} - \nu^{\text{IMHB}}{}_{\text{OH}}$) was used as the measure of the strength of the hydrogen bond since stronger IMHB causes the proton-donor (D–H) bond to be more elongated and weaker, hence, a larger shift is observed. Compound **16** [3-(tert-butoxy)propanol] displayed the strongest IMHB with a frequency difference value ($\Delta\nu$) of 112.[197]

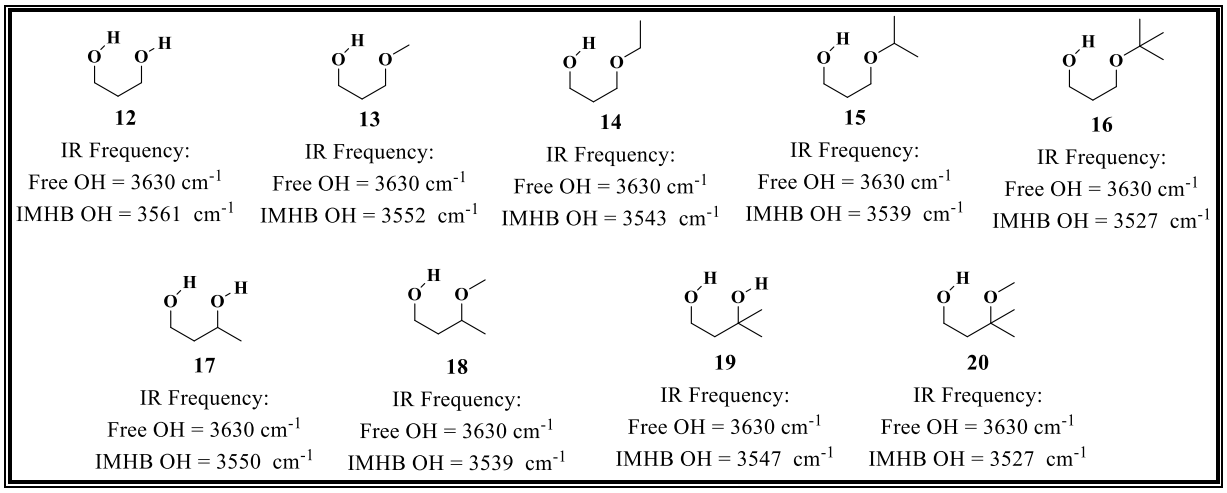

Figure 1.12: Chemical structures of acyclic alcohols assessed by IR for IMHB.

Direct experimental evidence of the presence of IMHB can be achieved by studying the molecule using single crystal X-ray diffraction. Crystallographic data are beneficial for retro prospective studies. This was chiefly shown by Kuhn and co-workers[183], who, also supported by Bilton et al.'s preliminary studies,[198] performed exhaustive searches in crystal structure databases and provided the probability for IMHB forming five- to eight-membered ring systems and their relevance in drug discovery (Figure 1.13). The probability of IMHB formation is higher for six-membered rings than for any other system. Moreover, a comparative analysis of X-ray structures crystallized from solvents with different polarities could highlight the impact of the environment on compounds' propensity to form IMHBs.

Pseudo-ring	Topology	Example	Propensity
5-membered	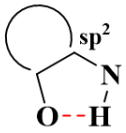	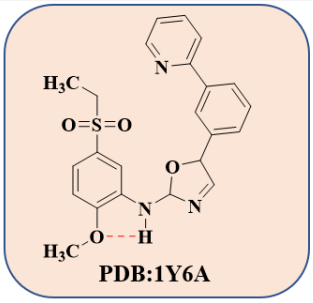 PDB:1Y6A	71%
6-membered	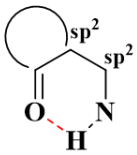	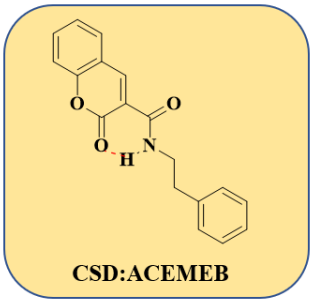 CSD:ACEMEB	93%
7-membered	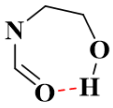	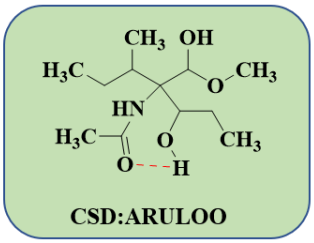 CSD:ARULOO	3%

Figure 1.13: Examples of Kuhn's topologies with their different tendency to form IMHB.[183]

An alternative option for diffraction experiments is neutron radiation. Neutrons can be diffracted like X-rays due to the particle/wave dualism, and depending on their energy, the wavelength can be modulated to deal with a specific issue. Neutrons interact with the nucleus of atoms but not the electron shell. Also, the scattering power does not directly increase with the atom number, unlike X-rays. In fact, the scattering lengths of elements seem to follow an arbitrary course, and even different isotopes of the same element can have utterly different scattering lengths. For instance, hydrogen has a coherent scattering length of −3.742 fm, while that of deuterium is 6.674 fm.[199] Like X-ray diffraction, neutron diffraction can be executed on single crystals as well as on powders. Meanwhile, without an initial X-ray model, it is rather challenging to ascertain crystal structures from the neutron diffraction due to the positive and negative nature of the scattering lengths, further complicating the assignment of phases. Nonetheless, neutron diffraction data gives valuable information about absolute atomic positions and bond lengths especially involving hydrogen.[200]

Density Functional Theory (DFT) methods are suitable for studies on intramolecular H-bonds. Basically, the geometries of the different species under investigation are optimized at the B3LYP/6-31G(d) level, which has been found to give results in good agreement with high-level ab initio calculations as far as the description of an intramolecular hydrogen bond is concerned.[201]

1.10.2 Antimalarials with an IMHB Motif

Earlier research work conducted by Burckhalter and co-workers on antimalarial α-aminocresols led to the discovery of 4-*tert*-butyl-2-dimethylaminomethyl phenol as an active compound against trophozoite-induced avian malaria (Figure 1.14).[202] Their work on α-aminocresols demonstrated the importance of having the hydroxyl group *ortho* to the α-amino group and the benefit of an additional hydrophobic substituent on the ring. This motif was later attached to the 7-chloroquinoline ring found in chloroquine to produce amodiaquine (Figure 1.15).[202] The use of amodiaquine is compromised by its hepatotoxicity and its ability to cause agranulocytosis. It has been shown that the toxicity of amodiaquine is related to the reactive metabolites formed by oxidation of its phenolic side chain, especially to the formation of a quinone imine by cytochrome P-450-catalysed biological oxidation. Pharmacological studies have revealed that the regioisomer of amodiaquine (isoquine), in which the positions of the groups on the hydroxyl aniline ring have been swapped, cannot be oxidized to the quinone imine and is comparatively less hepatotoxic (Figure 1.15).[203] Similar modifications were carried out on quinolinemethanols (obtained from quinine) through which the drug mefloquine (Figure 1.14) was obtained.[204] The common structural feature shared by these compounds is a basic nitrogen within hydrogen-bonding proximity to a hydroxyl group. Likely, the intramolecular hydrogen bonding between the basic nitrogen (H-bond acceptor) and the hydroxyl (H-bond donor) may be an essential feature for activity against chloroquine-resistant *P. falciparum*.[205]

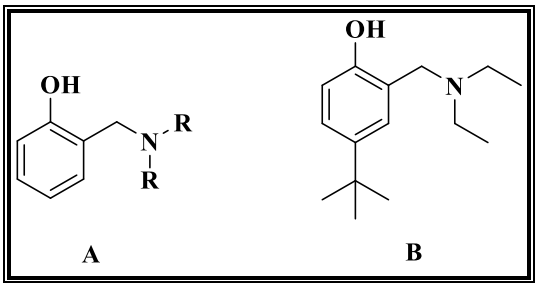

Figure 1.14: Generalized α-aminocresol (A) and 4-tert-butyl-2-dimethylaminomethylphenol (B).

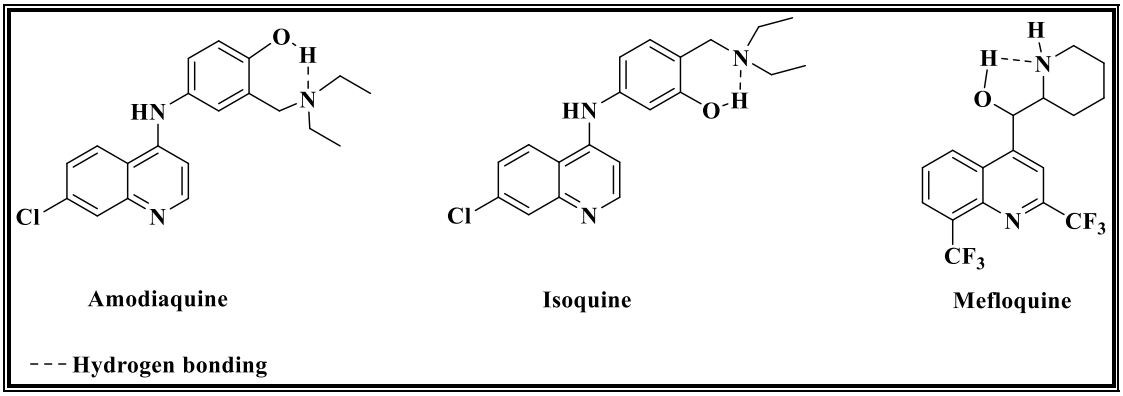

Figure 1.15: Amodiaquine, isoquine and mefloquine showing intramolecular hydrogen bonding.

Further research work was carried out on 4-aminoquinolines incorporating an intramolecular hydrogen bonding motif like the α-aminocresols in the side chain of these compounds.[205] It was reported that most of the compounds within this series were active against both chloroquine-sensitive (3D7) and multidrug-resistant parasite (W2) strains. This suggests that the aminocresol motif, when attached to the distal basic centre of quinolines, leads to potent compounds (Figure 1.16) against drug-resistant *P. falciparum*.

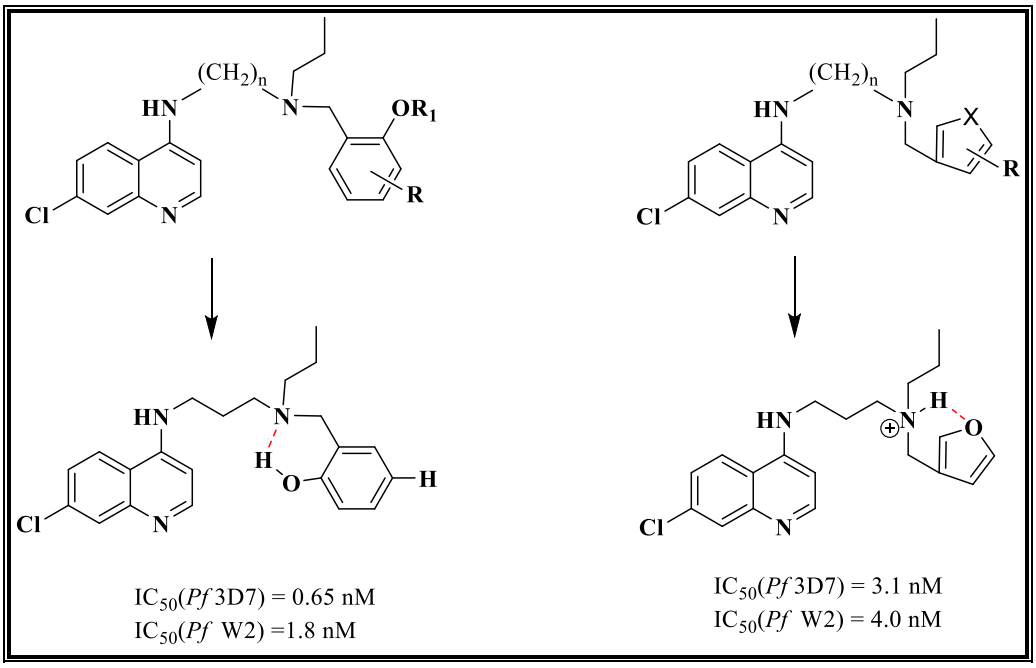

Figure 1.16: Potent 4-aminoquinolines with an intramolecular hydrogen bonding motif.

Previous reports on a new 2-aminomethylphenol, JPC-2997 (Figure 1.17), showed its high *in vitro* activity against chloroquine-sensitive (IC_{50}*Pf*D6 = 13 nM), chloroquine-resistant (IC_{50}*Pf*W2 = 6.6 nM) and multidrug-resistant (IC_{50}*Pf*TM90-C2B = 34 nM) *P. falciparum* strains, remarkable *in vivo* potency against *P. berghei* infections and high efficacy in the *Aotus* monkey *P. falciparum* model.[206,207] JPC-2997 is a derivative of the nonquinoline chlorophenylphenol WR-194,965, which was identified in the 1960s and 1970s with good antimalarial activity against rodent malaria but limited potency in humans. SAR studies revealed two other trifluoromethyl-substituted analogues, the pyrimidine JPC-3186 and the pyridine JPC-3210. Based on better *in vitro* activity against the multidrug-resistant *P. falciparum* strains, lower *in vitro* cytotoxicity in mammalian cell lines, favourable pharmacokinetic properties in mice and greater *in vivo* efficacy against murine malaria, JPC-3210 was selected as the lead compound for further preclinical development as a new antimalarial.[97]

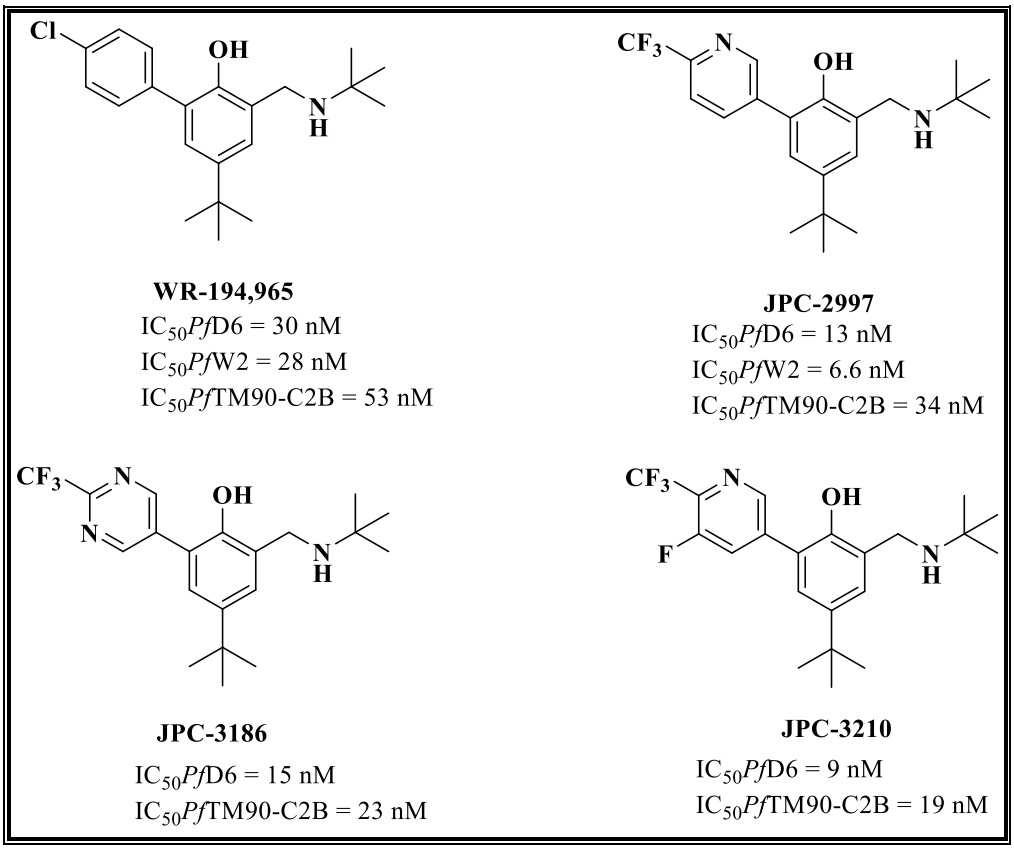

Figure 1.17: Chemical structures of 2-aminomethylphenols.

Nonimmune *Aotus* monkeys infected with *P. falciparum* and *P. vivax* were cured when treated with a single oral dose of 5 mg/kg and 10 mg/kg of JPC-3210, respectively. The blood elimination half-life of JPC-3210 in the monkeys is long, at approximately 21 days and biotransformation to its putative hydroxylated metabolite was low with a metabolic ratio of 1.3%. The pharmacokinetics of JPC-3210 suggests that it could be a suitable long-acting partner drug for a potential single-dose treatment as well as a prophylactic agent of malaria.[208]

1.11 Benzimidazoles and Imidazopyridines

1.11.1 Benzimidazoles

Benzimidazole is a heterocyclic aromatic compound that contains a benzene ring fused to an imidazole ring (Figure 1.18). It is an important pharmacophore in medicinal chemistry, which use dates many years back to the study of its structural modifications and their pharmacological actions.[209]

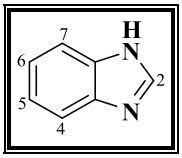

Figure 1.18: Chemical structure of benzimidazole.

Benzimidazole derivatives are of broad interest in drug discovery due to their diverse biological activities and clinical applications.[210] Compounds bearing different substituents on the benzimidazole structure are associated with a wide range of biological activities, including anticonvulsants, analgesics, antihistamine, antiulcer agents and antihelminthics (Figure 1.19).[211] For compounds that portray a given therapeutic action, the potency and pharmacokinetics can be modified by variations of the substituents around the parent molecule. This can be related to changes in the physicochemical properties of the compounds upon structural modifications.[212]

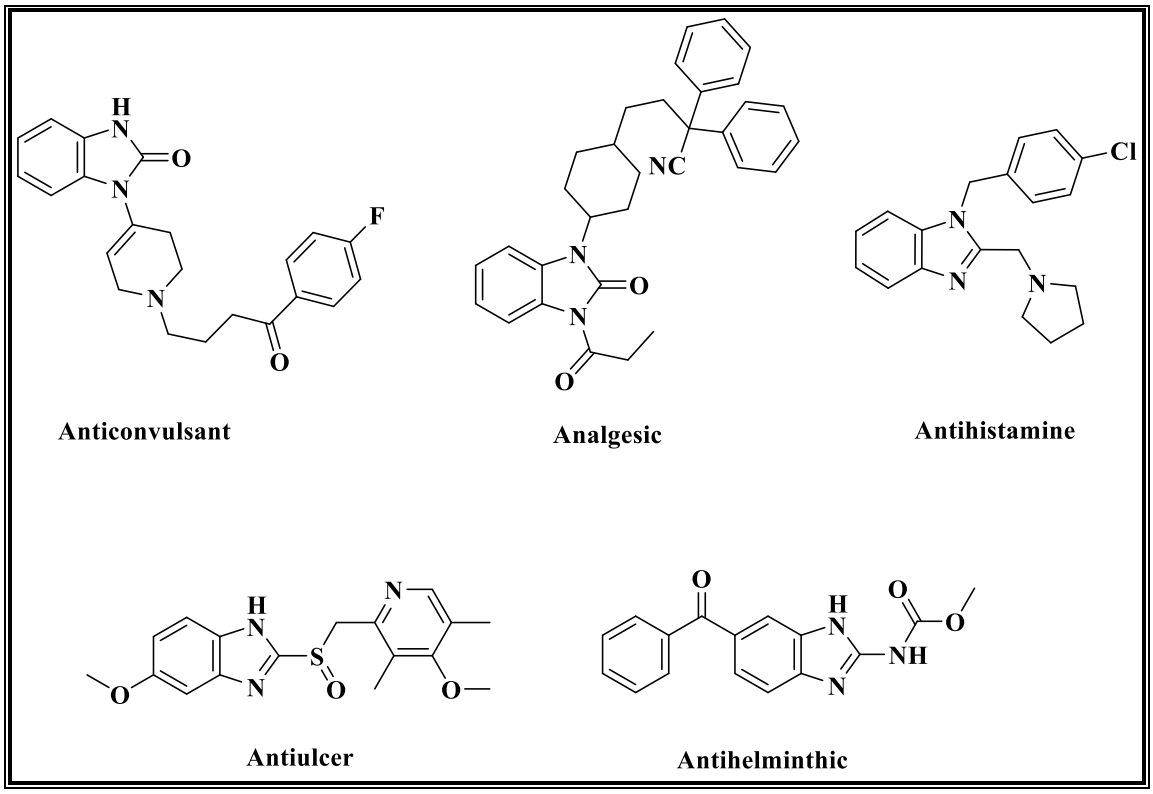

Figure 1.19: Chemical structures of some bioactive benzimidazole derivatives.

There are reports on the use of benzimidazoles as novel lead compounds for the potential treatment of malaria. Ramachandran and colleagues identified N-aryl-2-aminobenzimidazoles as novel hits against the asexual blood stage of *P. falciparum* through a phenotypic screening of AstraZeneca corporate compound library. Compound **21** (Figure 1.20) was identified as a lead molecule through medicinal chemistry optimization with good *in vivo* efficacy (98.9% activity of 4×30 mg/kg dose level at 96 hours p.o) in *P. berghei* infected mice. It also displayed an excellent pharmacokinetic profile with a long half-life of 19 hours in rats.[213] In general, this series of *N*-aryl-2-aminobenzimidazoles showed a fast killing rate equivalent to chloroquine in an *in vitro* parasite reduction ratio assay. Cross-resistance studies also suggest that they act through a novel mechanism of action, highlighting the promise of this novel chemical class for malaria treatment.[213]

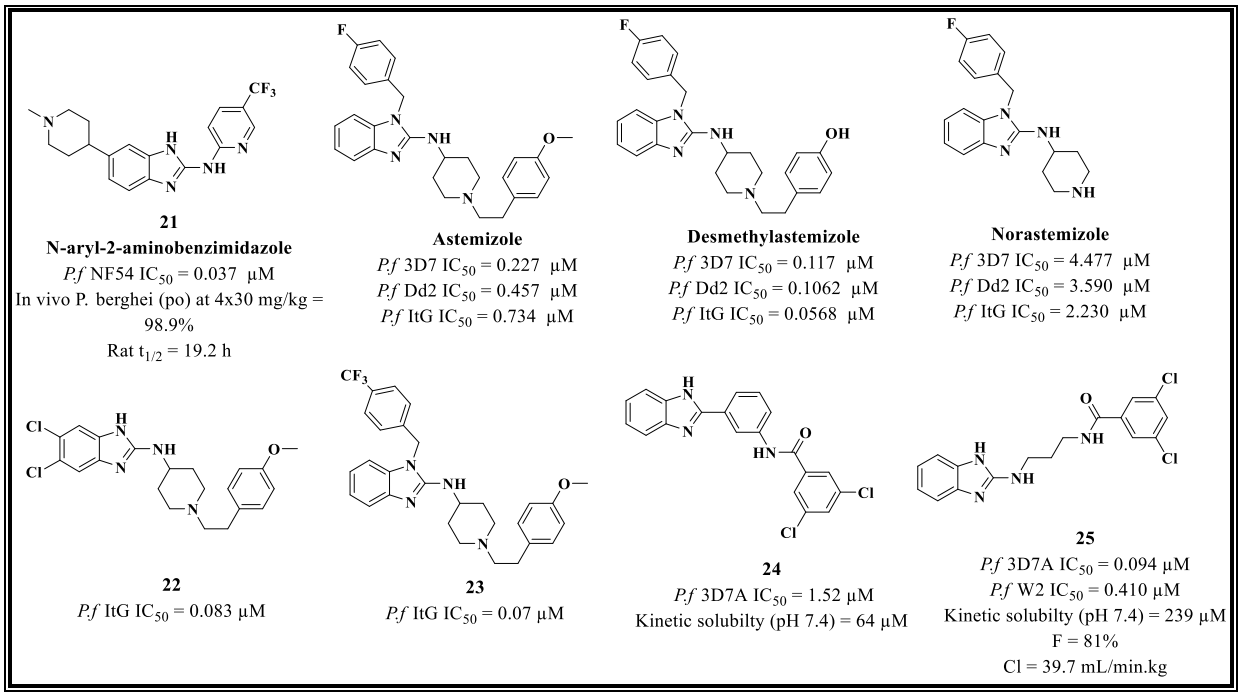

Figure 1.20: Examples of benzimidazole derivatives with antimalarial properties

The screening of existing drugs as potential antimalarial compounds from the Johns Hopkins Clinical Compound Library led to the identification of astemizole (Figure 1.20) as a drug that inhibits at sub-micromolar concentrations the proliferation of three *P.falciparum* parasite strains (ItG, Dd2 and 3D7) that differ in chloroquine sensitivity.[214] Astemizole undergoes rapid biotransformation by the hepatic cytochrome P450 enzyme primarily to desmethylastemizole, 6-hydroxydesmethylastemizole and norastemizole. Remarkably, desmethylastemizole was more potent in inhibiting *P. falciparum* due to its high abundance in plasma than astemizole, whereas norastemizole weakly inhibited the parasite. Both astemizole and desmethylastemizole showed inhibition against heme crystallization by concentrating within the food vacuole of *P. falciparum* and co-purifying with hemozoin in chloroquine-sensitive and multidrug-resistant parasites.[214] Astemizole as an antihistamine was voluntarily withdrawn from the market owing to safety concerns related to cardiovascular side effects due to the hERG channel blockade.

A series of compounds analogous to astemizole were designed and synthesized by Gheorghe and co-workers to determine their antiplasmodium activity. The report of the study stated that almost all the compounds showed good antiplasmodium activity ($IC_{50} < 0.4$ µM), with the most actives **22** and **23** (Figure 1.20) in the nanomolar range.[215] However, the presence of the

appropriate substituents at positions 1 and 2 (or the absence thereof) proved to be critical for their antiplasmodium activity. The study also noted that compounds having secondary amine functionality at position 2 selectively exhibited enhanced antiplasmodium potency. The fluoro replacement and the substitution of the benzene ring in the benzimidazole core of the astemizole structure could be used to disconnect the antihistaminic and the antimalarial activity of these compounds. Although the study lays the foundation for repositioning astemizole and its analogues as antimalarials, an extension of this investigation that exploits the present findings is needed to more accurately define the structural features required for a more active candidate while selectively improving toxicity towards the malaria parasite.[215]

Keurulainen and colleagues also identified a hit N-[3-[(benzimidazole-2-yl)amino]propyl]amide **24** (Figure 1.20) as an antimalarial agent through screening of benzimidazole-containing compounds from the University of Helsinki, which were initially designed as antichlamydial agents. However, the hit compound presented a weak antiplasmodial potency, a high degree of planarity because of the presence of several aromatic rings, high lipophilicity, scarce solubility and potential to deliver aniline-like genotoxic metabolites[216]. Optimization of this hit compound **24** led to a more potent compound **25** (Figure 1.19), which showed 1 order of magnitude improvement in potency [IC_{50} (*Pf* 3D7A) = 0.094µM] and a 3-fold increase in solubility (239 µM at pH 7.4). Gratifyingly, the oral bioavailability (F=81%), *in vivo* clearance in mice (Cl=39.7 mL/min.kg) and *in vitro* permeability (380 nm/s) data associated with the optimized compound were promising. The solubility in simulated fasting-intestine fluids (FaSSIF solubility) was found to be above 100 µg/mL)[216]. *In vivo*, compound **25** reduced parasitaemia under the limit of detection with just two doses, indicating a parasite clearance rate consistent with fast-acting antimalarials like dihydroartemisinin and piperaquine. Microscopic observations also suggest that it induces rapid *in vivo* killing of *P. falciparum* erythrocyte stages.

1.11.2 Imidazopyridines

Imidazopyridine scaffold is a foremost part of various biologically active compounds in plants, pharmaceuticals and human enzymes. It forms a class of compounds, similar to purine and benzimidazole.[217] Imidazopyridines are divided into four groups depending on the position of individual nitrogen atoms resulted from different annulations of imidazole and pyridine rings (Figure 1.21).[218]

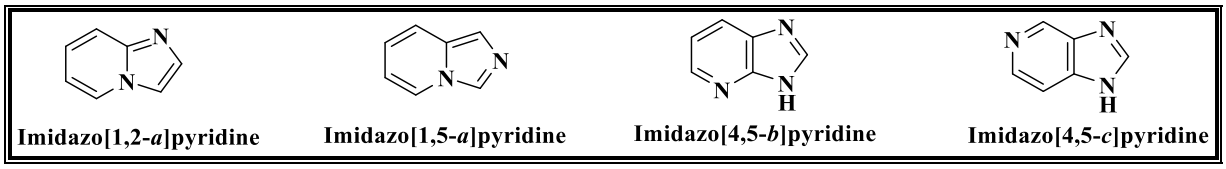

Figure 1.21: General structures of imidazopyridines.

Even though the individual scaffolds differ in structure and also in the number of nitrogen atoms, they are all categorized as imidazopyridines according to the correct nomenclature. Each of these core scaffolds differs in its physicochemical properties; thus, it may affect the ADME parameters of the compounds of biological interest in addition to influencing interactions with targets.[218] Pharmacological activities of imidazopyridines include anti-inflammatory[219,220], anticancer[221], antiviral[222], antiparasitic[223] and antihypertensive.[217] The use of imidazopyridine derivatives in psychiatry[224] and autoimmune[225] disorders have also been reported.

Apart from three published papers[226–228], there is no literature precedence concerning the exploration of imidazopyridines as antimalarial agents. More specifically, work on imidazopyridines documented in this Ph.D. thesis was motivated by studies undertaken by Nchinda *et al.*[227,228] This series of imidazopyridines, named SFK59, was identified from a phenotypic whole-cell high throughput screening (HTS) of a SoftFocus kinase library where two hit compounds exemplified by **26** and **27** (Figure 1.22) were found to display >50% inhibition of parasite growth at 2 µM but had a dose-response IC_{50} >1 µM against the drug-sensitive NF54 strain. However, two additional compounds, **28** and **29** (Figure 1.22), were synthesized for hit evaluation based on experience with a similar chemical series. It was established that N-demethylation of the core, as in **29** (*Pf* NF54 IC_{50} = 76 nM), resulted in potent compounds. Compound **29** was identified as a fast-acting compound in the *in vitro* speed assay.[229] It was also equipotent when tested against a panel of laboratory strains with mutations in identified targets, suggesting a potentially novel mechanism of action.[227]

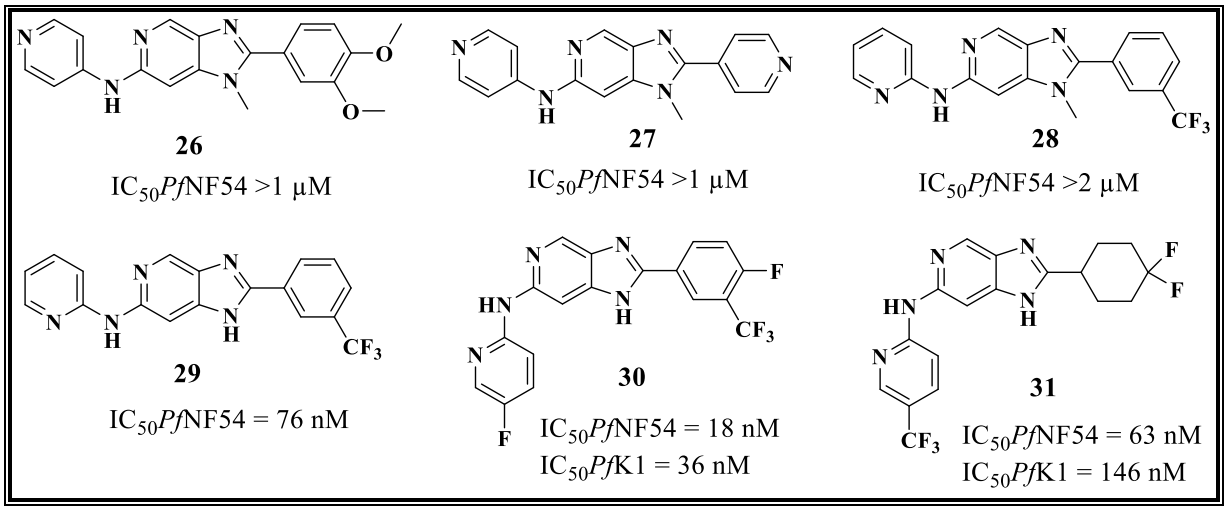

Figure 1.22: Chemical structures of antimalarial imidazopyridines from SFK59 series.

SAR studies and optimization of physicochemical properties based on compound **29** led to identifying two promising compounds **30** and **31** (Figure 1.22) that exhibited suitable *in vitro* properties and were further profiled *in vivo*. PK profiles in rats and mice were similar for both compounds. The volume of distribution in rats was moderate (2-3 L/kg), and intravenous (i.v) blood clearance was low to moderate (7.6 and 26.4 mL/min/kg for **30** and **31** respectively), resulting in elimination half-lives of 1 to 4 hours. Oral bioavailability was moderate to high for both compounds when they were dosed orally in rats. Compound **31** displayed a low blood clearance (11.7 mL/min/kg), a moderate volume of distribution and oral bioavailability of 51% in mice. In contrast, compound **30** had a dose-normalized area under the curve (AUC) twice as high as **31,** achieving a sustained oral exposure in mice. Based on their PK profiles, both compounds were tested *in vivo* in the *P. falciparum*-infected NOD-scid IL-2Rγ^{null} (SCID)[230] mouse model for malaria. They were efficacious with a 90% effective dose (ED_{90}) and related AUC_{ED90} of 4.2 mg/kg and 5.14 μg.h.ml^{-1}.day, and 5.6 mg/kg and 5.4 μg.h.ml^{-1}.day, for **30** and **31**, respectively. Flow cytometry and microscopy also suggested that both compounds were rapidly cidal *in vivo*, with fast parasite clearance and undetectable parasitaemia achieved on day 5, only 48 hours after the first dose was received. Altogether, both the *in vitro* and *in vivo* profiles of these compounds provide a good basis for further SAR studies and optimization.[227]

1.12 Research Programme

1.12.1 Justification of the study

As already mentioned, malaria continues to take an enormous toll on human health, particularly in tropical regions. Chemotherapy represents one of the most effective control measures to mitigate the malaria burden, with the WHO presently recommending the use of artemisinin combination therapies (ACTs) to treat uncomplicated malaria. However, there is compelling evidence from Southeast Asia describing the emergence and spread of ACT resistance, characterized by reduced clearance rates of *P. falciparum* parasites.[68,69] In some countries, resistance to partner drugs such as amodiaquine has been observed.[231,232] This highlights the crucial need to expand the antimalarial drug repository by exploring and developing new compound classes, ideally with a combination of novel modes of action, multistage activity, good safety profile, efficacy at low doses and a zero propensity to the development of resistance.

Benzimidazoles and imidazopyridines, as previously described, are privileged scaffolds due to their capacity to interact with numerous biological systems, leading to a wide variety of biological activities, including antimalarial activity. Further investigations into these two classes of chemotypes as novel antimalarial agents by the concept of incorporating an intramolecular hydrogen bonding (IMHB) motif is justified as this could offer an opportunity to target the malaria parasite through novel mechanisms of action. Meanwhile, IMHB considerations in drug discovery need robust and validated descriptors to verify the propensity of compounds to exhibit IMHBs experimentally. Thus, various techniques for studying intramolecular hydrogen bonding in molecules are employed in this thesis research work.

1.12.2 Research question

The research question is whether it will be possible to identify antimalarial benzimidazole and imidazopyridine analogues incorporating an IMHB with favourable safety, physicochemical and drug metabolism and pharmacokinetics (DMPK) properties.

1.12.3 Specific Aim

To utilize benzimidazoles and imidazopyridines as templates for the design and synthesis of potential novel antimalarial agents incorporating an IMHB.

1.12.4 Objectives

i. Perform the synthesis and structure-activity relationship (SAR) studies of various antimalarial benzimidazole and imidazopyridine analogues incorporating an IMHB motif.

ii. Profile synthesized compounds for solubility, cytotoxicity, hERG inhibition and *in vitro* metabolic stability.

iii. Use of various techniques to ascertain the presence of intramolecular hydrogen bonding in synthesized compounds.

iv. Contribute to the understanding of the underlying mode of action/resistance for these classes of compounds.

v. Demonstrate *in vivo* proof-of-concept for selected frontrunner compounds.

1.13 References

(1) Bynum, B. A History of Malaria. *Lancet* **2008**, *371* (9622), 1407–1408. https://doi.org/10.1016/S0140-6736(08)60612-1.

(2) Cox, F. E. History of the Discovery of the Malaria Parasites and Their Vectors. *Parasit. Vectors* **2010**, *3* (1), 5. https://doi.org/10.1186/1756-3305-3-5.

(3) Sherman, I. W. Chapter 2 An Introduction to Malaria Parasites. In *Advances in Parasitology*; 2008; pp 3–7. https://doi.org/10.1016/S0065-308X(08)00402-8.

(4) Escalante, A. A.; Ayala, F. J. Phylogeny of the Malarial Genus Plasmodium, Derived from RRNA Gene Sequences. *Proc. Natl. Acad. Sci.* **1994**, *91* (24), 11373–11377. https://doi.org/10.1073/pnas.91.24.11373.

(5) Escalante, A. A.; Cornejo, O. E.; Freeland, D. E.; Poe, A. C.; Durrego, E.; Collins, W. E.; Lal, A. A. A Monkey's Tale: The Origin of Plasmodium Vivax as a Human Malaria Parasite. *Proc. Natl. Acad. Sci.* **2005**, *102* (6), 1980–1985. https://doi.org/10.1073/pnas.0409652102.

(6) Jongwutiwes, S.; Putaporntip, C.; Iwasaki, T.; Ferreira, M. U.; Kanbara, H.; Hughes, A. L. Mitochondrial Genome Sequences Support Ancient Population Expansion in Plasmodium Vivax. *Mol. Biol. Evol.* **2005**, *22* (8), 1733–1739. https://doi.org/10.1093/molbev/msi168.

(7) Neafsey, D. E.; Galinsky, K.; Jiang, R. H. Y.; Young, L.; Sykes, S. M.; Saif, S.; Gujja, S.; Goldberg, J. M.; Young, S.; Zeng, Q.; et al. The Malaria Parasite Plasmodium Vivax Exhibits Greater Genetic Diversity than Plasmodium Falciparum. *Nat. Genet.* **2012**, *44* (9), 1046–1050. https://doi.org/10.1038/ng.2373.

(8) Liu, W.; Li, Y.; Learn, G. H.; Rudicell, R. S.; Robertson, J. D.; Keele, B. F.; Ndjango, J.-B. N.; Sanz, C. M.; Morgan, D. B.; Locatelli, S.; et al. Origin of the Human Malaria Parasite Plasmodium Falciparum in Gorillas. *Nature* **2010**, *467* (7314), 420–425. https://doi.org/10.1038/nature09442.

(9) Sundararaman, S. A.; Plenderleith, L. J.; Liu, W.; Loy, D. E.; Learn, G. H.; Li, Y.; Shaw, K. S.; Ayouba, A.; Peeters, M.; Speede, S.; et al. Genomes of Cryptic Chimpanzee Plasmodium Species Reveal Key Evolutionary Events Leading to Human Malaria. *Nat. Commun.* **2016**, *7* (1), 11078. https://doi.org/10.1038/ncomms11078.

(10) Liu, W.; Li, Y.; Shaw, K. S.; Learn, G. H.; Plenderleith, L. J.; Malenke, J. A.; Sundararaman, S. A.; Ramirez, M. A.; Crystal, P. A.; Smith, A. G.; et al. African Origin of the Malaria Parasite Plasmodium Vivax. *Nat. Commun.* **2014**, *5* (1), 3346. https://doi.org/10.1038/ncomms4346.

(11) Autino, B.; Noris, A.; Russo, R.; Castelli, F. Epidemiology of Malaria in Endemic Areas. *Mediterr. J. Hematol. Infect. Dis.* **2012**, *4* (1), e2012060. https://doi.org/10.4084/MJHID.2012.060.

(12) World Health Organisation. *Fact Sheet: World Malaria Report 2016*; 2016.

(13) World Health Organisation. *World Malaria Report 2020*; Geneva, Switzerland, 2020.

(14) Sheehy, T. W.; Reba, R. C. Complications of Falciparum Malaria and Their Treatment. *Ann. Intern. Med.* **1967**, *66* (4), 807–809.

(15) Chima, R. I.; Goodman, C. A.; Mills, A. The Economic Impact of Malaria in Africa: A Critical Review of the Evidence. *Health Policy* **2003**, *63* (1), 17–36.

(16) Sinka, M. E.; Bangs, M. J.; Manguin, S.; Rubio-Palis, Y.; Chareonviriyaphap, T.; Coetzee, M.; Mbogo, C. M.; Hemingway, J.; Patil, A. P.; Temperley, W. H.; et al. A Global Map of Dominant Malaria Vectors. *Parasit. Vectors* **2012**, *5* (1), 69. https://doi.org/10.1186/1756-3305-5-69.

(17) Matuschewski, K. Getting Infectious: Formation and Maturation of Plasmodium Sporozoites in the Anopheles Vector. *Cell. Microbiol.* **2006**, *8* (10), 1547–1556. https://doi.org/10.1111/j.1462-5822.2006.00778.x.

(18) Opare, D. . Congenital Malaria In Newborn Twins. *Ghana Med. J.* **2010**, 44,76-78.

(19) Owusu-Ofori, A.; Gadzo, D.; Bates, I. Transfusion-Transmitted Malaria: Donor Prevalence of Parasitaemia and a Survey of Healthcare Workers Knowledge and Practices in a District Hospital in Ghana. *Malar. J.* **2016**, *15* (1), 234. https://doi.org/10.1186/s12936-016-1289-3.

(20) Rodriguez, M.; Tome, S.; Vizcaino, L.; Fernandez-Castroagudin, J.; Otero-Anton, E.; Molina, E.; Martinez, J.; De la Rosa, G.; Lovo, J.; Varo, E. Malaria Infection through Multiorgan Donation: An Update from Spain. *Liver Transplant.* **2007**, *13* (9), 1302–1304. https://doi.org/10.1002/lt.21219.

(21) Biamonte, M. A.; Wanner, J.; Le Roch, K. G. Recent Advances in Malaria Drug Discovery. *Bioorg. Med. Chem. Lett.* **2013**, *23* (10), 2829–2843. https://doi.org/10.1016/j.bmcl.2013.03.067.

(22) Centers for Disease Control and Prevention. Biology. *Centers Dis. Control Prev.* **2016**.

(23) Raghavendra, K.; Barik, T. K.; Reddy, B. P. N.; Sharma, P.; Dash, A. P. Malaria Vector Control: From Past to Future. *Parasitol. Res.* **2011**, *108* (4), 757–779. https://doi.org/10.1007/s00436-010-2232-0.

(24) CAMERON, G. R. DDT: The Synthetic Insecticide. *Nature* **1946**, *158* (4011), 359–359. https://doi.org/10.1038/158359a0.

(25) World Health Organisation. *World Malaria Report 2018*; Geneva, 2018.

(26) Implications of Insecticide Resistance for Malaria Vector Control with Long-Lasting Insecticidal Nets: Trends in Pyrethroid Resistance during a WHO-Coordinated Multi-Country Prospective Study. *Parasit. Vectors* **2018**, *11* (1), 550. https://doi.org/10.1186/s13071-018-3101-4.

(27) Schlagenhauf, P.; Petersen, E. Malaria Chemoprophylaxis: Strategies for Risk Groups. *Clin. Microbiol. Rev.* **2008**, *21* (3), 466–472. https://doi.org/10.1128/CMR.00059-07.

(28) Schwartz, E. Prophylaxis of Malaria. *Mediterr. J. Hematol. Infect. Dis.* **2012**, e2012045. https://doi.org/10.4084/mjhid.2012.45.

(29) Malaria Prophylxis https://www.malariasite.com/prophylaxis/ (accessed Nov 1, 2019).

(30) Draper, S. J.; Sack, B. K.; King, C. R.; Nielsen, C. M.; Rayner, J. C.; Higgins, M. K.; Long, C. A.; Seder, R. A. Malaria Vaccines: Recent Advances and New Horizons. *Cell Host Microbe* **2018**, *24* (1), 43–56. https://doi.org/10.1016/j.chom.2018.06.008.

(31) World Health Organisation. *World Malaria Report 2016*; Geneva, 2016.

(32) Datoo, M. S.; Natama, M. H.; Somé, A.; Traoré, O.; Rouamba, T.; Bellamy, D.; Yameogo, P.; Valia, D.; Tegneri, M.; Ouedraogo, F.; et al. Efficacy of a Low-Dose Candidate Malaria Vaccine, R21 in Adjuvant Matrix-M, with Seasonal Administration to Children in Burkina Faso: A Randomised Controlled Trial. *Lancet* **2021**, *397* (10287), 1809–1818. https://doi.org/10.1016/S0140-6736(21)00943-0.

(33) Moorthy, V.; Binka, F. R21/Matrix-M: A Second Malaria Vaccine? *Lancet* **2021**, *397*

(10287), 1782–1783. https://doi.org/10.1016/S0140-6736(21)01065-5.

(34) Eisele, T. P. Mass Drug Administration Can Be a Valuable Addition to the Malaria Elimination Toolbox. *Malar. J.* **2019**, *18* (1), 281. https://doi.org/10.1186/s12936-019-2906-8.

(35) Hetzel, M. W.; Genton, B. Mass Drug Administration for Malaria Elimination: Do We Understand the Settings Well Enough? *BMC Med.* **2018**, *16* (1), 239. https://doi.org/10.1186/s12916-018-1230-4.

(36) Eisele, T. P.; Bennett, A.; Silumbe, K.; Finn, T. P.; Chalwe, V.; Kamuliwo, M.; Hamainza, B.; Moonga, H.; Kooma, E.; Chizema Kawesha, E.; et al. Short-Term Impact of Mass Drug Administration With Dihydroartemisinin Plus Piperaquine on Malaria in Southern Province Zambia: A Cluster-Randomized Controlled Trial. *J. Infect. Dis.* **2016**, *214* (12), 1831–1839. https://doi.org/10.1093/infdis/jiw416.

(37) von Seidlein, L.; Peto, T. J.; Landier, J.; Nguyen, T.-N.; Tripura, R.; Phommasone, K.; Pongvongsa, T.; Lwin, K. M.; Keereecharoen, L.; Kajeechiwa, L.; et al. The Impact of Targeted Malaria Elimination with Mass Drug Administrations on Falciparum Malaria in Southeast Asia: A Cluster Randomised Trial. *PLOS Med.* **2019**, *16* (2), e1002745. https://doi.org/10.1371/journal.pmed.1002745.

(38) Landier, J.; Kajeechiwa, L.; Thwin, M. M.; Parker, D. M.; Chaumeau, V.; Wiladphaingern, J.; Imwong, M.; Miotto, O.; Patumrat, K.; Duanguppama, J.; et al. Safety and Effectiveness of Mass Drug Administration to Accelerate Elimination of Artemisinin-Resistant Falciparum Malaria: A Pilot Trial in Four Villages of Eastern Myanmar. *Wellcome Open Res.* **2017**, *2*, 81. https://doi.org/10.12688/wellcomeopenres.12240.1.

(39) Achan, J.; Talisuna, A. O.; Erhart, A.; Yeka, A.; Tibenderana, J. K.; Baliraine, F. N.; Rosenthal, P. J.; D'Alessandro, U. Quinine, an Old Anti-Malarial Drug in a Modern World: Role in the Treatment of Malaria. *Malar. J.* **2011**, *10* (1), 144. https://doi.org/10.1186/1475-2875-10-144.

(40) PETERS, W. Antimalarial Drug Resistance: An Increasing Problem. *Br. Med. Bull.* **1982**, *38* (2), 187–192. https://doi.org/10.1093/oxfordjournals.bmb.a071757.

(41) Model List of Essential Medicines.

(42) Farooq, U.; Mahajan, R. C. Drug Resistance in Malaria. *J. Vector Borne Dis. 41* (3–4), 45–53.

(43) Klein, E. Y. Antimalarial Drug Resistance: A Review of the Biology and Strategies to Delay Emergence and Spread. *Int. J. Antimicrob. Agents* **2013**, *41* (4), 311–317. https://doi.org/10.1016/j.ijantimicag.2012.12.007.

(44) Packard, R. M. The Origins of Antimalarial-Drug Resistance. *N. Engl. J. Med.* **2014**, *371* (5), 397–399. https://doi.org/10.1056/NEJMp1403340.

(45) Antony, H.; Parija, S. Antimalarial Drug Resistance: An Overview. *Trop. Parasitol.* **2016**, *6* (1), 30. https://doi.org/10.4103/2229-5070.175081.

(46) Weina, P. J. From Atabrine in World War II to Mefloquine in Somalia: The Role of Education in Preventive Medicine. *Mil. Med.* **1998**, *163* (9), 635–639.

(47) Burgoine, K. L.; Bancone, G.; Nosten, F. The Reality of Using Primaquine. *Malar. J.* **2010**, *9* (1), 376. https://doi.org/10.1186/1475-2875-9-376.

(48) Clyde, D. F.; McCarthy, V. C.; Miller, R. M.; Hornick, R. B. Suppressive Activity of Mefloquine in Sporozoite-Induced Human Malaria. *Antimicrob. Agents Chemother.* **1976**, *9* (3), 384–386. https://doi.org/10.1128/AAC.9.3.384.

(49) Trenholme, C.; Williams, R.; Desjardins, R.; Frischer, H.; Carson, P.; Rieckmann, K.; Canfield, C. Mefloquine (WR 142,490) in the Treatment of Human Malaria. *Science (80-.).* **1975**, *190* (4216), 792–794. https://doi.org/10.1126/science.1105787.

(50) N. Burrows, J.; Chibale, K.; N.C. Wells, T. The State of the Art in Anti-Malarial Drug Discovery and Development. *Curr. Top. Med. Chem.* **2011**, *11* (10), 1226–1254. https://doi.org/10.2174/156802611795429194.

(51) Na-Bangchang, K.; Karbwang, J. Current Status of Malaria Chemotherapy and the Role of Pharmacology in Antimalarial Drug Research and Development. *Fundam. Clin. Pharmacol.* **2009**, *23* (4), 387–409. https://doi.org/10.1111/j.1472-8206.2009.00709.x.

(52) Nzila, A. The Past, Present and Future of Antifolates in the Treatment of Plasmodium Falciparum Infection. *J. Antimicrob. Chemother.* **2006**, *57* (6), 1043–1054. https://doi.org/10.1093/jac/dkl104.

(53) Gregson, A. Mechanisms of Resistance of Malaria Parasites to Antifolates. *Pharmacol.*

Rev. **2005**, *57* (1), 117–145. https://doi.org/10.1124/pr.57.1.4.

(54) Van Malderen, C.; Van Geertruyden, J.-P.; Machevo, S.; González, R.; Bassat, Q.; Talisuna, A.; Yeka, A.; Nabasumba, C.; Piola, P.; Daniel, A.; et al. Glucose-6-Phosphate Dehydrogenase Deficiency, Chlorproguanil-Dapsone with Artesunate and Post-Treatment Haemolysis in African Children Treated for Uncomplicated Malaria. *Malar. J.* **2012**, *11* (1), 139. https://doi.org/10.1186/1475-2875-11-139.

(55) Plowe, C. V.; Djimde, A.; Bouare, M.; Doumbo, O.; Wellems, T. E. Pyrimethamine and Proguanil Resistance-Conferring Mutations in Plasmodium Falciparum Dihydrofolate Reductase: Polymerase Chain Reaction Methods for Surveillance in Africa. *Am. J. Trop. Med. Hyg.* **1995**, *52* (6), 565–568. https://doi.org/10.4269/ajtmh.1995.52.565.

(56) Triglia, T.; Cowman, A. F. Primary Structure and Expression of the Dihydropteroate Synthetase Gene of Plasmodium Falciparum. *Proc. Natl. Acad. Sci.* **1994**, *91* (15), 7149–7153. https://doi.org/10.1073/pnas.91.15.7149.

(57) Brooks, D. R.; Wang, P.; Read, M.; Watkins, W. M.; Sims, P. F. G.; Hyde, J. E. Sequence Variation of the Hydroxymethyldihydropterin Pyrophosphokinase: Dihydropteroate Synthase Gene in Lines of the Human Malaria Parasite, Plasmodium Falciparum, with Differing Resistance to Sulfadoxine. *Eur. J. Biochem.* **1994**, *224* (2), 397–405. https://doi.org/10.1111/j.1432-1033.1994.00397.x.

(58) Michel, R. Comparative Study of the Association of Sulfalene and Pyrimethamine and of Sulfalene Alone in Mass Chemoprophylaxis of Malaria. *Med. Trop. (Mars). 28* (4), 488–494.

(59) Aviado, D. M.; Singh, G.; Berkley, R. Pharmacology of New Antimalarial Drugs Sulfonamides and Trimethoprim. *Chemotherapy* **1969**, *14* (1), 37–53. https://doi.org/10.1159/000220609.

(60) Gutman, J.; Mwandama, D.; Wiegand, R. E.; Ali, D.; Mathanga, D. P.; Skarbinski, J. Effectiveness of Intermittent Preventive Treatment With Sulfadoxine-Pyrimethamine During Pregnancy on Maternal and Birth Outcomes in Machinga District, Malawi. *J. Infect. Dis.* **2013**, *208* (6), 907–916. https://doi.org/10.1093/infdis/jit276.

(61) Rogerson, S. J.; Chaluluka, E.; Kanjala, M.; Mkundika, P.; Mhango, C.; Molyneux, M. E. Intermittent Sulfadoxine-Pyrimethamine in Pregnancy: Effectiveness against Malaria

Morbidity in Blantyre, Malawi, in 1997–1999. *Trans. R. Soc. Trop. Med. Hyg.* **2000**, *94* (5), 549–553. https://doi.org/10.1016/S0035-9203(00)90083-X.

(62) Antimalarial Studies on Qinghaosu. *Chin. Med. J. (Engl).* **1979**, *92* (12), 811–816.

(63) White, N. Antimalarial Drug Resistance and Combination Chemotherapy. *Philos. Trans. R. Soc. London. Ser. B Biol. Sci.* **1999**, *354* (1384), 739–749. https://doi.org/10.1098/rstb.1999.0426.

(64) Price, R. N.; Douglas, N. M. Artemisinin Combination Therapy for Malaria: Beyond Good Efficacy. *Clin. Infect. Dis.* **2009**, *49* (11), 1638–1640. https://doi.org/10.1086/647947.

(65) Eastman, R. T.; Fidock, D. A. Artemisinin-Based Combination Therapies: A Vital Tool in Efforts to Eliminate Malaria. *Nat. Rev. Microbiol.* **2009**, *7* (12), 864–874. https://doi.org/10.1038/nrmicro2239.

(66) Shandilya, A.; Chacko, S.; Jayaram, B.; Ghosh, I. A Plausible Mechanism for the Antimalarial Activity of Artemisinin: A Computational Approach. *Sci. Rep.* **2013**, *3* (1), 2513. https://doi.org/10.1038/srep02513.

(67) Mok, S.; Ashley, E. A.; Ferreira, P. E.; Zhu, L.; Lin, Z.; Yeo, T.; Chotivanich, K.; Imwong, M.; Pukrittayakamee, S.; Dhorda, M.; et al. Population Transcriptomics of Human Malaria Parasites Reveals the Mechanism of Artemisinin Resistance. *Science (80-.).* **2015**, *347* (6220), 431–435. https://doi.org/10.1126/science.1260403.

(68) Mbengue, A.; Bhattacharjee, S.; Pandharkar, T.; Liu, H.; Estiu, G.; Stahelin, R. V.; Rizk, S. S.; Njimoh, D. L.; Ryan, Y.; Chotivanich, K.; et al. A Molecular Mechanism of Artemisinin Resistance in Plasmodium Falciparum Malaria. *Nature* **2015**, *520* (7549), 683–687. https://doi.org/10.1038/nature14412.

(69) Ashley, E. A.; Dhorda, M.; Fairhurst, R. M.; Amaratunga, C.; Lim, P.; Suon, S.; Sreng, S.; Anderson, J. M.; Mao, S.; Sam, B.; et al. Spread of Artemisinin Resistance in Plasmodium Falciparum Malaria. *N. Engl. J. Med.* **2014**, *371* (5), 411–423. https://doi.org/10.1056/NEJMoa1314981.

(70) Uwimana, A.; Legrand, E.; Stokes, B. H.; Ndikumana, J.-L. M.; Warsame, M.; Umulisa, N.; Ngamije, D.; Munyaneza, T.; Mazarati, J.-B.; Munguti, K.; et al. Emergence and Clonal Expansion of in Vitro Artemisinin-Resistant Plasmodium Falciparum Kelch13

R561H Mutant Parasites in Rwanda. *Nat. Med.* **2020**, *26* (10), 1602–1608. https://doi.org/10.1038/s41591-020-1005-2.

(71) Uwimana, A.; Umulisa, N.; Venkatesan, M.; Svigel, S. S.; Zhou, Z.; Munyaneza, T.; Habimana, R. M.; Rucogoza, A.; Moriarty, L. F.; Sandford, R.; et al. Association of Plasmodium Falciparum Kelch13 R561H Genotypes with Delayed Parasite Clearance in Rwanda: An Open-Label, Single-Arm, Multicentre, Therapeutic Efficacy Study. *Lancet Infect. Dis.* **2021**, *21* (8), 1120–1128. https://doi.org/10.1016/S1473-3099(21)00142-0.

(72) Majori, G. Combined Antimalarial Therapy Using Artemisinin. *Parassitologia* **2004**, *46* (1–2), 85–87.

(73) Aweeka, F. T.; German, P. I. Clinical Pharmacology of Artemisinin-Based Combination Therapies. *Clin. Pharmacokinet.* **2008**, *47* (2), 91–102. https://doi.org/10.2165/00003088-200847020-00002.

(74) Fidock, D. A.; Rosenthal, P. J.; Croft, S. L.; Brun, R.; Nwaka, S. Antimalarial Drug Discovery: Efficacy Models for Compound Screening. *Nat. Rev. Drug Discov.* **2004**, *3* (6), 509–520. https://doi.org/10.1038/nrd1416.

(75) Cui, L.; Mharakurwa, S.; Ndiaye, D.; Rathod, P. K.; Rosenthal, P. J. Antimalarial Drug Resistance: Literature Review and Activities and Findings of the ICEMR Network. *Am. J. Trop. Med. Hyg.* **2015**, *93* (3_Suppl), 57–68. https://doi.org/10.4269/ajtmh.15-0007.

(76) Hewitt, S.; Delacollette, C.; Chavez, I. Malaria Situation in the Greater Mekong Subregion. *Southeast Asian J. Trop. Med. Public Health* **2013**, *44 Suppl 1*, 46–72; discussion 306-7.

(77) Khan, S. Y.; Khan, A.; Arshad, M.; Tahir, H. M.; Mukhtar, M. K.; Ahmad, K. R.; Arshad, N. Irrational Use of Antimalarial Drugs in Rural Areas of Eastern Pakistan: A Random Field Study. *BMC Public Health* **2012**, *12* (1), 941. https://doi.org/10.1186/1471-2458-12-941.

(78) Nsimba, S. E. D.; Massele, A. Y.; Eriksen, J.; Gustafsson, L. L.; Tomson, G.; Warsame, M. Case Management of Malaria in Under-Fives at Primary Health Care Facilities in a Tanzanian District. *Trop. Med. Int. Heal.* **2002**, *7* (3), 201–209. https://doi.org/10.1046/j.1365-3156.2002.00847.x.

(79) Franco-Paredes, C.; Santos-Preciado, J. I. Problem Pathogens: Prevention of Malaria in Travellers. *Lancet Infect. Dis.* **2006**, *6* (3), 139–149. https://doi.org/10.1016/S1473-3099(06)70410-8.

(80) Steffen, R.; Behrens, R. H. Travellers' Malaria. *Parasitol. Today* **1992**, *8* (2), 61–66. https://doi.org/10.1016/0169-4758(92)90091-F.

(81) Wells, T. N. C.; Alonso, P. L.; Gutteridge, W. E. New Medicines to Improve Control and Contribute to the Eradication of Malaria. *Nat. Rev. Drug Discov.* **2009**, *8* (11), 879–891. https://doi.org/10.1038/nrd2972.

(82) Beutler, E. G6PD Deficiency. *Blood* **1994**, *84* (11), 3613–3636.

(83) Olliaro, P.; Nevill, C.; LeBras, J.; Ringwald, P.; Mussano, P.; Garner, P.; Brasseur, P. Systematic Review of Amodiaquine Treatment in Uncomplicated Malaria. *Lancet* **1996**, *348* (9036), 1196–1201. https://doi.org/10.1016/S0140-6736(96)06217-4.

(84) Lind, D. E.; Levi, J. A.; Vincent, P. C. Amodiaquine-Induced Agranulocytosis: Toxic Effect of Amodiaquine in Bone Marrow Cultures In Vitro. *BMJ* **1973**, *1* (5851), 458–460. https://doi.org/10.1136/bmj.1.5851.458.

(85) Hatton, C. S. R.; Bunch, C.; Peto, T. E. A.; Pasvol, G.; Russell, S. J.; Singer, C. R. J.; Edwards, G.; Winstanley, P. Frequency of Severe Neutropenia Associated With Amodiaquine Prophylaxis Against Malaria. *Lancet* **1986**, *327* (8478), 411–414. https://doi.org/10.1016/S0140-6736(86)92371-8.

(86) Larrey, D. Amodiaquine-Lnduced Hepatitis. *Ann. Intern. Med.* **1986**, *104* (6), 801. https://doi.org/10.7326/0003-4819-104-6-801.

(87) Hood, J. E.; Jenkins, J. W.; Milatovic, D.; Rongzhu, L.; Aschner, M. Mefloquine Induces Oxidative Stress and Neurodegeneration in Primary Rat Cortical Neurons. *Neurotoxicology* **2010**, *31* (5), 518–523. https://doi.org/10.1016/j.neuro.2010.05.005.

(88) Ringqvist, Å.; Bech, P.; Glenthøj, B.; Petersen, E. Acute and Long-Term Psychiatric Side Effects of Mefloquine: A Follow-up on Danish Adverse Event Reports. *Travel Med. Infect. Dis.* **2015**, *13* (1), 80–88. https://doi.org/10.1016/j.tmaid.2014.10.021.

(89) Nevin, R. L. Limbic Encephalopathy and Central Vestibulopathy Caused by Mefloquine: A Case Report. *Travel Med. Infect. Dis.* **2012**, *10* (3), 144–151. https://doi.org/10.1016/j.tmaid.2012.03.006.

(90) Delves, M.; Plouffe, D.; Scheurer, C.; Meister, S.; Wittlin, S.; Winzeler, E. A.; Sinden, R. E.; Leroy, D. The Activities of Current Antimalarial Drugs on the Life Cycle Stages of Plasmodium: A Comparative Study with Human and Rodent Parasites. *PLoS Med.* **2012**, *9* (2), e1001169. https://doi.org/10.1371/journal.pmed.1001169.

(91) Flannery, E. L.; Chatterjee, A. K.; Winzeler, E. A. Antimalarial Drug Discovery — Approaches and Progress towards New Medicines. *Nat. Rev. Microbiol.* **2013**, *11* (12), 849–862. https://doi.org/10.1038/nrmicro3138.

(92) Barnett, D. S.; Guy, R. K. Antimalarials in Development in 2014. *Chem. Rev.* **2014**, *114* (22), 11221–11241. https://doi.org/10.1021/cr500543f.

(93) Alonso, P. L.; Brown, G.; Arevalo-Herrera, M.; Binka, F.; Chitnis, C.; Collins, F.; Doumbo, O. K.; Greenwood, B.; Hall, B. F.; Levine, M. M.; et al. A Research Agenda to Underpin Malaria Eradication. *PLoS Med.* **2011**, *8* (1), e1000406. https://doi.org/10.1371/journal.pmed.1000406.

(94) Burrows, J. N.; Hooft van Huijsduijnen, R.; Möhrle, J. J.; Oeuvray, C.; Wells, T. N. Designing the Next Generation of Medicines for Malaria Control and Eradication. *Malar. J.* **2013**, *12* (1), 187. https://doi.org/10.1186/1475-2875-12-187.

(95) Burrows, J. N.; Duparc, S.; Gutteridge, W. E.; Hooft van Huijsduijnen, R.; Kaszubska, W.; Macintyre, F.; Mazzuri, S.; Möhrle, J. J.; Wells, T. N. C. New Developments in Anti-Malarial Target Candidate and Product Profiles. *Malar. J.* **2017**, *16* (1), 26. https://doi.org/10.1186/s12936-016-1675-x.

(96) Medicines for Malaria Venture. MMV-supported projects https://www.mmv.org/research-development/mmv-supported-projects (accessed May 15, 2021).

(97) Chavchich, M.; Birrell, G. W.; Ager, A. L.; MacKenzie, D. O.; Heffernan, G. D.; Schiehser, G. A.; Jacobus, L. R.; Shanks, G. D.; Jacobus, D. P.; Edstein, M. D. Lead Selection of a New Aminomethylphenol, JPC-3210, for Malaria Treatment and Prevention. *Antimicrob. Agents Chemother.* **2016**, *60* (5), 3115–3118. https://doi.org/10.1128/AAC.03066-15.

(98) Birrell, G. W.; Heffernan, G. D.; Schiehser, G. A.; Anderson, J.; Ager, A. L.; Morales, P.; MacKenzie, D.; van Breda, K.; Chavchich, M.; Jacobus, L. R.; et al. Characterization

of the Preclinical Pharmacology of the New 2-Aminomethylphenol, JPC-3210, for Malaria Treatment and Prevention. *Antimicrob. Agents Chemother.* **2018**, *62* (4). https://doi.org/10.1128/AAC.01335-17.

(99) Birrell, G. W.; Challis, M. P.; De Paoli, A.; Anderson, D.; Devine, S. M.; Heffernan, G. D.; Jacobus, D. P.; Edstein, M. D.; Siddiqui, G.; Creek, D. J. Multi-Omic Characterization of the Mode of Action of a Potent New Antimalarial Compound, JPC-3210, Against Plasmodium Falciparum. *Mol. Cell. Proteomics* **2020**, *19* (2), 308–325. https://doi.org/10.1074/mcp.RA119.001797.

(100) Baragaña, B.; Hallyburton, I.; Lee, M. C. S.; Norcross, N. R.; Grimaldi, R.; Otto, T. D.; Proto, W. R.; Blagborough, A. M.; Meister, S.; Wirjanata, G.; et al. A Novel Multiple-Stage Antimalarial Agent That Inhibits Protein Synthesis. *Nature* **2015**, *522* (7556), 315–320. https://doi.org/10.1038/nature14451.

(101) Baragaña, B.; Norcross, N. R.; Wilson, C.; Porzelle, A.; Hallyburton, I.; Grimaldi, R.; Osuna-Cabello, M.; Norval, S.; Riley, J.; Stojanovski, L.; et al. Discovery of a Quinoline-4-Carboxamide Derivative with a Novel Mechanism of Action, Multistage Antimalarial Activity, and Potent in Vivo Efficacy. *J. Med. Chem.* **2016**, *59* (21), 9672–9685. https://doi.org/10.1021/acs.jmedchem.6b00723.

(102) Hameed P., S.; Solapure, S.; Patil, V.; Henrich, P. P.; Magistrado, P. A.; Bharath, S.; Murugan, K.; Viswanath, P.; Puttur, J.; Srivastava, A.; et al. Triaminopyrimidine Is a Fast-Killing and Long-Acting Antimalarial Clinical Candidate. *Nat. Commun.* **2015**, *6* (1), 6715. https://doi.org/10.1038/ncomms7715.

(103) Medicines for Malaria Venture. *MMV Annual Report*; Geneva, 2020.

(104) Wu, T.; Nagle, A.; Kuhen, K.; Gagaring, K.; Borboa, R.; Francek, C.; Chen, Z.; Plouffe, D.; Goh, A.; Lakshminarayana, S. B.; et al. Imidazolopiperazines: Hit to Lead Optimization of New Antimalarial Agents. *J. Med. Chem.* **2011**, *54* (14), 5116–5130. https://doi.org/10.1021/jm2003359.

(105) Nagle, A.; Wu, T.; Kuhen, K.; Gagaring, K.; Borboa, R.; Francek, C.; Chen, Z.; Plouffe, D.; Lin, X.; Caldwell, C.; et al. Imidazolopiperazines: Lead Optimization of the Second-Generation Antimalarial Agents. *J. Med. Chem.* **2012**, *55* (9), 4244–4273. https://doi.org/10.1021/jm300041e.

(106) Kuhen, K. L.; Chatterjee, A. K.; Rottmann, M.; Gagaring, K.; Borboa, R.; Buenviaje, J.; Chen, Z.; Francek, C.; Wu, T.; Nagle, A.; et al. KAF156 Is an Antimalarial Clinical Candidate with Potential for Use in Prophylaxis, Treatment, and Prevention of Disease Transmission. *Antimicrob. Agents Chemother.* **2014**, *58* (9), 5060–5067. https://doi.org/10.1128/AAC.02727-13.

(107) White, N. J.; Pukrittayakamee, S.; Phyo, A. P.; Rueangweerayut, R.; Nosten, F.; Jittamala, P.; Jeeyapant, A.; Jain, J. P.; Lefèvre, G.; Li, R.; et al. Spiroindolone KAE609 for Falciparum and Vivax Malaria. *N. Engl. J. Med.* **2014**, *371* (5), 403–410. https://doi.org/10.1056/NEJMoa1315860.

(108) Rottmann, M.; McNamara, C.; Yeung, B. K. S.; Lee, M. C. S.; Zou, B.; Russell, B.; Seitz, P.; Plouffe, D. M.; Dharia, N. V.; Tan, J.; et al. Spiroindolones, a Potent Compound Class for the Treatment of Malaria. *Science (80-.).* **2010**, *329* (5996), 1175–1180. https://doi.org/10.1126/science.1193225.

(109) van Pelt-Koops, J. C.; Pett, H. E.; Graumans, W.; van der Vegte-Bolmer, M.; van Gemert, G. J.; Rottmann, M.; Yeung, B. K. S.; Diagana, T. T.; Sauerwein, R. W. The Spiroindolone Drug Candidate NITD609 Potently Inhibits Gametocytogenesis and Blocks Plasmodium Falciparum Transmission to Anopheles Mosquito Vector. *Antimicrob. Agents Chemother.* **2012**, *56* (7), 3544–3548. https://doi.org/10.1128/AAC.06377-11.

(110) Zhou, Y.; Fomovska, A.; Muench, S.; Lai, B.-S.; Mui, E.; McLeod, R. Spiroindolone That Inhibits PfATPase4 Is a Potent, Cidal Inhibitor of Toxoplasma Gondii Tachyzoites In Vitro and In Vivo. *Antimicrob. Agents Chemother.* **2014**, *58* (3), 1789–1792. https://doi.org/10.1128/AAC.02225-13.

(111) Held, J.; Supan, C.; Salazar, C. L. O.; Tinto, H.; Bonkian, L. N.; Nahum, A.; Moulero, B.; Sié, A.; Coulibaly, B.; Sirima, S. B.; et al. Ferroquine and Artesunate in African Adults and Children with Plasmodium Falciparum Malaria: A Phase 2, Multicentre, Randomised, Double-Blind, Dose-Ranging, Non-Inferiority Study. *Lancet Infect. Dis.* **2015**, *15* (12), 1409–1419. https://doi.org/10.1016/S1473-3099(15)00079-1.

(112) Dubar, F.; Khalife, J.; Brocard, J.; Dive, D.; Biot, C. Ferroquine, an Ingenious Antimalarial Drug –Thoughts on the Mechanism of Action. *Molecules* **2008**, *13* (11), 2900–2907. https://doi.org/10.3390/molecules13112900.

(113) Chavain, N.; Vezin, H.; Dive, D.; Touati, N.; Paul, J.-F.; Buisine, E.; Biot, C. Investigation of the Redox Behavior of Ferroquine, a New Antimalarial. *Mol. Pharm.* **2008**, *5* (5), 710–716. https://doi.org/10.1021/mp800007x.

(114) Zheng, W.; Thorne, N.; McKew, J. C. Phenotypic Screens as a Renewed Approach for Drug Discovery. *Drug Discov. Today* **2013**, *18* (21–22), 1067–1073. https://doi.org/10.1016/j.drudis.2013.07.001.

(115) Shi, Y.; Inoue, H.; Wu, J. C.; Yamanaka, S. Induced Pluripotent Stem Cell Technology: A Decade of Progress. *Nat. Rev. Drug Discov.* **2017**, *16* (2), 115–130. https://doi.org/10.1038/nrd.2016.245.

(116) Fellmann, C.; Gowen, B. G.; Lin, P.-C.; Doudna, J. A.; Corn, J. E. Cornerstones of CRISPR–Cas in Drug Discovery and Therapy. *Nat. Rev. Drug Discov.* **2017**, *16* (2), 89–100. https://doi.org/10.1038/nrd.2016.238.

(117) Sioud, M. *Target Discovery and Validation Reviews and Protocols: Emerging Strategies for Targets and Biomarker Discovery*, Volume 1.; Humana Press Incorporation: Totowa, New Jersey, 2007.

(118) Comess, K. M.; McLoughlin, S. M.; Oyer, J. A.; Richardson, P. L.; Stöckmann, H.; Vasudevan, A.; Warder, S. E. Emerging Approaches for the Identification of Protein Targets of Small Molecules - A Practitioners' Perspective. *J. Med. Chem.* **2018**, *61* (19), 8504–8535. https://doi.org/10.1021/acs.jmedchem.7b01921.

(119) Aulner, N.; Danckaert, A.; Ihm, J.; Shum, D.; Shorte, S. L. Next-Generation Phenotypic Screening in Early Drug Discovery for Infectious Diseases. *Trends Parasitol.* **2019**, *35* (7), 559–570. https://doi.org/10.1016/j.pt.2019.05.004.

(120) Arrowsmith, J. Phase III and Submission Failures: 2007–2010. *Nat. Rev. Drug Discov.* **2011**, *10* (2), 87–87. https://doi.org/10.1038/nrd3375.

(121) Arrowsmith, J. Phase II Failures: 2008–2010. *Nat. Rev. Drug Discov.* **2011**, *10* (5), 328–329. https://doi.org/10.1038/nrd3439.

(122) Overington, J. P.; Al-Lazikani, B.; Hopkins, A. L. How Many Drug Targets Are There? *Nat. Rev. Drug Discov.* **2006**, *5* (12), 993–996. https://doi.org/10.1038/nrd2199.

(123) Rask-Andersen, M.; Almén, M. S.; Schiöth, H. B. Trends in the Exploitation of Novel Drug Targets. *Nat. Rev. Drug Discov.* **2011**, *10* (8), 579–590.

https://doi.org/10.1038/nrd3478.

(124) Moffat, J. G.; Vincent, F.; Lee, J. A.; Eder, J.; Prunotto, M. Opportunities and Challenges in Phenotypic Drug Discovery: An Industry Perspective. *Nat. Rev. Drug Discov.* **2017**, *16* (8), 531–543. https://doi.org/10.1038/nrd.2017.111.

(125) Lee, J. A.; Carragher, N. O.; Berg, E. L. Empirical Drug Discovery: A View from the Proteome. *Drug Discov. Today Technol.* **2017**, *23*, 1–5. https://doi.org/10.1016/j.ddtec.2017.05.003.

(126) Aubé, J. Drug Repurposing and the Medicinal Chemist. *ACS Med. Chem. Lett.* **2012**, *3* (6), 442–444. https://doi.org/10.1021/ml300114c.

(127) Klug, D. M.; Gelb, M. H.; Pollastri, M. P. Repurposing Strategies for Tropical Disease Drug Discovery. *Bioorg. Med. Chem. Lett.* **2016**, *26* (11), 2569–2576. https://doi.org/10.1016/j.bmcl.2016.03.103.

(128) Ashburn, T. T.; Thor, K. B. Drug Repositioning: Identifying and Developing New Uses for Existing Drugs. *Nat. Rev. Drug Discov.* **2004**, *3* (8), 673–683. https://doi.org/10.1038/nrd1468.

(129) Njoroge, M.; Njuguna, N. M.; Mutai, P.; Ongarora, D. S. B.; Smith, P. W.; Chibale, K. Recent Approaches to Chemical Discovery and Development Against Malaria and the Neglected Tropical Diseases Human African Trypanosomiasis and Schistosomiasis. *Chem. Rev.* **2014**, *114* (22), 11138–11163. https://doi.org/10.1021/cr500098f.

(130) Talevi, A.; Bellera, C. L. Challenges and Opportunities with Drug Repurposing: Finding Strategies to Find Alternative Uses of Therapeutics. *Expert Opin. Drug Discov.* **2020**, *15* (4), 397–401. https://doi.org/10.1080/17460441.2020.1704729.

(131) Leeson, P. D. Molecular Inflation, Attrition and the Rule of Five. *Adv. Drug Deliv. Rev.* **2016**, *101*, 22–33. https://doi.org/10.1016/j.addr.2016.01.018.

(132) Meanwell, N. A. Improving Drug Candidates by Design: A Focus on Physicochemical Properties As a Means of Improving Compound Disposition and Safety. *Chem. Res. Toxicol.* **2011**, *24* (9), 1420–1456. https://doi.org/10.1021/tx200211v.

(133) Gleeson, M. P.; Hersey, A.; Montanari, D.; Overington, J. Probing the Links between in Vitro Potency, ADMET and Physicochemical Parameters. *Nat. Rev. Drug Discov.* **2011**, *10* (3), 197–208. https://doi.org/10.1038/nrd3367.

(134) Lipinski, C. A. Lead- and Drug-like Compounds: The Rule-of-Five Revolution. *Drug Discov. Today Technol.* **2004**, *1* (4), 337–341. https://doi.org/10.1016/j.ddtec.2004.11.007.

(135) Savjani, K. T.; Gajjar, A. K.; Savjani, J. K. Drug Solubility: Importance and Enhancement Techniques. *ISRN Pharm.* **2012**, *2012*, 1–10. https://doi.org/10.5402/2012/195727.

(136) Di, L.; Fish, P. V.; Mano, T. Bridging Solubility between Drug Discovery and Development. *Drug Discov. Today* **2012**, *17* (9–10), 486–495. https://doi.org/10.1016/j.drudis.2011.11.007.

(137) Palucki, M.; Higgins, J. D.; Kwong, E.; Templeton, A. C. Strategies at the Interface of Drug Discovery and Development: Early Optimization of the Solid State Phase and Preclinical Toxicology Formulation for Potential Drug Candidates. *J. Med. Chem.* **2010**, *53* (16), 5897–5905. https://doi.org/10.1021/jm1002638.

(138) Waring, M. J. Lipophilicity in Drug Discovery. *Expert Opin. Drug Discov.* **2010**, *5* (3), 235–248. https://doi.org/10.1517/17460441003605098.

(139) Arnott, J. A.; Planey, S. L. The Influence of Lipophilicity in Drug Discovery and Design. *Expert Opin. Drug Discov.* **2012**, *7* (10), 863–875. https://doi.org/10.1517/17460441.2012.714363.

(140) Hughes, J. D.; Blagg, J.; Price, D. A.; Bailey, S.; DeCrescenzo, G. A.; Devraj, R. V.; Ellsworth, E.; Fobian, Y. M.; Gibbs, M. E.; Gilles, R. W.; et al. Physiochemical Drug Properties Associated with in Vivo Toxicological Outcomes. *Bioorg. Med. Chem. Lett.* **2008**, *18* (17), 4872–4875. https://doi.org/10.1016/j.bmcl.2008.07.071.

(141) Hou, T.; Wang, J.; Zhang, W.; Wang, W.; Xu, X. Recent Advances in Computational Prediction of Drug Absorption and Permeability in Drug Discovery. *Curr. Med. Chem.* **2006**, *13* (22), 2653–2667. https://doi.org/10.2174/092986706778201558.

(142) Veber, D. F.; Johnson, S. R.; Cheng, H.-Y.; Smith, B. R.; Ward, K. W.; Kopple, K. D. Molecular Properties That Influence the Oral Bioavailability of Drug Candidates. *J. Med. Chem.* **2002**, *45* (12), 2615–2623. https://doi.org/10.1021/jm020017n.

(143) Amidon, G. L.; Lennernäs, H.; Shah, V. P.; Crison, J. R. A Theoretical Basis for a Biopharmaceutic Drug Classification: The Correlation of in Vitro Drug Product

Dissolution and in Vivo Bioavailability. *Pharm. Res.* **1995**, *12* (3), 413–420.

(144) Kawabata, Y.; Wada, K.; Nakatani, M.; Yamada, S.; Onoue, S. Formulation Design for Poorly Water-Soluble Drugs Based on Biopharmaceutics Classification System: Basic Approaches and Practical Applications. *Int. J. Pharm.* **2011**, *420* (1), 1–10. https://doi.org/10.1016/j.ijpharm.2011.08.032.

(145) Wu, C.-Y.; Benet, L. Z. Predicting Drug Disposition via Application of BCS: Transport/Absorption/ Elimination Interplay and Development of a Biopharmaceutics Drug Disposition Classification System. *Pharm. Res.* **2005**, *22* (1), 11–23. https://doi.org/10.1007/s11095-004-9004-4.

(146) Löbenberg, R. Modern Bioavailability, Bioequivalence and Biopharmaceutics Classification System. New Scientific Approaches to International Regulatory Standards. *Eur. J. Pharm. Biopharm.* **2000**, *50* (1), 3–12. https://doi.org/10.1016/S0939-6411(00)00091-6.

(147) Hörter, D.; Dressman, J. . Influence of Physicochemical Properties on Dissolution of Drugs in the Gastrointestinal Tract1PII of Original Article: S0169-409X(96)00487-5. The Article Was Originally Published in Advanced Drug Delivery Reviews 25 (1997) 3–14.1. *Adv. Drug Deliv. Rev.* **2001**, *46* (1–3), 75–87. https://doi.org/10.1016/S0169-409X(00)00130-7.

(148) Leuner, C. Improving Drug Solubility for Oral Delivery Using Solid Dispersions. *Eur. J. Pharm. Biopharm.* **2000**, *50* (1), 47–60. https://doi.org/10.1016/S0939-6411(00)00076-X.

(149) Huang, Y.; Dai, W.-G. Fundamental Aspects of Solid Dispersion Technology for Poorly Soluble Drugs. *Acta Pharm. Sin. B* **2014**, *4* (1), 18–25. https://doi.org/10.1016/j.apsb.2013.11.001.

(150) Arrowsmith, J. E.; Campbell, S. F.; Cross, P. E.; Stubbs, J. K.; Burges, R. A.; Gardiner, D. G.; Blackburn, K. J. Long-Acting Dihydropyridine Calcium Antagonists. 1. 2-Alkoxymethyl Derivatives Incorporating Basic Substituents. *J. Med. Chem.* **1986**, *29* (9), 1696–1702. https://doi.org/10.1021/jm00159a022.

(151) Jordan, V. C. Tamoxifen: A Most Unlikely Pioneering Medicine. *Nat. Rev. Drug Discov.* **2003**, *2* (3), 205–213. https://doi.org/10.1038/nrd1031.

(152) Lundquist, J. T.; Harnish, D. C.; Kim, C. Y.; Mehlmann, J. F.; Unwalla, R. J.; Phipps, K. M.; Crawley, M. L.; Commons, T.; Green, D. M.; Xu, W.; et al. Improvement of Physiochemical Properties of the Tetrahydroazepinoindole Series of Farnesoid X Receptor (FXR) Agonists: Beneficial Modulation of Lipids in Primates. *J. Med. Chem.* **2010**, *53* (4), 1774–1787. https://doi.org/10.1021/jm901650u.

(153) Ishikawa, M.; Hashimoto, Y. Improvement in Aqueous Solubility in Small Molecule Drug Discovery Programs by Disruption of Molecular Planarity and Symmetry. *J. Med. Chem.* **2011**, *54* (6), 1539–1554. https://doi.org/10.1021/jm101356p.

(154) Ettmayer, P.; Amidon, G. L.; Clement, B.; Testa, B. Lessons Learned from Marketed and Investigational Prodrugs. *J. Med. Chem.* **2004**, *47* (10), 2393–2404. https://doi.org/10.1021/jm0303812.

(155) Stella, V. J.; Nti-Addae, K. W. Prodrug Strategies to Overcome Poor Water Solubility. *Adv. Drug Deliv. Rev.* **2007**, *59* (7), 677–694. https://doi.org/10.1016/j.addr.2007.05.013.

(156) Rautio, J.; Kumpulainen, H.; Heimbach, T.; Oliyai, R.; Oh, D.; Järvinen, T.; Savolainen, J. Prodrugs: Design and Clinical Applications. *Nat. Rev. Drug Discov.* **2008**, *7* (3), 255–270. https://doi.org/10.1038/nrd2468.

(157) Graham, D. Y.; Smith, J. L.; Holmes, G. I.; Davies, R. O. Nonsteroidal Anti-Inflammatory Effect of Sulindac Sulfoxide and Sulfide on Gastric Mucosa. *Clin. Pharmacol. Ther.* **1985**, *38* (1), 65–70. https://doi.org/10.1038/clpt.1985.136.

(158) Ferri, N.; Siegl, P.; Corsini, A.; Herrmann, J.; Lerman, A.; Benghozi, R. Drug Attrition during Pre-Clinical and Clinical Development: Understanding and Managing Drug-Induced Cardiotoxicity. *Pharmacol. Ther.* **2013**, *138* (3), 470–484. https://doi.org/10.1016/j.pharmthera.2013.03.005.

(159) Stevens, J. L.; Baker, T. K. The Future of Drug Safety Testing: Expanding the View and Narrowing the Focus. *Drug Discov. Today* **2009**, *14* (3–4), 162–167. https://doi.org/10.1016/j.drudis.2008.11.009.

(160) Roden, D. M. Drug-Induced Prolongation of the QT Interval. *N. Engl. J. Med.* **2004**, *350* (10), 1013–1022. https://doi.org/10.1056/NEJMra032426.

(161) Yap, Y. G. Drug Induced QT Prolongation and Torsades de Pointes. *Heart* **2003**, *89*

(11), 1363–1372. https://doi.org/10.1136/heart.89.11.1363.

(162) Valentin, J.-P. Reducing QT Liability and Proarrhythmic Risk in Drug Discovery and Development. *Br. J. Pharmacol.* **2010**, *159* (1), 5–11. https://doi.org/10.1111/j.1476-5381.2009.00547.x.

(163) Jamieson, C.; Moir, E. M.; Rankovic, Z.; Wishart, G. Medicinal Chemistry of HERG Optimizations: Highlights and Hang-Ups. *J. Med. Chem.* **2006**, *49* (17), 5029–5046. https://doi.org/10.1021/jm060379l.

(164) Hirose, H.; Yamasaki, T.; Ogino, M.; Mizojiri, R.; Tamura-Okano, Y.; Yashiro, H.; Muraki, Y.; Nakano, Y.; Sugama, J.; Hata, A.; et al. Discovery of Novel 5-Oxa-2,6-Diazaspiro[3.4]Oct-6-Ene Derivatives as Potent, Selective, and Orally Available Somatostatin Receptor Subtype 5 (SSTR5) Antagonists for Treatment of Type 2 Diabetes Mellitus. *Bioorg. Med. Chem.* **2017**, *25* (15), 4175–4193. https://doi.org/10.1016/j.bmc.2017.06.007.

(165) Mitcheson, J. S.; Chen, J.; Lin, M.; Culberson, C.; Sanguinetti, M. C. A Structural Basis for Drug-Induced Long QT Syndrome. *Proc. Natl. Acad. Sci.* **2000**, *97* (22), 12329–12333. https://doi.org/10.1073/pnas.210244497.

(166) Pearlstein, R. A.; Vaz, R. J.; Kang, J.; Chen, X.-L.; Preobrazhenskaya, M.; Shchekotikhin, A. E.; Korolev, A. M.; Lysenkova, L. N.; Miroshnikova, O. V; Hendrix, J.; et al. Characterization of HERG Potassium Channel Inhibition Using CoMSiA 3D QSAR and Homology Modeling Approaches. *Bioorg. Med. Chem. Lett.* **2003**, *13* (10), 1829–1835. https://doi.org/10.1016/S0960-894X(03)00196-3.

(167) Rajamani, R.; Tounge, B. A.; Li, J.; Reynolds, C. H. A Two-State Homology Model of the HERG K+ Channel: Application to Ligand Binding. *Bioorg. Med. Chem. Lett.* **2005**, *15* (6), 1737–1741. https://doi.org/10.1016/j.bmcl.2005.01.008.

(168) Blum, C. A.; Zheng, X.; De Lombaert, S. Design, Synthesis, and Biological Evaluation of Substituted 2-Cyclohexyl-4-Phenyl-1 H -Imidazoles: Potent and Selective Neuropeptide Y Y5-Receptor Antagonists. *J. Med. Chem.* **2004**, *47* (9), 2318–2325. https://doi.org/10.1021/jm030490g.

(169) Kim, D.; Wang, L.; Hale, J. J.; Lynch, C. L.; Budhu, R. J.; MacCoss, M.; Mills, S. G.; Malkowitz, L.; Gould, S. L.; DeMartino, J. A.; et al. Potent 1,3,4-Trisubstituted

Pyrrolidine CCR5 Receptor Antagonists: Effects of Fused Heterocycles on Antiviral Activity and Pharmacokinetic Properties. *Bioorg. Med. Chem. Lett.* **2005**, *15* (8), 2129–2134. https://doi.org/10.1016/j.bmcl.2005.02.030.

(170) Woosley, R. L. Cardiac Actions of Antihistamines. *Annu. Rev. Pharmacol. Toxicol.* **1996**, *36* (1), 233–252. https://doi.org/10.1146/annurev.pa.36.040196.001313.

(171) Rampe, D.; Wible, B.; Brown, A. M.; Dage, R. C. Effects of Terfenadine and Its Metabolites on a Delayed Rectifier K+ Channel Cloned from Human Heart. *Mol. Pharmacol.* **1993**, *44* (6), 1240–1245.

(172) Xu, J.; Wei, L.; Mathvink, R.; He, J.; Park, Y.-J.; He, H.; Leiting, B.; Lyons, K. A.; Marsilio, F.; Patel, R. A.; et al. Discovery of Potent and Selective Phenylalanine Based Dipeptidyl Peptidase IV Inhibitors. *Bioorg. Med. Chem. Lett.* **2005**, *15* (10), 2533–2536. https://doi.org/10.1016/j.bmcl.2005.03.055.

(173) Edmondson, S. D.; Mastracchio, A.; Beconi, M.; Colwell, L. F.; Habulihaz, B.; He, H.; Kumar, S.; Leiting, B.; Lyons, K. A.; Mao, A.; et al. Potent and Selective Proline Derived Dipeptidyl Peptidase IV Inhibitors. *Bioorg. Med. Chem. Lett.* **2004**, *14* (20), 5151–5155. https://doi.org/10.1016/j.bmcl.2004.07.056.

(174) Edmondson, S. D.; Mastracchio, A.; Duffy, J. L.; Eiermann, G. J.; He, H.; Ita, I.; Leiting, B.; Leone, J. F.; Lyons, K. A.; Makarewicz, A. M.; et al. Discovery of Potent and Selective Orally Bioavailable β-Substituted Phenylalanine Derived Dipeptidyl Peptidase IV Inhibitors. *Bioorg. Med. Chem. Lett.* **2005**, *15* (12), 3048–3052. https://doi.org/10.1016/j.bmcl.2005.04.028.

(175) Fernandez, D.; Ghanta, A.; Kauffman, G. W.; Sanguinetti, M. C. Physicochemical Features of the HERG Channel Drug Binding Site. *J. Biol. Chem.* **2004**, *279* (11), 10120–10127. https://doi.org/10.1074/jbc.M310683200.

(176) Waring, M. J.; Johnstone, C. A Quantitative Assessment of HERG Liability as a Function of Lipophilicity. *Bioorg. Med. Chem. Lett.* **2007**, *17* (6), 1759–1764. https://doi.org/10.1016/j.bmcl.2006.12.061.

(177) Bartolozzi, A.; Abeywardane, A.; Bosanac, T.; Broadwater, J. A.; Chen, Z.; Hutzler, J. M.; Huber, J. D.; Nemoto, P.; Olague, A.; Riether, D.; et al. Discovery and Optimization of Oxadiazole-Based FLAP Inhibitors. *Bioorg. Med. Chem. Lett.* **2017**, *27* (20), 4652–

4659. https://doi.org/10.1016/j.bmcl.2017.09.007.

(178) Furber, M.; Tiden, A.-K.; Gardiner, P.; Mete, A.; Ford, R.; Millichip, I.; Stein, L.; Mather, A.; Kinchin, E.; Luckhurst, C.; et al. Cathepsin C Inhibitors: Property Optimization and Identification of a Clinical Candidate. *J. Med. Chem.* **2014**, *57* (6), 2357–2367. https://doi.org/10.1021/jm401705g.

(179) Zolotoy, A.; Plouvier, B.; Beatch, G.; Hayes, E.; Wall, R.; Walker, M. Physicochemical Determinants for Drug Induced Blockade of HERG Potassium Channels: Effect of Charge and Charge Shielding. *Curr. Med. Chem. Hematol. Agents* **2003**, *1* (3), 225–241. https://doi.org/10.2174/1568016033477432.

(180) Zhang, H.-C.; Derian, C. K.; McComsey, D. F.; White, K. B.; Ye, H.; Hecker, L. R.; Li, J.; Addo, M. F.; Croll, D.; Eckardt, A. J.; et al. Novel Indolylindazolylmaleimides as Inhibitors of Protein Kinase C-β: Synthesis, Biological Activity, and Cardiovascular Safety †. *J. Med. Chem.* **2005**, *48* (6), 1725–1728. https://doi.org/10.1021/jm049478u.

(181) Jeffrey, G. A.; Saenger, W. *Hydrogen Bonding in Biological Structures*; Springer Berlin Heidelberg: Berlin, Heidelberg, 1991. https://doi.org/10.1007/978-3-642-85135-3.

(182) Caron, G.; Kihlberg, J.; Ermondi, G. Intramolecular Hydrogen Bonding: An Opportunity for Improved Design in Medicinal Chemistry. *Med. Res. Rev.* **2019**, *39* (5), 1707–1729. https://doi.org/10.1002/med.21562.

(183) Kuhn, B.; Mohr, P.; Stahl, M. Intramolecular Hydrogen Bonding in Medicinal Chemistry. *J. Med. Chem.* **2010**, *53* (6), 2601–2611. https://doi.org/10.1021/jm100087s.

(184) Desai, P. V.; Raub, T. J.; Blanco, M.-J. How Hydrogen Bonds Impact P-Glycoprotein Transport and Permeability. *Bioorg. Med. Chem. Lett.* **2012**, *22* (21), 6540–6548. https://doi.org/10.1016/j.bmcl.2012.08.059.

(185) Ettorre, A.; D'Andrea, P.; Mauro, S.; Porcelloni, M.; Rossi, C.; Altamura, M.; Catalioto, R. M.; Giuliani, S.; Maggi, C. A.; Fattori, D. HNK2 Receptor Antagonists. The Use of Intramolecular Hydrogen Bonding to Increase Solubility and Membrane Permeability. *Bioorg. Med. Chem. Lett.* **2011**, *21* (6), 1807–1809. https://doi.org/10.1016/j.bmcl.2011.01.074.

(186) Alex, A.; Millan, D. S.; Perez, M.; Wakenhut, F.; Whitlock, G. A. Intramolecular Hydrogen Bonding to Improve Membrane Permeability and Absorption in beyond Rule

of Five Chemical Space. *Medchemcomm* **2011**, *2* (7), 669. https://doi.org/10.1039/c1md00093d.

(187) Carrupt, P. A.; Testa, B.; Bechalany, A.; el Tayar, N.; Descas, P.; Perrissoud, D. Morphine 6-Glucuronide and Morphine 3-Glucuronide as Molecular Chameleons with Unexpected Lipophilicity. *J. Med. Chem.* **1991**, *34* (4), 1272–1275.

(188) Rafi, S. B.; Hearn, B. R.; Vedantham, P.; Jacobson, M. P.; Renslo, A. R. Predicting and Improving the Membrane Permeability of Peptidic Small Molecules. *J. Med. Chem.* **2012**, *55* (7), 3163–3169. https://doi.org/10.1021/jm201634q.

(189) Honda, T.; Nagahara, H.; Mogi, H.; Ban, M.; Aono, H. KDR Inhibitor with the Intramolecular Non-Bonded Interaction: Conformation–Activity Relationships of Novel Indole-3-Carboxamide Derivatives. *Bioorg. Med. Chem. Lett.* **2011**, *21* (6), 1782–1785. https://doi.org/10.1016/j.bmcl.2011.01.063.

(190) Liu, K. K. C.; Huang, X.; Bagrodia, S.; Chen, J. H.; Greasley, S.; Cheng, H.; Sun, S.; Knighton, D.; Rodgers, C.; Rafidi, K.; et al. Quinazolines with Intra-Molecular Hydrogen Bonding Scaffold (IMHBS) as PI3K/MTOR Dual Inhibitors. *Bioorg. Med. Chem. Lett.* **2011**, *21* (4), 1270–1274. https://doi.org/10.1016/j.bmcl.2010.12.026.

(191) Yang, X.; Zhong, J.; Zhang, Q.; Qian, J.; Song, K.; Ruan, C.; Xu, J.; Ding, K.; Zhang, J. Rational Design and Structure Validation of a Novel Peptide Inhibitor of the Adenomatous-Polyposis-Coli (APC)–Rho-Guanine-Nucleotide-Exchange-Factor-4 (Asef) Interaction. *J. Med. Chem.* **2018**, *61* (17), 8017–8028. https://doi.org/10.1021/acs.jmedchem.8b01112.

(192) Grabowski, S. J. Hydrogen Bonding Strength—Measures Based on Geometric and Topological Parameters. *J. Phys. Org. Chem.* **2004**, *17* (1), 18–31. https://doi.org/10.1002/poc.685.

(193) Caron, G.; Vallaro, M.; Ermondi, G. High Throughput Methods to Measure the Propensity of Compounds to Form Intramolecular Hydrogen Bonding. *Medchemcomm* **2017**, *8* (6), 1143–1151. https://doi.org/10.1039/C7MD00101K.

(194) George, J. *An Introduction to Hydrogen Bonding*, Illustrate.; Oxford University Press, 1997: New York, 1997.

(195) Abraham, M. H.; Abraham, R. J.; Acree, W. E.; Aliev, A. E.; Leo, A. J.; Whaley, W. L.

An NMR Method for the Quantitative Assessment of Intramolecular Hydrogen Bonding; Application to Physicochemical, Environmental, and Biochemical Properties. *J. Org. Chem.* **2014**, *79* (22), 11075–11083. https://doi.org/10.1021/jo502080p.

(196) Whaley, W. L.; Okoso-amaa, E. M.; Womack, C. L.; Vladimirova, A.; Rogers, L. B.; Risher, M. J.; Abraham, M. H. Summation Solute Hydrogen Bonding Acidity Values for Hydroxyl Substituted Flavones Determined by NMR Spectroscopy. *Nat. Prod. Commun.* **2013**, *8* (1), 1934578X1300800. https://doi.org/10.1177/1934578X1300800121.

(197) Karas, L. J.; Batista, P. R.; Viesser, R. V.; Tormena, C. F.; Rittner, R.; de Oliveira, P. R. Trends of Intramolecular Hydrogen Bonding in Substituted Alcohols: A Deeper Investigation. *Phys. Chem. Chem. Phys.* **2017**, *19* (25), 16904–16913. https://doi.org/10.1039/C7CP03572A.

(198) Bilton, C.; Allen, F. H.; Shields, G. P.; Howard, J. A. K. Intramolecular Hydrogen Bonds: Common Motifs, Probabilities of Formation and Implications for Supramolecular Organization. *Acta Crystallogr. Sect. B Struct. Sci.* **2000**, *56* (5), 849–856. https://doi.org/10.1107/S0108768100003694.

(199) Weller, M. T.; Henry, P. F.; Ting, V. P.; Wilson, C. C. Crystallography of Hydrogen-Containing Compounds: Realizing the Potential of Neutron Powder Diffraction. *Chem. Commun.* **2009**, No. 21, 2973. https://doi.org/10.1039/b821336d.

(200) Thomas, L. H.; Florence, A. J.; Wilson, C. C. Hydrogen Atom Behaviour Imaged in a Short Intramolecular Hydrogen Bond Using the Combined Approach of X-Ray and Neutron Diffraction. *New J. Chem.* **2009**, *33* (12), 2486. https://doi.org/10.1039/b908915b.

(201) Mó, O.; Yáñez, M. Substituent Effects on the Strength of the Intramolecular Hydrogen Bond of Thiomalonaldehyde. *J. Org. Chem.* **1999**, *64* (7), 2314–2321. https://doi.org/10.1021/jo981982h.

(202) Burckhalter, J. H.; Tendick, F. H.; Jones, E. M.; Holcomb, W. F.; Rawlins, A. L. Aminoalkylphenols as Antimalarials. I. Simply Substituted α-Aminocresols 1. *J. Am. Chem. Soc.* **1946**, *68* (10), 1894–1901. https://doi.org/10.1021/ja01214a008.

(203) O'Neill, P. M.; Mukhtar, A.; Stocks, P. A.; Randle, L. E.; Hindley, S.; Ward, S. A.;

Storr, R. C.; Bickley, J. F.; O'Neil, I. A.; Maggs, J. L.; et al. Isoquine and Related Amodiaquine Analogues: A New Generation of Improved 4-Aminoquinoline Antimalarials. *J. Med. Chem.* **2003**, *46* (23), 4933–4945. https://doi.org/10.1021/jm030796n.

(204) Rieckmann, K. H.; Trenholme, G. M.; Williams, R. L.; Carson, P. E.; Frischer, H.; Desjardins, R. E. Prophylactic Activity of Mefloquine Hydrochloride (WR 142490) in Drug-Resistant Malaria. *Bull. World Health Organ.* **1974**, *51* (4), 375–377.

(205) Madrid, P. B.; Liou, A. P.; DeRisi, J. L.; Guy, R. K. Incorporation of an Intramolecular Hydrogen-Bonding Motif in the Side Chain of 4-Aminoquinolines Enhances Activity against Drug-Resistant P. f Alciparum. *J. Med. Chem.* **2006**, *49* (15), 4535–4543. https://doi.org/10.1021/jm0600951.

(206) Birrell, G. W.; Chavchich, M.; Ager, A. L.; Shieh, H.-M.; Heffernan, G. D.; Zhao, W.; Krasucki, P. E.; Saionz, K. W.; Terpinski, J.; Schiehser, G. A.; et al. JPC-2997, a New Aminomethylphenol with High In Vitro and In Vivo Antimalarial Activities against Blood Stages of Plasmodium. *Antimicrob. Agents Chemother.* **2015**, *59* (1), 170–177. https://doi.org/10.1128/AAC.03762-14.

(207) McCallum, F.; Harris, I.; van Breda, K.; De, S. L.; Stanisic, D. I.; Good, M. F.; Jacobus, D. P.; Edstein, M. D. Evaluation of the 2-Aminomethylphenol JPC-2997 in Aotus Monkeys Infected with Plasmodium Falciparum: TABLE 1. *Antimicrob. Agents Chemother.* **2016**, *60* (3), 1948–1949. https://doi.org/10.1128/AAC.02799-15.

(208) McCallum, F. J.; Birrell, G. W.; Chavchich, M.; Harris, I.; Obaldia, N.; Van Breda, K.; Heffernan, G. D.; Jacobus, D. P.; Shanks, D.; Edstein, M. D. In Vivo Efficacy and Pharmacokinetics of the 2-Aminomethylphenol Antimalarial JPC-3210 in the Aotus Monkey-Human Malaria Model. *Antimicrob. Agents Chemother.* **2019**, *64* (3). https://doi.org/10.1128/AAC.01538-19.

(209) Preethi, P. J.; Karthikeyan, E.; Lohita, M.; Teja, P. G.; Subhash, M.; Shaheena, P.; Prashanth, Y.; Sai, N. K. Benzimidazole: An Important Scaffold in Drug Discovery. *Asian J. Pharm. Technol.* **2015**, *5* (3), 138. https://doi.org/10.5958/2231-5713.2015.00021.5.

(210) Ansari, K. F.; Lal, C. Synthesis, Physicochemical Properties and Antimicrobial Activity of Some New Benzimidazole Derivatives. *Eur. J. Med. Chem.* **2009**, *44* (10), 4028–

4033. https://doi.org/10.1016/j.ejmech.2009.04.037.

(211) Kalyankar T.M ; Pekamwar SS, W. S. T. P. and S. G. Review on Benzimidazole Derivative. *Int. J. Chem. Pharm. Sci.* **2012**, *3* (4), 1–10.

(212) Enumula S, Pangal A, Gazge M, Shaikh J. A, A. K. Diverse Pharmacological Aspects of Benzimidazole Derivatives: A Review. *Res. J. Chem. Sci.* **2014**, *4* (4), 78–88.

(213) Ramachandran, S.; Hameed P, S.; Srivastava, A.; Shanbhag, G.; Morayya, S.; Rautela, N.; Awasthy, D.; Kavanagh, S.; Bharath, S.; Reddy, J.; et al. N-Aryl-2-Aminobenzimidazoles: Novel, Efficacious, Antimalarial Lead Compounds. *J. Med. Chem.* **2014**, *57* (15), 6642–6652. https://doi.org/10.1021/jm500715u.

(214) Chong, C. R.; Chen, X.; Shi, L.; Liu, J. O.; Sullivan, D. J. A Clinical Drug Library Screen Identifies Astemizole as an Antimalarial Agent. *Nat. Chem. Biol.* **2006**, *2* (8), 415–416. https://doi.org/10.1038/nchembio806.

(215) Roman, G.; Crandall, I. E.; Szarek, W. A. Synthesis and Anti- Plasmodium Activity of Benzimidazole Analogues Structurally Related to Astemizole. *ChemMedChem* **2013**, *8* (11), 1795–1804. https://doi.org/10.1002/cmdc.201300172.

(216) Keurulainen, L.; Vahermo, M.; Puente-Felipe, M.; Sandoval-Izquierdo, E.; Crespo-Fernández, B.; Guijarro-López, L.; Huertas-Valentín, L.; de las Heras-Dueña, L.; Leino, T. O.; Siiskonen, A.; et al. A Developability-Focused Optimization Approach Allows Identification of in Vivo Fast-Acting Antimalarials: N -[3-[(Benzimidazol-2-Yl)Amino]Propyl]Amides. *J. Med. Chem.* **2015**, *58* (11), 4573–4580. https://doi.org/10.1021/acs.jmedchem.5b00114.

(217) Dymińska, L. Imidazopyridines as a Source of Biological Activity and Their Pharmacological Potentials—Infrared and Raman Spectroscopic Evidence of Their Content in Pharmaceuticals and Plant Materials. *Bioorg. Med. Chem.* **2015**, *23* (18), 6087–6099. https://doi.org/10.1016/j.bmc.2015.07.045.

(218) Vanda, D.; Zajdel, P.; Soural, M. Imidazopyridine-Based Selective and Multifunctional Ligands of Biological Targets Associated with Psychiatric and Neurodegenerative Diseases. *Eur. J. Med. Chem.* **2019**, *181*, 111569. https://doi.org/10.1016/j.ejmech.2019.111569.

(219) Langheinrich, A. C.; Sedding, D. G.; Kampschulte, M.; Moritz, R.; Wilhelm, J.;

Haberbosch, W. G.; Ritman, E. L.; Bohle, R. M. 3-Deazaadenosine Inhibits Vasa Vasorum Neovascularization in Aortas of ApoE−/−/LDL−/− Double Knockout Mice. *Atherosclerosis* **2009**, *202* (1), 103–110. https://doi.org/10.1016/j.atherosclerosis.2008.04.008.

(220) Fujita, M.; Nakao, Y.; Matsunaga, S.; Seiki, M.; Itoh, Y.; Yamashita, J.; van Soest, R. W. M.; Fusetani, N. Ageladine A: An Antiangiogenic Matrixmetalloproteinase Inhibitor from the Marine Sponge Agelas n Akamurai 1. *J. Am. Chem. Soc.* **2003**, *125* (51), 15700–15701. https://doi.org/10.1021/ja038025w.

(221) Hayden, A.; Johnson, P. W. M.; Packham, G.; Crabb, S. J. S-Adenosylhomocysteine Hydrolase Inhibition by 3-Deazaneplanocin A Analogues Induces Anti-Cancer Effects in Breast Cancer Cell Lines and Synergy with Both Histone Deacetylase and HER2 Inhibition. *Breast Cancer Res. Treat.* **2011**, *127* (1), 109–119. https://doi.org/10.1007/s10549-010-0982-0.

(222) Burgeson, J. R.; Moore, A. L.; Gharaibeh, D. N.; Larson, R. A.; Cerruti, N. R.; Amberg, S. M.; Hruby, D. E.; Dai, D. Discovery and Optimization of Potent Broad-Spectrum Arenavirus Inhibitors Derived from Benzimidazole and Related Heterocycles. *Bioorg. Med. Chem. Lett.* **2013**, *23* (3), 750–756. https://doi.org/10.1016/j.bmcl.2012.11.093.

(223) Tatipaka, H. B.; Gillespie, J. R.; Chatterjee, A. K.; Norcross, N. R.; Hulverson, M. A.; Ranade, R. M.; Nagendar, P.; Creason, S. A.; McQueen, J.; Duster, N. A.; et al. Substituted 2-Phenylimidazopyridines: A New Class of Drug Leads for Human African Trypanosomiasis. *J. Med. Chem.* **2014**, *57* (3), 828–835. https://doi.org/10.1021/jm401178t.

(224) Wanner, M. J.; Deghati, P. Y. F.; Rodenko, B.; Koomen, G. J. New Nucleoside Analogs, Synthesis, and Biological Properties. *Pure Appl. Chem.* **2000**, *72* (9), 1705–1708. https://doi.org/10.1351/pac200072091705.

(225) Arbuckle, W.; Baugh, M.; Belshaw, S.; Bennett, D. J.; Bruin, J.; Cai, J.; Cameron, K. S.; Claxton, C.; Dempster, M.; Everett, K.; et al. 1H-Imidazo[4,5-c]Pyridine-4-Carbonitrile as Cathepsin S Inhibitors: Separation of Desired Cellular Activity from Undesired Tissue Accumulation through Optimization of Basic Nitrogen Pka. *Bioorg. Med. Chem. Lett.* **2011**, *21* (3), 932–935. https://doi.org/10.1016/j.bmcl.2010.12.065.

(226) Large, J. M.; Birchall, K.; Bouloc, N. S.; Merritt, A. T.; Smiljanic-Hurley, E.; Tsagris,

D. J.; Wheldon, M. C.; Ansell, K. H.; Coombs, P. J.; Kettleborough, C. A.; et al. Potent Inhibitors of Malarial P. Falciparum Protein Kinase G: Improving the Cell Activity of a Series of Imidazopyridines. *Bioorg. Med. Chem. Lett.* **2019**, *29* (3), 509–514. https://doi.org/10.1016/j.bmcl.2018.11.039.

(227) Nchinda, A. T.; Le Manach, C.; Paquet, T.; Gonzàlez Cabrera, D.; Wicht, K. J.; Brunschwig, C.; Njoroge, M.; Abay, E.; Taylor, D.; Lawrence, N.; et al. Identification of Fast-Acting 2,6-Disubstituted Imidazopyridines That Are Efficacious in the in Vivo Humanized Plasmodium Falciparum NODscidIL2Rγ Null Mouse Model of Malaria. *J. Med. Chem.* **2018**, *61* (9), 4213–4227. https://doi.org/10.1021/acs.jmedchem.8b00382.

(228) Le Manach, C.; Paquet, T.; Wicht, K.; Nchinda, A. T.; Brunschwig, C.; Njoroge, M.; Gibhard, L.; Taylor, D.; Lawrence, N.; Wittlin, S.; et al. Antimalarial Lead-Optimization Studies on a 2,6-Imidazopyridine Series within a Constrained Chemical Space To Circumvent Atypical Dose–Response Curves against Multidrug Resistant Parasite Strains. *J. Med. Chem.* **2018**, *61* (20), 9371–9385. https://doi.org/10.1021/acs.jmedchem.8b01333.

(229) Le Manach, C.; Scheurer, C.; Sax, S.; Schleiferböck, S.; Cabrera, D.; Younis, Y.; Paquet, T.; Street, L.; Smith, P.; Ding, X. C.; et al. Fast in Vitro Methods to Determine the Speed of Action and the Stage-Specificity of Anti-Malarials in Plasmodium Falciparum. *Malar. J.* **2013**, *12* (1), 424. https://doi.org/10.1186/1475-2875-12-424.

(230) Jiménez-Díaz, M. B.; Mulet, T.; Viera, S.; Gómez, V.; Garuti, H.; Ibáñez, J.; Alvarez-Doval, A.; Shultz, L. D.; Martínez, A.; Gargallo-Viola, D.; et al. Improved Murine Model of Malaria Using Plasmodium Falciparum Competent Strains and Non-Myelodepleted NOD-Scid IL2Rγnull Mice Engrafted with Human Erythrocytes. *Antimicrob. Agents Chemother.* **2009**, *53* (10), 4533–4536. https://doi.org/10.1128/AAC.00519-09.

(231) Ajayi, N. A.; Ukwaja, K. N. Possible Artemisinin-Based Combination Therapy-Resistant Malaria in Nigeria: A Report of Three Cases. *Rev. Soc. Bras. Med. Trop. 46* (4), 525–527. https://doi.org/10.1590/0037-8682-0098-2013.

(232) Folarin, O. A.; Bustamante, C.; Gbotosho, G. O.; Sowunmi, A.; Zalis, M. G.; Oduola, A. M. J.; Happi, C. T. In Vitro Amodiaquine Resistance and Its Association with Mutations in Pfcrt and Pfmdr1 Genes of Plasmodium Falciparum Isolates from Nigeria.

Acta Trop. **2011**, *120* (3), 224–230. https://doi.org/10.1016/j.actatropica.2011.08.013.

CHAPTER 2

DESIGN, SYNTHESIS AND CHARACTERIZATION OF TARGET COMPOUNDS

2.1 Chapter Overview

Chapter 2 presents the medicinal chemistry plans leading to the synthesis of the target compounds. The chapter is divided into two broad sections; one that covers benzimidazoles and the other highlighting imidazopyridines. Brief descriptions of the chemistry employed, some relevant reaction mechanisms and characterization of both intermediates and target compounds are presented.

2.2 Design, Synthesis and Characterization of benzimidazole analogues

2.2.1 Design and Synthesis

As previously mentioned in chapter 1, the benzimidazole scaffold has been recognized as a potential antimalarial chemotype.[1–4] In the current study, benzimidazole-based analogues with an intramolecular hydrogen bonding motif were explored. Three sites for alteration, as depicted in Figure 2.1, were scouted to introduce structural diversity around the benzimidazole core by implementing modifications at the highlighted positions.

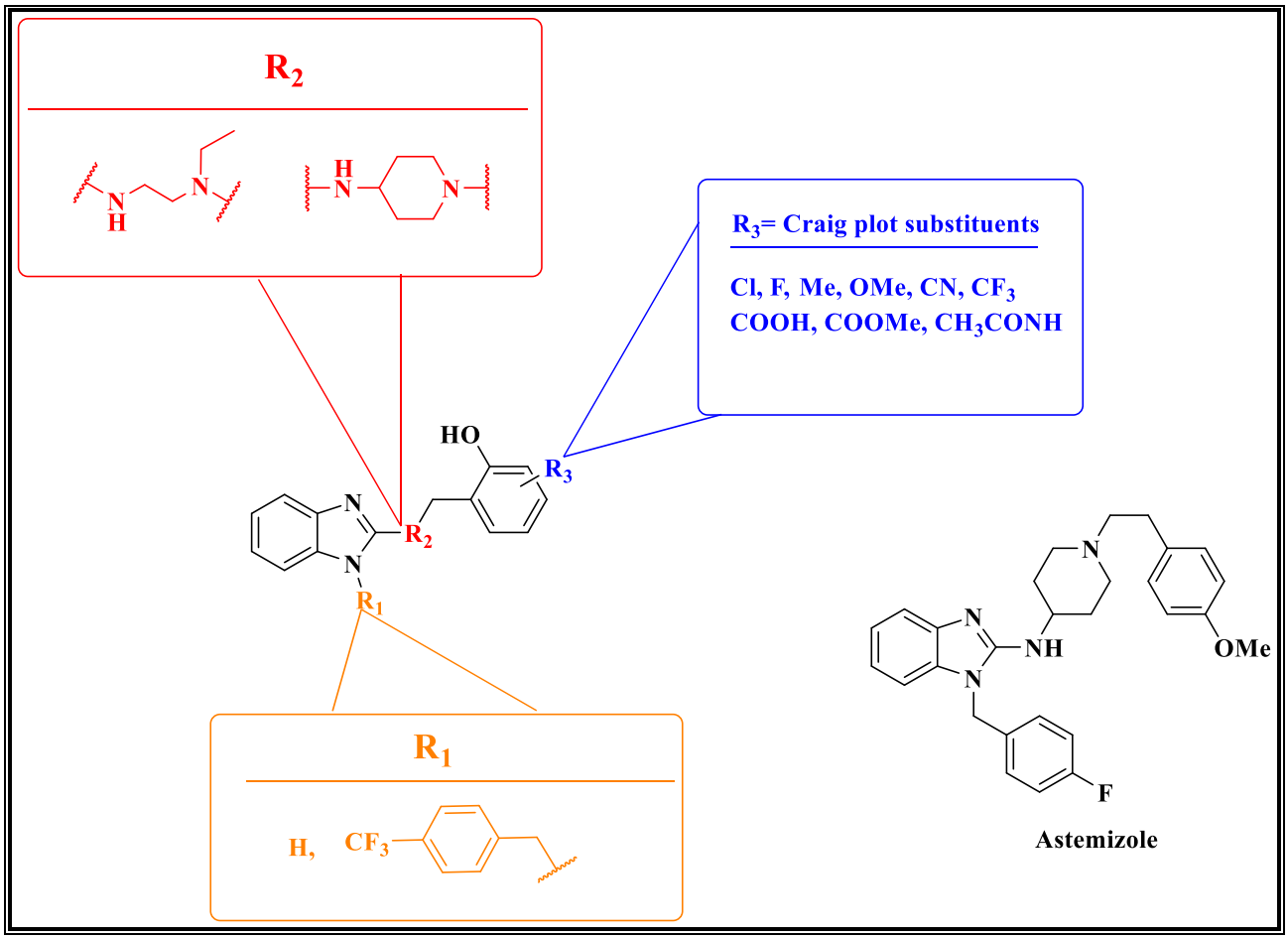

Figure 2.1: Medicinal chemistry plan for benzimidazole analogues.

The SAR was to explore the benzimidazole scaffold without any substitution on the core, thus, keeping **R_1** as hydrogen and assessing the effect of a benzyl moiety as exemplified in the antihistamine drug astemizole. The choice of **R_2** was based on the hypothesis that having a flexible linker between the benzimidazole core and the phenyl moiety can result in compounds with good solubility. The **R_3** substituents on the phenyl ring were based on creating diversity in electronic properties and hydrophobicity of the target compounds. Thus, the Craig plot (Figure 2.2) was used as a guide in the selection of various aromatic substituents such that all the four quadrants were well represented.[5,6]

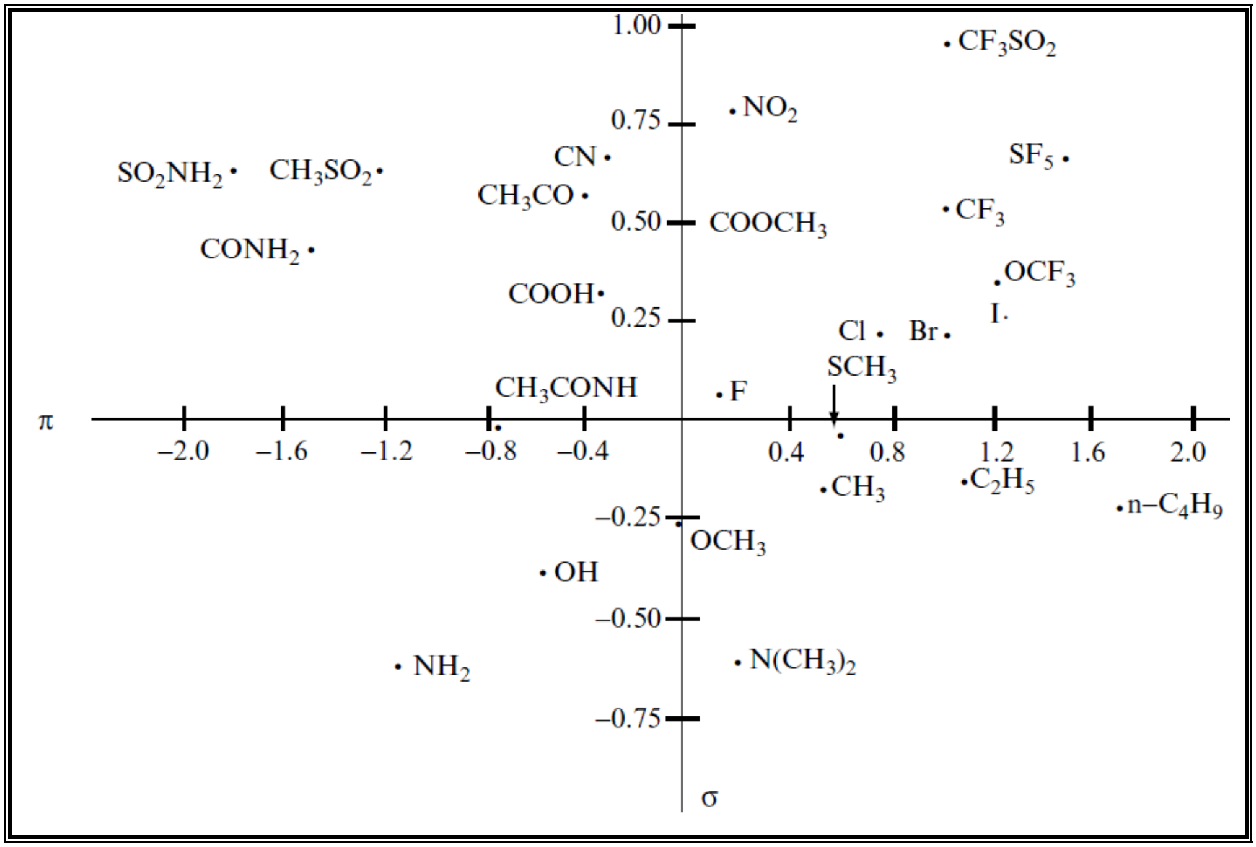

Figure 2.2: Craig plot of electronic effects (σ) against hydrophobicity (π) values.[6]

Benzimidazole analogues studied in this thesis work were synthesized as outlined in Scheme 2.1. Target compounds **1.1 - 1.12** were synthesized through an initial addition-elimination nucleophilic aromatic substitution reaction of commercially available 2-chlorobenzimidazole and *N*^{1}-ethylethane-1,2-diamine in the presence of triethylamine (Et_3N) to give the desired intermediate **1a** in a moderate yield. Reductive amination of appropriate aldehydes using intermediate **1a** was achieved in the presence of sodium borohydride ($NaBH_4$) to afford the respective target compounds in moderate to excellent yields.

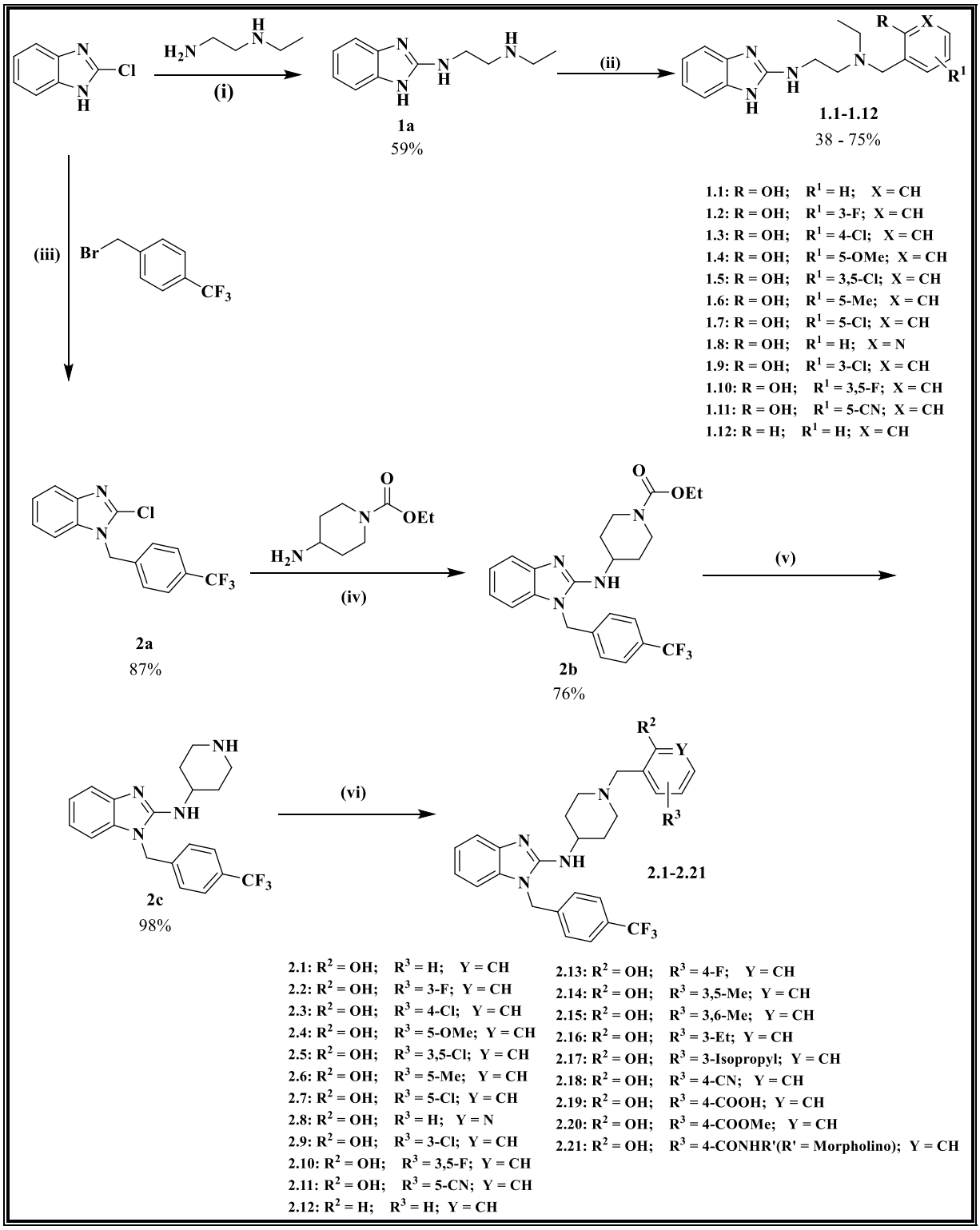

Scheme 2.1: Synthetic protocol towards benzimidazole target compounds.[4,7–9] ***Reagents and conditions***: (**i**) Et_3N, reflux, 140 °C, 16 h; (**ii**) Aldehyde, MeOH, $NaBH_4$, 25 °C, 16 h; (**iii**) K_2CO_3, CH_3CN, reflux, 85 °C, 2 h; (**iv**) reflux, 170 °C, 48 h; (**v**) 48% Aqueous HBr, reflux, 2 h (**vi**) Aldehyde, MeOH, $NaBH_4$, 25 °C, 16 –48 h (for compounds **2.1 – 2.12**) or (**vi**) HCHO, Phenol, EtOH, 85 °C, 2 h (for compounds **2.13 – 2.21**).

Similarly, the target compounds **2.1 – 2.21** were obtained through an initial nucleophilic substitution reaction between 2-chlorobenzimidazole and 4-(trifluoromethyl)benzyl bromide to afford intermediate **2a** followed by an addition-elimination reaction with ethyl-4-amino-1-piperidine carboxylate to give intermediate **2b** (Scheme 2.1). Intermediate **2b** was subjected to deprotection of the ethyl carboxylate group, which resulted in a cyclic secondary amine as intermediate **2c**. Reductive amination of various aldehydes using this intermediate was also achieved in the presence of $NaBH_4$ to afford target compounds (**2.1 -2.12**) in moderate to excellent yields. Compounds **2.13 – 2.21** were obtained in relatively high yields by subjecting intermediate **2c** to a Mannich reaction in the presence of formaldehyde and the appropriate phenol in ethanol.

2.2.2 Proposed Reaction Mechanisms and Characterization

Some relevant mechanisms associated with the reactions carried out are proposed and backed by literature. All compounds were characterized using proton nuclear magnetic resonance (^{1}H NMR) and high-pressure liquid chromatography-mass spectrometry (HPLC-MS), while final target compounds were also characterized using carbon-13 NMR (^{13}C NMR). The ^{1}H NMR and ^{13}C NMR spectra, HPLC chromatograms and mass spectra are presented for representative compounds.

2.2.2.1 Nucleophilic Substitution: Step (i), Scheme 2.1

As depicted in scheme 2.2, the less nucleophilic but sterically unhindered amino nitrogen of N^1-ethylethane-1,2-diamine attacks the electron-deficient carbon of the 2-chlorobenzimidazole to form intermediate **I**. This is followed by the elimination of hydrogen chloride (HCl), which is mopped up by triethylamine to yield the secondary amine intermediate **1a**.

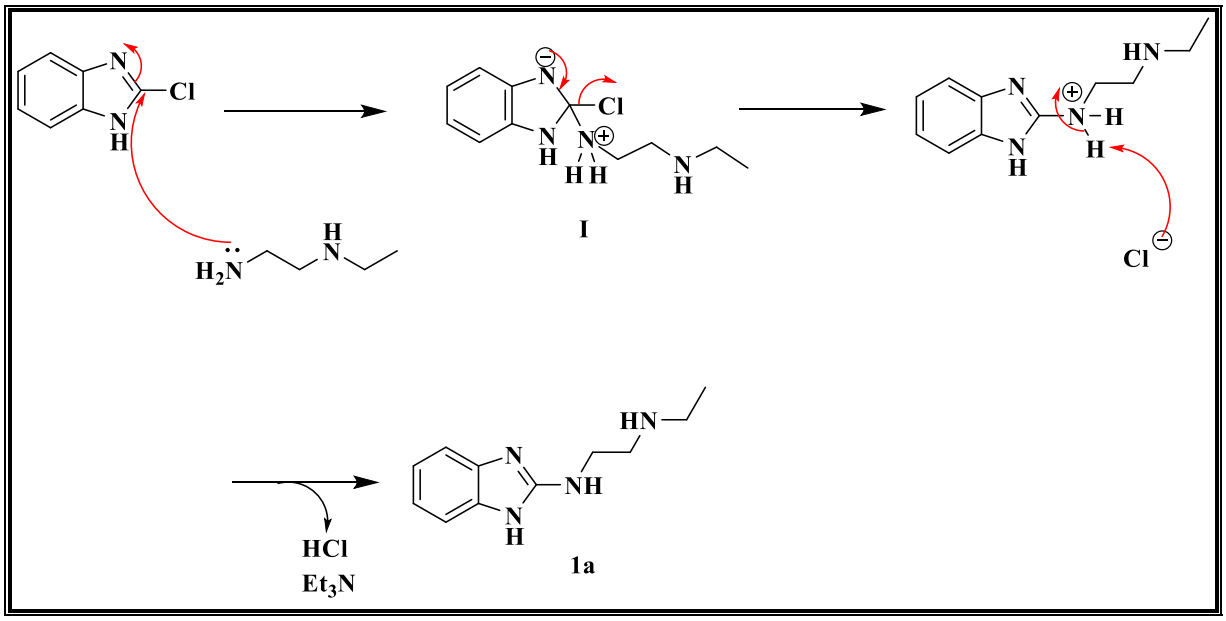

Scheme 2.2: Proposed mechanism for the formation of intermediate **1a**.

The successful synthesis of intermediate **1a** was confirmed by ^{1}H NMR (Figure 2.3) with the appearance of the aliphatic protons with chemical shifts between δ 3.49 and 1.14 ppm. HPLC-MS (ESI/APCI : m/z $[M+H]^{+}$ = 205.1, t_R = 0.218 min) also confirmed the formation of this intermediate.

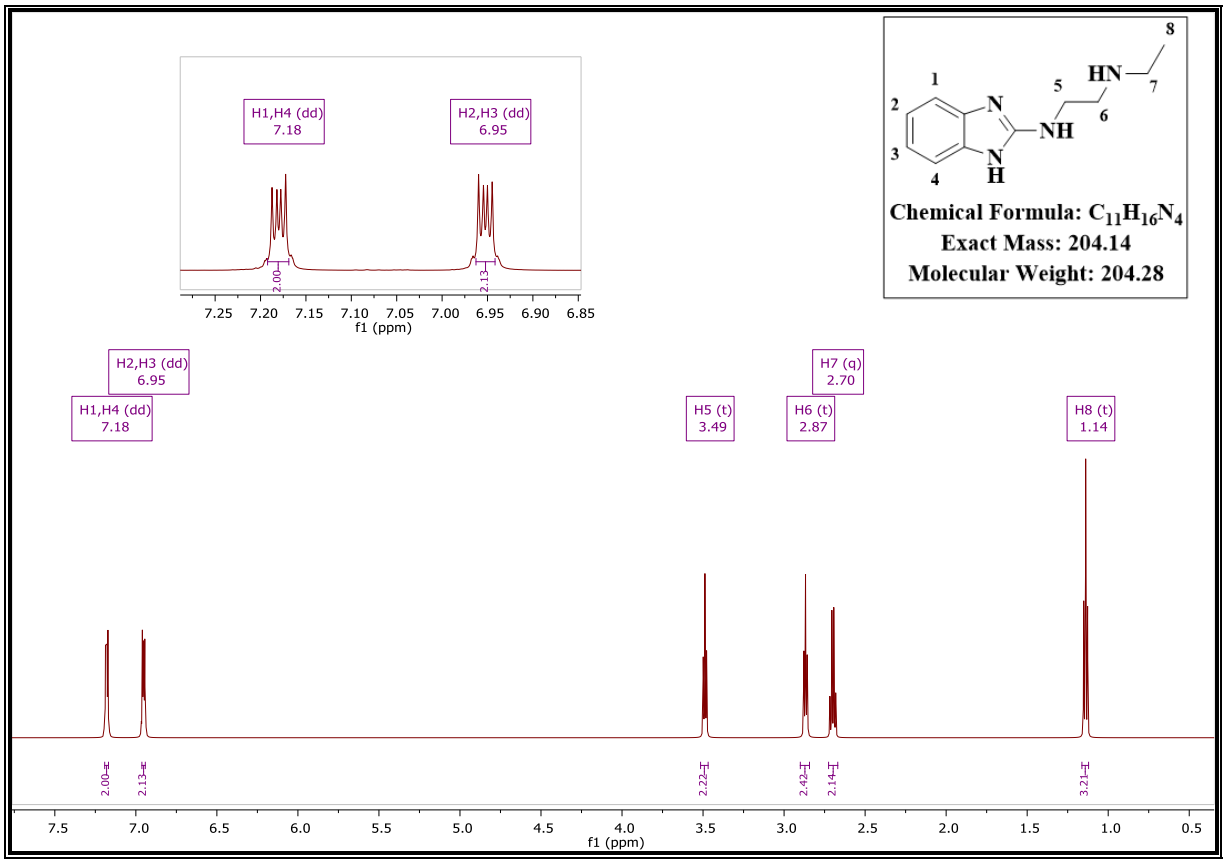

Figure 2.3: ^{1}H NMR spectrum of **1a** at 600 MHz in MeOD.

2.2.2.2 Reductive Amination: Step (ii), Scheme 2.1

The formation of target compounds **1.1 – 1.12** involves a nucleophilic addition reaction of intermediate **1a** to the carbonyl carbon of the aldehyde to yield an intermediate carbinolamine (scheme 2.3).[10,11] This carbinolamine loses water to form an N-protonated iminium ion, which is subsequently reduced by sodium borohydride to form the desired tertiary amine product.

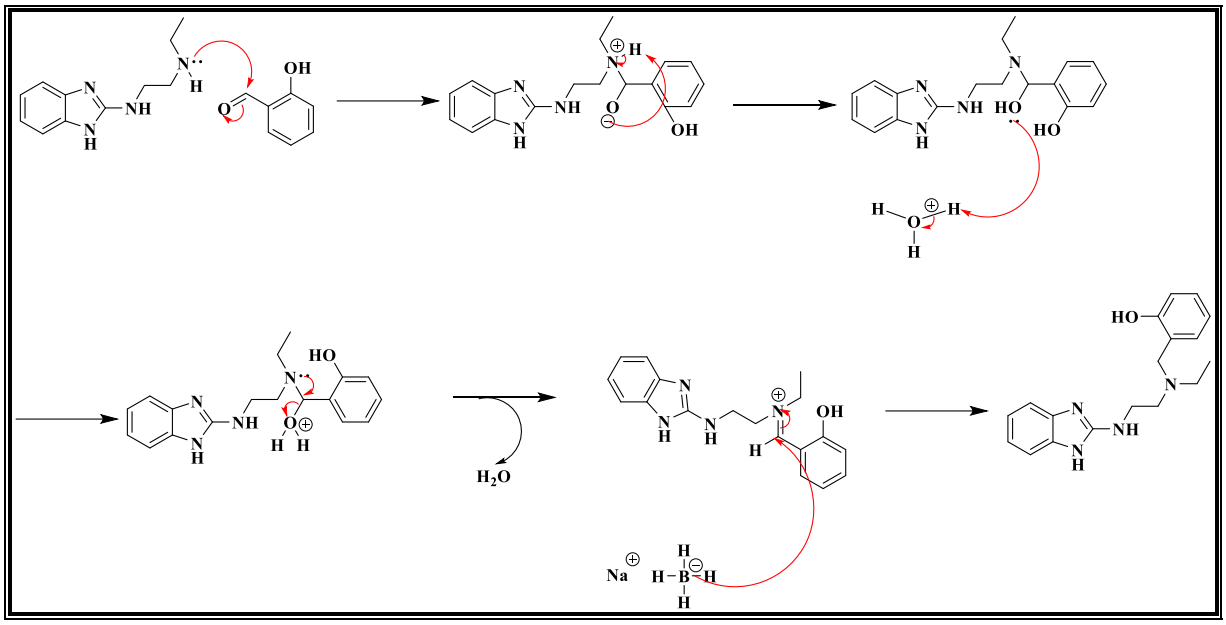

Scheme 2.3: Proposed mechanism of reductive amination.

The ^{1}H NMR spectrum (Figure 2.4) of the representative analogue **1.1** showed additional protons diagnostic of the benzyl protons (H9) exhibiting a methylene singlet, resonating downfield at δ 3.79 ppm. Also, a well-resolved multiplicity pattern was observed upfield, showing the presence of additional aromatic protons.

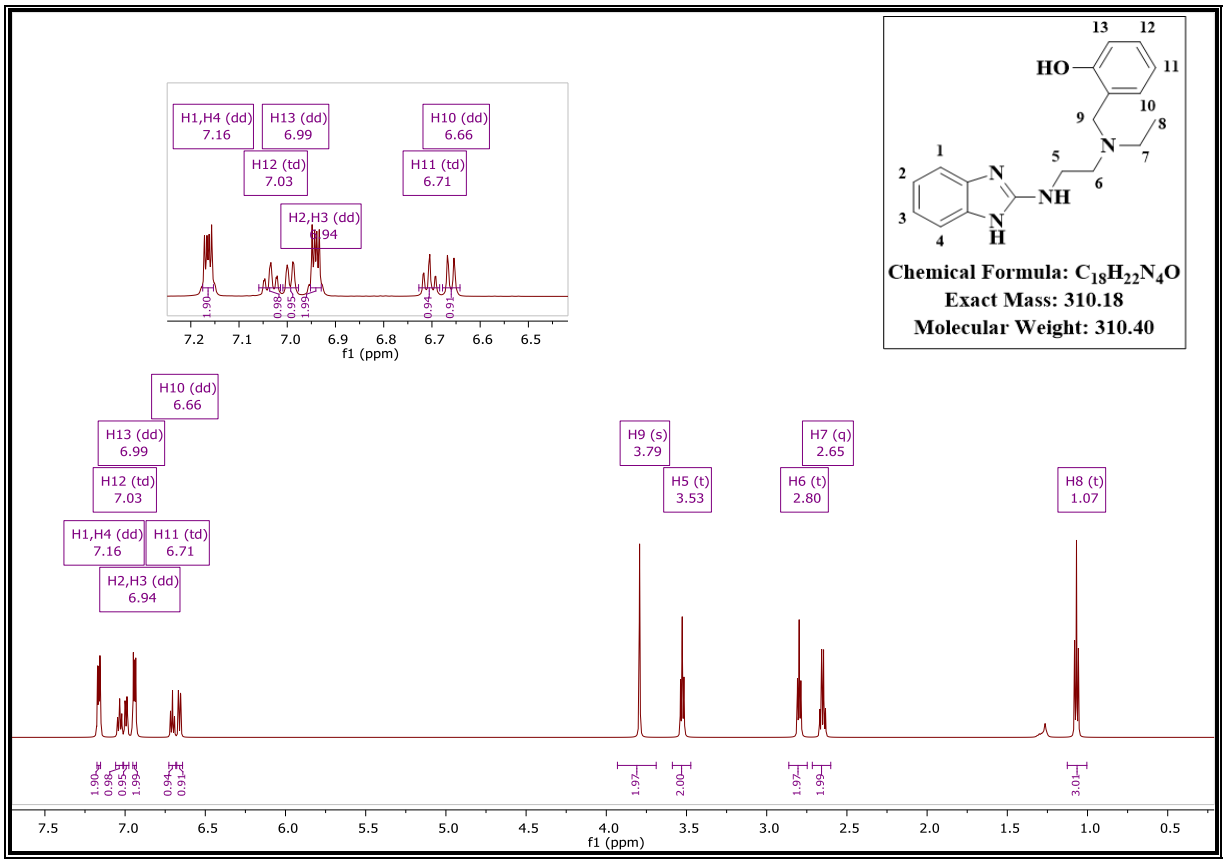

Figure 2.4: ^{1}H NMR spectrum of **1.1** at 600 MHz in MeOD.

The ^{13}C NMR spectrum (Figure 2.5) for the representative compound **1.1** showed diagnostic peaks which comprised the additional aromatic carbon peaks between δ 130-116 ppm, the aromatic carbon bearing the hydroxyl group (C-OH) at δ 158.60 ppm and the methylene carbon (C-9) peak at δ 53.49 ppm.

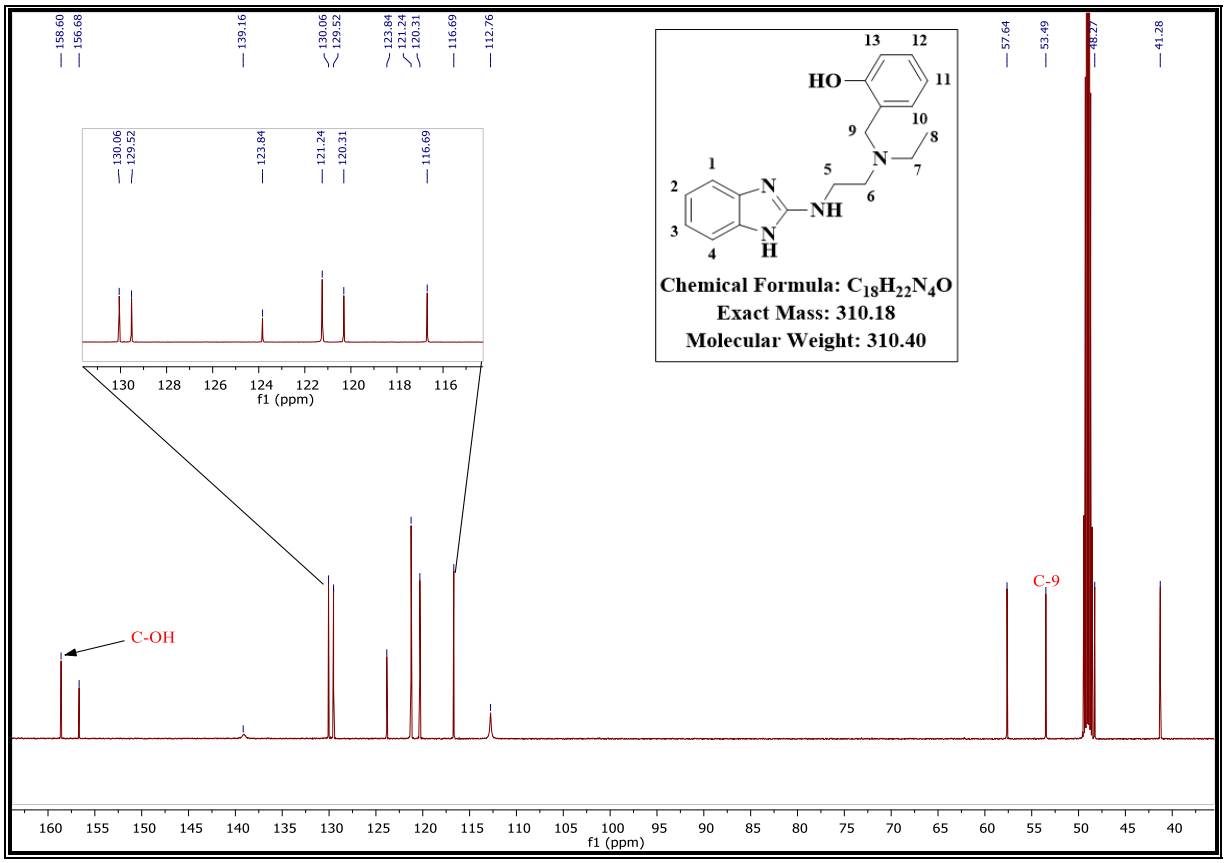

Figure 2.5: ^{13}C NMR spectrum of **1.1** at 151 MHz in MeOD.

HPLC-MS analysis further confirmed the successful synthesis of analogue **1.1** with a pseudo-molecular ion $[M+H]^+$ observed at *m/z* = 310.9 at a retention time, t_R = 2.078 min (Figure 2.6).

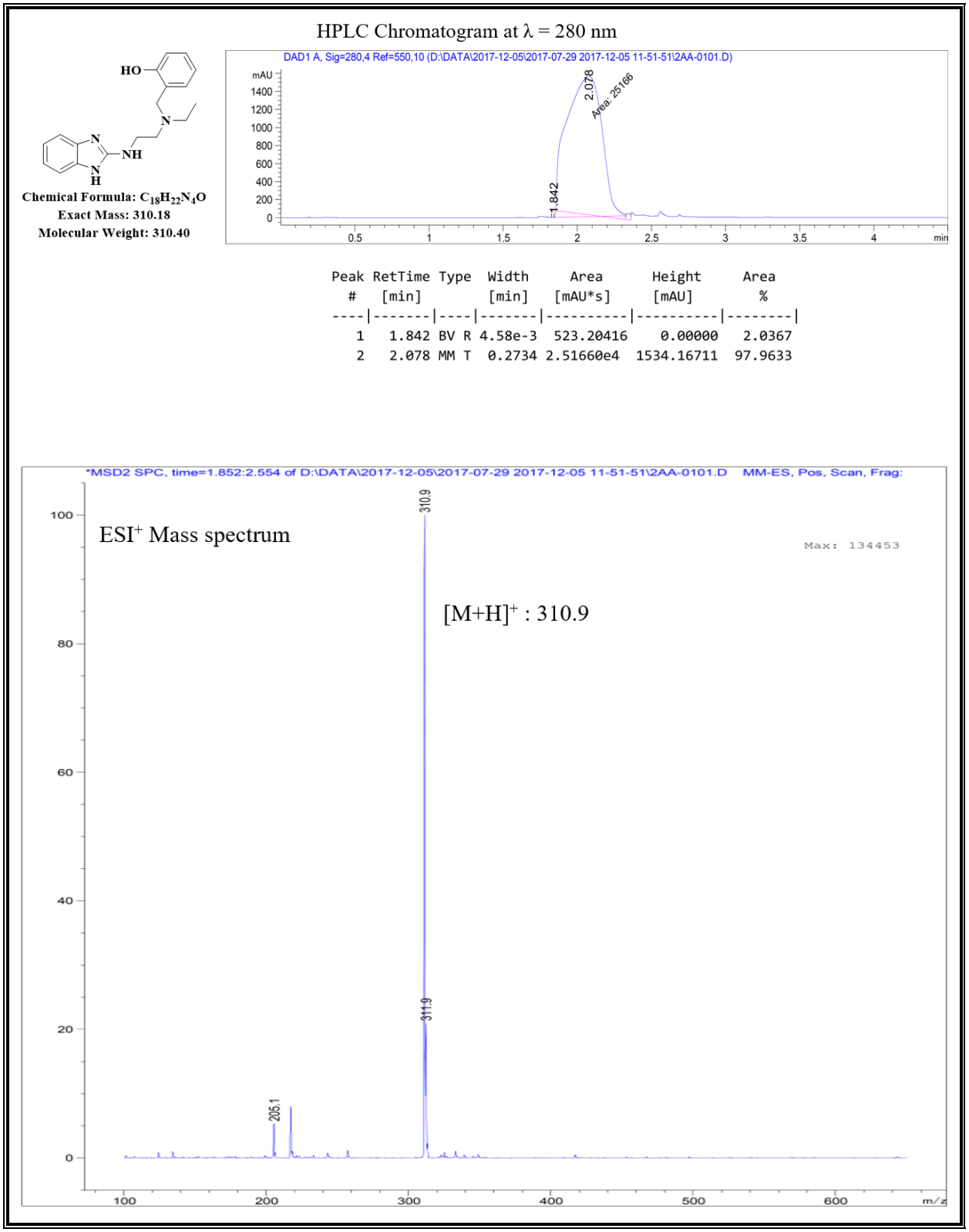

Figure 2.6: HPLC chromatogram and ESI$^+$ mass spectrum of **1.1**.

2.2.2.3 Benzylation Reaction: Step (iii), Scheme 2.1

Intermediate **2a** was obtained through a benzylation reaction between 2-chlorobenzimidazole and 4-trifluoromethylbenzyl bromide. HPLC-MS and ^{1}H NMR (Figure 2.7) analyses provided evidence of successful product formation. The benzyl protons resonated as two doublets, each integrating for two protons at δ 7.73 (H7 and H8) and 7.40 ppm (H6 and H9), respectively. The signals exhibited equal coupling constants (J = 8.1 Hz), as expected. The methylene protons H5 also resonated at δ 5.67 ppm as a singlet. In addition, a characteristic $[M+H]^{+}$ value (m/z = 310.8) was observed for this benzylated intermediate on the HPLC-MS.

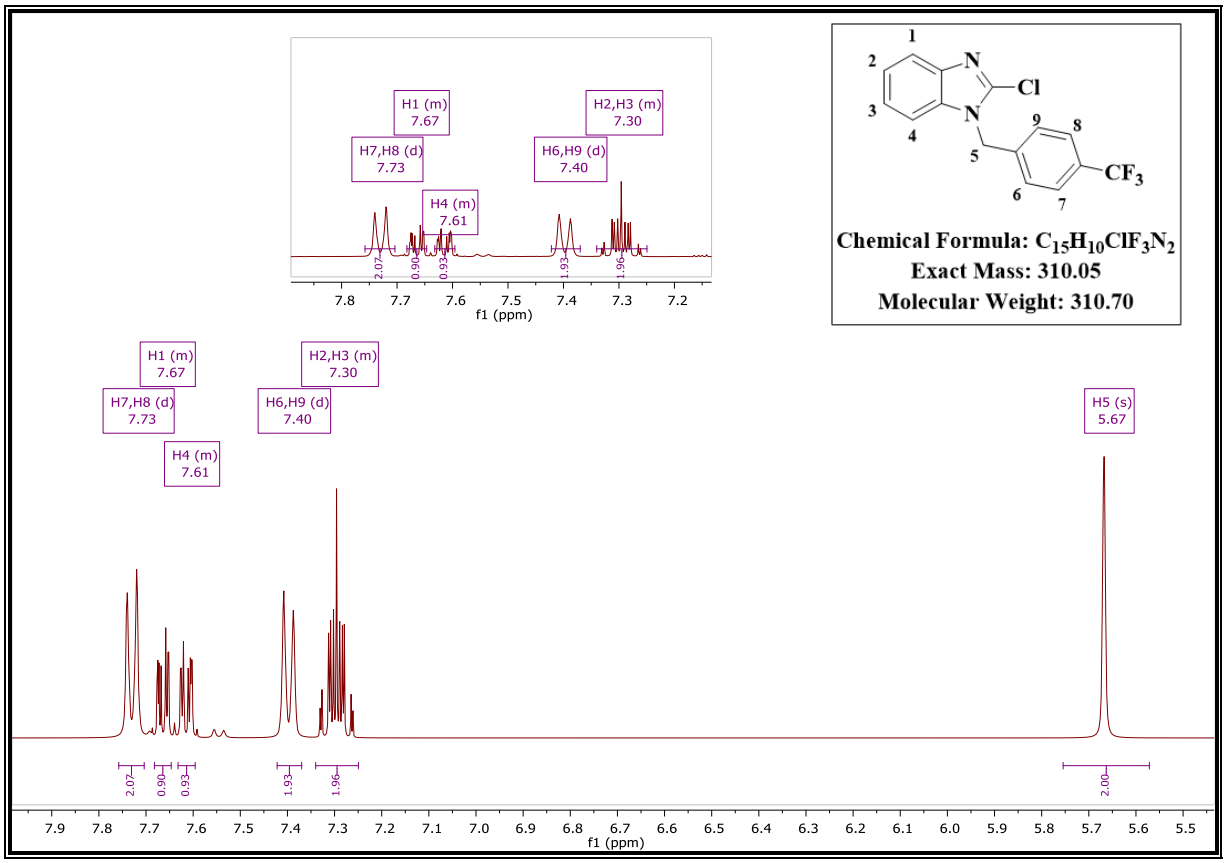

Figure 2.7: ^{1}H NMR spectrum of **2a** at 400 MHz in DMSO.

2.2.2.4 Nucleophilic Substitution: Step (iv), Scheme 2.1

The benzylated intermediate **2a** was subjected to nucleophilic substitution with ethyl 4-amino-1-piperidine carboxylate to afford the aminated intermediate **2b**. The mechanism for this reaction is the same as described in section 2.2.2.1. The ^{1}H NMR (Figure 2.8) exhibited aliphatic signals corresponding to protons of the piperidine ring, and since piperidine mostly assumes the chair conformation, the axial (a) and equatorial (e) protons resonated at different

chemical shifts. Notably, the piperidinyl protons resonated as multiplets due to a multiplicity of coupling, including geminal (J^2) and vicinal (J^3) coupling.[12] The methine proton H10 was observed resonating at δ 4.00 ppm. The triplet signal integrating for three protons (H16) at δ 1.27 ppm also indicates the presence of the ethyl carboxylate.

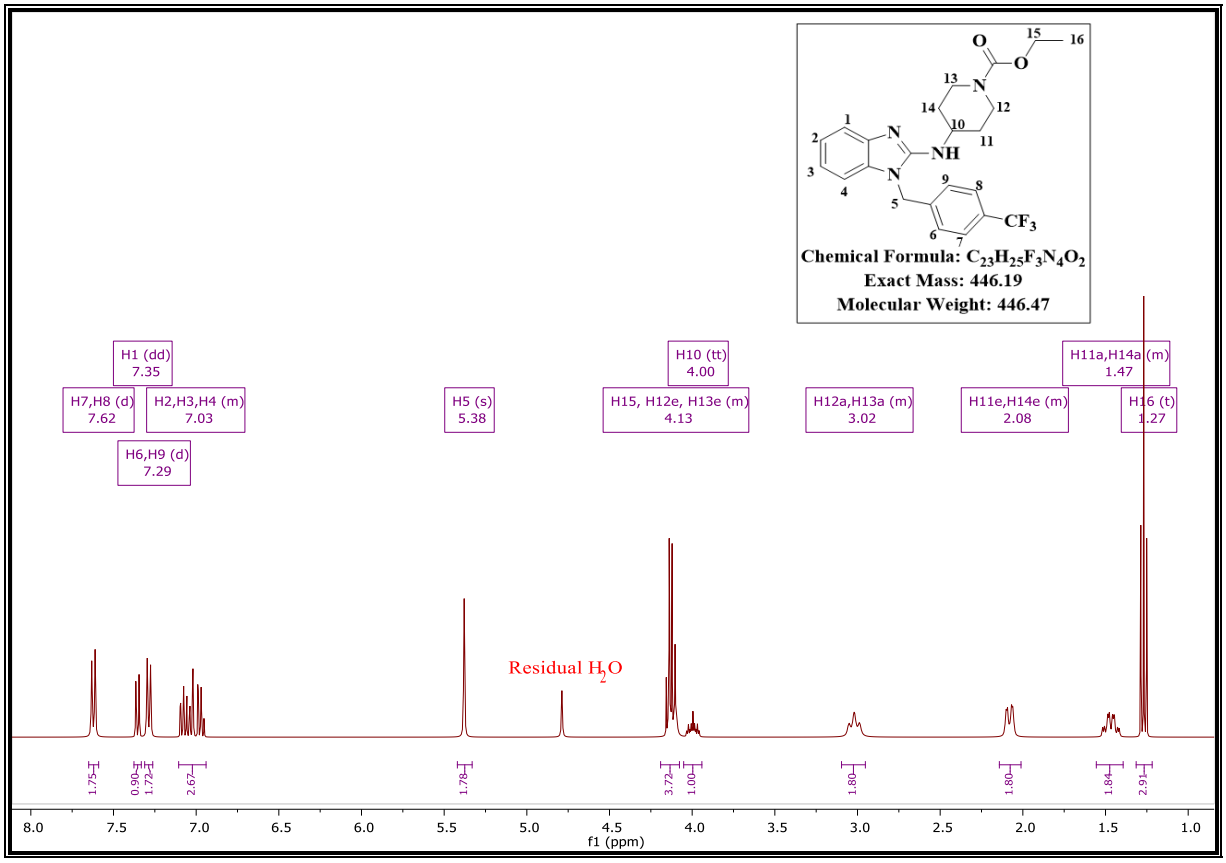

Figure 2.8: [1]H NMR spectrum of **2b** at 400 MHz in MeOD.

2.2.2.5 Acid-catalyzed Decarboxylation: Step (v), Scheme 2.1

Acid-catalyzed hydrolysis of intermediate **2b** furnished the free amine intermediate **2c**. Evidence of successful decarboxylation was deduced from [1]H NMR, which was in congruence with the disappearance of the ethyl carboxylate protons (Figure 2.9). Resolved multiplicity patterns were observed for both aromatic and aliphatic protons. HPLC-MS showed a quasi-molecular ion $[M+H]^+$ value (m/z = 374.9) for this secondary amine intermediate.

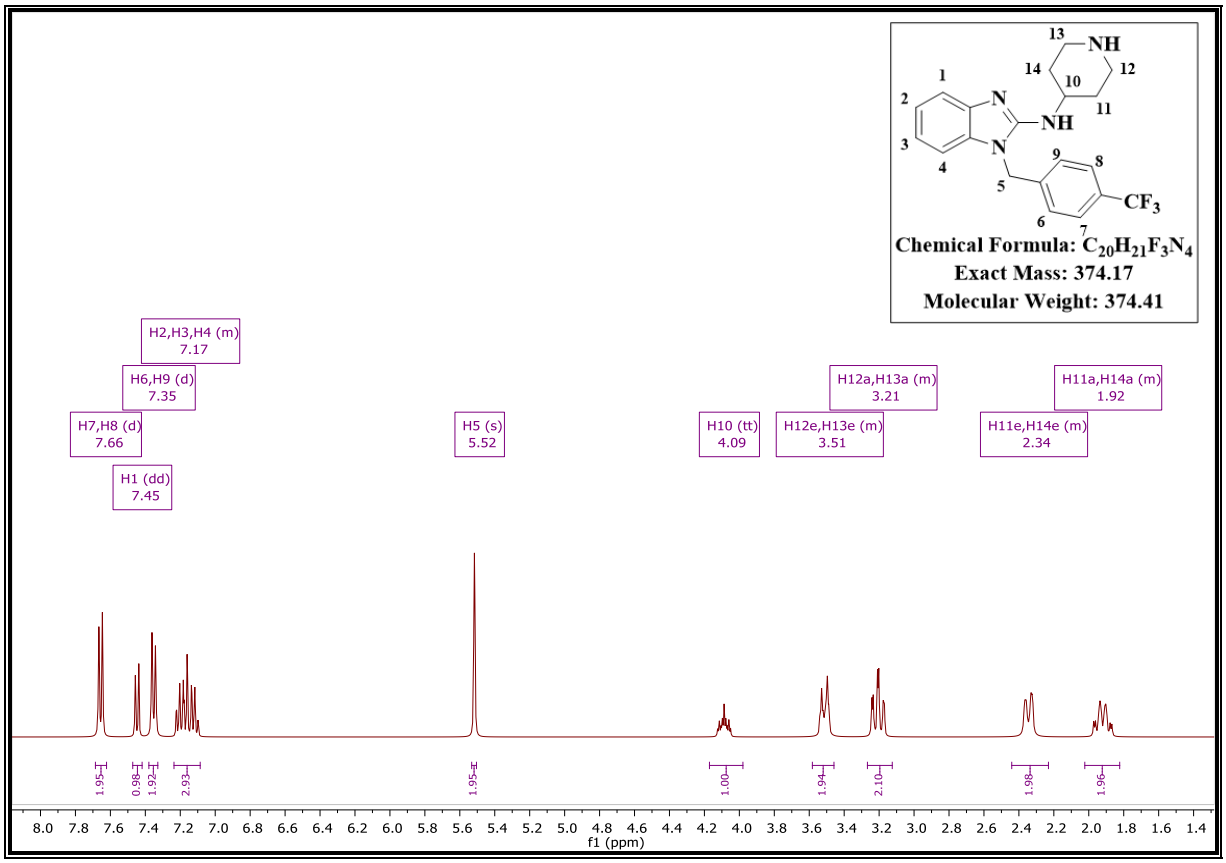

Figure 2.9: ^{1}H NMR spectrum of **2c** at 400 MHz in MeOD.

2.2.2.6 The Mannich Reaction: Step (vi), Scheme 2.1

The Mannich reaction involves the combination of an aldehyde (mostly formaldehyde) with either a primary or secondary amine and a compound that has activated hydrogen (a phenol in this case) to form a Mannich base.[13] The reaction proceeds via nucleophilic addition of the amine to formaldehyde, followed by dehydration to form a Schiff base (Scheme 2.4). Electrophilic addition of the Schiff base to the enol affords the desired product.

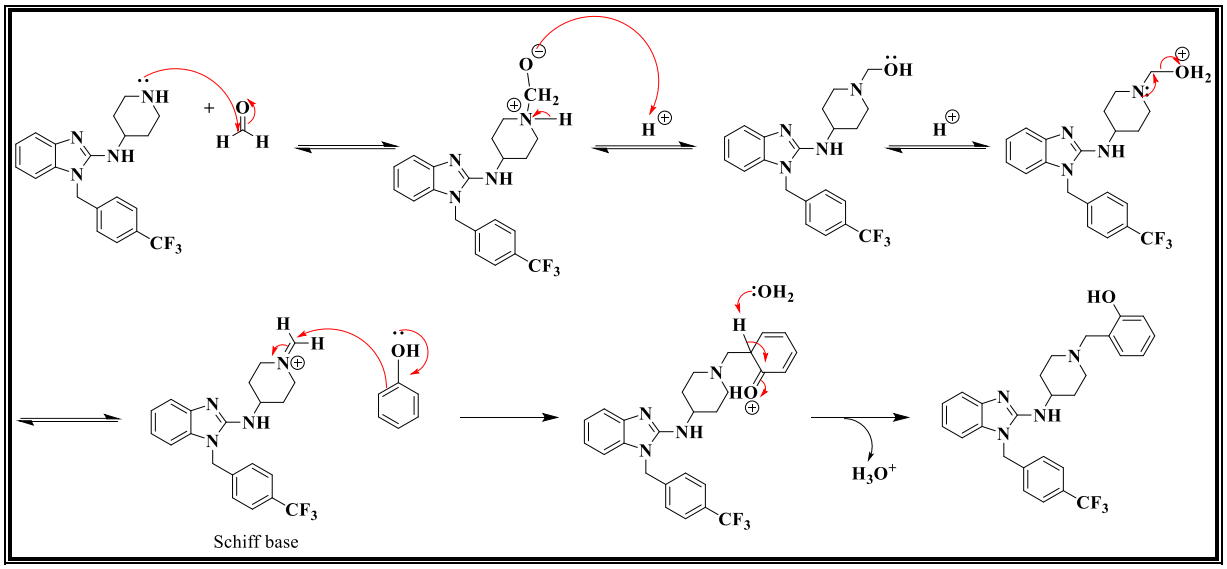

Scheme 2.4: Proposed mechanism of the Mannich reaction.

The ^{1}H NMR spectra of the 1-(4-trifluoromethylbenzyl) benzimidazole analogues (**2.1 – 2.21**) were generally of a similar pattern; thus, the spectrum for analogue **2.13** (Figure 2.10) is shown as a representative example. Additional aromatic protons and a methylene singlet resonating at δ 3.67 ppm were observed, indicating the successful formation of this target compound.

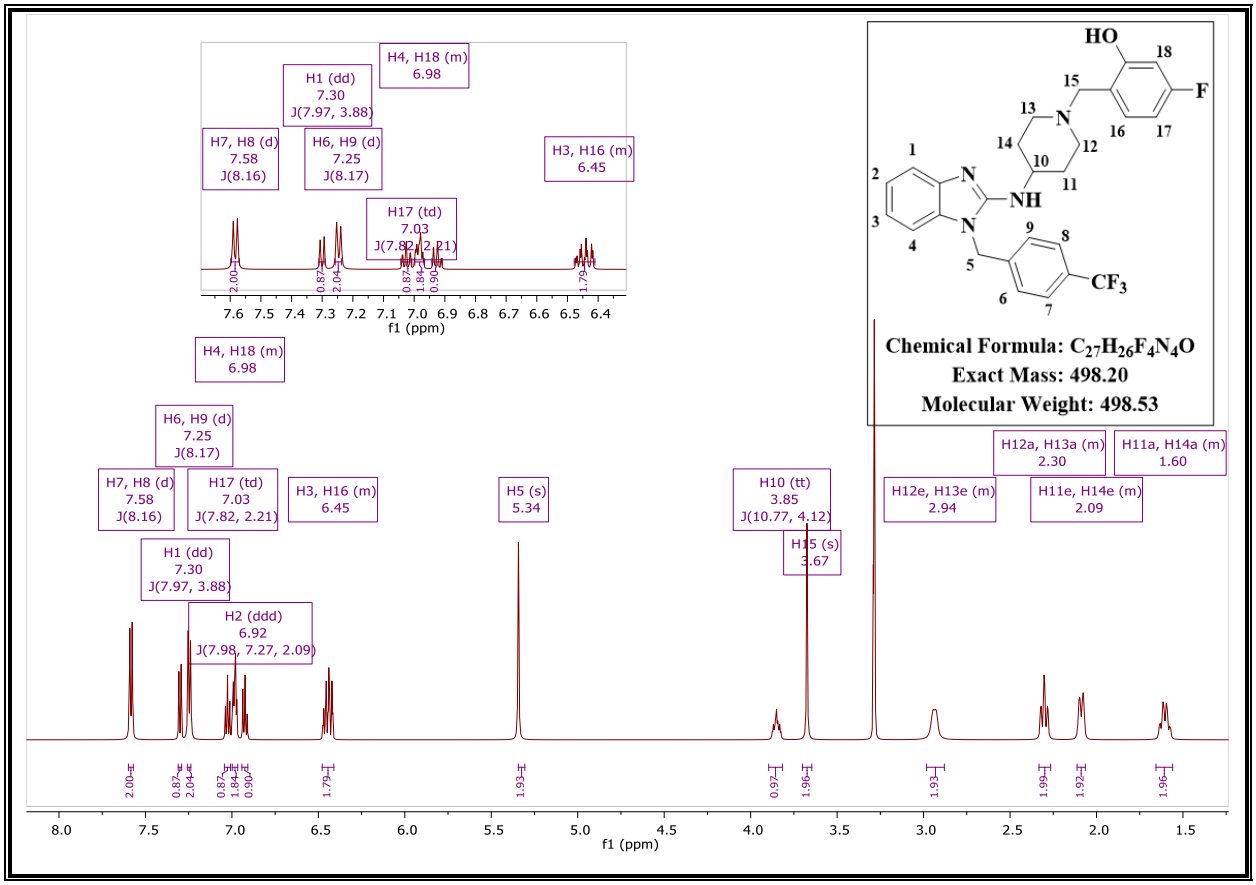

Figure 2.10: ^{1}H NMR spectrum of **2.13** at 600 MHz in MeOD.

The ^{13}C NMR spectrum (Figure 2.11) of **2.13** exhibited signals that reinforced the structure assignment and all 27 carbons were accounted. The diagnostic signal is the most deshielded carbon, which bears the fluorine atom (C-F) resonating downfield at δ 164.04 ppm. The carbon-bearing the trifluoromethyl moiety (C-CF_3) was observed at δ 125.22 ppm while the trifluoromethyl carbon itself (CF_3) resonated at δ 117.68 ppm.

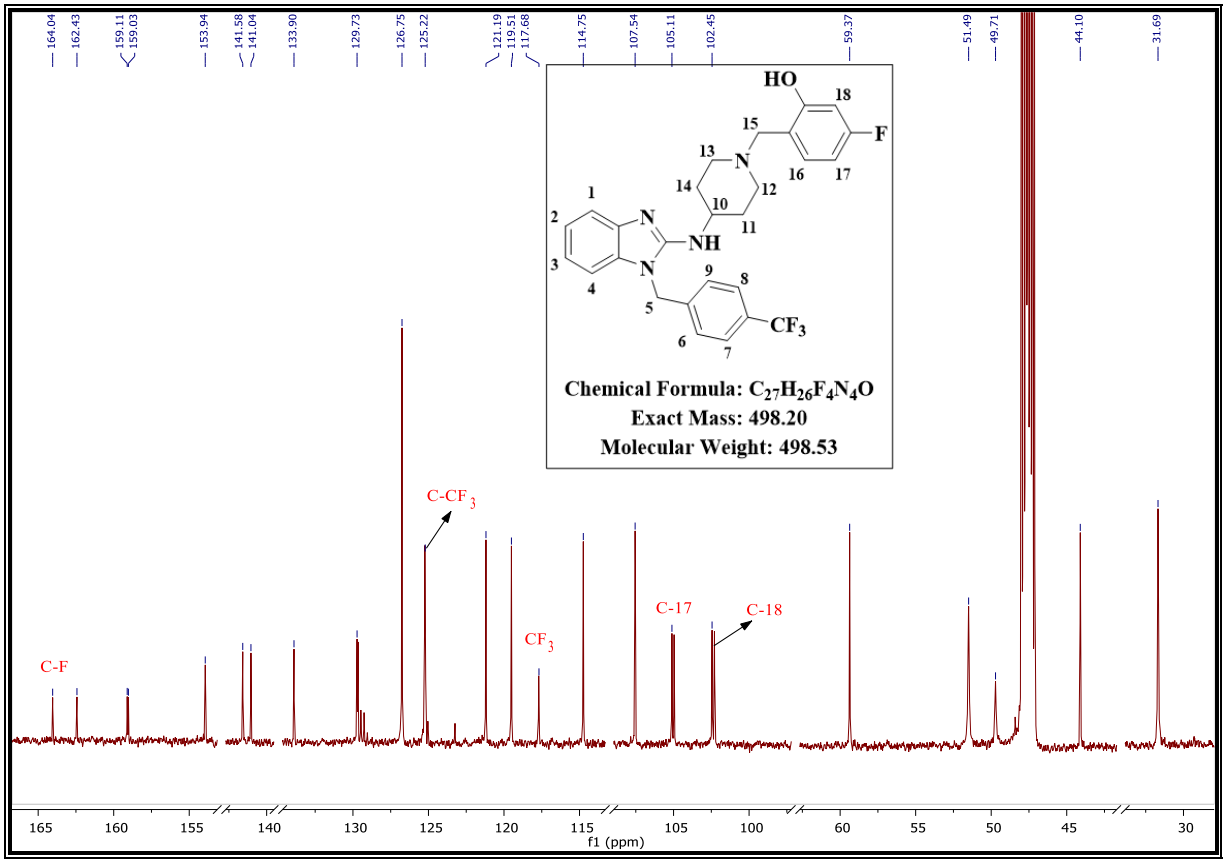

Figure 2.11: ^{13}C NMR spectrum of **2.13** at 151 MHz in MeOD.

The HPLC-MS spectrum (Figure 2.12) further supported the formation of compound **2.13** with a molecular ion $[M+H]^+$ of *m/z* = 498.8.

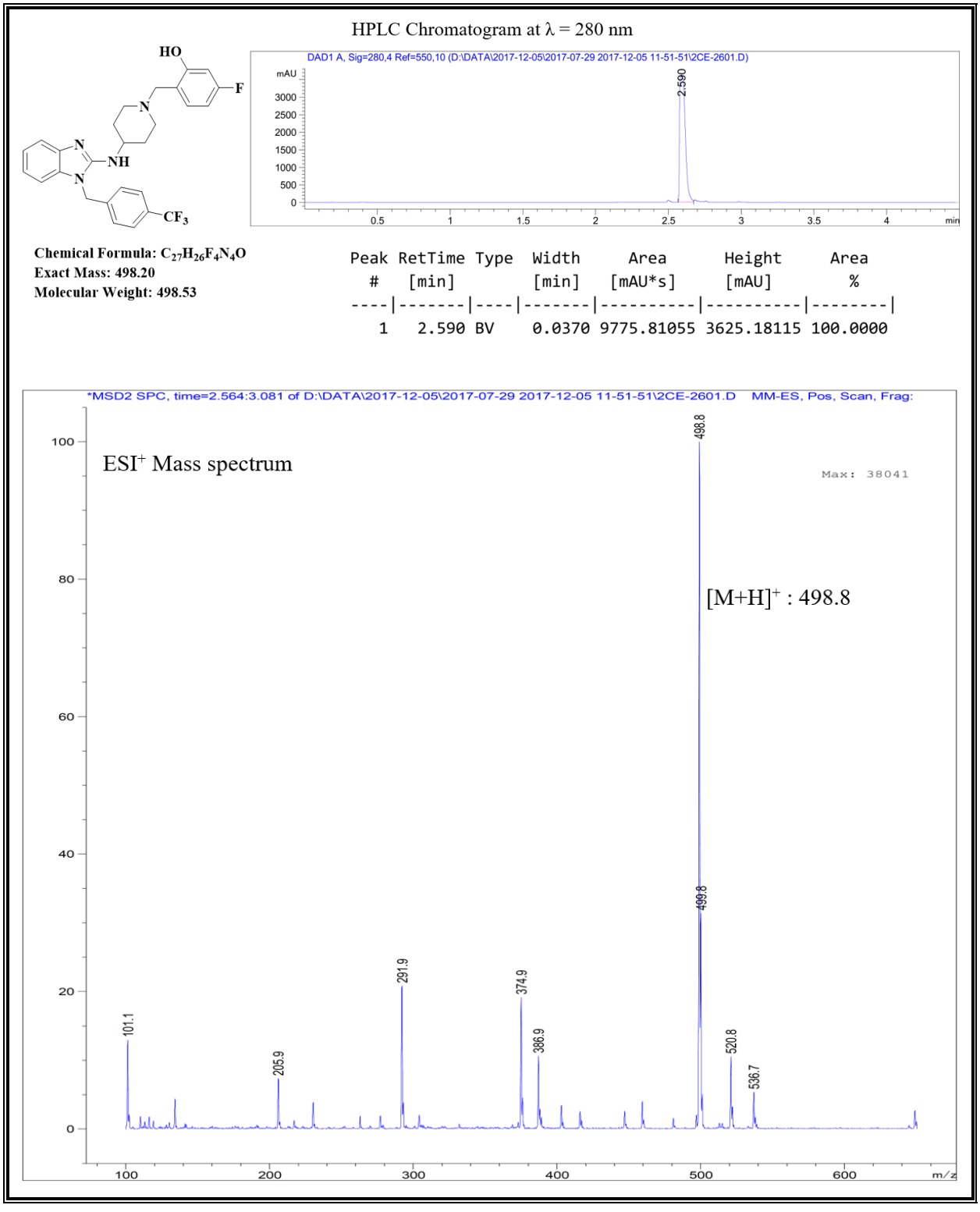

Figure 2.12: HPLC chromatogram and ESI$^+$ mass spectrum of **2.13**.

2.3 Design, Synthesis and Characterization of Imidazopyridine analogues

2.3.1 Design and Synthesis

Using the benzimidazole frontrunner compound **1.3** as a guide, the SAR plan outlined in Figure 2.13 was pursued to produce diverse analogues arising from modifications around the core scaffold.

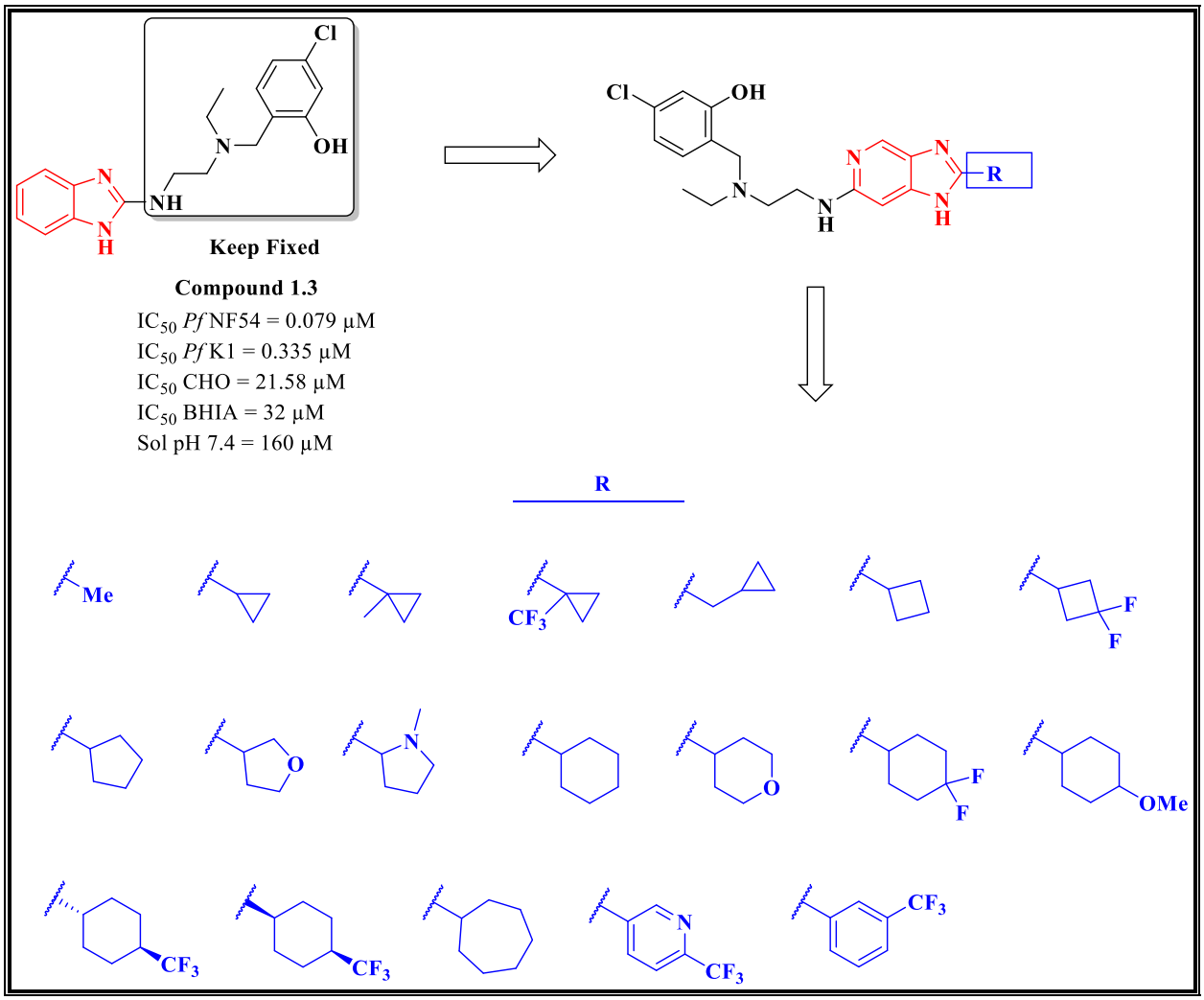

Figure 2.13: Design of imidazopyridine analogues.

CHO: Chinese hamster ovarian cells; BHIA: β-hematin inhibition activity; sol: solubility.

The choice of **R** substituents was aimed at introducing structural diversity around the imidazopyridine core and reducing the lipophilicity of target compounds. The **R** group was also informed by the commercial availability of the relevant carboxylic acid starting materials. The core scaffold modification involved a scaffold hopping approach wherein the benzimidazole core was replaced with an imidazopyridine core based on its presence in previously described antimalarial agents.[14,15]

Synthetic protocols reported in the literature were adapted to access the target compounds. The general protocol followed an eight-step synthetic route from commercially available 2,4-dichloro-5-nitropyridine (Scheme 2.5). A nucleophilic substitution was first performed to introduce a *para*-methoxybenzyl (PMB) amino-protecting group to form the 2-chloro-N-(4-methoxybenzyl)-5-nitropyridin-4-amine intermediate **3a** in quantitative yield. This intermediate was subjected to a second nucleophilic substitution reaction under microwave irradiation with *tert*-butyl (2-aminoethyl)(ethyl)carbamate in the presence of triethylamine and *N*, *N*-dimethylformamide (DMF) to produce *tert*-butylethyl(2-((4-((4-methoxybenzyl)amino)-5-nitropyridin-2 yl)amino)ethyl)carbamate **3b**. The nitro group was then reduced with palladium on carbon (10% Pd/C) under H_2 gas to deliver the corresponding amine **3c**. This amine intermediate was reacted with the appropriate carboxylic acids in the presence of 1-ethyl-3-(3-dimethylaminopropyl)carbodiimide, hydrochloride (EDCI.HCl), and a catalytic amount of 4-dimethylaminopyridine (DMAP) in dichloromethane (DCM) to produce the amide intermediates **3d**. At this stage, the imidazole ring was allowed to form by heating in 2M aqueous NaOH and absolute ethanol at 80 °C to yield intermediate **3e**. The appropriate cyclized intermediate was subjected to boc-deprotection followed by reductive amination with 4-chloro-2-hydroxybenzaldehyde in the presence of sodium borohydride to yield the penultimate intermediate **3f**. Finally, the PMB group was removed using neat trifluoroacetic acid (TFA) to afford the desired imidazopyridine analogues **3.1-3.19** in moderate yields (50-75%).

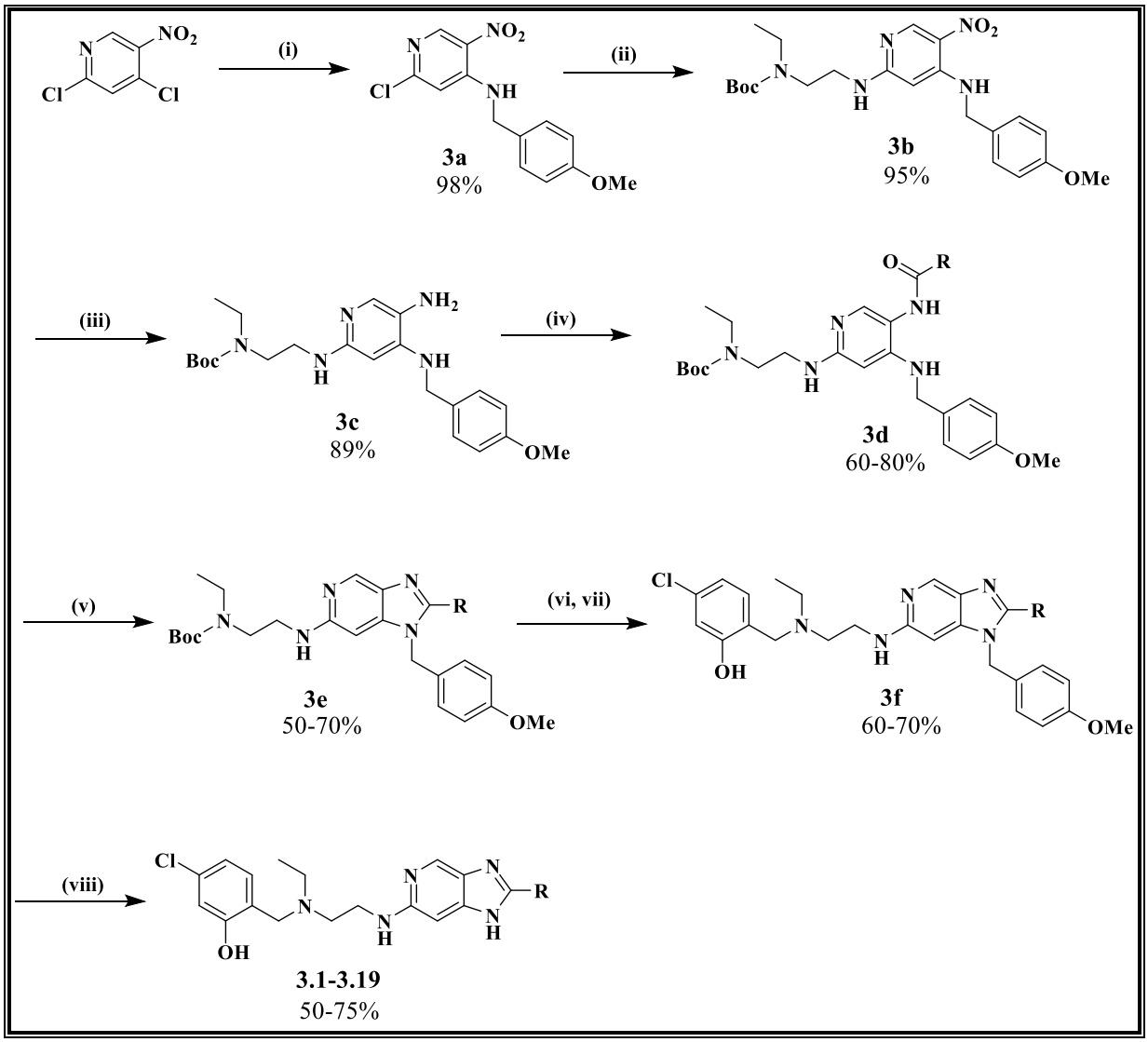

Scheme 2.5: General synthetic approach for imidazopyridine analogues. ***Reagents and conditions***: (**i**) PMB-NH_2 (1.8 eq), DIPEA (1.8 eq), THF, 0–25 °C, 30 min, 98%; (**ii**) tert-butyl (2-aminoethyl)(ethyl)carbamate (1.5 eq), Et_3N (2 eq), DMF, µW 100 °C, 1 h, 60%; (**iii**) 10% Pd/C H_2(g) 25 °C; (**iv**) R-COOH (1.3 eq) 85%, EDCI.HCl (1.5 eq), DMAP (0.1eq), DCM, 25 °C, 12, 60-80%; (**v**) 2 M NaOH, EtOH, 80 °C, 12-72 h 50-70%; (**vi**) 4 M HCl/dioxane 60-75%; (**vii**) 4-chloro-2-hydroxybenzaldehyde, $NaBH_4$, 25 °C, 24 h, 60-70%; (**viii**) TFA, 100 °C, 12 h, 50-75%.

2.3.2 Proposed Reaction Mechanisms and Characterization

2.3.2.1 Nucleophilic Substitution: Step (i), Scheme 2.5

The PMB-intermediate **3a**, obtained in this step, was confirmed by both ^{1}H NMR and HPLC-MS. The ^{1}H NMR (Figure 2.14) revealed the diagnostic methylene protons H3 resonating upfield at δ 4.57 ppm as a doublet (J = 6.15 Hz) because of its coupling to the amino proton H4 (NH; J = 6.14 Hz). The aromatic protons of the benzyl moiety were also observed as

doublets at δ 7.29 ppm (J = 8.73 Hz, 2H, H5 and H6) and δ 6.89 ppm (J = 8.73 Hz, 2H, H7 and H8) integrating for two protons each due to the symmetry of the benzyl group.

The mass spectrum of intermediate **3a** exhibited a pseudo-molecular ion peak at m/z = 294.0.

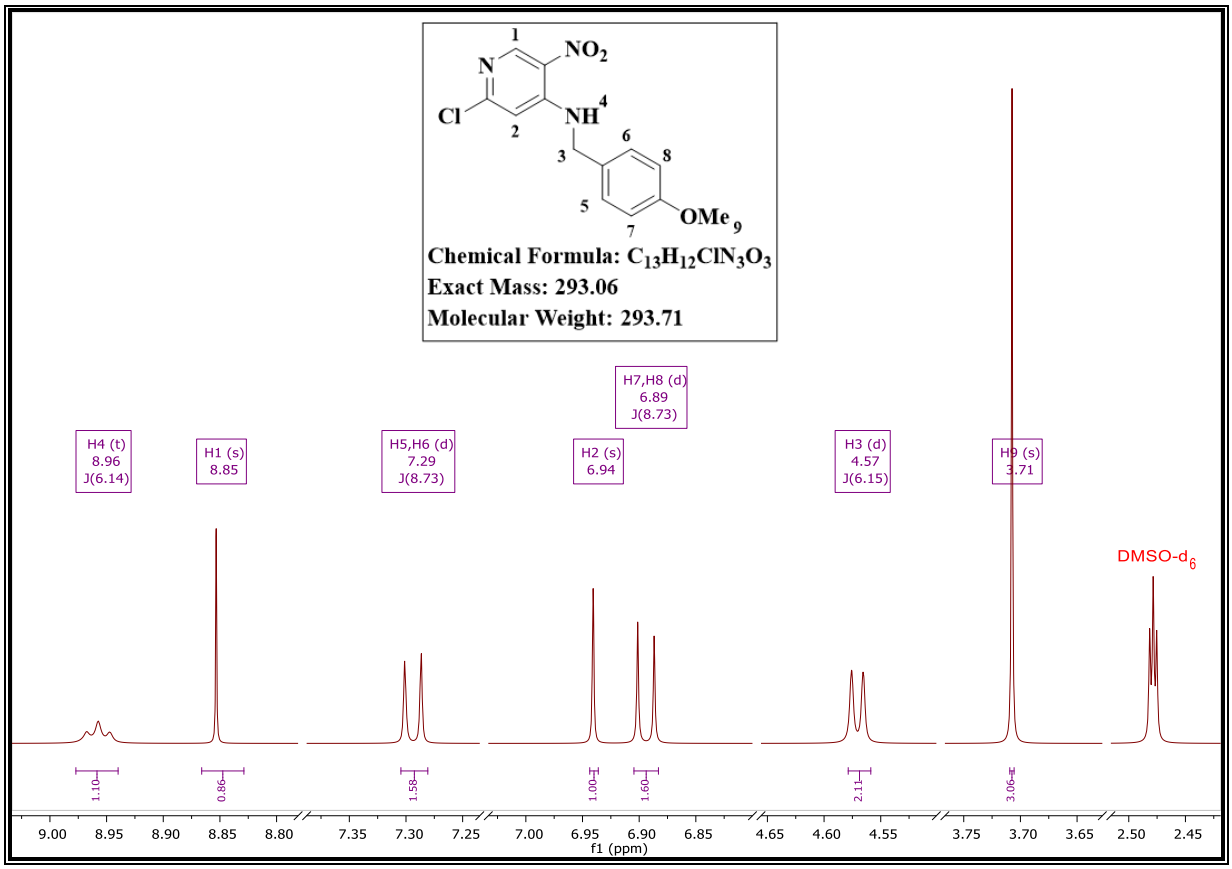

Figure 2.14: ^{1}H NMR spectrum of intermediate **3a** at 600 MHz in DMSO.

2.3.2.2 Nucleophilic Substitution: Step (ii), Scheme 2.5

Taking advantage of the electron-withdrawing nitro group, a second nucleophilic substitution reaction was carried out with *tert*-butyl (2-aminoethyl)(ethyl)carbamate to displace the second chloro group. The ^{1}H NMR for intermediate **3b** is captured in Figure 2.15 below. The splitting pattern of the aromatic protons remained almost the same as that for the preceding intermediate **3a**. Additional aliphatic protons were observed, but the signals for the H9 and H10 protons were not well resolved; thus, this was recognized as a multiplet integrating for four protons. The shielded nine protons of the boc group (H13) resonated as a very intense singlet at δ 1.41 ppm.

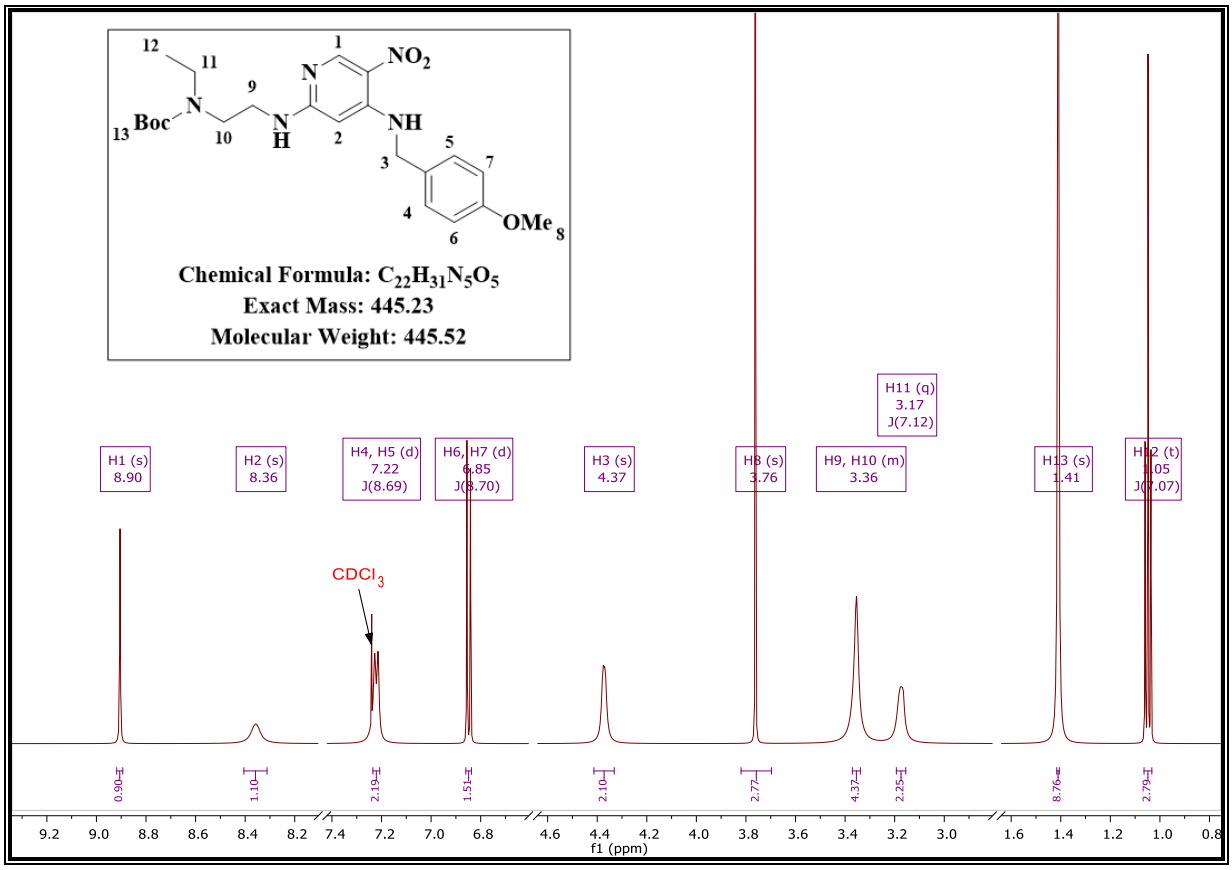

Figure 2.15: ^{1}H NMR spectrum of intermediate **3b** at 600 MHz in $CDCl_3$.

The molecular ion peak of **3b** was observed at *m/z* = 446.2, corresponding to the protonated (M+H) molecule at a retention time t_R = 2.677 min.

2.3.2.3 Reduction of the Nitro Group: Step (iii), Scheme 2.5

The Pd/C-mediated reduction of the nitro group in the presence of H_2 gas afforded the intermediate amine **3c**. The reduction of the nitro group resulted in a significant upfield shift of the aromatic protons H1 and H2 observed in the ^{1}H NMR spectrum (Figure 2.16). The aliphatic signals also retained a similar splitting pattern observed in the preceding intermediate. More evidently, a successful nitro reduction was obtained from the HPLC-MS measurements, which showed a pseudo-molecular ion m/z = 416.2 for intermediate **3c**.

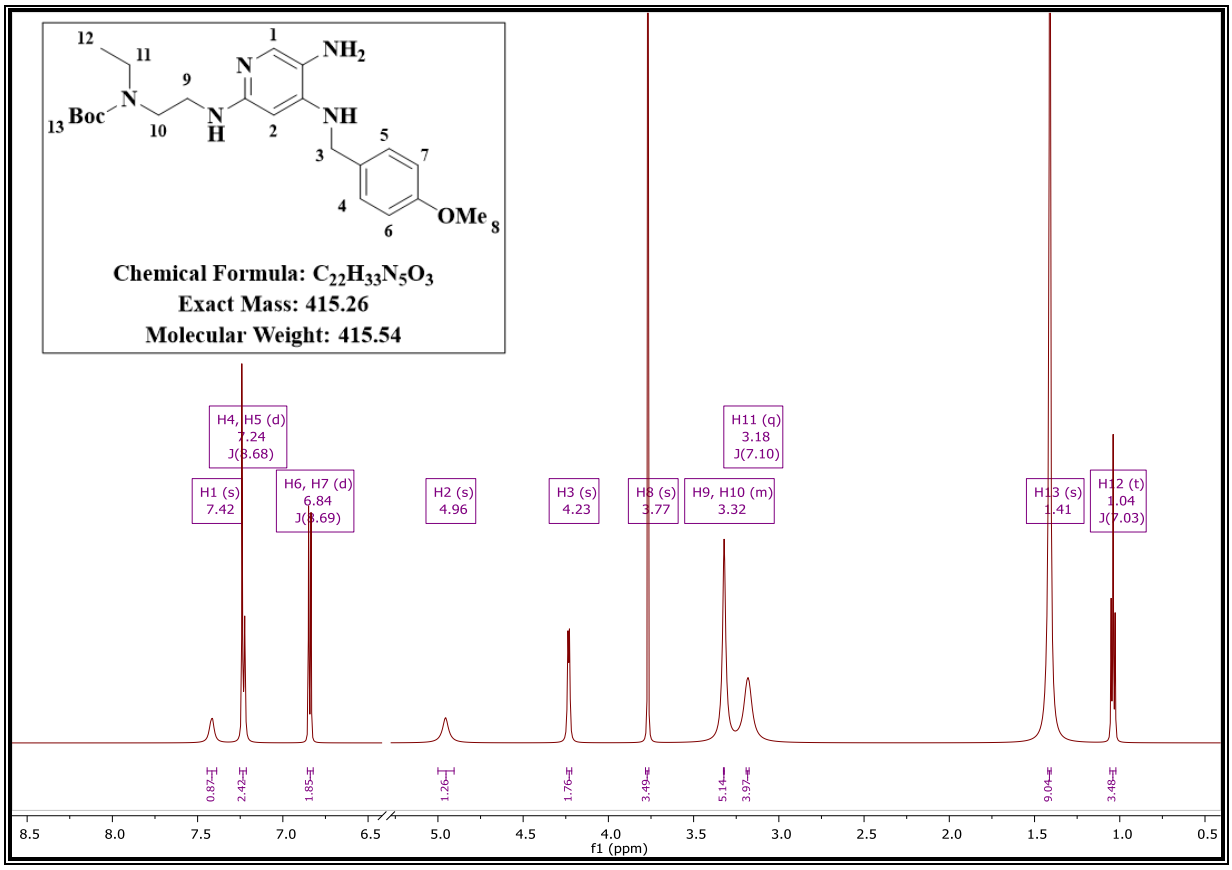

Figure 2.16: ^{1}H NMR spectrum of intermediate **3c** at 600 MHz in $CDCl_3$.

2.3.2.4 Amide Bond Formation: Step (iv), Scheme 2.5

The formation of the imidazole ring proceeds via an initial amide bond formation whose mechanism is detailed in Scheme 2.6 below.[16–18] The first step in amide bond formation involves deprotonation of the carboxylic acid. The carboxylate attacks the carbodiimide carbon of EDCI, resulting in the formation of the *O*-acylisourea mixed ester intermediate rendering the carbonyl carbon more susceptible to nucleophilic attack. The amine then reacts with the activated *O*-acylisourea mixed ester intermediate to form the desired amide bond and a urea by-product. Meanwhile, a commonly encountered undesirable side reaction usually occurs, which significantly compromises the yield of amide bond reactions. The reactive and unstable *O*-acylisourea mixed ester intermediate could rearrange via an acetyl transfer to the stable *N*-acylurea. This side reaction is considerably averted by the addition of DMAP, which reacts with the *O*-acylisourea mixed ester at a relatively faster rate compared to the rearrangement. The formation of all the amide intermediates was only confirmed by the HPLC-MS, and they were used in the cyclodehydration reaction without any further purification.

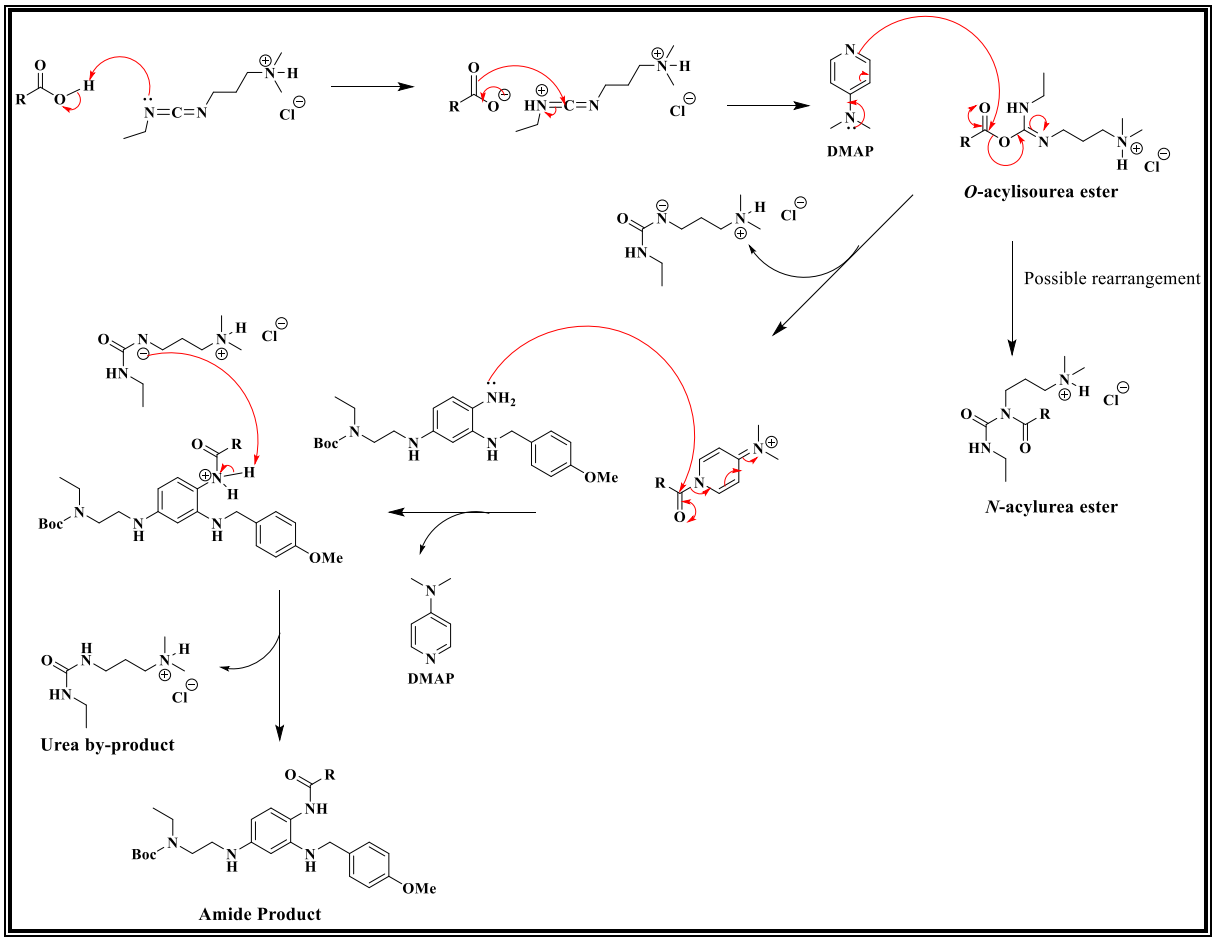

Scheme 2.6: Proposed mechanism of amide bond formation.[16–18]

2.3.2.5 Base-catalyzed Cyclodehydration Reaction: Step (v), Scheme 2.5

The amino benzyl initiates the cyclization by directly attacking the amide carbonyl to form a cyclized enol intermediate, as depicted in Scheme 2.7. The hydroxyl from the sodium hydroxide then deprotonates the amino group resulting in aromatization and a subsequent loss of the hydroxyl on the adjacent carbon and the loss of water as a by-product.

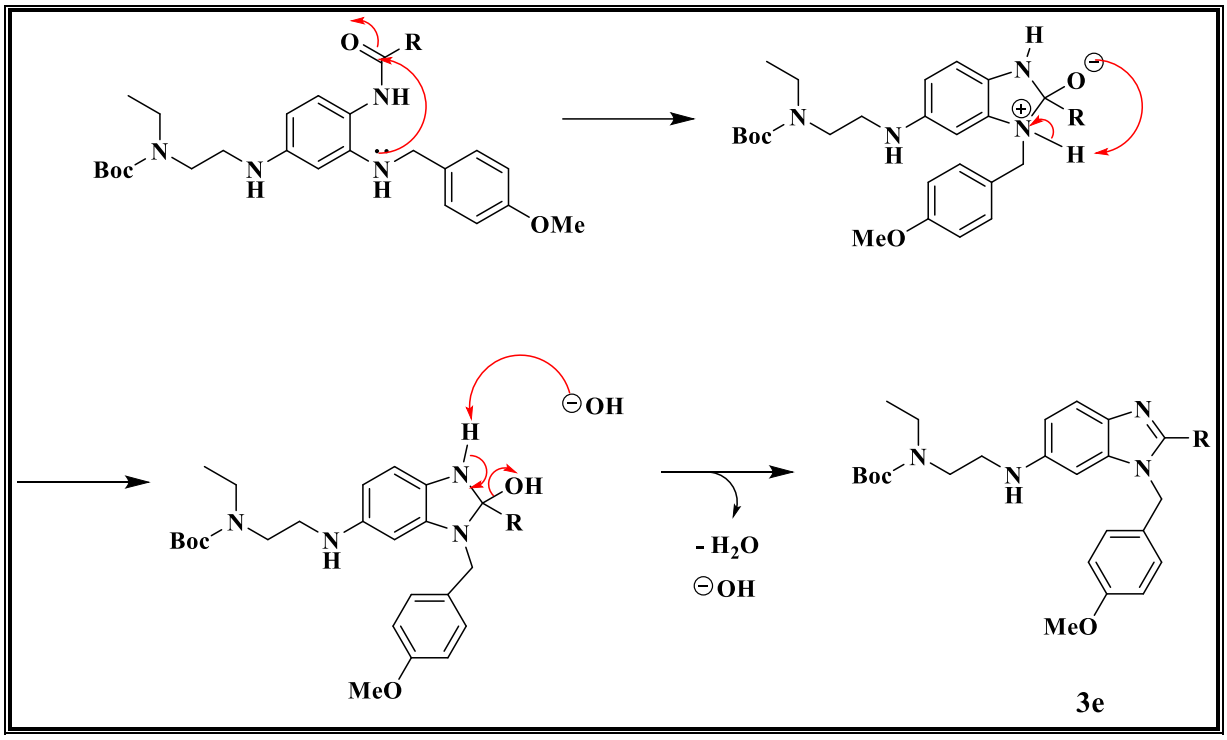

Scheme 2.7: Proposed mechanism of base-catalyzed cyclodehydration.

The ^{1}H NMR spectra acquired for these intermediates confirmed a successful cyclodehydration from the respective amide intermediates. A representative ^{1}H NMR spectrum for intermediate **3e.1** is shown in Figure 2.17 below. The most diagnostic feature in this spectrum is the additional aliphatic signals corresponding to the cyclopentyl moiety. The HPLC-MS also confirmed a successful cyclodehydration with a pseudo-molecular ion peak $[M+H]^{+}$ at *m/z* = 494.2 in the positive ionization mode.

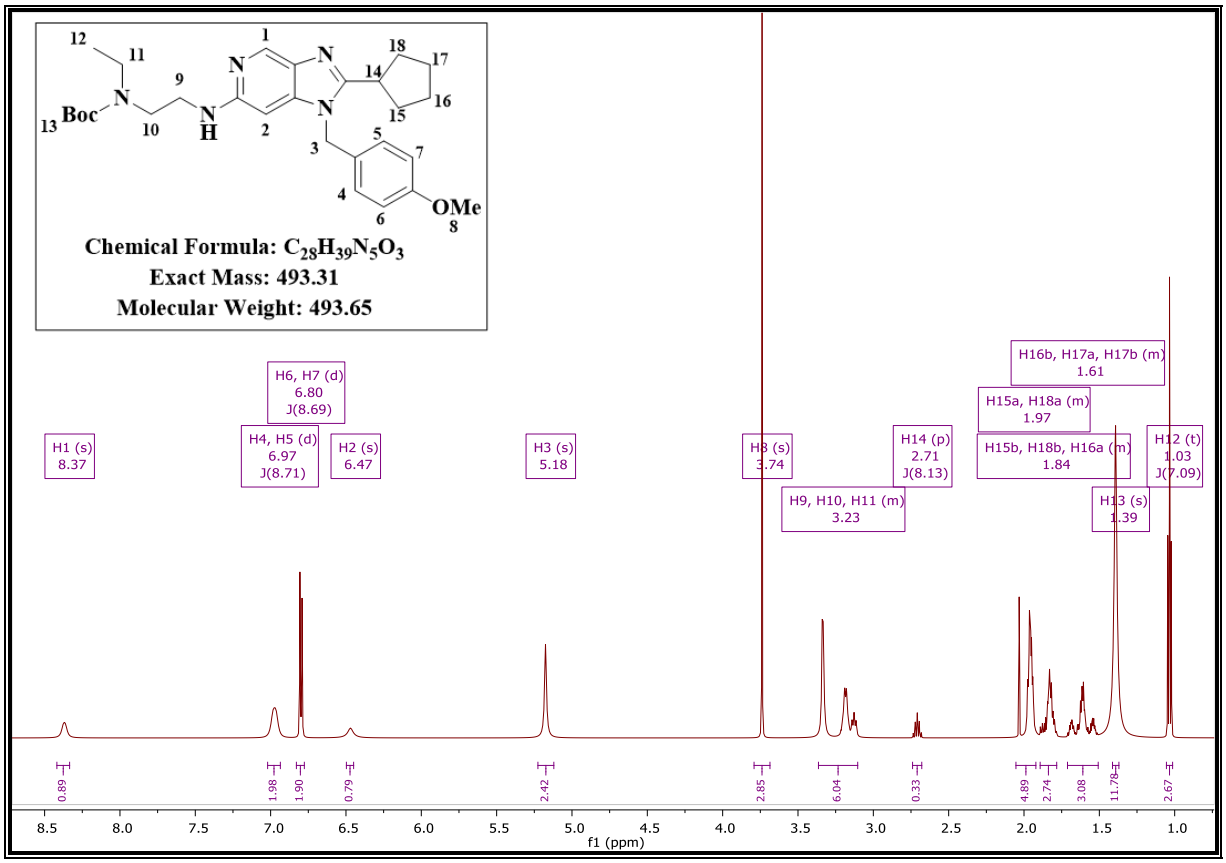

Figure 2.17: ^{1}H NMR spectrum of intermediate **3e.1** at 600 MHz in $CDCl_3$.

2.3.2.6 *N*-Boc-deprotection and Reductive amination: Steps (vi and vii), Scheme 2.5

The *N*-boc-deprotection step affords a free amine intermediate, which is subsequently used in a reductive amination reaction with 4-chloro-2-hydroxybenzaldehyde. The ^{1}H NMR spectrum of intermediate **3f.1** is shown as a representative example (Figure 2.18). The spectrum was accompanied by the disappearance of the upfield signal of the *tert*-butyl group and the appearance of a methylene singlet (H13) resonating at δ 3.72 ppm. Additional aromatic protons were also observed.

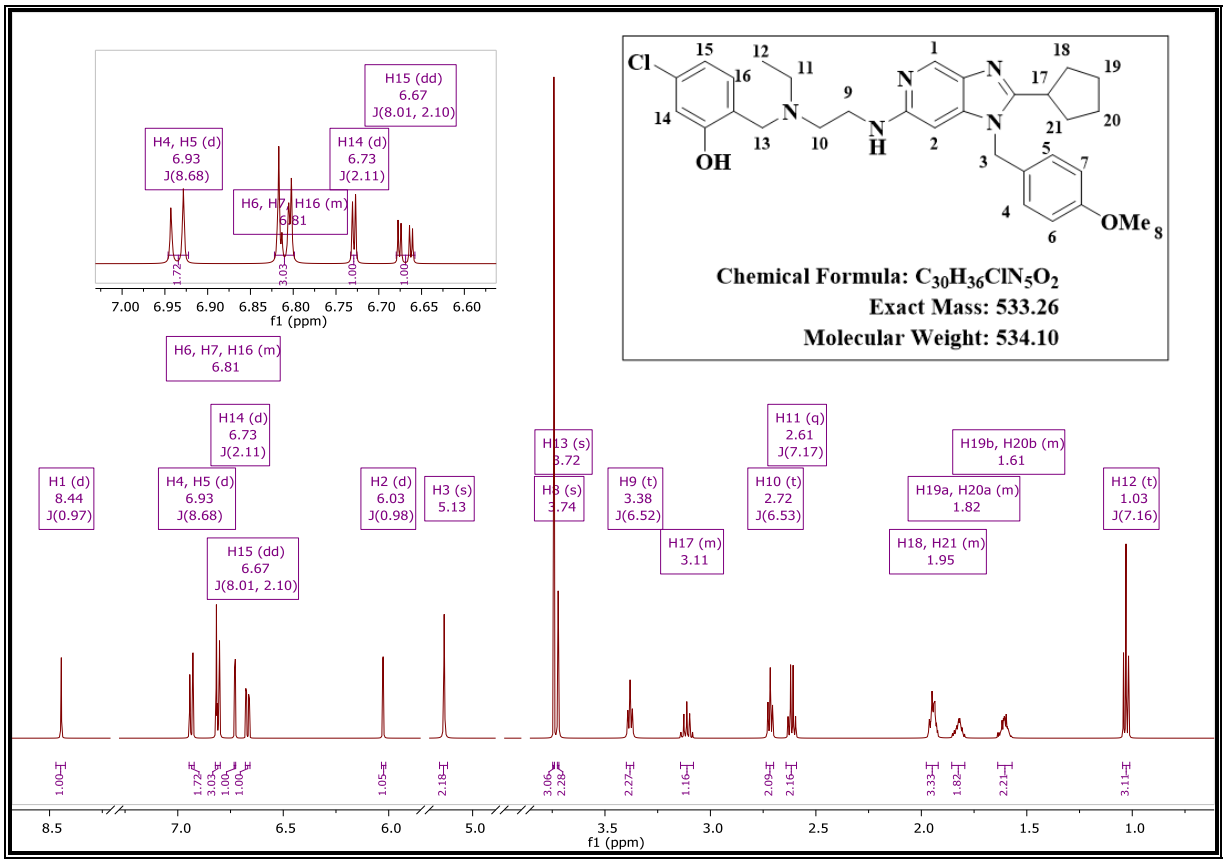

Figure 2.18: ^{1}H NMR spectrum of intermediate **3f.1** at 600 MHz in $CDCl_3$.

The mass spectrum, on the other hand, afforded a pseudo-molecular ion [M+H] at *m/z* = 534.3. In this case, the mass spectrum also exhibited a pattern characteristic of a compound containing a chloro group due to the two isotopes of chlorine.

2.3.2.7 Acid-catalyzed Cleavage of PMB group: Step (viii), Scheme 2.5

The acid-catalyzed cleavage of the p-methoxybenzyl moiety was attained by heating the appropriate intermediate in trifluoroacetic acid (TFA) under reflux to afford the target compounds **3.1-3.19**. The benzyl nitrogen is firstly protonated, and then the C-N bond is broken by the delocalization of electrons through the benzyl ring system from the methoxy oxygen, as depicted in Scheme 2.8 below. The free amine was then obtained by using Amberlyst A21 free base resin.

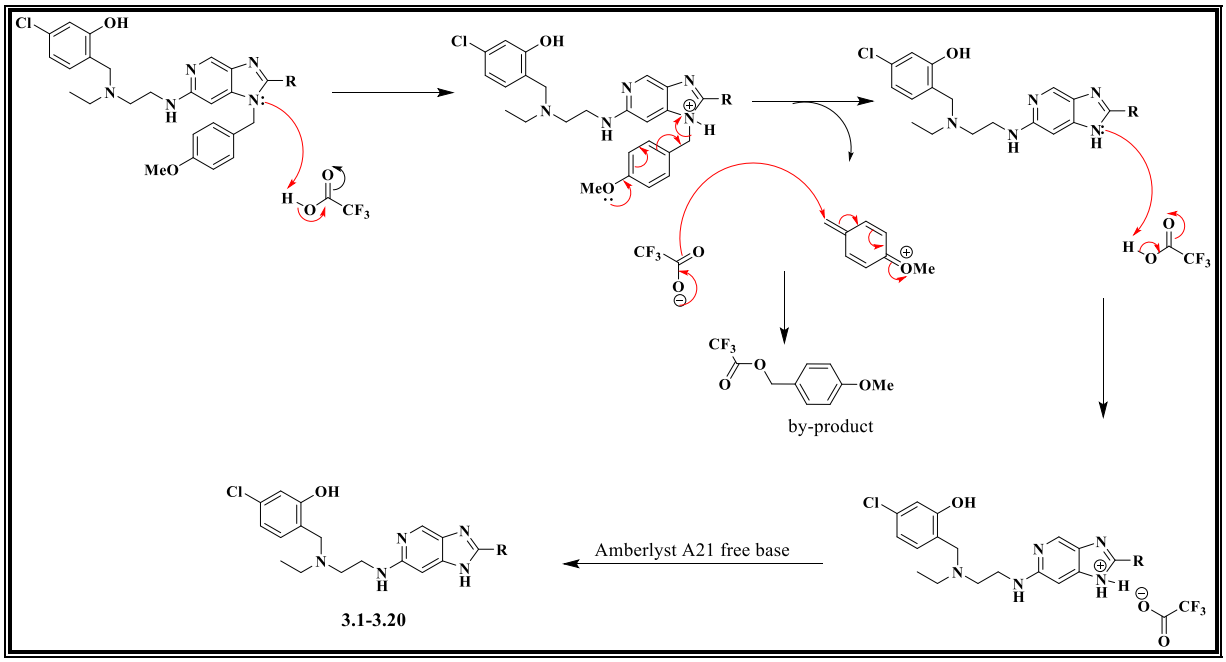

Scheme 2.8: Proposed mechanism of acid-catalyzed cleavage of the p-methoxybenzyl moiety.

Successful cleavage of the p-methoxybenzyl moiety was confirmed by ^{1}H NMR, which showed the loss of the p-methoxybenzyl moiety. The ^{1}H NMR spectrum of analogue **3.1** is shown as a representative example in Figure 2.19. The aliphatic region retained a similar pattern of signals as observed for the precursor of this final compound.

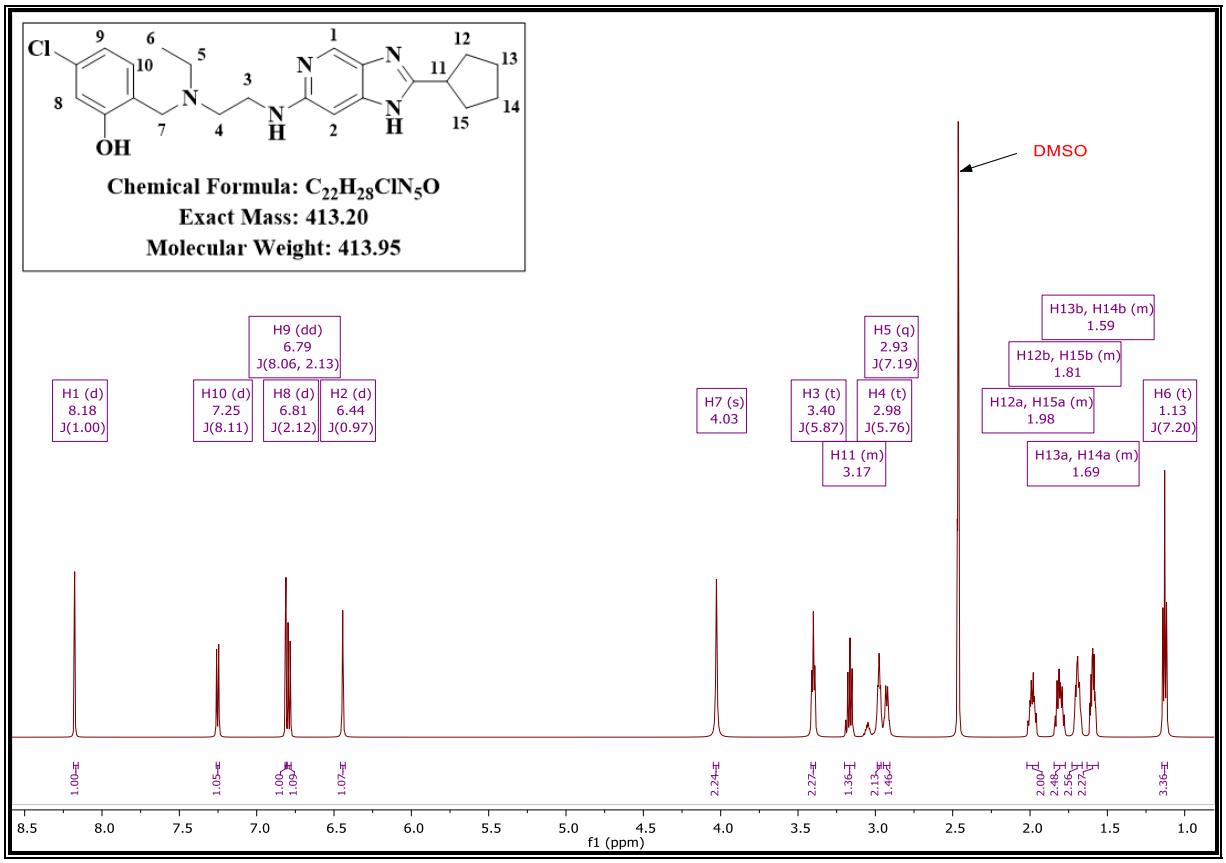

Figure 2.19: ^{1}H NMR spectrum of **3.1** at 600 MHz in DMSO.

In addition, ^{13}C NMR spectroscopy was used to provide further evidence to support the chemical structure of compound **3.1** (Figure 2.20). Although 20 distinct signals were obtained, the chemical shift-equivalent pairs of carbons in the cyclopentyl moiety resonated at the same chemical shifts; thus, all 22 carbons were ascertained.

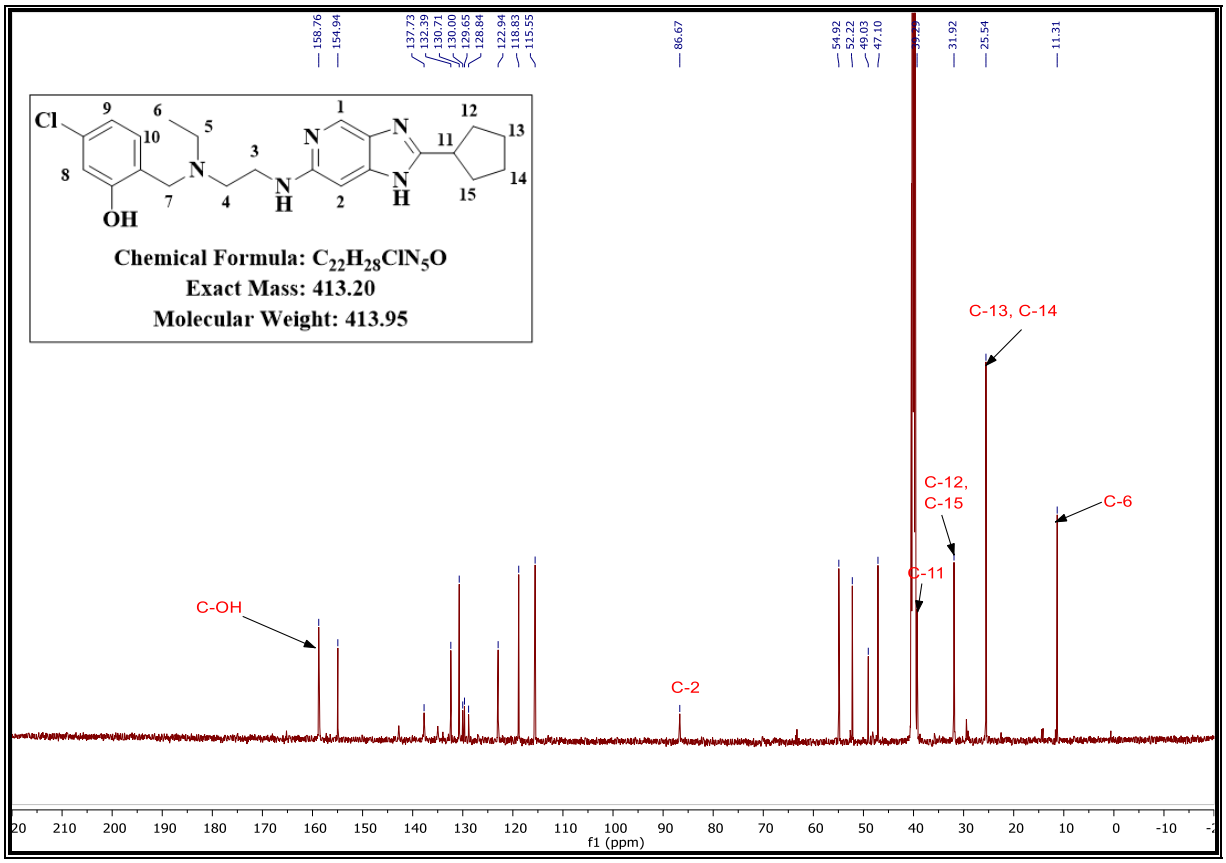

Figure 2.20: ^{13}C NMR spectrum of 3.1 at 151 MHz in DMSO.

Compound **3.1** was further characterized using HPLC-MS and displayed a retention time of 2.300 min with a pseudo-molecular ion [M+H] at m/z = 414.1 detected under ESI mode (Figure 2.21).

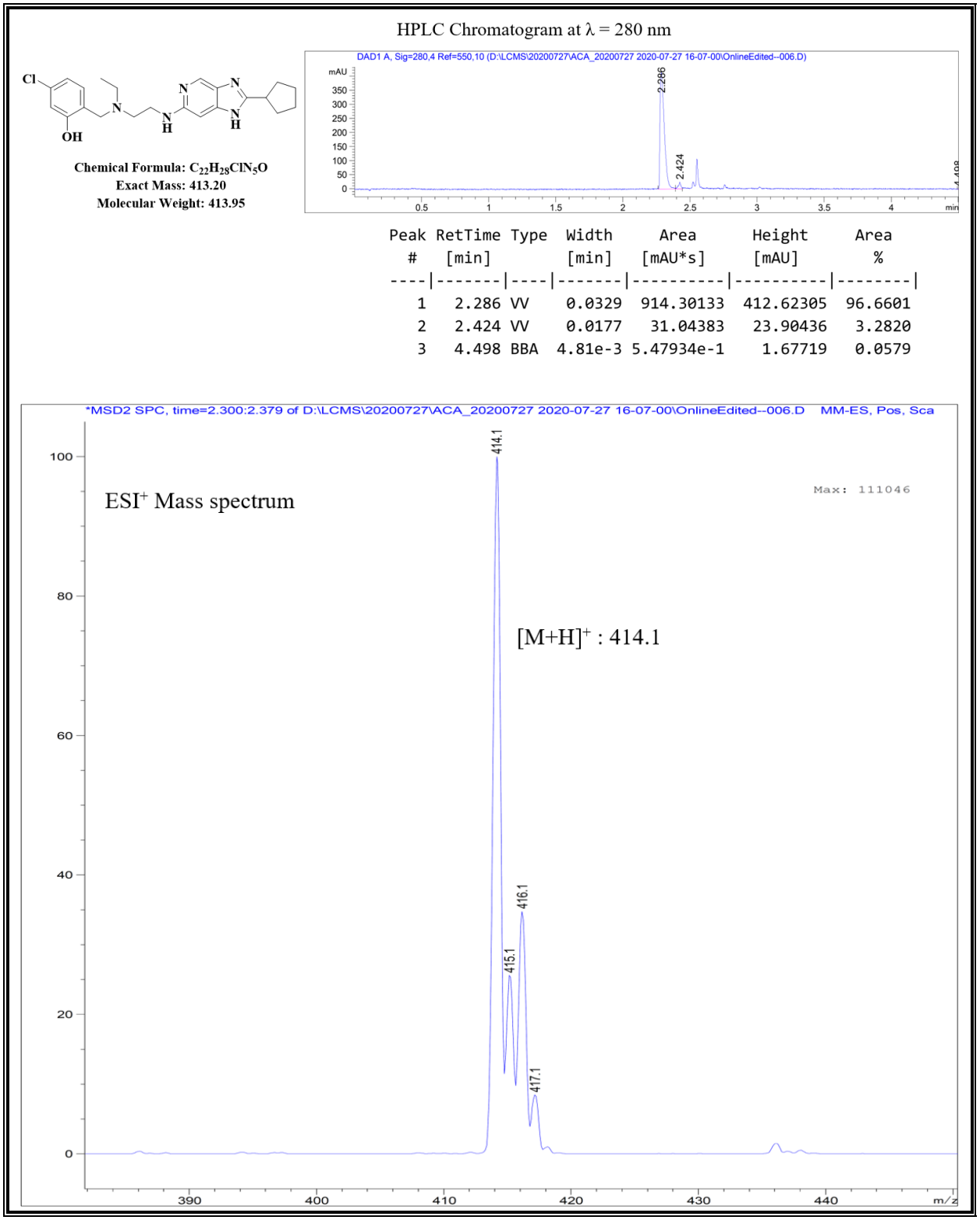

Figure 2.21: HPLC chromatogram and ESI$^+$ mass spectrum of **3.1**.

2.4 Design and Synthesis of Fluorescent Probes

Fluorescent probes of compounds **1.3** and **3.14** were designed and synthesized by connecting a fluorophore [7-nitrobenz-2-oxa-1,3-diazole (NBD)] on the ethylenediamine side chain via an ethyl linker such that the alteration of binding sites was minimized. As illustrated in Scheme 2.9, the **1.3-NBD** probe was synthesized from commercially available 2-chlorobenzimidazole in six steps. Intermediate **4a** was first synthesized by nucleophilic substitution of 2-chlorobenzimidazole with *N*-boc ethylenediamine using triethylamine as the base in toluene. The boc-protecting group was then removed with 4N HCl/Dioxane followed by reductive amination of 4-chloro-2-hydroxybenzaldehyde to yield intermediate **4b**. A second reductive amination was carried out on intermediate **4b** with *N*-boc glycinal in the presence of sodium cyanoborohydride resulting in the penultimate intermediate **4c**. Finally, removing the boc group followed by a nucleophilic substitution reaction with NBD-chloride yielded the target fluorescent probe **1.3-NBD**. ^{1}H NMR was used to confirm the successful formation of the probe (Figure 2.22).

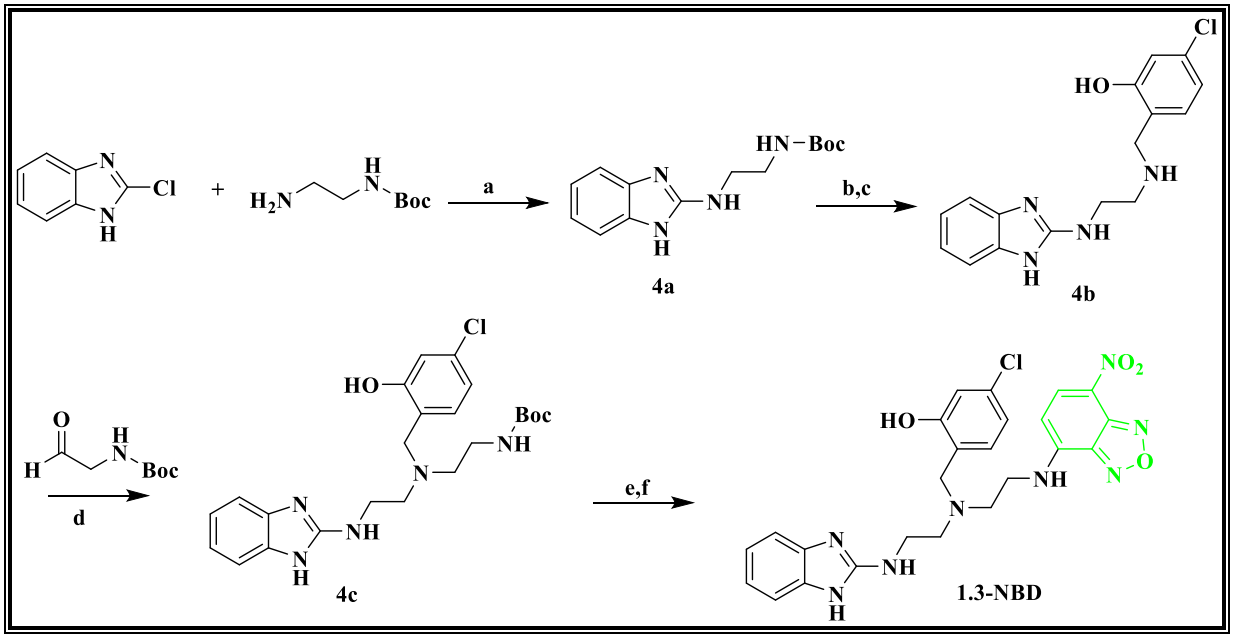

Scheme 2.9: Synthetic scheme of fluorescent analogue **1.3-NBD**. ***Reagents and conditions*:** (**a**) Et_3N (3 eq), Toluene 150°C, 16 hrs, quantitative; (**b**) 4N HCl/Dioxane 25°C, 2hr, 80%; (**c**) 4-chloro-2-hydroxybenzaldehyde, $NaBH_4$, 25°C, 3 hrs, 70%; (**d**) $NaBH_3CN$, cat. AcOH, MeOH, 80°C, 16 hrs 86%; (**e**) 4M HCl/Dioxane, 25°C ; (**f**) NBD-Chloride, $NaHCO_3$, EtOAc, 60°C, 24h, 60%.

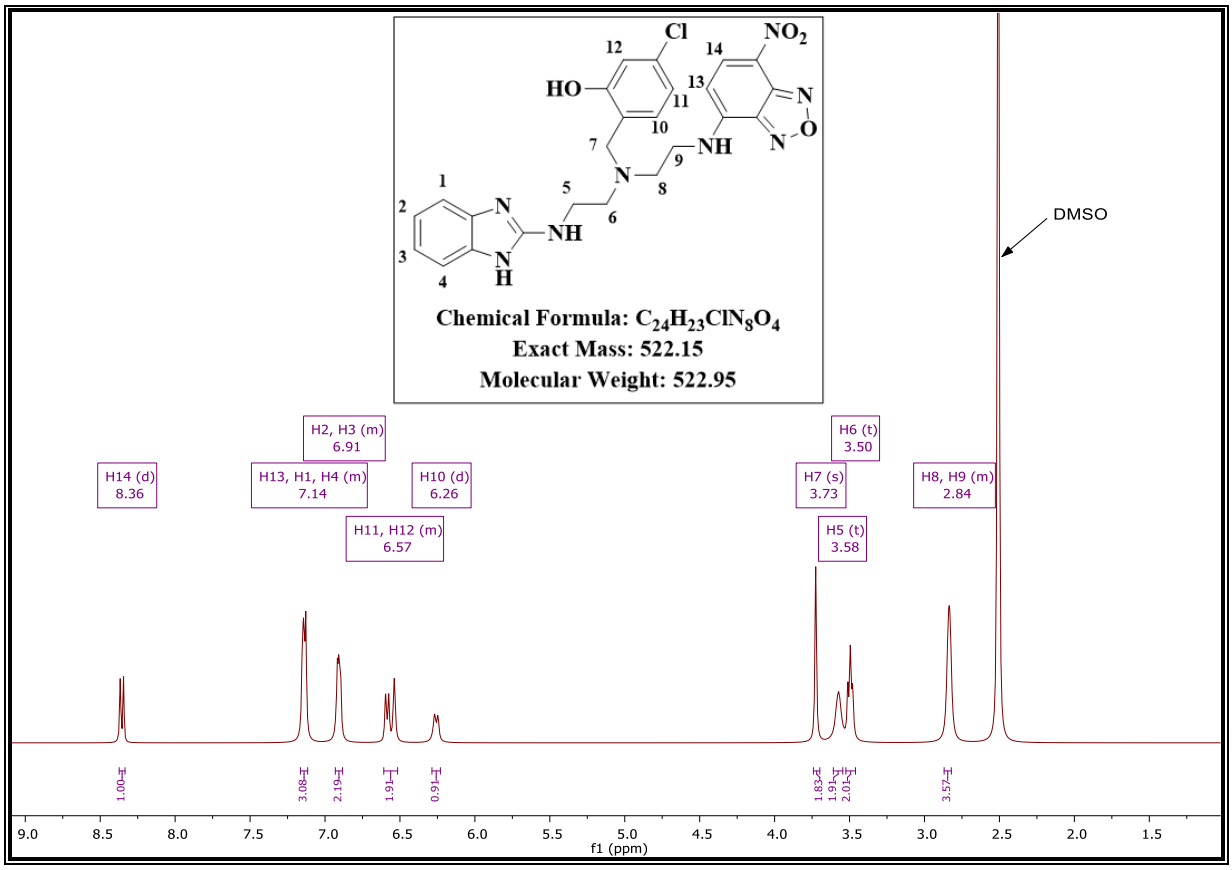

Figure 2.22: ^{1}H NMR spectrum of fluorescent probe **1.3-NBD**.

On the other hand, the synthetic protocol used in obtaining the fluorescent probe **3.14-NBD** followed an eleven-step synthetic route from commercially available 2,4-dichloro-5-nitropyridine (Scheme 2.10).

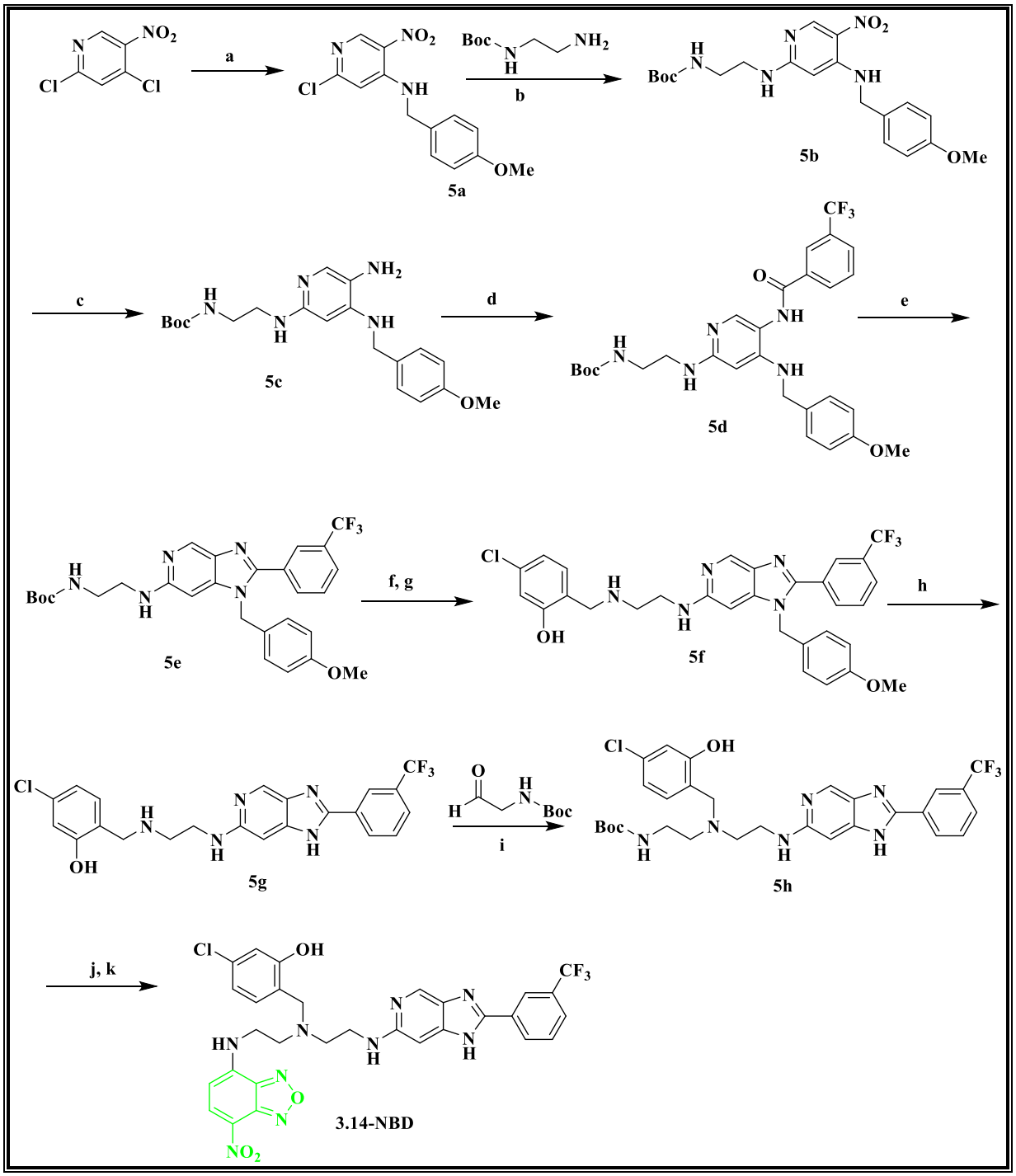

Scheme 2.10: Synthetic scheme for the synthesis of fluorescent analogue **3.14-NBD**. ***Reagents and conditions*****:** (**a**) PMB-NH_2 (1.8 eq), DIPEA (1.8 eq), THF, 0°C to 25°C, 30 min, quantitative; (**b**) N-Boc ethylenediamine (1.5 eq), Et_3N (2 eq), DMF, µW 90°C, 1hr, 75%; (**c**) Zn/AcOH, DCM, 25°C, 30 min (**d**) 3-trifluoromethyl benzoic acid (1.3 eq), EDCI.HCl (1.5 eq), DMAP (0.1eq), DCM, 25°C, 12hrs; (**e**) 2M NaOH, EtOH, 80°C, 16hrs, 65%; (**f**) 4N HCl/Dioxane; (**g**) 4-chloro-2-hydroxybenzaldehyde, $NaBH_4$, 25°C, 6hrs, 65%; (**h**) TFA, 100°C, 12h, 75%; (**i**) $NaBH_3CN$, cat. AcOH, MeOH, 80°C, 16hrs, 70%; (**j**) 4N HCl/Dioxane, 25°C; (**k**) NBD-Chloride, $NaHCO_3$, EtOAc, 60°C, 24hrs, 50%.

A nucleophilic substitution was first performed to introduce a *para*-methoxybenzyl (PMB) amino-protecting group to form the 2-chloro-N-(4-methoxybenzyl)-5-nitropyridin-4-amine intermediate **5a** in quantitative yield. The 2-chloro-N-(4-methoxybenzyl)-5-nitropyridin-4-amine intermediate was subjected to a second nucleophilic substitution under microwave irradiation with *N*-boc ethylenediamine in the presence of triethylamine and *N*, *N*-dimethylformamide (DMF) to produce intermediate **5b**. The nitro group was then reduced with Zn in acetic acid to deliver the corresponding amine intermediate **5c**. This intermediate was reacted with 3-trifluoromethyl benzoic acid in the presence of 1-ethyl-3-(3-dimethylaminopropyl)carbodiimide, hydrochloride (EDCI.HCl), and a catalytic amount of 4-dimethylaminopyridine (DMAP) in dichloromethane (DCM) to produce the amide intermediate **5d**. At this stage, the imidazole ring was allowed to form by heating in 2M aqueous NaOH and absolute ethanol at 80 °C to yield intermediate **5e**. The cyclized intermediate was subjected to boc-deprotection followed by reductive amination with 4-chloro-2-hydroxybenzaldehyde in the presence of sodium borohydride to deliver the intermediate **5f**. The PMB group was then removed using neat trifluoroacetic acid (TFA), resulting in intermediate **5g**. Reductive amination of N-boc glycinal was then carried out in sodium cyanoborohydride to deliver the penultimate intermediate **5h**. Finally, removing the boc group, followed by a nucleophilic substitution reaction with NBD-chloride, yielded the target fluorescent probe **3.14-NBD**. ^{1}H NMR (Figure 2.23) confirmed the formation of this fluorescent probe of interest.

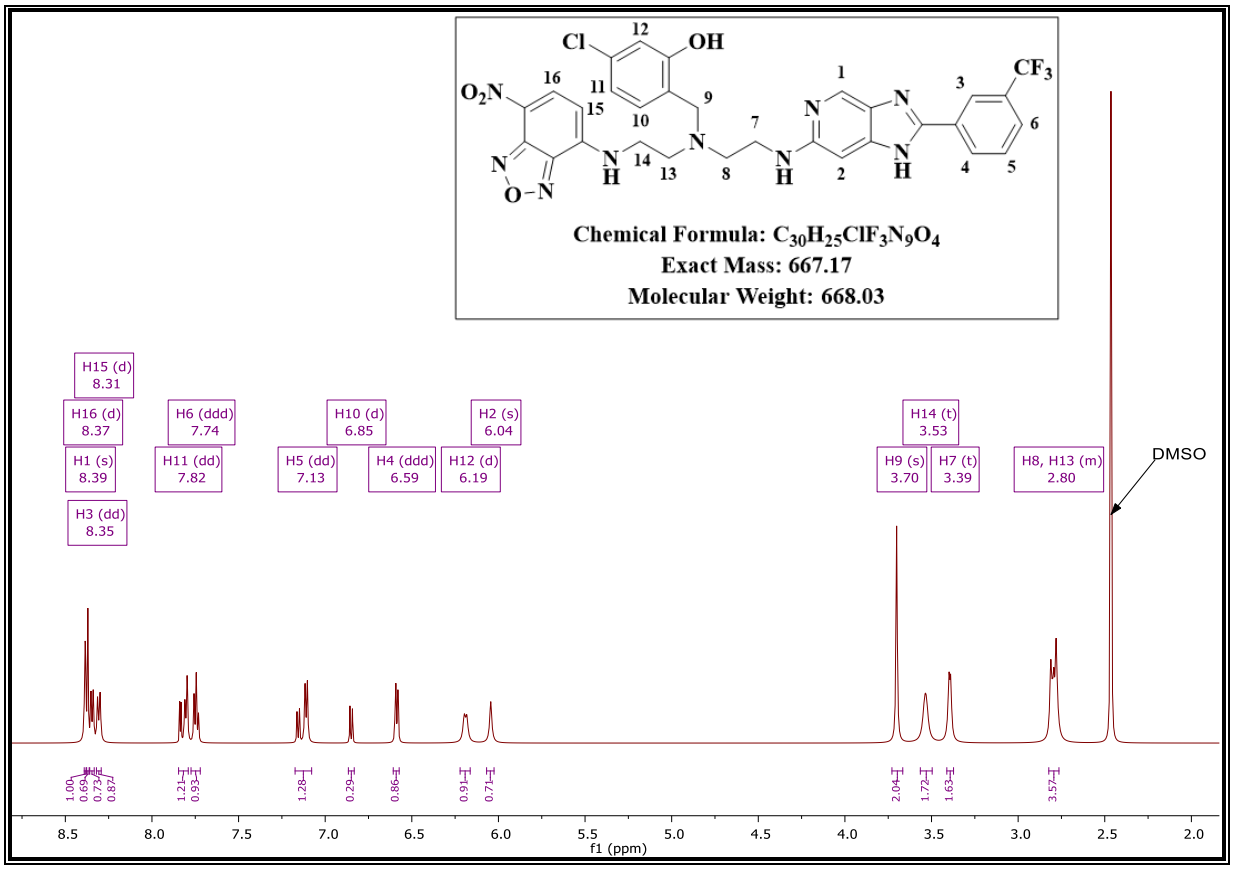

Figure 2.23: ^{1}H NMR spectrum of fluorescent probe **3.14-NBD**.

2.5 Concluding Remarks

Overall, the rationale for designing the synthesized target compounds has been outlined and selected relevant mechanisms for the various reactions performed have also been described. The target compounds were fully characterized by spectroscopic techniques such as NMR and chromatographic methods such as the HPLC-MS. It was ensured that the target compounds were of acceptable purity (≥ 95%) for biological evaluation.

2.6 References

(1) Ramachandran, S.; Hameed P, S.; Srivastava, A.; Shanbhag, G.; Morayya, S.; Rautela, N.; Awasthy, D.; Kavanagh, S.; Bharath, S.; Reddy, J.; et al. N-Aryl-2-Aminobenzimidazoles: Novel, Efficacious, Antimalarial Lead Compounds. *J. Med. Chem.* **2014**, *57* (15), 6642–6652. https://doi.org/10.1021/jm500715u.

(2) Chong, C. R.; Chen, X.; Shi, L.; Liu, J. O.; Sullivan, D. J. A Clinical Drug Library Screen Identifies Astemizole as an Antimalarial Agent. *Nat. Chem. Biol.* **2006**, *2* (8), 415–416. https://doi.org/10.1038/nchembio806.

(3) Roman, G.; Crandall, I. E.; Szarek, W. A. Synthesis and Anti- Plasmodium Activity of Benzimidazole Analogues Structurally Related to Astemizole. *ChemMedChem* **2013**, *8* (11), 1795–1804. https://doi.org/10.1002/cmdc.201300172.

(4) Keurulainen, L.; Vahermo, M.; Puente-Felipe, M.; Sandoval-Izquierdo, E.; Crespo-Fernández, B.; Guijarro-López, L.; Huertas-Valentín, L.; de las Heras-Dueña, L.; Leino, T. O.; Siiskonen, A.; et al. A Developability-Focused Optimization Approach Allows Identification of in Vivo Fast-Acting Antimalarials: N -[3-[(Benzimidazol-2-Yl)Amino]Propyl]Amides. *J. Med. Chem.* **2015**, *58* (11), 4573–4580. https://doi.org/10.1021/acs.jmedchem.5b00114.

(5) Craig, P. N. Interdependence between Physical Parameters and Selection of Substituent Groups for Correlation Studies. *J. Med. Chem.* **1971**, *14* (8), 680–684. https://doi.org/10.1021/jm00290a004.

(6) Ritchie, T. J.; Ertl, P.; Lewis, R. The Graphical Representation of ADME-Related Molecule Properties for Medicinal Chemists. *Drug Discov. Today* **2011**, *16* (1–2), 65–72. https://doi.org/10.1016/j.drudis.2010.11.002.

(7) Ntuli, N. A. New Aminoquinoline Antimalarial Cysteine Protease Inhibitors Based on the Isatin Natural Product Scaffold, University of Cape Town, South Africa, 2005.

(8) Pan, W.; Hu, K.; Bai, P.; Yu, L.; Ma, Q.; Li, T.; Zhang, X.; Chen, C.; Peng, K.; Liu, W.; et al. Design, Synthesis and Evaluation of Novel Ferulic Acid-Memoquin Hybrids as Potential Multifunctional Agents for the Treatment of Alzheimer's Disease. *Bioorg. Med. Chem. Lett.* **2016**, *26* (10), 2539–2543. https://doi.org/10.1016/j.bmcl.2016.03.086.

(9) Ishikawa, M.; Kubota, D.; Yamamoto, M.; Kuroda, C.; Iguchi, M.; Koyanagi, A.; Murakami, S.; Ajito, K. Tricyclic Pharmacophore-Based Molecules as Novel Integrin Avβ3 Antagonists. Part 2: Synthesis of Potent Avβ3/AIIbβ3 Dual Antagonists. *Bioorg. Med. Chem.* **2006**, *14* (7), 2109–2130. https://doi.org/10.1016/j.bmc.2005.10.061.

(10) Borch, R. F.; Bernstein, M. D.; Durst, H. D. Cyanohydridoborate Anion as a Selective Reducing Agent. *J. Am. Chem. Soc.* **1971**, *93* (12), 2897–2904. https://doi.org/10.1021/ja00741a013.

(11) Tadanier, J.; Hallas, R.; Martin, J. R.; Stanaszek, R. S. Observations Relevant to the Mechanism of the Reductive Aminations of Ketones with Sodium Cyanoborohydride and Ammonium Acetate. *Tetrahedron* **1981**, *37* (7), 1309–1316. https://doi.org/10.1016/S0040-4020(01)92446-9.

(12) 1H NMR Properties of Piperidine Derivatives; 1991; pp 34–87. https://doi.org/10.1016/B978-0-444-88348-3.50007-6.

(13) Cummings, T. F.; Shelton, J. R. Mannich Reaction Mechanisms. *J. Org. Chem.* **1960**, *25* (3), 419–423. https://doi.org/10.1021/jo01073a029.

(14) Nchinda, A. T.; Le Manach, C.; Paquet, T.; Gonzàlez Cabrera, D.; Wicht, K. J.; Brunschwig, C.; Njoroge, M.; Abay, E.; Taylor, D.; Lawrence, N.; et al. Identification of Fast-Acting 2,6-Disubstituted Imidazopyridines That Are Efficacious in the in Vivo Humanized Plasmodium Falciparum NODscidIL2Rγ Null Mouse Model of Malaria. *J. Med. Chem.* **2018**, *61* (9), 4213–4227. https://doi.org/10.1021/acs.jmedchem.8b00382.

(15) Le Manach, C.; Paquet, T.; Wicht, K.; Nchinda, A. T.; Brunschwig, C.; Njoroge, M.; Gibhard, L.; Taylor, D.; Lawrence, N.; Wittlin, S.; et al. Antimalarial Lead-Optimization Studies on a 2,6-Imidazopyridine Series within a Constrained Chemical Space To Circumvent Atypical Dose-Response Curves against Multidrug-Resistant Parasite Strains. *J. Med. Chem.* **2018**, *61* (20), 9371–9385. https://doi.org/10.1021/acs.jmedchem.8b01333.

(16) Montalbetti, C. A. G. N.; Falque, V. Amide Bond Formation and Peptide Coupling. *Tetrahedron* **2005**, *61* (46), 10827–10852. https://doi.org/10.1016/j.tet.2005.08.031.

(17) Rebek, J.; Feitler, D. Improved Method for the Study of Reaction Intermediates. Mechanism of Peptide Synthesis Mediated by Carbodiimides. *J. Am. Chem. Soc.* **1973**,

95 (12), 4052–4053. https://doi.org/10.1021/ja00793a039.

(18) Rebek, J.; Feitler, D. Mechanism of the Carbodiimide Reaction. II. Peptide Synthesis on the Solid Phase. *J. Am. Chem. Soc.* **1974**, *96* (5), 1606–1607. https://doi.org/10.1021/ja00812a061.

CHAPTER 3

BIOLOGICAL EVALUATION

3.1 Chapter Overview

This chapter discusses the various biological studies conducted on the synthesized target compounds. These studies were undertaken following the screening cascade depicted in Figure 3.1. The cascade portrays the criteria that informed the progression of compounds from one biological assay to the other.

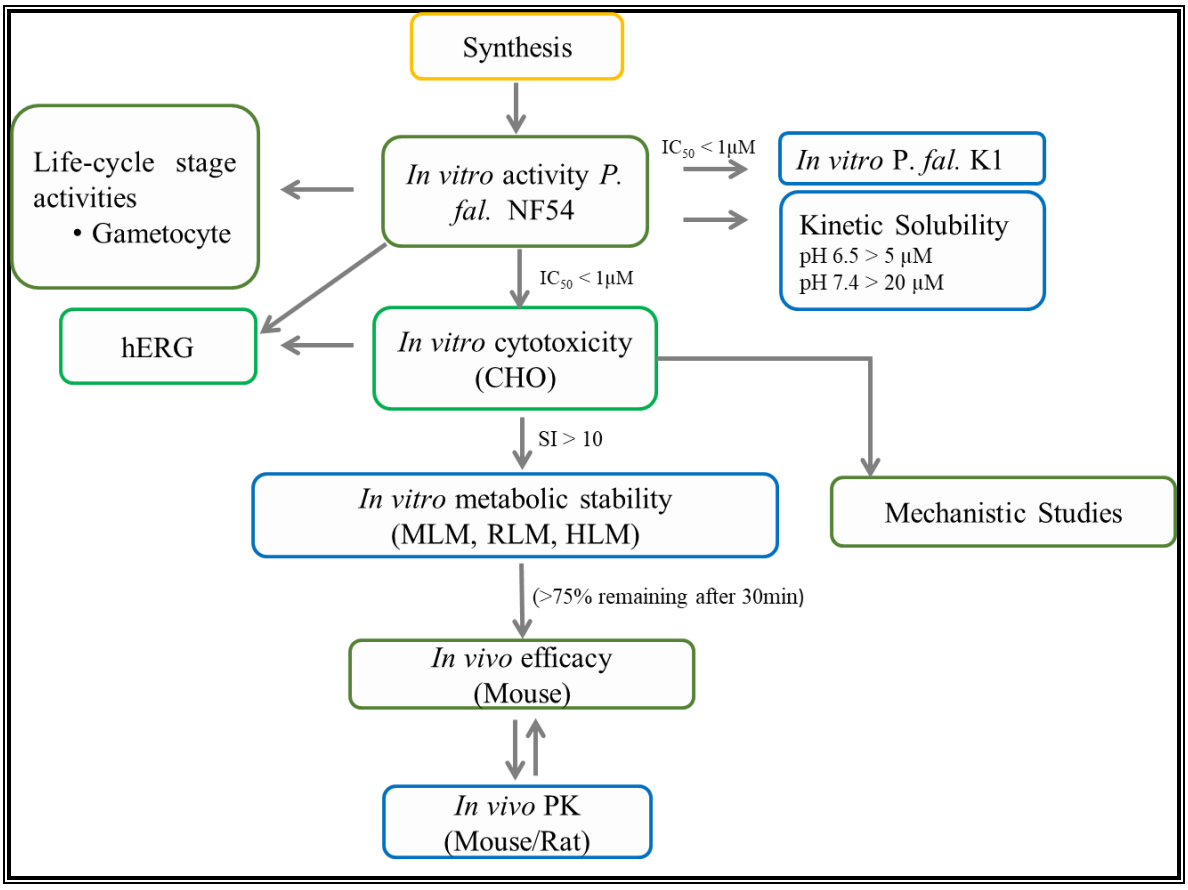

Figure 3.1: The screening cascade adapted for the biological evaluation of target compounds.

This chapter begins with a description of the *in vitro* asexual blood-stage antiplasmodium activity of all the benzimidazole analogues, followed by a discussion of the *in vitro* gametocytocidal activity and cytotoxicity of selected analogues. The hERG inhibition results of the astemizole-based analogues and microsomal metabolic stability studies on selected benzimidazole analogues are also described. For the imidazopyridine analogues, *in vitro* antiplasmodium activity, cytotoxicity and metabolic stability studies are outlined.

3.2 Benzimidazoles

3.2.1 *In vitro* Asexual Blood Stage Antiplasmodium Activity

All target compounds, once synthesized, were primarily evaluated *in vitro* for their antiplasmodium activity against the drug-sensitive strain (NF54) of *P. falciparum*. Compounds that displayed IC_{50} < 1 µM were further evaluated against the multidrug-resistant strain (K1) of the parasite. The experiments were carried out either at the Drug Discovery and Development (H3D) Centre housed within the Division of Clinical Pharmacology, Department of Medicine, University of Cape Town (UCT) or at the Swiss Tropical and Public Health Institute (STPH), University of Basel, Switzerland, following established protocols.

Experiments performed at UCT involved the measurement of the parasites' lactate dehydrogenase (pLDH) activity. Lactate dehydrogenase plays a significant role in the metabolism of glucose in the human malaria parasite. In the final step of anaerobic respiration, the glycolytic redox enzyme LDH converts lactate to pyruvate and NAD^+, reduced to NADH and is necessary for ATP production.[1,2] Decreased metabolic activities, including glycolysis, are reflected in diminished LDH function when parasite growth is inhibited. The NADH produced in this reaction can then react with a probe substrate, creating a colour that is detected and quantified spectrophotometrically.[3–5] The spectrophotometric readouts are converted to non-linear dose-response curves from which the half-maximum inhibitory concentration (IC_{50}) is determined.

The modified [^{3}H]-hypoxanthine incorporation assay[6–8] was employed for *in vitro* antiplasmodium studies carried out at the Swiss TPH. This assay takes advantage of the *Plasmodium* parasites' inability to synthesize bases such as purine *de novo*. Thus, the parasites scavenge for these bases through a process known as the salvage pathway of DNA synthesis.[9–11] When radiolabelled purine, hypoxanthine, is supplemented in the parasite cultures, proliferating parasites take up the hypoxanthine, allowing growth to be quantified through radioactivity by a scintillating counter.[8] Both assay methods are described in detail in the experimental chapter 7, sections 7.3.1.1 and 7.3.1.2 of this thesis.

3.2.1.1 SAR of 1*H*-benzimidazole Analogues

Structural modifications on the benzimidazole resulted in compounds that may be classified broadly into either the 1*H*-benzimidazole or the *N*-benzyl benzimidazole (astemizole-based) series as earlier described in Chapter 2. In the 1*H*-benzimidazole series, the benzimidazole moiety is linked to a hydroxyphenyl ring through an N^1-ethylethylene amine linker. Both

lipophilic and electronic features of substitutions around the hydroxyphenyl ring influenced the observed antiplasmodium activity. The *in vitro* antiplasmodium activities (IC_{50} values) displayed by this series of target compounds are outlined in Table 3.1 below.

Table 3.1: *In vitro* antiplasmodium activities of 1*H*-benzimidazole analogues.

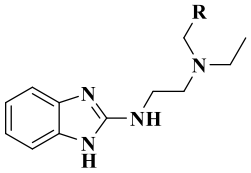

Compound Code	R	*In vitro* antiplasmodium activity IC_{50} (µM)[a]		Resistance index (RI)[b]
		*Pf*NF54 strain	*Pf*K1 strain	
1.1	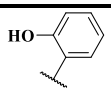	0.474	2.658	6
1.2	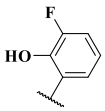	0.299	1.487	5
1.3	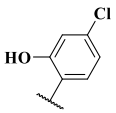	0.079	0.335	4
1.4	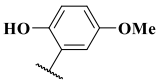	0.320	3.042	10
1.5	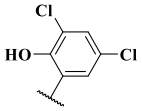	0.400	1.397	3
1.6	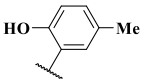	0.408	2.425	6
1.7	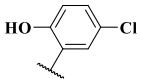	0.110	0.762	7
1.8	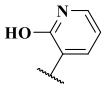	>10	>10	>1
1.9	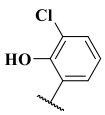	0.521	1.252	2
1.10	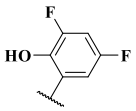	0.222	0.952	4

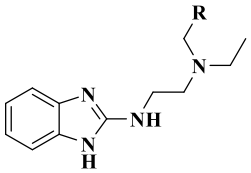

Compound Code	R	*In vitro* antiplasmodium activity IC_{50} (µM)[a]		Resistance index (RI)[b]
		***Pf*NF54 strain**	***Pf*K1 strain**	
1.11	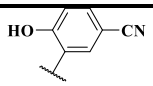	0.968	>10	10
1.12		3.604	ND	ND
Chloroquine	-	0.012	0.431	36
Artesunate	-	0.007	0.0029	0

[a] Determined from n ≥ 3 independent [^{3}H]-hypoxanthine incorporation experiments with multidrug-resistant (K1) and chloroquine-sensitive (NF54) strains of *P. falciparum*.

[b] RI (resistance index) =IC_{50} *Pf*K1/ IC_{50} *Pf*NF54

All the target compounds in this series except **1.8** and **1.12** exhibited sub-micromolar potencies against the chloroquine-sensitive NF54 strain of *P. falciparum*, with IC_{50} values between 0.079 µM and 0.968 µM. Against the multidrug-resistant strain of *P. falciparum* (K1), these compounds displayed between 4 and 10-fold less activity, an observation that may suggest the possibility of cross-resistance with drugs like chloroquine. Considering structure-activity relationships, replacing the phenyl ring with pyridine as represented in compound **1.8** was detrimental to the potency. Overall, the most active compounds were those with electron-withdrawing and lipophilic phenyl substituents with a *meta* substituted chloro, compound **1.3** (IC_{50} = 0.079 µM), portraying the best activity. A di-substituted chloro analogue (compound **1.9,** IC_{50} = 0.521 µM) resulted in a decrease in potency compared to the mono-substituted chloro analogues **1.3** and **1.7** (IC_{50} =0.11 µM). Conversely, a di-substituted fluoro analogue (compound **1.10**, IC_{50} = 0.222 µM) was well tolerated. Removal of the hydroxyl substituent as in compound **1.12** (IC_{50} = 3.604 µM) resulted in a loss of potency, indicating the importance of the hydroxyl substituent (an IMHB motif) in these analogues. To assess the potential of these compounds to manifest cross-resistance with chloroquine, the fold change in the IC_{50} between drug-sensitive and drug-resistant strains was determined in the form of the resistance index (RI), calculated as the ratio of IC_{50}*Pf*K1 to IC_{50}*Pf*NF54. The results suggest that the parasites'

resistant to chloroquine are cross-resistant to these compounds, as shown by the great shift in potency between the drug-sensitive and drug-resistant parasite strains.

3.2.1.2 SAR of *N*-benzyl benzimidazole (Astemizole-based) Analogues

All analogues based on the *N*-benzyl benzimidazole (astemizole) scaffold exhibited sub-micromolar activity against the chloroquine-sensitive strain of *P.falciparum*, except compounds **2.8** (IC_{50} *Pf*NF54 = 2.285 µM) and **2.11** (IC_{50} *Pf*NF54 = 2.324 µM). Table 3.2 summarizes all antiplasmodium activity results for this series of analogues. Activity trends were generally maintained across both strains of the parasite. Thus, potent compounds retained their potency while inactive compounds in the drug-sensitive (NF54) strain also exhibited inactivity in the drug-resistant (K1) strain. Compound **2.3** displayed the highest potency (IC_{50} *Pf*NF54 = 0.029 µM) within this series. Replacing the chloro group with carboxylic acid (analogue **2.19**) or an amide (analogue **2.21**) led to a decrease in potency. Meanwhile, the fluoro (**2.13**), cyano (**2.18**) and the ester (**2.20**) analogues had potencies quite comparable to **2.3**.

Table 3.2: *In vitro* antiplasmodium activities of *N*-benzyl benzimidazole analogues.

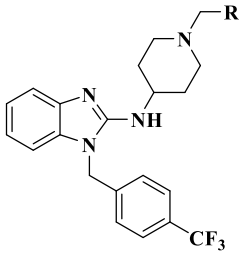

Compound Code	R	*In vitro* antiplasmodium activity IC_{50} (µM)[a]		Resistance index (RI)[b]
		*Pf*NF54 strain	*Pf*K1 strain	
2.1	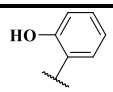	0.095	0.267	3
2.2	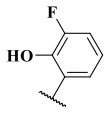	0.121	0.450	4
2.3	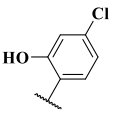	0.029	0.117	4

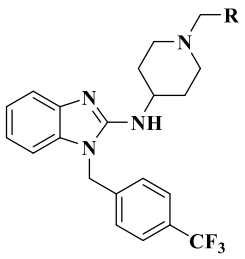

Compound Code	R	*In vitro* antiplasmodium activity IC_{50} (µM)[a]		Resistance index (RI)[b]
		***Pf*NF54 strain**	***Pf*K1 strain**	
2.4	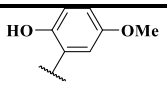	0.087	0.359	4
2.5	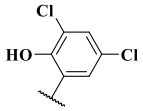	0.226	1.385	6
2.6	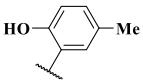	0.085	0.453	5
2.7	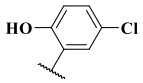	0.055	0.215	4
2.8	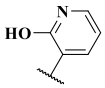	2.285	2.814	1
2.9	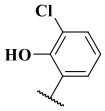	0.187	0.372	2
2.10	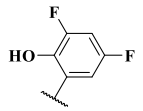	0.086	0.470	5
2.11	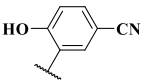	2.324	3.183	1
2.12		0.297	1.057	4
2.13	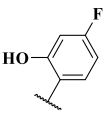	0.043	0.116	3
2.14	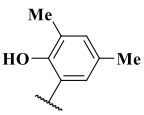	0.219	ND	ND

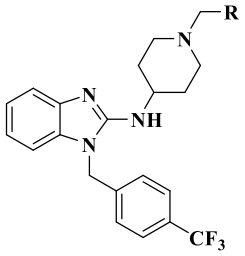

Compound Code	R	*In vitro* antiplasmodium activity IC_{50} (µM)[a]		Resistance index (RI)[b]
		***Pf*NF54 strain**	***Pf*K1 strain**	
2.15	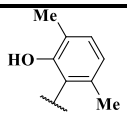	0.525	ND	ND
2.16	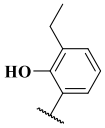	0.509	ND	ND
2.17	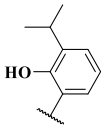	0.504	ND	ND
2.18	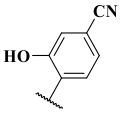	0.034	ND	ND
2.19	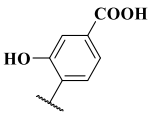	0.417	ND	ND
2.20	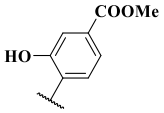	0.030	0.133	4
2.21	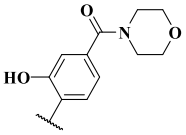	0.186	0.737	4
Chloroquine	-	0.012	0.431	36
Artesunate	-	0.007	0.0029	0

[a] Determined from n ≥ 3 independent [^{3}H]-hypoxanthine incorporation experiments with multidrug-resistant (K1) and chloroquine-sensitive (NF54) strains of *P. falciparum*.

[b] RI (resistance index) =IC_{50} *Pf*K1/ IC_{50} *Pf*NF54

ND- Not determined.

3.2.2 *In vitro* Gametocytocidal Activity

As part of the malaria eradication agenda, new TPPs for novel antimalarials have been outlined by the malaria community. One of these is the need to deliver antimalarials that target multiple stages of the *Plasmodium* parasite development.[12,13] In conformity with this requirement, a selected number of benzimidazole analogues were evaluated *in vitro* for their transmission-blocking potential. The *in vitro* gametocytocidal activity employed both early and late-stage gametocyte assays. The luciferase reporter assay, as described by Reader *et al.*[5] was used to establish accurate, reliable and quantifiable investigations of the stage-specific activity of the compounds for the early and late gametocyte marker cell line NF54-PfS16-GFP-Luc. The compounds were evaluated against both the early and late stages of gametocyte development since each stage displays differential susceptibility to drugs.[14,15] In this assay, parasites were exposed to test compounds for 48 hours, after which luciferase activity was determined by adding luciferin substrate to the parasite lysate and then measuring the resulting bioluminescence.[5]

For the initial screen, 20 benzimidazole analogues were selected (compounds **1.1-1.7, 1.9-1.11**, **2.1-2.7** and **2.9-2.11** in Tables 3.1 and 3.2) for their percentage inhibition at two different concentrations of 1 and 5 µM. Compounds that showed good activity (>70% inhibition at 5µM and >50% inhibition at 1 µM) in the initial dual point screen were to be prioritized for a full-dose response IC_{50} determination (with n = 3 independent experiments). Those with moderate activity (>70% inhibition at 5 µM and <50% inhibition at 1 µM; <70% inhibition at 5 µM and >50% inhibition at 1 µM; 50-70% inhibition at 5 µM and <50% inhibition at 1 µM) were to be prioritized for a single IC_{50} determination (n = 1 experiment). Methylene blue (5 µM) and an internal project-specific control (MMV390048, 5 µM) were used as controls in the experiment.

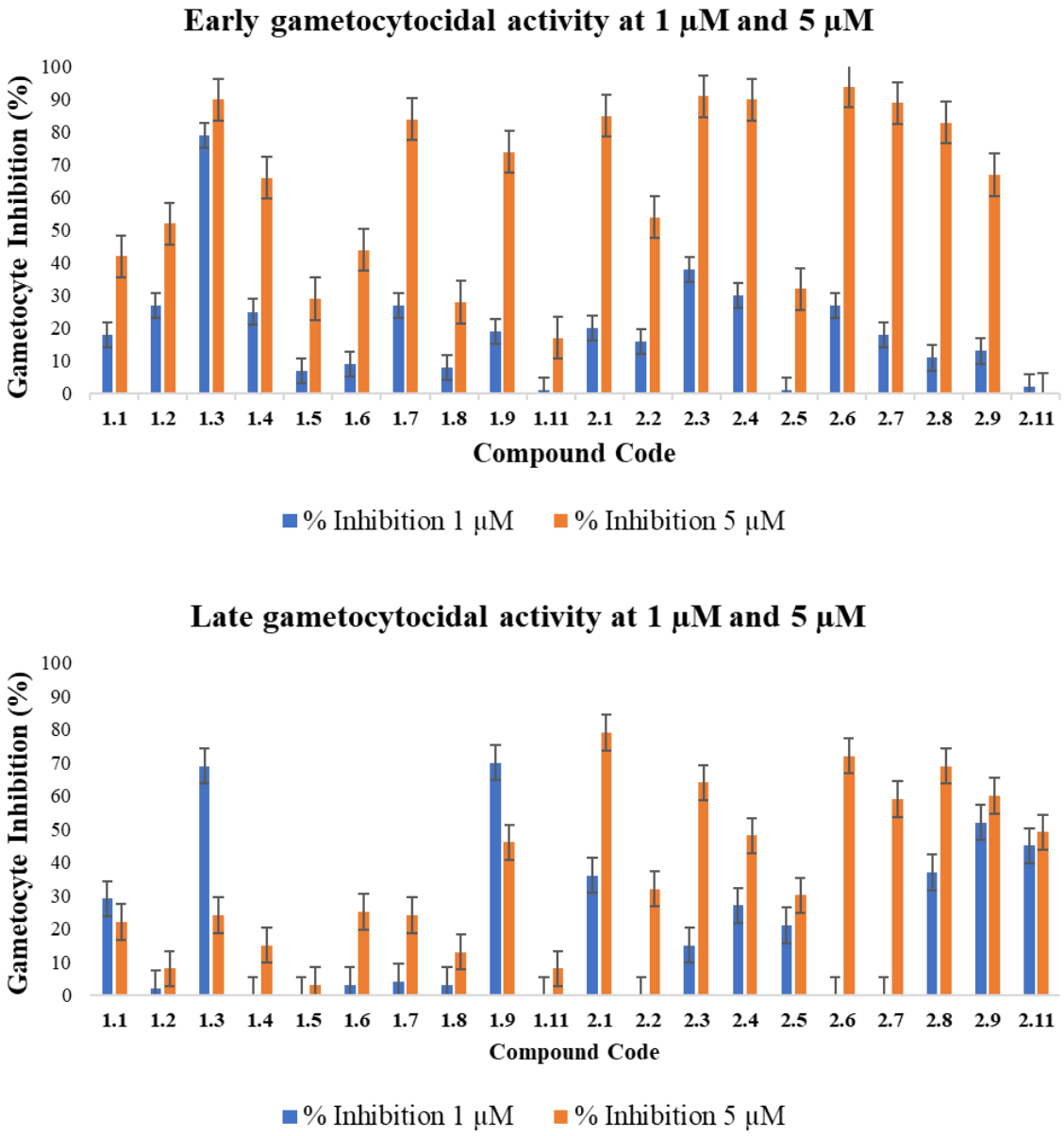

Figure 3.2: Gametocytocidal activity of selected benzimidazole compounds.

Compound **1.3** (79% and 90% inhibition at 1 µM and 5 µM, respectively) was the only compound that exhibited good activity in the primary dual point screen against the early gametocytes. The inhibition activity of **1.3** and its regioisomer **1.9** against the late gametocytes was moderate (69% and 70% respectively) at 1 µM and minimal (24% and 46% respectively) at 5 µM. When evaluated for dose-response, compound **1.3** displayed sub-micromolar potency (IC_{50} = 0.382 µM) against early-stage gametocytes. Overall, the benzimidazole analogues displayed poor activity against the gametocyte stage of the *Plasmodium* parasite in comparison to the asexual blood stage.

3.2.3 *In vitro* Mammalian Cytotoxicity

Compounds exhibiting sub-micromolar (IC_{50} <1 µM) *in vitro* asexual blood-stage potency were evaluated for *in vitro* cytotoxicity against the mammalian Chinese Hamster Ovary (CHO) cell line to determine their selectivity for antiplasmodium activity. The MTT [3-(4,5-dimethylthiazol-2-yl)-2,5-diphenyltetrazolium bromide] assay[16] which calorimetrically measures cellular growth and survival, was used to assess the cytotoxicity of the compounds. The MTT assay works based on converting the water-soluble tetrazolium dye to the insoluble coloured formazan by redox enzymes present in living cells. The formazan is then solubilized, and its amount is spectrophotometrically detected. Dose-response curves, which enabled the determination of IC_{50} values (Tables 3.3 and 3.4), were generated using triplicate serial dilutions of six concentrations. The reference drug used in this assay was emetine. The Selectivity Index (SI), which represents the ratio of the IC_{50} of the compound in *Plasmodium* parasites to that in the CHO cells, was derived. A higher ratio signifies that the compound is more selective for the *Plasmodium* parasite than the healthy cells. In the context of the screening cascade used for this work, a selectivity index of 10 was the cut-off.

Table 3.3: *In vitro* mammalian cytotoxicity and BHIA of 1*H*-benzimidazole analogues.

Compound Code	Structure	*Pf*NF54 IC_{50}, µM	Cytotoxicity[c] CHO cells		BHIA[e] IC_{50}, µM
			IC_{50}, µM	SI[d]	
1.1	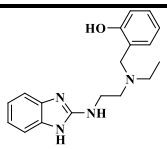	0.474	50	105	452
1.2	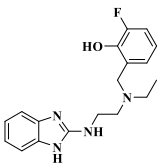	0.299	50	167	161
1.3	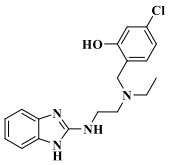	0.079	22	273	32
1.4	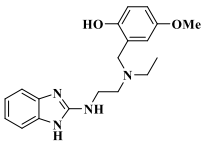	0.320	50	156	489

Compound Code	Structure	*Pf*NF54 IC_{50}, µM	Cytotoxicity[c] CHO cells		BHIA[e] IC_{50}, µM
			IC_{50}, µM	SI[d]	
1.5	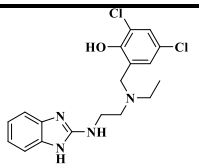	0.400	50	125	30
1.6	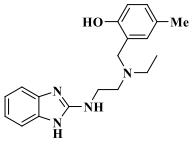	0.408	25	60	4223
1.7	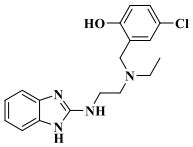	0.110	25	228	125
1.9	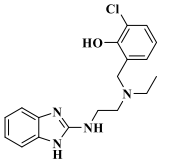	0.521	50	96	130
1.10	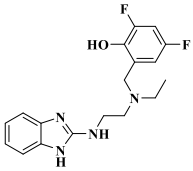	0.222	50	225	68
1.11	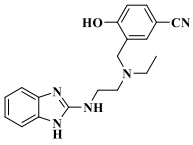	0.968	50	52	250

[c] Determined from n = 3 independent experiments; Emetine was used as a reference drug (IC_{50} = 0.059 µM)

[d] SI (selectivity index) =IC_{50} CHO/ IC_{50} *Pf*NF54. BHIA: Beta-hematin inhibition activity

[e]Mean from n = 3 independent experiments; Controls: Chloroquine (IC_{50} = 53 µM) and Amodiaquine (IC_{50} = 13 µM).

Gratifyingly, all the compounds demonstrated selectivity indices above the cut-off of 10. However, the *N*-benzyl benzimidazole analogues (Table 3.4) generally showed higher selectivity in comparison to their 1*H*-benzimidazole congeners (Table 3.3). Compound **2.3** displayed the best selectivity for *P. falciparum* against CHO cells with a selectivity index of 1500, while the di-methyl substituted analogue **2.14** had the least selectivity (SI = 20).

Table 3.4: *In vitro* mammalian cytotoxicity, BHIA and hERG inhibition of *N*-benzyl benzimidazole analogues.

Compound Code	Structure	*Pf*NF54 IC_{50}, µM	Cytotoxicity[c] CHO cells		BHIA[e] IC_{50}, µM	hERG[f] IC_{50}, µM (SD)[g]
			IC_{50}, µM	SI[d]		
2.1	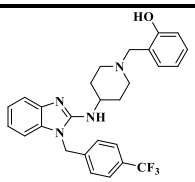	0.095	39	408	49	1.71(0.15)
2.2	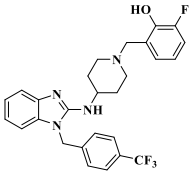	0.121	45	369	31	2.70(0.27)
2.3	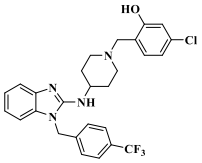	0.029	44	1500	14	2.28(0.82)
2.4	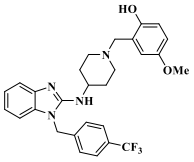	0.087	42	482	31	2.23(0.46)
2.5	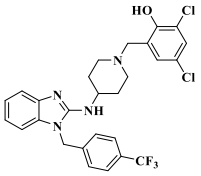	0.226	47	208	16	>10(0)
2.6	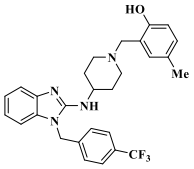	0.085	41	482	17	0.96(0.17)
2.7	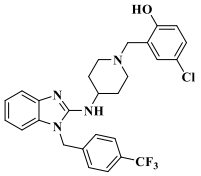	0.055	44	794	16	4.34(0.82)
2.8	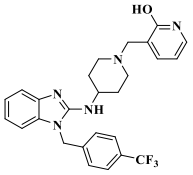	2.285	ND	ND	5830	3.85(0.76)

Compound Code	Structure	*Pf*NF54 IC_{50}, µM	Cytotoxicity[c] CHO cells		BHIA[e] IC_{50}, µM	hERG[f] IC_{50}, µM (SD)[g]
			IC_{50}, µM	SI[d]		
2.9	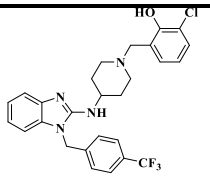	0.187	50	267	9	3.82(0.76)
2.10	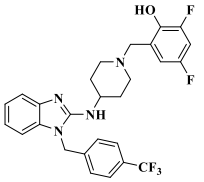	0.086	46	530	16	2.90(0.19)
2.11	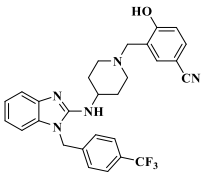	2.324	ND	ND	344	>10(0)
2.12	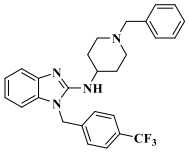	0.297	27	89	269	1.61(0.53)
2.13	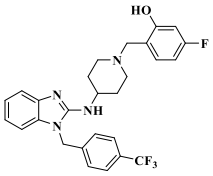	0.074	43	579	22	2.17(0.29)
2.14	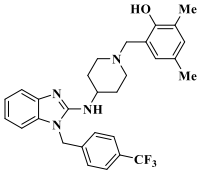	0.219	>50	20	25	9.54(2.44)
2.15	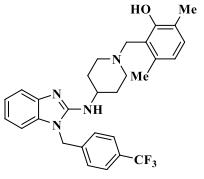	0.714	>50	>70	64	4.89(1.02)
2.16	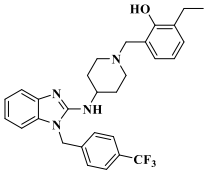	0.509	>50	>44	17	5.68(1.14)

Compound Code	Structure	*Pf*NF54 IC_{50}, µM	Cytotoxicity[c] CHO cells		BHIA[e] IC_{50}, µM	hERG[f] IC_{50}, µM (SD)[g]
			IC_{50}, µM	SI[d]		
2.17	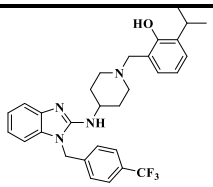	0.940	>50	>53	16	13.24(0.22)
2.18	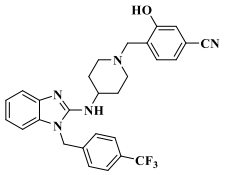	0.290	>50	>172	16	1.04(0.42)
2.19	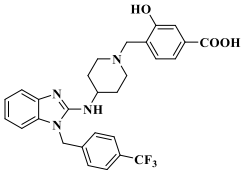	0.809	31	39	46	2.35(0.25)
2.20	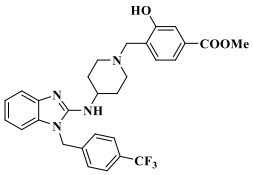	0.045	45	994	16	4.93(1.34)
2.21	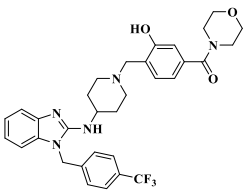	0.250	18	74	242	1.33(0.19)

[c] Determined from n = 3 independent experiments; Emetine was used as a reference drug (IC_{50} = 0.059 µM)

[d] SI (selectivity index) =IC_{50} CHO/ IC_{50} *Pf*NF54.

[e]Mean from n = 3 independent experiments; Controls: Chloroquine (IC_{50} = 53 µM) and Amodiaquine (IC_{50} = 13 µM).

[f]Mean from n = 3 independent experiments; Verapamil was used as a positive control (IC_{50} = 0.58 ± 0.13 µM).

[g]SD = Standard deviation

3.2.4 hERG Inhibition Activity

To assess the potential risk emerging from interactions with the hERG potassium ion channel whose inhibition could lead to fatal cardiac arrhythmias, the astemizole-based analogues were profiled against this channel. It is noteworthy that astemizole was withdrawn from the market due to this liability. The hERG inhibition assay was performed by Metrion Biosciences, Cambridge, United Kingdom. The CHO cell line, which stably expresses the hERG channel on

a QPatch gigaseal automated patch clamp, was employed for the study. Compounds were screened in triplicate in dose-response mode at four concentrations for IC_{50} determination. At the highest tested concentration (10 µM), any compound with <40% hERG inhibition was assigned an arbitrary IC_{50} value of >10 µM and considered inactive. Table 3.4 summarizes the hERG inhibition results for the astemizole-based compounds, and verapamil was used as a positive reference control.

All the compounds except **2.5** and **2.11** produced >40% inhibition against the hERG ion channel at the highest test concentration with potency values ranging between 0.96 and 13.24 µM. Compound **2.6** exhibited the highest hERG potency (IC_{50} = 0.96 µM). However, di-methyl substitutions as in the case of **2.14** (IC_{50} = 9.54 µM) and **2.15** (IC_{50} = 4.89 µM) detuned hERG activity by 10-fold and 5-fold, respectively. Also, hERG activity was further significantly reduced following a *meta*-to-*para* positional change of the cyano group (IC_{50} = 1.04 µM for **2.18** and IC_{50} = >10 µM for **2.11**). In general, this series of compounds showed less potential to cause cardiotoxicity than verapamil (IC_{50} = 0.58 µM), which was used as a positive control drug in the experiment.

3.2.5 Beta-hematin Inhibition Activity (BHIA)

Assessment of the target compounds in this assay was informed by the research work conducted by Wright and co-workers.[17] In their work, they reported various types of benzimidazoles as potent inhibitors of beta-hematin formation. The beta-hematin assay is a cell-free assay that mimics the whole-cell process of hemozoin formation. The target compounds were evaluated using the Nonidet P-40 (NP-40) mediated assay previously described by Sandlin et al.[18]

In summary, stock solutions of the test compounds were made in DMSO from which serially diluted concentrations were obtained. NP-40 detergent was used as a lipid source to mediate the formation of beta-hematin in a test mixture that contained predetermined compound concentrations, HEPES buffer (pH 4.8), hematin and pyridine solution. The inhibition potency of the compounds against beta-hematin formation was assessed spectrophotometrically by measuring the absorbance of the pyridine-hematin complex formed. A higher absorbance signifies greater compound potency against beta-hematin formation. Tables 3.3 and 3.4 outlines the BHIA results of the benzimidazole target compounds.

Most of the analogues displayed good beta-hematin inhibition activity (IC_{50} <100 µM). Amongst the 1*H*-benzimidazole series (Table 3.3), only compounds **1.3** (IC_{50} = 32 µM) and

1.5 (IC_{50} = 30 µM) exhibited the greatest potencies. Meanwhile, most of the astemizole-based analogues (17 out of 21) demonstrated beta-hematin inhibition activity in the preferred range (<100 µM), with compound **2.9** (Table 3.4) being the most potent (IC_{50} = 9 µM). As previously mentioned, the beta-hematin assay is a cell-free assay in which the test compound is in direct contact with hemin while antiplasmodium evaluation is carried out in a whole cell. Hence, to establish the correlation (or lack thereof) between the ability of these compounds to inhibit the formation of beta-hematin and their antiplasmodium activities, further assays such as the cell-based heme fractionation assay are warranted.

3.2.6 Metabolic Stability Studies of Selected Benzimidazole Analogues

Hepatic metabolism is the principal mechanism for eliminating most drugs and xenobiotics, although various tissues like the kidneys, lungs, intestinal wall, skin and blood are prospective sites for metabolism.[19] Metabolic stability data enables the logical prediction of pharmacokinetics, such as bioavailability, clearance, and elimination half-life of a xenobiotic.[20] The extent of hepatic metabolism of compounds is usually studied in an *in vitro* assay in which liver microsomes are employed. The mouse liver microsomes (MLM), rat liver microsomes (RLM) and human liver microsomes (HLM) are mainly utilized to determine any interspecies disparities. These liver microsomes generally consist of membrane-bound enzymes such as the cytochrome P450 (CYP450) metabolizing enzymes that are responsible for Phase I metabolism.[21]

Conversely, the S9 fraction, which has both Phases I and II metabolizing enzymes compared to microsomes, can be used to assess metabolic stability. The cytosol, which mainly consists of soluble Phase II enzymes, can also be used. In this study, however, the single-point metabolic stability assay was employed.[22] Selected compounds were incubated with the various liver microsomes (MLM, RLM and HLM) for half an hour, after which the incubation mixture is investigated for any metabolic transformations.

Briefly, the test compounds are appropriately diluted to 0.1 µM with a phosphate buffer at pH 7.4. The microsomes are then added with the required co-factors, including NADPH, to initiate enzymatic reactions. The mixture is incubated at 37 °C for 30 minutes while shaking. The reaction is stopped by adding ice-cold acetonitrile and subsequently centrifuged to remove proteins as sediments. The supernatant is then analyzed using a liquid chromatography-mass spectrometry (LC-MS), whereby the percentage of the compound remaining is calculated. The test compound's metabolic stability is subsequently assigned based on the criteria; (i) >75% of

compound remaining for highly stable compounds, (ii) 50-74% of compound remaining for moderately stable compounds and (iii) <50% of compound remaining for unstable compounds. In this regard, selected benzimidazole analogues were evaluated for metabolic stability in mouse, rat and human liver microsomes (Table 3.5). The three different liver microsomes were employed due to specific reasons. The MLM was used in anticipation of conducting *in vivo* efficacy studies in mice models. The RLM, on the other hand, is used to conduct *in vivo* pharmacokinetic studies. Even though mice models can be used for *in vivo* pharmacokinetics, rat models are usually preferred because rats have more blood than mice. The HLM, however, was employed because the overarching goal is to obtain a pharmacologically active compound for human use.

Table 3.5: Microsomal metabolic stability of selected benzimidazole analogues.

Compound Code	Structure	% Remaining after 30 min	Projected $t_{1/2}$ (min)
		$M^h/R^i/H^j$	$M^h/R^i/H^j$
1.3	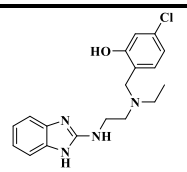	0.47/2.54/4.13	3.87/5.56/6.04
2.1	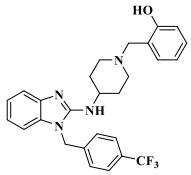	12.36/1.40/17.18	9.91/4.87/11.77
2.3	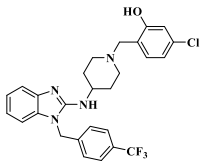	45.65/42.38/71.30	26.46/24.04/59.92
2.4	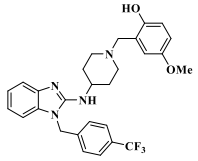	45.75/28.17/58.38	26.57/16.38/37.54
2.7	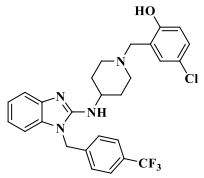	9.66/21.76/32.44	8.90/13.62/18.46

^{h}M, mouse; ^{i}R, rat; ^{j}H, human.

All the tested compounds generally displayed low microsomal metabolic stability, with compound **1.3** being the least stable. The low metabolic stability of **1.3** could be attributed to the metabolically labile *N*-ethyl moiety, which could undergo rapid deethylation by the microsomal enzymes. Metabolic stability for compounds **2.3** and **2.4** was consistent across the three species. All the astemizole analogues (**2.1**, **2.3**, **2.4** and **2.7**) were more metabolically stable in human liver microsomes than mice and rats, indicating a potential species difference in their metabolism. The low metabolic stability of these compounds, especially in MLM, suggests that they could display poor exposure and possibly low efficacy in an *in vivo* mouse model.

3.2.7 Metabolite Identification Studies on Compounds 1.3 and 2.3

Metabolite identification studies were conducted on selected compounds **1.3** and **2.3** due to their enhanced predisposition to drug-metabolizing enzymes. The studies were conducted to understand the nature of the biotransformation, identify the putative metabolites and the metabolic hotspots of the compounds to guide future optimization studies to address the metabolic instability liability.

Concisely, the compounds were incubated in mouse liver microsomes (male mouse CD1, Lot No. 1510043, XenoTech) with NADPH, magnesium chloride and potassium phosphate buffer (pH 7.4) as required co-factors to mimic the physiological conditions while shaking for 60 minutes at 37 °C. The samples were then precipitated by ice-cold acetonitrile, centrifuged and filtered for LC-MS/MS analysis. Control experiments in which microsomes, test compounds or NADPH were individually excluded were prepared as described for the test compounds. Experiments in which microsomes and test compounds were excluded aided the assessment of background instability which is likely due to compound degradation in the experimental medium. The exclusion of NADPH from the experiment, on the other hand, facilitated the assessment of non-CYP450-mediated metabolism. Tentative identification of the metabolites was deduced by comparing the product ion spectra of the $[M+H]^+$ ions of the metabolites with that of the parent compound.

The incubation of compound **1.3** in mouse liver microsomes (MLM) identified five (5) metabolites arising from hydroxylation of the aminobenzimidazole moiety (Figure 3.3). However, a subsequent hydroxylation on the 3-chlorophenol moiety yielded the major metabolite (P+32) with a product ion $[M+H]^+$ of 377. The absence of *N*-dealkylation metabolites for this compound was notable, given that this metabolic pathway was

hypothesized. Thus, this route of metabolism is either absent or is much slower than hydroxylation resulting in metabolites below the level of detection. It is also noteworthy that the formation of the metabolites required NADPH, indicating that the metabolic transformation required CYP450 catalysis.

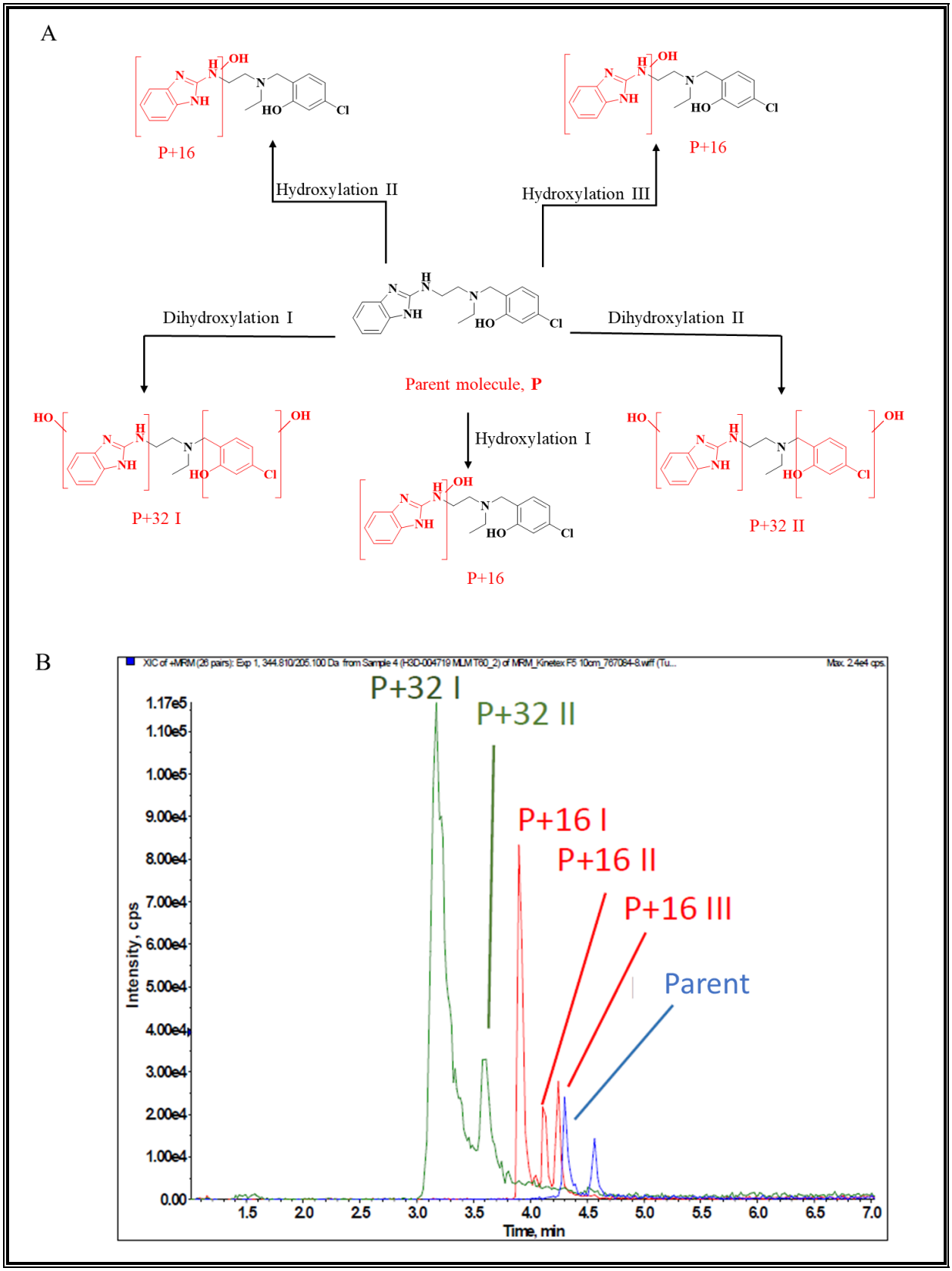

Figure 3.3: (A) Identified metabolites from the metabolism of compound **1.3** MLM; (B) XIC plot showing the relative abundance of the identified metabolites from compound **1.3**.

Three (3) metabolites were identified from the metabolism of compound **2.3** in mouse liver microsomes, with the primary metabolite (P+16) arising from the hydroxylation of the benzimidazole core (Figure 3.4). This metabolic pathway is similar to that of astemizole, as previously reported in the literature.[23]

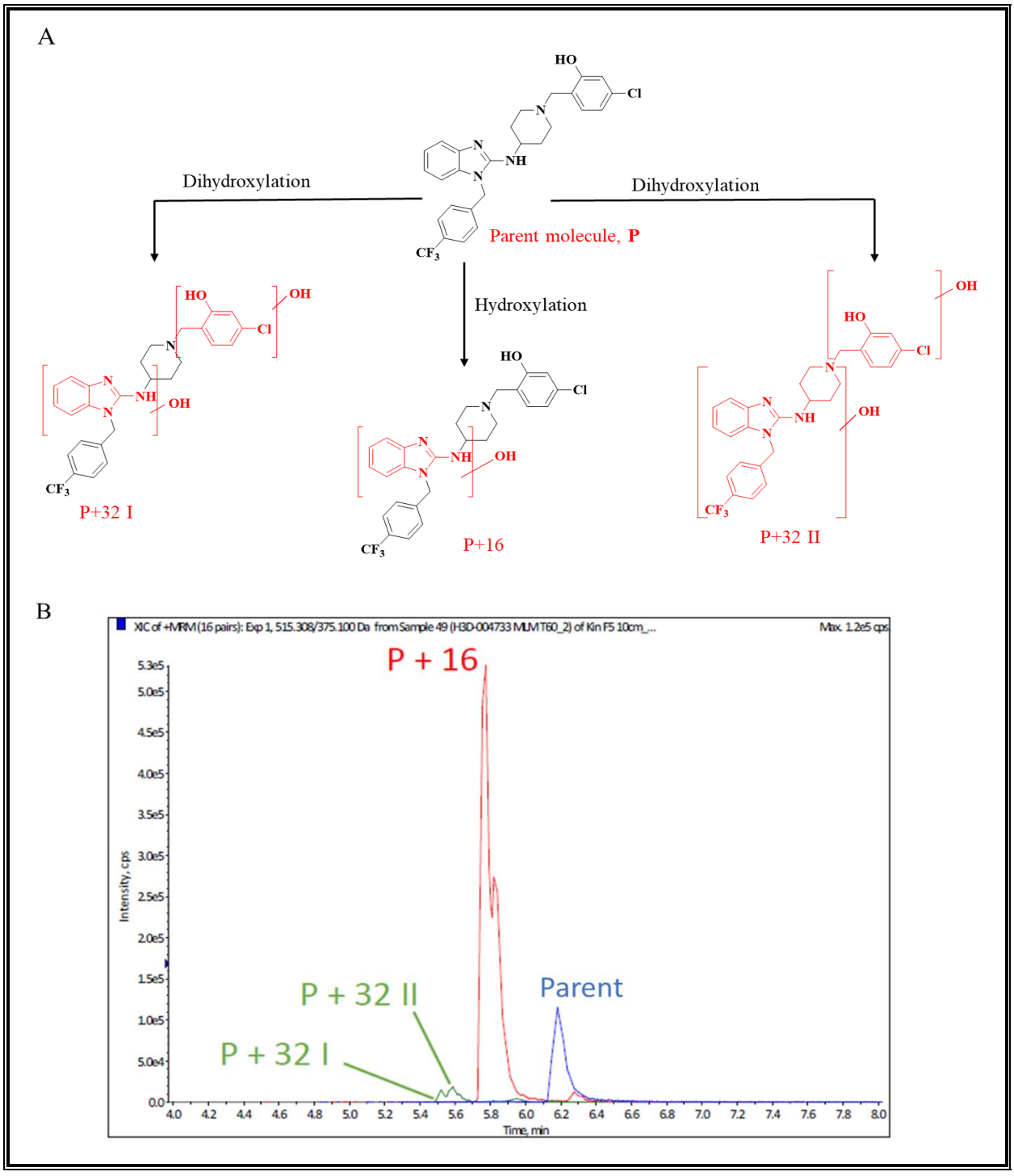

Figure 3.4: (A) Identified metabolites from the metabolism of compound **2.3** MLM; (B) XIC plot showing the relative abundance of the identified metabolites from compound **2.3**.

3.3 Imidazopyridines

3.3.1 *In vitro* Asexual Blood Stage Antiplasmodium Activity

The imidazopyridine analogues were tested for *in vitro* asexual blood-stage antiplasmodium activity against both the NF54 and K1 strains of P. *falciparum*. The lactate dehydrogenase assay was used for this class of compounds, and the SAR is discussed with respect to IC_{50} values on the chloroquine-sensitive NF54 strain.

Table 3.6: *In vitro* antiplasmodium activities of imidazopyridine analogues.

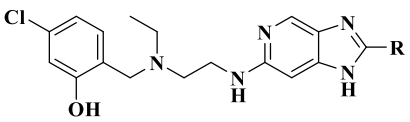

Compound Code	R	*In vitro* antiplasmodium activity IC_{50} (µM)[a]		Resistance index (RI)[b]
		*Pf*NF54 strain	*Pf*K1 strain	
3.1		0.34	1.35	4
3.2		1.67	1.61	1
3.3		2.37	4.19	2
3.4		2.53	4.11	2
3.5		0.39	0.48	1
3.6		0.49	6.00	12
3.7		1.67	1.82	1
3.8		0.56	6.00	11
3.9		0.67	6.00	9
3.10	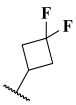	0.86	5.27	6
3.11		0.69	2.12	3

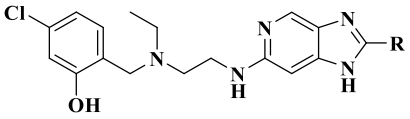

Compound Code	R	*In vitro* antiplasmodium activity IC_{50} (μM)[a]		Resistance index (RI)[b]
		*Pf*NF54 strain	*Pf*K1 strain	
3.12	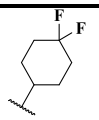	0.93	3.68	4
3.13		1.03	3.90	4
3.14	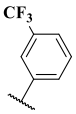	0.08	0.10	1
3.15		0.67	2.48	4
3.16	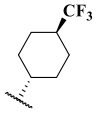	0.56	ND	ND
3.17	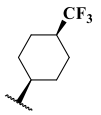	0.95	ND	ND
3.18	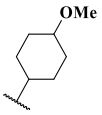	2.91	2.34	1
3.19	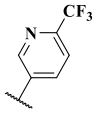	0.38	0.36	1
Chloroquine	-	0.015	0.530	35

[a] Determined from n ≥ 3 independent pLDH experiments with multidrug-resistant (K1) and chloroquine-sensitive (NF54) strains of *P. falciparum*.

[b] RI (resistance index) =IC_{50} *Pf*K1/ IC_{50} *Pf*NF54; ND- Not determined.

The SAR was explored with various aliphatic and 2 aromatic groups. The compounds with aromatic groups bearing small non-polar *meta*- or *para*- electron-withdrawing substituents displayed better antiplasmodium potency, with compound **3.14** (IC_{50} = 0.08 μM) having the highest potency. Incorporation of heteroatoms in the saturated cyclic substituents as exemplified in compounds **3.2** (IC_{50} = 1.67 μM), **3.3** (IC_{50} = 2.37 μM) and **3.13** (IC_{50} = 1.03

μM) was detrimental to antiplasmodium activity. Electron-withdrawing substituents such as a fluoro (-F) or a trifluoromethyl (-CF_3) on the saturated rings also led to the loss of antiplasmodium activity in comparison to their unsubstituted congeners. Electron-releasing groups such as methyl (-CH_3), on the other hand, were more tolerable. Additionally, the results suggest that parasites that are resistant to chloroquine are cross-resistant to the imidazopyridine analogues as indicated by the IC_{50} potency shifts (resistance indices) between the sensitive and resistant strains of the parasite.

3.3.2 *In vitro* Mammalian Cytotoxicity

The cytotoxicity of the imidazopyridine analogues was determined against the Chinese Hamster Ovary (CHO) cell line using the MTT assay. All the compounds showed a favorable cytotoxicity profile (Table 3.7) on account of their selectivity indices (SI > 10), with compound **3.14** (SI = 466) exhibiting the highest SI.

Table 3.7: *In vitro* mammalian cytotoxicity and BHIA results for imidazopyridine analogues.

Compound Code	Structure	*Pf*NF54 IC_{50}, μM	BHIA[f] IC_{50}, μM	Cytotoxicity[c] CHO cells	
				IC_{50}, μM	SI[d]
3.1	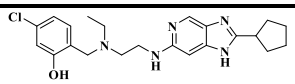	0.34	18	27	80
3.2	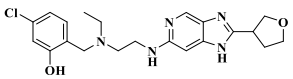	1.67	225	>50	>30
3.3	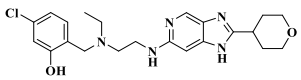	2.37	722	>50	>21
3.4	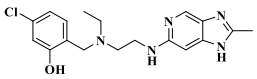	2.53	257	>50	>20
3.5	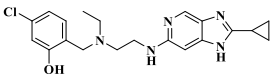	0.39	16	46	119
3.6	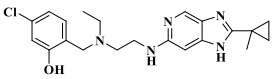	0.49	33	>50	>102
3.7	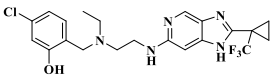	1.67	275	>50	>30
3.8	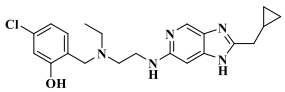	0.56	444	>50	>89

Compound Code	Structure	*Pf*NF54 IC_{50}, µM	BHIA[f] IC_{50}, µM	Cytotoxicity[c] CHO cells	
				IC_{50}, µM	SI[d]
3.9	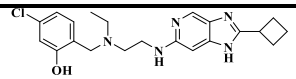	0.67	128	>50	>75
3.10	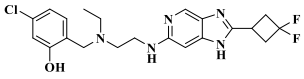	0.86	76	>50	>58
3.11	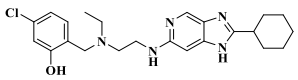	0.69	80	>50	>73
3.12	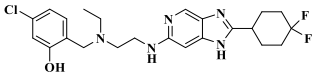	1.03	31	>50	>49
3.13	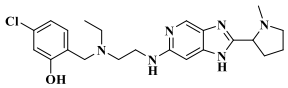	1.03	285	>50	>49
3.14	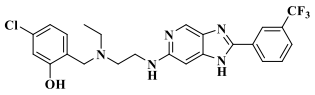	0.08	9	37	466
3.15	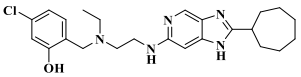	0.67	137	50	75
3.16	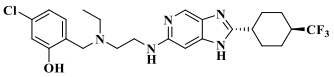	0.56	127	>50	>89
3.17	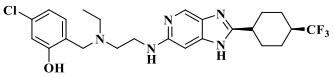	0.95	239	49	52
3.18	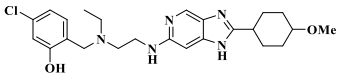	2.91	18	>50	>17
3.19	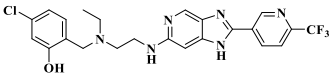	0.38	65	>50	>132

[c] Determined from n = 3 independent experiments; Emetine was used as a reference drug (IC_{50} = 0.059 µM)

[d] SI (selectivity index) =IC_{50} CHO/ IC_{50} *Pf*NF54.

[f]Mean from n = 3 independent experiments; Controls: Chloroquine (IC_{50} = 32 µM) and Amodiaquine (IC_{50} = 5 µM).

3.3.3 Beta-hematin Inhibition Activity

The potential of the imidazopyridine analogues to inhibit hemozoin formation was assessed *in vitro* by inquiring about their ability to inhibit the formation of beta-hematin (Table 3.7). Literature precedence[24,25] informed the investigation of the analogues in this assay. Using the discriminatory cut-off of < 100 µM, only nine compounds: **3.1** (18 µM), **3.5** (16 µM), **3.6** (33 µM), **3.10** (76 µM), **3.11** (80 µM), **3.12** (31 µM), **3.14** (9 µM), **3.18** (18 µM) and **3.19** (65 µM)

exhibited beta-hematin activity in the preferred range, with compound **3.14** showing the greatest potency. However, the cellular heme fractionation assay will be necessary to establish these analogues as hemozoin inhibitors confidently.

3.3.4 Metabolic Stability Studies of Selected Imidazopyridine Analogues

Selected imidazopyridine analogues exhibiting submicromolar *in vitro* asexual blood-stage antiplasmodium activity (IC_{50} < 1 µM), suitable solubility (> 50 µM) and an acceptable selectivity over the mammalian Chinese Hamster Ovary cell line (SI > 10) were evaluated for metabolic stability in mouse, rat and human liver microsomes (Table 3.8). Like the benzimidazoles, these compounds were generally not stable across all three species of microsomes. However, they were more metabolically stable in the human liver microsomes than the mouse and rat liver microsomes.

Table 3.8: Microsomal metabolic stability of selected imidazopyridine analogues.

Compound Code	Structure	% Remaining after 30 min	Projected $t_{1/2}$ (min)
		$M^h/R^i/H^j$	$M^h/R^i/H^j$
3.1	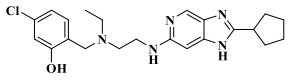	14.65/18.48/73.25	10.82/12.31/66.78
3.5	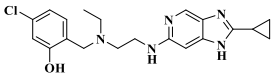	31.71/22.29/78.86	18.08/13.85/86.96
3.6	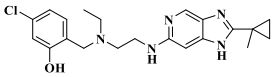	8.56/21.11/60.51	8.45/13.36/41.25
3.14	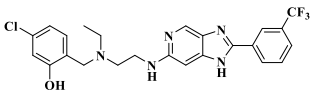	31.38/27.36/30.42	17.92/16.04/17.47
3.19	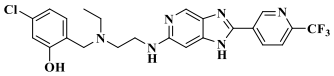	24.92/13.75/45.11	14.96/10.48/26.12

^{h}M, mouse; ^{i}R, rat; ^{j}H, human

3.3.5 Metabolite Identification Studies on Compound 3.14

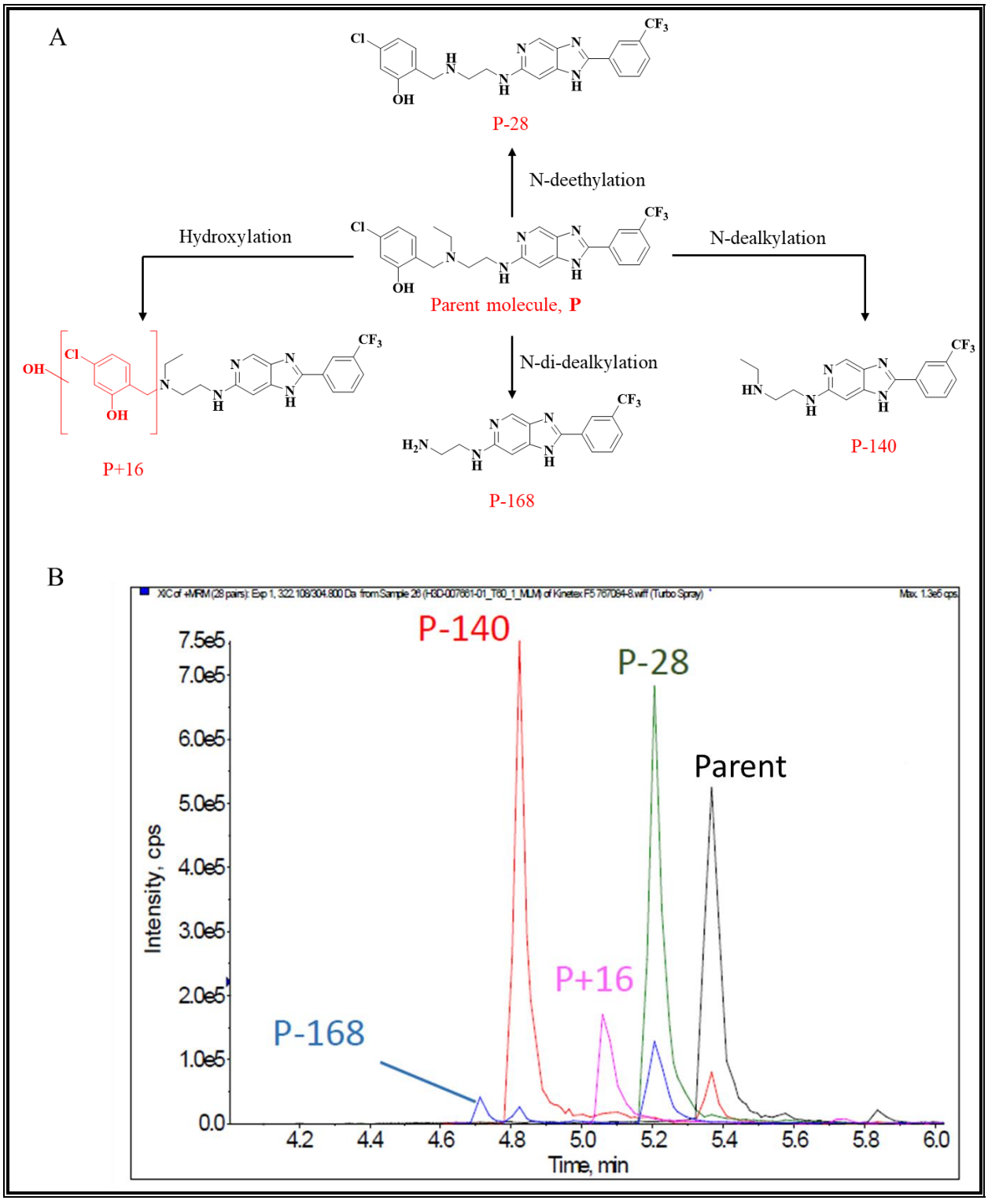

Figure 3.5: (A) Identified metabolites from the metabolism of compound **3.14** MLM; (B) XIC plot showing the relative abundance of the identified metabolites from compound **3.14**.

Four (4) metabolites were identified from the metabolism of **3.14** in mouse liver microsomes with the primary metabolites (P-28 and P-140) arising from dealkylation of the side chain N-alkyl groups (Figure 3.5). The low relative abundances of the *N*-di-dealkylation metabolite (P-168) and the hydroxylation metabolite (P+16) suggest that their formation does not occur rapidly. It is noteworthy that the formation of the metabolites required NADPH suggesting the presence of microsomes and the involvement of CYP450 enzymes, indicating that they were products of metabolism and not chemical degradation.

3.4 Conclusions

This chapter described the antiplasmodium activities of benzimidazoles and imidazopyridines, incorporating an intramolecular hydrogen bonding (IMHB) motif. The benzimidazole analogues showed suitable antiplasmodium activity (IC_{50} < 1 μM) against both the chloroquine-sensitive (NF54) and multidrug-resistant (K1) strains of *P. falciparum*. Meanwhile, they displayed relatively poor potency against the sexual gametocyte stage. These analogues exhibited good selectivity (SI >10) over the mammalian Chinese Hamster Ovary cells. In addition, *N*-benzyl benzimidazoles with an encouraging hERG inhibition profile (IC_{50} >1 μM) were identified. The imidazopyridine analogues also displayed antiplasmodium activity with IC_{50} < 1 μM against the asexual blood stage of the parasite. Like the benzimidazoles, a favourable cytotoxicity profile was observed for this class of compounds.

Nonetheless, selected potent analogues of both the benzimidazoles and imidazopyridines were metabolically unstable when evaluated against mouse, rat and human liver microsomes. Hence, they were not progressed for *in vivo* efficacy studies. Furthermore, metabolite identification studies were carried out to identify the metabolic hotspots in these compounds. Overall, it was observed that the presence of an IMHB motif was necessary for the antiplasmodium activity of these compounds since the absence thereof led to a loss of activity.

3.5 References

(1) Basco, L. K.; Marquet, F.; Makler, M. M.; Lebras, J. Plasmodium Falciparum and Plasmodium Vivax: Lactate-Dehydrogenase Activity and Its Application for in Vitro Drug Susceptibility Assay. *Exp. Parasitol.* **1995**, *80* (2), 260–271. https://doi.org/10.1006/expr.1995.1032.

(2) Hinrichs, D. J.; Makler, M. T. Measurement of the Lactate Dehydrogenase Activity of Plasmodium Falciparum as an Assessment of Parasitemia. *Am. J. Trop. Med. Hyg.* **1993**, *48* (2), 205–210. https://doi.org/10.4269/ajtmh.1993.48.205.

(3) Knobloch, J.; Henk, M. Screening for Malaria by Determination of Parasite-Specific Lactate Dehydrogenase. *Trans. R. Soc. Trop. Med. Hyg.* **1995**, *89* (3), 269–270. https://doi.org/10.1016/0035-9203(95)90533-2.

(4) Houzé, S.; Wentworth, L.; Chiodini, P.; Hunt-Cooke, A.; Piper, R.; Makler, M.; Lebras, J. Immunocapture Diagnostic Assays for Malaria Using Plasmodium Lactate Dehydrogenase (PLDH). *Am. J. Trop. Med. Hyg.* **1999**, *60* (1), 109–118. https://doi.org/10.4269/ajtmh.1999.60.109.

(5) Reader, J.; Botha, M.; Theron, A.; Lauterbach, S. B.; Rossouw, C.; Engelbrecht, D.; Wepener, M.; Smit, A.; Leroy, D.; Mancama, D.; et al. Nowhere to Hide: Interrogating Different Metabolic Parameters of Plasmodium Falciparum Gametocytes in a Transmission Blocking Drug Discovery Pipeline towards Malaria Elimination. *Malar. J.* **2015**, *14* (1), 213. https://doi.org/10.1186/s12936-015-0718-z.

(6) Chulay, J. D.; Haynes, J. D.; Diggs, C. L. Plasmodium Falciparum: Assessment of in Vitro Growth by [3H]Hypoxanthine Incorporation. *Exp. Parasitol.* **1983**, *55* (1), 138–146. https://doi.org/10.1016/0014-4894(83)90007-3.

(7) de Cózar, C.; Caballero, I.; Colmenarejo, G.; Sanz, L. M.; Álvarez-Ruiz, E.; Gamo, F.-J.; Cid, C. Development of a Novel High-Density [3 H]Hypoxanthine Scintillation Proximity Assay To Assess Plasmodium Falciparum Growth. *Antimicrob. Agents Chemother.* **2016**, *60* (10), 5949–5956. https://doi.org/10.1128/AAC.00433-16.

(8) Arnold, M. S. J.; Engel, J. A.; Chua, M. J.; Fisher, G. M.; Skinner-Adams, T. S.;

Andrews, K. T. Adaptation of the [3 H]Hypoxanthine Uptake Assay for In Vitro - Cultured Plasmodium Knowlesi Malaria Parasites. *Antimicrob. Agents Chemother.* **2016**, *60* (7), 4361–4363. https://doi.org/10.1128/AAC.02948-15.

(9) Downie, M. J.; Kirk, K.; Mamoun, C. Ben. Purine Salvage Pathways in the Intraerythrocytic Malaria Parasite Plasmodium Falciparum. *Eukaryot. Cell* **2008**, *7* (8), 1231–1237. https://doi.org/10.1128/EC.00159-08.

(10) Ting, L.-M.; Shi, W.; Lewandowicz, A.; Singh, V.; Mwakingwe, A.; Birck, M. R.; Ringia, E. A. T.; Bench, G.; Madrid, D. C.; Tyler, P. C.; et al. Targeting a Novel Plasmodium Falciparum Purine Recycling Pathway with Specific Immucillins. *J. Biol. Chem.* **2005**, *280* (10), 9547–9554. https://doi.org/10.1074/jbc.M412693200.

(11) Hyde, J. E. Exploring the Folate Pathway in Plasmodium Falciparum. *Acta Trop.* **2005**, *94* (3), 191–206. https://doi.org/10.1016/j.actatropica.2005.04.002.

(12) Burrows, J. N.; Hooft van Huijsduijnen, R.; Möhrle, J. J.; Oeuvray, C.; Wells, T. N. Designing the Next Generation of Medicines for Malaria Control and Eradication. *Malar. J.* **2013**, *12* (1), 187. https://doi.org/10.1186/1475-2875-12-187.

(13) Wells, T. N. C.; van Huijsduijnen, R. H.; Van Voorhis, W. C. Malaria Medicines: A Glass Half Full? *Nat. Rev. Drug Discov.* **2015**, *14* (6), 424–442. https://doi.org/10.1038/nrd4573.

(14) Delves, M. J.; Ruecker, A.; Straschil, U.; Lelièvre, J.; Marques, S.; López-Barragán, M. J.; Herreros, E.; Sinden, R. E. Male and Female Plasmodium Falciparum Mature Gametocytes Show Different Responses to Antimalarial Drugs. *Antimicrob. Agents Chemother.* **2013**, *57* (7), 3268–3274. https://doi.org/10.1128/AAC.00325-13.

(15) Buchholz, K.; Burke, T. A.; Williamson, K. C.; Wiegand, R. C.; Wirth, D. F.; Marti, M. A High-Throughput Screen Targeting Malaria Transmission Stages Opens New Avenues for Drug Development. *J. Infect. Dis.* **2011**, *203* (10), 1445–1453. https://doi.org/10.1093/infdis/jir037.

(16) Mosmann, T. Rapid Colorimetric Assay for Cellular Growth and Survival: Application to Proliferation and Cytotoxicity Assays. *J. Immunol. Methods* **1983**, *65* (1–2), 55–63. https://doi.org/10.1016/0022-1759(83)90303-4.

(17) Sandlin, R. D.; Fong, K. Y.; Wicht, K. J.; Carrell, H. M.; Egan, T. J.; Wright, D. W.

Identification of β-Hematin Inhibitors in a High-Throughput Screening Effort Reveals Scaffolds with in Vitro Antimalarial Activity. *Int. J. Parasitol. Drugs Drug Resist.* **2014**, *4* (3), 316–325. https://doi.org/10.1016/j.ijpddr.2014.08.002.

(18) Sandlin, R. D.; Carter, M. D.; Lee, P. J.; Auschwitz, J. M.; Leed, S. E.; Johnson, J. D.; Wright, D. W. Use of the NP-40 Detergent-Mediated Assay in Discovery of Inhibitors of β-Hematin Crystallization. *Antimicrob. Agents Chemother.* **2011**, *55* (7), 3363–3369. https://doi.org/10.1128/AAC.00121-11.

(19) Remmer, H. The Role of the Liver in Drug Metabolism. *Am. J. Med.* **1970**, *49* (5), 617–629. https://doi.org/10.1016/S0002-9343(70)80129-2.

(20) Thompson, T. Early ADME in Support of Drug Discovery: The Role of Metabolic Stability Studies. *Curr. Drug Metab.* **2000**, *1* (3), 215–241. https://doi.org/10.2174/1389200003339018.

(21) Masimirembwa, C. M.; Bredberg, U.; Andersson, T. B. Metabolic Stability for Drug Discovery and Development. *Clin. Pharmacokinet.* **2003**, *42* (6), 515–528. https://doi.org/10.2165/00003088-200342060-00002.

(22) Le Manach, C.; Paquet, T.; Gonzàlez Cabrera, D.; Younis, Y.; Taylor, D.; Wiesner, L.; Lawrence, N.; Schwager, S.; Waterson, D.; Witty, M. J.; et al. Medicinal Chemistry Optimization of Antiplasmodial Imidazopyridazine Hits from High Throughput Screening of a SoftFocus Kinase Library: Part 2. *J. Med. Chem.* **2014**, *57* (21), 8839–8848. https://doi.org/10.1021/jm500887k.

(23) Matsumoto, S.; Yamazoe, Y. Involvement of Multiple Human Cytochromes P450 in the Liver Microsomal Metabolism of Astemizole and a Comparison with Terfenadine. *Br. J. Clin. Pharmacol.* **2001**, *51* (2), 133–142. https://doi.org/10.1111/j.1365-2125.2001.01292.x.

(24) Nchinda, A. T.; Le Manach, C.; Paquet, T.; Gonzàlez Cabrera, D.; Wicht, K. J.; Brunschwig, C.; Njoroge, M.; Abay, E.; Taylor, D.; Lawrence, N.; et al. Identification of Fast-Acting 2,6-Disubstituted Imidazopyridines That Are Efficacious in the in Vivo Humanized Plasmodium Falciparum NODscidIL2Rγ Null Mouse Model of Malaria. *J. Med. Chem.* **2018**, *61* (9), 4213–4227. https://doi.org/10.1021/acs.jmedchem.8b00382.

(25) Horatscheck, A.; Andrijevic, A.; Nchinda, A. T.; Le Manach, C.; Paquet, T.; Khonde,

L. P.; Dam, J.; Pawar, K.; Taylor, D.; Lawrence, N.; et al. Identification of 2,4-Disubstituted Imidazopyridines as Hemozoin Formation Inhibitors with Fast-Killing Kinetics and In Vivo Efficacy in the Plasmodium Falciparum NSG Mouse Model. *J. Med. Chem.* **2020**, *63* (21), 13013–13030. https://doi.org/10.1021/acs.jmedchem.0c01411.

CHAPTER 4

PHYSICOCHEMICAL PROFILING AND METHODS OF ASSESSING INTRAMOLECULAR HYDROGEN BONDING (IMHB)

4.1 Chapter Overview

Chapter 4 covers the physicochemical evaluation and the analysis of factors influencing the solubility of the compounds described in this thesis. The chapter highlights the impact of physicochemical parameters on drug-likeness, followed by an outline of the *in silico* and experimental physicochemical properties of the synthesized final target molecules. An assessment of the drug-likeness of the compounds with prominence on Lipinski's Rule of Five (RO5) and Veber's rule is described. Correlation studies aimed at unravelling the factors responsible for the observed aqueous solubility of the target compounds are also outlined. The chapter concludes with the methods used to assess intramolecular hydrogen bonds in representative analogues **1.2** and **2.2**.

4.2 The Impact of Physicochemical Properties on Drug-likeness

Physicochemical and molecular properties significantly contribute to the pharmacokinetics, pharmacodynamic and safety profiles exhibited by drugs. Formulation challenges and unfavourable ADMET profiles are usually attributed to poor physicochemical properties, especially permeability and aqueous solubility.[1–3] The relationship between physicochemical properties and drug-likeness has also been revealed by various studies. To this effect, different sets of acceptable cut-off values for the fundamental molecular descriptors considered paramount in predicting suitable physicochemical properties for an oral drug-like space have been devised.[4]

The Lipinski's rule of five (RO5), which needs to be noted is only a guideline, hypothesizes that an orally administered drug is more likely to exhibit good absorption and permeability when molecular weight (MW) ≤ 500 Daltons (Da); cLogP ≤ 5; the number of hydrogen-bond donors (HBD) ≤ 5; and the number of hydrogen-bond acceptors ≤ 10.[5,6] In addition, Veber et al., proposed that a compound has an increased chance of achieving an acceptable oral bioavailability when it has ten or less rotatable bonds (RB) [a measure of molecular flexibility], a topological polar surface area (tPSA) ≤ 140 $Å^2$ and the total number of both HBD and HBA

≤ 12.[7] The rule of three (RO3) which is relevant to fragment-based drug discovery and an extension of the RO5 have also been put forward.[8]

4.3 Evaluation of Physicochemical Properties

The previously mentioned physicochemical parameters (MW, cLogP, tPSA, HBD and HBA) in relation to the compounds synthesized in this thesis work were predicted using StarDrop™ 6.6 and ChemDraw Professional 18.2 software. Other parameters [melting point, HPLC retention time (t_R), TLC retardation factor (R_f) and solubility] were determined experimentally. To assess the compliance of the compounds to Lipinski's RO5, frequency distribution histograms were plotted for the predicted parameters cLogP, tPSA and MW. However, the assessment of RO5 compliance regarding the number of HBDs and HBAs was done by inspection.

As previously alluded to, a drug's oral bioavailability is mostly influenced by aqueous solubility, permeability and metabolic stability. In relation to drug discovery, solubility significantly influences bioassays, intestinal absorption, and formulation for *in vivo* dosing.[9] Accordingly, the kinetic solubility of the target compounds was determined by the turbidimetric assay method[10] and the miniaturized shake flask method.[11] Briefly, the turbidimetric assay involves preparing solutions of the test compounds in DMSO. Aliquots of the solutions are then added to a phosphate-buffered saline (PBS) at pH 7.4 to give nominal serial dilutions. The concentration value above which the test compound yields turbidity by precipitating out of solution is then recorded as the approximate solubility. A UV-Visible spectrophotometer is used to detect the turbidity of the compound by measuring the absorbance at 620 nm, the wavelength at which the compound is not expected to absorb electromagnetic radiation. The turbidimetric assay method is fast, simple, cost-effective and suitable for high throughput screening of a large number of compounds. However, this method is far less accurate because the observed values only depend on turbidity. Another drawback is the use of DMSO, which can increase the solubility to an unpredictable and unknown extent.

The miniaturized shake flask method, on the other hand, also involves making a stock solution of the test compound in DMSO. The stock solution is then used to spike duplicate aqueous samples in PBS at the desired pH. Unlike the turbidimetric assay method, the DMSO is dried off, after which the sample is incubated while shaking to prevent particle aggregation. The solution is filtered to separate the saturated solution from the solute phase. HPLC is used to

analyze the saturated solution, after which a calibration curve (using a calibration standard) is plotted to determine the solubility of the sample. The advantage of using this method is that the HPLC can detect impurities and any instability which the spectrophotometric method cannot detect.[12]

Factors affecting the recorded solubility values were investigated by assessing solubility as a function of different physicochemical parameters [cLogP, tPSA, melting point, HPLC retention time (t_R) and TLC retardation factor (R_f)]. These factors were used as a measure of a peculiar inherent compound characteristic, which influences aqueous solubility. For instance, t_R and R_f were used as a measure of polarity, melting point as a measure of crystal packing energy and cLogP as a measure of lipophilicity. For comparable data among the compounds, similar HPLC and TLC methods were applied for all the compounds in each class studied in this thesis work.

4.3.1 Results and Discussion

The calculated and experimentally determined physicochemical parameters of the benzimidazole and imidazopyridine-based compounds are outlined in Tables 4.1-4.3 below.

Table 4.1: Physicochemical properties of 1*H*-benzimidazole analogues.

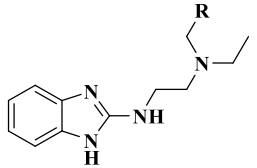

Compound Code	R	Calculated physicochemical properties					Experimental physicochemical properties			
		MW,[a] g/mol	cLogP[b]	tPSA,[a] Å^2	HBD[a]	HBA[a]	R_f[c]	t_R[d] (min)	m.p.[e] (°C)	Solubility[f] (µM)
1.1	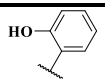	310.4	3.91	64.18	3	5	0.35	0.421	79.7	>200
1.2	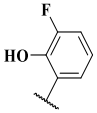	328.4	4.15	64.18	3	5	0.43	0.401	105.2	160
1.3	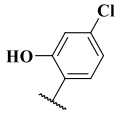	344.8	4.92	64.18	3	5	0.43	1.536	103.0	160
1.4	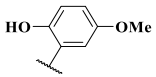	340.4	4.01	73.41	3	6	0.29	0.263	103.0	160
1.5	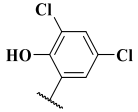	379.3	5.41	64.18	3	5	0.53	2.352	72.0	160
1.6	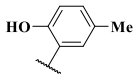	324.4	4.41	64.18	3	5	0.31	0.465	83.4	>200

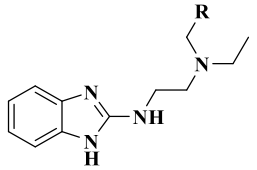

Compound Code	R	Calculated physicochemical properties					Experimental physicochemical properties			
		MW,[a] g/mol	cLogP[b]	tPSA,[a] Å^2	HBD[a]	HBA[a]	R_f[c]	t_R[d] (min)	m.p.[e] (°C)	Solubility[f] (µM)
1.7	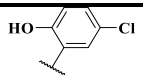	344.8	4.92	64.18	3	5	0.46	0.702	145.2	160
1.8		311.4	3.37	77.07	3	6	0.10	0.149	75.2	>200
1.9	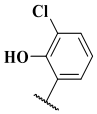	344.8	4.59	64.18	3	5	0.53	1.031	88.8	160
1.10	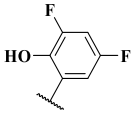	346.4	4.39	64.18	3	5	0.45	1.027	172.5	140
1.11	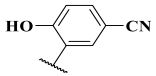	335.4	4.03	87.97	3	6	0.38	0.325	72.6	160
1.12		294.4	4.63	43.95	2	4	0.34	0.281	95.0	140

[a]MW, molecular weight; tPSA, topological polar surface area; HBD, hydrogen bond donor, HBA, hydrogen bond acceptor: Calculated using StarDrop™ 6.6

[b]cLogP, calculated log P: Calculated using ChemDraw Professional 18.2.

[c]R_f, Retardation factor: Analytical TLC with 10% methanol in dichloromethane as the mobile phase.

[d] t_R, Retention time: Measured using HPLC-MS (method described in chapter 7).

[e] m.p., melting point (values are averages between the upper and lower limit values of the melting range): Measured using a Stuart automatic melting point machine SMP40.

[f] Determined using kinetic (turbidimetric) solubility assay at pH 7.4 (method described in chapter 7).

Table 4.2: Physicochemical properties of *N*-benzyl benzimidazole (astemizole-based) analogues.

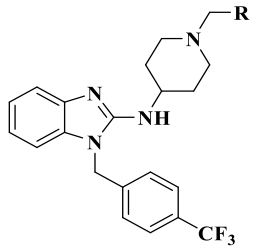

Compound Code	R	Calculated physicochemical properties					Experimental physicochemical properties			
		MW,[a] g/mol	cLogP[b]	tPSA,[a] Å^2	HBD[a]	HBA[a]	R_f[c]	t_R[d] (min)	m.p.[e] (°C)	Solubility[f] (µM)
2.1	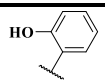	480.5	5.63	53.32	2	5	0.74	2.378	209.8	140
2.2	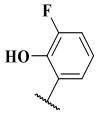	498.5	5.87	53.32	2	5	0.79	2.431	204.9	140
2.3	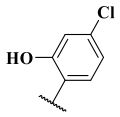	515.0	6.64	53.32	2	5	0.81	2.466	203.5	160

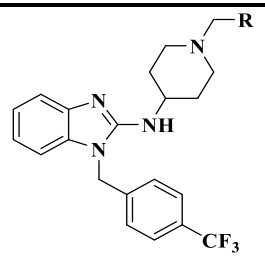

Compound Code	R	Calculated physicochemical properties					Experimental physicochemical properties			
		MW,[a] g/mol	cLogP[b]	tPSA,[a] Å^2	HBD[a]	HBA[a]	R_f[c]	t_R[d] (min)	m.p.[e] (°C)	Solubility[f] (µM)
2.4	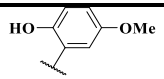	510.6	5.73	62.55	2	6	0.75	2.387	193.8	>200
2.5	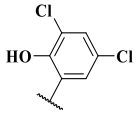	549.4	7.12	53.32	2	5	0.86	2.703	157.7	140
2.6	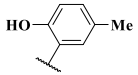	494.6	6.13	53.32	2	5	0.76	2.431	158.4	>200
2.7	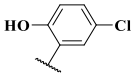	515.0	6.64	53.32	2	5	0.86	2.501	110.8	160
2.8	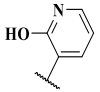	481.5	5.08	66.21	2	6	0.13	2.282	188.2	>200
2.9	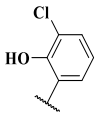	515.0	6.31	53.32	2	5	0.88	2.483	165.9	160

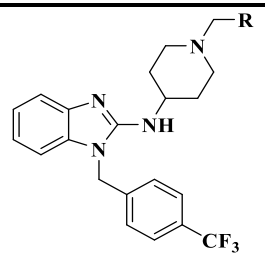

Compound Code	R	Calculated physicochemical properties					Experimental physicochemical properties			
		MW,[a] g/mol	cLogP[b]	tPSA,[a] Å^2	HBD[a]	HBA[a]	R_f[c]	t_R[d] (min)	m.p.[e] (°C)	Solubility[f] (µM)
2.10	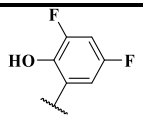	516.5	6.11	53.32	2	5	0.86	2.475	153.7	160
2.11	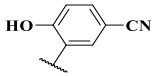	505.5	5.75	77.11	2	6	0.84	2.405	204.5	160
2.12		464.5	6.34	33.09	1	4	0.69	2.404	157.6	140
2.13	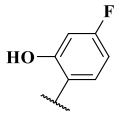	498.5	6.07	53.32	2	5	0.81	2.404	207.1	140
2.14	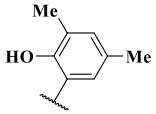	508.6	6.58	53.32	2	5	0.90	2.545	160.05	160
2.15	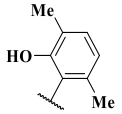	508.6	6.53	53.32	2	5	0.90	2.598	162.5	160

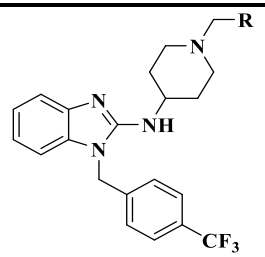

Compound Code	R	Calculated physicochemical properties					Experimental physicochemical properties			
		MW,[a] g/mol	cLogP[b]	tPSA,[a] Å^2	HBD[a]	HBA[a]	R_f[c]	t_R[d] (min)	m.p.[e] (°C)	Solubility[f] (µM)
2.16	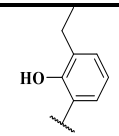	508.6	6.61	53.32	2	5	0.88	2.598	177.2	140
2.17	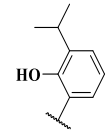	522.6	6.71	53.32	2	5	0.89	2.650	201.9	80
2.18	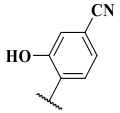	505.5	5.75	77.11	2	6	0.80	2.501	171.9	160
2.19	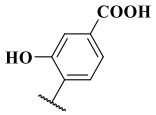	524.5	3.44	90.62	3	7	0.19	2.325	179.8	>200
2.20	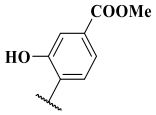	538.6	6.14	79.62	2	7	0.79	2.466	197.7	160

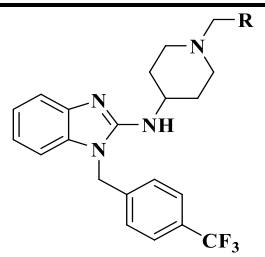

Compound Code	R	Calculated physicochemical properties					Experimental physicochemical properties			
		MW,[a] g/mol	cLogP[b]	tPSA,[a] Å^2	HBD[a]	HBA[a]	R_f[c]	t_R[d] (min)	m.p.[e] (°C)	Solubility[f] (µM)
2.21	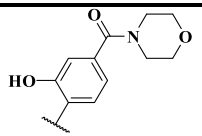	593.6	4.8	82.86	2	8	0.64	2.387	176.2	160

[a]MW, molecular weight; tPSA, topological polar surface area; HBD, hydrogen bond donor, HBA, hydrogen bond acceptor: Calculated using StarDrop™ 6.6

[b]cLogP, calculated log P: Calculated using ChemDraw Professional 18.2.

[c]R_f, Retardation factor: Analytical TLC with 10% methanol in dichloromethane as the mobile phase.

[d]t_R, Retention time: Measured using HPLC-MS (method described in chapter 7).

[e]m.p., melting point (values are averages between the upper and lower limit values of the melting range): Measured using a Stuart automatic melting point machine SMP40.

[f]Determined using kinetic (turbidimetric) solubility assay at pH 7.4 (method described in chapter 7).

Table 4.3: Physicochemical properties of imidazopyridine analogues.

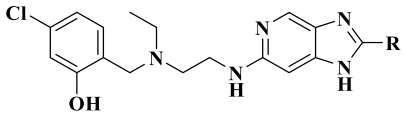

Compound Code	R	Calculated physicochemical properties					Experimental physicochemical properties			
		MW,[a] g/mol	cLogP[b]	tPSA,[a] Å^2	HBD[a]	HBA[a]	R_f[c]	t_R[d] (min)	m.p.[e] (°C)	Solubility[g] (µM)
3.1		413.9	6.1	77.07	3	6	0.30	2.203	[h]ND	15
3.2		415.9	3.98	86.3	3	7	0.18	0.298	ND	125
3.3		429.9	4.26	86.3	3	7	0.18	0.430	ND	120
3.4		359.9	4.54	77.07	3	6	0.13	0.219	ND	135
3.5		385.9	4.98	77.07	3	6	0.16	2.211	ND	25
3.6		399.9	5.51	77.07	3	6	0.25	0.755	ND	200
3.7		453.9	5.36	77.07	3	6	0.28	2.194	ND	175
3.8		399.9	5.51	77.07	3	6	0.28	0.588	ND	185
3.9		399.9	5.54	77.07	3	6	0.28	0.921	ND	170

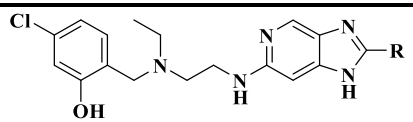

Compound Code	R	Calculated physicochemical properties					Experimental physicochemical properties			
		MW,[a] g/mol	cLogP[b]	tPSA,[a] Å^2	HBD[a]	HBA[a]	R_f[c]	t_R[d] (min)	m.p.[e] (°C)	Solubility[g] (µM)
3.10		435.9	4.93	77.07	3	6	0.26	1.808	ND	175
3.11		428.0	6.66	77.07	3	6	0.30	2.238	ND	140
3.12	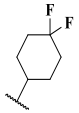	464.0	6.05	77.07	3	6	0.33	2.150	ND	<5
3.13		429.0	4.73	80.31	3	7	0.18	0.141	ND	175
3.14	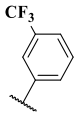	489.9	7.26	77.07	3	6	0.36	2.422	ND	65
3.15		442.0	7.22	77.07	3	6	0.36	2.413	ND	150
3.16	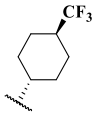	496.0	6.45	77.07	3	6	0.36	2.413	ND	135

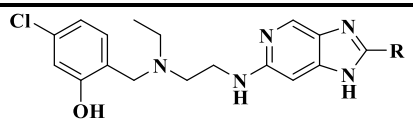

Compound Code	R	Calculated physicochemical properties					Experimental physicochemical properties			
		MW,[a] g/mol	cLogP[b]	tPSA,[a] Å^2	HBD[a]	HBA[a]	R_f[c]	t_R[d] (min)	m.p.[e] (°C)	Solubility[g] (µM)
3.17	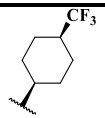	496.0	6.45	77.07	3	6	0.31	2.343	ND	135
3.18	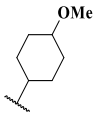	458.0	5.29	86.3	3	7	0.29	2.124	ND	120
3.19	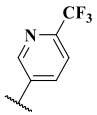	490.9	5.96	89.96	3	7	0.34	2.352	ND	140

[a]MW, molecular weight; tPSA, topological polar surface area; HBD, hydrogen bond donor, HBA, hydrogen bond acceptor: Calculated using StarDrop™ 6.6

[b]cLogP, calculated log P: Calculated using ChemDraw Professional 18.2.

[c]R_f, Retardation factor: Analytical TLC with 10% methanol in dichloromethane as the mobile phase.

[d]t_R, Retention time: Measured using HPLC-MS (method described in chapter 7).

[e]m.p., melting point (values are averages between the upper and lower limit values of the melting range): Measured using a Stuart automatic melting point machine SMP40.

[g]Determined using miniaturized shake flask method at pH 6.5 (method described in chapter 7).

[h]Not determined (compounds were isolated as either semi-solids or viscous oils).

Table 4.4: Comparison of calculated physicochemical properties to drug-like guidelines

Compound class	MW, g/mol	cLogP	tPSA, Å^2	HBD	HBA
1*H*-benzimidazoles	294.4 – 379.3	3.37 – 5.41	43.95 – 87.97	2 - 3	4 - 6
Astemizoles	464.5 – 593.6	3.44 – 7.12	33.09 – 90.62	1 - 3	4 – 8
Imidazopyridines	359.9 – 496.0	3.98 – 7.26	77.07 – 89.96	3	6 – 7
Targeted criteria[i]	≤ 500	≤ 5	≤ 140	≤ 5	≤ 10

[i] Targeted criteria are defined according to Lipinski's RO5 and Veber's rule on tPSA.

4.3.1.1 Compliance Assessment of RO5 for the 1*H*-benzimidazoles

Four out of the five calculated molecular features of the 1*H*-benzimidazole analogues complied with the RO5. These molecular features, as depicted in Table 4.4, include MW (294.4-379.3 g/mol), tPSA (43.95-87.97 Å^2), HBD (2-3) and HBA (4-6). Except for analogue **1.5** (cLogP = 5.41), all the other analogues have cLogP values less than five, which conforms to Lipinski's RO5. According to the molecular weight frequency distribution (Figure 4.1A), most analogues possess molecular weights in the range 341-350 g/mol. Similarly, the majority of the analogues (8 out of 12) have tPSA values in the range 61-65 Å^2 (Figure 4.1C). The cLogP values, on the other hand, were mostly distributed over the range 4.1-5.0, as shown in Figure 4.1B.

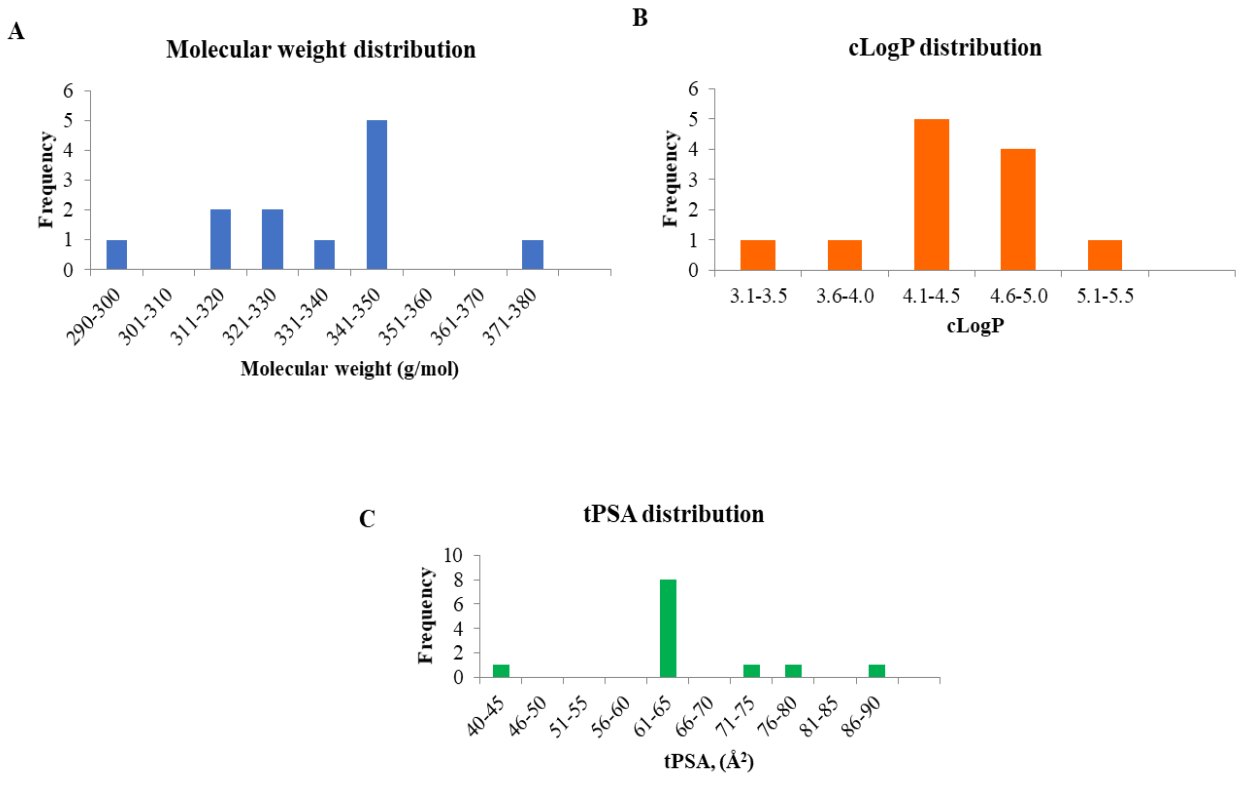

Figure 4.1: Frequency distribution of physicochemical parameters for 1H-benzimidazole analogues: (A) Molecular weight; (B) Calculated Log P and (C) Topological polar surface area.

4.3.1.2 Compliance Assessment of RO5 for the Astemizole analogues

For the astemizole analogues, the physicochemical parameters tPSA (33.09-90.62 $Å^2$), HBD (1-3), HBA (4-8) were RO5 compliant. The frequency distribution plot showed most of the analogues have molecular weights in the range 501-520 g/mol (Figure 4.2A). Additionally, most analogues possess cLogP values in the range of 5.6-7. The tPSA values were predominantly in the range of 51-55 $Å^2$. Like the 1*H*-benzimidazoles, the HBD and HBA values of the astemizoles varied over a narrow range; thus, their frequency distribution graphs were not plotted.

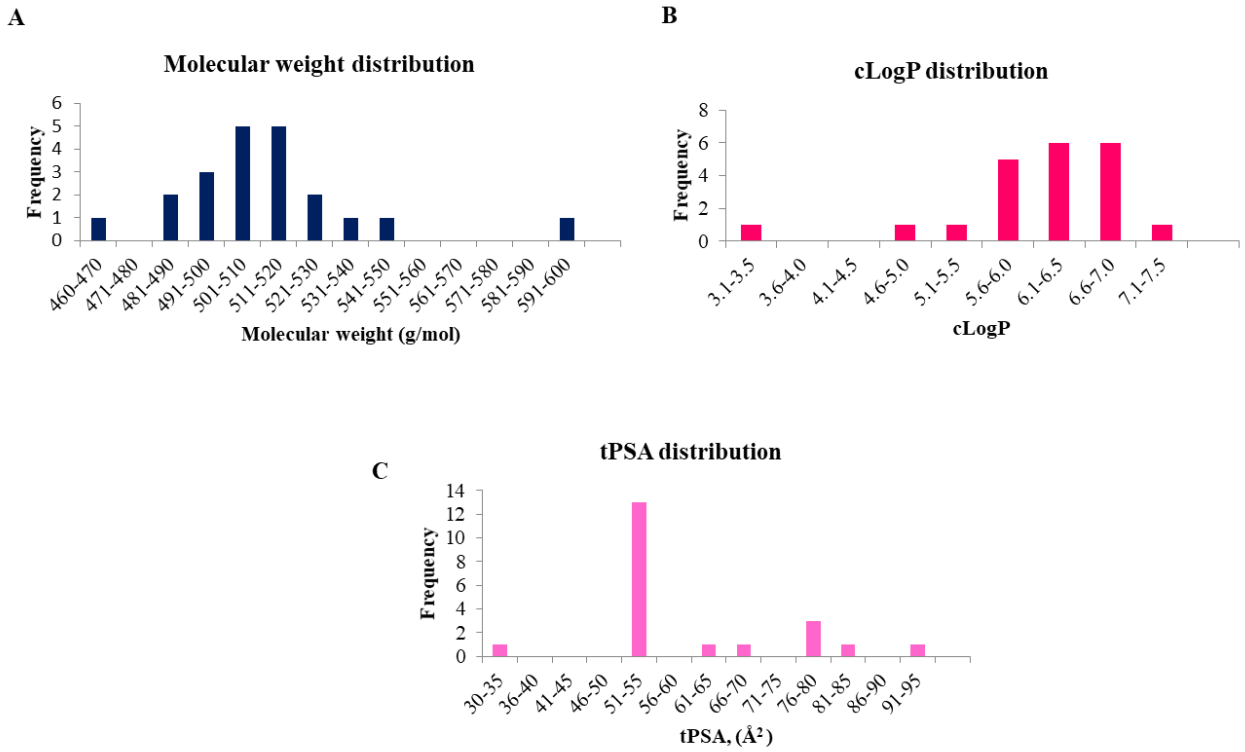

Figure 4.2: Frequency distribution of physicochemical parameters for Astemizole analogues: (A) Molecular weight; (B) Calculated Log P and (C) Topological polar surface area.

4.3.1.3 Compliance Assessment of RO5 for the Imidazopyridines

Out of the five calculated physicochemical parameters of the imidazopyridines, four were RO5 compliant. These parameters are the MW (359.9-496.0), tPSA (77.07-89.96), HBD (3) and HBA (6-7). According to the frequency distribution analysis, the molecular weight and cLogP

values of these analogues were distributed over a wide range (Figure 4.3A and 4.3B). On the other hand, about 70% of the analogues (14 out of 19) have tPSA values in the range of 75-80 $Å^2$.

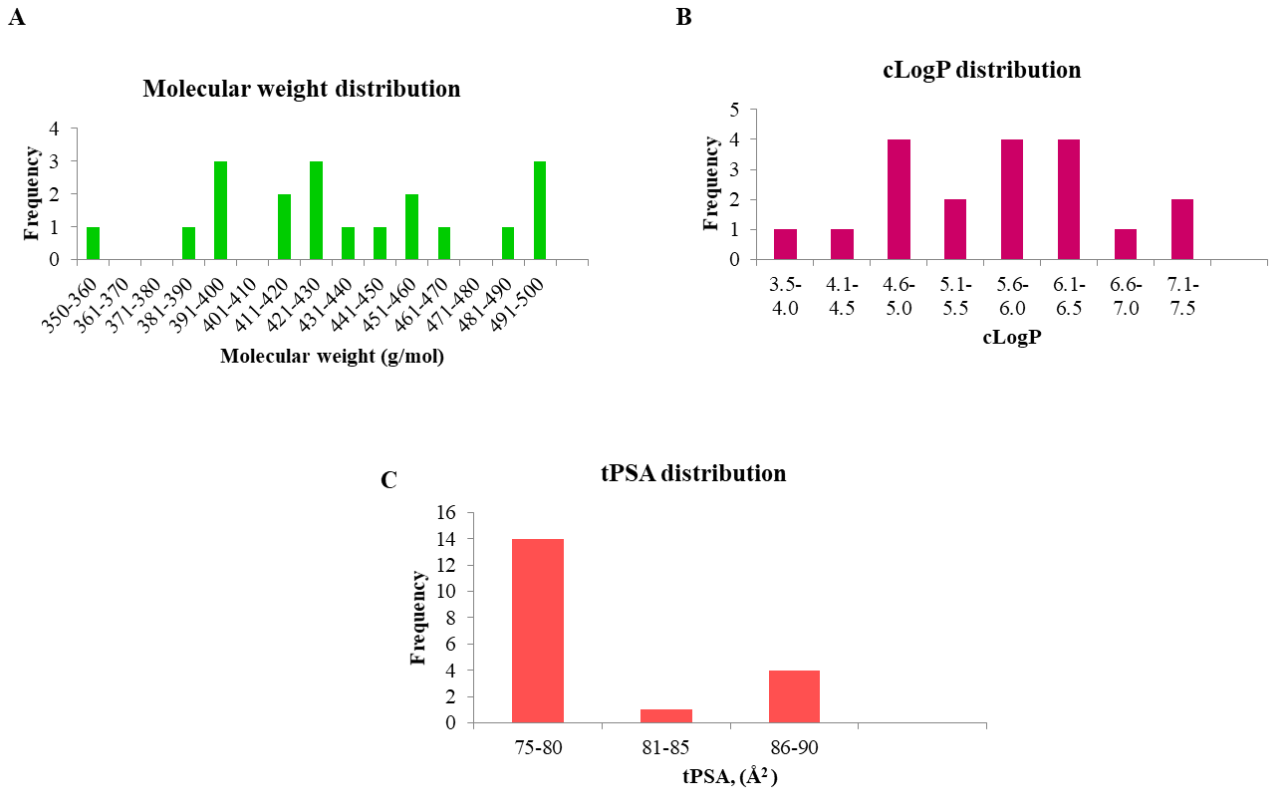

Figure 4.3: Frequency distribution of physicochemical parameters for Imidazopyridine analogues: (A) Molecular weight; (B) Calculated Log P and (C) Topological polar surface area.

4.3.1.4 Analysis of Factors Influencing the Solubility of 1*H*-Benzimidazoles

Various factors anticipated to inherently influence solubility were analyzed through correlation plots. For the 1*H*-benzimidazoles, the factor that appears to impact solubility largely is the TLC retardation factor (Figure 4.4C). Although weak (R^2 = 0.3286), the observed negative correlation was anticipated. A similar trend was also observed for melting point (Figure 4.4A), which was in congruence with previous literature.[13,14] More specifically, a high melting point is a measure of efficient crystal packing and high crystal packing energy, which discourages the dissolution of a compound in an aqueous medium. HPLC retention time exhibited almost no correlation with solubility (R^2 = 0.0838). Furthermore, a weak correlation was observed between solubility and cLogP, a surrogate measure of a compound's lipophilicity. In general,

the correlation plots for these analogues suggests that many other factors simultaneously affect their solubility.

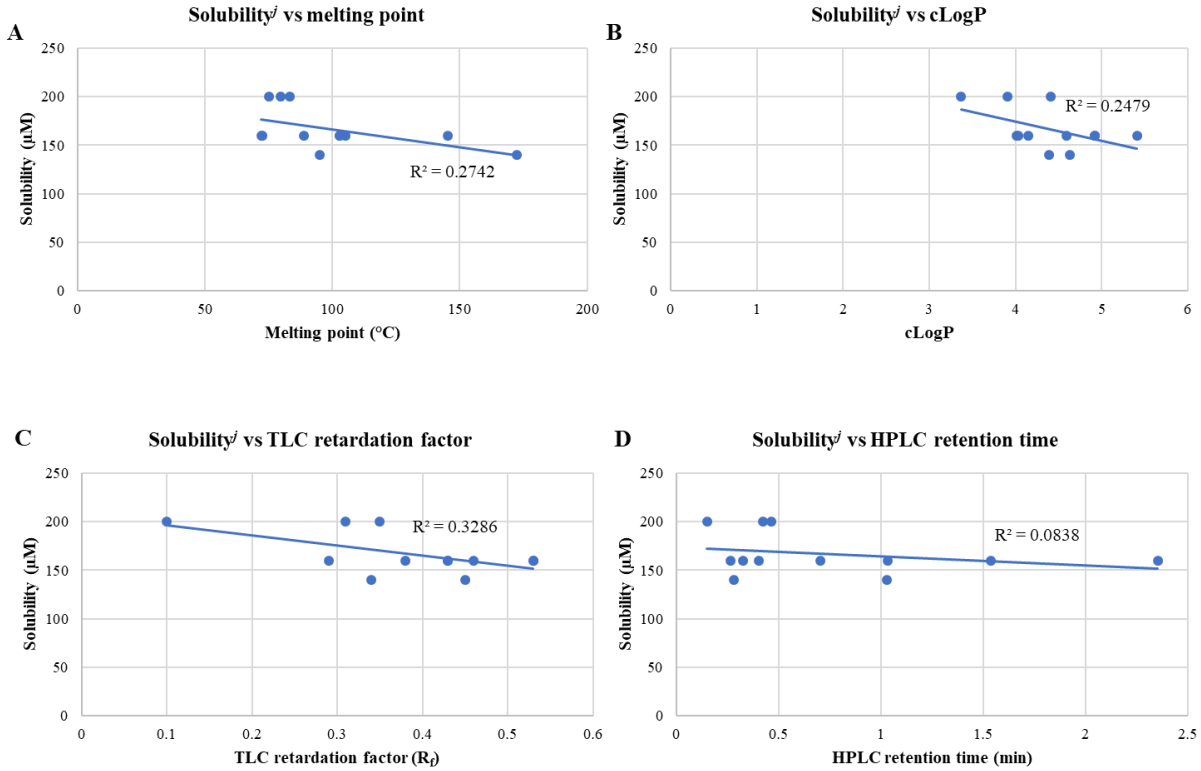

Figure 4.4: Correlation plots of solubility expressed in µM against: (A) melting point; (B) cLogP; (C) TLC retardation factor (D) HLPC retention time. [j]Solubility was determined by the turbidimetric method using PBS at pH 7.4. For the purposes of plotting the correlations, all compounds with uncertain solubility values, i.e., <5 and >200 µM, were assigned definite values of 0 and 200 µM, respectively.

4.3.1.5 Analysis of Factors Influencing the Solubility of Astemizole analogues

HPLC retention time was established to be a significant factor influencing solubility compared to TLC retardation factor, cLogP and melting point for the astemizole analogues. A negative correlation between solubility and HPLC retention time, as depicted in Figure 4.5D, was expected, albeit the correlation was weak ($R^2 = 0.3582$). Characteristically, the HPLC retention time is used as a proxy measure of the compound's capability to interact with the aqueous media of the reversed-phase HPLC column. Hence, it is a more pragmatic measure of a compound's polarity. The mobile phase of a reversed-phase HPLC is more polar than the stationary phase of the column; thus, each gradient run starts with a high percentage of the aqueous media, allowing more polar compounds to elute faster than less polar compounds.[15]

Melting point displayed no correlation with solubility (R^2 = 0.0336), and that could be due to other factors playing a role in reducing the effect of crystal packing energy on solubility.

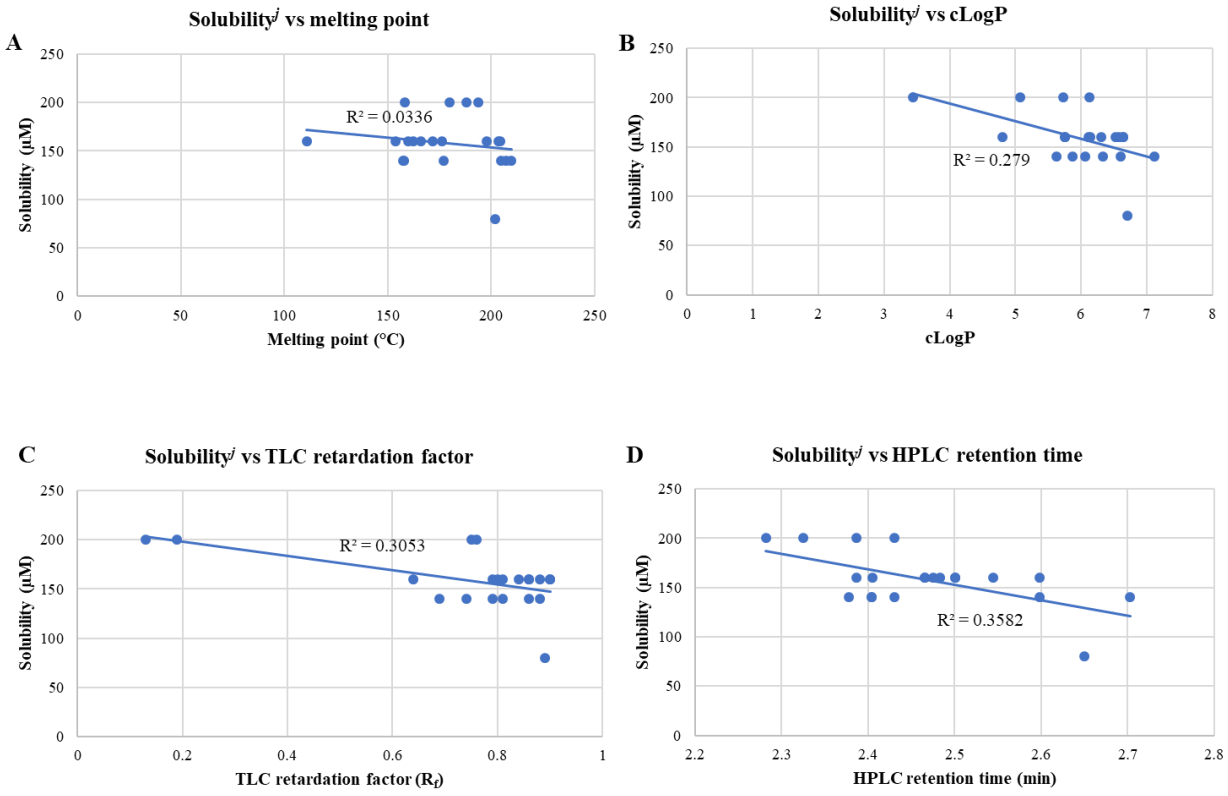

Figure 4.5: Correlation plots of solubility expressed in µM against: (A) melting point; (B) cLogP; (C) TLC retardation factor (D) HLPC retention time. [j]Solubility was determined by the turbidimetric method using PBS at pH 7.4. For the purposes of plotting the correlations, all compounds with uncertain solubility values, i.e., <5 and >200 µM, were assigned definite values of 0 and 200 µM, respectively.

4.3.1.6 Analysis of Factors Influencing the Solubility of Imidazopyridines

For this compound class, the melting point parameter could not be described because the compounds were isolated as either semi-solids or viscous oils. In this regard, the factors analyzed through correlation plots are cLogP, TLC retardation factor and HPLC retention time. TLC retardation factor and cLogP exhibited almost no correlation with solubility. Although weak (R^2 = 0.1684), HPLC retention time negatively correlated with solubility as expected (Figure 4.6C). Altogether, these correlation studies indicate that many factors simultaneously affect the solubility of compounds across a specific class of compounds. It may be crucial to examine the factors responsible for aqueous solubility based on individual cases rather than an entire class of compounds.

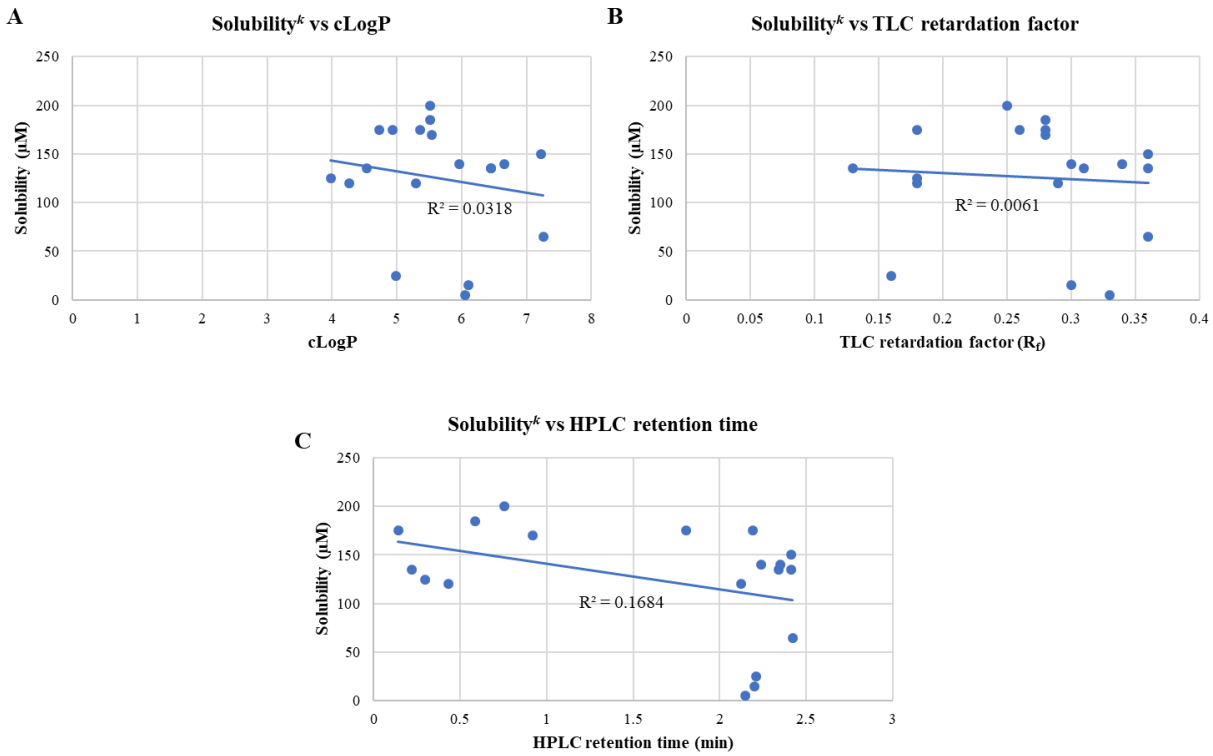

Figure 4.6: Correlation plots of solubility expressed in µM against (A) cLogP; (B) TLC retardation factor (C) HLPC retention time. [k]Solubility was determined by the miniaturized shake flask method at pH 6.5. For the purposes of plotting the correlations, all compounds with uncertain solubility values, i.e., <5 µM, were assigned a definite value of 0 µM.

4.4 Methods of Assessing Intramolecular Hydrogen Bonding (IMHB)

As previously mentioned in section 1.10.1 of chapter 1, the successful implementation of IMHB considerations in medicinal chemistry and drug discovery as a whole requires experimental tools that assess the formation of IMHB in molecules. In this thesis work, the experimental tools used to investigate the formation of IMHB include X-ray diffraction, infrared spectroscopy and density functional theory.

4.4.1 Single Crystal X-ray Diffraction (XRD) Analysis

Crystal structures furnish information on the intrinsic properties of compounds such as the molecular geometry, polymorphism, solvation profile, π-π stacking and hydrogen bond interactions.[16] To elucidate the crystal structures of representative compounds **1.2** and **2.2**, experiments to obtain the crystal structures were initiated. Both compounds were crystallized by the slow evaporation method in a mixture of dichloromethane and hexane to produce

crystals of adequate size and quality for X-ray diffraction experiments. Single crystal X-ray diffraction data were acquired on a Bruker KAPPA APEX II DUO diffractometer using graphite-monochromated Mo-Kα radiation (χ = 0.71073 Å). Data collection was carried out at 173 K. Temperature was controlled by an Oxford Cryostream cooling system (Oxford Cryostat). Data reduction and cell refinement were performed using the program SAINT.[17] The data were scaled, and absorption correction was performed using SADABS.[18] The crystal structure was solved by employing SHELXS-97[18] and refined by full-matrix least-squares methods based on F^2 using SHELXL-2014[18] and applying the graphics interface program X-Seed.[19,20] The programs X-Seed and POV-Ray[21] were used to prepare molecular graphic images.

4.4.1.1 Single Crystal XRD Studies of Compound 1.2

The single crystal XRD and refinement data for compound **1.2** hydrate are summarized in Table 4.5 below.

Table 4.5: Data-collection and refinement parameters for **1.2** hydrate.

Parameter	**Value**
Molecular Formula	$C_{18}H_{21}FN_4O•H_2O$
Formula Weight	346.40
Crystal System	monoclinic
Space Group	P21/c
a (Å)	13.6252(16)
b (Å)	10.5144(12)
c (Å)	12.6246(13)
α (º)	90
β (º)	96.075(2)
γ (º)	90
V ($Å^3$)	1798.5(3)
Z	4
D (calc) ($g.cm^{-3}$)	1.279
μ (MoKα) (mm^{-1})	0.093
F (000)	736
Crystal Size (mm^3)	0.07 x 0.26 x 0.27
Temperature (K)	173
Radiation (Å)	MoKα 0.71073
θ Min–Max (º)	1.5-27.5
Index ranges ±*h*, ±*k*, ±*l*	-17: 17; -13: 13; -8: 16
Reflections (total)	13245
Reflections (unique)	4132
R (int)	0.045
Reflections with I>2σ(I)	2914

Nref, Npar	4132,247
R1, w*R*2, S	0.0432, 0.1137, 1.02
Max. and Av. Shift/Error	0.00, 0.00
Δρmin, max (e Å^{-3})	-0.27, 0.18

The crystal structure of compound **1.2** hydrate is illustrated in Figure 4.7. The geometrical data (bond lengths, bond angles, torsion angles etc.) for this crystal structure were obtained in the form of crystallographic information (CIF) files.

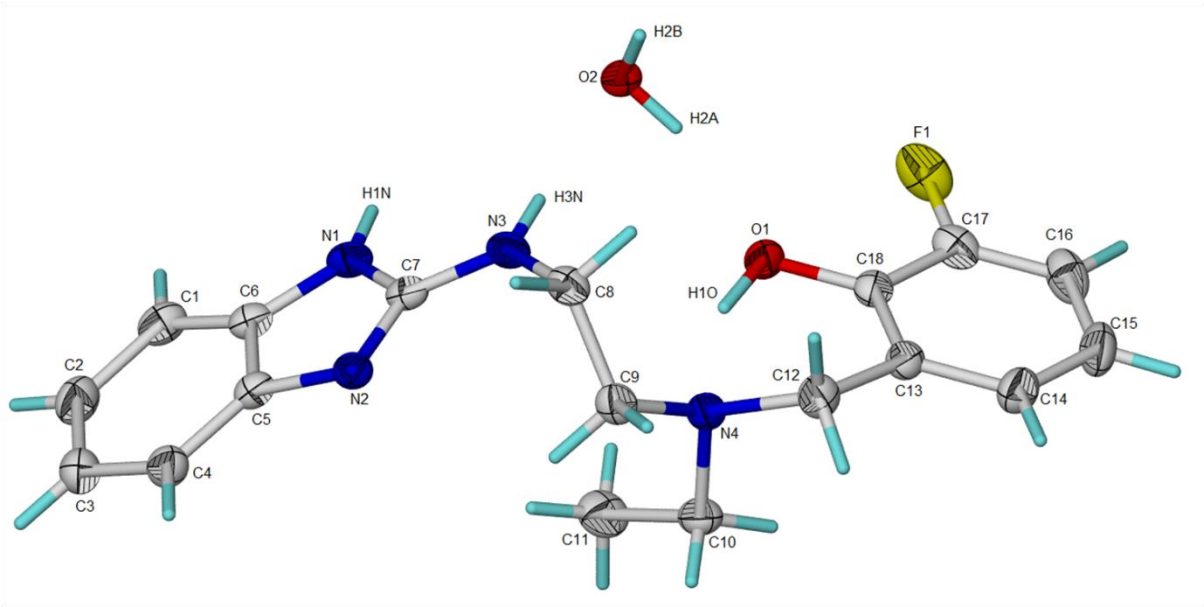

Figure 4.7: Single crystal X-ray structure of compound **1.2** hydrate, where thermal ellipsoids are drawn at 40% probability level.

All non-hydrogen atoms of compound **1.2** were refined anisotropically. Except for the functional hydrogen atoms, all hydrogen atoms were placed in idealized positions and refined in riding models with U_{iso} assigned 1.2 or 1.5 times U_{eq} of their parent atoms. The bond distances were constrained from 0.95 to 0.99 Å. The hydrogen atoms H1N and H3N on N1 and N3 respectively were located in different density maps. They were also refined independently without restraints. The hydroxyl hydrogen H1O and the water hydrogen atoms H2A and H2B were located in different density maps, refined with simple O-H bond length restraints. The crystal structure was refined to an R factor of 0.0432. The principal hydrogen bonding interactions are outlined in Table 4.6. The intramolecular hydrogen bond that exists in compound **1.2** is described by O1−H10•••N4 with a bond angle of 157.5°. The distance

between the nitrogen N4 and hydrogen H10 is 1.62 Å, which is shorter than the total of their Van der Waals radii (2.75 Å), making this intramolecular hydrogen bond quite significant.

Table 4.6: Hydrogen bonding interactions for compound **1.2** hydrate.

D−H•••A(Interactions)	**d(D−H)**	**d(H•••A)**	**d(D•••A)**	**∠D−H•••A**
N1−H1•••O2	0.875(18)	1.991(18)	2.8319(17)	160.6(17)
O1−H10•••N4[intra]	0.974(19)	1.616(18)	2.5435(16)	157.5(19)
O2−H2A•••O1	0.954(14)	1.828(15)	2.7505(15)	161.8(13)
O2−H2B•••N2	0.955(16)	1.809(15)	2.7627(16)	176(2)
N3−H3N•••O2	0.868(18)	2.132(18)	2.9986(18)	176.5(14)
C12−H12A•••F1	0.9900	2.4800	3.253(2)	135.00
C16−H16•••F1	0.9500	2.5500	3.439(2)	157.00

D = Donor; A = Acceptor; d = distance (Å); ∠ = angle (º).

4.4.1.2 Single Crystal XRD Studies of Compound 2.2

The single crystal XRD and refinement data for compound **2.2** are outlined in Table 4.7 below.

Table 4.7: Data-collection and refinement parameters for compound **2.2**.

Parameter	**Value**
Molecular Formula	$C_{27}H_{26}F_4N_4O$
Formula Weight	498.52
Crystal System	triclinic
Space Group	P-1
a (Å)	10.5950(6)
b (Å)	11.1515(7)
c (Å)	11.4711(7)
α (º)	69.862(1)
β (º)	74.979(1)
γ (º)	82.623(1)
V ($Å^3$)	1227.83(13)
Z	2
D (calc) ($g.cm^{-3}$)	1.348
μ (MoKα) (mm^{-1})	0.105
F (000)	520
Crystal Size (mm^3)	0.17 x 0.19 x 0.27
Temperature (K)	173
Radiation (Å)	MoKα 0.71073
θ Min–Max (º)	1.9-28.4
Index ranges ±*h*, ±*k*, ±*l*	-14:14; -14:14; -15:15
Reflections (total)	33037
Reflections (unique)	6097
R (int)	0.039
Reflections with I>2σ(I)	4601
Nref, Npar	609,390

R1, w*R*2, S	0.0427,0.1094,1.04
Max. and Av. Shift/Error	0.03, 0.00
Δρmin, max (e Å^{-3})	-0.25, 0.24

The crystal structure of compound **2.2** (Figure 4.8) was conclusively refined to an acceptable level despite the disorder in the trifluoromethyl group. The geometrical data were also obtained in the form of CIF files.

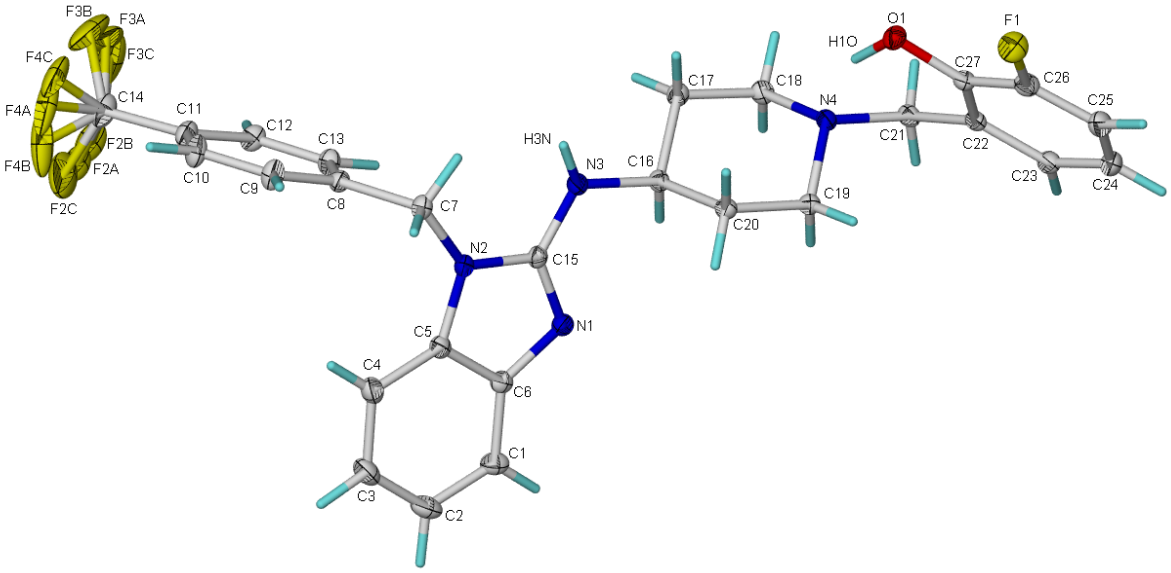

Figure 4.8: Single crystal X-ray structure of compound **2.2**, where thermal ellipsoids are drawn at 30% probability level.

All non-hydrogen atoms were refined anisotropically. All hydrogen atoms, except H10 on O1 and H3N on N3, were placed in idealized positions and refined in riding models with U_{iso} assigned 1.2 or 1.5 times U_{eq} of their parent atoms. The bond distances were constrained from 0.95 to 1.00 Å. The hydrogen atoms H10 and H3N were located in different density maps and refined independently without restraints. The trifluoromethyl (CF_3) group was disordered over three positions with refined site occupancy factors of 0.460(3), 0.216(3) and 0.324(3), respectively. The structure was refined to an R factor of 0.0427. The predominant hydrogen bonding interactions in the crystal structure of compound **2.2** are summarized in Table 4.8. The distance between the nitrogen N4 and hydrogen H10 is 1.71 Å. The bond angle for the intramolecular hydrogen bond O1−H10•••N4 is 154.1°, making the bond quite noteworthy.

Table 4.8: Hydrogen bonding interactions for compound **2.2**.

D−H•••A(Interactions)	d(D−H)	d(H•••A)	d(D•••A)	∠D−H•••A
O1−H10•••N4[intra]	0.97(2)	1.71(2)	2.6194(15)	154.1(19)
N3−H3N•••O1	0.861(18)	2.327(18)	3.1445(16)	158.7(15)
C24−H24•••N1	0.9500	2.5900	3.534(2)	170.00
C25−H25•••F1	0.9500	2.5400	3.4024(18)	151.00

D = Donor; A = Acceptor; d = distance (Å); ∠ = angle (º).

4.4.2 Infrared (IR) Spectroscopy Analysis

The IR absorption intensity and frequency of hydroxy (OH) stretching vibrations show a rigorous change due to the formation of hydrogen bonds. Intermolecular hydrogen bond formation results in an enhancement of the OH absorption intensity and a reduction in the vibrational frequency. On the contrary, an OH band involved in an intramolecular hydrogen bond usually has a weak vibrational intensity, and its frequency is reduced drastically.[22] In this thesis work, IR experiments were performed on compounds **1.2** and **2.2** to ascertain the presence of IMHB. IR spectroscopy was conducted on a Perkin-Elmer Spectrum 100 FT-IR spectrometer using Attenuated Total Reflectance (ATR) with bond vibrations measured in reciprocal centimetres (cm^{-1}). The IR samples of these compounds were made by mixing them thoroughly with dry potassium bromide (KBr) to obtain a KBr disk which was then placed in the sample holder of the spectrometer.

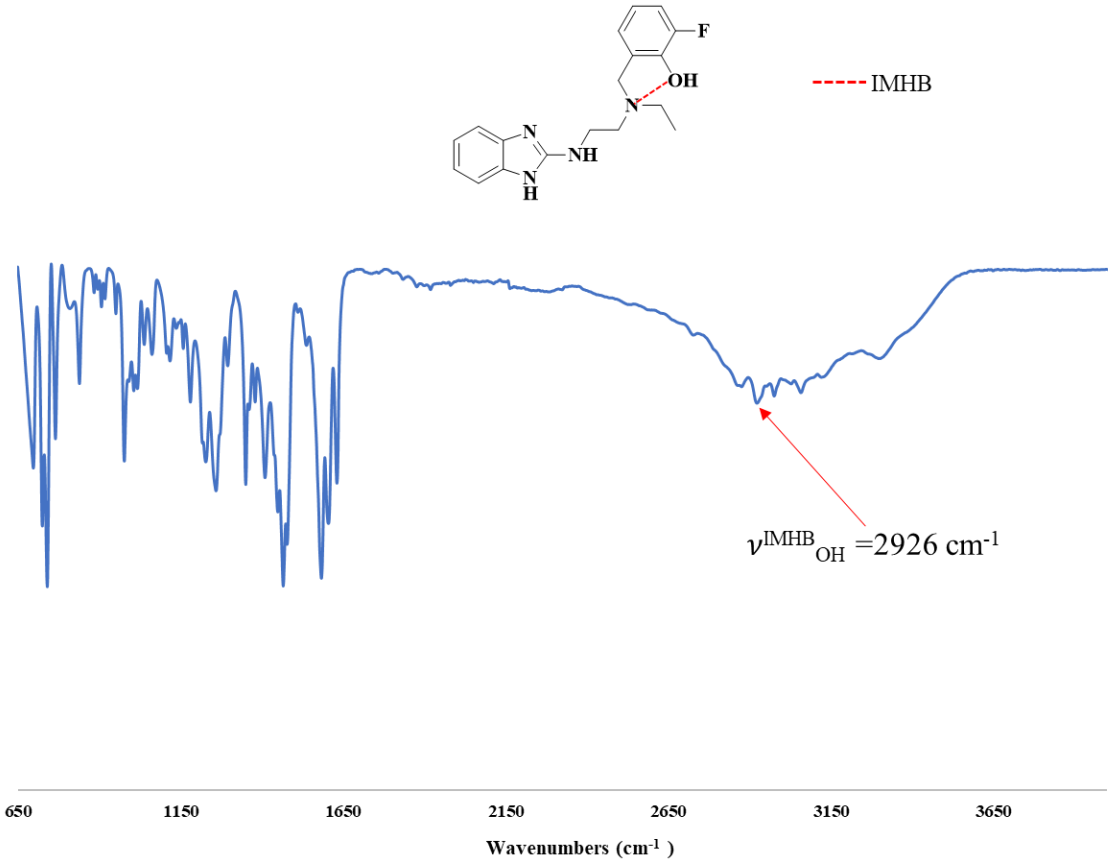

Figure 4.9: IR spectrum of compound **1.2**.

In the IR spectrum of compound **1.2** (Figure 4.9), the νOH band is found at 2926 cm^{-1}. This band is broad and considerably shifted towards a lower frequency. The lower frequency indicates an intramolecular hydrogen bond, which is quite significant. Similarly, the IR spectrum of compound **2.2** (Figure 4.10) shows a weak frequency νOH band at 2947 cm^{-1}, indicating the presence of IMHB in the molecule.

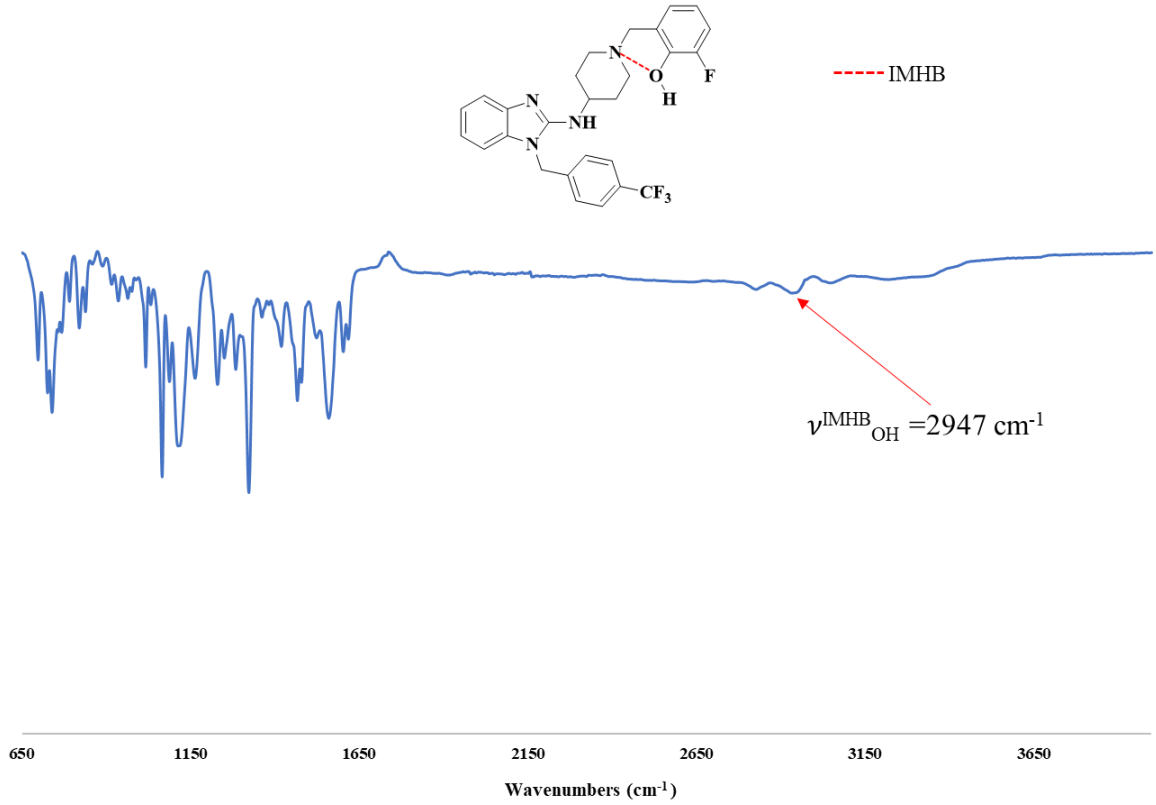

Figure 4.10: IR spectrum of compound **2.2**.

4.4.3 Density Functional Theory (DFT)

Optimized structures of compounds **1.2** and **2.2** were calculated at the B3LYP/6-31+G** level of theory using the crystal structures of both compounds as the starting input for the calculations. The primary rationale of the calculations was to ensure that the compounds were able to form an intramolecular hydrogen bond.

4.4.3.1 Optimised Structure of Compound 1.2 using DFT

The DFT calculation output of compound **1.2** (Figure 4.11) displayed an IMHB from the hydroxyl group to the tertiary amine with a bond length of 1.692 Å and a bond angle of 153.35°. Since the interest of the calculation was to find an IMHB, the crystal water molecule was removed before the optimization at the B3LYP/6-31+G** level of theory, followed by a frequency calculation to ensure that there was no imaginary frequency.

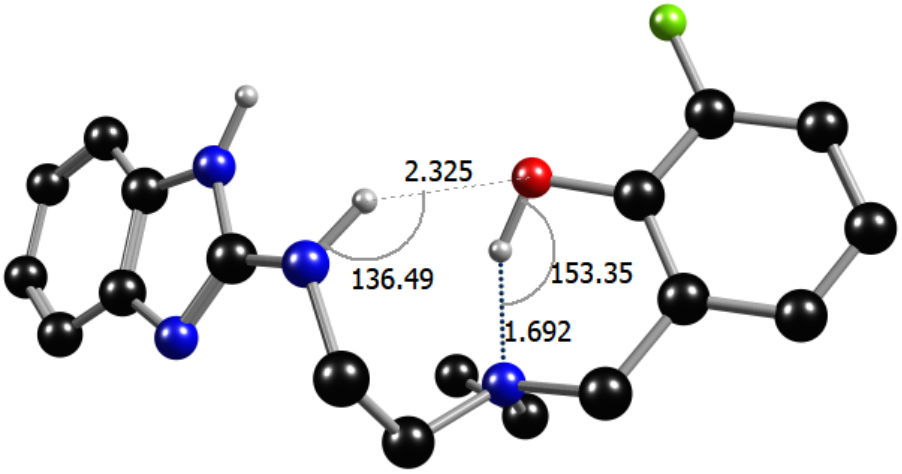

Figure 4.11: Optimized structure of compound **1.2** at the B3LYP/6-31+G** level of theory.

An overlay of the crystal structure and the optimized structure of compound **1.2** (Figure 4.12) resulted in a good root mean square deviation (RMSD) of 0.501 for both geometries. The deviation was mainly due to the ethylene linker of the molecule. The dihedral angle of the C-N-C-C (starting from the benzimidazole ring) was 72.3° for the crystal structure and 70.9° for the B3LYP/6-31+G** result.

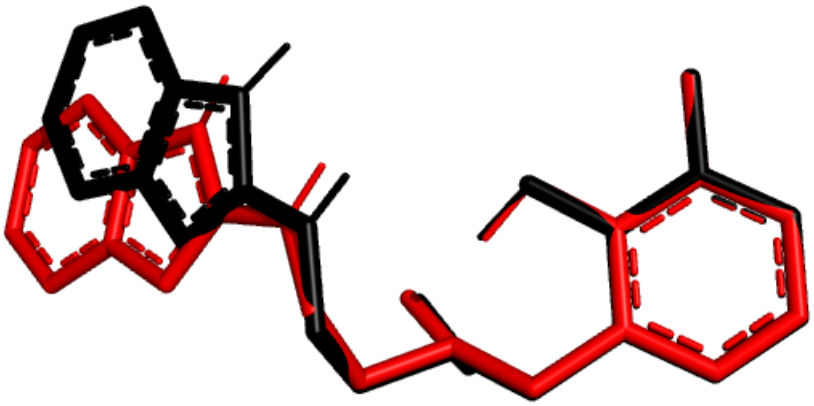

Figure 4.12: Overlay of the crystal structure (red) and the optimized structure (black) of compound **1.2**.

4.4.3.2 Optimised Structure of Compound 2.2 using DFT

The B3LYP/6-31+G** was used to simulate the crystal structure output of compound **2.2,** which displayed an IMHB between the hydroxyl group and the piperidine nitrogen, with a bond length of 1.804 Å and a bond angle of 149.21°.

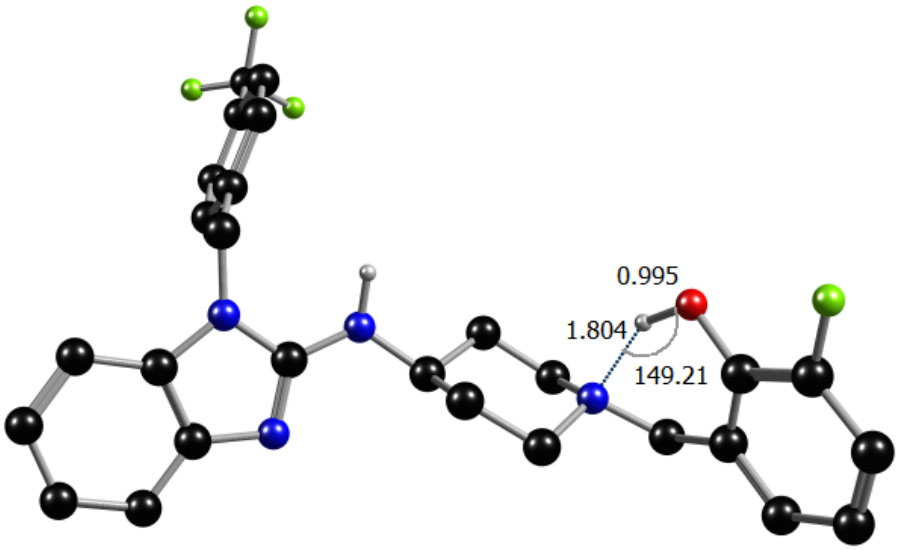

Figure 4.13: Optimized structure of compound **2.2** at the B3LYP/6-31+G** level of theory.

The B3LYP/6-31+G** optimized structure in an overlay with the crystal structure of compound **2.2** yielded an RMSD value of 0.198, which indicates an excellent overlay over the heavy atoms of the molecule. Figure 4.14 below shows the overlay of the two structures.

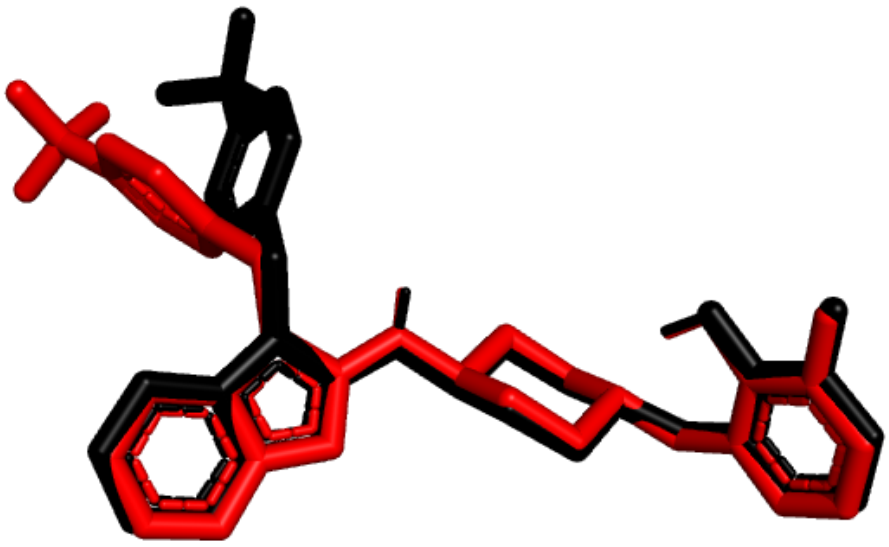

Figure 4.14: Overlay of the crystal structure (red) and the optimized structure (black) of compound **2.2**.

4.4.3.3 IR Spectra Predictions of Compound 1.2 using DFT

The IR spectra of the molecules under scrutiny were calculated at the B3LYP/6-31+G** level of theory. For compound **1.2**, the IMHB between the hydroxyl group and the aliphatic tertiary amine showed a vibrational frequency peak at 2919 cm^{-1} (Figure 4.15A). The optimal dihedral

angles for this interaction were found to be 14.52° (C-O-H-N), -18.02° (C-C-O-H), and 38.90° (C-C-C-N). Once the dihedral angle of C-C-C-N changed from 38.90° to -161.53°, the IMHB was lost, and the 2919 cm^{-1} peak was shifted to 3825$cm^{-1,}$ which is indicative of a normal O-H stretching vibration without the presence of an IMHB (Figure 4.15B). The relative stabilization energies obtained for both conformations (0 kcal/mol for IMHB and 9.56 kcal/mol for non-IMHB) show that compound **1.2** has a high propensity to form an IMHB.

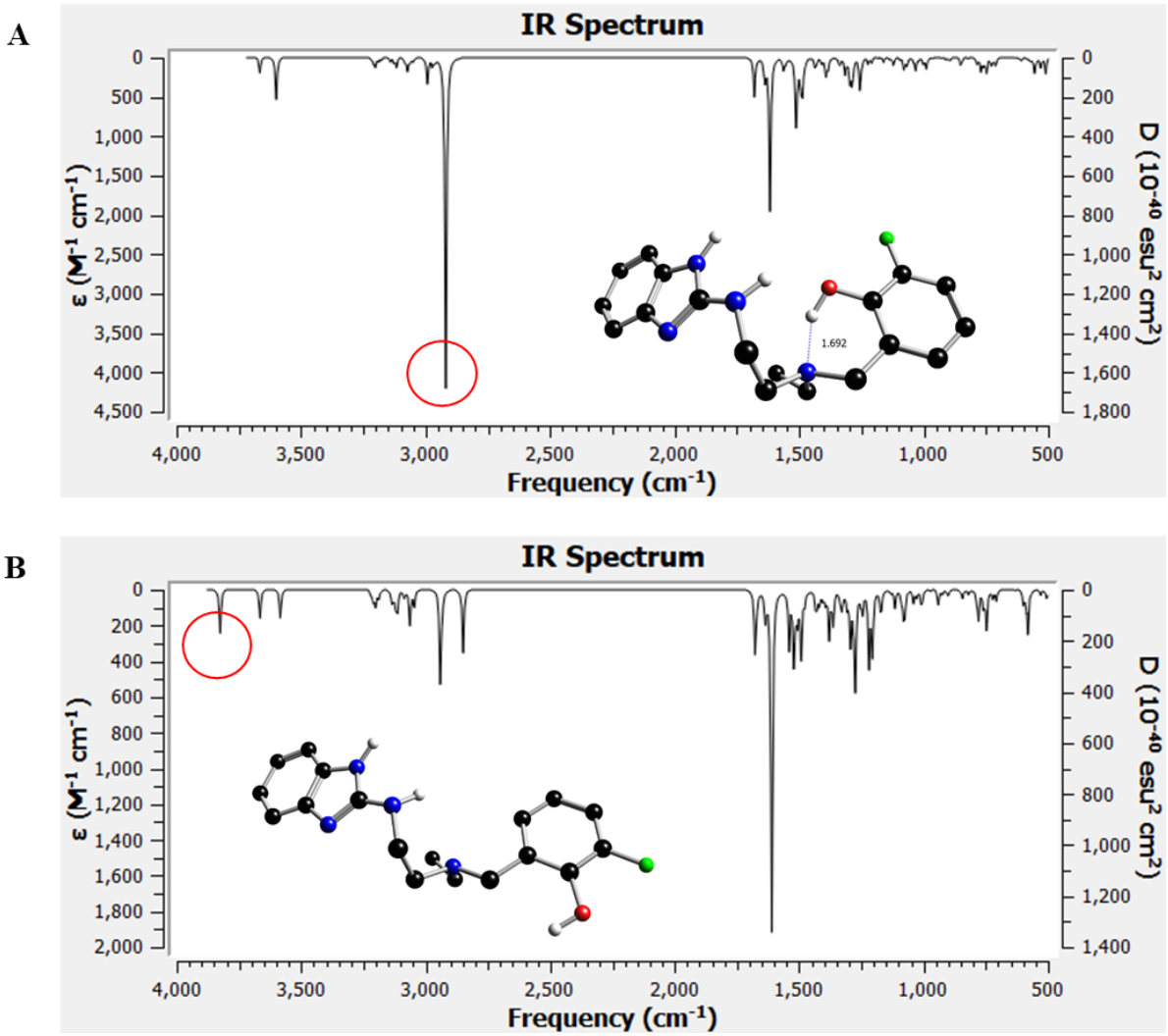

Figure 4.15: Predicted IR spectra of compound **1.2** at B3LYP/6-31+G** level of theory (A) Spectrum with the presence of IMHB (B) Spectrum without IMHB.

4.4.3.4 IR Spectra Predictions of Compound 2.2 using DFT

Similar IR spectra predictions were carried out on compound **2.2**. The IMHB between the hydroxyl group and the piperidine nitrogen showed a vibrational frequency peak at 3244 cm^{-1} with dihedral angles of 1.10° (C-O-H-N), 15.40° (C-C-O-H), and -42.52° (C-C-C-N). Again,

this IMHB was lost once the dihedral angle of C-C-C-N changed from -42.52° to 112.81° and the peak at 3244 cm-^{1} shifted to 3814 cm^{-1} (Figure 4.16B). Furthermore, the tendency of compound **2.2,** forming an IMHB, was confirmed by the relative stabilization energies obtained for both conformations (0 kcal/mol for IMHB and 8.36 kcal/mol for non-IMHB).

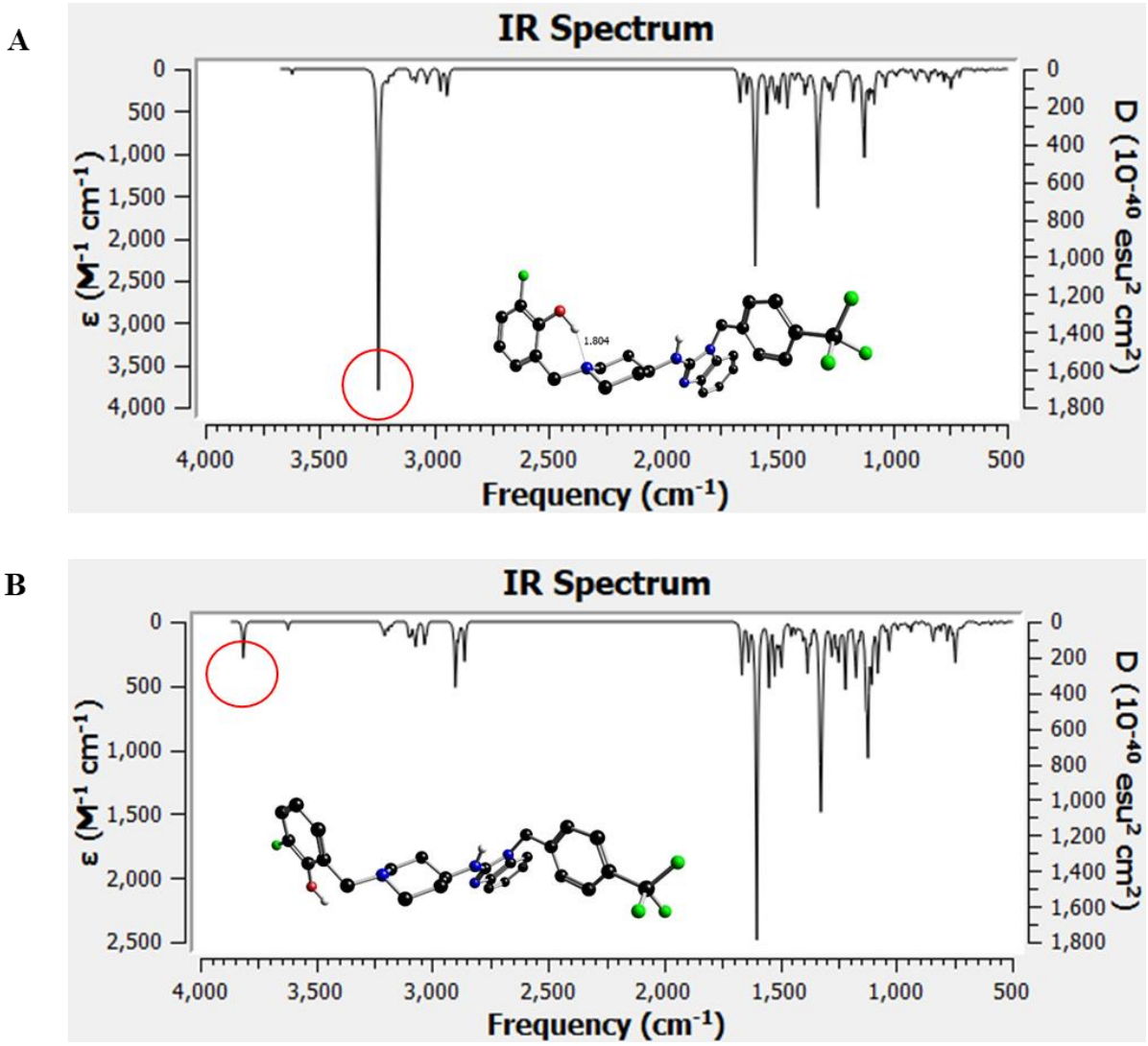

Figure 4.16: Predicted IR spectra of compound **2.2** at B3LYP/6-31+G** level of theory (A) Spectrum with the presence of IMHB (B) Spectrum without IMHB.

4.5 Conclusions

Studies conducted in relation to physicochemical profiling and methods of assessing intramolecular hydrogen bonds in molecules were described in this chapter. The physicochemical assessment revealed that both the benzimidazoles and the imidazopyridines had very few violations of Lipinski's RO5 and no violation of Veber's rule. Additionally, evaluation of the factors affecting solubility for each class of compounds showed that many

factors simultaneously affect the solubility of compounds across a specific class; hence, it may be crucial to assess the factors responsible for aqueous solubility based on individual cases rather than an entire class of compounds.

To assess the presence of IMHB in the molecules, compounds **1.2** and **2.2** were used as representative analogues for the studies. Single crystal X-ray analysis, IR spectroscopy and DFT calculations ascertained the presence of IMHB in these compounds.

4.6 References

(1) Waring, M. J. Lipophilicity in Drug Discovery. *Expert Opin. Drug Discov.* **2010**, *5* (3), 235–248. https://doi.org/10.1517/17460441003605098.

(2) Schuster, D.; Laggner, C.; Langer, T. Why Drugs Fail - A Study on Side Effects in New Chemical Entities. *Curr. Pharm. Des.* **2005**, *11* (27), 3545–3559. https://doi.org/10.2174/138161205774414510.

(3) Meanwell, N. A. Improving Drug Candidates by Design: A Focus on Physicochemical Properties As a Means of Improving Compound Disposition and Safety. *Chem. Res. Toxicol.* **2011**, *24* (9), 1420–1456. https://doi.org/10.1021/tx200211v.

(4) Vistoli, G.; Pedretti, A.; Testa, B. Assessing Drug-Likeness – What Are We Missing? *Drug Discov. Today* **2008**, *13* (7–8), 285–294. https://doi.org/10.1016/j.drudis.2007.11.007.

(5) Lipinski, C. A. Drug-like Properties and the Causes of Poor Solubility and Poor Permeability. *J. Pharmacol. Toxicol. Methods 44* (1), 235–249.

(6) Lipinski, C. A.; Lombardo, F.; Dominy, B. W.; Feeney, P. J. Experimental and Computational Approaches to Estimate Solubility and Permeability in Drug Discovery and Development Settings 1PII of Original Article: S0169-409X(96)00423-1. The Article Was Originally Published in Advanced Drug Delivery Reviews 23 (1997). *Adv. Drug Deliv. Rev.* **2001**, *46* (1–3), 3–26. https://doi.org/10.1016/S0169-409X(00)00129-0.

(7) Veber, D. F.; Johnson, S. R.; Cheng, H.-Y.; Smith, B. R.; Ward, K. W.; Kopple, K. D. Molecular Properties That Influence the Oral Bioavailability of Drug Candidates. *J. Med. Chem.* **2002**, *45* (12), 2615–2623. https://doi.org/10.1021/jm020017n.

(8) Congreve, M.; Carr, R.; Murray, C.; Jhoti, H. A 'Rule of Three' for Fragment-Based Lead Discovery? *Drug Discov. Today* **2003**, *8* (19), 876–877. https://doi.org/10.1016/S1359-6446(03)02831-9.

(9) Kerns, E.; Di, L.; Carter, G. In Vitro Solubility Assays in Drug Discovery. *Curr. Drug Metab.* **2008**, *9* (9), 879–885. https://doi.org/10.2174/138920008786485100.

(10) Bevan, C. D.; Lloyd, R. S. A High-Throughput Screening Method for the Determination of Aqueous Drug Solubility Using Laser Nephelometry in Microtiter Plates. *Anal. Chem.* **2000**, *72* (8), 1781–1787. https://doi.org/10.1021/ac9912247.

(11) Hill, A. P.; Young, R. J. Getting Physical in Drug Discovery: A Contemporary Perspective on Solubility and Hydrophobicity. *Drug Discov. Today* **2010**, *15* (15–16), 648–655. https://doi.org/10.1016/j.drudis.2010.05.016.

(12) Glomme, A.; März, J.; Dressman, J. B. Comparison of a Miniaturized Shake-Flask Solubility Method with Automated Potentiometric Acid/Base Titrations and Calculated

Solubilities. *J. Pharm. Sci.* **2005**, *94* (1), 1–16. https://doi.org/10.1002/jps.20212.

(13) Banerjee, S.; Yalkowsky, S. H.; Valvani, C. Water Solubility and Octanol/Water Partition Coefficients of Organics. Limitations of the Solubility-Partition Coefficient Correlation. *Environ. Sci. Technol.* **1980**, *14* (10), 1227–1229. https://doi.org/10.1021/es60170a013.

(14) Jain, N.; Yalkowsky, S. H. Estimation of the Aqueous Solubility I: Application to Organic Nonelectrolytes. *J. Pharm. Sci.* **2001**, *90* (2), 234–252. https://doi.org/10.1002/1520-6017(200102)90:2<234::AID-JPS14>3.0.CO;2-V.

(15) Aguilar, M.-I. Reversed-Phase High-Performance Liquid Chromatography. In *HPLC of Peptides and Proteins*; Humana Press: New Jersey; pp 9–22. https://doi.org/10.1385/1-59259-742-4:9.

(16) Aitipamula, S.; Banerjee, R.; Bansal, A. K.; Biradha, K.; Cheney, M. L.; Choudhury, A. R.; Desiraju, G. R.; Dikundwar, A. G.; Dubey, R.; Duggirala, N.; et al. Correction for Polymorphs, Salts and Cocrystals: What's in a Name? *Cryst. Growth Des.* **2012**, *12* (8), 4290–4291. https://doi.org/10.1021/cg300704b.

(17) SAINT Version 7.60a, Bruker AXS Inc. Madison, WI, USA 2006.

(18) Sheldrick G. M. SHELXS-97, SHELXL-2014 and SADABS Version 2.05. University of Göttingen, Germany 1997.

(19) Barbour, L. J. X-Seed — A Software Tool for Supramolecular Crystallography. *J. Supramol. Chem.* **2001**, *1* (4–6), 189–191. https://doi.org/10.1016/S1472-7862(02)00030-8.

(20) Atwood, J. L.; Barbour, L. J. Molecular Graphics: From Science to Art. *Cryst. Growth Des.* **2003**, *3* (1), 3–8. https://doi.org/10.1021/cg020063o.

(21) The Persistence of Vision Raytracer http://www.povray.org.

(22) Mitsuzuka, A.; Fujii, A.; Ebata, T.; Mikami, N. Infrared Spectroscopy of Intramolecular Hydrogen-Bonded OH Stretching Vibrations in Jet-Cooled Methyl Salicylate and Its Clusters. *J. Phys. Chem. A* **1998**, *102* (48), 9779–9784. https://doi.org/10.1021/jp9830934.

CHAPTER 5

MECHANISTIC STUDIES

5.1 Chapter Overview

In this chapter, mechanistic studies of frontrunner compounds **1.3** and **3.14** are discussed. The chapter commences with the various approaches used towards deconvoluting the mechanism of action of phenotypically active compounds. This is followed by the discussion of results

from photophysical, pharmacological and fluorescence live-cell imaging studies on previously synthesized fluorescent probes. Finally, the results from docking the parent compounds **1.3** and **3.14** against the β-hematin surface, and their evaluation in the cellular heme fractionation assay are presented and discussed.

5.2 Introduction

As previously described in section 1.7 of chapter 1, the phenotypic-based approach to drug discovery enables discovering lead compounds for many diseases where the drug target(s) have not been identified or validated. Nonetheless, identifying the target has also proven to be a practical approach to discovering drugs for understudied diseases.[1] Even though mechanistic deconvolution of hits or leads is a very challenging facet of the phenotypic drug discovery approach, the emergence of various new technologies in the areas of fluorescent drug localization studies, genomics and chemical proteomics has aided in identifying and validating suitable targets of phenotypically active leads, along with understanding their mechanism of action (MoA).[2–4]

In the genomics approach to target identification, information generated from sequencing the genome of humans and other organisms is employed to understand the biological convolution of various human diseases, identify and authenticate new targets.[5] Chemical proteomics, on the contrary, relies on the interplay between biology, chemistry, biochemistry, structural biology and bioinformatics to identify proteins that bind to small molecules and provide appropriate starting points for the discovery of new chemical entities.[6,7] Efforts of the omics-based approaches of target identification have been complemented by fluorescence live-cell imaging studies. Over the years, live-cell imaging tools have provided insight into understanding the subcellular localization and associated phenotypes of chemical therapeutics.[8,9] To undertake fluorescence imaging, a fluorescent molecule must be present in the experimental sample. Even though intrinsic fluorescent molecules in cells such as tryptophan, NADPH and flavins have been used in these studies[10–12], external fluorophores, in most cases, are employed either genetically or chemically.

5.3 Fluorescence Drug Localization Studies

As part of contributing towards understanding the mechanism of action of the class of compounds studied in this thesis work, fluorescence drug localization studies was employed as

the starting point to logically probe into the subcellular localization of the target compounds within *Plasmodium falciparum*. Compounds **1.3** (IC_{50}*Pf*NF54 = 0.079 μM) and **3.14** (IC_{50}*Pf*NF54 = 0.08 μM) were used as representative analogues for the benzimidazoles and imidazopyridines, respectively. These compounds were selected based on their nanomolar *in vitro* asexual blood-stage antiplasmodium activity, acceptable cytotoxicity profile against the mammalian Chinese Hamster Ovary cell line, solubility and their beta-hematin inhibition activity.

In the absence of an intrinsic fluorescence property for both compounds, fluorescent probes of compounds **1.3** and **3.14** were synthesized with the extrinsic fluorophore 7-nitrobenz-2-oxa-1,3-diazole (NBD) (Figure 5.1) as described in Chapter 2. The selection of NBD as a suitable fluorophore was based on various reasons. Firstly, it is an inexpensive small fluorophore; hence, it is expected to cause the least perturbation to biological activity upon conjugation to the target compounds. Also, the fluorescence of NBD is stable over a biologically relevant pH range even though its fluorescence is intensified in non-aqueous environments.[13] Finally, despite the solvatochromic nature of NBD, its excitation and emission maxima in aqueous media are approximately 470 and 540 nm, respectively; thus, these bands are expected to minimally overlap with the Soret region of Fe(III)PPIX, should the compounds accumulate in the digestive vacuole of *P. falciparum*.[13]

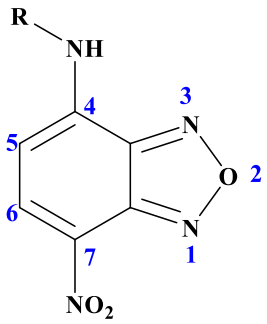

Figure 5.1: Structure of 7-nitrobenz-2-oxa-1,3-diazole (NBD) fluorophore with an amine substitution at 4-position.

5.3.1 Photophysical and Pharmacological Evaluation of Fluorescent Probes

The photophysical characterization of both fluorescent probes revealed that they possess similar photophysical properties. In the case of **1.3-NBD**, three absorption maxima were observed corresponding to the absorbance of the benzimidazole core (occurring at 350 nm), the 3-chlorophenol moiety (at 270 nm) and the absorption due to NBD. However, as shown in Figure 5.2A, the maximum fluorescence absorption is due to the NBD reporter fluorophore

occurring at 485 nm. This absorbance occurs in the visible region of the electromagnetic spectrum and is suitable for probing the subcellular accumulation of the compounds in *P. falciparum*.

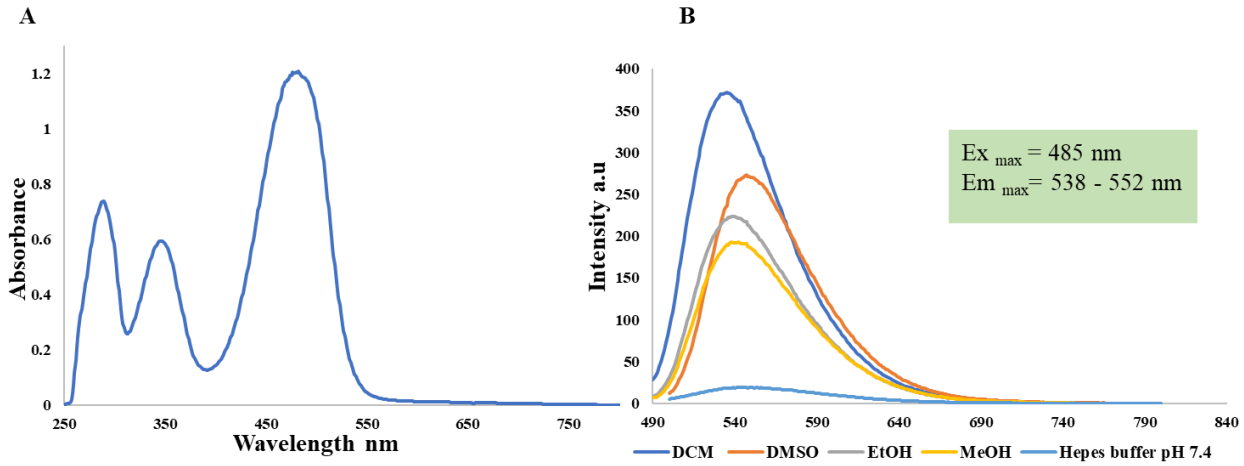

Figure 5.2: (A) Excitation spectrum of **1.3-NBD** in DMSO (B) Emission spectrum of **1.3-NBD** in varying solvents.

Following the excitation at the maximum absorption, fluorescence emission was observed around 540 nm (Figure 5.2B). Fluorescence emission exhibited a slight solvatochromic shift from 538-550 nm over five solvents. As expected, the fluorescence of NBD fluorophore was brightest in non-polar environments and very weak in aqueous solvents. Therefore the interaction of these fluorescent derivatives with the phospholipid bilayers or neutral lipid components should be easily detected during imaging studies. Furthermore, both fluorescent analogues retained pharmacological activity against *Plasmodium falciparum*, making them suitable representatives of the parent compounds to probe their sub-cellular accumulation.

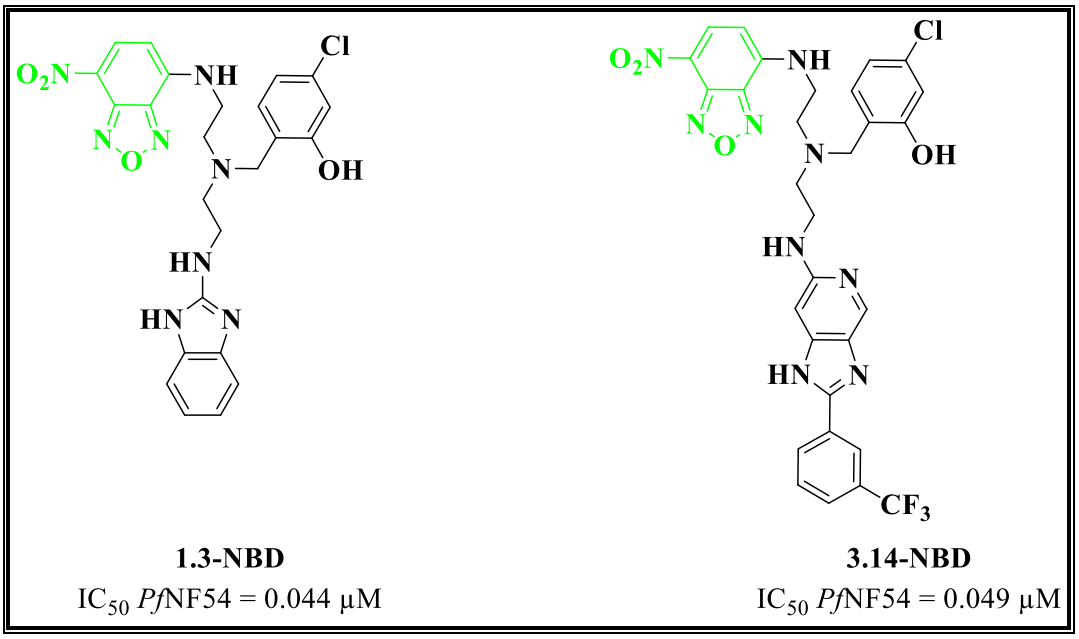

Figure 5.3: Antiplasmodium activity of fluorescent probes **1.3-NBD** and **3.14-NBD**.

5.3.2 Fluorescence Live-cell Microscopy

Fluorescence live-cell subcellular localization and colocalization studies with commercially available organelle trackers were undertaken. Several available tracker dyes have been used to co-illuminate cellular compartments or subcellular structures in *P. falciparum*. More specifically, the dyes employed in this work have previously been used and reported in literature[14,15] hence justifying their use. These dyes (chemical structures in Figure 5.4) include an acidotrophic dye Lysotracker Red that illuminates the acidic organelles in live cells such as the digestive vacuole, an anthraquinone dye DRAQ 5 with a high affinity for double-stranded DNA, a MitoTracker Deep Red fluorescent dye used to illuminate the mitochondrion of the parasite, an ER-Tracker Red dye which is made up of glibenclamide, linked to BODIPY reporter fluorophore. Glibenclamide binds to the sulfonylurea receptors of ATP-sensitive K^+, prominent on the endoplasmic reticulum (ER).[16]

Finally, Nile Red, a lipophilic dye known and commonly used to illuminate lipids in cells, was also utilized. It is highly solvatochromic in non-polar environments and entirely quenched in water.[17] This dye has previously been used to identify neutral lipid bodies within *P. falciparum,* which have been implicated in hemozoin formation.[18] Nile Red has broad excitation and emission spectra, allowing one to distinguish between different chemical environments. However, the disadvantage of this property is that crosstalk is frequently observed when Nile Red is used in conjunction with other green dyes that require high-energy excitation. For

instance, when excited using a 561 nm laser and monitored for fluorescence in the red region of the visible spectrum (650-710 nm), Nile Red emits a signal corresponding to the fluorescence from a phospholipid-rich environment. However, when the dye is excited at lower wavelengths (575-630 nm), the resulting emission corresponds to an environment characterized by neutral lipids.

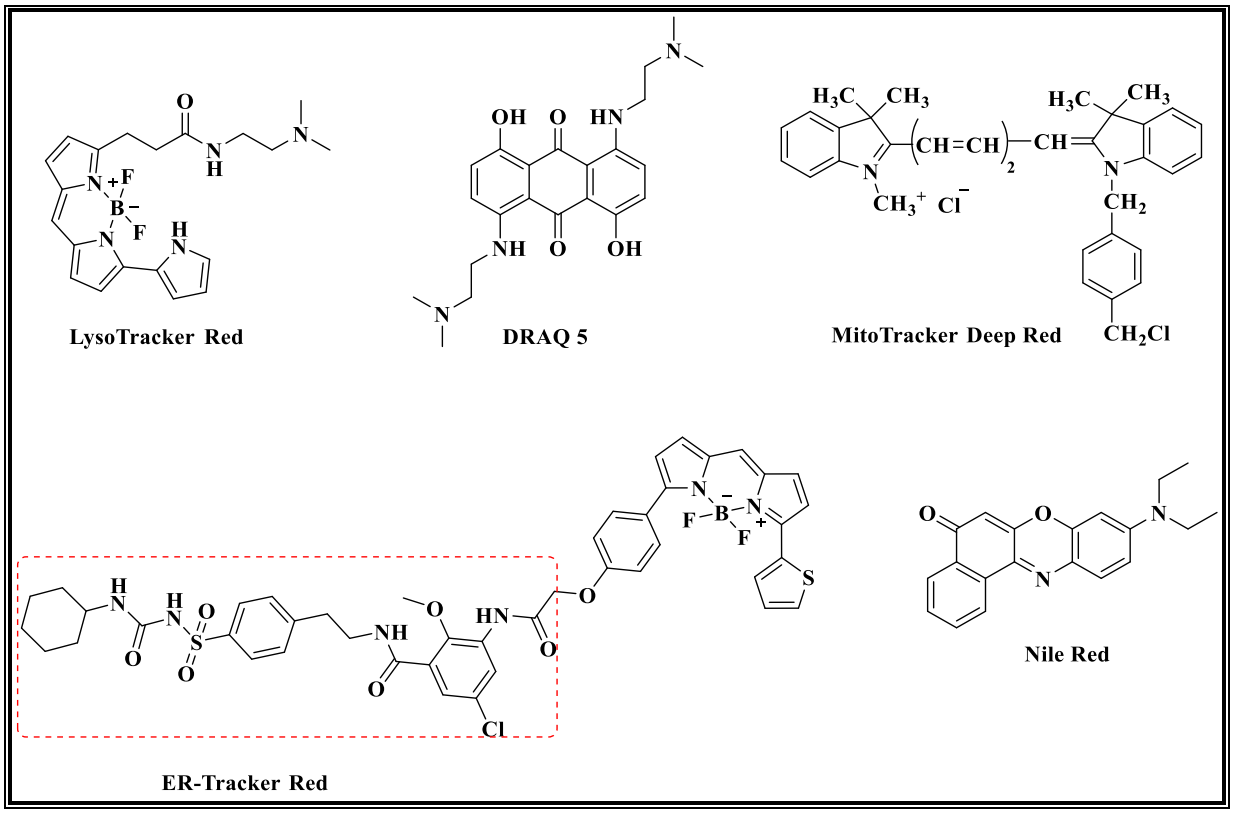

Figure 5.4: Chemical structures of the commercially available tracker dyes used in this study. The sulfonylurea drug glibenclamide is shown in the red dashed box in its derivatized amide form.

5.3.2.1 Confocal Fluorescence Microscopy

Infected red blood cells were resuspended in Ringer's solution and incubated at 37 °C for live-cell imaging.[19] Confocal fluorescence microscopy was used for the initial examination of the red blood cells infected with the chloroquine-sensitive (NF54) strain of *P. falciparum*. Infected erythrocytes were easily identified under transmitted light by the hemozoin pigment (Panels **A** and **B** in Figure 5.5). The detection of both **1.3-NBD** and **3.14-NBD** was carried out following several optimizations of drug concentrations.

Cytoplasmic or plasma membrane staining in the infected host cell was observed for both compounds (Panels **A** and **B** in Figure 5.5). However, no signal for these compounds was detected in the uninfected erythrocytes (Panel **C** in Figure 5.5). This suggests no accumulation

of the compounds in uninfected red blood cells and that their activity is specific to *P. falciparum.* Although there are some differences in the host plasma membrane composition between infected and uninfected red blood cells[20], that alone is probably not responsible for the compound's selectivity for the infected red blood cells. The tendency of the compounds to accumulate in *P. falciparum* and not uninfected red blood cells suggests that their site of action is in the *Plasmodium* parasite and not in the host red blood cell, assuming the site of accumulation corresponds to the site of action.

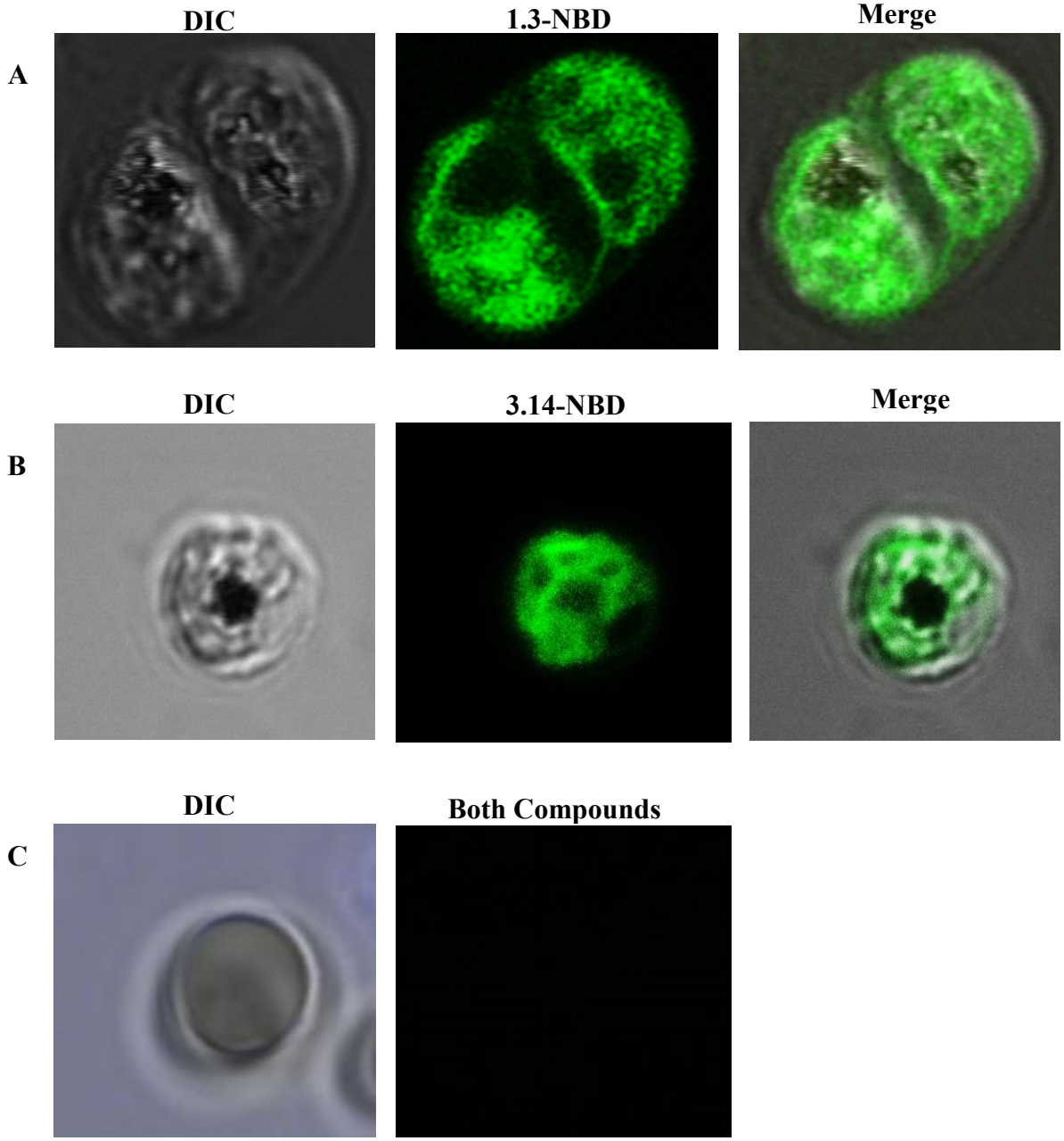

Figure 5.5: Panels A and B represent *P. falciparum*-infected erythrocytes incubated with **1.3-NBD** and **3.14-NBD**. Panel C represents an uninfected erythrocyte incubated with **1.3-NBD** and **3.14-NBD**. Scale bars represent 5 μm.

5.3.2.2 Colocalization Studies

Since the parent compounds **1.3** (BHIA IC_{50} = 32 μM) and **3.14** (BHIA IC_{50} = 9 μM) were potent beta-hematin inhibitors in the cell-free assay, the earlier hypothesis was that their mode of action might be closely linked to the parasite's heme detoxification pathway. Hence, the trophozoite stage of the parasite was ideal for subcellular accumulation studies. During the trophozoites stage, all organelles are fully developed, making their visualization easier. Also, haem detoxification is a process peculiar to the trophozoite stage of the parasite. Besides the digestive vacuole, other organelles such as the endoplasmic reticulum (ER), the mitochondrion, and the plastids (apicoplast) play crucial roles during the intraerythrocytic stage of *P. falciparum*. Unlike the digestive vacuole, these organelles persist in all stages of the intraerythrocytic cycle of the parasite.

Furthermore, these organelles have been implicated as drug targets in other clinically relevant antimalarials. For example, the antimalarial atovaquone inhibits *P. falciparum*'s mitochondrial electron transporter. Consequently, the accumulation of the ER Tracker and the MitoTracker was studied with the fluorescent analogues.

Colocalization studies of fluorescent signals of **1.3-NBD** and the Lysotracker Red in *Plasmodium falciparum* revealed a strong interaction between the two signals. The tracker dye colocalized completely with **1.3-NBD** with intense fluorescence accumulation in the digestive vacuole shown by the arrow in Figure 5.6. However, it should be noted that NBD has the least fluorescence in aqueous media. Hence, observing such intense signals in the digestive vacuole implies that significant accumulation should have occurred. Compound **3.14-NBD,** on the other hand, showed relatively partial colocalization with the Lysotracker dye.

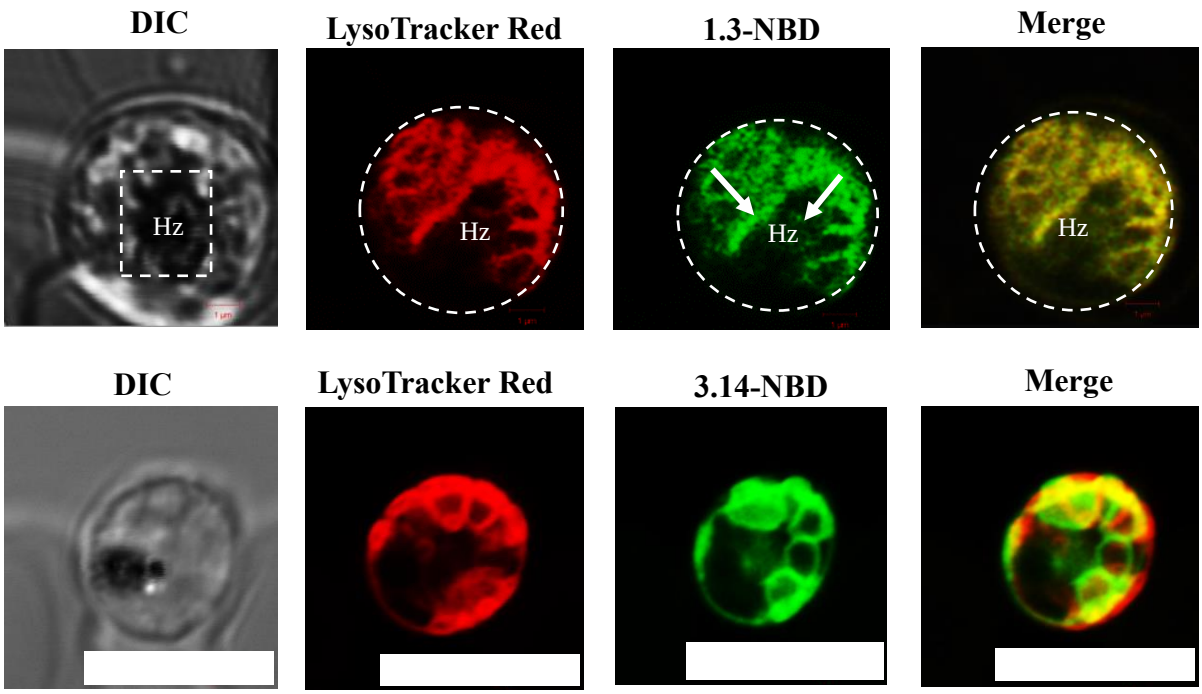

Figure 5.6: Subcellular accumulation of **1.3-NBD** and **3.14-NBD** with LysoTracker Red in *P. falciparum*. Scale bars represent 1 µm.

Both compounds showed no accumulation in the nucleus when incubated with the nuclear marker DRAQ 5. This suggests that both **1.3-NBD** and **3.14-NBD** do not act in the nucleus of the parasite (Figure 5.7).

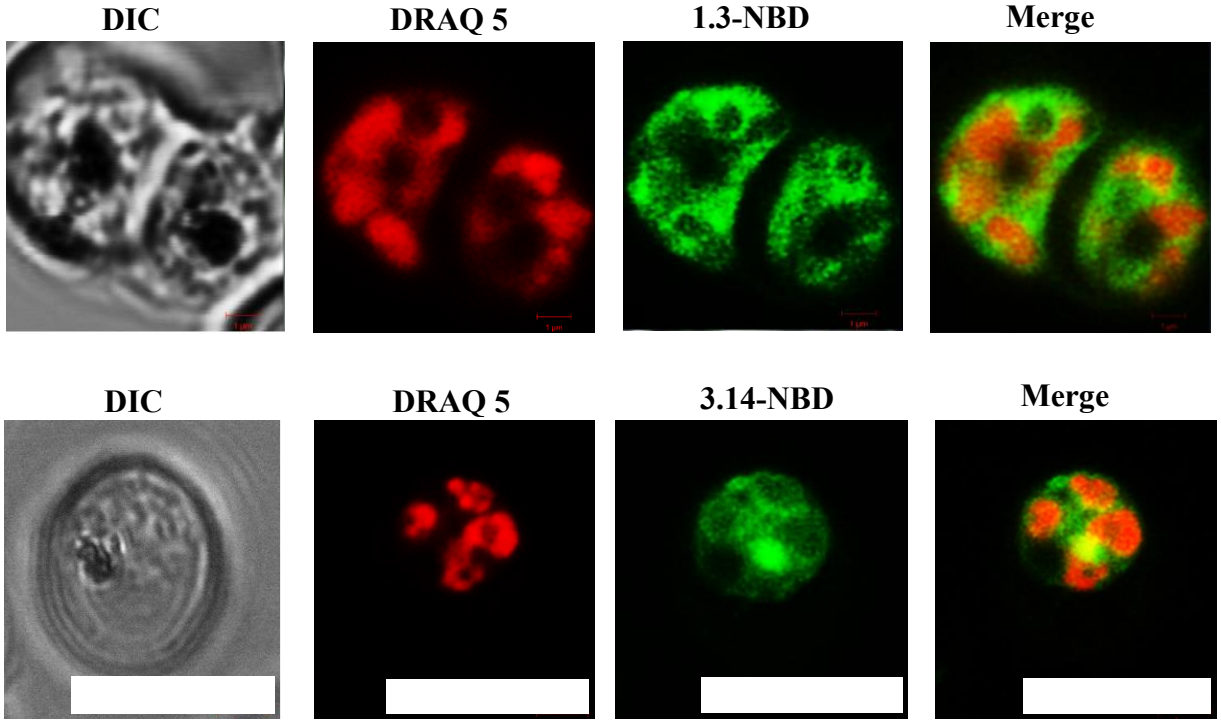

Figure 5.7: Subcellular accumulation of **1.3-NBD** and **3.14-NBD** with nuclear dye DRAQ 5 in *P. falciparum*. Scale bars represent 1 µm.

To probe the association of **1.3-NBD** and **3.14-NBD** with the endoplasmic reticulum and the mitochondrion of the parasite, the ER-Tracker Red and the MitoTracker Deep Red were incubated with the compounds in the parasite. Confocal imaging showed intense accumulation of the dyes, which broadly colocalized with the compounds. For the ER, a punctuate-like structure adjacent to the digestive vacuole was illuminated by both the ER tracker dye and the compounds. This suggests that **1.3-NBD** and **3.14-NBD** accumulate significantly in the ER (Figure 5.8). Similarly, a strong fluorescence signal was observed within the mitochondrion of the parasite. Although very diffused, the signal from the MitoTracker Deep Red colocalizes extensively with that of **1.3-NBD** and **3.14-NBD** (Figure 5.9).

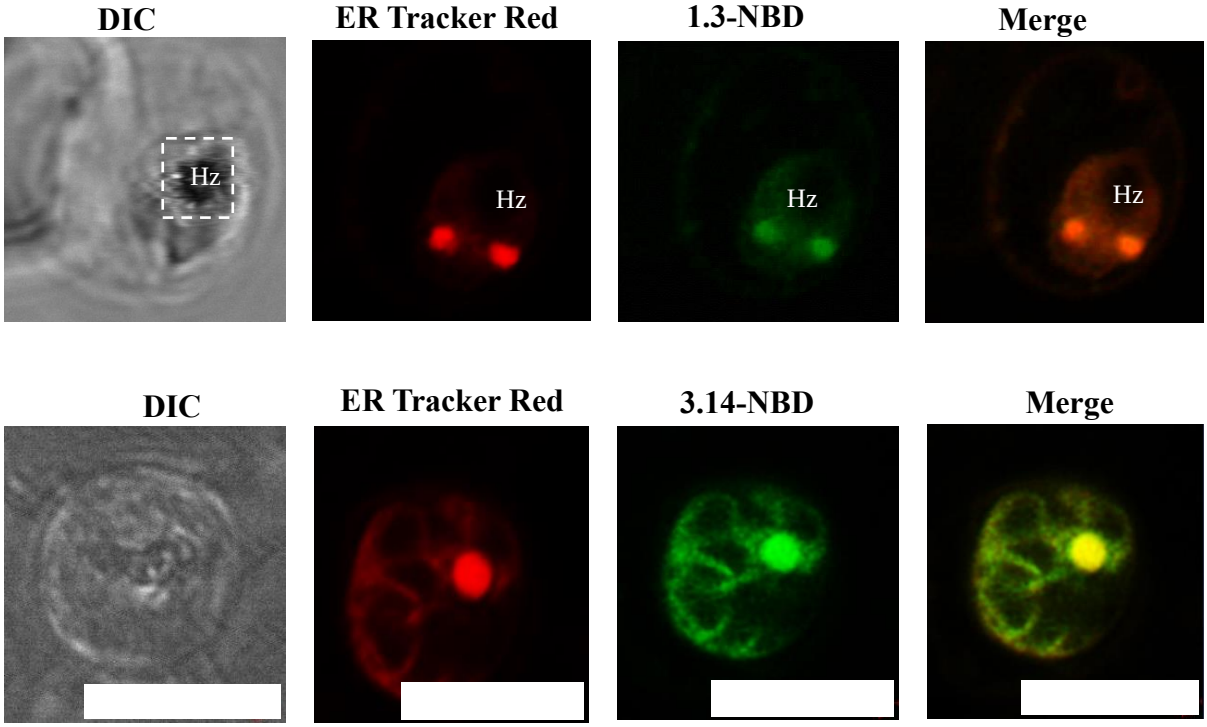

Figure 5.8: Subcellular accumulation of **1.3-NBD** and **3.14-NBD** with ER-Tracker Red in *P. falciparum*. Scale bars represent 1 µm.

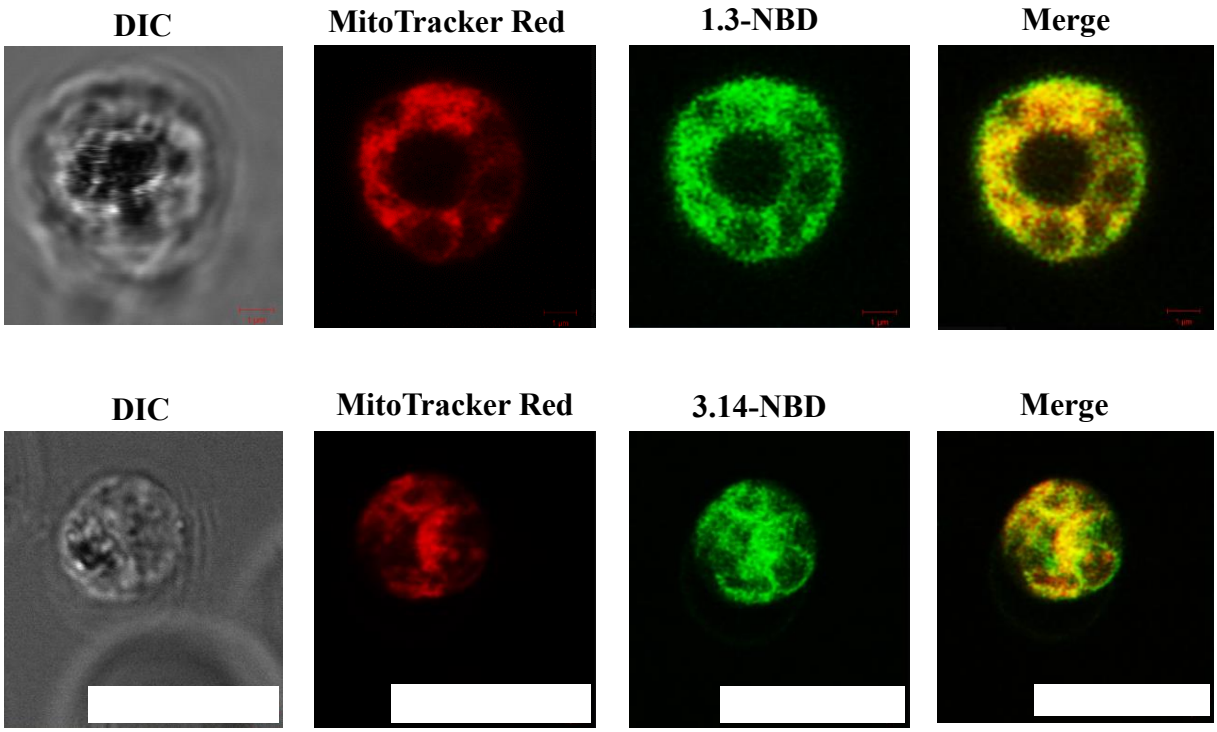

Figure 5.9: Subcellular accumulation of **1.3-NBD** and **3.14-NBD** with MitoTracker Deep Red in *P. falciparum*. Scale bars represent 1 µm.

Nile Red, as previously mentioned, is useful in identifying neutral lipids in *P. falciparum.* Neutral lipid droplets have been implicated in mediating the formation of hemozoin. They can be found concentrated within the parasite's digestive vacuole and located close to hemozoin crystals.[21] Furthermore, molecular dynamic simulations have demonstrated that the lipophilic environment of the lipid body would serve to stabilize the hemozoin precursor dimer and that the formation of hemozoin would be favoured at the lipid/aqueous interface.[22]

When **1.3-NBD** and **3.14-NBD** were incubated with Nile Red, some punctuate structures were observed, which were believed to be neutral lipid droplets. These lipid droplets are formed in the parasite's cytosol and transported into the digestive vacuole to aid in converting heme to hemozoin. Also, neutral lipid droplets are only observed during the trophozoite stage of the parasite's life cycle. As shown in Figure 5.10, **1.3-NBD** and **3.14-NBD** colocalized with these lipid droplets as they form in the parasite's cytosol and are transported into the digestive vacuole.

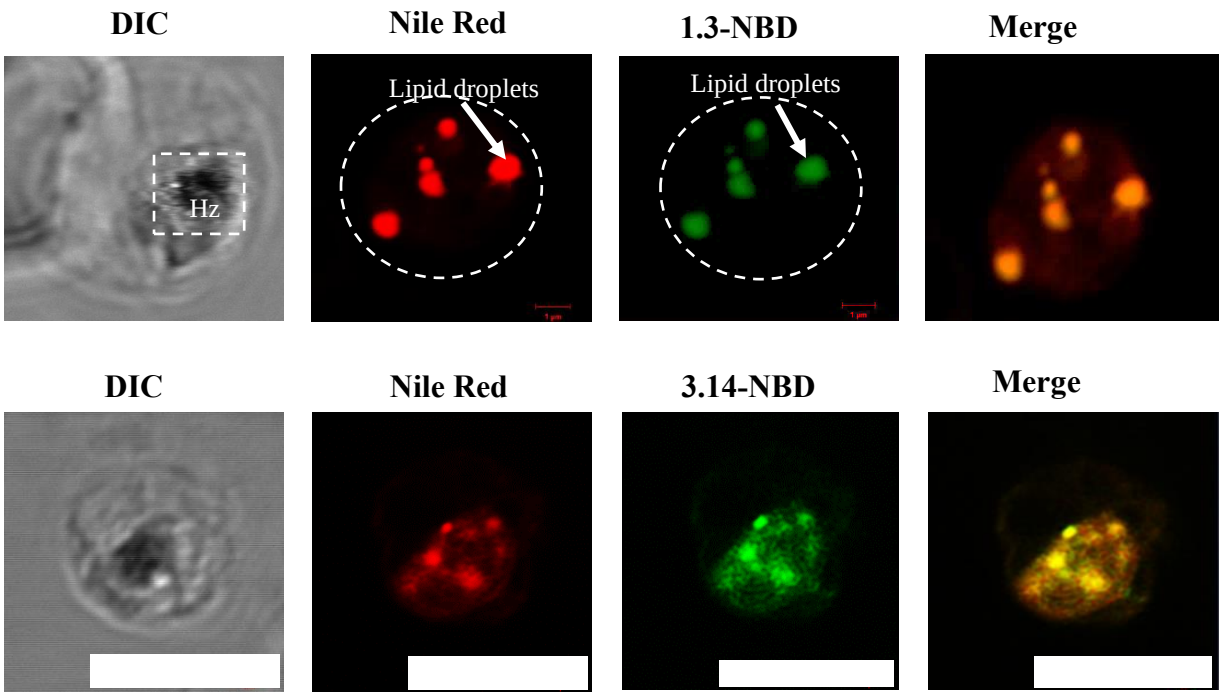

Figure 5.10: Subcellular accumulation of **1.3-NBD** with Nile Red in *P. falciparum*. Scale bars represent 1 µm.

Apart from the nucleus, both compounds seem to interact significantly with all the studied organelles in the parasite, suggesting that their site of action could be any of these organelles except the nucleus. More importantly, a significant amount of both **1.3-NBD** and **3.14-NBD** accumulated in the digestive vacuole and could interfere with hemozoin formation. Although the fluorescent probes have been validated pharmacologically with respect to antiplasmodium activity, there are still concerns regarding the effect of the NBD reporter fluorophore on the accumulation of the compound and whether or not the accumulation pattern observed is due to the compound only.

5.4 Docking Studies

During the intraerythrocytic stage of its's life cycle, the parasite degrades nearly all of its host cell's hemoglobin to obtain nutrients. This catabolic process occurs in the acidic, oxygen-rich, lysosome-like digestive vacuole (DV).[23,24] As a consequence of this process, large quantities of heme are released into the DV as a by-product. Due to the toxicity of heme to the parasite, it immediately sequesters the released heme by converting it into an insoluble and relatively unreactive microcrystalline dimer known as hemozoin.[25–27] Thus, the heme detoxification pathway is a unique target for antimalarial chemotherapy, as demonstrated by the 4-

aminoquinolines.[28] They have been shown to inhibit hemozoin formation by either capping the growing hemozoin crystals, thereby retarding the deposition of heme onto the crystal surface or complexing with free heme in the lumen of the digestive vacuole.[29]

Some intermolecular interactions permit this association with the hemozoin surface, including π–π-stacking interactions between the inhibitor and heme or hemozoin, hydrogen bonding between the propionate group of heme and a protonated nitrogen of the inhibitor as well as coordination of the deprotonated hydroxyl groups to the iron(III) centre of the heme monomer. Based on the results from the live-cell imaging and the beta-hematin inhibition activity of **1.3** and **3.14**, it was hypothesized that both compounds could be inhibiting the formation of hemozoin. To investigate this hypothesis, docking studies was employed to predict whether **1.3** and **3.14** are likely hemozoin inhibitors. The compounds were docked against the β-hematin surface using the 3D crystal structure previously published by Pagola et al. [26] (Figures 5.11 and 5.12).

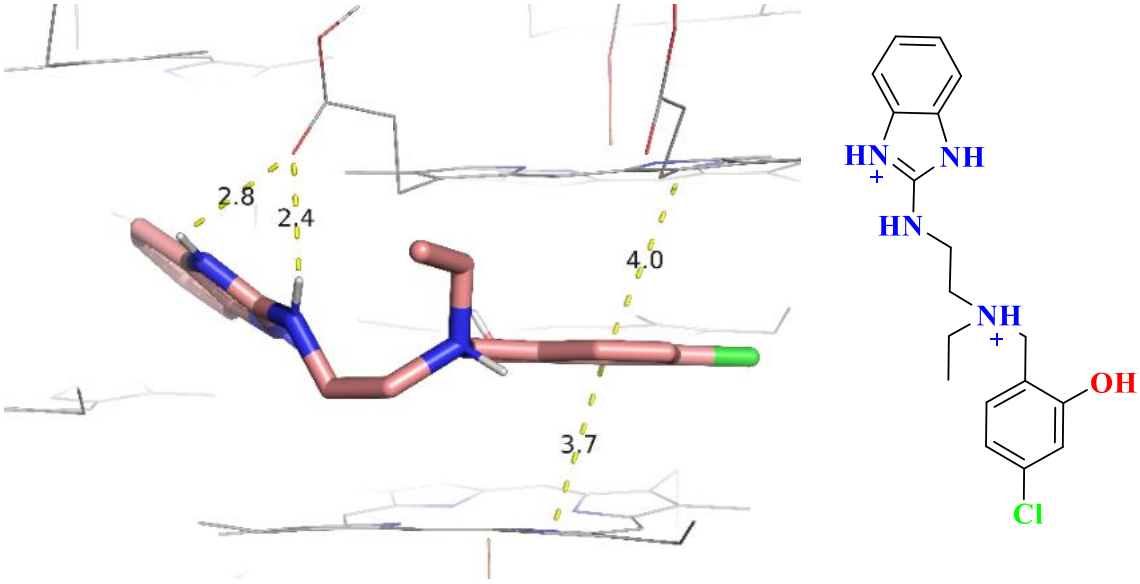

Figure 5.11: Predicted binding mode with the 001 face of β-hematin showing hydrogen bonding interactions between the protonated tertiary amine, the imidazole N-H and the propionate group of β-hematin at pH 4.5 (2.4 and 2.8 Å respectively) and π–π-stacking interactions shown between the porphyrin ring of the heme and the 3-chlorophenol moiety of **1.3** (4.0 Å).

Intermolecular interactions were observed between **1.3** and the crystal surface of β-hematin. The 3-chlorophenol moiety of the compound interacts through π–π stacking with the porphyrin ring of β-hematin. The basic nitrogen of the imidazole ring and the tertiary nitrogen on the side chain of the compound form hydrogen bonds with the propionate group of β-hematin when

protonated at pH 4.5, the biologically relevant pH in the digestive vacuole (Figure 5.11). It has been shown via live-cell imaging that significant amounts of the compound accumulate in the parasite's digestive vacuole. The docking studies also predict that once in the DV, intermolecular interactions occur between the compound and the heme/hemozoin surfaces to inhibit hemozoin formation, leading to the accumulation of heme and, consequently, death of the parasite.

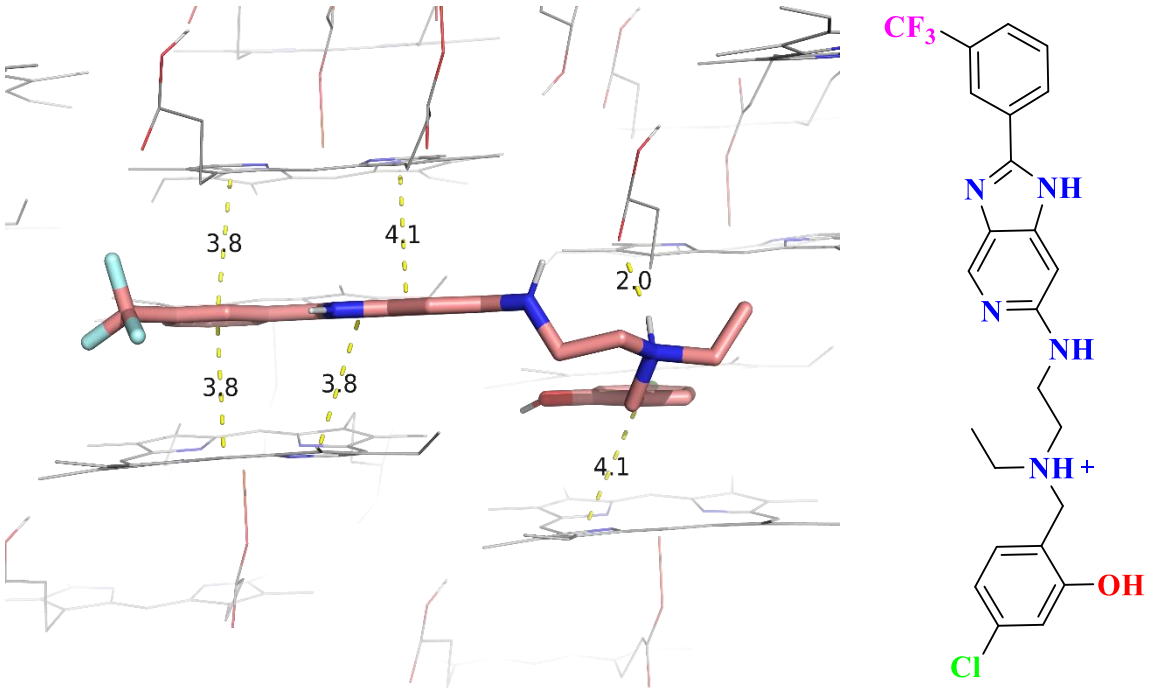

Figure 5.12: Predicted binding mode with the 001 face of β-hematin showing hydrogen bonding interactions between the protonated tertiary amine and the propionate group of β-hematin at pH 4.5 (2.0 Å) and π–π-stacking interactions shown between the porphyrin ring of the heme and the 3-chlorophenol moiety (4.1 Å), 3-trifluoromethylphenyl moiety (3.8 Å) and imidazopyridine core (4.1 Å).

A similar docking pose was observed for compound **3.14** (Figure 5.12). The imidazopyridine core, the 3-trifluoromethylphenyl and the 3-chlorophenol moieties of the compound interact through π–π stacking with the porphyrin ring of β-hematin. Also, the basic nitrogen of the tertiary amine on the side chain of the compound forms a hydrogen bond with the propionate group of β-hematin when protonated at pH 4.5.

5.5 Heme Fractionation Studies

The results obtained from the live-cell imaging implicate all organelles in the *Plasmodium* parasite as possible sites of action except the nucleus. However, this result, taken together with the beta-hematin inhibition activity and the docking studies, suggests that hemozoin inhibition could likely be the MoA or a contributory MoA of both compounds **1.3** and **3.14**. Therefore, the heme fractionation assay was carried out to further investigate the effect of the compound on heme and hemozoin levels at increasing concentrations of the compound, according to methods previously described by Combrinck et al.[30] The assay results indicate that as the concentration of **1.3** increases, heme levels increase steadily and hemozoin levels decrease concomitantly (Figure 5.13). This demonstrates that the exposure of *P. falciparum* to **1.3** in a dose-dependent manner causes the build-up of toxic heme, which leads to parasite death. Consequently, the inhibition of hemozoin formation has been identified as a mechanism of action of **1.3**. However, further experiments such as resistance selection and chemical proteomics are required to identify any other MoA (s) as the inhibition of hemozoin formation is likely a contributing mechanism.

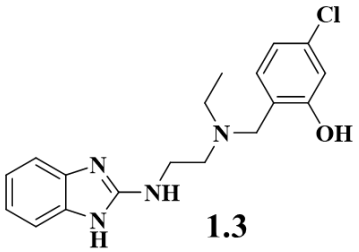

1.3

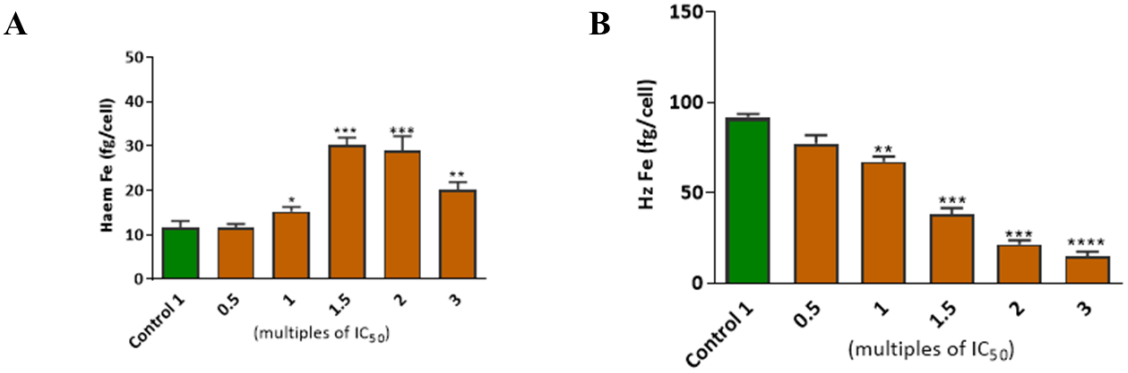

Figure 5.13: Heme fractionation profile of **1.3**. The amount of "free" heme Fe (A) and hemozoin (Hz); (B) Fe at increasing concentrations of the compound. Significance levels are depicted with asterisks, where * = $p < 0.05$, ** = $p < 0.01$, *** = $p < 0.001$ and **** = $p < 0.0001$.

Conversely, no significant change in heme levels was observed with increasing concentrations of **3.14** (Figure 5.14). However, a statistically significant dose-response decrease in hemozoin levels was observed, indicating that **3.14** could be targeting different digestive vacuole processes, although it may not be a direct hemozoin inhibitor. It is noteworthy that a true hemozoin inhibitor causes an increase in free heme and a corresponding decrease in hemozoin.

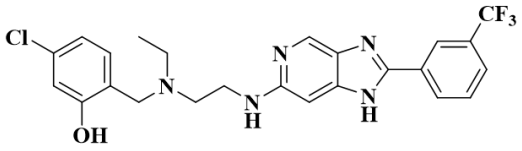

3.14

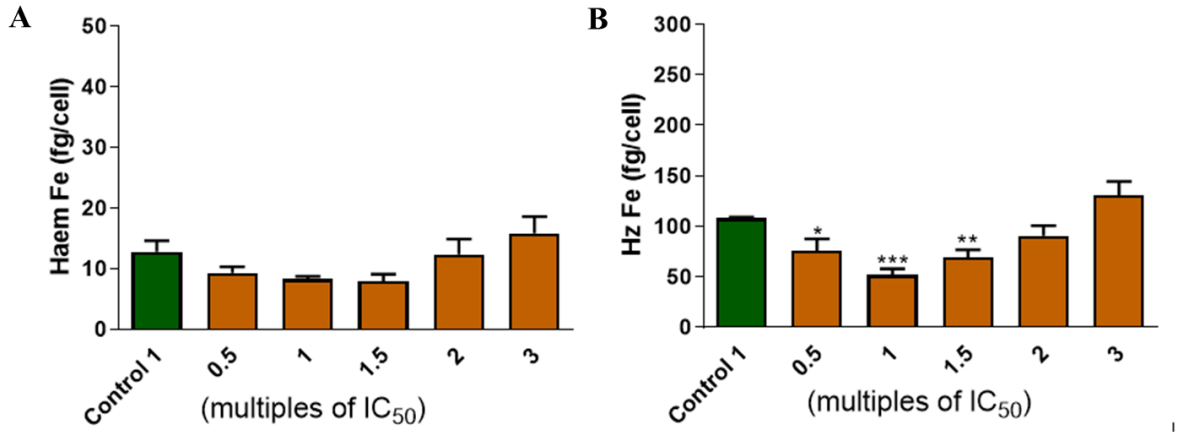

Figure 5.14: Heme fractionation profile of **3.14**. The amount of "free" heme Fe (A) and hemozoin (Hz); (B) Fe at increasing concentrations of the compound. Significance levels are depicted with asterisks, where * = $p < 0.05$, ** = $p < 0.01$ and *** = $p < 0.001$.

5.6 Conclusions

In summary, novel fluorescent analogues (**1.3-NBD** and **3.14-NBD**) of the frontrunner compounds (**1.3** and **3.14**) have been identified as suitable probes for live-cell imaging. Their use as fluorescent probes of the parent compounds was photophysically and pharmacologically evaluated. Live-cell microscopy showed no localization of both **1.3-NBD** and **3.14-NBD** in the nucleus of the parasite, eliminating the nucleus as the site of antiplasmodium activity of these compounds. However, localization in the phospholipid structures such as the membranes was observed. This observation suggests possible effects of the compounds in membraneous structures and their associated organelles due to the extensive localization observed in the ER and the mitochondrion. Despite much weaker fluorescence in an aqueous medium, localization in the digestive vacuole was evident. This is also supported by their localization within neutral

lipid bodies, which have been implicated in hemozoin formation. Docking studies predicted intermolecular interactions between the parent compounds (**1.3** and **3.14**) and the heme/hemozoin surfaces to inhibit hemozoin formation. The heme fractionation studies of **1.3** showed a dose-dependent increase in heme levels with a subsequent decrease in hemozoin levels. Altogether, these observations support hemozoin inhibition as a mechanism of action of compound **1.3** while pointing to additional targets within the parasite based on widespread association with other organelles. Compound **3.14**, however, is not a hemozoin inhibitor but could be targeting different digestive vacuole processes.

5.7 References

(1) Butera, J. A. Phenotypic Screening as a Strategic Component of Drug Discovery Programs Targeting Novel Antiparasitic and Antimycobacterial Agents: An Editorial. *J. Med. Chem.* **2013**, *56* (20), 7715–7718. https://doi.org/10.1021/jm400443k.

(2) Bantscheff, M.; Drewes, G. Chemoproteomic Approaches to Drug Target Identification and Drug Profiling. *Bioorg. Med. Chem.* **2012**, *20* (6), 1973–1978. https://doi.org/10.1016/j.bmc.2011.11.003.

(3) Guiguemde, W. A.; Shelat, A. A.; Bouck, D.; Duffy, S.; Crowther, G. J.; Davis, P. H.; Smithson, D. C.; Connelly, M.; Clark, J.; Zhu, F.; et al. Chemical Genetics of Plasmodium Falciparum. *Nature* **2010**, *465* (7296), 311–315. https://doi.org/10.1038/nature09099.

(4) Hartwig, C. L.; Lauterwasser, E. M. W.; Mahajan, S. S.; Hoke, J. M.; Cooper, R. A.; Renslo, A. R. Investigating the Antimalarial Action of 1,2,4-Trioxolanes with Fluorescent Chemical Probes. *J. Med. Chem.* **2011**, *54* (23), 8207–8213. https://doi.org/10.1021/jm2012003.

(5) Zheng, X. F. S.; Chan, T.-F. Chemical Genomics: A Systematic Approach in Biological Research and Drug Discovery. *Curr. Issues Mol. Biol.* **2002**, *4* (2), 33–43.

(6) Graves, P. R.; Haystead, T. A. J. Molecular Biologist's Guide to Proteomics. *Microbiol. Mol. Biol. Rev.* **2002**, *66* (1), 39–63. https://doi.org/10.1128/MMBR.66.1.39-63.2002.

(7) Yates, J. R.; Eng, J. K.; McCormack, A. L.; Schieltz, D. Method to Correlate Tandem Mass Spectra of Modified Peptides to Amino Acid Sequences in the Protein Database. *Anal. Chem.* **1995**, *67* (8), 1426–1436. https://doi.org/10.1021/ac00104a020.

(8) Terai, T.; Nagano, T. Small-Molecule Fluorophores and Fluorescent Probes for Bioimaging. *Pflügers Arch. - Eur. J. Physiol.* **2013**, *465* (3), 347–359. https://doi.org/10.1007/s00424-013-1234-z.

(9) Yun, S.-W.; Kang, N.-Y.; Park, S.-J.; Ha, H.-H.; Kim, Y. K.; Lee, J.-S.; Chang, Y.-T. Diversity Oriented Fluorescence Library Approach (DOFLA) for Live Cell Imaging Probe Development. *Acc. Chem. Res.* **2014**, *47* (4), 1277–1286. https://doi.org/10.1021/ar400285f.

(10) Eng, J.; Lynch, R. M.; Balaban, R. S. Nicotinamide Adenine Dinucleotide Fluorescence Spectroscopy and Imaging of Isolated Cardiac Myocytes. *Biophys. J.* **1989**, *55* (4), 621–630. https://doi.org/10.1016/S0006-3495(89)82859-0.

(11) Reinert, K. C.; Dunbar, R. L.; Gao, W.; Chen, G.; Ebner, T. J. Flavoprotein Autofluorescence Imaging of Neuronal Activation in the Cerebellar Cortex In Vivo. *J.*

Neurophysiol. **2004**, *92* (1), 199–211. https://doi.org/10.1152/jn.01275.2003.

(12) Skala, M. C.; Riching, K. M.; Gendron-Fitzpatrick, A.; Eickhoff, J.; Eliceiri, K. W.; White, J. G.; Ramanujam, N. In Vivo Multiphoton Microscopy of NADH and FAD Redox States, Fluorescence Lifetimes, and Cellular Morphology in Precancerous Epithelia. *Proc. Natl. Acad. Sci.* **2007**, *104* (49), 19494–19499. https://doi.org/10.1073/pnas.0708425104.

(13) Lavis, L. D.; Raines, R. T. Bright Ideas for Chemical Biology. *ACS Chem. Biol.* **2008**, *3* (3), 142–155. https://doi.org/10.1021/cb700248m.

(14) Woodland, J. G.; Hunter, R.; Smith, P. J.; Egan, T. J. Shining New Light on Ancient Drugs: Preparation and Subcellular Localisation of Novel Fluorescent Analogues of Cinchona Alkaloids in Intraerythrocytic Plasmodium Falciparum. *Org. Biomol. Chem.* **2017**, *15* (3), 589–597. https://doi.org/10.1039/C6OB02110G.

(15) Korkor, C. M.; Garnie, L. F.; Amod, L.; Egan, T. J.; Chibale, K. Intrinsic Fluorescence Properties of Antimalarial Pyrido[1,2- a]Benzimidazoles Facilitate Subcellular Accumulation and Mechanistic Studies in the Human Malaria Parasite Plasmodium Falciparum. *Org. Biomol. Chem.* **2020**, *18* (42), 8668–8676. https://doi.org/10.1039/D0OB01730B.

(16) Wiederschain, G. Y. The Molecular Probes Handbook. A Guide to Fluorescent Probes and Labeling Technologies. *Biochem.* **2011**, *76* (11), 1276–1276. https://doi.org/10.1134/S0006297911110101.

(17) Greenspan, P.; Mayer, E. P.; Fowler, S. D. Nile Red: A Selective Fluorescent Stain for Intracellular Lipid Droplets. *J. Cell Biol.* **1985**, *100* (3), 965–973. https://doi.org/10.1083/jcb.100.3.965.

(18) Ambele, M. A.; Egan, T. J. Neutral Lipids Associated with Haemozoin Mediate Efficient and Rapid β-Haematin Formation at Physiological PH, Temperature and Ionic Composition. *Malar. J.* **2012**, *11* (1), 337. https://doi.org/10.1186/1475-2875-11-337.

(19) Fitch, C. D.; Chevli, R.; Banyal, H. S.; Phillips, G.; Pfaller, M. A.; Krogstad, D. J. Lysis of Plasmodium Falciparum by Ferriprotoporphyrin IX and a Chloroquine-Ferriprotoporphyrin IX Complex. *Antimicrob. Agents Chemother.* **1982**, *21* (5), 819–822. https://doi.org/10.1128/AAC.21.5.819.

(20) Chou, A. C.; Fitch, C. D. Mechanism of Hemolysis Induced by Ferriprotoporphyrin IX. *J. Clin. Invest.* **1981**, *68* (3), 672–677. https://doi.org/10.1172/JCI110302.

(21) Pisciotta, J. M.; Coppens, I.; Tripathi, A. K.; Scholl, P. F.; Shuman, J.; Bajad, S.; Shulaev, V.; Sullivan, D. J. The Role of Neutral Lipid Nanospheres in Plasmodium

Falciparum Haem Crystallization. *Biochem. J.* **2007**, *402* (1), 197–204. https://doi.org/10.1042/BJ20060986.

(22) Ketchum, M. A.; Lee, A. M.; Vekilov, P. G.; Rimer, J. D. Biomimetic Assay for Hematin Crystallization Inhibitors: A New Platform To Screen Antimalarial Drugs. *Cryst. Growth Des.* **2017**, *17* (1), 197–206. https://doi.org/10.1021/acs.cgd.6b01424.

(23) Sullivan, D. J. Theories on Malarial Pigment Formation and Quinoline Action. *Int. J. Parasitol.* **2002**, *32* (13), 1645–1653. https://doi.org/10.1016/S0020-7519(02)00193-5.

(24) Francis, S. E.; Sullivan, D. J.; Goldberg, and D. E. Hemoglobin Metabolism in the Malaria Parasite Plasmodium Falciparum. *Annu. Rev. Microbiol.* **1997**, *51* (1), 97–123. https://doi.org/10.1146/annurev.micro.51.1.97.

(25) Slater, A. F.; Swiggard, W. J.; Orton, B. R.; Flitter, W. D.; Goldberg, D. E.; Cerami, A.; Henderson, G. B. An Iron-Carboxylate Bond Links the Heme Units of Malaria Pigment. *Proc. Natl. Acad. Sci.* **1991**, *88* (2), 325–329. https://doi.org/10.1073/pnas.88.2.325.

(26) Pagola, S.; Stephens, P. W.; Bohle, D. S.; Kosar, A. D.; Madsen, S. K. The Structure of Malaria Pigment β-Haematin. *Nature* **2000**, *404* (6775), 307–310. https://doi.org/10.1038/35005132.

(27) Egan, T. J.; Ncokazi, K. K. Quinoline Antimalarials Decrease the Rate of β-Hematin Formation. *J. Inorg. Biochem.* **2005**, *99* (7), 1532–1539. https://doi.org/10.1016/j.jinorgbio.2005.04.013.

(28) Slater, A. F. G.; Cerami, A. Inhibition by Chloroquine of a Novel Haem Polymerase Enzyme Activity in Malaria Trophozoites. *Nature* **1992**, *355* (6356), 167–169. https://doi.org/10.1038/355167a0.

(29) Kapishnikov, S.; Staalsø, T.; Yang, Y.; Lee, J.; Pérez-Berná, A. J.; Pereiro, E.; Yang, Y.; Werner, S.; Guttmann, P.; Leiserowitz, L.; et al. Mode of Action of Quinoline Antimalarial Drugs in Red Blood Cells Infected by Plasmodium Falciparum Revealed in Vivo. *Proc. Natl. Acad. Sci.* **2019**, *116* (46), 22946–22952. https://doi.org/10.1073/pnas.1910123116.

(30) Combrinck, J. M.; Fong, K. Y.; Gibhard, L.; Smith, P. J.; Wright, D. W.; Egan, T. J. Optimization of a Multi-Well Colorimetric Assay to Determine Haem Species in Plasmodium Falciparum in the Presence of Anti-Malarials. *Malar. J.* **2015**, *14* (1), 253. https://doi.org/10.1186/s12936-015-0729-9.

CHAPTER 6

SUMMARY, CONCLUSIONS AND RECOMMENDATIONS FOR FUTURE WORK

6.1 Summary and Conclusions

The overarching goal of this thesis work was to incorporate an intramolecular hydrogen bonding (IMHB) motif in known antimalarial chemotypes exemplified by benzimidazole and imidazopyridine scaffolds . Medicinal chemistry principles and strategies were employed to achieve the intended objective of exploring the antiplasmodium structure-activity relationship profiles. An accompanying aim of the project was to conduct mechanistic studies on the frontrunner compounds of each scaffold. The target compounds were synthesized by various literature protocols and characterized through chromatographic methods (TLC and HPLC-MS) and spectroscopic techniques (NMR spectroscopy). Physicochemical parameters such as aqueous solubility and melting point were also used to characterize the target compounds. The compounds were pharmacologically evaluated for their *in vitro* antiplasmodium activity, cytotoxicity and microsomal metabolic stability profiles.

Due to structural modifications on the benzimidazole chemotype, analogues from this scaffold were classified into 1*H*-benzimidazole and *N*-benzyl benzimidazole (astemizole-based) series. Accordingly, the 1*H*-benzimidazole analogues manifested sub-micromolar potencies against the chloroquine-sensitive NF54 strain of *P. falciparum*, with IC_{50} values between 0.079 µM and 0.968 µM. The most potent analogue within this series was compound **1.3** with an IC_{50} of 0.079 µM against the chloroquine-sensitive strain and 0.335 µM against the multidrug-resistant (K1) strain. The astemizole-based analogues also exhibited sub-micromolar activity against the chloroquine-sensitive strain of the parasite, with compound **2.3** displaying the highest potency (IC_{50} *Pf*NF54 = 0.029 µM and IC_{50} *Pf*K1 = 0.117 µM) within the series. Overall, the benzimidazole analogues displayed poor activity against the sexual gametocyte stage of the *Plasmodium* parasite in comparison to the asexual blood stage. However, compound **1.3** displayed sub-micromolar potency (IC_{50} = 0.382 µM) against early-stage gametocytes. In addition, the selected potent analogues exhibited a low cytotoxicity profile against the mammalian Chinese Hamster Ovary (CHO) cell line.

The astemizole-based analogues expressed >40% inhibition against the hERG ion channel at the highest test concentration with potencies between 0.96 and 13.24 µM. In general, this series of analogues showed an improved cardiotoxicity risk relative to verapamil (IC_{50} = 0.58 µM).

Furthermore, selected potent analogues evaluated for microsomal metabolic stability were unstable across all three species (mouse, rat and human) of liver microsomes. This impeded the advancement of these potent analogues to *in vivo* efficacy studies. Meanwhile, metabolite identification studies provided insight on the metabolic hotspots, and this information could be used to synthesize analogues that would address this liability.

The SAR of the imidazopyridine analogues was explored with both aromatic and aliphatic groups. Compound **3.14** (IC_{50} *Pf*NF54 = 0.08 μM) displayed the highest potency within this series while incorporating heteroatoms in the saturated cyclic substituents was detrimental to antiplasmodium activity. Also, these compounds showed a favourable cytotoxicity profile against the CHO cell line. Nonetheless, like the benzimidazoles, these compounds were metabolically labile; hence, they were not progressed for *in vivo* efficacy studies.

A physicochemical assessment revealed that both the benzimidazoles and the imidazopyridines complied with Lipinski's RO5 and Veber's rule. Additionally, evaluating the factors affecting solubility showed that various factors simultaneously affect the solubility of compounds across a specific class; hence, it may be crucial to assess these factors based on individual cases rather than an entire class of compounds. Using compounds **1.2** and **2.2** as representative analogues, single crystal X-ray analysis, IR spectroscopy, and DFT calculations were used to ascertain the presence of IMHB in these compounds.

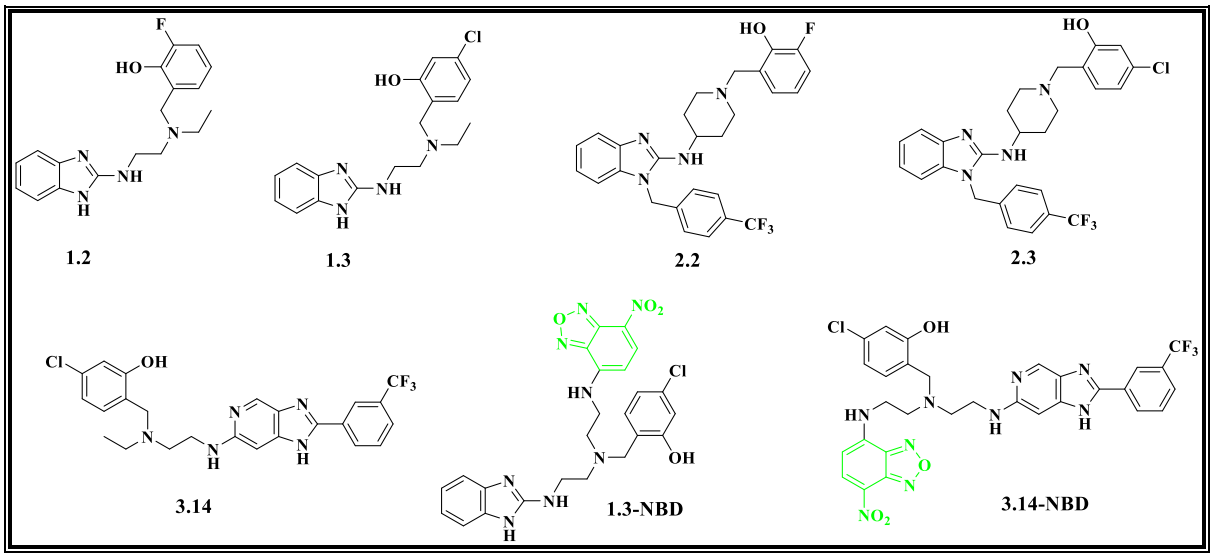

Figure 6.1: Chemical structures of frontrunner analogues and fluorescent probes.

To probe the mechanism of action, novel fluorescent analogues (**1.3-NBD** and **3.14-NBD**) of the frontrunner compounds **1.3** and **3.14** were identified as suitable probes for fluorescence

live-cell imaging. The fluorescent probes were assessed pharmacologically to ensure that potency against *P. falciparum* was maintained. Live-cell microscopy showed localization of both probes in all the studied organelles except the nucleus, eliminating it as a site of action for antiplasmodium activity. Docking studies predicted intermolecular interactions between the parent compounds (**1.3** and **3.14**) and the heme/hemozoin surfaces to inhibit hemozoin formation. The heme fractionation studies of **1.3** showed a dose-dependent increase in heme levels with a subsequent decrease in hemozoin levels. Essentially, these observations support hemozoin inhibition as a mechanism of action of compound **1.3** while pointing to other targets within the parasite based on widespread association with other organelles. Compound **3.14**, however, is not a hemozoin inhibitor but could be targeting different digestive vacuole processes.

In conclusion, this Ph.D. thesis presents the synthesis, biological evaluation and physicochemical assessment of novel benzimidazole and imidazopyridine analogues with an intramolecular hydrogen bonding (IMHB) motif. It was observed that the absence of an IMHB motif led to a loss in antiplasmodium activity, and this shows the importance of this motif in the target compounds. Meanwhile, the frontrunner compounds **1.3** and **3.14** presented issues of microsomal metabolic stability, which impeded their progression to *in vivo* efficacy studies. The presence of IMHB in these molecules was also established through single crystal X-ray analysis, IR spectroscopy and DFT calculations. In addition, fluorescence live-cell microscopy, docking studies and cellular heme fractionation studies were employed to investigate the mechanism of action of the frontrunner compounds **1.3** and **3.14**.

6.2 Recommendations for Future Work

Based on the results obtained from this study, more benzimidazole and imidazopyridine analogues can be designed by adapting strategies to address the issues of low microsomal metabolic stability and subsequently performing an *in vivo* efficacy study. Also, to establish the spectrum of antiplasmodium activity of these class of compounds, a broad panel of *Plasmodium* parasite strains need to be tested.

It is recommended that chemical proteomics and resistance selection studies are carried out to elucidate the putative targets of these compounds. Also, resistance selection experiments should facilitate the unravelling of the resistance potential of the *Plasmodium* parasite towards these compounds. This information will provide insight into any differences or similarities in the mechanism(s) of resistance of these compounds compared to known antimalarial drugs.

CHAPTER 7

EXPERIMENTAL

7.1 Chemistry

7.1.1 Reagents, Solvents and Spectroscopic Characterization

All commercially available chemicals were purchased from either Sigma-Aldrich (South Africa) or Combi-Blocks Limited (USA). These chemicals were of analytical grade and used without further purification. Reported compounds were characterized via ^{1}H NMR, ^{13}C NMR, and high-performance liquid chromatography-mass spectrometry (HPLC-MS).

^{1}H NMR spectra were recorded on Varian Mercury (300 MHz), Bruker Ultrashield-Plus (400 MHz), or a Bruker Ascend™ (600 MHz) instrument. ^{13}C NMR spectra were recorded on the same instruments at 101 MHz or 151 MHz, and samples were dissolved in deuterated dimethyl sulfoxide (DMSO-d_6), methanol (Methanol-d_4) or chloroform ($CDCl_3$). Chemical shifts (δ) are reported in parts per million (ppm) and rounded off to two decimal places. Coupling constants (*J*) are reported in Hertz (Hz) and rounded to one decimal place. Abbreviations used in assigning ^{1}H NMR signals are d (doublet), dd (doublet of doublets), ddd (doublet of doublet of doublets), m (multiplet), q (quartet), s (singlet), t (triplet), or td (triplet of doublets).

The mass spectra of target compounds used to determine peak purities were acquired on an Agilent HPLC system equipped with Agilent 1260® Infinity Binary Pump, Agilent 1260® Infinity Diode Array Detector, Agilent 1290® Infinity Column Compartment, Agilent 1260® Infinity Autosampler, Agilent 6120® Quadrupole LC/MS, and Peak Scientific® Genius 1050 Nitrogen Generator. The column used was a Kinetex Core C18 column (2.6 μM, 3 x 50 mm, 100 Å) maintained at 40 °C. The composition and gradient conditions of the mobile phase used at a flow rate of 0.7 mL/min are summarized in Table 7.1. The injection volume was 2 μL, and the mass spectra were obtained in either positive or negative modes using electrospray ionization (ESI) and atmospheric pressure chemical ionization (APCI). The diode array detector was programmed to scan the eluents at an absorption wavelength range of 210 - 640 nm.

Table 7.1: High-performance liquid chromatography (HPLC) gradient conditions

Time (min)	% A	% B
0.00	85	15
0.30	85	15
1.20	0	100
4.50	0	100

A: 10 mM NH_4OAc in buffer (0.4 % acetic acid) in H_2O; B: 10 mM NH_4OAc in buffer (0.4 % acetic acid) in HPLC-grade CH_3OH.

Reactions were monitored by thin-layer chromatography (TLC) using Fluka or Merck F254 aluminium-backed pre-coated silica gel plates and were visualized under ultraviolet light at 254 or 366 nm. Silica gel column chromatography was performed using Merck kieselgel 60: 70-230 mesh by gravity column chromatography or flash column chromatography on a Biotage Isolera™ system (Biotage AB, Uppsala, Sweden). The mobile phase solvents for column chromatography were purchased as analytical reagent (AR) grade and used without prior distillation. Melting points were determined using the Automatic STUART® SMP 40 melting point apparatus.

7.2 Synthesis and Characterization

7.2.1 Benzimidazoles

7.2.1.1 Procedure for the synthesis of intermediate 1a (Scheme 2.1)

A mixture of 2-chlorobenzimidazole (1 eq), ethylethane-1,2-diamine (10 eq), triethylamine (0.3 eq) and potassium carbonate (0.3 eq) was stirred under reflux at 140 ºC for 16 hours. Excess amine was distilled off, and 1.0 M NaOH (30 mL) was added to the residue. The resulting mixture was extracted with warm ethyl acetate (5 × 20mL). The combined organic layer was washed with brine and dried over anhydrous Na_2SO_4. The solvent was evaporated *in vacuo*, and the crude product was obtained.

N^1-(1H-benzo[*d*]imidazol-2-yl)-N^2-ethylethane-1, 2-diamine (1a):

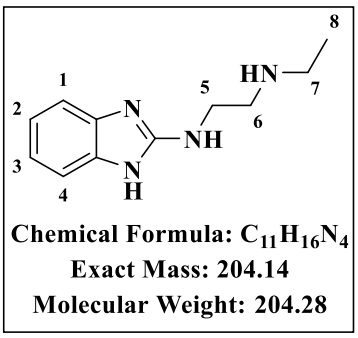

Obtained from 2-chlorobenzimidazole (2.00 g, 13.11 mmols) and ethylethane-1, 2-diamine (13.31 mL, 131.1 mmols) as a white solid (59%, 1.5708 g); R_f (DCM: MeOH: NH_4OH, 8:2:0.5) 0.47; ^{1}H NMR (600 MHz, MeOH-d_4) δ 7.18 (dd, J = 5.8, 3.2 Hz, 2H, $H^1$and H^4), 6.95 (dd, J = 5.8, 3.2 Hz, 2H, H^2 and H^3), 3.49 (t, J = 6.2 Hz, 2H, H^5), 2.87 (t, J = 6.2 Hz, 2H, H^6), 2.70 (q, J = 7.2 Hz, 2H, H^7), 1.14 (t, J = 7.2 Hz, 3H, H^8). ^{13}C NMR (151 MHz, MeOH-d_4) δ 156.90, 139.12 (2C), 121.32 (2C), 112.80 (2C), 49.66, 44.49, 43.04, 14.54. HPLC-MS (ESI): Purity = 98%, t_R = 0.218 min, m/z $[M+H]^+$ = 205.1

7.2.1.2 General procedure for the synthesis of target compounds 1.1-1.11 (Scheme 2.1)

To a solution of intermediate **1a** (1 eq) in methanol (6 mL) was added the appropriate aldehyde (1.1 eq), and the resulting mixture was stirred at 25 °C for 6 hours. The mixture was cooled at 0 °C, and $NaBH_4$ (5 eq) was added. The reaction solution was then stirred at 25 °C for 16 hours, quenched with distilled water and concentrated *in vacuo* to remove methanol. The residue was diluted with 5 mL of distilled water and extracted with dichloromethane (4 x 20mL). The combined organic layer was washed with brine, dried over anhydrous Na_2SO_4 and solvent was evaporated *in vacuo* to afford the desired compound. The crude product obtained was purified by column chromatography (DCM/MeOH).

2-(((2-((1H-benzo[*d*]imidazol-2-yl)amino)ethyl)(ethyl)amino)methyl)phenol(1.1):

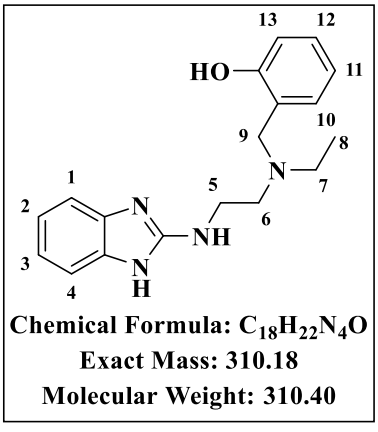

Obtained from intermediate **1a** (150 mg, 0.73 mmols) and salicylaldehyde (0.09 mL, 0.80 mmols) as a yellow solid(48%, 108.2 mg); R_f (DCM: MeOH: NH_4OH, 9.5:0.5:0.05) 0.48; ^{1}H NMR (600 MHz, MeOH-d_4) δ 7.20 – 7.13 (dd, J = 5.8, 3.2 Hz, 2H, H^1 and H^4), 7.03 (td, J = 7.7, 1.7 Hz, 1H, H^{12}), 6.99 (dd, J = 7.5, 1.6 Hz, 1H, H^{13}), 6.96 – 6.92 (dd, J = 5.8, 3.2 Hz, 2H, H^2 and H^3), 6.71 (td, J = 7.4, 1.2 Hz, 1H, H^{11}), 6.66 (dd, J = 8.1, 1.2 Hz, 1H, H^{10}), 3.79 (s, 2H, H^9), 3.53 (t, J = 6.3 Hz, 2H, H^5), 2.80 (t, J = 6.3 Hz, 2H, H^6), 2.65 (q, J = 7.2 Hz, 2H, H^7), 1.07 (t, J = 7.1 Hz, 3H, H^8). ^{13}C NMR (151 MHz, MeOH-d_4) δ 158.61(C-OH), 156.69, 139.17 (2C), 130.06, 129.53, 123.84, 121.25 (2C), 120.32, 116.70, 112.77 (2C), 57.65, 53.50, 48.28, 41.29, 11.35. HPLC-MS (ESI): Purity = 98%, t_R = 2.079 min, m/z $[M+H]^+$ = 310.9.

2-(((2-((1H-benzo[*d*]imidazol-2-yl)amino)ethyl)(ethyl)amino)methyl)-6-fluorophenol (1.2):

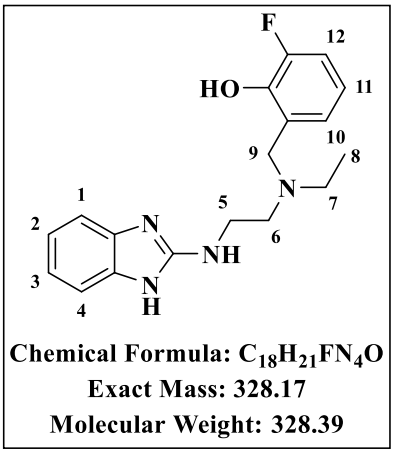

Chemical Formula: $C_{18}H_{21}FN_4O$
Exact Mass: 328.17
Molecular Weight: 328.39

Obtained from intermediate **1a** (150 mg, 0.73 mmols) and 3-fluorosalicylaldehyde (112.08 mg, 0.80 mmols) as an off-white solid (63%, 151.9 mg); R_f (DCM: MeOH: NH_4OH, 9.5:0.5:0.05) 0.32; ^{1}H NMR (600 MHz, MeOH-d_4) δ 7.17 (dd, J = 5.8, 3.2 Hz, 2H, H^1 and H^4), 6.94 (dd, J = 5.8, 3.1 Hz, 2H, H^2 and H^3), 6.86 (ddd, J = 10.6, 8.3, 1.5 Hz, 1H, H^{12}), 6.81 (d, J = 7.6 Hz, 1H, H^{10}), 6.63 (td, J = 7.9, 4.8 Hz, 1H, H^{11}), 3.87 (s, 2H, H^9), 3.55 (t, J = 6.3 Hz, 2H, H^5), 2.84 (t, J = 6.3 Hz, 2H, H^6), 2.69 (q, J = 7.2 Hz, 2H, H^7), 1.09 (t, J = 7.2 Hz, 3H, H^8). ^{13}C NMR (151 MHz, MeOH-d_4) δ 156.58 (C-OH), 153.58 (C-F), 151.98, 147.12, 139.17 (2C), 126.39, 125.19, 121.27 (2C), 119.53, 115.82, 112.79 (2C), 57.22, 53.39, 41.08, 11.23. HPLC-MS (ESI): Purity = 98%, t_R = 2.028 min, m/z $[M+H]^+$ = 328.9.

2-(((2-((1H-benzo[*d*]imidazol-2-yl)amino)ethyl)(ethyl)amino)methyl)-5-chlorophenol (1.3):

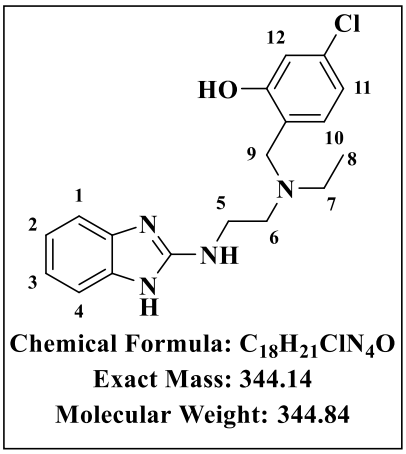

Chemical Formula: $C_{18}H_{21}ClN_4O$
Exact Mass: 344.14
Molecular Weight: 344.84

Obtained from intermediate **1a** (150 mg, 0.73 mmols) and 4-chlorosalicylaldehyde (125.28 mg, 0.80 mmols) as a yellow solid (74%, 186.6 mg); R_f (DCM: MeOH: NH_4OH, 9.5:0.5:0.05) 0.35; ^{1}H NMR (600 MHz, MeOH-d_4) δ 7.20 – 7.12 (dd, J = 5.8, 3.2 Hz, 2H, H^1 and H^4), 6.99 – 6.89 (m, 3H, H^2, $H^3$and H^{10}), 6.68 (dd, J = 8.0, 2.1 Hz, 1H, H^{11}), 6.64 (d, J = 2.1 Hz, 1H, H^{12}), 3.77 (s, 2H, H^9), 3.52 (t, J = 6.3 Hz, 2H, H^5), 2.80 (t, J = 6.3 Hz, 2H, H^6), 2.65 (q, J = 7.2 Hz, 2H, H^7), 1.07 (t, J = 7.2 Hz, 3H, H^8). ^{13}C NMR (151 MHz, MeOH-d_4) δ 158.58 (C-OH), 155.25, 137.69 (C-Cl), 133.41 (2C), 129.70, 121.34 (2C), 119.92, 118.58, 115.53, 111.40 (2C), 55.59, 52.01, 46.90, 39.78, 9.90. HPLC-MS (ESI): Purity = 98%, t_R = 2.267 min, m/z $[M+H]^+$ = 344.9.

2-(((2-((1H-benzo[*d*]imidazol-2-yl)amino)ethyl)(ethyl)amino)methyl)-4-methoxyphenol (1.4):

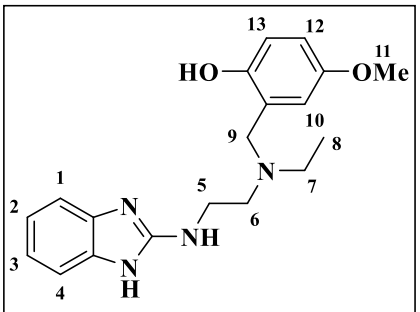

Obtained from intermediate **1a** (150 mg, 0.73 mmols) and 5-methoxysalicylaldehyde (0.1 mL, 0.80 mmols) as a pale-orange solid (53%, 132.5 mg); R_f (DCM: MeOH: NH_4OH, 9.5:0.5:0.05) 0.21; ^1H NMR (600 MHz, MeOH-d_4) δ 7.16 (dd, J = 5.8, 3.2 Hz, 2H, H^1 and H^4), 6.94 (dd, J = 5.8, 3.1 Hz, 2H, H^2 and H^3), 6.65 – 6.55 (m, 3H, H^{10}, H^{12} and H^{13}), 3.75 (s, 2H, H^9), 3.64 (s, 3H, H^{11}), 3.51 (t, J = 6.3 Hz, 2H, H^5), 2.79 (t, J = 6.3 Hz, 2H, H^6), 2.65 (q, J = 7.1 Hz, 2H, H^7), 1.08 (t, J = 7.1 Hz, 3H, H^8). ^{13}C NMR (151 MHz, MeOH-d_4) δ 156.66 (C-OCH_3), 154.20 (C-OH), 152.21, 139.18 (2C), 124.69, 121.22 (2C), 117.16, 115.81, 114.59, 112.76 (2C), 57.69 (-OCH_3), 56.14, 53.51, 48.43, 41.30, 11.47. HPLC-MS (ESI): Purity = 96%, t_R = 2.390 min, m/z $[M+H]^+$ = 340.9.

2-(((2-((1H-benzo[*d*]imidazol-2-yl)amino)ethyl)(ethyl)amino)methyl)-4,6-dichlorophenol (1.5):

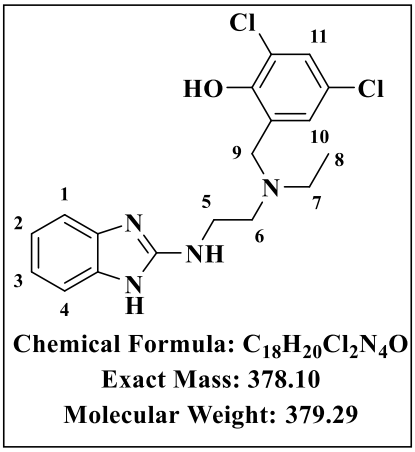

Obtained from intermediate **1a** (150 mg, 0.73 mmols) and 3,5-dichlorosalicylaldehyde (152.8 mg, 0.80 mmols) as a pale-yellow solid (38%, 105.7 mg); R_f (DCM: MeOH: NH_4OH, 9.5:0.5:0.05) 0.20; ^1H NMR (600 MHz, MeOH-d_4) δ 7.20 (dd, J = 5.8, 3.2 Hz, 2H, H^1 and H^4), 7.12 (d, J = 2.5 Hz, 1H, H^{11}), 7.00 – 6.96 (m, 3H, H^2, H^3 and H^{10}), 3.89 (s, 2H, H^9), 3.59 (t, J = 6.2 Hz, 2H, H^5), 2.91 (d, J = 6.2 Hz, 2H, H^6), 2.76 (d, J = 7.2 Hz, 2H, H^7), 1.13 (d, J = 7.2 Hz, 3H, H^8). ^{13}C NMR (151 MHz, MeOH-d_4) δ 156.28 (C-OH), 155.02, 138.95 (2C), 129.25, 128.22 (C-Cl), 126.03, 123.52, 122.65 (C-Cl), 121.34 (2C), 112.85 (2C), 57.51, 53.15, 48.37, 40.73, 10.97. HPLC-MS (ESI): Purity = 98%, t_R = 2.574 min, m/z $[M+H]^+$ = 378.8.

2-(((2-((1H-benzo[*d*]imidazol-2-yl)amino)ethyl)(ethyl)amino)methyl)-4-methylphenol (1.6):

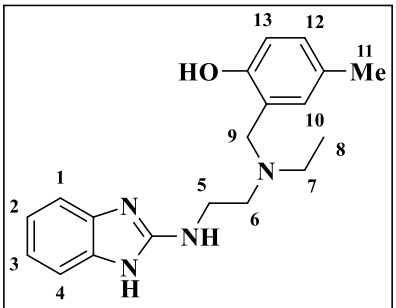

Obtained from intermediate **1a** (300 mg, 1.47 mmols) and 5-methylsalicylaldehyde (220.48 mg, 1.62 mmols) as an off-white solid (42%, 125.6 mg); R_f (DCM: MeOH: NH_4OH, 9.5:0.5:0.05) 0.24; ^1H NMR (400 MHz, MeOH-d_4) δ 7.19 (dd, J = 5.9, 3.2 Hz, 2H, H^1 and H^4), 6.97 (dd, J = 5.9, 3.2 Hz, 2H, H^2 and H^3), 6.89 – 6.84 (m, 2H, H^{10} and H^{12}), 6.58 (d, J = 8.0 Hz, 1H, H^{13}), 3.81 (s, 2H, H^9), 3.56 (t, J = 6.3 Hz, 2H, H^5), 2.84 (t, J = 6.3 Hz, 2H, H^6), 2.71 (q, J = 7.2 Hz, 2H, H^7), 2.18 (s, 3H, H^{11}), 1.12 (t, J = 7.2 Hz, 3H, H^8). ^{13}C NMR (101 MHz, MeOH-d_4) δ 155.33 (C-OH), 154.74, 129.16 (2C), 128.49 (C-CH_3), 128.14, 126.03, 122.23, 119.84 (2C), 115.10, 111.25 (2C), 56.34, 52.16, 47.01, 39.96, 19.07 (-CH_3), 10.03. HPLC-MS (ESI): Purity=98%, t_R = 2.290 min, m/z $[M+H]^+$ = 324.9.

2-(((2-((1H-benzo[*d*]imidazol-2-yl)amino)ethyl)(ethyl)amino)methyl)-4-chlorophenol (1.7):

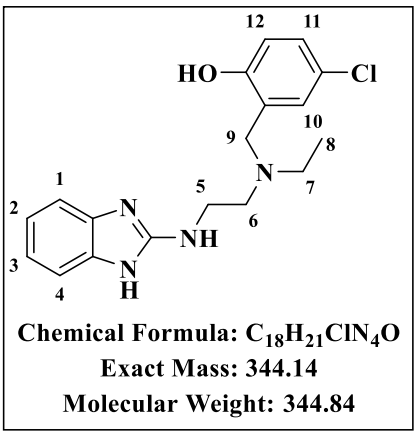

Obtained from intermediate **1a** (300 mg, 1.47 mmols) and 5-chlorosalicylaldehyde (253.69 mg, 1.62 mmols) as an off-white solid(75%, 223.6 mg); R_f (DCM: MeOH: NH_4OH, 9.5:0.5:0.05) 0.16; ^1H NMR (400 MHz, MeOH-d_4) δ 7.19 (dd, J = 5.9, 3.2 Hz, 2H, H^1 and H^4), 7.07 (d, J = 2.7 Hz, 1H, H^{10}), 7.01 (dd, J = 8.6, 2.7 Hz, 1H, H^{11}), 6.98 (dd, J = 5.8, 3.2 Hz, 2H, H^2 and H^3), 6.63 (d, J = 8.6 Hz, 1H, H^{12}), 3.83 (s, 2H, H^9), 3.56 (t, J = 6.3 Hz, 2H, H^5), 2.86 (t, J = 6.3 Hz, 2H, H^6), 2.72 (q, J = 7.2 Hz, 2H, H^7), 1.13 (t, J = 7.1 Hz, 3H, H^8). ^{13}C NMR (101 MHz, MeOH-d_4) δ 156.13 (C-OH), 155.22, 128.33 (2C), 127.78 (C-Cl), 126.82, 124.45, 123.35, 119.90 (2C), 116.70, 111.39 (2C), 55.67, 52.17, 47.06, 39.84, 9.94. HPLC-MS (ESI): Purity= 99 %, t_R = 2.376 min, m/z $[M+H]^+$ = 344.9.

3-(((2-((1H-benzo[*d*]imidazol-2-yl)amino)ethyl)(ethyl)amino)methyl)pyridin-2-ol (1.8):

Obtained from intermediate **1a** (300 mg, 1.47 mmols) and 2-hydroxynicotinaldehyde (199.42 mg, 1.62 mmols) as an off-white solid (44%, 130.5 mg); R_f (DCM: MeOH: NH_4OH, 9:1:0.1)

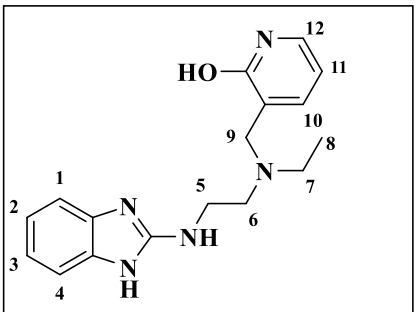

0.45; ^{1}H NMR (400 MHz, MeOH-d_4) δ 7.63 (dd, J = 6.7, 2.1 Hz, 1H, H^{12}), 7.33 (dd, J = 6.5, 2.1 Hz, 1H, H^{10}), 7.23 (dd, J = 5.8, 3.2 Hz, 2H, H^{1} and H^{4}), 7.02 (dd, J = 5.9, 3.2 Hz 2H, H^{2} and H^{3}), 6.31 (t, J = 6.7 Hz, 1H, H^{11}), 3.66 (s, 2H, H^{9}), 3.53 (t, J = 6.4 Hz, 2H, H^{5}), 2.87 (t, J = 6.4 Hz, 2H, H^{6}), 2.70 (q, J = 7.1 Hz, 2H, H^{7}), 1.09 (t, J = 7.1 Hz, 3H, H^{8}). ^{13}C NMR (101 MHz, MeOH-d_4) δ 163.75 (C-OH), 155.02, 141.32, 136.46 (2C), 133.51, 128.43 (2C), 120.39, 111.34, 106.67 (2C), 53.16, 52.58, 47.17, 40.61, 10.29. HPLC-MS (ESI): Purity = 99.0 %, t_R = 0.239 min, m/z $[M+H]^+$ = 311.9.

2-(((2-((1H-benzo[d]imidazol-2-yl)amino)ethyl)(ethyl)amino)methyl)-6-chlorophenol (1.9):

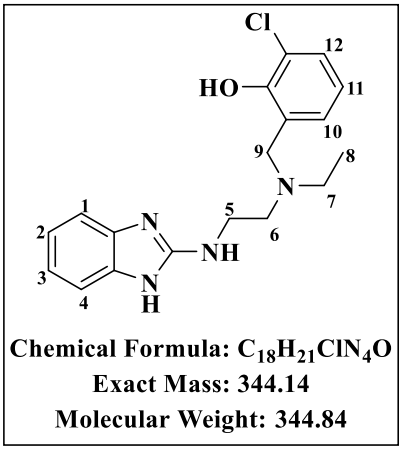

Obtained from intermediate **1a** (300 mg, 1.47 mmols) and 3-chlorosalicylaldehyde (253.69 mg, 1.62 mmols) as an off-white solid (63%, 319.36 mg); R_f (DCM: MeOH: NH_4OH, 9.5:0.5:0.05) 0.35; ^{1}H NMR (600 MHz, MeOH-d_4) δ 7.17 (dd, J = 5.8, 3.2 Hz, 2H, H^{1} and H^{4}), 7.11 (dd, J = 7.7, 2.3 Hz, 1H, H^{12}), 6.94 (dd, J = 5.9, 3.1 Hz, 2H, H^{2} and H^{3}), 6.91 (dd, J = 7.4, 2.3 Hz, 1H, H^{10}), 6.63 (t, J = 7.7 Hz, 1H, H^{11}), 3.85 (s, 2H, H^{9}), 3.56 (t, J = 6.3 Hz, 2H, H^{5}), 2.85 (t, J = 6.3 Hz, 2H, H^{6}), 2.68 (q, J = 7.1 Hz, 2H, H^{7}), 1.08 (t, J = 7.1 Hz, 3H, H^{8}). ^{13}C NMR (151 MHz, MeOH-d_4) δ 156.43 (C-OH), 155.35, 139.10 (2C), 129.91, 128.35, 124.98, 121.80, 121.31 (2C), 120.13 (C-Cl), 112.82 (2C), 57.90, 53.19, 48.20, 40.93, 11.06. HPLC-MS (ESI): Purity = 98 %, t_R = 2.393 min, m/z $[M+H]^+$ = 344.9.

2-(((2-((1H-benzo[d]imidazol-2-yl)amino)ethyl)(ethyl)amino)methyl)-4,6-difluorophenol (1.10):

Obtained from intermediate **1a** (300 mg, 1.47 mmols) and 3,5- difluoro salicylaldehyde (256.12 mg, 1.62 mmols) as an off-white solid (48%, 244.41 mg); R_f (DCM: MeOH: NH_4OH,

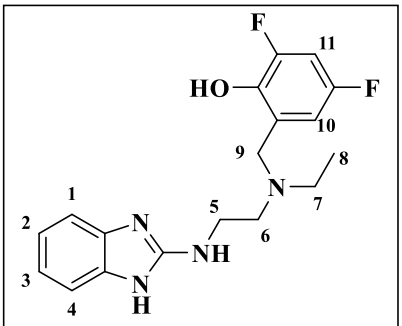

Chemical Formula: $C_{18}H_{20}F_2N_4O$
Exact Mass: 346.16
Molecular Weight: 346.38

9.5:0.5:0.05) 0.40; ^{1}H NMR (600 MHz, MeOH-*d*$_4$) δ 7.16 (dd, *J* = 5.8, 3.2 Hz, 2H, H^1 and H^4), 6.95 (dd, *J* = 5.8, 3.2 Hz, 2H, H^2 and H^3), 6.72 – 6.64 (m, 2H, H^{10} and H^{11}), 3.84 (s, 2H, H^9), 3.54 (t, *J* = 6.2 Hz, 2H, H^5), 2.84 (t, *J* = 6.2 Hz, 2H, H^6), 2.69 (q, *J* = 7.2 Hz, 2H, H^7), 1.10 (t, *J* = 7.2 Hz, 3H, H^8); ^{13}C NMR (151 MHz, MeOH-*d*$_4$) δ 156.54 (C-F), 155.16 (C-OH), 152.93 (C-F), 151.24, 143.20, 138.95 (2C), 127.23, 121.27 (2C), 112.80, 111.37 (2C), 103.84, 56.87, 53.45, 41.08, 11.34. HPLC-MS (ESI): Purity = 98 %, t_R = 2.341 min, m/z $[M+H]^+$ = 346.9.

3-(((2-((1H-benzo[d]imidazol-2-yl)amino)ethyl)(ethyl)amino)methyl)-4 hydroxybenzonitrile (1.11):

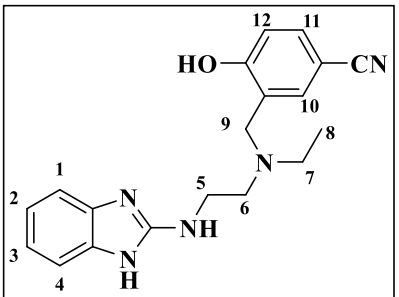

Chemical Formula: $C_{19}H_{21}N_5O$
Exact Mass: 335.17
Molecular Weight: 335.41

Obtained from intermediate **1a** (300 mg, 1.47 mmols) and 3-formyl-4-hydroxybenzonitrile (238.30 mg, 1.62 mmols) as a yellow solid (74%, 364.86 mg); R_f (DCM: MeOH: NH_4OH, 9.5:0.5:0.05) 0.38; ^{1}H NMR (600 MHz, MeOH-*d*$_4$) δ 7.38 (d, *J* = 2.1 Hz, 1H, H^{10}), 7.31 (dd, *J* = 8.5, 2.2 Hz, 1H, H^{11}), 7.16 (dd, *J* = 5.8, 3.2 Hz, 2H, H^1 and H^4), 6.95 (dd, *J* = 5.8, 3.1 Hz, 2H, H^2 and H^3), 6.65 (d, *J* = 8.5 Hz, 1H, H^{12}), 3.88 (s, 2H, H^9), 3.55 (t, *J* = 6.1 Hz, 2H, H^5), 2.88 (t, *J* = 6.1 Hz, 2H, H^6), 2.74 (q, *J* = 7.2 Hz, 2H, H^7), 1.12 (t, *J* = 7.1 Hz, 3H, H^8). ^{13}C NMR (151 MHz, MeOD-*d*$_4$) δ 164.85 (C-OH), 156.41, 138.96 (2C), 134.31, 134.18, 125.02, 121.34 (2C), 120.63 (-CN), 118.24, 112.81 (2C), 101.64 (C-CN), 56.76, 53.27, 48.42, 40.81, 11.04. HPLC-MS (ESI): Purity = 98 %, t_R = 2.169 min, m/z $[M+H]^+$ = 335.9.

7.2.1.3 Procedure for the synthesis of intermediate 2a (Scheme 2.1)

A mixture of 2-chlorobenzimidazole (1 eq), (4-trifluoromethyl)benzyl bromide (1.1 eq) and potassium carbonate (2 eq) in acetonitrile (20 mL) was stirred under reflux at 85 ºC for 2 hours with the completion of the reaction being monitored by TLC and LCMS. The reaction was quenched with water, and the resulting mixture was extracted with DCM (5 × 20 mL). The combined organic layer was washed with brine and dried over anhydrous Na_2SO_4. The solvent

was evaporated *in vacuo* to afford a white solid, which was used in the subsequent reaction without further purification.

2-chloro-1-(4-(trifluoromethyl)benzyl)-1H-benzo[d]imidazole (2a):

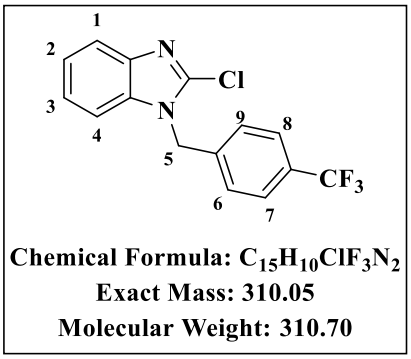

Chemical Formula: $C_{15}H_{10}ClF_3N_2$
Exact Mass: 310.05
Molecular Weight: 310.70

Obtained from 2-chlorobenzimidazole (5.00 g, 32.8 mmols) and (4-trifluoromethyl)benzyl bromide (8.63 g, 36.1 mmols) as a white solid (87%, 8.91 g); R_f (DCM: MeOH: 9.5:0.5) 0.77; ^{1}H NMR (400 MHz, DMSO-d_6) δ 7.73 (d, J = 8.1, 2H, H^7 and H^8), 7.68 – 7.65 (m, 1H, H^1), 7.63 – 7.60 (m, 1H, H^4), 7.40 (d, J = 8.1 Hz, 2H, H^6 and H^9), 7.34 – 7.25 (m, 2H, H^2 and H^3), 5.67 (s, 2H, H^5). ^{13}C NMR (101 MHz, DMSO) δ 141.68, 141.19 (C-CF_3), 140.51, 135.58, 128.76, 128.02 (2C), 126.26 (-CF_3), 123.84 (2C), 123.22 (2C), 119.32, 111.13, 47.06. HPLC-MS (ESI): Purity = 92 %, t_R = 2.779 min, m/z $[M+H]^+$ = 310.8.

7.2.1.4 Procedure for the synthesis of intermediate 2b (Scheme 2.1)

A mixture of intermediate **2a** (1 eq) and ethyl 4-amino-1-piperidine carboxylate (2 eq) was stirred under reflux at 170 ºC for 48 hours with the completion of the reaction being monitored by TLC and LCMS. The reaction mixture was dissolved in DCM/MeOH (95%: 5%) and washed with saturated $NaHCO_3$. More extraction was done with DCM/MeOH (95%: 5%) (4 × 20 mL), and the organic layer was dried over anhydrous Na_2SO_4. The solvent was evaporated *in vacuo* to give a sticky brown solid, washed initially with DCM/Et_2O to eliminate the excess amine, followed by Et_2O wash to afford an off-white solid in quantitative yield. This compound was used in the next reaction without further purification.

Ethyl 4-((1-(4-(trifluoromethyl)benzyl)-1H-benzo[d]imidazol-2-yl)amino)piperidine-1-carboxylate (2b):

Obtained from intermediate **2a** (2.00 g, 6.44 mmols) and ethyl 4-amino-1-piperidine carboxylate (2.20 mL, 12.88 mmols) as an off-white solid (76%, 2.18 g); R_f (DCM: MeOH:

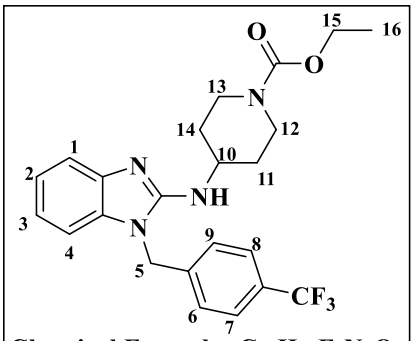

9.5:0.5) 0.45; ^{1}H NMR (400 MHz, MeOH-d_4) δ 7.63 (d, 2H, H^7 and H^8), 7.35 (dd, J = 7.7, 3.8 Hz, 1H, H^1), 7.29 (d, 2H, H^6 and H^9), 7.11 – 6.94 (m, 3H, H^2, H^3 and H^4), 5.38 (s, 2H, H^5), 4.19 – 4.08 (m, 4H, H^{15}, H^{12e} and H^{13e}), 4.00 (tt, J = 11.0, 4.0 Hz, 1H, H^{10}), 3.10 – 2.95 (m, 2H, H^{12a} and H^{13a}), 2.14 – 2.01 (m, 2H, H^{11e} and H^{14e}), 1.56 – 1.39 (m, 2H, H^{11a} and H^{14a}), 1.27 (t, J = 7.1 Hz, 3H, H^{16}). ^{13}C NMR (101 MHz, MeOH-d_4) δ 155.86 (C=O), 153.91, 141.63, 141.03, 133.96 (C-CF_3), 129.60 (2C), 126.77 (2C), 125.27 (-CF_3), 121.25, 119.58, 114.85, 107.62, 61.28, 50.07, 44.18, 42.70 (2C), 31.72 (2C), 13.52. HPLC-MS (ESI): Purity = 98 %, t_R = 2.680 min, m/z $[M+H]^+$ = 446.8.

7.2.1.4 Procedure for the synthesis of intermediate 2c (Scheme 2.1)

A mixture of intermediate **2b** in HBr (48% aq) was stirred under reflux at 120 ºC for 3 hours, with the completion of the reaction being monitored by TLC and LCMS. The mixture was allowed to cool to room temperature and treated with 3N NaOH to basify the excess HBr (pH = 9). Extraction was done with DCM (7 × 30mL), and the combined organic layer was dried over anhydrous Na_2SO_4. The solvent was evaporated *in vacuo* to afford an off-white solid, which was used in the next reaction without further purification.

N-(piperidin-4-yl)-1-(4-(trifluoromethyl)benzyl)-1H-benzo[d]imidazol-2-amine (2c):

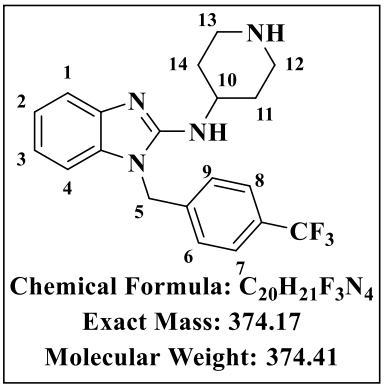

Obtained from intermediate **2b** (1.90 g, 4.26 mmols) and 48% $HBr_{(aq)}$ (16.00 ml, 29.46 mmols) as an off-white solid (98%, 1.75 g); R_f (DCM: MeOH:NH_4OH 9:1:0.05) 0.35; ^{1}H NMR (400 MHz, MeOH-d_4) δ 7.66 (d, J = 8.2 Hz, 2H, H^7 and H^8), 7.45 (dd, J = 8.0, 3.8 Hz, 1H, H^1), 7.35 (d, J = 8.1 Hz, 2H, H^6 and H^9), 7.24 – 7.09 (m, 3H, H^2, H^3 and H^4), 5.52 (s, 2H, H^5), 4.09 (tt, J = 10.9, 4.0 Hz, 1H, H^{10}), 3.58 – 3.46 (dt, J = 13.6, 3.7 Hz, 2H, H^{12e} and H^{13e}), 3.27 – 3.12 (td, J = 12.9, 3.0 Hz, 2H, H^{12a} and H^{13a}), 2.44 – 2.23 (m, 2H, H^{11e} and H^{14e}), 2.02 – 1.82 (m, 2H, H^{11a} and H^{14a}). ^{13}C NMR (101 MHz, MeOH-d_4) δ 152.80, 140.08, 139.03, 132.84 (C-CF_3), 128.90 (2C), 126.82 (2C), 125.42 (-CF_3), 122.42, 121.31, 116.43, 113.90, 108.69, 49.98, 44.69 (2C), 43.02, 28.53 (2C). HPLC-MS (ESI): Purity = 98 %, t_R = 2.426 min, m/z $[M+H]^+$ = 374.9.

7.2.1.5 General procedure for the synthesis of target compounds 2.1-2.12 (Scheme 2.1)

To a solution of intermediate **2c** (1 eq) in methanol (10 mL) was added the appropriate aldehyde (1.1 eq) and the resulting mixture stirred at 25 °C for 6 hours. The mixture was cooled at 0 °C, and $NaBH_4$ (5 eq) was added. The reaction solution was then stirred at 25 °C for 48 hours, quenched with distilled water and concentrated *in vacuo* to remove methanol. The residue was diluted with 5ml of distilled water and extracted with dichloromethane (4 x 20mL). The combined organic layer was washed with brine, dried over anhydrous Na_2SO_4 and solvent was evaporated *in vacuo* to afford the desired compound. The crude product obtained was purified by column chromatography (DCM/MeOH).

2-((4-((1-(4-(trifluoromethyl)benzyl)-1H-benzo[d]imidazol-2-yl)amino)piperidin-1-yl)methyl)phenol (2.1):

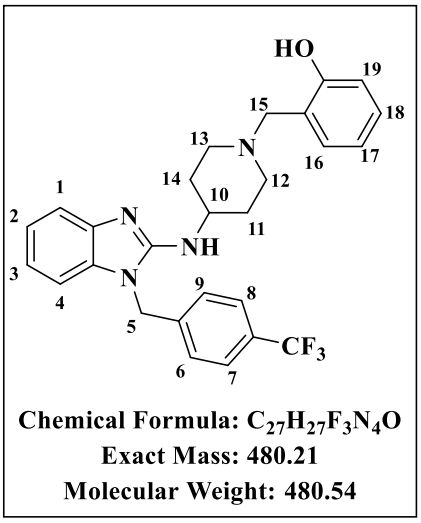

Chemical Formula: $C_{27}H_{27}F_3N_4O$
Exact Mass: 480.21
Molecular Weight: 480.54

Obtained from intermediate **2c** (200 mg, 0.53 mmols) and salicylaldehyde (0.06 mL, 0.58 mmols) as a white solid (85%, 217.7 mg); R_f (DCM: MeOH: 9.5:0.5) 0.75; ^{1}H NMR (400 MHz, MeOH-d_4) δ 7.62 (d, J = 8.2 Hz, 2H, H^7 and H^8), 7.35 (dd, J = 7.9, 3.8 Hz, 1H, H^1), 7.29 (d, J = 8.2 Hz, 2H, H^6 and H^9), 7.16 – 6.93 (m, 5H, H^2, H^3, H^4, H^{17} and H^{19}), 6.85 – 6.71 (m, 2H, H^{16} and H^{18}), 5.38 (s, 2H, H^5), 3.89 (tt, J = 10.9, 4.2 Hz, 1H, H^{10}), 3.73 (s, 2H, H^{15}), 3.07 – 2.89 (m, 2H, H^{12e} and H^{13e}), 2.41 – 2.27 (m, 2H, H^{12a} and H^{13a}), 2.18 – 2.06 (m, 2H, H^{11e} and H^{14e}), 1.75 – 1.56 (m, 2H, H^{11a} and H^{14a}). ^{13}C NMR (101 MHz, MeOH-d_4) δ 157.28 (C-OH), 154.00, 141.66, 141.05, 133.96, 128.67, 128.22 (2C), 127.88 (C-CF_3), 126.80 (2C), 125.23 (-CF_3), 121.74, 121.22, 119.53, 118.96, 115.22, 114.82, 114.59, 107.57, 60.16, 51.60, 49.79 (2C), 44.17, 31.81 (2C). HPLC-MS (ESI): Purity = 99%, t_R = 2.589 min, m/z $[M+H]^+$ = 480.8.

2-fluoro-6-((4-((1-(4-(trifluoromethyl)benzyl)-1H-benzo[d]imidazol-2-yl)amino)piperidin-1-yl)methyl)phenol (2.2):

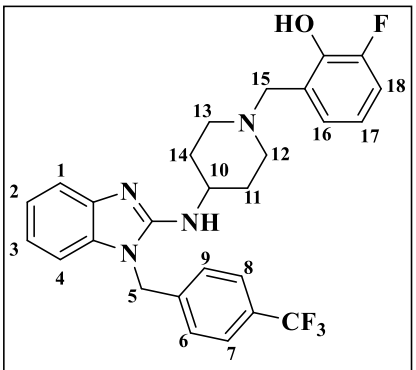

Chemical Formula: $C_{27}H_{26}F_4N_4O$
Exact Mass: 498.20
Molecular Weight: 498.53

Obtained from intermediate **2c** (200 mg, 0.53 mmols) and 3-fluorosalicyladehyde (81.26mg, 0.58mmols) as an off-white solid (55%, 145.4 mg); R_f (DCM: MeOH: 9.5:0.5) 0.53; ^{1}H NMR (400 MHz, MeOH-d_4) δ 7.63 (d, J = 8.2 Hz, 2H, H^7 and H^8), 7.35 (dd, J = 8.0, 3.8 Hz, 1H, H^1), 7.29 (d, J = 8.1 Hz, 2H, H^6 and H^9), 7.12 – 6.93 (m, 5H, H^2, H^4, H^{16}, $H^{17}$and H^{18}), 6.88 – 6.69 (m, 1H, H^3), 5.39 (s, 2H, H^5), 3.91 (tt, J = 10.9, 4.1 Hz, 1H, H^{10}), 3.81 (s, 2H, H^{15}), 3.08 – 2.94 (m, 2H, H^{12e} and H^{13e}), 2.47 – 2.33 (m, 2H, H^{12a} and H^{13a}), 2.21 – 2.09 (m, 2H, H^{11e} and H^{14e}), 1.76 – 1.59 (m, 2H, H^{11a} and H^{14a}). ^{13}C NMR (101 MHz, MeOH-d_4) δ 153.98 (C-OH), 152.46 (C-F), 150.06, 145.54, 141.77, 141.04, 133.95 (2C), 129.48 (C-CF_3), 126.80 (2C), 125.27 (-CF_3), 124.17, 123.79, 121.23, 119.55, 118.78, 118.32, 114.82, 107.59, 59.67, 51.60, 49.66 (2C), 44.18, 31.69 (2C). HPLC-MS (ESI): Purity = 98%, t_R = 2.590 min, m/z $[M+H]^+$ = 498.8.

5-chloro-2-((4-((1-(4-(trifluoromethyl)benzyl)-1H-benzo[d]imidazol-2-yl)amino)piperidin-1-yl)methyl)phenol (2.3):

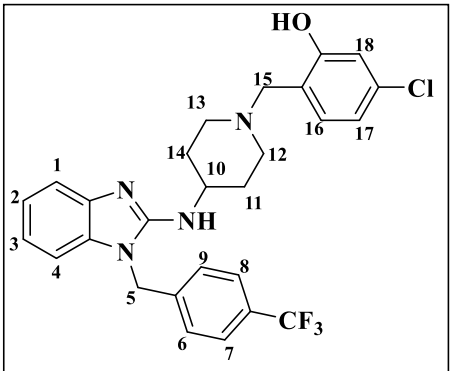

Chemical Formula: $C_{27}H_{26}ClF_3N_4O$
Exact Mass: 514.17
Molecular Weight: 514.98

Obtained from intermediate **2c** (200 mg, 0.53 mmols) and 4-chlorosalicyladehyde (90.83 mg, 0.58 mmols) as an off-white solid (49%, 134.35 mg); R_f (DCM: MeOH: 9.5:0.5) 0.43; ^{1}H NMR (400 MHz, MeOH-d_4) δ 7.62 (d, J = 8.1 Hz, 2H, H^7 and H^8), 7.35 (d, J = 8.1 Hz, 1H, H^{16}), 7.28 (d, J = 8.0 Hz, 2H, H^6 and H^9), 7.10 – 6.93 (m, 4H, H^1, H^2, H^4 and H^{17}), 6.77 (d, J = 2.1 Hz, 1H, H^{18}), 6.76 – 6.74 (m, 1H, H^3), 5.38 (s, 2H, H^5), 3.89 (tt, J = 10.8, 4.2 Hz, 1H, H^{10}), 3.71 (s, 2H, H^{15}), 3.02 – 2.90 (m, 2H, H^{12e} and H^{13e}), 2.42 – 2.26 (m, 2H, H^{12a} and H^{13a}), 2.19 – 2.04 (m, 2H, H^{11e} and H^{14e}), 1.75 – 1.56 (m, 2H, H^{11a} and H^{14a}). ^{13}C NMR (101 MHz, MeOH-d_4) δ 158.57 (C-OH), 153.98, 141.64, 141.03 (C-Cl), 133.96 (2C), 133.50, 129.75, 126.80 (2C), 125.23 (-CF_3), 123.79, 121.23, 120.57, 119.55, 118.68, 118.28, 115.40, 114.83, 107.58, 59.44, 51.56, 49.71 (2C), 44.18, 31.72 (2C). HPLC-MS (ESI): Purity = 98%, t_R = 2.681 min, m/z $[M+H]^+$ = 514.8.

4-methoxy-2-((4-((1-(4-(trifluoromethyl)benzyl)-1H-benzo[d]imidazol-2-yl)amino)piperidin-1-yl)methyl)phenol (2.4):

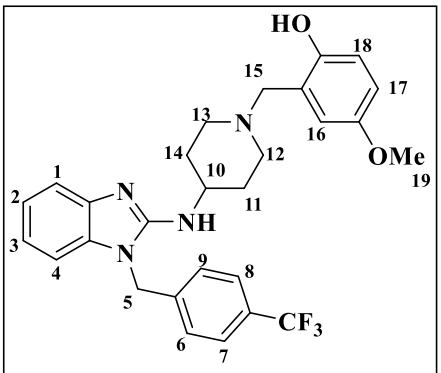

Chemical Formula: $C_{28}H_{29}F_3N_4O_2$
Exact Mass: 510.22
Molecular Weight: 510.56

Obtained from intermediate **2c** (200 mg, 0.53 mmols) and 5-methoxysalicylaldehyde (0.07 mL, 0.58 mmols) as pale- orange solid (40%, 106.7mg); R_f (DCM: MeOH: 9.5:0.5) 0.75; ^{1}H NMR (400 MHz, MeOH-d_4) δ 7.63 (d, J = 8.1 Hz, 2H, H^7 and H^8), 7.35 (dd, J = 8.0, 3.8 Hz, 1H, H^1), 7.29 (d, J = 8.1 Hz, 2H, H^6 and H^9), 7.10 – 6.93 (m, 3H, H^2, H^3 and H^4), 6.76 – 6.64 (m, 3H, H^{16}, H^{17} and H^{18}), 5.39 (s, 2H, H^5), 3.95 – 3.83 (m, 1H, H^{10}), 3.73 (s, 3H, H^{19}), 3.70 (s, 2H, H^{15}), 3.04 – 2.90 (m, 2H, H^{12e} and H^{13e}), 2.42 – 2.27 (m, 2H, H^{12a} and H^{13a}), 2.20 – 2.07 (m, 2H, H^{11e} and H^{14e}), 1.75 – 1.54 (m, 2H, H^{11a} and H^{14a}). ^{13}C NMR (101 MHz, MeOH-d_4) δ 154.17 (C-OCH_3), 152.88 (C-OH), 150.94, 141.65, 141.06, 139.68 (C-CF_3), 133.96 (2C), 132.53, 126.80 (2C), 125.19 (-CF_3), 122.43, 121.21, 119.53, 115.68, 114.81, 114.37, 113.51, 107.56, 60.15 (-OCH_3), 54.84, 51.63, 49.79 (2C), 44.17, 31.81 (2C). HPLC-MS (ESI): Purity = 99%, t_R = 2.577 min, m/z $[M+H]^+$ = 510.8.

2,4-dichloro-6-((4-((1-(4-(trifluoromethyl)benzyl)-1H-benzo[d]imidazol-2-yl)amino)piperidin-1-yl)methyl)phenol (2.5):

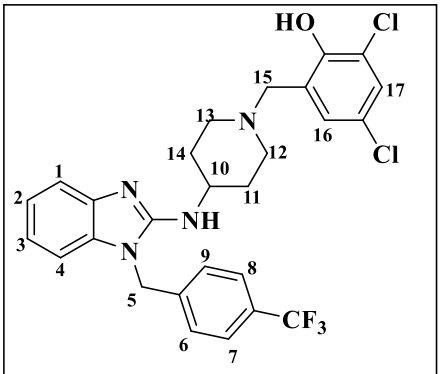

Chemical Formula: $C_{27}H_{25}Cl_2F_3N_4O$
Exact Mass: 548.14
Molecular Weight: 549.42

Obtained from intermediate **2c** (200 mg, 0.53 mmols) and 3,5-dichlorosalicylaldehyde (110.78 mg, 0.58 mmols) as yellow solid (33%, 95.9 mg); R_f (DCM: MeOH: 9.5:0.5) 0.52; ^{1}H NMR (400 MHz, MeOH-d_4) δ 7.63 (d, J = 8.2 Hz, 2H, H^7 and H^8), 7.35 (dd, J = 7.8, 3.7 Hz, 1H, H^1), 7.29 (d, J = 8.1 Hz, 2H, H^6 and H^9), 7.26 (d, J = 2.5 Hz, 1H, H^{17}), 7.11 – 6.94 (m, 4H, H^2, H^3, H^4 and H^{16}), 5.39 (s, 2H, H^5), 3.92 (tt, J = 10.8, 4.0 Hz, 1H, H^{10}), 3.80 (s, 2H, H^{15}), 3.06 – 2.93 (m, 2H, H^{12e} and H^{13e}), 2.52 – 2.38 (m, 2H, H^{12a} and H^{13a}), 2.21 – 2.09 (m, 2H, H^{11e} and H^{14e}), 1.78 – 1.59 (m, 2H, H^{11a} and H^{14a}). ^{13}C NMR (101 MHz, MeOH-d_4) δ 153.93 (C-OH), 153.11, 141.59, 141.02, 133.95 (2C), 132.53 (C-Cl) 129.32, 127.93, 126.80 (2C), 125.28 (-CF_3), 124.20, 122.75, 121.25, 121.05, 119.59 (C-Cl), 114.84, 107.62, 59.80, 51.42, 49.47, 47.81(2C), 44.19, 31.57 (2C). HPLC-MS (ESI): Purity = 98%, t_R = 2.892 min, m/z $[M+H]^+$ = 548.7.

4-methyl-2-((4-((1-(4-(trifluoromethyl)benzyl)-1H-benzo[d]imidazol-2-yl)amino)piperidin-1-yl)methyl)phenol (2.6):

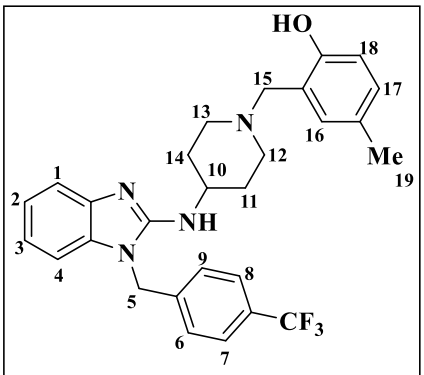

Chemical Formula: $C_{28}H_{29}F_3N_4O$
Exact Mass: 494.23
Molecular Weight: 494.56

Obtained from intermediate **2c** (200 mg, 0.53 mmols) and 5-methylsalicylaldehyde (78.94 mg, 0.58 mmols) as yellow solid (77%, 202.50 mg); R_f (DCM: MeOH: 9.5:0.5) 0.70; ^{1}H NMR (400 MHz, MeOH-d_4) δ 7.62 (d, J = 8.0 Hz, 2H, H^7 and H^8), 7.34 (dd, J = 8.0, 3.7 Hz, 1H, H^1), 7.29 (d, J = 7.9 Hz, 2H, H^6 and H^9), 7.11 – 6.84 (m, 5H, H^2, H^3, H^4, H^{16} and H^{17}), 6.65 (d, J = 7.8 Hz, 1H, H^{18}), 5.38 (s, 2H, H^5), 3.89 (tt, J = 10.9, 5.5 Hz, 1H, H^{10}), 3.68 (s, 2H, H^{15}), 3.03 – 2.88 (m, 2H, H^{12e} and H^{13e}), 2.37 – 2.27 (m, 2H, H^{12a} and H^{13a}), 2.23 (s, 3H, H^{19}), 2.17 – 2.07 (m, 2H, H^{11e} and H^{14e}), 1.71 – 1.58 (m, 2H, H^{11a} and H^{14a}). ^{13}C NMR (101 MHz, MeOH-d_4) δ 154.81 (C-OH), 154.00, 141.66, 141.06, 133.96 (2C), 129.15 (C-CF_3), 128.57 (C-Me), 128.14 (2C), 126.79 (2C), 125.27 (-CF_3), 125.23, 121.42, 121.21, 119.52, 114.99, 114.81, 107.56, 60.20, 59.89, 54.86, 51.61 (2C), 49.81, 44.16, 31.82 (2C), 19.09 (-Me). HPLC-MS (ESI): Purity = 99%, t_R = 2.611 min, m/z $[M+H]^+$ = 494.8.

4-chloro-2-((4-((1-(4-(trifluoromethyl)benzyl)-1H-benzo[d]imidazol-2-yl)amino)piperidin-1-yl)methyl)phenol (2.7):

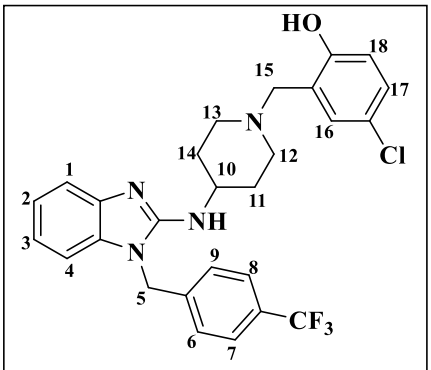

Chemical Formula: $C_{27}H_{26}ClF_3N_4O$
Exact Mass: 514.17
Molecular Weight: 514.98

Obtained from intermediate **2c** (200 mg, 0.53 mmols) and 5-chlorosalicylaldehyde (90.83 g, 0.58 mmols) as an off-white solid (48%, 132.10 mg); R_f (DCM: MeOH: 9.5:0.5) 0.49; ^{1}H NMR (400 MHz, MeOH-d_4) δ 7.62 (d, J = 8.0 Hz, H^7 and H^8), 7.35 (d, J = 3.1 Hz, 1H, H^{16}), 7.29 (d, J = 8.1 Hz, 2H, H^6 and H^9), 7.13 – 6.94 (m, 5H, H^1, H^2, H^3, H^4 and H^{17}), 6.73 (d, J = 8.8 Hz, 1H, H^{18}), 5.38 (s, 2H, H^5), 3.90 (tt, J = 11.0, 4.1 Hz, 1H, H^{10}), 3.71 (s, 2H, H^{15}), 3.01 – 2.88 (m, 2H, H^{12e} and H^{13e}), 2.41 – 2.30 (m, 2H, H^{12a} and H^{13a}), 2.19 – 2.07 (m, 2H, H^{11e} and H^{14e}), 1.72 – 1.57 (m, 2H, H^{11a} and H^{14a}). ^{13}C NMR (101 MHz, MeOH-d_4) δ 153.93 (C-OH), 153.11, 141.59, 141.02, 133.95, 129.32, 127.93 (2C), 126.80 (2C), 125.28, 125.25 (-CF_3), 124.20, 122.75, 121.25, 121.05, 119.59 (C-Cl), 114.84, 107.62, 59.80, 51.42 , 49.47 (2C), 47.81, 44.19, 31.57 (2C). HPLC-MS (ESI): Purity = 98%, t_R = 2.658 min, m/z $[M+H]^+$ = 514.8.

3-((4-((1-(4-(trifluoromethyl)benzyl)-1H-benzo[d]imidazol-2-yl)amino)piperidin-1-yl)methyl)pyridin-2-ol (2.8):

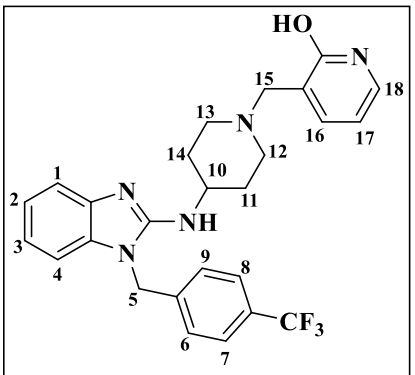

Chemical Formula: $C_{26}H_{26}F_3N_5O$
Exact Mass: 481.21
Molecular Weight: 481.52

Obtained from intermediate **2c** (200 mg, 0.53 mmols) and 2-hydroxynicotinaldehyde (71.40 mg, 0.58 mmols) as a white solid (44%, 112.50 mg); R_f (DCM: MeOH: 9.5:0.5) 0.20; ^{1}H NMR (400 MHz, MeOH-d_4) δ 7.62 (dd, J = 7.2, 4.7 Hz, 3H, H^7, H^8 and H^{18}), 7.38 (dd, J = 6.5, 2.1 Hz, 1H, H^1), 7.34 (dd, J = 7.9, 2.9 Hz, 1H, H^4), 7.28 (d, J = 8.1 Hz, 2H, H^6 and H^9), 7.10 – 6.93 (m, 3H, H^2, H^3 and H^{16}), 6.40 (t, J = 6.7 Hz, 1H, H^{17}), 5.38 (s, 2H, H^5), 3.85 (tt, J = 10.9, 4.1 Hz, 1H, H^{10}), 3.50 (s, 2H, H^{15}), 3.06 – 2.85 (m, 2H, 2H, H^{12e} and H^{13e}), 2.42 – 2.26 (m, 2H, 2H, H^{12a} and H^{13a}), 2.15 – 2.01 (m, 2H, H^{11e} and H^{14e}), 1.74 – 1.54 (m, 2H, H^{11a} and H^{14a}). ^{13}C NMR (101 MHz, MeOH-d_4) δ 163.71 (C-OH), 154.05, 141.68, 141.07, 138.08, 137.69, 133.94, 133.39, 127.80 (2C), 126.78 (2C), 125.26 (-CF_3), 125.22, 121.18, 119.47, 114.79, 107.53, 106.54, 55.57, 52.16, 49.95 (2C), 44.15, 31.54 (2C). HPLC-MS (ESI): Purity = 98%, t_R = 2.475 min, m/z $[M+H]^+$ = 481.8.

2-chloro-6-((4-((1-(4-(trifluoromethyl)benzyl)-1H-benzo[d]imidazol-2-yl)amino)piperidin-1-yl)methyl)phenol (2.9):

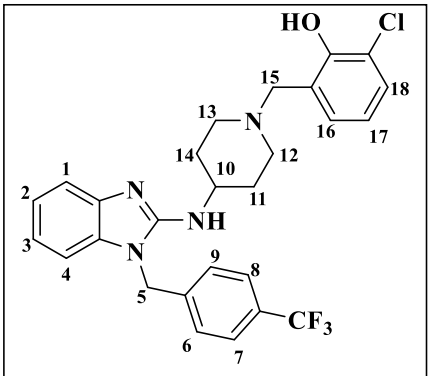

Chemical Formula: $C_{27}H_{26}ClF_3N_4O$
Exact Mass: 514.17
Molecular Weight: 514.98

Obtained from intermediate **2c** (200 mg, 0.53 mmols) and 3-chlorosalicylaldehyde (90.83 mg, 0.58 mmols) as an off-white solid (41%, 112.50 mg); R_f (DCM: MeOH: 9.5:0.5) 0.60; ^{1}H NMR (400 MHz, MeOH-d_4) δ 7.63 (d, J = 8.1 Hz, 2H, H^7 and H^8), 7.35 (dd, J = 7.7, 2.9 Hz, 1H, H^1), 7.29 (d, J = 8.0 Hz, 2H, H^6 and H^9), 7.22 (dd, J = 8.0, 6.9 Hz, 1H, H^{17}), 7.11 – 6.92 (m, 4H, H^2, H^4, H^{16} and H^{18}), 6.74 (t, J = 7.7 Hz, 1H, H^3), 5.39 (s, 2H, H^5), 3.92 (tt, J = 10.7, 4.1 Hz, 1H, H^{10}), 3.79 (s, 2H, H^{15}), 3.08 – 2.90 (m, 2H, H^{12e} and H^{13e}), 2.48 – 2.32 (m, 2H, H^{12a} and H^{13a}), 2.23 – 2.10 (m, 2H, H^{11e} and H^{14e}), 1.77 – 1.57 (m, 2H, H^{11a} and H^{14a}). ^{13}C NMR (101 MHz, MeOH-d_4) δ 153.96 (C-OH), 153.69, 141.61, 141.04, 138.02, 133.95, 128.60 (2C), 126.93 (2C), 126.80, 125.28, 125.25 (-CF_3), 123.08 (C-Cl), 121.24, 120.28, 119.57, 119.03, 114.82, 107.61, 60.29, 51.47, 49.62 (2C), 44.18, 31.70 (2C). HPLC-MS (ESI): Purity = 99%, t_R = 2.686 min, m/z $[M+H]^+$ = 514.8.

2,4-difluoro-6-((4-((1-(4-(trifluoromethyl)benzyl)-1H-benzo[d]imidazol-2-yl)amino)piperidin-1-yl)methyl)phenol (2.10):

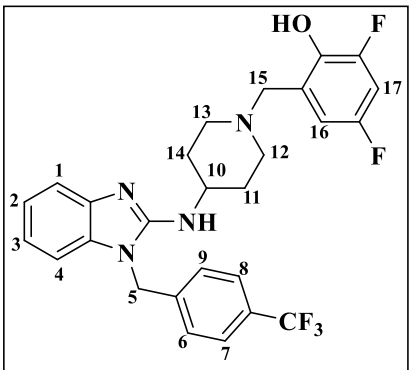

Chemical Formula: $C_{27}H_{25}F_5N_4O$
Exact Mass: 516.19
Molecular Weight: 516.52

Obtained from intermediate **2c** (200mg, 0.53 mmols) and 3,5-difluorosalicylaldehyde (91.70 mg, 0.58 mmols) as an off-white solid (42%, 114.70 mg); R_f (DCM: MeOH: 9.5:0.5) 0.52; ^{1}H NMR (400 MHz, MeOH-d_4) δ 7.63 (d, J = 8.1 Hz, 2H, H^7 and H^8), 7.35 (d, J = 3.8 Hz, 1H, H^{16}), 7.29 (d, J = 8.0 Hz, 2H, H^6 and H^9), 7.11 – 6.93 (m, 3H, H^1, H^2 and H^4), 6.84 (d, J = 3.8 Hz, 1H, H^{17}), 6.70 (dd, J = 8.9, 7.9 Hz, 1H, H^3), 5.38 (s, 2H, H^5), 3.90 (tt, J = 10.9, 4.1 Hz, 1H, H^{10}), 3.77 (s, 2H, H^{15}), 3.05 – 2.92 (m, 2H, 2H, H^{12e} and H^{13e}), 2.47 – 2.30 (m, 2H, 2H, H^{12a} and H^{13a}), 2.20 – 2.08 (m, 2H, H^{11e} and H^{14e}), 1.76 – 1.58 (m, 2H, 2H, H^{11a} and H^{14a}). ^{13}C NMR (101 MHz, MeOH-d_4) δ 155.95 (C-F), 153.95 (C-F), 141.58 (C-OH), 141.02, 138.08, 133.94, 128.11 (2C),126.79 (2C), 125.27, 125.24 (-CF_3), 124.88, 121.25, 119.58, 114.82, 110.19, 109.96, 107.60, 102.67, 59.31, 51.66, 49.63 (2C), 44.18, 31.68 (2C). HPLC-MS (ESI): Purity = 99%, t_R = 2.638 min, m/z $[M+H]^+$ = 516.8.

4-hydroxy-3-((4-((1-(4-(trifluoromethyl)benzyl)-1H-benzo[d]imidazol-2-yl)amino)piperidin-1-yl)methyl)benzonitrile (2.11):

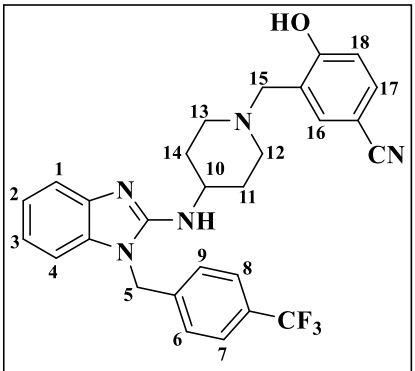

Chemical Formula: $C_{28}H_{26}F_3N_5O$
Exact Mass: 505.21
Molecular Weight: 505.55

Obtained from intermediate **2c** (200 mg, 0.53 mmols) and 3-formyl-4-hydroxybenzonitrile (85.32 mg, 0.58 mmols) as yellow solid (42%, 115.50 mg); R_f (DCM: MeOH: 9.5:0.5) 0.77; ^{1}H NMR (600 MHz, Methanol-d_4) δ 7.60 (d, J = 8.2 Hz, 2H, H^7 and H^8), 7.47 (dd, J = 8.4, 2.2 Hz, 1H, H^{17}), 7.43 (d, J = 2.1 Hz, 1H, H^{16}), 7.32 (dd, J = 7.8, 2.6 Hz, 1H, H^1), 7.27 (d, J = 8.1 Hz, 2H, H^6 and H^9), 7.05 (td, J = 7.8, 2.6 Hz, 1H, H^2), 7.01 (dd, J = 7.7, 2.6 Hz, 1H, H^4), 6.94 (td, J = 7.8, 2.6 Hz, 1H, H^3), 6.81 (d, J = 8.4 Hz, 1H, H^{18}), 5.37 (s, 2H, H^5), 3.89 (tt, J = 10.9, 4.1 Hz, 1H, H^{10}), 3.79 (s, 2H, H^{15}), 3.04 – 2.90 (m, 2H, H^{12e} and H^{13e}), 2.46 – 2.35 (m, 2H, H^{12a} and H^{13a}), 2.19 – 2.07 (m, 2H, H^{11e} and H^{14e}), 1.70 – 1.57 (m, 2H, H^{11a} and H^{14a}). ^{13}C NMR (151 MHz, MeOH-d_4) δ 164.52 (C-OH), 155.34, 142.47, 138.08, 135.34, 134.39, 130.91, 130.70, 128.11 (2C), 126.65 (2C), 124.67, 124.53 (-CF_3), 122.64, 120.97, 120.54 (-CN), 118.09, 116.21, 109.00, 102.17, 60.39, 52.92 (2C), 50.92, 45.55, 32.93 (2C). HPLC-MS (ESI): Purity = 99%, t_R = 2.594 min, m/z $[M+H]^+$ = 505.8.

N-(1-benzylpiperidin-4-yl)-1-(4-(trifluoromethyl)benzyl)-1H-benzo[d]imidazol-2-amine (2.12):

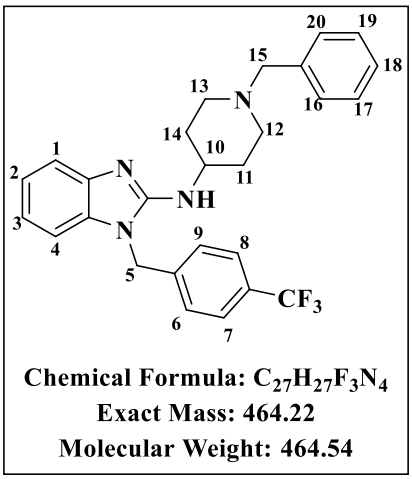

Obtained from intermediate **2c** (200 mg, 0.53 mmols) and benzaldehyde (61.55 mg, 0.58 mmols) as a white solid (31%, 75.60 mg); R_f (DCM: MeOH: 9.5:0.5) 0.38; ^{1}H NMR (400 MHz, MeOH-d_4) δ 7.61 (d, J = 8.1 Hz, 2H, H^7 and H^8), 7.38 – 7.24 (m, 8H, H^1, H^6, H^9, H^{16}, H^{17}, H^{18}, H^{19} and H^{20}), 7.10 – 6.91 (m, 3H, $H^2H^3H^4$), 5.37 (s, 2H, H^5), 3.83 (tt, J = 10.9, 4.2 Hz, 1H, H^{10}), 3.55 (s, 2H, H^{15}), 2.99 – 2.81 (m, 2H, $H^{12e}H^{13e}$), 2.31 – 2.15 (m, 2H, $H^{12a}H^{13a}$),), 2.13 – 2.00 (m, 2H, $H^{11e}H^{14e}$), 1.71 – 1.54 (m, 2H, $H^{11a}H^{14a}$). ^{13}C NMR (101 MHz, MeOH-d_4) δ 154.03, 141.67, 141.06, 137.05, 133.95, 129.36 (2C), 128.07 (2C) 127.89 (2C), 127.04, 126.78 (2C), 125.25, 125.22 (-CF_3), 121.19, 119.49, 114.79, 107.53, 62.60, 52.09 (2C), 49.99, 44.14, 31.42 (2C). HPLC-MS (ESI): Purity = 98%, t_R = 2.584 min, m/z $[M+H]^+$ = 464.8.

7.2.1.6 General procedure for the Mannich reaction of target compounds 2.13-2.21 (Scheme 2.1)

A mixture of intermediate **2c** (1 eq), 37% aq paraformaldehyde (1.2 eq) and the appropriate phenol (1.2 eq) in ethanol (3 mL) was refluxed at 85 °C for 16 h. When the reaction had completed, the solvent was removed *in vacuo*, and the residue was purified via column chromatography to obtain the desired product.

5-fluoro-2-((4-((1-(4-(trifluoromethyl)benzyl)-1H-benzo[d]imidazol-2-yl)amino)piperidin-1-yl)methyl)phenol (2.13):

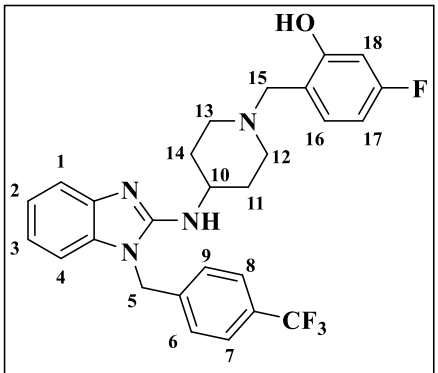

Chemical Formula: $C_{27}H_{26}F_4N_4O$
Exact Mass: 498.20
Molecular Weight: 498.53

Obtained from intermediate **2c** (100 mg, 0.27 mmol) and 3-fluorophenol (0.03 mL, 0.32 mmol) as a white solid (83%, 111.1 mg); Rf (DCM:MeOH, 9:1) 0.58; ^{1}H-NMR (600 MHz, Methanol-d_4) δ 7.58 (d, J = 8.2 Hz, 2H, H^7 and H^8), 7.30 (dd, J = 8.0, 3.9 Hz, 1H, H^1), 7.25 (d, J = 8.2 Hz, 2H, H^6 and H^9), 7.03 (td, J = 7.8, 2.2 Hz, 1H, H^{17}), 7.00–6.97 (m, 2H, H^4 and H^{18}), 6.92 (ddd, J = 8.0, 7.3, 2.1 Hz, 1H, H^2), 6.48–6.41 (m, 2H, H^3 and H^{16}), 5.34 (s, 2H, H^5), 3.85 (tt, J = 10.8, 4.1 Hz, 1H, H^{10}), 3.67 (s, 2H, H^{15}), 2.98–2.88 (m, 2H, H^{12e} and H^{13e}), 2.33–2.27 (m, 2H, H^{12a} and H^{13a}), 2.11–2.06 (m, 2H, H^{11e} and H^{14e}), 1.66–1.56 (m, 2H, H^{11a} and H^{14a}). ^{13}C-NMR (151 MHz, MeOD) δ 164.04, 162.43, 159.11, 159.03, 153.94, 141.58, 141.04, 133.90, 129.73 (2C), 126.75 (2C), 125.22, 121.19, 119.51, 117.68, 114.75, 107.54, 105.11, 102.45, 59.37, 51.49, 49.71, 44.10 (2C), 31.69 (2C). HPLC-MS (ESI): Purity = 98%, t_R = 2.404 min, *m/z* [M+H]$^+$ = 499.2.

2,4-dimethyl-6-((4-((1-(4-(trifluoromethyl)benzyl)-1H-benzo[d]imidazol-2-yl)amino)piperidin-1-yl)methyl)phenol (2.14):

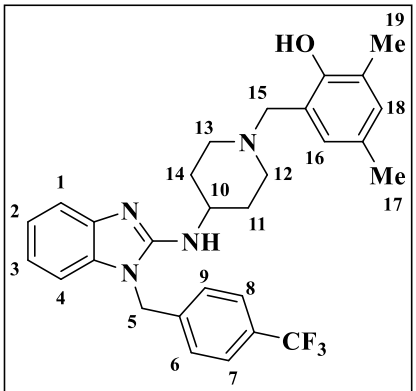

Chemical Formula: $C_{29}H_{31}F_3N_4O$
Exact Mass: 508.24
Molecular Weight: 508.59

Obtained from intermediate **2c** (100 mg, 0.27 mmol) and 2,4-dimethylphenol (0.03 mL, 0.32 mmol) as a white solid (90%, 123.4 mg); Rf (DCM:MeOH, 9:1) 0.63; ^{1}H-NMR (600 MHz, Methanol-d_4) δ 7.57 (d, J = 8.1 Hz, 2H, H^7 and H^8), 7.31 (dd, J = 7.9, 3.8 Hz, 1H, H^1), 7.25 (d, J = 8.0 Hz, 2H, H^6 and H^9), 7.04–6.90 (m, 3H, H^2, H^3 and H^4), 6.77 (d, J = 2.2 Hz, 1H, H^{18}), 6.60 (d, J = 2.2 Hz, 1H, H^{16}), 5.32 (s, 2H, H^5), 3.87 (tt, J = 10.7, 4.2 Hz, 1H, H^{10}), 3.60 (s, 2H, H^{15}), 2.90–2.86 (m, 2H, H^{12e} and H^{13e}), 2.29–2.23 (m, 2H, H^{12a} and H^{13a}), 2.14 (s, 3H, H^{19}), 2.09 (s, 3H, H^{17}), 2.08–2.03 (m, 2H, H^{11e} and H^{14e}), 1.65–1.56 (m, 2H, H^{11a} and H^{14a}). ^{13}C-NMR (151 MHz, MeOD) δ 154.02, 152.95, 141.72, 140.99, 134.01, 129.90 (2C), 129.61, 129.40, 127.58, 126.80 (2C),

126.36, 125.21, 123.83, 121.18, 120.70, 119.50, 114.89, 107.54, 60.77, 51.49, 49.81, 44.23 (2C), 31.87 (2C), 19.02, 14.16. HPLC-MS (ESI): Purity = 98%, t_R = 2.545 min, *m/z* $[M+H]^+$ = 509.2.

3,6-dimethyl-2-((4-((1-(4-(trifluoromethyl)benzyl)-1H-benzo[d]imidazol-2-yl)amino)piperidin-1-yl)methyl)phenol (2.15):

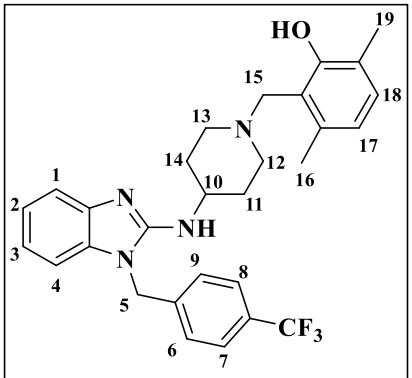

Chemical Formula: $C_{29}H_{31}F_3N_4O$
Exact Mass: 508.24
Molecular Weight: 508.59

Obtained from intermediate **2c** (100 mg, 0.27 mmol) and 2,5-dimethylphenol (0.03 mL, 0.32 mmol) as a white solid (70%, 96.6 mg); Rf (DCM:MeOH, 9:1) 0.61; ^{1}H-NMR (600 MHz, Methanol-d_4) δ 7.59 (d, *J* = 8.2 Hz, 2H, H^7 and H^8), 7.30 (dd, *J* = 7.9, 3.9 Hz, 1H, H^1), 7.25 (d, *J* = 8.2 Hz, 2H, H^6 and H^9), 7.05–6.90 (m, 3H, H^2, H^3 and H^4), 6.82 (d, *J* = 7.6 Hz, 1H, H^{18}), 6.49 (d, *J* = 7.6 Hz, 1H, H^{17}), 5.35 (s, 2H, H^5), 3.87 (tt, *J* = 11.1, 5.3 Hz, 1H, H^{10}), 3.71 (s, 2H, H^{15}), 2.99–2.88 (m, 2H, H^{12e} and H^{13e}), 2.34–2.28 (m, 2H, H^{12a} and H^{13a}), 2.18 (s, 3H, H^{19}), 2.11–2.09 (m, 2H, H^{11e} and H^{14e}), 2.08 (s, 3H, H^{16}), 1.66–1.58 (m, 2H, H^{11a} and H^{14a}). ^{13}C-NMR (151 MHz, MeOD) δ 155.80, 153.96, 141.60, 141.05, 133.90, 133.61, 129.48, 129.26, 128.75 (2C), 126.76 (2C), 125.21, 121.98, 121.19, 120.36, 119.50, 118.73, 114.74, 107.54, 56.53, 51.47, 49.94, 44.10 (2C), 31.85 (2C), 18.21, 14.28. HPLC-MS (ESI): Purity = 97%, t_R = 2.598 min, *m/z* $[M+H]^+$ = 509.2.

2-ethyl-6-((4-((1-(4-(trifluoromethyl)benzyl)-1H-benzo[d]imidazol-2-yl)amino)piperidin-1-yl)methyl)phenol (2.16):

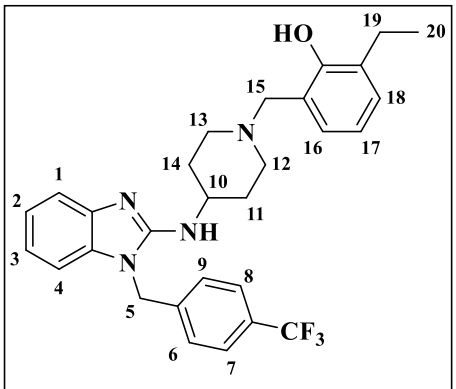

Chemical Formula: $C_{29}H_{31}F_3N_4O$
Exact Mass: 508.24
Molecular Weight: 508.59

Obtained intermediate **2c** (100 mg, 0.27 mmol) and 2-ethylphenol (0.03 mL, 0.32 mmol) as a white solid (92%, 125.7 mg); Rf (DCM:MeOH, 9:1) 0.74; ^{1}H-NMR (600 MHz, Methanol-d_4) δ 7.57 (d, J = 8.1 Hz, 2H, H^7 and H^8), 7.30 (dd, J = 7.9, 3.8 Hz, 1H, H^1), 7.24 (d, J = 8.1 Hz, 2H, H^6 and H^9), 7.05–6.89 (m, 4H, H^2, H^3, H^4 and H^{16}), 6.79 (dd, J = 7.5, 3.7 Hz, 1H, H^{18}), 6.65 (t, J = 7.6 Hz, 1H, H^{17}), 5.33 (s, 2H, H^5), 3.85 (tt, J = 10.7, 4.8 Hz, 1H, H^{10}), 3.65 (s, 2H, H^{15}), 2.95–2.86 (m, 2H, H^{12e} and H^{13e}), 2.56 (q, J = 7.2 Hz, 2H, H^{19}), 2.29–2.23 (m, 2H, H^{12a} and H^{13a}), 2.10–2.06 (m, 2H, H^{11e} and H^{14e}), 1.64–1.57 (m, 2H, H^{11a} and H^{14a}), 1.13 (t, J = 7.2 Hz, 3H, H^{20}). ^{13}C-NMR (151 MHz, MeOD) δ 155.08, 153.95, 141.60, 141.02, 133.91, 130.32, 129.26, 127.78 (2C), 126.77 (2C), 125.95, 125.22, 121.20, 121.02, 119.50, 118.60, 114.76, 107.54, 89.70, 60.82, 51.50, 49.81, 44.11 (2C), 31.87 (2C), 22.44, 13.26. HPLC-MS (ESI): Purity = 98%, t_R = 2.598 min, *m/z* $[M+H]^+$ = 509.2.

2-isopropyl-6-((4-((1-(4-(trifluoromethyl)benzyl)-1H-benzo[d]imidazol-2-yl)amino)piperidin-1-yl)methyl)phenol (2.17):

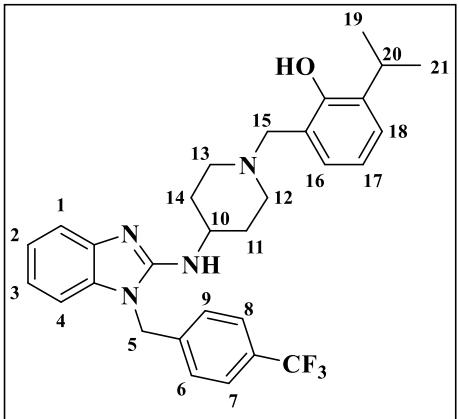

Chemical Formula: $C_{30}H_{33}F_3N_4O$
Exact Mass: 522.26
Molecular Weight: 522.62

Obtained from intermediate **2c** (100 mg, 0.27 mmol) and 2-isopropylphenol (0.04 mL, 0.32 mmol) as a white solid (99%, 139.7 mg); Rf (DCM:MeOH, 9:1) 0.69; ^{1}H-NMR (600 MHz, Methanol-d_4) δ 7.58 (d, J = 8.2 Hz, 2H, H^7 and H^8), 7.30 (dd, J = 7.7, 3.7 Hz, 1H, H^1), 7.25 (d, J = 8.1 Hz, 2H, H^6 and H^9), 7.05–6.89 (m, 4H, H^2, H^3, H^4 and H^{16}), 6.79 (dd, J = 7.5, 3.6 Hz, 1H, H^{18}), 6.69 (t, J = 7.5 Hz, 1H, H^{17}), 5.34 (s, 2H, H^5), 3.86 (tt, J = 10.9, 4.3 Hz, 1H, H^{10}), 3.67 (s, 2H, H^{15}), 3.27–3.22 (m, 1H, H^{20}), 2.95–2.90 (m, 2H, H^{12e} and H^{13e}), 2.30–2.25 (m, 2H, H^{12a} and H^{13a}), 2.12–2.06 (m, 2H, H^{11e} and H^{14e}), 1.66–1.58 (m, 2H, H^{11a} and H^{14a}), 1.17 (d, J = 7.0 Hz, 3H, H^{19}), 1.16 (d, J = 7.0 Hz, 3H, H^{21}). ^{13}C-NMR (151 MHz, MeOD) δ 154.58, 153.96,

141.60, 141.04, 134.61, 133.91 (2C), 129.48, 126.77 (2C), 125.74, 125.22, 124.69, 121.19, 121.06, 119.49, 118.63, 114.75, 107.54, 89.70, 60.92, 51.48, 49.82, 44.11 (2C), 31.87 (2C), 26.30, 21.57 (2C). HPLC-MS (ESI): Purity = 97%, t_R = 2.650 min, *m/z* $[M+H]^+$ = 523.2.

3-hydroxy-4-((4-((1-(4-(trifluoromethyl)benzyl)-1H-benzo[d]imidazol-2-yl)amino)piperidin-1-yl)methyl)benzonitrile (2.18):

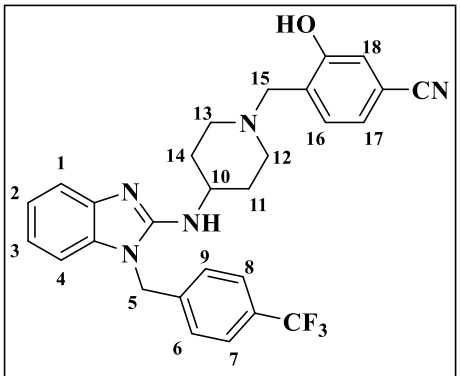

Chemical Formula: $C_{28}H_{26}F_3N_5O$
Exact Mass: 505.21
Molecular Weight: 505.55

Obtained from intermediate **2c** (2.00 g, 5.34 mmol) and 4-formyl-3-hydroxybenzonitrile (863.48 mg, 5.87 mmol) as an off-white solid (50%, 1.35 g); Rf (DCM:MeOH, 9:1) 0.61; ^{1}H-NMR (600 MHz, Methanol-d_4) δ 7.59 (d, *J* = 8.2 Hz, 2H, H^7 and H^8), 7.33 (dd, *J* = 7.9, 3.9 Hz, 1H, H^1), 7.26 (d, *J* = 8.1 Hz, 2H, H^6 and H^9), 7.23 (d, *J* = 7.7 Hz, 1H, H^{16}), 7.10 (dd, *J* = 7.7, 1.6 Hz, 1H, H^{17}), 7.08–6.95 (m, 4H, H^2, H^3, H^4 and H^{18}), 5.36 (s, 2H, H^5), 3.88 (tt, *J* = 10.9, 4.2 Hz, 1H, H^{10}), 3.84 (s, 2H, H^{15}), 3.00–2.96 (m, 2H, H^{12e} and H^{13e}), 2.50–2.43 (m, 2H, H^{12a} and H^{13a}), 2.15–2.10 (m, 2H, H^{11e} and H^{14e}), 1.72–1.62 (m, 2H, H^{11a} and H^{14a}). ^{13}C-NMR (151 MHz, MeOD) δ 173.87, 158.17, 153.45, 140.69, 140.36, 133.65, 130.13 (2C), 127.20, 126.79 (2C), 125.26, 122.51, 121.54, 120.03, 118.34, 118.24, 114.58, 111.89, 107.86, 59.03, 51.56, 49.52, 44.34 (2C), 31.26, 19.38 (2C). HPLC-MS (ESI): Purity = 98%, t_R = 2.501 min, *m/z* $[M+H]^+$ = 506.2.

3-hydroxy-4-((4-((1-(4-(trifluoromethyl)benzyl)-1H-benzo[d]imidazol-2-yl)amino)piperidin-1-yl)methyl)benzoic acid (2.19):

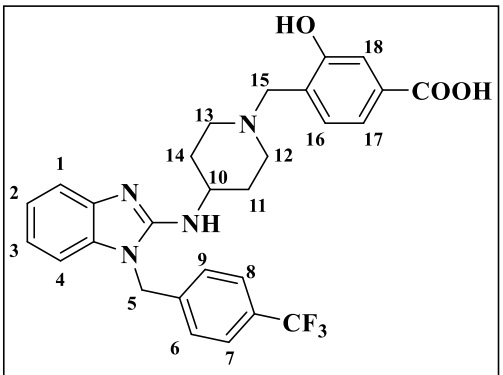

Chemical Formula: $C_{28}H_{27}F_3N_4O_3$
Exact Mass: 524.20
Molecular Weight: 524.54

Obtained from 3-hydroxy-4-((4-((1-(4-(trifluoromethyl)benzyl)-1H-benzo[d]imidazol-2-yl)amino)piperidin-1-yl)methyl)benzonitrile (1.00 g, 5.34 mmol) as a white solid (73%, 761.3 mg); Rf (DCM:MeOH, 9:1) 0.25; ^{1}H-NMR (600 MHz, Methanol-d_4) δ 7.64 (d, J = 8.1 Hz, 2H, H^7 and H^8), 7.58 (dd, J = 8.4, 1.5 Hz, 1H, H^{17}), 7.56 (d, J = 1.6 Hz, 1H, H^{18}), 7.53 (d, J = 8.1 Hz, 2H, H^6 and H^9), 7.43–7.37 (m, 3H, H^1, H^2 and H^4), 7.34 (ddd, J = 8.2, 5.9, 2.7 Hz, 1H, H^3), 7.29 (d, J = 8.4 Hz, 1H, H^{16}), 5.61 (s, 2H, H^5), 4.42 (s, 2H, H^{15}), 4.14 (tt, J = 10.3, 4.4 Hz, 1H, H^{10}), 3.68–3.61 (m, 2H, H^{12e} and H^{13e}), 3.39–3.31 (m, 2H, H^{12a} and H^{13a}), 2.38–2.30 (m, 2H, H^{11e} and H^{14e}), 2.24–2.13 (m, 2H, H^{11a} and H^{14a}). ^{13}C-NMR (151 MHz, MeOD) δ 169.94, 167.42, 156.68, 149.10, 138.31, 134.18, 132.77 (2C), 130.61, 129.03, 126.97 (2C), 125.59, 124.36, 124.02, 120.74, 118.45, 116.21, 114.64, 111.76, 110.24, 56.91, 51.33, 45.46 (2C), 28.74, 16.89 (2C). HPLC-MS (ESI): Purity = 98%, t_R = 2.325 min, *m/z* $[M+H]^+$ = 525.2.

Methyl 3-hydroxy-4-((4-((1-(4-(trifluoromethyl)benzyl)-1H-benzo[d]imidazol-2-yl)amino)piperidin-1-yl)methyl)benzoate (2.20):

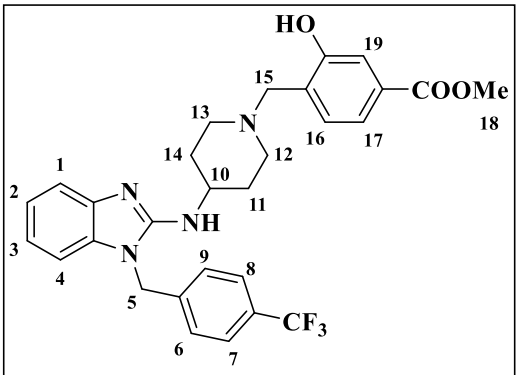

Chemical Formula: $C_{29}H_{29}F_3N_4O_3$
Exact Mass: 538.22
Molecular Weight: 538.57

Obtained from 3-hydroxy-4-((4-((1-(4-(trifluoromethyl)benzyl)-1H-benzo[d]imidazol-2-yl)amino)piperidin-1-yl)methyl)benzoic acid (100 mg, 0.19 mmol) as an off- white solid (94%, 96.1 mg); Rf (DCM:MeOH, 9:1) 0.56; ^{1}H-NMR (600 MHz, DMSO) δ 6.84 (d, J = 8.1 Hz, 2H, H^7 and H^8), 6.63 (dd, J = 7.8, 1.7 Hz, 1H, H^{17}), 6.54 (d, J = 1.7 Hz, 1H, H^{19}), 6.53–6.50 (m, 3H, H^1, H^6 and H^9), 6.38 (d, J = 7.9 Hz, 1H, H^{16}), 6.27–6.23 (m, 2H, H^2, H^4), 6.15 (ddd, J = 8.1, 7.3, 1.1 Hz, 1H, H^3), 4.59 (s, 2H, H^5), 3.09 (tt, J = 10.3, 4.3 Hz, 1H, H^{10}), 3.07 (s, 3H, H^{18}), 2.99 (s, 2H, H^{15}), 2.20–2.14 (m,

2H, H^{12e} and H^{13e}), 1.59–1.52 (m, 2H, H^{12a} and H^{13a}), 1.34–1.30 (m, 2H, H^{11e} and H^{14e}), 0.91–0.82 (m, 2H, H^{11a} and H^{14a}). ^{13}C-NMR (151 MHz, DMSO) δ 165.53, 156.81, 153.26, 140.98, 140.52, 133.22, 129.50, 128.53, 128.31, 128.20 (2C), 126.74, 126.25 (2C), 124.63, 120.49, 119.18, 118.75, 115.22, 114.10, 106.36, 58.32, 51.01, 50.51, 48.93 (2C), 43.03, 32.00 (2C). HPLC-MS (ESI): Purity = 98%, t_R = 2.466 min, *m/z* $[M+H]^+$ = 539.2.

(3-hydroxy-4-((4-((1-(4-(trifluoromethyl)benzyl)-1H-benzo[d]imidazol-2-yl)amino)piperidin-1-yl)methyl)phenyl)(morpholino)methanone (2.21):

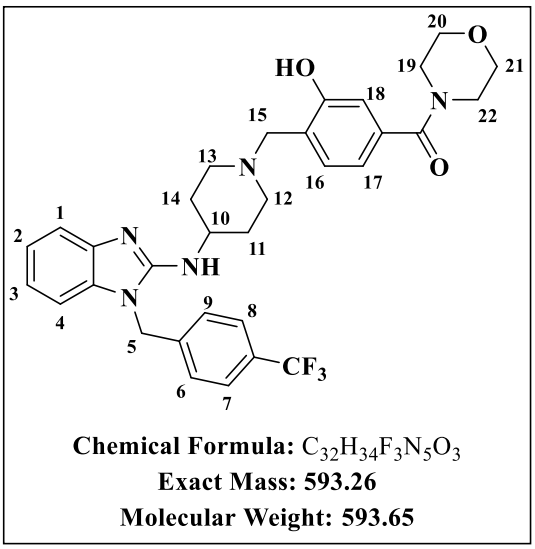

Obtained from 3-hydroxy-4-((4-((1-(4-(trifluoromethyl)benzyl)-1H-benzo[d]imidazol-2-yl)amino)piperidin-1-yl)methyl)benzoic acid (100 mg, 0.19 mmol) and morpholine (0.02 mL, 0.25 mmol) as a pale yellow solid (94%, 80.8 mg); Rf (DCM:MeOH, 9:1) 0.58; ^{1}H-NMR (600 MHz, MeOD) δ 7.60 (d, *J* = 8.2 Hz, 2H, H^7 and H^8), 7.32 (dd, *J* = 7.9, 1.6 Hz, 1H, H^{17}), 7.26 (d, *J* = 8.2 Hz, 2H, H^6 and H^9), 7.13 (d, *J* = 7.9 Hz, 1H, H^{16}), 7.04 (ddd, *J* = 8.0, 1.3, 0.6 Hz, 1H, H^1), 7.00 (ddd, *J* = 8.0, 7.8, 1.4 Hz, 1H, H^2), 6.94 (ddd, *J* = 7.9, 1.4, 0.6 Hz, 1H, H^4), 6.81 (ddd, *J* = 7.9, 7.8, 1.3 Hz, 1H, H^3), 6.77 (d, *J* = 1.6 Hz, 1H, H^{18}), 5.36 (s, 2H, H^5), 3.87 (tt, *J* = 10.8, 4.2 Hz, 1H, H^{10}), 3.75 (s, 2H, H^{15}), 3.74–3.55 (m, 4H, H^{20} and H^{21}), 3.52–3.38 (m, 4H, H^{19} and H^{22}), 2.99–2.92 (m, 2H, H^{12e} and H^{13e}), 2.38–2.29 (m, 2H, H^{12a} and H^{13a}), 2.13–2.08 (m, 2H, H^{11e} and H^{14e}), 1.67–1.59 (m, 2H, H^{11a} and H^{14a}). ^{13}C-NMR (151 MHz, MeOD) δ 170.98, 157.75, 153.93, 141.57, 141.04, 135.37, 133.91, 129.47, 129.26, 128.62 (2C), 126.76 (2C), 125.19, 123.93, 121.21, 119.53, 117.25, 114.76, 113.02, 107.15, 66.36 (2C), 59.70, 52.14 (2C), 49.67, 44.12 (2C), 42.42, 32.16 (2C). HPLC-MS (ESI): Purity = 97%, t_R = 2.387 min, *m/z* $[M+H]^+$ = 594.2.

7.2.2 Imidazopyridines

7.2.2.1 Procedure for the synthesis of intermediate 3a (Scheme 2.5)

A mixture of p-methoxybenzyl amine and *N*,*N*-Diisopropylethylamine (DIPEA) in tetrahydrofuran (THF) was added dropwise to a 0 °C solution of 2,4-dichloro-5-nitropyridine in THF. The solution was then warmed up to 25 °C and stirred for an additional 30 min. Water

was then added, and the resulting mixture was extracted with ethyl acetate. The combined organic layer was dried over anhydrous Na_2SO_4 and concentrated under reduced pressure to produce the desired intermediate as a yellow solid in 98% yield.

2-chloro-N-(4-methoxybenzyl)-5-nitropyridin-4-amine (3a):

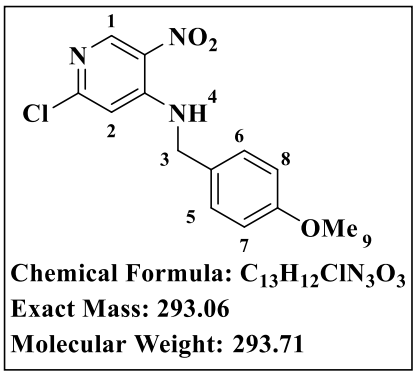

Obtained from 2,4-dichloro-5-nitropyridine (2.00 g, 10.36 mmol) and p-methoxybenzyl amine (2.56 g, 18.65 mmol) as a yellow solid (98%, 3.54 g); Rf (Hex: EtOAc, 1:1) 0.54; ^{1}H-NMR (600 MHz, DMSO-d_6) δ 8.96 (t, J = 6.1 Hz, 1H, H^4), 8.85 (s, 1H, H^1), 7.29 (d, J = 8.7 Hz, 2H, H^5 and H^6), 6.94 (s, 1H, H^2), 6.89 (d, J = 8.7 Hz, 2H, H^7 and H^8), 4.57 (d, J = 6.1 Hz, 2H, H^3), 3.71 (s, 3H, H^9). ^{13}C-NMR (151 MHz, DMSO) δ 159.91, 155.92, 150.57, 150.08, 130.29, 129.76 (2C), 115.42 (2C), 108.83, 56.41, 46.26. HPLC-MS (ESI): Purity = 98%, t_R = 2.457 min, *m/z* $[M-H]^+$ = 294.0.

7.2.2.2 Procedure for the synthesis of intermediate 3b (Scheme 2.5)

A mixture of 2-chloro-N-(4-methoxybenzyl)-5-nitropyridin-4-amine (**3a**), *tert*-butyl (2-aminoethyl)(ethyl)carbamate, and triethylamine was made in *N*,*N*-dimethylformamide (DMF). The mixture was heated under microwave radiation at 100 °C for 1 hour. When the reaction had completed, water was added, and the mixture was extracted with ethyl acetate (4 × 30 mL). The combined organic layer was dried over anhydrous Na_2SO_4, concentrated under reduced pressure, and purified via column chromatography. A yellow solid was obtained as the product.

***Tert*-butylethyl(2-((4-((4-methoxybenzyl)amino)-5-nitropyridin-2 yl)amino)ethyl)carbamate (3b):**

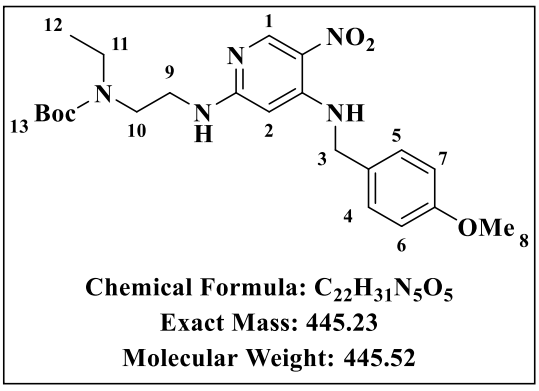

Obtained from intermediate **3a** (5.00 g, 17.02 mmol) and *tert*-butyl (2-aminoethyl)(ethyl)carbamate (4.81 g, 25.53 mmol) as a yellow solid (95%, 7.24 g); Rf (Hex: EtOAc, 1:1) 0.44; ^{1}H-NMR (600 MHz, Chloroform-*d*) δ 8.90 (s, 1H, H^1), 8.36 (s, 1H, H^2), 7.22 (d, J = 8.7 Hz, 2H, H^4 and H^5), 6.85 (d, J = 8.7 Hz, 2H, H^6 and H^7), 4.37 (s, 2H, H^3), 3.76 (s,

3H, H^8), 3.37–3.34 (m, 4H, H^9 and H^{10}), 3.17 (q, *J* = 7.1 Hz, 2H, H^{11}), 1.41 (s, 9H, H^{13}), 1.05 (t, *J* = 7.1 Hz, 3H, H^{12}). ^{13}C-NMR (151 MHz, $CDCl_3$) δ 161.22, 159.20, 156.45, 150.82, 149.91, 128.71, 128.49 (2C), 124.63, 114.31(2C), 83.65, 79.91, 55.26, 46.20, 45.70, 43.02, 41.73, 28.37 (3C), 13.87. HPLC-MS (ESI): Purity = 99%, t_R = 2.641 min, *m/z* $[M+H]^+$ = 446.2.

7.2.2.3 Procedure for the synthesis of intermediate 3c (Scheme 2.5)

A mixture of *tert*-butyl ethyl(2-((4-((4-methoxybenzyl)amino)-5-nitropyridin-2 yl)amino)ethyl)carbamate (**3b**) and 10% Pd/C in methanol was stirred for 16 hours at 25 °C under hydrogen gas. After the reaction had been completed, the mixture was filtered through a pad of celite and concentrated *in vacuo* to obtain the product, which was used in the next reaction without any further purification.

***Tert*-butyl(2-((5-amino-4-((4-methoxybenzyl)amino)pyridin-2-yl)amino)ethyl)(ethyl)carbamate (3c):**

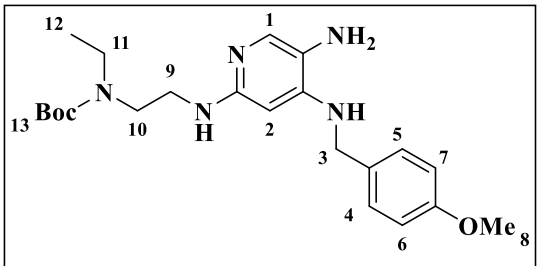

Chemical Formula: $C_{22}H_{33}N_5O_3$
Exact Mass: 415.26
Molecular Weight: 415.54

Obtained from intermediate **3b** (6.00 g, 13.47 mmol) as a wine-colored solid (89%, 4.98 g); Rf (DCM:MeOH, 9:1); ^{1}H-NMR (600 MHz, Chloroform-*d*) δ 7.42 (s, 1H, H^1), 7.24 (d, *J* = 8.7 Hz, 2H, H^4 and H^5), 6.84 (d, *J* = 8.7 Hz, 2H, H^6 and H^7), 4.96 (s, 1H, H^2), 4.23 (s, 2H, H^3), 3.77 (s, 3H, H^8), 3.32–3.32 (m, 4H, H^9 and H^{10}), 3.18 (q, *J* = 7.1 Hz, 2H, H^{11}), 1.41 (s, 9H, H^{13}), 1.04 (t, *J* = 7.0 Hz, 3H, H^{12}). ^{13}C-NMR (151 MHz, $CDCl_3$) δ 158.99, 155.78, 149.34, 130.21, 129.99, 128.75 (2C), 119.97, 114.10 (2C), 87.26, 79.42, 55.29, 55.23, 46.61, 46.21, 41.54, 29.65, 28.42 (3C), 13.86. HPLC-MS (ESI): Purity = 97%, t_R = 2.334 min, *m/z* $[M+H]^+$ = 416.2.

7.2.2.4 General procedure for the synthesis of intermediates 3d and 3e (Scheme 2.5)

(a) Amide coupling (intermediate 3d): Intermediate **3c** (1 eq) was dissolved in DCM with the appropriate carboxylic acid (1.3 eq) and 4-dimethylaminopyridine (DMAP, 0.1 eq). 1-Ethyl-3-(3-dimethylaminopropyl)carbodiimide hydrochloride (EDCI.HCl, 1.5 eq) was then added, and the reaction mixture was stirred at 25 °C for 16 hours. Water was added, and the solution was extracted with ethyl acetate, dried over anhydrous Na_2SO_4, and concentrated

under reduced pressure. The residue was used in the subsequent reaction without any further purification.

(b) Cyclization (intermediate 3e): The corresponding amide intermediate **3d** was dissolved in ethanol (10 mL), and 2 M NaOH solution (10 mL) was added. The resulting mixture was heated at 80 °C for 24–72 hours, depending on the amide intermediate. When the reaction had gone to completion, the solvent was removed *in vacuo,* and saturated citric acid was added to the residue. Extraction was done with DCM (2 × 20 mL), and the combined organic extract was dried over anhydrous Na_2SO_4, filtered, and concentrated *in vacuo*. The residue was purified via column chromatography (DCM/MeOH) to obtain the corresponding product.

***Tert*-butyl(2-((2-cyclopentyl-1-(4-methoxybenzyl)-1H-imidazo[4,5-c]pyridin-6-yl)amino)ethyl)(ethyl)carbamate (3e.1):**

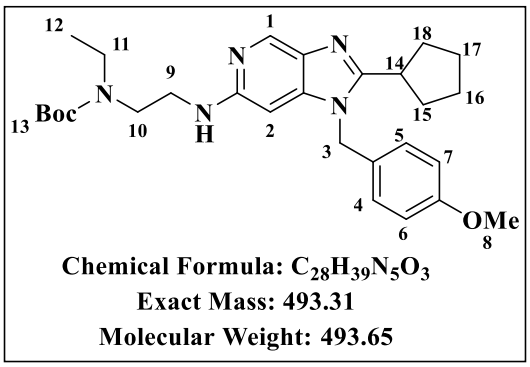

Obtained from intermediat**e 3c** (500 mg, 1.20 mmol) and cyclopentane carboxylic acid (0.16 mL, 1.56 mmol) as a wine-colored sticky solid (46%, 270.4 mg); Rf (DCM:MeOH, 9:1) 0.64; ^{1}H-NMR (600 MHz, Chloroform-*d*) δ 8.37 (s, 1H, H^1), 6.97 (d, *J* = 8.7 Hz, 2H, H^4 and H^5), 6.80 (d, *J* = 8.7 Hz, 2H, H^6 and H^7), 6.47 (s, 1H, H^2), 5.18 (s, 2H, H^3), 3.74 (s, 3H, H^8), 3.36–3.10 (m, 6H, H^9, H^{10} and H^{11}), 2.71 (p, *J* = 8.1 Hz, 1H, H^{14}), 2.05–1.92 (m, 2H, H^{15a} and H^{18a}), 1.89–1.78 (m, 3H, H^{15b}, H^{18b} and H^{16a}), 1.71–1.51 (m, 3H, H^{16b}, H^{17a} and H^{17b}), 1.39 (s, 9H, H^{13}), 1.03 (t, *J* = 7.1 Hz, 3H, H^{12}). ^{13}C-NMR (151 MHz, $CDCl_3$) δ 181.48, 159.28, 154.15, 127.56, 127.42 (2C), 114.35 (2C), 85.09, 79.49, 55.24, 46.30, 45.90, 44.64, 43.14, 41.82, 37.16, 32.08 (2C), 30.17, 28.39 (3C), 25.86 (2C), 25.76 (2C), 13.93. HPLC-MS (ESI): Purity = 98%, t_R = 2.598 min, *m/z* $[M+H]^+$ = 494.3.

***Tert*-butylethyl(2-((1-(4-methoxybenzyl)-2-(tetrahydrofuran-3-yl)-1H-imidazo[4,5-c]pyridin-6-yl)amino)ethyl)carbamate (3e.2):**

Obtained from intermediat**e 3c** (500 mg, 1.20 mmol) and tetrahydrofuran-3-carboxylic acid (0.14 mL, 1.56 mmol) as a wine-colored sticky solid (68%, 401.7 mg); Rf (DCM:MeOH, 9:1) 0.57; ^{1}H-NMR (600 MHz, Chloroform-*d*) δ 8.45 (s, 1H, H^1), 6.96 (d, *J* = 8.7 Hz, 2H, H^4 and H^5), 6.81 (d, *J* = 8.7 Hz, 2H, H^6 and H^7), 6.45 (s, 1H, H^2), 5.17 (s, 2H, H^3), 4.04–3.98 (m, 2H, H^{16a} and H^{17a}), 3.93–3.86 (m, 2H, H^{16b} and H^{17b}), 3.74 (s, 3H, H^8), 3.50–3.44 (m, 1H, H^{14}),

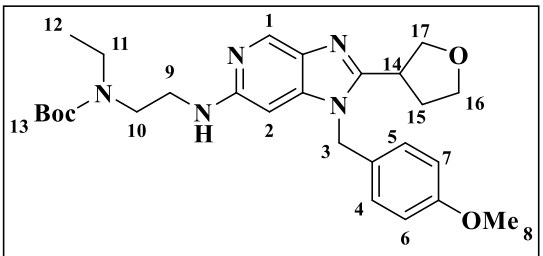

Chemical Formula: $C_{27}H_{37}N_5O_4$
Exact Mass: 495.28
Molecular Weight: 495.62

3.39–3.33 (m, 4H, H^9 and H^{10}), 3.20 (q, *J* = 7.2 Hz, 2H, H^{11}), 2.37–2.30 (m, 1H, H^{15a}), 2.24–2.16 (m, 1H, H^{15b}), 1.40 (s, 9H, H^{13}), 1.05 (t, *J* = 7.1 Hz, 3H, H^{12}). ^{13}C-NMR (151 MHz, $CDCl_3$) δ 159.43, 156.14, 154.68, 137.64, 133.55, 127.48, 127.27 (2C), 114.48 (2C), 84.86, 79.53, 71.93, 70.92, 68.33, 55.27, 46.34, 45.97, 43.07, 41.98, 37.14, 31.86, 29.65, 28.40 (3C), 13.89. HPLC-MS (ESI): Purity = 98%, t_R = 2.448 min, *m/z* $[M+H]^+$ = 496.3.

Tert-butylethyl(2-((1-(4-methoxybenzyl)-2-(tetrahydro-2H-pyran-4-yl)-1H-imidazo[4,5-c]pyridin-6-yl)amino)ethyl)carbamate (3e.3):

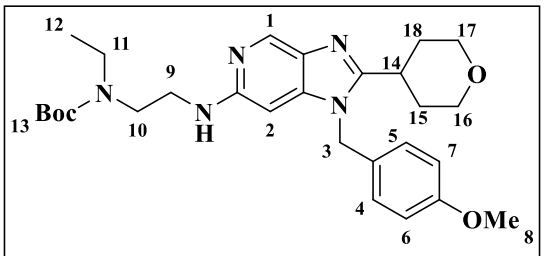

Chemical Formula: $C_{28}H_{39}N_5O_4$
Exact Mass: 509.30
Molecular Weight: 509.65

Obtained from intermediat**e 3c** (500 mg, 1.20 mmol) and tetrahydro-2H-pyran-4-carboxylic acid (202.96 mg, 1.56 mmol) as a wine-colored sticky solid (98%, 599.12 mg); Rf (DCM:MeOH, 9:1) 0.56; ^{1}H-NMR (600 MHz, Chloroform-*d*) δ 8.44 (s, 1H, H^1), 6.93 (d, *J* = 8.7 Hz, 2H, H^4 and H^5), 6.78 (d, *J* = 8.7 Hz, 2H, H^6 and H^7), 6.34 (s, 1H, H^2), 5.15 (s, 2H, H^3), 4.02–3.96 (m, 2H, H^{16a} and H^{17a}), 3.71 (s, 3H, H^8), 3.42–3.36 (m, 2H, H^{16e} and H^{17e}), 3.34–3.30 (m, 4H, H^9 and H^{10}), 3.16 (q, *J* = 7.3 Hz, 2H, H^{11}), 2.93 (tt, *J* = 11.5, 3.7 Hz, 1H, H^{14}), 2.08–1.99 (m, 2H, H^{15a} and H^{18a}), 1.68–1.63 (m, 2H, H^{15e} and H^{18e}), 1.37 (s, 9H, H^{13}), 1.01 (t, *J* = 7.1 Hz, 3H, H^{12}). ^{13}C-NMR (151 MHz, $CDCl_3$) δ 159.34, 157.79, 154.73, 127.39 (2C), 114.43 (2C), 84.91, 79.47, 67.50, 67.45 (2C), 55.24, 46.23, 45.96, 42.99, 41.99, 33.78, 31.26, 31.21 (2C), 29.62, 29.26, 28.47, 28.38 (3C), 13.86. HPLC-MS (ESI): Purity = 97%, t_R = 2.457 min, *m/z* $[M+H]^+$ = 510.2.

Tert-butylethyl(2-((1-(4-methoxybenzyl)-2-methyl-1H-imidazo[4,5-c]pyridin-6-yl)amino)ethyl)carbamate (3e.4):

Obtained from intermediat**e 3c** (500 mg, 1.20 mmol) and acetic acid (0.02 mg, 1.56 mmol) as a wine-colored sticky solid (43%, 228.2 mg); Rf (DCM:MeOH, 9:1) 0.53; ^{1}H-NMR (600 MHz, Chloroform-*d*) δ 8.37 (s, 1H, H^1), 6.97 (d, *J* = 8.7 Hz, 2H, H^4 and H^5), 6.78 (d, *J* = 8.7 Hz, 2H, H^6 and H^7), 6.36 (s, 1H, H^2), 5.07 (s, 2H, H^3), 3.71 (s, 3H, H^8), 3.37–3.32 (m, 4H, H^9 and H^{10}),

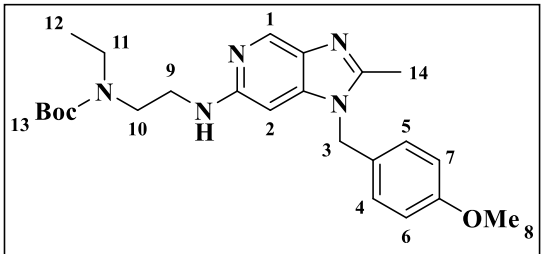

3.18 (q, *J* = 7.3 Hz, 2H, H^{11}), 2.43 (s, 3H, H^{14}), 1.38 (s, 9H, H^{13}), 1.02 (t, *J* = 7.1 Hz, 3H, H^{12}). ^{13}C-NMR (151 MHz, $CDCl_3$) δ 159.33, 156.09, 154.66, 152.26, 144.07, 137.58, 133.73, 127.77, 127.29 (2C), 114.38 (2C), 84.77, 79.47, 55.23, 46.55, 46.00, 42.98, 41.98, 29.62, 28.39 (3C), 13.93. HPLC-MS (ESI): Purity = 97%, t_R = 2.422 min, *m/z* $[M+H]^+$ = 440.2.

Tert-butyl(2-((cyclopropyl-1-(4-methoxybenzyl)-1H-imidazo[4,5-c]pyridin-6-yl)amino)ethyl)(ethyl)carbamate (3e.5):

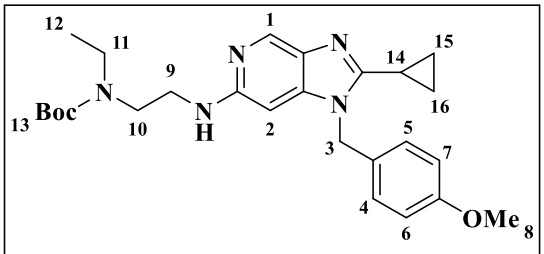

Obtained from intermediat**e 3c** (500 mg, 1.20 mmol) and cyclopropane carboxylic acid (286.0 mg, 1.56 mmol) as a wine-colored sticky solid (51%, mg); Rf (DCM:MeOH, 9:1) 0.58; ^{1}H-NMR (600 MHz, Chloroform-*d*) δ 8.14 (s, 1H, H^1), 7.13 (d, *J* = 8.7 Hz, 2H, H^4 and H^5), 6.96 (s, 1H, H^2), 6.77 (d, *J* = 8.7 Hz, 2H, H^6 and H^7), 5.25 (s, 2H, H^3), 3.69 (s, 3H, H^8), 3.30–3.26 (m, 4H, H^9 and H^{10}), 3.17 (q, *J* = 7.1 Hz, 2H, H^{11}), 1.51 (tt, *J* = 8.0, 4.6 Hz, 1H, H^{14}), 1.38 (s, 9H, H^{13}), 1.01 (t, *J* = 7.0 Hz, 3H, H^{12}), 0.92–0.89 (m, 2H, H^{15a} and H^{16a}), 0.73–0.70 (m, 2H, H^{15b} and H^{16b}). ^{13}C-NMR (151 MHz, $CDCl_3$) δ 179.93, 177.01, 159.37, 155.81, 153.27, 146.39, 132.22, 128.26 (2C), 127.16, 114.33 (2C), 85.19, 79.42, 55.20, 46.48, 45.58, 43.33, 41.26, 28.36 (3C), 22.23, 13.53, 8.83, 7.94. HPLC-MS (ESI): Purity = 98%, t_R = 2.483 min, *m/z* $[M+H]^+$ = 466.2.

Tert-butylethyl(2-((1-(4-methoxybenzyl)-2-(1-methylcyclopropyl)-1H-imidazo[4,5-c]pyridin-6-yl)amino)ethyl)carbamate (3e.6):

Obtained from intermediat**e 3c** (500 mg, 1.20 mmol) and 1-methylcyclopropane-1-carboxylic acid (0.13 mL, 1.56 mmol) as a wine-colored sticky solid (59%, 338.56 mg); Rf (DCM:MeOH, 9:1) 0.60; ^{1}H-NMR (400 MHz, Chloroform-*d*) δ 8.19 (s, 1H, H^1), 7.02 (d, *J* = 8.2 Hz, 2H, H^4 and H^5), 6.87–6.83 (m, 3H, H^2, H^6 and H^7), 5.45 (s, 2H, H^3), 3.77 (s, 3H, H^8), 3.46–3.17 (m, 6H, H^9, H^{10} and H^{11}), 1.42 (s, 9H, H^{13}), 1.24 (t, *J* = 7.1 Hz, 3H, H^{12}), 1.14 (s, 3H, H^{16}), 1.11–

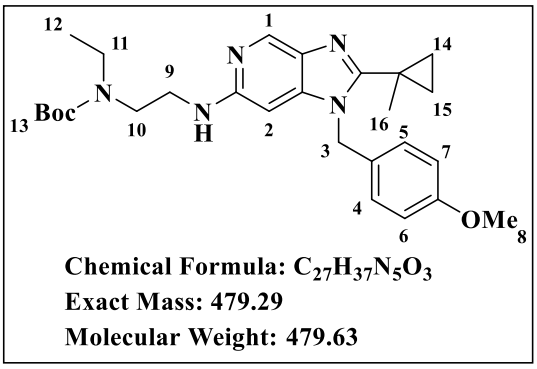

1.03 (m, 2H, H^{14a} and H^{15a}), 0.90–0.86 (m, 2H, H^{14b} and H^{15b}). ^{13}C-NMR (101 MHz, CDCl3) δ 159.55, 151.30, 132.47, 128.34, 127.62 (2C), 126.01, 114.55 (2C), 87.14, 79.77, 60.31, 55.27, 53.38, 47.41, 47.25, 45.41, 43.64, 41.26, 29.63, 28.36 (3C), 23.18, 14.38, 14.15, 13.63. HPLC-MS (ESI): Purity = 97%, t_R = 2.554 min, *m/z* $[M+H]^+$ = 480.3.

Tert-butylethyl(2-((1-(4-methoxybenzyl)-2-(1-(trifluoromethyl)cyclopropyl)-1H-imidazo[4,5-c]pyridin-6-yl)amino)ethyl)carbamate (3e.7):

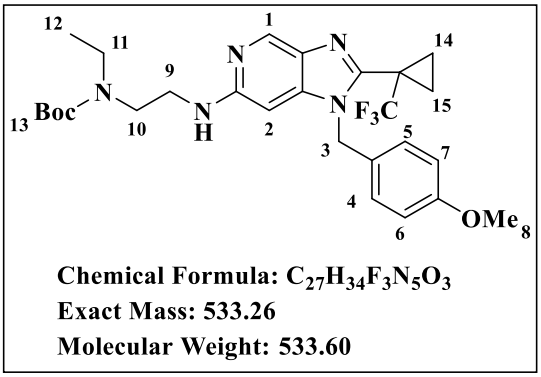

Obtained from intermediat**e 3c** (500 mg, 1.20 mmol) and 1-(trifluoromethyl)cyclopropane-1-carboxylic acid (240.40 mg, 1.56 mmol) as a wine-colored sticky solid (22%, 140 mg); Rf (DCM:MeOH, 9:1) 0.59; ^{1}H-NMR (400 MHz, Chloroform-*d*) δ 8.52 (s, 1H, H^1), 6.95 (d, *J* = 8.7 Hz, 2H, H^4 and H^5), 6.90 (s, 1H, H^2), 6.86 (d, *J* = 8.7 Hz, 2H, H^6 and H^7), 5.42 (s, 2H, H^3), 3.80 (s, 3H, H^8), 3.36–3.18 (m, 6H, H^9, H^{10} and H^{11}), 1.44 (s, 9H, H^{13}), 1.25–1.04 (m, 7H, H^{12}, H^{14} and H^{15}). ^{13}C-NMR (101 MHz, CDCl3) δ 159.38, 154.75, 149.39, 143.79, 138.12, 131.91, 127.40 (2C), 126.68, 114.46 (2C), 108.53, 97.98, 79.55, 55.27, 53.36, 48.32, 47.35, 45.79, 44.38, 41.84, 28.40 (3C), 22.05, 12.24, 10.31. HPLC-MS (ESI): Purity = 96%, t_R = 2.659 min, *m/z* $[M+H]^+$ = 534.2.

Tert-butyl(2-((2-(cyclopropylmethyl)-1-(4-methoxybenzyl)-1H-imidazo[4,5-c]pyridin-6-yl)amino)ethyl)(ethyl)carbamate (3e.8):

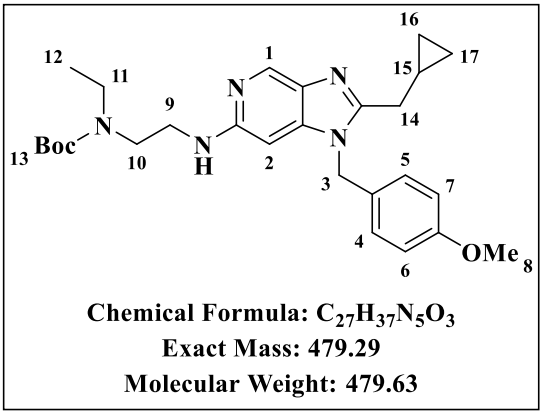

Obtained from intermediat**e 3c** (500 mg, 1.20 mmol) and 2-cyclopropylacetic acid (0.13 mL, 1.56 mmol) as a wine-colored sticky solid (96%, 552.4 mg); Rf (DCM:MeOH, 9:1) 0.57; ^{1}H-NMR (600 MHz, Chloroform-*d*) δ 8.34 (s, 1H, H^1), 6.96 (d, *J* = 8.7 Hz, 2H, H^4 and H^5), 6.82–6.67 (m, 3H, H^2, H^6 and H^7), 5.24 (s, 2H, H^3), 3.72 (s, 3H, H^8), 3.34–3.31 (m, 4H, H^9 and H^{10}), 3.18 (q, *J* = 7.2

Hz, 2H, H^{11}), 2.69 (d, *J* = 6.8 Hz, 2H, H^{14}), 1.39 (s, 9H, H^{13}), 1.15–1.10 (m, 1H, H^{15}), 1.03 (t, *J* = 7.1 Hz, 3H, H^{12}), 0.57–0.53 (m, 2H, H^{16a} and H^{17a}), 0.52–0.47 (m, 2H, H^{16b} and H^{17b}). ^{13}C-NMR (151 MHz, $CDCl_3$) δ 178.61, 159.35, 154.07, 135.08, 127.77 (2C), 127.08, 114.36 (2C), 85.21, 79.42, 55.26, 53.38, 46.51, 45.79, 43.23, 41.68, 40.64, 32.38, 28.38 (3C), 14.02, 8.67, 7.24, 4.98, 4.37. HPLC-MS (ESI): Purity = 96%, t_R = 2.580 min, *m/z* $[M+H]^+$ = 480.3.

Tert-butyl(2-((2-cyclobutyl-1-(4-methoxybenzyl)-1H-imidazo[4,5-c]pyridin-6-yl)amino)ethyl)(ethyl)carbamate (3e.9):

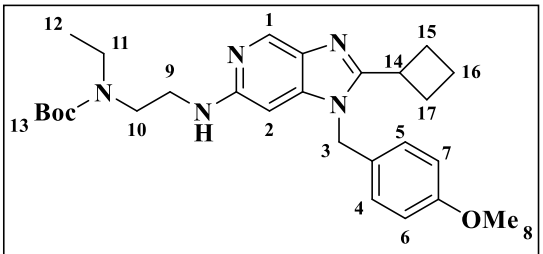

Obtained from intermediat**e 3c** (500 mg, 1.20 mmol) and cyclobutane carboxylic acid (0.15 mL, 1.56 mmol) as a wine-colored sticky solid (78%, 446.7 mg); Rf (DCM:MeOH, 9:1) 0.57; ^{1}H-NMR (600 MHz, Chloroform-*d*) δ 8.50 (s, 1H, H^1), 6.92 (d, *J* = 8.6 Hz, 2H, H^4 and H^5), 6.77 (d, *J* = 8.6 Hz, 2H, H^6 and H^7), 6.15 (s, 1H, H^2), 5.01 (s, 2H, H^3), 3.71 (s, 3H, H^8), 3.38–3.29 (m, 5H, H^9, H^{10} and H^{14}), 3.19 (q, *J* = 7.1 Hz, 2H, H^{11}), 2.52–2.43 (m, 2H, H^{15a} and H^{17a}), 2.28–2.22 (m, 2H, H^{15b} and H^{17b}), 2.04–1.88 (m, 2H, H^{16}), 1.38 (s, 9H, H^{13}), 1.02 (t, *J* = 7.1 Hz, 3H, H^{12}). ^{13}C-NMR (151 MHz, $CDCl_3$) δ 159.22, 158.00, 156.06, 154.76, 143.88, 139.08, 134.09, 128.46, 127.63 (2C), 127.45, 114.27 (2C), 84.66, 79.44, 55.19, 53.38, 46.05, 42.88, 42.11, 32.32, 28.38 (3C), 27.14, 18.53, 14.14. HPLC-MS (ESI): Purity = 96%, t_R = 2.571 min, *m/z* $[M+H]^+$ = 480.2.

Tert-butyl(2-((2-(3,3-difluorocyclobutyl)-1-(4-methoxybenzyl)-1H-imidazo[4,5-c]pyridin-6-yl)amino)ethyl)(ethyl)carbamate (3e.10):

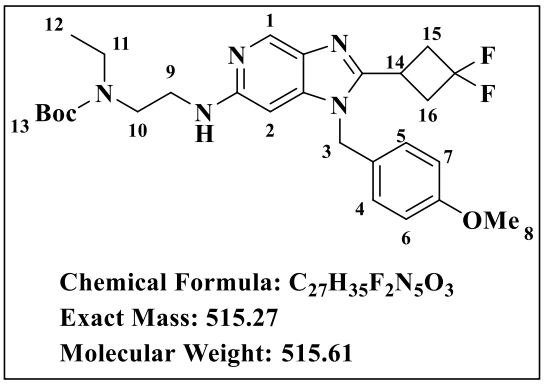

Obtained from intermediat**e 3c** (500 mg, 1.20 mmol) and 3,3-difluorocyclobutane-1-carboxylic acid (212.32 mg, 1.56 mmol) as a wine-colored sticky solid (79%, 491.3 mg); Rf (DCM:MeOH, 9:1) 0.57; ^{1}H-NMR (600 MHz, Chloroform-*d*) δ 8.35 (s, 1H, H^1), 6.98 (d, *J* = 8.7 Hz, 2H, H^4 and H^5), 6.85–6.79 (m, 3H, H^2, H^6 and H^7), 5.13 (s, 2H, H^3), 3.75 (s, 3H, H^8), 3.42–3.31 (m, 4H, H^9 and H^{10}), 3.21 (q, *J* = 7.1 Hz, 2H, H^{11}), 3.07–2.96 (m, 1H, H^{14}), 2.84–2.73 (m, 4H, H^{15} and H^{16}), 1.39 (s, 9H, H^{13}), 1.05 (t, *J* = 7.1 Hz, 3H, H^{12}). ^{13}C-NMR (151 MHz, $CDCl_3$) δ 159.60, 156.04, 146.54, 134.04, 132.87, 127.71, 126.63

(2C), 120.47, 118.57, 116.80, 114.57 (2C), 85.67, 79.63, 55.28, 46.58, 45.69, 43.34, 41.71, 40.37, 39.03, 28.38 (3C), 21.83, 14.05. HPLC-MS (ESI): Purity = 98%, t_R = 2.589 min, *m/z* $[M+H]^+$ = 516.2.

***Tert*-butyl(2-((2-cyclohexyl-1-(4-methoxybenzyl)-1H-imidazo[4,5-c]pyridin-6-yl)amino)ethyl)(ethyl)carbamate (3e.11):**

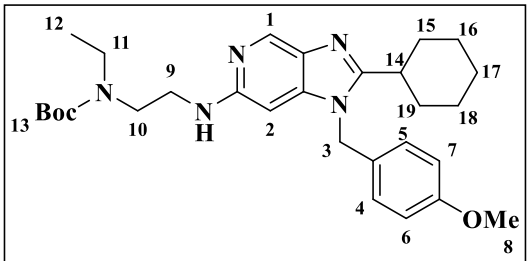

Obtained from intermediat**e 3c** (500 mg, 1.20 mmol) and cyclohexane carboxylic acid (200 mg, 1.56 mmol) as a wine-colored sticky solid (68%, 411.5 mg); Rf (DCM:MeOH, 9:1) 0.57; ^{1}H-NMR (600 MHz, Chloroform-*d*) δ 8.19 (s, 1H, H^1), 7.43 (s, 1H, H^2), 7.03 (d, *J* = 8.7 Hz, 2H, H^4 and H^5), 6.80 (d, *J* = 8.7 Hz, 2H, H^6 and H^7), 5.21 (s, 2H, H^3), 3.73 (s, 3H, H^8), 3.38–3.27 (m, 4H, H^9 and H^{10}), 3.19 (q, *J* = 7.1 Hz, 2H, H^{11}), 2.80–2.71 (m, 1H, H^{14}), 1.86–1.79 (m, 4H, H^{15} and H^{19}), 1.74–1.64 (m, 3H, H^{16a}, H^{17a} and H^{18a}), 1.39 (s, 9H, H^{13}), 1.31–1.26 (m, 3H, H^{16e}, H^{17e} and H^{18e}), 1.04 (t, *J* = 7.1 Hz, 3H, H^{12}). ^{13}C-NMR (151 MHz, $CDCl_3$) δ 164.23, 159.54, 155.97, 151.78, 147.27, 133.11, 129.45, 127.92 (2C), 126.60, 114.50 (2C), 86.72, 79.73, 55.26, 46.63, 45.47, 43.56, 41.32, 36.56, 31.49 (2C), 28.36 (3C), 25.98 (2C), 25.53, 14.12. HPLC-MS (ESI): Purity = 97%, t_R = 2.668 min, *m/z* $[M+H]^+$ = 508.3.

***Tert*-butyl(2-((2-(4,4-difluorocyclohexyl)-1-(4-methoxybenzyl)-1H-imidazo[4,5-c]pyridin-6-yl)amino)ethyl)(ethyl)carbamate (3e.12):**

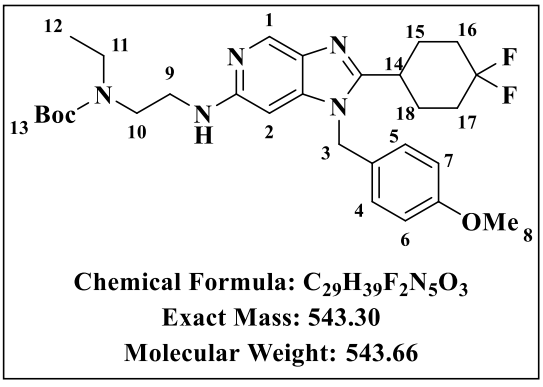

Obtained from intermediat**e 3c** (500 mg, 1.20 mmol) and 4,4-difluorocyclohexane-1-carboxylic acid (256.00 mg, 1.56 mmol) as a wine-colored sticky solid (92%, 603.2 mg); Rf (DCM:MeOH, 9:1) 0.59; ^{1}H-NMR (600 MHz, Chloroform-*d*) δ 8.44 (s, 1H, H^1), 6.96 (d, *J* = 8.7 Hz, 2H, H^4 and H^5), 6.82 (d, *J* = 8.7 Hz, 2H, H^6 and H^7), 6.47 (s, 1H, H^2), 5.17 (s, 2H, H^3), 3.75 (s, 3H, H^8), 3.40–3.32 (m, 4H, H^9 and H^{10}), 3.20 (q, *J* = 7.1 Hz, 2H, H^{11}), 2.84–2.77 (m, 1H, H^{14}), 2.24–2.18 (m, 2H, H^{15a} and H^{18a}), 2.11–2.01 (m, 2H, H^{15e} and H^{18e}), 1.91–1.83 (m, 2H, H^{16a} and H^{17a}), 1.83–1.68 (m, 2H, H^{16e} and H^{17e}), 1.40 (s, 9H, H^{13}), 1.05 (t, *J* = 7.1 Hz, 3H, H^{12}). ^{13}C-NMR (151 MHz, $CDCl_3$) δ 159.45, 157.88, 156.10,

154.48, 137.04, 133.57, 127.26 (2C), 123.94, 122.34, 120.74, 114.51 (2C), 85.17, 79.53, 55.28, 46.37, 45.94, 43.08, 41.99, 34.11, 33.17 (2C), 28.40 (3C), 27.68 (2C), 13.93. HPLC-MS (ESI): Purity = 97%, t_R = 2.615 min, *m/z* $[M+H]^+$ = 544.3.

Tert-butylethyl(2-((1-(4-methoxybenzyl)-2-(1-methylpyrrolidin-2-yl)-1H-imidazo[4,5-c]pyridin-6-yl)amino)ethyl)carbamate (3e.13):

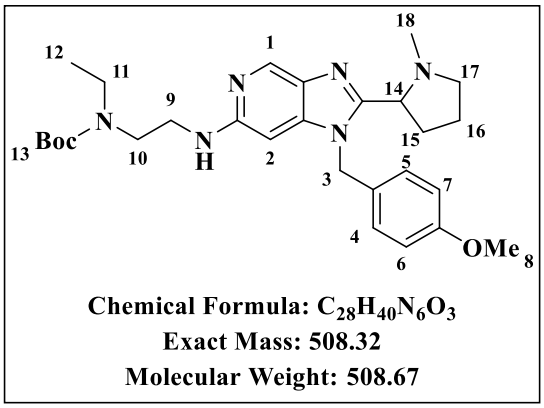

Obtained from intermediat**e 3c** (500 mg, 1.20 mmol) and 1-methylproline (201.55 mg, 1.56 mmol) as a wine-colored sticky solid (20%, 124.6 mg); Rf (DCM:MeOH, 9:1) 0.58; ^{1}H-NMR (600 MHz, Chloroform-*d*) δ 8.49 (s, 1H, H^1), 6.97 (d, *J* = 8.6 Hz, 2H, H^4 and H^5), 6.80 (d, *J* = 8.6 Hz, 2H, H^6 and H^7), 6.19 (s, 1H, H^2), 4.88 (s, 2H, H^3), 3.74 (s, 3H, H^8), 3.62 (dd, *J* = 8.2, 4.4 Hz, 1H, H^{14}), 3.38–3.32 (m, 4H, H^9 and H^{10}), 3.18 (q, *J* = 7.1 Hz, 2H, H^{11}), 2.31–2.25 (m, 2H, H^{17}), 2.23 (s, 3H, H^{18}), 2.16–2.08 (m, 1H, H^{15a}), 1.91–1.83 (m, 2H, H^{16}), 1.81–1.75 (m, 1H, H^{15b}), 1.39 (s, 9H, H^{13}), 1.05 (t, *J* = 7.1 Hz, 3H, H^{12}). ^{13}C-NMR (151 MHz, $CDCl_3$) δ 159.25, 159.05, 155.36, 154.72, 144.68, 133.93, 129.19, 128.09, 127.43 (2C), 114.17 (2C), 86.63, 79.57, 64.97, 56.55, 55.23, 46.72, 45.99, 44.03, 42.03, 40.79, 30.93, 28.40 (3C), 23.07, 13.86. HPLC-MS (ESI): Purity = 96%, t_R = 2.255 min, *m/z* $[M+H]^+$ = 509.3.

Tert-butylethyl(2-((1-(4-methoxybenzyl)-2-(3-(trifluoromethyl)phenyl)-1H-imidazo[4,5-c]pyridin-6-yl)amino)ethyl)carbamate (3e.14):

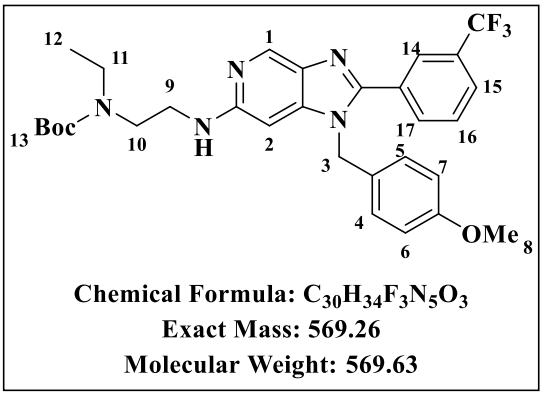

Obtained from intermediat**e 3c** (500 mg, 1.20 mmol) and 3-(trifluoromethyl)benzoic acid (296.56 mg, 1.56 mmol) as a wine-colored sticky solid (70%, 481.1 mg); Rf (DCM:MeOH, 9:1) 0.59; ^{1}H-NMR (600 MHz, Chloroform-*d*) δ 8.49 (s, 1H, H^1), 8.36 (ddd, *J* = 1.6, 1.5, 0.8 Hz, 1H, H^{14}), 8.27 (ddd, *J* = 7.8, 1.6, 1.3 Hz, 1H, H^{17}), 7.92 (s, 1H, H^2), 7.73 (d, *J* = 8.7 Hz, 2H, H^4 and H^5), 7.60 (ddd, *J* = 8.6, 1.5, 1.3 Hz, 1H, H^{15}), 7.53 (ddd, *J* = 8.6, 7.8, 0.8 Hz, 1H, H^{16}), 6.99 (d, *J* = 8.7 Hz, 2H, H^6 and H^7), 5.32 (s, 2H, H^3), 3.76 (s, 3H, H^8), 3.42–3.39 (m, 4H, H^9 and H^{10}), 3.24 (q, *J* = 7.1 Hz, 2H, H^{11}), 1.40 (s, 9H, H^{13}), 1.08 (t, *J* = 7.1 Hz, 3H, H^{12}). ^{13}C-NMR (151 MHz,

$CDCl_3$) δ 170.61, 159.53, 134.48, 134.06, 132.87, 132.28, 129.89, 129.53, 128.59 (2C), 128.23, 127.75, 127.24, 126.86, 126.65, 126.21, 114.56 (2C), 86.37, 79.61, 55.85, 48.06, 45.50, 44.34, 43.44, 41.52, 28.37 (3C), 14.13. HPLC-MS (ESI): Purity = 98%, t_R = 2.712 min, *m/z* $[M+H]^+$ = 570.2.

***Tert*-butyl(2-((2-cycloheptyl-1-(4-methoxybenzyl)-1H-imidazo[4,5-c]pyridin-6-yl)amino)ethyl)(ethyl)carbamate (3e.15):**

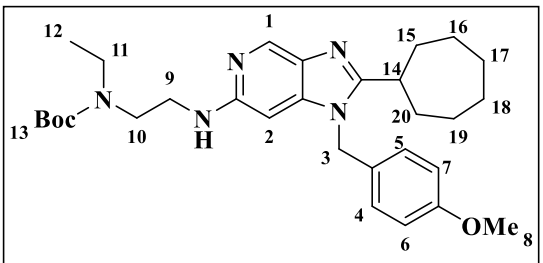

Obtained from intermediat**e 3c** (500 mg, 1.20 mmol) and cycloheptane carboxylic acid (0.21 mL, 1.56 mmol) as a wine-colored sticky solid (37%, 232.2 mg); Rf (DCM:MeOH, 9:1) 0.53; ^{1}H-NMR (600 MHz, Chloroform-*d*) δ 8.30 (s, 1H, H^1), 7.02 (d, *J* = 8.7 Hz, 2H, H^4 and H^5), 6.80 (d, *J* = 8.7 Hz, 2H, H^6 and H^7), 6.66 (s, 1H, H^2), 5.16 (s, 2H, H^3), 3.74 (s, 3H, H^8), 3.40–3.38 (m, 1H, H^{14}), 3.36–3.28 (m, 4H, H^9 and H^{10}), 3.19 (q, *J* = 7.1 Hz, 2H, H^{11}), 1.98–1.93 (m, 2H, H^{15a} and H^{20a}), 1.90–1.86 (m, 2H, H^{15b} and H^{20b}), 1.82–1.75 (m, 2H, H^{16a} and H^{19a}), 1.73–1.63 (m, 2H, H^{16b} and H^{19b}), 1.61–1.57 (m, 2H, H^{17a} and H^{18a}), 1.56–1.47 (m, 2H, H^{17b} and H^{18b}), 1.43 (s, 9H, H^{13}), 1.04 (t, *J* = 7.1 Hz, 3H, H^{12}). ^{13}C-NMR (151 MHz, $CDCl_3$) δ 181.97, 163.18, 162.53, 159.34, 155.88, 153.90, 134.43, 127.77 (2C), 127.34, 114.38 (2C), 85.36, 79.43, 55.25, 46.37, 45.49, 37.94, 33.36, 30.97 (2C), 28.39 (3C), 28.29, 27.91, 26.69, 26.45 (2C), 12.64. HPLC-MS (ESI): Purity = 98%, t_R = 2.791 min, *m/z* $[M+H]^+$ = 522.3.

***Tert*-butylethyl(2-((1-(4-methoxybenzyl)-2-((1r,4r)-4-(trifluoromethyl)cyclohexyl)-1H-imidazo[4,5-c]pyridin-6-yl)amino)ethyl)carbamate (3e.16):**

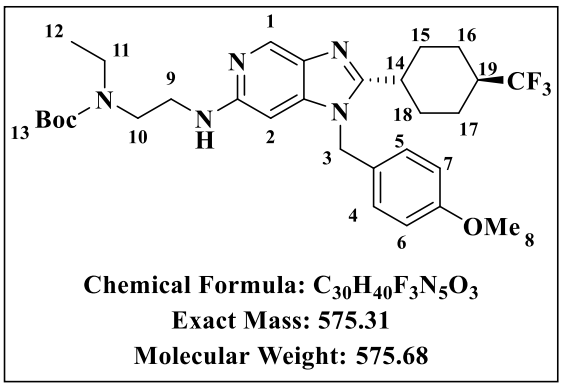

Obtained from intermediat**e 3c** (500 mg, 1.20 mmol) and (1r,4r)-4-(trifluoromethyl)cyclohexane-1-carboxylic acid (306.03 mg, 1.56 mmol) as a wine-colored sticky solid (27%, 183.7 mg); Rf (DCM:MeOH, 9:1) 0.64; ^{1}H-NMR (600 MHz, Chloroform-*d*) δ 8.45 (s, 1H, H^1), 6.96 (d, *J* = 8.7 Hz, 2H, H^4 and H^5), 6.81 (d, *J* = 8.7 Hz, 2H, H^6 and H^7), 6.41 (s, 1H, H^2), 5.15 (s, 2H, H^3), 3.75 (s, 3H, H^8), 3.37–3.35 (m, 5H, H^9, H^{10} and H^{14}), 3.21 (q, *J* = 7.1 Hz, 2H, H^{11}), 2.69 (tt, *J* = 11.9, 3.4 Hz,

1H, H^{19}), 2.05–2.00 (m, 2H, H^{15a} and H^{18a}), 1.95–1.90 (m, 2H, H^{15e} and H^{18e}), 1.81–1.72 (m, 2H, H^{16a} and H^{17a}), 1.40 (s, 9H, H^{13}), 1.36–1.30 (m, 2H, H^{16e} and H^{17e}), 1.04 (t, *J* = 7.1 Hz, 3H, H^{12}). ^{13}C-NMR (151 MHz, $CDCl_3$) δ 162.57, 159.40, 156.26, 154.60, 144.28, 137.61, 133.92, 128.40, 127.40 (2C), 126.55, 114.46 (2C), 85.11, 79.52, 55.26, 46.26, 45.98, 44.36, 42.02, 41.05, 38.15, 35.44, 30.00 (2C), 28.40 (3C), 24.68, 12.66. HPLC-MS (ESI): Purity = 98%, t_R = 2.703 min, *m/z* $[M+H]^+$ = 576.3.

***Tert*-butylethyl(2-((1-(4-methoxybenzyl)-2-((1r,4r)-4-(trifluoromethyl)cyclohexyl)-1H-imidazo[4,5-c]pyridin-6-yl)amino)ethyl)carbamate (3e.17):**

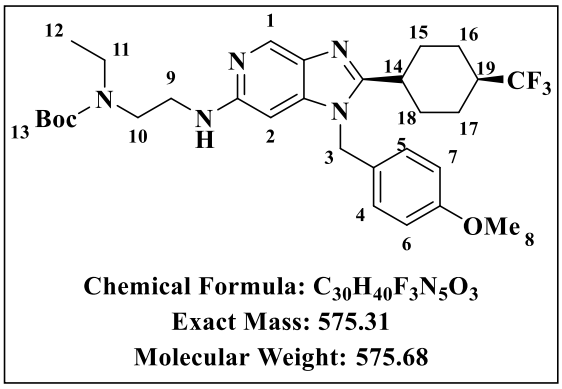

Obtained from intermediat**e 3c** (500 mg, 1.20 mmol) and (1s,4s)-4-(trifluoromethyl)cyclohexane-1-carboxylic acid (306.03 mg, 1.56 mmol) as a wine-colored sticky solid (34%, 233.7 mg); Rf (DCM:MeOH, 9:1) 0.53; ^{1}H-NMR (600 MHz, Chloroform-*d*) δ 8.29 (s, 1H, H^1), 6.93 (d, *J* = 8.7 Hz, 2H, H^4 and H^5), 6.82 (d, *J* = 8.7 Hz, 2H, H^6 and H^7), 6.43 (s, 1H, H^2), 5.21 (s, 2H, H^3), 3.75 (s, 3H, H^8), 3.42–3.29 (m, 5H, H^9, H^{10} and H^{14}), 3.21 (q, *J* = 7.1 Hz, 2H, H^{11}), 2.64 (tt, *J* = 11.8, 3.5 Hz, 1H, H^{19}), 2.25–2.22 (m, 2H, H^{15a} and H^{18a}), 2.14–2.10 (m, 2H, H^{15e} and H^{18e}), 2.01–1.97 (m, 2H, H^{16a} and H^{17a}), 1.79–1.75 (m, 2H, H^{16e} and H^{17e}), 1.43 (s, 9H, H^{13}), 1.05 (t, *J* = 7.1 Hz, 3H, H^{12}). ^{13}C-NMR (151 MHz, $CDCl_3$) δ 180.16, 178.97, 176.40, 159.54, 146.11, 132.66, 128.60, 127.77 (2C), 126.76, 114.51 (2C), 85.72, 79.53, 55.26, 46.48, 42.92, 41.15, 38.76, 35.67, 29.81, 28.37 (3C), 27.55, 25.76 (2C), 24.25, 21.75, 12.62. HPLC-MS (ESI): Purity = 97%, t_R = 2.703 min, *m/z* $[M+H]^+$ = 576.3.

***Tert*-butylethyl(2-((1-(4-methoxybenzyl)-2-(4-methoxycyclohexyl)-1H-imidazo[4,5-c]pyridin-6-yl)amino)ethyl)carbamate (3e.18):**

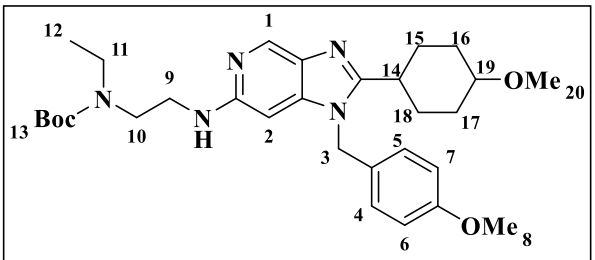

Chemical Formula: $C_{30}H_{43}N_5O_4$
Exact Mass: 537.33
Molecular Weight: 537.71

Obtained from intermediat**e 3c** (500 mg, 1.20 mmol) and 4-methoxycyclohexane-1-carboxylic acid (0.23 mL, 1.56 mmol) as a wine-colored sticky solid (15%, 98.8 mg); Rf (DCM:MeOH, 9:1) 0.45; ^{1}H-NMR (600 MHz, Chloroform-*d*) δ 8.27 (s, 1H, H^{1}), 7.03 (d, *J* = 8.7 Hz, 2H, H^{4} and H^{5}), 6.82 (d, *J* = 8.7 Hz, 2H, H^{6} and H^{7}), 6.41 (s, 1H, H^{2}), 5.20 (s, 2H, H^{3}), 3.75 (s, 3H, H^{8}), 3.41–3.39 (m, 1H, H^{19}), 3.35–3.32 (m, 4H, H^{9} and H^{10}), 3.28 (s, 3H, H^{20}), 3.22 (q, *J* = 7.2 Hz, 2H, H^{11}), 3.12 (tt, *J* = 10.6, 4.0 Hz, 1H, H^{14}), 2.20–2.14 (m, 2H, H^{15a} and H^{18a}), 1.79–1.74 (m, 2H, H^{15e} and H^{18e}), 1.68–1.64 (m, 2H, H^{16a} and H^{17a}), 1.40 (s, 9H, H^{13}), 1.24–1.21 (m, 2H, H^{16e} and H^{17e}), 1.09 (t, *J* = 7.2 Hz, 3H, H^{12}). ^{13}C-NMR (151 MHz, $CDCl_3$) δ 179.95, 179.68, 163.07, 159.50, 127.74 (2C), 126.96, 114.49 (2C), 79.58, 78.42, 75.15, 55.45, 44.33, 42.52, 41.64, 38.26, 31.51, 30.81, 29.71, 28.65 (2C), 28.39 (3C), 27.05, 25.51, 23.69 (2C), 12.66. HPLC-MS (ESI): Purity = 97%, t_R = 2.554 min, *m/z* $[M+H]^+$ = 538.3.

***Tert*-butylethyl(2-((1-(4-methoxybenzyl)-2-(6-(trifluoromethyl)pyridin-3-yl)-1H-imidazo[4,5-c]pyridin-6-yl)amino)ethyl)carbamate (3e.19):**

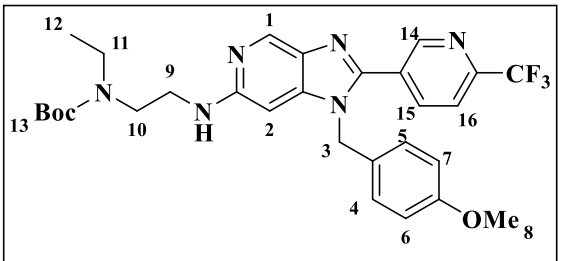

Chemical Formula: $C_{29}H_{33}F_3N_6O_3$
Exact Mass: 570.26
Molecular Weight: 570.62

Obtained from intermediat**e 3c** (500 mg, 1.20 mmol) and 6-(trifluoromethyl)nicotinic acid (298.12 mg, 1.56 mmol) as a wine-colored sticky solid (18%, 121.4 mg); Rf (DCM:MeOH, 9:1) 0.53; ^{1}H-NMR (600 MHz, Chloroform-*d*) δ 8.95 (d, *J* = 2.1 Hz, 1H, H^{14}), 8.65 (s, 1H, H^{1}), 8.16 (d, *J* = 8.2 Hz, 1H, H^{16}), 7.73 (dd, *J* = 8.2, 2.1 Hz, 1H, H^{15}), 7.24 (s, 1H, H^{2}), 6.95 (d, *J* = 8.7 Hz, 2H, H^{4} and H^{5}), 6.82 (d, *J* = 8.7 Hz, 2H, H^{6} and H^{7}), 5.27 (s, 2H, H^{3}), 3.75 (s, 3H, H^{8}), 3.40–3.37 (m, 4H, H^{9} and H^{10}), 3.21 (q, *J* = 7.2 Hz, 2H, H^{11}), 1.43 (s, 9H, H^{13}), 1.05 (t, *J* = 7.1 Hz, 3H, H^{12}). ^{13}C-NMR (151 MHz, $CDCl_3$) δ 162.54, 159.49, 155.62, 149.42, 149.24, 144.61, 140.68, 137.86, 134.49, 128.93, 128.54, 127.05 (2C), 122.13, 120.38, 114.73 (2C), 113.88, 79.61, 64.84, 55.28, 47.84, 45.92, 44.37, 38.04, 28.36 (3C), 12.66. HPLC-MS (ESI): Purity = 98%, t_R = 2.668 min, *m/z* $[M+H]^+$ = 571.2.

7.2.2.5 General procedure for the synthesis of intermediate 3f (Scheme 2.5)

(a) Boc-deprotection: The appropriate intermediate **3e** was dissolved in 4 M HCl/dioxane, and the mixture was stirred at 25 °C for 2 hours. When the reaction was complete, the solvent was removed *in vacuo,* and the residue was neutralized with Amberlyst A21 in a mixture of DCM and methanol. The Amberlyst was filtered off, the solvent was removed *in vacuo,* and the residue was used in the next reaction without further purification.

(b) Reductive amination: The crude product from step (a) above and 4-chloro-2-hydroxybenzaldehyde in methanol was stirred at 25 °C for 6 hours. The mixture was cooled at 0 °C, and sodium borohydride ($NaBH_4$) was added portion-wise. After the addition, the reaction was allowed to warm to room temperature (25 °C) for 2 hours. The solvent was removed *in vacuo,* and the residue was diluted with deionized water. The compound was extracted with DCM and dried over anhydrous sodium sulphate. The solvent was removed *in vacuo,* and the residue was purified via column chromatography to obtain the desired product.

5-chloro-2-(((2-((2-cyclopentyl-1-(4-methoxybenzyl)-1H-imidazo[4,5-c]pyridin-6-yl)amino)ethyl)(ethyl)amino)methyl)phenol (3f.1):

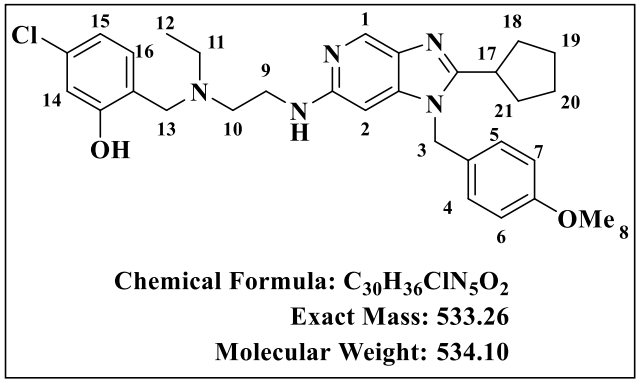

Obtained from intermediate **3e.1** (160 mg, 0.41 mmol) and 4-chloro-2-hydroxybenzaldehyde (76.42 mg, 0.49 mmol) as a pale yellow sticky solid (53%, 115.9 mg); Rf (DCM:MeOH, 9:1) 0.50; ^{1}H-NMR (600 MHz, Chloroform-*d*) δ 8.44 (d, *J* = 1.0 Hz, 1H, H^1), 6.93 (d, *J* = 8.7 Hz, 2H, H^4 and H^5), 6.82–6.80 (m, 3H, H^6, H^7 and H^{16}), 6.73 (d, *J* = 2.1 Hz, 1H, H^{14}), 6.67 (dd, *J* = 8.0, 2.1 Hz, 1H, H^{15}), 6.03 (d, *J* = 1.0 Hz, 1H, H^2), 5.13 (s, 2H, H^3), 3.74 (s, 3H, H^8), 3.72 (s, 2H, H^{13}), 3.38 (t, *J* = 6.5 Hz, 2H, H^9), 3.14–3.08 (m, 1H, H^{17}), 2.72 (t, *J* = 6.5 Hz, 2H, H^{10}), 2.61 (q, *J* = 7.2 Hz, 2H, H^{11}), 1.98–1.92 (m, 4H, H^{18} and H^{21}), 1.86–1.79 (m, 2H, H^{19a} and H^{20a}), 1.64–1.57 (m, 2H, H^{19b} and H^{20b}), 1.03 (t, *J* = 7.2 Hz, 3H, H^{12}). ^{13}C-NMR (151 MHz, $CDCl_3$) δ 159.80, 159.29, 158.80, 154.09, 143.91, 138.46, 134.01, 133.98, 129.25, 128.58, 127.48, 127.39 (2C), 119.13, 116.42, 114.40 (2C), 85.32, 57.12, 55.27, 52.13, 47.60, 46.25, 40.48, 37.14, 32.10 (2C), 25.75 (2C), 10.91. HPLC-MS (ESI): Purity = 98%, t_R = 2.450 min, *m/z* $[M+H]^+$ = 534.2.

5-chloro-2-((ethyl(2-((1-(4-methoxybenzyl)-2-(tetrahydrofuran-3-yl)-1H-imidazo[4,5-c]pyridin-6-yl)amino)ethyl)amino)methyl)phenol (3f.2):

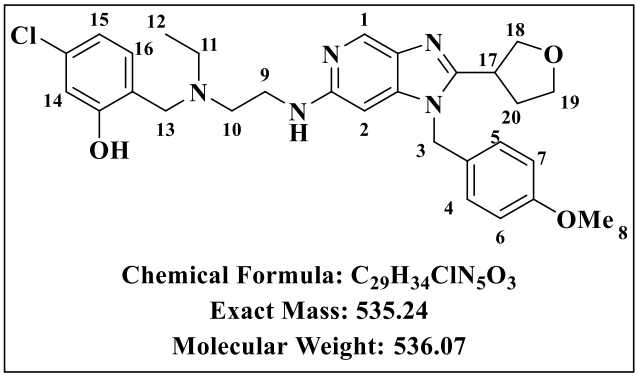

Obtained from intermediate **3e.2** (140 mg, 0.35 mmol) and 4-chloro-2-hydroxybenzaldehyde (65.77 mg, 0.42 mmol) as an orange-colored sticky solid (60%, 113.3 mg); Rf (DCM:MeOH, 9:1) 0.53; ^{1}H-NMR (600 MHz, Chloroform-*d*) δ 8.48 (d, *J* = 1.0 Hz, 1H, H^{1}), 6.93 (d, *J* = 8.7 Hz, 2H, H^{4} and H^{5}), 6.82–6.80 (m, 3H, H^{6}, H^{7} and H^{16}), 6.72 (d, *J* = 2.1 Hz, 1H, H^{14}), 6.66 (dd, *J* = 8.0, 2.1 Hz, 1H, H^{15}), 6.08 (d, *J* = 1.0 Hz, 1H, H^{2}), 5.13 (s, 2H, H^{3}), 4.02–3.95 (m, 3H, H^{17}, H^{18a} and H^{19a}), 3.93–3.84 (m, 2H, H^{18b} and H^{19b}), 3.74 (s, 3H, H^{8}), 3.74 (s, 2H, H^{13}), 3.42 (t, *J* = 6.5 Hz, 2H, H^{9}), 2.75 (t, *J* = 6.5 Hz, 2H, H^{10}), 2.64 (q, *J* = 7.2 Hz, 2H, H^{11}), 2.35–2.26 (m, 1H, H^{20a}), 2.23–2.13 (m, 1H, H^{20b}), 1.05 (t, *J* = 7.1 Hz, 3H, H^{12}). ^{13}C-NMR (151 MHz, $CDCl_3$) δ 159.44, 158.78, 155.83, 154.36, 143.95, 139.07, 134.00, 129.31, 127.39 (2C), 127.28, 120.34, 119.14, 116.41, 114.52 (2C), 85.13, 71.92, 68.32, 57.08, 55.28, 52.16, 47.66, 46.28, 40.41, 37.12, 31.87, 29.65, 10.91. HPLC-MS (ESI): Purity = 98%, t_R = 2.542 min, *m/z* $[M+H]^+$ = 536.2.

5-chloro-2-((ethyl(2-((1-(4-methoxybenzyl)-2-(tetrahydro-2H-pyran-4-yl)-1H-imidazo[4,5-c]pyridin-6-yl)amino)ethyl)amino)methyl)phenol (3f.3):

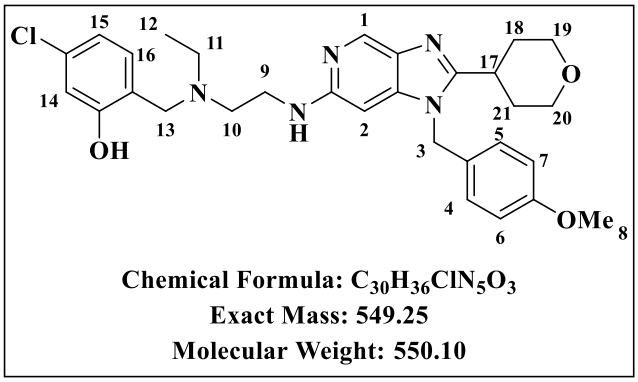

Obtained from intermediate **3e.3** (90 mg, 0.22 mmol) and 4-chloro-2-hydroxybenzaldehyde (40.72 mg, 0.26 mmol) as an orange-colored sticky solid (54%, 65.5 mg); Rf (DCM:MeOH, 9:1) 0.44; ^{1}H-NMR (600 MHz, Chloroform-*d*) δ 8.49 (d, *J* = 1.0 Hz, 1H, H^{1}), 6.92 (d, *J* = 8.7 Hz, 2H, H^{4} and H^{5}), 6.84–6.79 (m, 3H, H^{6}, H^{7} and H^{16}), 6.72 (d, *J* = 2.1 Hz, 1H, H^{14}), 6.66 (dd, *J* = 8.0, 2.1 Hz, 1H, H^{15}), 6.05 (d, *J* = 1.0 Hz, 1H, H^{2}), 5.13 (s, 2H, H^{3}), 4.04–3.97 (m, 2H, H^{19a} and H^{20a}), 3.74 (s, 3H, H^{8}), 3.73 (s, 2H, H^{13}), 3.43–3.38 (m, 4H, H^{9}, H^{19e} and H^{20e}), 2.93 (tt, *J* = 11.5, 3.7 Hz, 1H, H^{17}), 2.74 (t, *J* = 6.4 Hz, 2H, H^{10}), 2.63 (q, *J* = 7.1 Hz, 2H, H^{11}), 2.09–

2.00 (m, 2H, H^{18a} and H^{21a}), 1.70–1.63 (m, 2H, H^{18e} and H^{21e}), 1.04 (t, *J* = 7.1 Hz, 3H, H^{12}). ^{13}C-NMR (151 MHz, $CDCl_3$) δ 159.39, 158.79, 157.69, 154.31, 143.61, 139.03, 133.98, 129.32, 127.38, 127.33 (2C), 125.25, 120.35, 119.12, 116.39, 114.49 (2C), 85.35, 67.48 (2C), 57.04, 55.27, 52.15, 47.64, 46.22, 40.40, 33.80, 31.24 (2C), 10.90. HPLC-MS (ESI): Purity = 98%, t_R = 2.531 min, *m/z* $[M+H]^+$ = 550.2.

5-chloro-2-((ethyl(2-((1-(4-methoxybenzyl)-2-methyl-1H-imidazo[4,5-c]pyridin-6-yl)amino)ethyl)amino)methyl)phenol (3f.4):

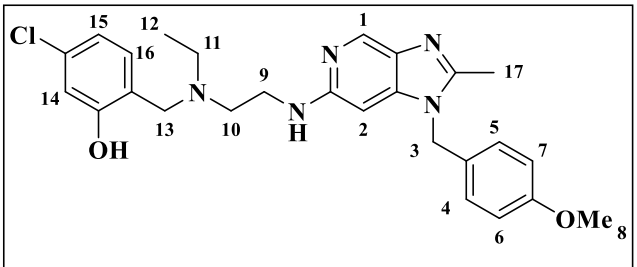

Chemical Formula: $C_{26}H_{30}ClN_5O_2$
Exact Mass: 479.21
Molecular Weight: 480.01

Obtained from intermediate **3e.4** (70 mg, 0.21 mmol) and 4-chloro-2-hydroxybenzaldehyde (39.15 mg, 0.25 mmol) as a wine-colored sticky solid (65%, 65.8 mg); Rf (DCM:MeOH, 9:1) 0.63; ^{1}H-NMR (600 MHz, Chloroform-*d*) δ 8.35 (d, *J* = 1.0 Hz, 1H, H^1), 6.97 (d, *J* = 8.7 Hz, 2H, H^4 and H^5), 6.86–6.81 (m, 3H, H^6, H^7 and H^{16}), 6.74 (d, *J* = 2.1 Hz, 1H, H^{14}), 6.68 (dd, *J* = 8.0, 2.1 Hz, 1H, H^{15}), 6.10 (d, *J* = 1.0 Hz, 1H, H^2), 5.08 (s, 2H, H^3), 3.77 (s, 2H, H^{13}), 3.76 (s, 3H, H^8), 3.41 (t, *J* = 6.6 Hz, 2H, H^9), 2.78 (t, *J* = 6.5 Hz, 2H, H^{10}), 2.68 (q, *J* = 7.2 Hz, 2H, H^{11}), 2.46 (s, 3H, H^{17}), 1.08 (t, *J* = 7.1 Hz, 3H, H^{12}). ^{13}C-NMR (151 MHz, $CDCl_3$) δ 159.49, 158.68, 153.51, 153.41, 144.59, 136.35, 134.18, 133.92, 129.53, 127.68 (2C), 126.84, 120.08, 119.24, 116.47, 114.53 (2C), 85.45, 56.89, 55.30, 52.08, 47.88, 46.68, 40.48, 14.06, 10.85. HPLC-MS (ESI): Purity = 97%, t_R = 2.299 min, *m/z* $[M+H]^+$ = 480.2.

5-chloro-2-(((2-((2-cyclopropyl-1-(4-methoxybenzyl)-1H-imidazo[4,5-c]pyridin-6-yl)amino)ethyl)(ethyl)amino)methyl)phenol (3f.5):

Obtained from intermediate **3e.5** (550 mg, 1.50 mmol) and 4-chloro-2-hydroxybenzaldehyde (281.88 mg, 1.80 mmol) as a wine-colored sticky solid (46%, 350.8 mg); Rf (DCM:MeOH,

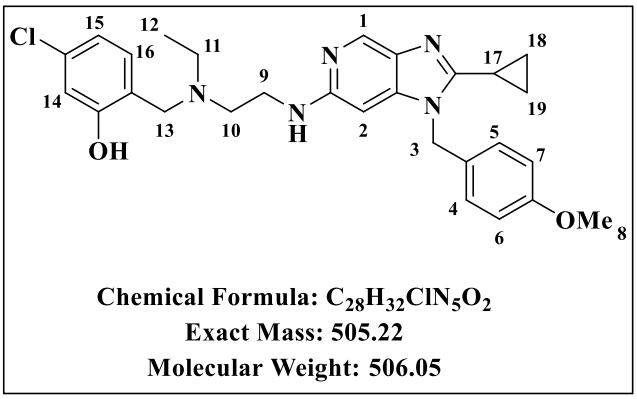

9:1) 0.56; ^{1}H-NMR (600 MHz, Chloroform-*d*) δ 8.40 (d, *J* = 1.0 Hz, 1H, H^1), 7.03 (d, *J* = 8.7 Hz, 2H, H^4 and H^5), 6.85–6.81 (m, 3H, H^6, H^7 and H^{16}), 6.75 (d, *J* = 2.1 Hz, 1H, H^{14}), 6.68 (dd, *J* = 8.0, 2.1 Hz, 1H, H^{15}), 6.08 (d, *J* = 1.0 Hz, 1H, H^2), 5.22 (s, 2H, H^3), 3.75 (s, 3H, H^8), 3.75 (s, 2H, H^{13}), 3.42 (t, *J* = 6.5 Hz, 2H, H^9), 2.75 (t, *J* = 6.5 Hz, 2H, H^{10}), 2.64 (q, *J* = 7.2 Hz, 2H, H^{11}), 1.84 (tt, *J* = 8.2, 4.9 Hz, 1H, H^{17}), 1.16–1.13 (m, 2H, H^{18a} and H^{19a}), 1.05 (t, *J* = 7.2 Hz, 3H, H^{12}), 1.02–0.98 (m, 2H, H^{18b} and H^{19b}). ^{13}C-NMR (151 MHz, $CDCl_3$) δ 159.33, 158.81, 157.42, 153.93, 144.03, 138.03, 134.00, 133.98, 129.27, 127.69 (2C), 127.59, 120.40, 119.15, 116.44, 114.40 (2C), 85.15, 57.15, 55.28, 52.18, 47.65, 46.29, 40.48, 10.94, 8.20 (2C), 7.71. HPLC-MS (ESI): Purity = 98%, t_R = 2.352 min, *m/z* $[M+H]^+$ = 506.2.

5-chloro-2-((ethyl(2-((1-(4-methoxybenzyl)-2-(1-methylcyclopropyl)-1H-imidazo[4,5-c]pyridin-6-yl)amino)ethyl)amino)methyl)phenol (3f.6):

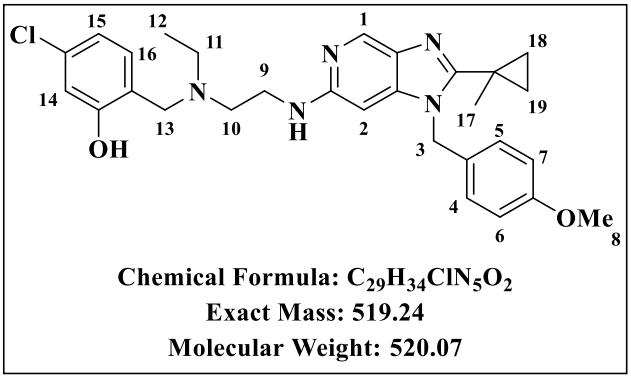

Obtained from intermediate **3e.6** (440 mg, 1.16 mmol) and 4-chloro-2-hydroxybenzaldehyde (272.48 mg, 1.74 mmol) as an orange-colored sticky solid (63%, 380.9 mg); Rf (DCM:MeOH, 9:1) 0.52; ^{1}H-NMR (600 MHz, Chloroform-*d*) δ 8.44 (d, *J* = 1.0 Hz, 1H, H^1), 6.95 (d, *J* = 8.7 Hz, 2H, H^4 and H^5), 6.84–6.80 (m, 3H, H^6, H^7 and H^{16}), 6.74 (d, *J* = 2.1 Hz, 1H, H^{14}), 6.68 (dd, *J* = 8.0, 2.1 Hz, 1H, H^{15}), 5.89 (d, *J* = 1.0 Hz, 1H, H^2), 5.33 (s, 2H, H^3), 3.75 (s, 3H, H^8), 3.72 (s, 2H, H^{13}), 3.36 (t, *J* = 6.5 Hz, 2H, H^9), 2.71 (t, *J* = 6.5 Hz, 2H, H^{10}), 2.61 (q, *J* = 7.1 Hz, 2H, H^{11}), 1.35 (s, 3H, H^{17}), 1.10–1.07 (m, 2H, H^{18a} and H^{19a}), 1.03 (t, *J* = 7.2 Hz, 3H, H^{12}), 0.80–0.77 (m, 2H, H^{18b} and H^{19b}). ^{13}C-NMR (151 MHz, $CDCl_3$) δ 159.21, 158.78, 158.62, 154.05, 143.98, 138.70, 134.01, 129.27, 127.33 (2C), 127.27, 120.34, 119.12, 116.44, 114.42, 114.38 (2C), 85.79, 57.08, 55.26, 52.09, 47.64, 46.83, 40.35, 23.73, 14.16, 13.33 (2C), 10.90. HPLC-MS (ESI): Purity = 98%, t_R = 2.571 min, *m/z* $[M+H]^+$ = 520.2.

5-chloro-2-((ethyl(2-((1-(4-methoxybenzyl)-2-(1-(trifluoromethyl)cyclopropyl)-1H-imidazo[4,5-c]pyridin-6-yl)amino)ethyl)amino)methyl)phenol (3f.7):

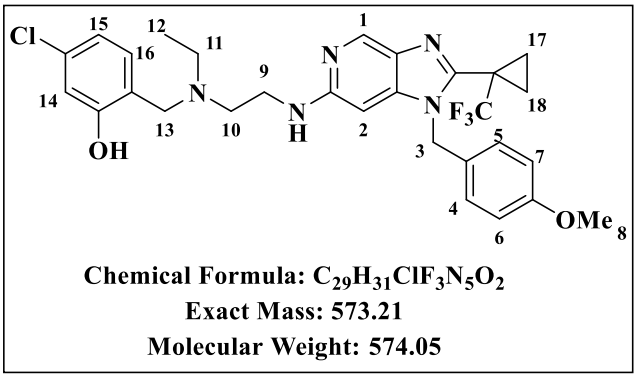

Obtained from intermediate **3e.7** (89 mg, 0.21 mmol) and 4-chloro-2-hydroxybenzaldehyde (50.11 mg, 0.32 mmol) as an orange-colored sticky solid (49%, 58.8 mg); Rf (DCM:MeOH, 9:1) 0.56; ^{1}H-NMR (600 MHz, Chloroform-*d*) δ 8.49 (d, *J* = 1.0 Hz, 1H, H^1), 6.90 (d, *J* = 8.7 Hz, 2H, H^4 and H^5), 6.84–6.80 (m, 3H, H^6, H^7 and H^{16}), 6.75 (d, *J* = 2.1 Hz, 1H, H^{14}), 6.68 (dd, *J* = 8.0, 2.1 Hz, 1H, H^{15}), 5.88 (d, *J* = 1.0 Hz, 1H, H^2), 4.78 (s, 2H, H^3), 3.75 (s, 3H, H^8), 3.74 (s, 2H, H^{13}), 3.35 (t, *J* = 6.3 Hz, 2H, H^9), 2.75 (t, *J* = 6.3 Hz, 2H, H^{10}), 2.67 (q, *J* = 7.2 Hz, 2H, H^{11}), 1.50–1.47 (m, 2H, H^{17a} and H^{18a}), 1.11–1.09 (m, 2H, H^{17b} and H^{18b}), 1.07 (t, *J* = 7.2 Hz, 3H, H^{12}). ^{13}C-NMR (151 MHz, $CDCl_3$) δ 159.35, 158.51, 157.05, 154.35, 143.80, 139.59, 129.69, 128.58, 127.40, 126.59 (2C), 123.88, 119.77, 119.30, 116.71, 114.47 (2C), 86.22, 72.27, 71.12, 63.56, 61.68, 55.27, 52.18, 42.84, 40.11, 10.68 (2C), 10.29. HPLC-MS (ESI): Purity = 97%, t_R = 2.483 min, *m/z* $[M+H]^+$ = 574.2.

5-chloro-2-(((2-((2-(cyclopropylmethyl)-1-(4-methoxybenzyl)-1H-imidazo[4,5-c]pyridin-6-yl)amino)ethyl)(ethyl)amino)methyl)phenol (3f.8):

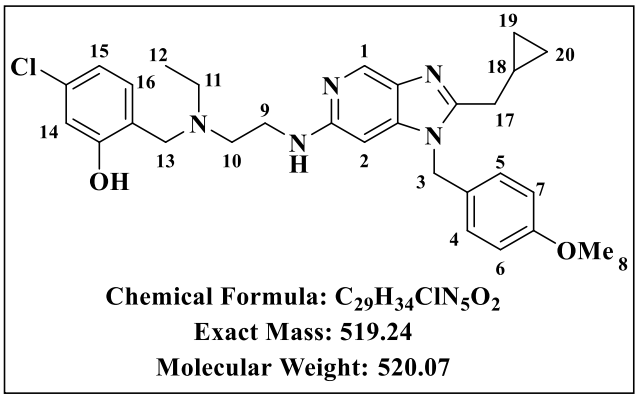

Obtained from intermediate **3e.8** (270 mg, 0.71 mmol) and 4-chloro-2-hydroxybenzaldehyde (167.56 mg, 1.07 mmol) as a wine-colored sticky solid (65%, 239.1 mg); Rf (DCM:MeOH, 9:1) 0.59; ^{1}H-NMR (600 MHz, Chloroform-*d*) δ 8.50 (d, *J* = 1.0 Hz, 1H, H^1), 6.94 (d, *J* = 8.7 Hz, 2H, H^4 and H^5), 6.83–6.78 (m, 3H, H^6, H^7 and H^8), 6.74 (d, *J* = 2.1 Hz, 1H, H^{14}), 6.67 (dd, *J* = 8.0, 2.1 Hz, 1H, H^{15}), 6.04 (d, *J* = 1.0 Hz, 1H, H^2), 5.11 (s, 2H, H^3), 3.74 (s, 3H, H^8), 3.73 (s, 2H, H^{13}), 3.41 (t, *J* = 6.5 Hz, 2H, H^9), 2.74 (t, *J* = 6.5 Hz, 2H, H^{10}), 2.67 (d, *J* = 6.8 Hz, 2H, H^{17}), 2.63 (q, *J* = 7.2 Hz, 2H, H^{11}), 1.15–1.10 (m, 1H, H^{18}), 1.04 (t, *J* = 7.2 Hz, 3H, H^{12}), 0.57–0.53 (m, 2H, H^{19a} and H^{20a}), 0.21–

0.17 (m, 2H, H^{19b} and H^{20b}). ^{13}C-NMR (151 MHz, $CDCl_3$) δ 159.31, 158.82, 155.31, 154.21, 143.65, 138.98, 134.32, 133.97, 129.26, 127.45 (2C), 127.35, 120.42, 119.12, 116.41, 114.40 (2C), 85.31, 57.13, 55.27, 52.17, 47.60, 46.36, 40.44, 32.41, 10.92, 8.75, 4.98 (2C). HPLC-MS (ESI): Purity = 98%, t_R = 2.598 min, *m/z* $[M+H]^+$ = 520.2.

5-chloro-2-(((2-((2-cyclobutyl-1-(4-methoxybenzyl)-1H-imidazo[4,5-c]pyridin-6-yl)amino)ethyl)(ethyl)amino)methyl)phenol (3f.9):

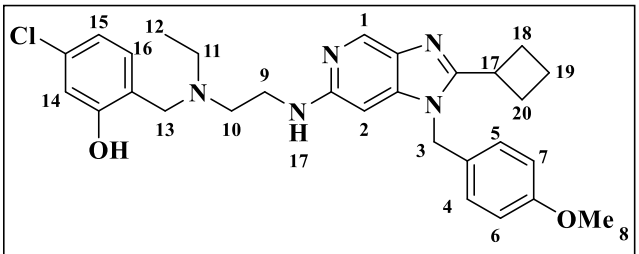

Obtained from intermediate **3e.9** (400 mg, 1.05 mmol) and 4-chloro-2-hydroxybenzaldehyde (247.43 mg, 1.58 mmol) as an orange-colored sticky solid (57%, 311.3 mg); Rf (DCM:MeOH, 9:1) 0.53; ^{1}H-NMR (400 MHz, Chloroform-*d*) δ 8.55 (d, *J* = 1.0 Hz, 1H, H^1), 6.96 (d, *J* = 8.7 Hz, 2H, H^4 and H^5), 6.87–6.82 (m, 3H, H^6, H^7 and H^{16}), 6.78 (d, *J* = 2.1 Hz, 1H, H^{14}), 6.71 (dd, *J* = 8.0, 2.1 Hz, 1H, H^{15}), 6.07 (d, *J* = 1.0 Hz, 1H, H^2), 5.05 (s, 2H, H^3), 3.78 (s, 3H, H^8), 3.77 (s, 2H, H^{13}), 3.65–3.54 (m, 1H, H^{17}), 3.45 (t, *J* = 6.5 Hz, 2H, H^9), 2.78 (t, *J* = 6.5 Hz, 2H, H^{10}), 2.66 (q, *J* = 7.1 Hz, 2H, H^{11}), 2.56–2.47 (m, 2H, H^{18a} and H^{20a}), 2.35–2.26 (m, 2H, H^{18b} and H^{20b}), 2.11–1.95 (m, 2H, H^{19}), 1.08 (t, *J* = 7.2 Hz, 3H, H^{12}). ^{13}C-NMR (101 MHz, $CDCl_3$) δ 159.34, 158.87, 158.40, 154.24, 143.96, 138.91, 134.34, 133.99, 129.24, 127.56, 127.46 (2C), 120.48, 119.12, 116.45, 114.40 (2C), 85.26, 57.20, 55.28, 52.28, 47.64, 46.22, 40.49, 32.39, 27.16 (2C), 18.57, 10.96. HPLC-MS (ESI): Purity = 98%, t_R = 2.624 min, *m/z* $[M+H]^+$ = 520.2.

5-chloro-2-(((2-((2-(3,3-difluorocyclobutyl)-1-(4-methoxybenzyl)-1H-imidazo[4,5-c]pyridin-6-yl)amino)ethyl)(ethyl)amino)methyl)phenol (3f.10):

Obtained from intermediate **3e.10** (350 mg, 0.84 mmol) and 4-chloro-2-hydroxybenzaldehyde (197.32 mg, 1.26 mmol) as a wine-colored sticky solid (59%, 274.1 mg); Rf (DCM:MeOH,

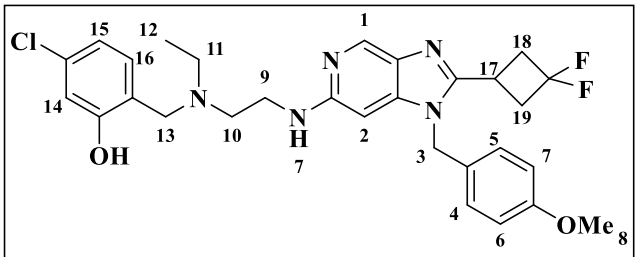

Chemical Formula: $C_{29}H_{32}ClF_2N_5O_2$
Exact Mass: 555.22
Molecular Weight: 556.05

9:1) 0.49; ^{1}H-NMR (600 MHz, Chloroform-*d*) δ 8.51 (d, *J* = 1.0 Hz, 1H, H^1), 6.91 (d, *J* = 8.7 Hz, 2H, H^4 and H^5), 6.83–6.80 (m, 3H, H^6, H^7 and H^{16}), 6.72 (d, *J* = 2.1 Hz, 1H, H^{14}), 6.67 (dd, *J* = 8.0, 2.1 Hz, 1H, H^{15}), 6.08 (d, *J* = 1.0 Hz, 1H, H^2), 5.05 (s, 2H, H^3), 3.75 (s, 3H, H^8), 3.74 (s, 2H, H^{13}), 3.43 (t, *J* = 6.5 Hz, 2H, H^9), 3.36–3.28 (m, 1H, H^{17}), 3.07–2.95 (m, 4H, H^{18} and H^{19}), 2.75 (t, *J* = 6.4 Hz, 3H, H^{10}), 2.64 (q, *J* = 7.2 Hz, 2H, H^{11}), 1.05 (t, *J* = 7.2 Hz, 3H, H^{12}). ^{13}C-NMR (151 MHz, $CDCl_3$) δ 159.49, 158.78, 155.33, 154.58, 144.18, 139.48, 133.99, 133.84, 129.29, 127.40 (2C), 127.09, 120.38, 119.15, 116.41, 114.54 (2C), 84.97, 57.12, 55.29, 52.17, 47.65, 46.29, 40.52, 40.40, 40.21, 20.95 (2C), 10.93. HPLC-MS (ESI): Purity = 97%, t_R = 2.580 min, *m/z* $[M+H]^+$ = 556.2.

5-chloro-2-(((2-((2-cyclohexyl-1-(4-methoxybenzyl)-1H-imidazo[4,5-c]pyridin-6-yl)amino)ethyl)(ethyl)amino)methyl)phenol (3f.11):

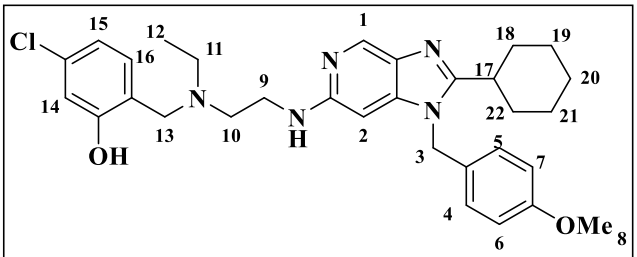

Chemical Formula: $C_{31}H_{38}ClN_5O_2$
Exact Mass: 547.27
Molecular Weight: 548.13

Obtained from intermediate **3e.11** (220 mg, 0.54 mmol) and 4-chloro-2-hydroxybenzaldehyde (126.85 mg, 0.81 mmol) as a wine-colored sticky solid (93%, 274.1 mg); Rf (DCM:MeOH, 9:1) 0.51; ^{1}H-NMR (400 MHz, Chloroform-*d*) δ 8.52 (d, *J* = 0.9 Hz, 1H, H^1), 6.99 (d, *J* = 8.8 Hz, 2H, H^4 and H^5), 6.89–6.85 (m, 3H, H^6, H^7 and H^{16}), 6.79 (d, *J* = 2.1 Hz, 1H, H^{14}), 6.72 (dd, *J* = 8.0, 2.1 Hz, 1H, H^{15}), 6.08 (d, *J* = 1.0 Hz, 1H, H^2), 5.17 (s, 2H, H^3), 3.80 (s, 3H, H^8), 3.79 (s, 2H, H^{13}), 3.46 (t, *J* = 6.5 Hz, 2H, H^9), 2.79 (t, *J* = 6.5 Hz, 2H, H^{10}), 2.76–2.71 (m, 1H, H^{17}), 2.68 (q, *J* = 7.1 Hz, 2H, H^{11}), 1.90–1.85 (m, 4H, H^{18} and H^{22}), 1.79–1.72 (m, 3H, H^{19a}, H^{20a} and H^{21a}), 1.36–1.31 (m, 3H, H^{19e}, H^{20e} and H^{21e}), 1.10 (t, *J* = 7.1 Hz, 3H, H^{12}). ^{13}C-NMR (101 MHz, $CDCl_3$) δ 160.08, 159.39, 158.85, 153.91, 143.72, 138.23, 134.35, 134.05, 129.28, 127.56, 127.47 (2C), 120.43, 119.16, 116.48, 114.48 (2C), 85.55, 57.19, 55.30, 52.25, 47.73, 46.27, 40.53, 36.45, 31.74 (2C), 26.21 (2C), 25.71, 10.95. HPLC-MS (ESI): Purity = 97%, t_R = 2.685 min, *m/z* $[M+H]^+$ = 548.2.

5-chloro-2-(((2-((2-(4,4-difluorocyclohexyl)-1-(4-methoxybenzyl)-1H-imidazo[4,5-c]pyridin-6-yl)amino)ethyl)(ethyl)amino)methyl)phenol (3f.12):

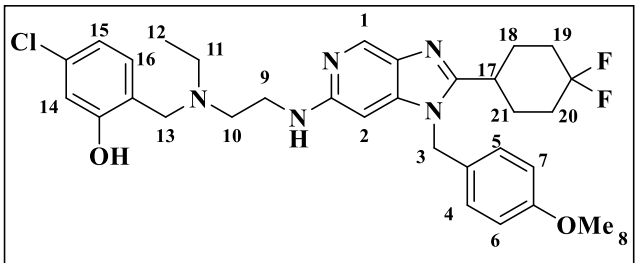

Obtained from intermediate **3e.12** (480 mg, 1.08 mmol) and 4-chloro-2-hydroxybenzaldehyde (253.69 mg, 1.62 mmol) as a wine-colored sticky solid (60%, 381.3 mg); Rf (DCM:MeOH, 9:1) 0.55; ^{1}H-NMR (400 MHz, Chloroform-*d*) δ 8.54 (d, *J* = 1.0 Hz, 1H, H^1), 6.97 (d, *J* = 8.7 Hz, 2H, H^4 and H^5), 6.87–6.83 (m, 3H, H^6, H^7 and H^{16}), 6.76 (d, *J* = 2.1 Hz, 1H, H^{14}), 6.70 (dd, *J* = 8.0, 2.1 Hz, 1H, H^{15}), 6.10 (d, *J* = 1.0 Hz, 1H, H^2), 5.16 (s, 2H, H^3), 3.78 (s, 3H, H^8), 3.77 (s, 2H, H^{13}), 3.46 (t, *J* = 6.5 Hz, 2H, H^9), 2.85–2.80 (m, 1H, H^{17}), 2.77 (t, *J* = 6.5 Hz, 2H, H^{10}), 2.66 (q, *J* = 7.2 Hz, 2H, H^{11}), 2.25–2.20 (m, 2H, H^{18a} and H^{21a}), 2.14–2.02 (m, 2H, H^{18e} and H^{21e}), 1.92–1.65 (m, 4H, H^{19} and H^{20}), 1.08 (t, *J* = 7.2 Hz, 3H, H^{12}). ^{13}C-NMR (101 MHz, $CDCl_3$) δ 159.48, 158.86, 157.04, 154.49, 143.46, 139.39, 134.19, 133.96, 129.27, 127.45, 127.36 (2C), 120.51, 119.12, 116.42, 114.56 (2C), 85.27, 57.17, 55.30, 52.27, 47.64, 46.30, 40.47, 34.08, 33.44, 33.20 (2C), 27.80 (2C), 10.94. HPLC-MS (ESI): Purity = 98%, t_R = 2.589 min, *m/z* $[M+H]^+$ = 584.2.

5-chloro-2-((ethyl(2-((1-(4-methoxybenzyl)-2-(1-methylpyrrolidin-2-yl)-1H-imidazo[4,5-c]pyridin-6-yl)amino)ethyl)amino)methyl)phenol (3f.13):

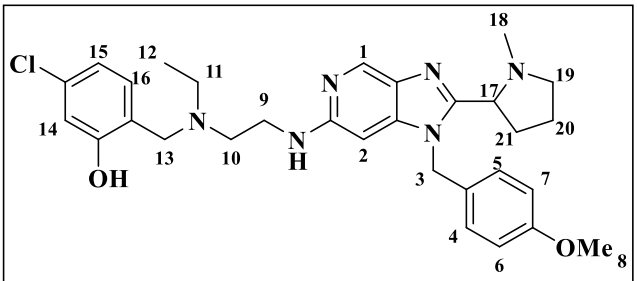

Obtained from intermediate **3e.13** (100 mg, 0.24 mmol) and 4-chloro-2-hydroxybenzaldehyde (56.38 mg, 0.36 mmol) as a yellow sticky solid (39%, 50.9 mg); Rf (DCM:MeOH, 9:1) 0.47; ^{1}H-NMR (400 MHz, Chloroform-*d*) δ 8.52 (d, *J* = 1.0 Hz, 1H, H^1), 7.01 (d, *J* = 8.6 Hz, 2H, H^4 and H^5), 6.87–6.84 (m, 3H, H^6, H^7 and H^{16}), 6.79 (d, *J* = 2.1 Hz, 1H, H^{14}), 6.72 (dd, *J* = 8.0, 2.2 Hz, 1H, H^{15}), 6.05 (d, *J* = 1.0 Hz, 1H, H^2), 4.90 (s, 2H, H^3), 3.80 (s, 3H, H^8), 3.79 (s, 2H, H^{13}), 3.43 (t, *J* = 6.5 Hz, 2H, H^9), 3.23 (t, *J* = 8.1 Hz, 1H, H^{17}), 2.79 (t, *J* = 6.4 Hz, 2H, H^{10}), 2.68 (q, *J* = 7.1 Hz, 2H, H^{11}), 2.40–2.32

(m, 1H, H^{19a}), 2.29 (s, 3H, H^{18}), 2.21–2.13 (m, 1H, H^{19b}), 1.99–1.81 (m, 4H, H^{20} and H^{21}), 1.10 (t, *J* = 7.1 Hz, 3H, H^{12}). ^{13}C-NMR (101 MHz, $CDCl_3$) δ 159.21, 158.81, 154.12, 144.73, 138.77, 134.10, 129.31, 128.91, 127.46 (2C), 120.33, 119.17, 116.49, 114.31 (2C), 85.63, 64.77, 57.12, 56.52, 55.28, 52.26, 47.74, 46.81, 44.11, 40.70, 40.03, 30.99, 25.35, 23.10, 10.91. HPLC-MS (ESI): Purity = 97%, t_R = 2.027 min, *m/z* $[M+H]^+$ = 549.2.

5-chloro-2-((ethyl(2-((1-(4-methoxybenzyl)-2-(3-(trifluoromethyl)phenyl)-1H-imidazo[4,5-c]pyridin-6-yl)amino)ethyl)amino)methyl)phenol (3f.14):

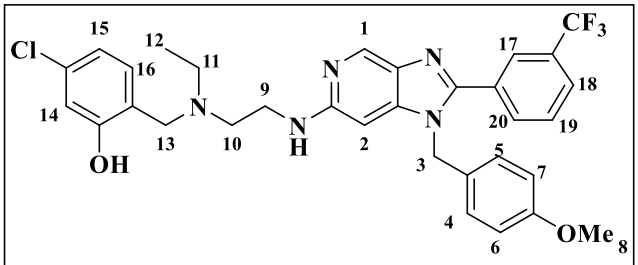

Obtained from intermediate **3e.14** (420 mg, 0.89 mmol) and 4-chloro-2-hydroxybenzaldehyde (209.84 mg, 1.34 mmol) as a wine-colored sticky solid (42%, 230.5 mg); Rf (DCM:MeOH, 9:1) 0.50 ; ^{1}H-NMR (400 MHz, Chloroform-*d*) δ 8.66 (d, *J* = 1.0 Hz, 1H, H^1), 7.95 (dd, *J* = 2.1, 1.5 Hz, 1H, H^{17}), 7.83 (ddd, *J* = 7.9, 2.1, 1.6 Hz, 1H, H^{20}), 7.75 (ddd, *J* = 7.7, 1.6, 1.5 Hz, 1H, H^{18}), 7.59 (dd, *J* = 7.9, 7.7 Hz, 1H, H^{19}), 7.01 (d, *J* = 8.7 Hz, 2H, H^4 and H^5), 6.91–6.86 (m, 3H, H^6, H^7 and H^{16}), 6.80 (d, *J* = 2.1 Hz, 1H, H^{14}), 6.73 (dd, *J* = 8.0, 2.1 Hz, 1H, H^{15}), 6.18 (d, *J* = 1.0 Hz, 1H, H^2), 5.25 (s, 2H, H^3), 3.83 (s, 2H, H^{13}), 3.81 (s, 3H, H^8), 3.52 (t, *J* = 6.4 Hz, 2H, H^9), 2.86 (t, *J* = 6.4 Hz, 2H, H^{10}), 2.74 (q, *J* = 7.1 Hz, 2H, H^{11}), 1.14 (t, *J* = 7.2 Hz, 3H, H^{12}). ^{13}C-NMR (101 MHz, $CDCl_3$) δ 159.50, 158.71, 156.41, 154.58, 152.85, 144.62, 139.85, 134.60, 134.25, 132.16, 131.60, 131.27, 130.53, 129.53, 129.32, 127.33 (2C), 126.69, 126.17, 124.96, 120.08, 119.28, 116.58, 114.67 (2C), 85.74, 56.97, 55.32, 52.27, 47.92, 40.32, 10.86. HPLC-MS (ESI): Purity = 98%, t_R = 2.677 min, *m/z* $[M+H]^+$ = 610.2.

5-chloro-2-(((2-((2-cycloheptyl-1-(4-methoxybenzyl)-1H-imidazo[4,5-c]pyridin-6-yl)amino)ethyl)(ethyl)amino)methyl)phenol (3f.15):

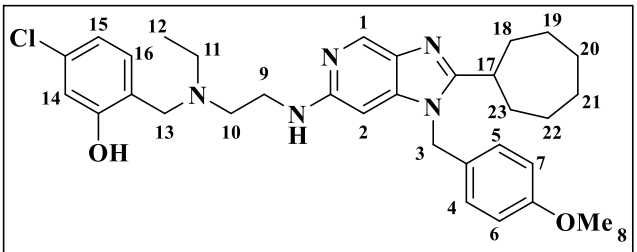

Chemical Formula: $C_{32}H_{40}ClN_5O_2$
Exact Mass: 561.29
Molecular Weight: 562.16

Obtained from intermediate **3e.15** (150 mg, 0.36 mmol) and 4-chloro-2-hydroxybenzaldehyde (84.56 mg, 0.54 mmol) as a wine-colored sticky solid (37%, 75.8 mg); Rf (DCM:MeOH, 9:1); ^{1}H-NMR (600 MHz, Chloroform-*d*) δ 8.45 (d, *J* = 1.0 Hz, 1H, H^1), 6.95 (d, *J* = 8.7 Hz, 2H, H^4 and H^5), 6.83–6.81 (m, 3H, H^6, H^7 and H^{16}), 6.74 (d, *J* = 2.1 Hz, 1H, H^{14}), 6.67 (dd, *J* = 8.0, 2.1 Hz, 1H, H^{15}), 6.04 (d, *J* = 1.0 Hz, 1H, H^2), 5.11 (s, 2H, H^3), 3.75 (s, 3H, H^8), 3.74 (s, 2H, H^{13}), 3.41 (t, *J* = 6.6 Hz, 2H, H^9), 2.92–2.85 (m, 1H, H^{17}), 2.75 (t, *J* = 6.5 Hz, 2H, H^{10}), 2.64 (q, *J* = 7.1 Hz, 2H, H^{11}), 1.91–1.86 (m, 4H, H^{18} and H^{23}), 1.82–1.76 (m, 2H, H^{19a} and H^{22a}), 1.60 (dd, *J* = 5.3, 3.3 Hz, 4H, H^{20} and H^{21}), 1.44–1.41 (m, 2H, H^{19b} and H^{22b}), 1.05 (t, *J* = 7.2 Hz, 3H, H^{12}). ^{13}C-NMR (151 MHz, $CDCl_3$) δ 161.20, 159.38, 158.83, 153.94, 143.74, 138.12, 134.25, 134.02, 129.23, 127.55, 127.47 (2C), 120.41, 119.12, 116.45, 114.46 (2C), 85.43, 57.17, 55.27, 52.22, 47.70, 46.30, 40.54, 37.91, 33.45 (2C), 27.96 (2C), 26.70 (2C), 10.91. HPLC-MS (ESI): Purity = 98%, t_R = 2.729 min, *m/z* $[M+H]^+$ = 562.2.

5-chloro-2-((ethyl(2-((1-(4-methoxybenzyl)-2-((1r,4r)-4-(trifluoromethyl)cyclohexyl)-1H-imidazo[4,5-c]pyridin-6-yl)amino)ethyl)amino)methyl)phenol (3f.16):

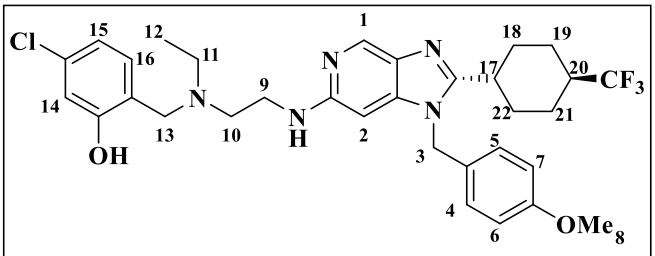

Chemical Formula: $C_{32}H_{37}ClF_3N_5O_2$
Exact Mass: 615.26
Molecular Weight: 616.13

Obtained from intermediate **3e.16** (150 mg, 0.32 mmol) and 4-chloro-2-hydroxybenzaldehyde (75.17 mg, 0.48 mmol) as a wine-colored sticky solid (41%, 81.40 mg); Rf (DCM:MeOH, 9:1) 0.50; ^{1}H-NMR (600 MHz, Chloroform-*d*) δ 8.47 (d, *J* = 1.0 Hz, 1H, H^1), 6.94 (d, *J* = 8.7 Hz, 2H, H^4 and H^5), 6.84–6.81 (m, 3H, H^6, H^7 and H^{16}), 6.73 (d, *J* = 2.2 Hz, 1H, H^{14}), 6.67 (dd, *J* = 8.0, 2.3 Hz, 1H, H^{15}), 6.06 (d, *J* = 1.0 Hz, 1H, H^2), 5.12 (s, 2H, H^3), 3.75 (s, 3H, H^8), 3.74 (s, 2H, H^{13}), 3.42 (t, *J* = 6.5 Hz, 2H, H^9), 2.75 (t, *J* = 6.5 Hz, 2H, H^{10}), 2.70–2.67 (m, 1H, H^{17}), 2.65 (q, *J* = 7.2 Hz, 2H, H^{11}), 2.14–2.06 (m, 1H, H^{20}), 2.04–2.01 (m, 2H, H^{18a} and

H^{22a}), 1.94–1.89 (m, 2H, H^{18e} and H^{22e}), 1.80–1.72 (m, 2H, H^{19a} and H^{21a}), 1.38–1.30 (m, 2H, H^{19e} and H^{21e}), 1.05 (t, *J* = 7.2 Hz, 3H, H^{12}). ^{13}C-NMR (151 MHz, $CDCl_3$) δ 159.49, 158.79, 158.44, 154.22, 143.60, 138.69, 134.13, 134.05, 129.27, 127.39 (2C), 120.36, 119.15, 116.44, 114.55 (2C), 85.36, 57.13, 55.27, 52.26, 47.72, 46.26, 41.93, 41.87, 41.27, 41.09, 40.48, 35.47, 30.00 (2C), 24.70, 10.89. HPLC-MS (ESI): Purity = 97%, t_R = 2.694 min, *m/z* $[M+H]^+$ = 616.2.

5-chloro-2-((ethyl(2-((1-(4-methoxybenzyl)-2-((1r,4r)-4-(trifluoromethyl)cyclohexyl)-1H-imidazo[4,5-c]pyridin-6-yl)amino)ethyl)amino)methyl)phenol (3f.17):

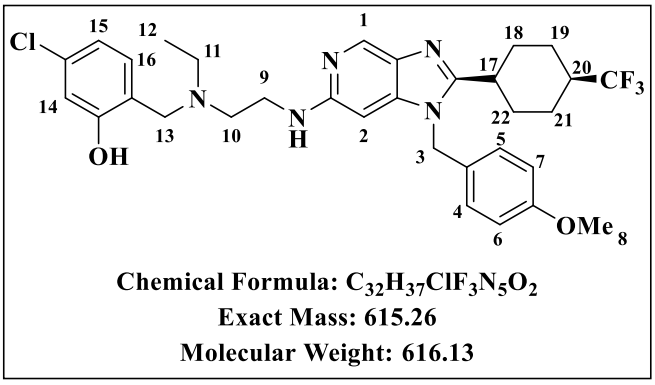

Obtained from intermediate **3e.17** (170 mg, 0.36 mmol) and 4-chloro-2-hydroxybenzaldehyde (84.56 mg, 0.54 mmol) as a wine-colored sticky solid (35%, 76.70 mg); Rf (DCM:MeOH, 9:1) 0.63; ^{1}H-NMR (600 MHz, Chloroform-*d*) δ 8.47 (d, *J* = 1.0 Hz, 1H, H^1), 6.94 (d, *J* = 8.7 Hz, 2H, H^4 and H^5), 6.83–6.81 (m, 3H, H^6, H^7 and H^{16}), 6.73 (d, *J* = 2.1 Hz, 1H, H^{14}), 6.67 (dd, *J* = 8.0, 2.1 Hz, 1H, H^{15}), 6.06 (d, *J* = 1.0 Hz, 1H, H^2), 5.12 (s, 2H, H^3), 3.75 (s, 3H, H^8), 3.75 (s, 2H, H^{13}), 3.42 (t, *J* = 6.5 Hz, 2H, H^9), 2.76 (t, *J* = 6.5 Hz, 2H, H^{10}), 2.70–2.67 (m, 1H, H^{17}), 2.65 (q, *J* = 7.2 Hz, 3H, H^{11}), 2.13–2.07 (m, 1H, H^{20}), 2.04–2.01 (m, 2H, H^{18a} and H^{22a}), 1.94–1.89 (m, 2H, H^{18e} and H^{22e}), 1.80–1.72 (m, 2H, H^{19a} and H^{21a}), 1.38–1.30 (m, 2H, H^{19e} and H^{21e}), 1.06 (t, *J* = 7.2 Hz, 3H, H^{12}). ^{13}C-NMR (151 MHz, $CDCl_3$) δ 159.44, 158.78, 158.52, 154.20, 143.67, 138.51, 134.04, 134.02, 129.32, 127.39 (2C), 127.19, 120.34, 119.14, 116.42, 114.51 (2C), 85.28, 57.08, 55.29, 52.10, 47.69, 46.36, 46.24, 41.06, 40.44, 35.44, 29.99 (2C), 27.40, 24.69, 10.89. HPLC-MS (ESI): Purity = 98%, t_R = 2.878 min, *m/z* $[M+H]^+$ = 616.2.

5-chloro-2-((ethyl(2-((1-(4-methoxybenzyl)-2-(4-methoxycyclohexyl)-1H-imidazo[4,5-c]pyridin-6-yl)amino)ethyl)amino)methyl)phenol (3f.18):

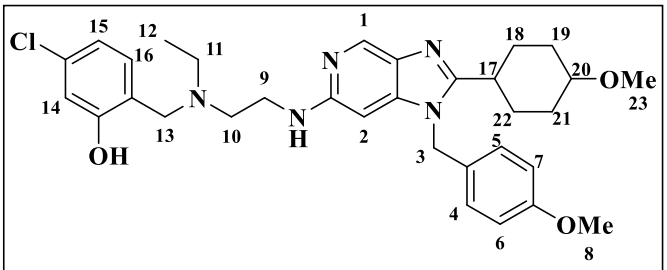

Chemical Formula: $C_{32}H_{40}ClN_5O_3$
Exact Mass: 577.28
Molecular Weight: 578.15

Obtained from intermediate **3e.18** (80 mg, 0.18 mmol) and 4-chloro-2-hydroxybenzaldehyde (42.28 mg, 0.27 mmol) as an orange-colored sticky solid (70%, 73 mg); Rf (DCM:MeOH, 9:1) 0.47; ^{1}H-NMR (600 MHz, Chloroform-*d*) δ 8.42 (d, *J* = 1.0 Hz, 1H, H^1), 6.95 (d, *J* = 8.7 Hz, 2H, H^4 and H^5), 6.85–6.81 (m, 3H, H^6, H^7 and H^{16}), 6.74 (d, *J* = 2.1 Hz, 1H, H^{14}), 6.67 (dd, *J* = 8.0, 2.1 Hz, 1H, H^{15}), 6.07 (d, *J* = 1.0 Hz, 1H, H^2), 5.13 (s, 2H, H^3), 3.77 (s, 3H, H^8), 3.76 (s, 2H, H^{13}), 3.47 (tt, *J* = 11.3, 4.3 Hz, 1H, H^{20}), 3.42 (t, *J* = 6.4 Hz, 2H, H^9), 3.34 (s, 3H, H^{23}), 3.19 (tt, *J* = 10.7, 4.2 Hz, 1H, H^{17}), 2.78 (t, *J* = 6.4 Hz, 2H, H^{10}), 2.68 (q, *J* = 7.2 Hz, 2H, H^{11}), 2.18–2.13 (m, 2H, H^{18a} and H^{22a}), 1.90–1.84 (m, 2H, H^{18e} and H^{22e}), 1.81–1.72 (m, 2H, H^{19a} and H^{21a}), 1.25–1.21 (m, 2H, H^{19e} and H^{21e}), 1.08 (t, *J* = 7.2 Hz, 3H, H^{12}). ^{13}C-NMR (151 MHz, $CDCl_3$) δ 159.47, 158.69, 153.50, 144.28, 136.87, 134.14, 129.50, 127.52 (2C), 127.40, 119.22, 116.44, 114.53 (2C), 85.54, 78.32, 73.57, 56.94, 55.77, 55.30, 52.01, 47.89, 46.39, 40.43, 35.67, 31.57 (2C), 29.79 (2C), 29.00, 25.57, 10.87. HPLC-MS (ESI): Purity = 97%, t_R = 2.650 min, *m/z* $[M+H]^+$ = 578.2.

5-chloro-2-((ethyl(2-((1-(4-methoxybenzyl)-2-(6-(trifluoromethyl)pyridin-3-yl)-1H-imidazo[4,5-c]pyridin-6-yl)amino)ethyl)amino)methyl)phenol (3f.19):

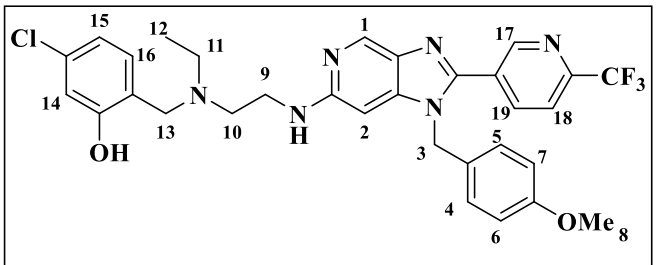

Chemical Formula: $C_{31}H_{30}ClF_3N_6O_2$
Exact Mass: 610.21
Molecular Weight: 611.07

Obtained from intermediate **3e.19** (87 mg, 0.18 mmol) and 4-chloro-2-hydroxybenzaldehyde (42.28 mg, 0.27 mmol) as a wine-colored sticky solid (50%, 54.9 mg); Rf (DCM:MeOH, 9:1) 0.58; ^{1}H-NMR (600 MHz, Chloroform-*d*) δ 8.95 (d, *J* = 1.0 Hz, 1H, H^1), 8.63 (d, *J* = 1.8 Hz, 1H, H^{17}), 8.15 (d, *J* = 8.2 Hz, 1H, H^{18}), 7.73 (dd, *J* = 8.2, 1.8 Hz, 1H, H^{19}), 6.95 (d, *J* = 8.7 Hz, 2H, H^4 and H^5), 6.86–6.83 (m, 3H, H^6, H^7 and H^{16}), 6.73 (d, *J* = 2.1 Hz, 1H, H^{14}), 6.68 (dd, *J* = 8.0, 2.1 Hz, 1H, H^{15}), 6.12

(d, J = 1.0 Hz, 1H, H^2), 5.24 (s, 2H, H^3), 3.78 (s, 2H, H^{13}), 3.76 (s, 3H, H^8), 3.47 (t, J = 6.3 Hz, 2H, H^9), 2.81 (t, J = 6.3 Hz, 2H, H^{10}), 2.70 (q, J = 7.2 Hz, 2H, H^{11}), 1.08 (t, J = 7.2 Hz, 3H, H^{12}). ^{13}C-NMR (151 MHz, $CDCl_3$) δ 159.54, 158.60, 155.00, 149.46, 144.49, 140.74, 137.88, 134.69, 134.25, 129.57, 128.82, 127.04 (2C), 126.84, 120.39, 120.37, 119.88, 119.26, 116.50, 114.79 (2C), 85.39, 56.84, 55.31, 53.23, 52.20, 47.84, 41.84, 38.57, 12.62, 10.77. HPLC-MS (ESI): Purity = 98%, t_R = 2.975 min, *m/z* $[M+H]^+$ = 611.1.

7.2.2.6 General procedure for the synthesis of target compounds 3.1-3.19 (Scheme 2.5)

The appropriate intermediate **3f** was stirred in neat TFA (10 mL) at 100 °C for 16 hours. Once the reaction was complete, TFA was removed under reduced pressure. The residue was dissolved in DCM/MeOH (9:1) and stirred with Amberlyst A21 for 1 hour. The resin was filtered off and the filtrate concentrated under reduced pressure. The residue was purified via column chromatography to obtain the final product.

5-chloro-2-(((2-((2-cyclopentyl-1H-imidazo[4,5-c]pyridin-6-yl)amino)ethyl)(ethyl)amino)methyl)phenol (3.1):

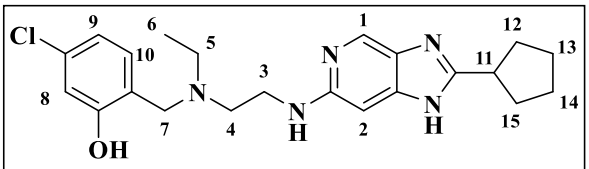

Chemical Formula: $C_{22}H_{28}ClN_5O$
Exact Mass: 413.20
Molecular Weight: 413.95

Obtained from intermediate **3f.1** (115.90 mg, 0.22 mmol) as an off-white sticky solid (68%, 61.3 mg); Rf (DCM:MeOH, 9:1) 0.38; ^{1}H-NMR (600 MHz, DMSO-d_6) δ 8.18 (d, J = 1.0 Hz, 1H, H^1), 7.25 (d, J = 8.1 Hz, 1H, H^{10}), 6.81 (d, J = 2.1 Hz, 1H, H^8), 6.79 (dd, J = 8.1, 2.1 Hz, 1H, H^9), 6.44 (d, J = 1.0 Hz, 1H, H^2), 4.03 (s, 2H, H^7), 3.40 (t, J = 5.9 Hz, 2H, H^3), 3.20–3.13 (m, 1H, H^{11}), 2.98 (t, J = 5.8 Hz, 2H, H^4), 2.93 (q, J = 7.2 Hz, 2H, H^5), 2.02–1.95 (m, 2H, H^{12a} and H^{15a}), 1.84–1.77 (m, 2H, H^{12b} and H^{15b}), 1.73–1.66 (m, 2H, H^{13a} and H^{14a}), 1.63–1.56 (m, 2H, H^{13b} and H^{14b}), 1.13 (t, J = 7.2 Hz, 3H, H^6). ^{13}C-NMR (151 MHz, DMSO) δ 158.76, 154.94, 137.73, 132.39, 130.71, 130.00, 129.65, 128.84, 122.94, 118.83, 115.55, 86.67, 54.92, 52.22, 49.03, 47.10, 39.29, 31.92 (2C), 25.54 (2C), 11.31. HPLC-MS (ESI): Purity = 98%, t_R = 2.203 min, *m/z* $[M+H]^+$ = 414.1.

5-chloro-2-((ethyl(2-((2-(tetrahydrofuran-3-yl)-1H-imidazo[4,5-c]pyridin-6-yl)amino)ethyl)amino)methyl)phenol (3.2):

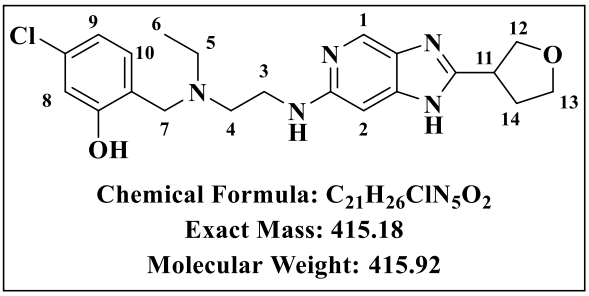

Obtained from intermediate **3f.2** (113.3 mg, 0.21 mmol) as an off-white sticky solid (74%, 65.30 mg); Rf (DCM:MeOH, 9:1) 0.34; ^{1}H-NMR (600 MHz, DMSO-d_6) δ 8.21 (d, J = 1.0 Hz, 1H, H^{1}), 7.08 (d, J = 8.0 Hz, 1H, H^{10}), 6.73 (d, J = 2.1 Hz, 1H, H^{8}), 6.71 (dd, J = 8.0, 2.1 Hz, 1H, H^{9}), 6.32 (d, J = 1.0 Hz, 1H, H^{2}), 4.02–3.99 (m, 1H, H^{12a}), 3.83 (t, J = 6.7 Hz, 2H, H^{3}), 3.78–3.73 (m, 1H, H^{12b}), 3.71 (s, 2H, H^{7}), 3.56–3.49 (m, 1H, H^{11}), 3.35–3.31 (m, 2H, H^{13}), 2.65 (t, J = 6.7 Hz, 2H, H^{4}), 2.56 (q, J = 7.1 Hz, 2H, H^{5}), 2.28–2.17 (m, 2H, H^{14}), 0.98 (t, J = 7.1 Hz, 3H, H^{6}). ^{13}C-NMR (151 MHz, DMSO) δ 158.75, 155.54, 155.12, 142.76, 138.05, 134.83, 132.38, 130.70, 130.00, 122.96, 118.83, 115.55, 86.69, 71.63, 67.89, 54.93, 52.19, 49.03, 47.10, 31.48, 11.32. HPLC-MS (ESI): Purity = 98%, t_R = 0.298 min, *m/z* $[M+H]^+$ = 416.2.

5-chloro-2-((ethyl(2-((2-(tetrahydro-2H-pyran-4-yl)-1H-imidazo[4,5-c]pyridin-6-yl)amino)ethyl)amino)methyl)phenol (3.3):

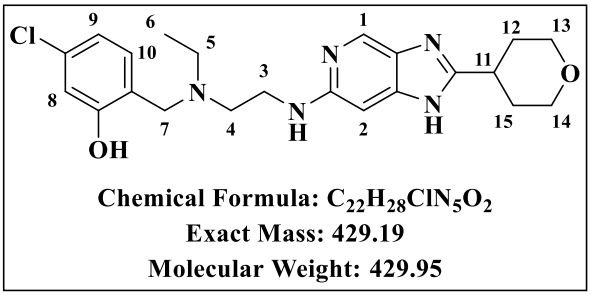

Obtained from intermediate **3f.3** (65.5 mg, 0.12 mmol) as an off-white sticky solid (80%, 40.80 mg); Rf (DCM:MeOH, 9:1) 0.29; ^{1}H-NMR (600 MHz, DMSO-d_6) δ 8.21 (d, J = 1.0 Hz, 1H, H^{1}), 7.15 (d, J = 7.9 Hz, 1H, H^{10}), 6.76 (d, J = 2.1 Hz, 1H, H^{8}), 6.74 (dd, J = 7.9, 2.1 Hz, 1H, H^{9}), 6.38 (d, J = 1.0 Hz, 1H, H^{2}), 3.91–3.86 (m, 2H, H^{13a} and H^{14a}), 3.83 (s, 2H, H^{7}), 3.44–3.39 (m, 2H, H^{13e} and H^{14e}), 3.36 (t, J = 6.4 Hz, 2H, H^{3}), 3.03–2.96 (m, 1H, H^{11}), 2.78 (t, J = 6.4 Hz, 2H, H^{4}), 2.71 (q, J = 7.2 Hz, 2H, H^{5}), 1.90–1.85 (m, 2H, H^{12a} and H^{15a}), 1.79–1.72 (m, 2H, H^{12e} and H^{15e}), 1.04 (t, J = 7.1 Hz, 3H, H^{6}). ^{13}C-NMR (151 MHz, DMSO) δ 158.55, 154.84, 142.80, 137.40, 133.97, 133.06, 131.58, 130.00, 129.68, 128.96, 119.01, 115.57, 66.96 (2C), 54.16, 52.89, 49.03, 47.44, 35.17, 31.12 (2C), 10.84. HPLC-MS (ESI): Purity = 97%, t_R = 0.430 min, *m/z* $[M+H]^+$ = 430.2.

5-chloro-2-((ethyl(2-((2-methyl-1H-imidazo[4,5-c]pyridin-6-yl)amino)ethyl)amino)methyl)phenol (3.4):

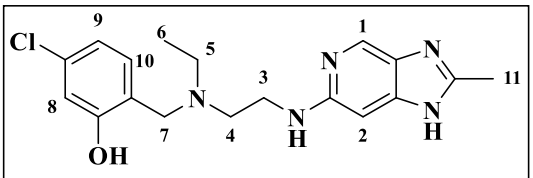

Chemical Formula: $C_{18}H_{22}ClN_5O$
Exact Mass: 359.15
Molecular Weight: 359.86

Obtained from intermediate **3f.4** (65.80 mg, 0.14 mmol) as an off-white sticky solid (71%, 35.8 mg); Rf (DCM:MeOH, 9:1) 0.26; ^{1}H-NMR (600 MHz, DMSO-d_6) δ 8.15 (d, J = 1.0 Hz, 1H, H^1), 7.08 (d, J = 8.0 Hz, 1H, H^{10}), 6.73 (d, J = 2.1 Hz, 1H, H^8), 6.71 (dd, J = 8.0, 2.1 Hz, 1H, H^9), 6.29 (d, J = 1.0 Hz, 1H, H^2), 3.70 (s, 2H, H^7), 3.32 (t, J = 6.4 Hz, 2H, H^3), 2.64 (t, J = 6.4 Hz, 2H, H^4), 2.55 (q, J = 7.2 Hz, 2H, H^5), 2.35 (s, 3H, H^{11}), 0.98 (t, J = 7.1 Hz, 3H, H^6). ^{13}C-NMR (151 MHz, DMSO) δ 158.75, 154.96, 151.25, 137.45, 132.35, 130.69, 130.01, 123.02, 118.83, 115.55, 86.62, 63.28, 54.92, 52.20, 49.04, 47.10, 15.01, 11.35. HPLC-MS (ESI): Purity = 98%, t_R = 0.219 min, *m/z* $[M+H]^+$ = 360.1.

5-chloro-2-(((2-((2-cyclopropyl-1H-imidazo[4,5-c]pyridin-6-yl)amino)ethyl)(ethyl)amino)methyl)phenol (3.5):

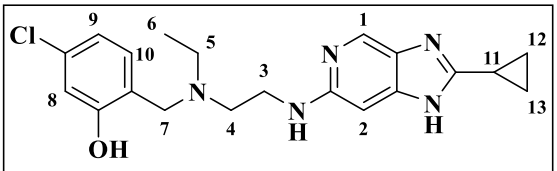

Chemical Formula: $C_{20}H_{24}ClN_5O$
Exact Mass: 385.17
Molecular Weight: 385.90

Obtained from intermediate **3f.5** (350.80 mg, 0.69 mmol) as an off-white sticky solid (68%, 180.50 mg); Rf (DCM:MeOH, 9:1) 0.30; ^{1}H-NMR (600 MHz, DMSO-d_6) δ 8.11 (d, J = 1.0 Hz, 1H, H^1), 7.10 (d, J = 8.0 Hz, 1H, H^{10}), 6.74 (d, J = 2.2 Hz, 1H, H^8), 6.72 (dd, J = 8.0, 2.1 Hz, 1H, H^9), 6.31 (d, J = 1.0 Hz, 1H, H^2), 3.74 (s, 2H, H^7), 3.32 (t, J = 6.7 Hz, 2H, H^3), 2.68 (t, J = 6.7 Hz, 2H, H^4), 2.59 (q, J = 7.2 Hz, 2H, H^5), 2.01–1.96 (m, 1H, H^{11}), 0.99 (t, J = 7.1 Hz, 3H, H^6), 0.95–0.93 (m, 4H, H^{12} and H^{13}). ^{13}C-NMR (151 MHz, DMSO) δ 158.69, 157.15, 154.78, 142.64, 137.07, 132.58, 130.97, 130.00, 122.52, 118.88, 115.56, 86.76, 54.69, 52.44, 49.03, 47.20, 11.18, 9.83 (2C), 8.93. HPLC-MS (ESI): Purity = 98%, t_R = 2.211 min, *m/z* $[M+H]^+$ = 386.1.

5-chloro-2-((ethyl(2-((2-(1-methylcyclopropyl)-1H-imidazo[4,5-c]pyridin-6-yl)amino)ethyl)amino)methyl)phenol (3.6):

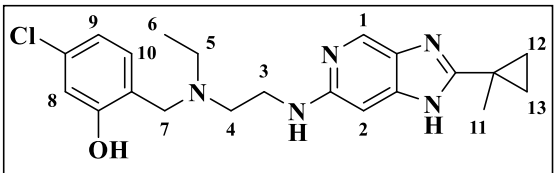

Obtained from intermediate **3f.6** (380.90 mg, 0.73 mmol) as an off-white sticky solid (86%, 250.18 mg); Rf (DCM:MeOH, 9:1) 0.29; ^{1}H-NMR (400 MHz, DMSO-d_6) δ 8.37 (d, J = 1.0 Hz, 1H, H^1), 7.40 (d, J = 8.2 Hz, 1H, H^{10}), 6.92 (d, J = 2.1 Hz, 1H, H^8), 6.87 (dd, J = 8.2, 2.1 Hz, 1H, H^9), 6.73 (d, J = 1.0 Hz, 1H, H^2), 4.30 (s, 2H, H^7), 3.66 (t, J = 6.1 Hz, 2H, H^3), 3.28 (t, J = 6.0 Hz, 2H, H^4), 3.22 (q, J = 7.2 Hz, 1H, H^5), 1.53 (s, 3H, H^{11}), 1.31–1.26 (m, 5H, H^6, H^{12a} and H^{13a}), 1.04–1.01 (m, 2H, H^{12b} and H^{13b}). ^{13}C-NMR (101 MHz, DMSO) δ 158.06, 152.70, 149.17, 143.15, 140.46, 135.35, 134.45, 131.71, 127.66, 116.35, 115.81, 108.67, 90.14, 51.45, 48.64, 38.07, 20.88, 17.89, 15.68 (2C), 9.19. HPLC-MS (ESI): Purity = 98%, t_R = 0.755 min, *m/z* $[M+H]^+$ = 400.2.

5-chloro-2-((ethyl(2-((2-(1-(trifluoromethyl)cyclopropyl)-1H-imidazo[4,5-c]pyridin-6-yl)amino)ethyl)amino)methyl)phenol (3.7):

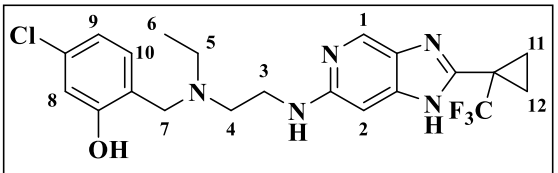

Obtained from intermediate **3f.7** (58.8 mg, 0.10 mmol) as an off-white sticky solid (77%, 35.16 mg); Rf (DCM:MeOH, 9:1) 0.30; ^{1}H-NMR (400 MHz, DMSO-d_6) δ 8.50 (d, J = 1.0 Hz, 1H, H^1), 7.41 (d, J = 8.2 Hz, 1H, H^{10}), 6.93 (d, J = 2.1 Hz, 1H, H^8), 6.88 (dd, J = 8.1, 2.1 Hz, 1H, H^9), 6.74 (d, J = 1.0 Hz, 1H, H^2), 4.32 (s, 2H, H^7), 3.65 (t, J = 5.9 Hz, 2H, H^3), 3.30 (t, J = 5.9 Hz, 2H, H^4), 3.24 (q, J = 7.1 Hz, 2H, H^5), 1.60–1.55 (m, 4H, H^{11} and H^{12}), 1.29 (t, J = 7.2 Hz, 3H, H^6). ^{13}C-NMR (101 MHz, DMSO) δ 158.05, 152.50, 149.26, 146.22, 141.57, 135.40, 134.48, 129.93, 124.43, 119.59, 116.31, 115.81, 111.78, 51.57, 48.70, 38.22, 31.43, 23.37, 12.03 (2C), 9.18. HPLC-MS (ESI): Purity = 98%, t_R = 2.194 min, *m/z* $[M+H]^+$ = 454.1.

5-chloro-2-(((2-((2-(cyclopropylmethyl)-1H-imidazo[4,5-c]pyridin-6-yl)amino)ethyl)(ethyl)amino)methyl)phenol (3.8):

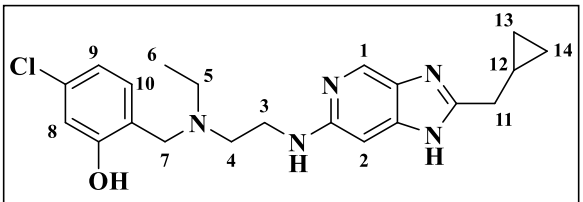

Obtained from intermediate **3f.8** (239.10 mg, 0.46 mmol) as an off-white sticky solid (88%, 161.96 mg); Rf (DCM:MeOH, 9:1) 0.35; ^{1}H-NMR (400 MHz, DMSO-d_6) δ 8.46 (d, J = 1.0 Hz, 1H, H^{1}), 7.41 (d, J = 8.2 Hz, 1H, H^{10}), 6.94 (d, J = 2.1 Hz, 1H, H^{8}), 6.87 (dd, J = 8.1, 2.1 Hz, 1H, H^{9}), 6.79 (d, J = 1.0 Hz, 1H, H^{2}), 4.31 (s, 2H, H^{7}), 3.68 (t, J = 6.0 Hz, 2H, H^{3}), 3.30 (t, J = 6.0 Hz, 2H, H^{4}), 3.24 (q, J = 7.2 Hz, 2H, H^{5}), 2.80 (d, J = 7.0 Hz, 2H, H^{11}), 1.30 (t, J = 7.2 Hz, 3H, H^{6}), 1.20–1.15 (m, 1H, H^{12}), 0.57–0.52 (m, 2H, H^{13a} and H^{14a}), 0.34–0.29 (m, 2H, H^{13b} and H^{14b}). ^{13}C-NMR (101 MHz, DMSO) δ 159.52, 158.11, 152.35, 146.06, 135.35, 134.43, 131.03, 125.99, 119.54, 116.36, 115.84, 89.98, 56.56, 52.04, 51.47, 48.64, 38.03, 33.06, 9.19, 4.94 (2C). HPLC-MS (ESI): Purity = 98%, t_R = 0.588 min, *m/z* $[M+H]^+$ = 400.2.

5-chloro-2-(((2-((2-cyclobutyl-1H-imidazo[4,5-c]pyridin-6-yl)amino)ethyl)(ethyl)amino)methyl)phenol (3.9):

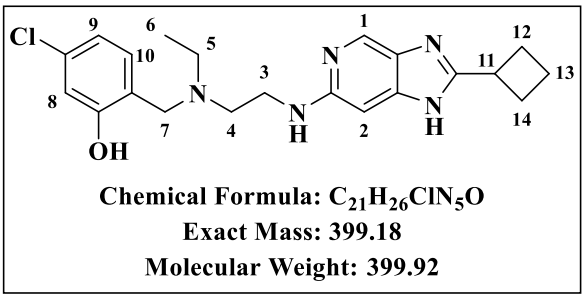

Obtained from intermediate **3f.9** (311.30 mg, 0.60 mmol) as an off-white sticky solid (79%, 190.50 mg); Rf (DCM:MeOH, 9:1) 0.31; ^{1}H-NMR (400 MHz, DMSO-d_6) δ 8.45 (d, J = 1.0 Hz, 1H, H^{1}), 7.41 (d, J = 8.2 Hz, 1H, H^{10}), 6.94 (d, J = 2.1 Hz, 1H, H^{8}), 6.85 (dd, J = 8.2, 2.1 Hz, 1H, H^{9}), 6.78 (d, J = 1.0 Hz, 1H, H^{2}), 4.31 (s, 2H, H^{7}), 3.83–3.72 (m, 1H, H^{11}), 3.69 (t, J = 6.1 Hz, 2H, H^{3}), 3.29 (t, J = 6.0 Hz, 2H, H^{4}), 3.23 (q, J = 7.2 Hz, 2H, H^{5}), 2.46–2.34 (m, 4H, H^{12} and H^{14}), 2.15–2.02 (m, 1H, H^{13a}), 2.00–1.89 (m, 1H, H^{13b}), 1.30 (t, J = 7.1 Hz, 3H, H^{6}). ^{13}C-NMR (101 MHz, DMSO) δ 163.14, 159.51, 158.11, 151.94, 135.38, 134.37, 119.50, 116.27, 115.86, 89.93, 79.09, 51.89, 51.45, 48.65, 40.46, 38.02, 33.40, 27.37 (2C), 18.60, 9.19. HPLC-MS (ESI): Purity = 98%, t_R = 0.921 min, *m/z* $[M+H]^+$ = 400.2.

5-chloro-2-(((2-((2-(3,3-difluorocyclobutyl)-1H-imidazo[4,5-c]pyridin-6-yl)amino)ethyl)(ethyl)amino)methyl)phenol (3.10):

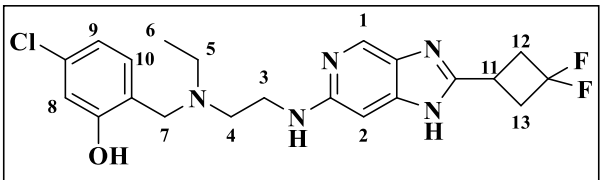

Obtained from intermediate **3f.10** (274.10 mg, 0.49 mmol) as an off-white sticky solid (84%, 178.80 mg); Rf (DCM:MeOH, 9:1) 0.29; ^{1}H-NMR (600 MHz, DMSO-d_6) δ 8.51 (d, *J* = 1.0 Hz, 1H, H^{1}), 7.37 (d, *J* = 8.2 Hz, 1H, H^{10}), 6.88 (d, *J* = 2.1 Hz, 1H, H^{8}), 6.84 (dd, *J* = 8.2, 2.1 Hz, 1H, H^{9}), 6.80 (d, *J* = 1.0 Hz, 1H, H^{2}), 4.28 (s, 2H, H^{7}), 3.66 (t, *J* = 6.3 Hz, 2H, H^{3}), 3.64–3.60 (m, 1H, H^{11}), 3.27 (t, *J* = 6.2 Hz, 2H, H^{4}), 3.20 (q, *J* = 7.2 Hz, 2H, H^{5}), 3.10–2.94 (m, 4H, H^{12} and H^{13}), 1.26 (t, *J* = 7.2 Hz, 3H, H^{6}). ^{13}C-NMR (151 MHz, DMSO) δ 159.36, 158.02, 150.81, 147.81, 135.40, 134.50, 133.25, 122.12, 120.25, 119.58, 118.45, 116.14, 115.75, 89.93, 63.24, 51.32, 48.61, 37.86, 21.96 (2C), 9.11. HPLC-MS (ESI): Purity = 99%, t_R = 1.808 min, *m/z* $[M+H]^+$ = 436.1.

5-chloro-2-(((2-((2-cyclohexyl-1H-imidazo[4,5-c]pyridin-6-yl)amino)ethyl)(ethyl)amino)methyl)phenol (3.11):

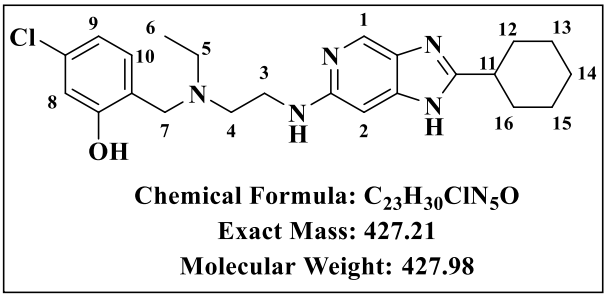

Obtained from intermediate **3f.11** (274.1 mg, 0.50 mmol) as an off-white sticky solid (71%, 151.80 mg); Rf (DCM:MeOH, 9:1) 0.32; ^{1}H-NMR (600 MHz, DMSO-d_6) δ 8.44 (d, *J* = 1.0 Hz, 1H, H^{1}), 7.36 (d, *J* = 8.2 Hz, 1H, H^{10}), 6.88 (d, *J* = 2.1 Hz, 1H, H^{8}), 6.82 (dd, *J* = 8.2, 2.1 Hz, 1H, H^{9}), 6.76 (d, *J* = 1.0 Hz, 1H, H^{2}), 4.26 (s, 2H, H^{7}), 3.65 (t, *J* = 6.2 Hz, 2H, H^{3}), 3.25 (t, *J* = 6.2 Hz, 2H, H^{4}), 3.19 (q, *J* = 7.2 Hz, 2H, H^{5}), 2.89 (tt, *J* = 11.7, 3.7 Hz, 1H, H^{11}), 2.01–1.96 (m, 2H, H^{12a} and H^{16a}), 1.77–1.73 (m, 2H, H^{12e} and H^{16e}), 1.67–1.63 (m, 1H, H^{14a}), 1.59–1.52 (m, 2H, H^{13a} and H^{15a}), 1.39–1.30 (m, 2H, H^{13e} and H^{15e}), 1.25 (t, *J* = 7.2 Hz, 3H, H^{6}), 1.23–1.17 (m, 1H, H^{14e}). ^{13}C-NMR (151 MHz, DMSO) δ 164.77, 159.42, 158.04, 151.60, 146.44, 135.37, 134.44, 130.11, 126.08, 119.51, 116.14, 115.75, 110.92, 89.86, 51.33, 48.63, 37.63, 30.78 (2C), 25.69, 25.57 (2C), 9.09. HPLC-MS (ESI): Purity = 97%, t_R = 2.238 min, *m/z* $[M+H]^+$ = 428.2.

5-chloro-2-(((2-((2-(4,4-difluorocyclohexyl)-1H-imidazo[4,5-c]pyridin-6-yl)amino)ethyl)(ethyl)amino)methyl)phenol (3.12):

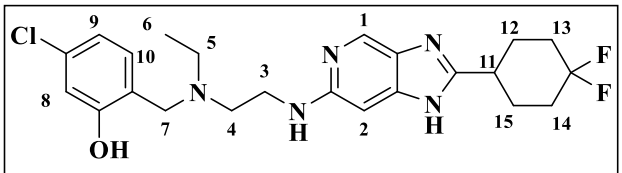

Obtained from intermediate **3f.12** (381 mg, 0.65 mmol) as an off-white sticky solid (83%, 250 mg); Rf (DCM:MeOH, 9:1) 0.37; ^{1}H-NMR (600 MHz, DMSO-d_6) δ 8.46 (d, J = 1.0 Hz, 1H, H^{1}), 7.36 (d, J = 8.2 Hz, 1H, H^{10}), 6.89 (d, J = 2.1 Hz, 1H, H^{8}), 6.81 (dd, J = 8.2, 2.1 Hz, 1H, H^{9}), 6.80 (d, J = 1.0 Hz, 1H, H^{2}), 4.27 (s, 2H, H^{7}), 3.76–3.70 (m, 1H, H^{11}), 3.67 (t, J = 6.3 Hz, 2H, H^{3}), 3.27 (t, J = 6.2 Hz, 2H, H^{4}), 3.19 (q, J = 7.1 Hz, 2H, H^{5}), 3.12–3.06 (m, 1H, H^{13a}), 2.11–2.07 (m, 4H, H^{12} and H^{15}), 2.01–1.89 (m, 1H, H^{14a}), 1.88–1.80 (m, 2H, H^{13e} and H^{14e}), 1.25 (t, J = 7.2 Hz, 3H, H^{6}). ^{13}C-NMR (151 MHz, DMSO) δ 158.09, 150.96, 135.35, 134.42, 129.70, 125.56, 123.97, 122.38, 119.46, 116.12, 115.78, 89.88, 62.47, 51.26, 48.62, 37.80, 35.06, 32.56, 27.12 (2C), 25.84 (2C), 9.08. HPLC-MS (ESI): Purity = 98%, t_R = 2.150 min, *m/z* $[M+H]^+$ = 464.2.

5-chloro-2-((ethyl(2-((2-(1-methylpyrrolidin-2-yl)-1H-imidazo[4,5-c]pyridin-6-yl)amino)ethyl)amino)methyl)phenol (3.13):

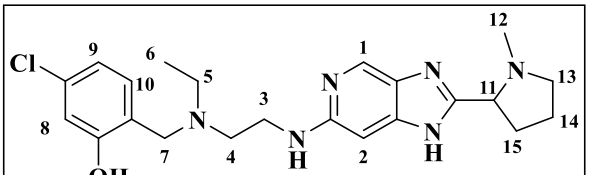

Obtained from intermediate **3f.13** (50.90 mg, 0.10 mmol) as a yellow sticky solid (71%, 30.50 mg); Rf (DCM:MeOH, 9:1) 0.20; ^{1}H-NMR (600 MHz, DMSO-d_6) δ 8.44 (d, J = 1.0 Hz, 1H, H^{1}), 7.38 (d, J = 8.2 Hz, 1H, H^{10}), 6.92 (d, J = 2.1 Hz, 1H, H^{8}), 6.83 (dd, J = 8.2, 2.1 Hz, 1H, H^{9}), 6.66 (d, J = 1.0 Hz, 1H, H^{2}), 4.77 (dd, J = 8.1, 4.3 Hz, 1H, H^{11}), 4.27 (s, 2H, H^{7}), 3.58 (t, J = 5.9 Hz, 2H, H^{3}), 3.24 (t, J = 5.9 Hz, 2H, H^{4}), 3.20 (q, J = 7.2 Hz, 2H, H^{5}), 2.94–2.86 (m, 2H, H^{13}), 2.60–2.53 (m, 2H, H^{14}), 2.27–1.98 (m, 2H, H^{15}), 1.72 (s, 3H, H^{12}), 1.24 (t, J = 7.2 Hz, 3H, H^{6}). ^{13}C-NMR (151 MHz, DMSO) δ 172.03, 159.23, 158.81, 158.11, 153.85, 135.31, 134.45, 120.46, 119.47, 118.48, 116.50, 116.33, 115.80, 114.52, 52.89, 51.50, 48.58, 38.13, 29.75, 22.88, 22.29, 9.14. HPLC-MS (ESI): Purity = 97%, t_R = 0.141 min, *m/z* $[M+H]^+$ = 429.2

5-chloro-2-((ethyl(2-((2-(3-(trifluoromethyl)phenyl)-1H-imidazo[4,5-c]pyridin-6-yl)amino)ethyl)amino)methyl)phenol (3.14):

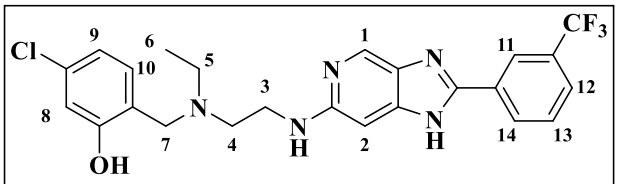

Chemical Formula: $C_{24}H_{23}ClF_3N_5O$
Exact Mass: 489.15
Molecular Weight: 489.93

Obtained from intermediate **3f.14** (230.50 mg, 0.38 mmol) as an off-white sticky solid (81%, 150.50 mg); Rf (DCM:MeOH, 9:1) 0.30; ^{1}H-NMR (600 MHz, DMSO-d_6) δ 8.53 (d, J = 1.0 Hz, 1H, H^1), 8.47 (dd, J = 2.1, 1.5 Hz, 1H, H^{11}), 8.44 (ddd, J = 7.8, 1.6, 1.5 Hz, 1H, H^{12}), 7.88 (ddd, J = 7.8, 2.1, 1.6 Hz, 1H, H^{14}), 7.79 (t, J = 7.8 Hz, 1H, H^{13}), 7.41 (d, J = 8.2 Hz, 1H, H^{10}), 6.90 (d, J = 2.1 Hz, 1H, H^8), 6.85 (dd, J = 8.2, 2.1 Hz, 1H, H^9), 6.75 (d, J = 1.0 Hz, 1H, H^2), 4.28 (s, 2H, H^7), 3.64 (t, J = 6.0 Hz, 2H, H^3), 3.26 (t, J = 5.9 Hz, 2H, H^4), 3.21 (q, J = 7.2 Hz, 2H, H^5), 1.27 (t, J = 7.2 Hz, 3H, H^6). ^{13}C-NMR (151 MHz, DMSO) δ 158.96, 158.75, 158.54, 158.32, 158.04, 135.32, 134.55, 131.14, 130.85, 130.47, 127.62, 125.27, 123.74, 120.50, 120.36, 119.56, 118.39, 116.28, 115.75, 51.39, 48.58, 38.16, 22.91, 9.16. HPLC-MS (ESI): Purity = 98%, t_R = 2.422 min, *m/z* $[M+H]^+$ = 490.1.

5-chloro-2-(((2-((2-cycloheptyl-1H-imidazo[4,5-c]pyridin-6-yl)amino)ethyl)(ethyl)amino)methyl)phenol (3.15):

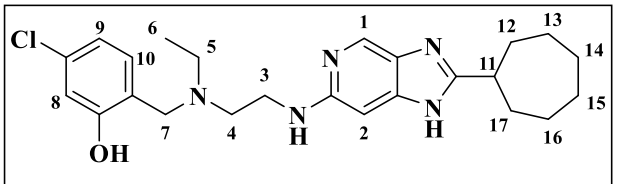

Chemical Formula: $C_{24}H_{32}ClN_5O$
Exact Mass: 441.23
Molecular Weight: 442.00

Obtained from intermediate **3f.15** (75.80 mg, 0.14 mmol) as an off-white sticky solid (92%, 56.80 mg); Rf (DCM:MeOH, 9:1) 0.38; ^{1}H-NMR (600 MHz, DMSO-d_6) δ 8.41 (d, J = 1.0 Hz, 1H, H^1), 7.37 (d, J = 8.2 Hz, 1H, H^{10}), 6.89 (d, J = 2.2 Hz, 1H, H^8), 6.82 (dd, J = 8.2, 2.1 Hz, 1H, H^9), 6.74 (d, J = 1.0 Hz, 1H, H^2), 4.26 (s, 2H, H^7), 3.64 (t, J = 6.2 Hz, 2H, H^3), 3.25 (t, J = 6.2 Hz, 2H, H^4), 3.19 (q, J = 7.2 Hz, 2H, H^5), 3.07 (tt, J = 9.4, 4.4 Hz, 1H, H^{11}), 2.03–1.96 (m, 2H, H^{12a} and H^{17a}), 1.84–1.76 (m, 2H, H^{12b} and H^{17b}), 1.62–1.56 (m, 4H, H^{13} and H^{16}), 1.55–1.48 (m, 4H, H^{14} and H^{15}), 1.25 (t, J = 7.1 Hz, 3H, H^6). ^{13}C-NMR (151 MHz, DMSO) δ 172.01, 159.28, 159.06, 158.85, 158.64, 158.06, 135.31, 134.44, 119.49, 118.40, 116.22, 115.76, 89.77, 51.31, 48.60, 37.84, 32.67 (2C), 28.14 (2C), 26.17 (2C), 22.88, 9.12. HPLC-MS (ESI): Purity = 99%, t_R = 2.413 min, *m/z* $[M+H]^+$ = 442.2.

5-chloro-2-((ethyl(2-((2-((1r,4r)-4-(trifluoromethyl)cyclohexyl)-1H-imidazo[4,5-c]pyridin-6-yl)amino)ethyl)amino)methyl)phenol (3.16):

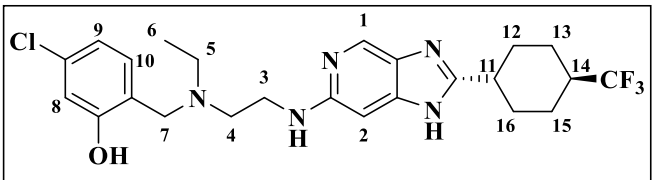

Obtained from intermediate **3f.16** (81.40 mg, 0.13 mmol) as an off-white sticky solid (88%, 56.70 mg); Rf (DCM:MeOH, 9:1) 0.38; ^{1}H-NMR (600 MHz, DMSO-d_6) δ 8.42 (d, *J* = 1.0 Hz, 1H, H^{1}), 7.37 (d, *J* = 8.2 Hz, 1H, H^{10}), 6.89 (d, *J* = 2.1 Hz, 1H, H^{8}), 6.82 (dd, *J* = 8.2, 2.1 Hz, 1H, H^{9}), 6.76 (d, *J* = 1.0 Hz, 1H, H^{2}), 4.26 (s, 2H, H^{7}), 3.64 (t, *J* = 6.2 Hz, 2H, H^{3}), 3.25 (t, *J* = 6.2 Hz, 2H, H^{4}), 3.18 (q, *J* = 7.2 Hz, 2H, H^{5}), 2.89 (tt, *J* = 12.1, 3.6 Hz, 1H, H^{11}), 2.36–2.27 (m, 1H, H^{14}), 2.16–2.12 (m, 2H, H^{12a} and H^{16a}), 1.98–1.94 (m, 2H, H^{12e} and H^{16e}), 1.66–1.58 (m, 2H, H^{13a} and H^{15a}), 1.45–1.35 (m, 2H, H^{13e} and H^{15e}), 1.25 (t, *J* = 7.2 Hz, 3H, H^{6}). ^{13}C-NMR (151 MHz, $CDCl_3$) δ 159.44, 158.78, 154.20, 143.67, 138.51, 134.04, 134.02, 129.32, 127.19, 120.34, 119.14, 116.42, 85.28, 57.08, 55.29, 52.10, 47.69, 46.36, 46.24, 41.06, 35.44, 29.99 (2C), 10.89. HPLC-MS (ESI): Purity = 98%, t_R = 2.413 min, *m/z* $[M+H]^+$ = 496.2.

5-chloro-2-((ethyl(2-((2-((1r,4r)-4-(trifluoromethyl)cyclohexyl)-1H-imidazo[4,5-c]pyridin-6-yl)amino)ethyl)amino)methyl)phenol (3.17):

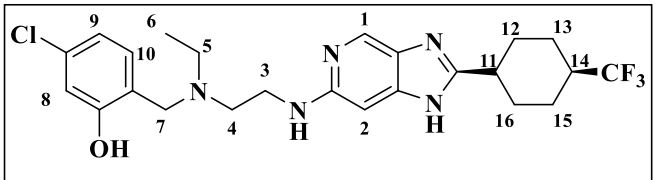

Obtained from intermediate **3f.17** (76.70 mg, 0.12 mmol) as an off-white sticky solid (78%, 46.50 mg); Rf (DCM:MeOH, 9:1) 0.36; ^{1}H-NMR (600 MHz, DMSO) δ 8.40 (d, *J* = 1.0 Hz, 1H, H^{1}), 7.36 (d, *J* = 8.2 Hz, 1H, H^{10}), 6.87 (d, *J* = 2.2 Hz, 1H, H^{8}), 6.83 (dd, *J* = 8.2, 2.1 Hz, 1H, H^{9}), 6.71 (d, *J* = 1.0 Hz, 1H, H^{2}), 4.26 (s, 2H, H^{7}), 3.25–3.22 (m, 4H, H^{3}, H^{4}), 3.18 (q, *J* = 7.2 Hz, 2H, H^{5}), 2.88 (tt, *J* = 12.3, 3.7 Hz, 1H, H^{11}), 2.37–2.28 (m, 1H, H^{14}), 2.17–2.12 (m, 2H, H^{12a} and H^{16a}), 1.99–1.94 (m, 2H, H^{12e} and H^{16e}), 1.66–1.58 (m, 2H, H^{13a} and H^{15a}), 1.45–1.36 (m, 2H, H^{13e} and H^{15e}), 1.24 (t, *J* = 7.2 Hz, 3H, H^{6}). ^{13}C-NMR (151 MHz, $CDCl_3$) δ 159.44, 158.78, 154.20, 143.67, 138.51, 134.04, 134.02, 129.32, 127.19, 120.34, 119.14, 116.42, 85.28, 57.08, 55.29, 52.10, 47.69, 46.36, 46.24, 41.06, 35.44, 29.99 (2C), 10.89. HPLC-MS (ESI): Purity = 97%, t_R = 2.343 min, *m/z* $[M+H]^+$ = 496.2.

5-chloro-2-((ethyl(2-((2-(4-methoxycyclohexyl)-1H-imidazo[4,5-c]pyridin-6-yl)amino)ethyl)amino)methyl)phenol (3.18):

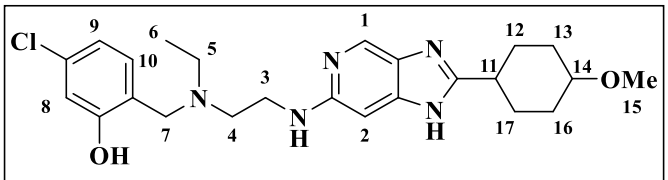

Chemical Formula: $C_{24}H_{32}ClN_5O_2$
Exact Mass: 457.22
Molecular Weight: 458.00

Obtained from intermediate **3f.18** (73 mg, 0.13 mmol) as an off-white sticky solid (77%, 45.80 mg); Rf (DCM:MeOH, 9:1) 0.50; ^{1}H-NMR (600 MHz, DMSO) δ 8.37 (d, *J* = 1.0 Hz, 1H, H^1), 8.13 (d, *J* = 8.1 Hz, 1H, H^{10}), 6.89 (d, *J* = 2.1 Hz, 1H, H^8), 6.83 (dd, *J* = 8.2, 2.1 Hz, 1H, H^9), 6.62 (d, *J* = 1.0 Hz, 1H, H^2), 4.25 (s, 2H, H^7), 3.64–3.53 (m, 1H, H^{14}), 3.22 (s, 3H, H^{15}), 3.12 (tt, *J* = 10.88, 4.11 Hz, 1H, H^{11}), 2.92 (t, *J* = 6.2 Hz, 2H, H^3), 2.81 (t, *J* = 6.2 Hz, 2H, H^4), 2.58 (q, *J* = 7.2 Hz, 2H, H^5), 2.08–2.02 (m, 2H, H^{12a} and H^{17a}), 1.88–1.77 (m, 2H, H^{12e} and H^{17e}), 1.75–1.71 (m, 2H, H^{13a} and H^{16a}), 1.63–1.47 (m, 2H, H^{13e} and H^{16e}), 1.23 (t, *J* = 7.2 Hz, 3H, H^6). ^{13}C-NMR (151 MHz, $CDCl_3$) δ 159.47, 153.50, 144.28, 136.87, 134.14, 129.50, 127.40, 119.22, 116.44, 85.54, 78.32, 73.57, 56.94, 55.77, 55.30, 52.01, 47.89, 40.43, 35.67, 31.57 (2C), 29.79 (2C), 10.87. HPLC-MS (ESI): Purity = 97%, t_R = 2.124 min, *m/z* $[M+H]^+$ = 458.2.

5-chloro-2-((ethyl(2-((2-(6-(trifluoromethyl)pyridin-3-yl)-1H-imidazo[4,5-c]pyridin-6-yl)amino)ethyl)amino)methyl)phenol (3.19):

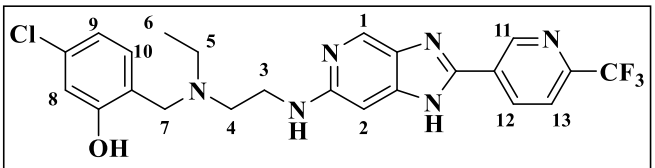

Chemical Formula: $C_{23}H_{22}ClF_3N_6O$
Exact Mass: 490.15
Molecular Weight: 490.92

Obtained from intermediate **3f.19** (54.90 mg, 0.09 mmol) as an off-white solid (81%, 35.60 mg); Rf (DCM:MeOH, 9:1) 0.38; ^{1}H-NMR (600 MHz, DMSO-d_6) δ 9.44 (d, *J* = 2.1 Hz, 1H, H^{11}), 8.70 (dd, *J* = 8.2, 2.1 Hz, 1H, H^{12}), 8.52 (d, *J* = 1.0 Hz, 1H, H^1), 8.09 (d, *J* = 8.2 Hz, 1H, H^{13}), 7.38 (d, *J* = 8.2 Hz, 1H, H^{10}), 6.89 (d, *J* = 2.1 Hz, 1H, H^8), 6.85 (dd, *J* = 8.2, 2.1 Hz, 1H, H^9), 6.67 (d, *J* = 1.0 Hz, 1H, H^2), 4.28 (s, 2H, H^7), 3.59 (t, *J* = 5.8 Hz, 2H, H^3), 3.25 (t, *J* = 5.9 Hz, 2H, H^4), 3.21 (q, *J* = 7.2 Hz, 2H, H^5), 1.27 (t, *J* = 7.2 Hz, 3H, H^6). ^{13}C-NMR (151 MHz, $CDCl_3$) δ 159.54, 158.60, 155.00, 149.46, 144.49, 140.74, 137.88, 134.69, 134.25, 129.57, 128.82, 126.84, 120.39, 119.88, 119.26, 114.79, 85.39, 56.84, 55.31, 52.20, 47.84, 41.84, 10.77. HPLC-MS (ESI): Purity = 98%, t_R = 2.352 min, *m/z* $[M+H]^+$ = 491.1.

7.2.3 Benzimidazole Fluorescent Probe

7.2.3.1 Procedure for the synthesis of intermediate 4a (Scheme 2.9)

A mixture of 2-chlorobenzimidazole (1 eq), N-boc ethylenediamine (2 eq) and triethylamine (3 eq) in toluene was stirred under reflux at 150 ºC for 16 hours. After cooling to room temperature, toluene was removed and the residue diluted with ethyl acetate and 1M NaOH solution. The organic layer was washed with brine, dried over anhydrous Na_2SO_4 and concentrated. The residue was purified by column chromatography, and an off-white solid was obtained as the product.

***Tert*-butyl (2-((1H-benzo[d]imidazol-2-yl)amino)ethyl)carbamate (4a):**

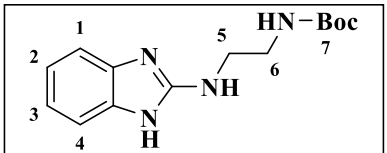

Chemical Formula: $C_{14}H_{20}N_4O_2$
Exact Mass: 276.16
Molecular Weight: 276.34

Obtained from 2-chlorobenzimidazole (1.00 g, 6.55 mmols) and N-boc ethylenediamine (2.10 g, 13.11 mmols) as an off-white solid (96%, 1.7443 g); R_f (DCM: MeOH, 9:1) 0.47; ^{1}H NMR (400 MHz, MeOH-d_4) δ 7.20 (dd, J = 6.1, 3.4 Hz, 2H, H^1 and H^4), 6.98 (dd, J = 6.0, 3.3 Hz, 2H, H^2 and H^3), 3.45 (t, J = 6.2 Hz, 2H, H^5), 3.32 (t, J = 6.2 Hz, 2H, H^6), 1.43 (s, 9H, H^7). ^{13}C NMR (101 MHz, MeOD) δ 157.34, 155.35, 137.54, 130.08, 119.89, 118.35, 115.40, 111.34, 78.80, 42.42, 39.93, 27.31(3C). HPLC-MS (ESI): Purity = 98%, t_R = 1.720 min, m/z $[M+H]^+$ = 277.2.

7.2.3.2 Procedure for the synthesis of intermediate 4b (Scheme 2.9)

(a) Boc-deprotection: Intermediate **4a** was dissolved in 4 M HCl/dioxane, and the mixture was stirred at 25 °C for 2 hours. When the reaction was complete, the solvent was removed *in vacuo,* and the residue was neutralized with Amberlyst A21 in a mixture of DCM and methanol. The Amberlyst was filtered off, the solvent was removed *in vacuo,* and the residue was used in the next reaction without further purification.

(b) Reductive amination: The crude product from step (a) above and 4-chloro-2-hydroxybenzaldehyde in methanol was stirred at 25 °C for 6 hours. The mixture was cooled at 0 °C, and sodium borohydride ($NaBH_4$) was added portion-wise. After the addition, the reaction was allowed to warm to room temperature (25 °C) for 3 hours. The solvent was removed *in vacuo,* and the residue was diluted with deionized water. The compound was extracted with DCM and dried over anhydrous sodium sulphate. The solvent was removed *in vacuo,* and the residue was purified via column chromatography to obtain the desired product.

2-(((2-((1H-benzo[d]imidazol-2-yl)amino)ethyl)amino)methyl)-5-chlorophenol (4b):

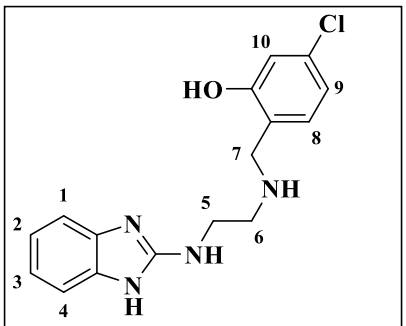

Chemical Formula: $C_{16}H_{17}ClN_4O$
Exact Mass: 316.11
Molecular Weight: 316.79

Obtained from intermediate **4a** (1.50 g, 8.51 mmols) and 4-chloro-2-hydroxybenzaldehyde (1.60 g, 10.21 mmols) as an off-white solid (70%, 1.1143 g); R_f (DCM: MeOH, 9:1) 0.25; ^{1}H NMR (400 MHz, DMSO-d_6) δ 7.14 – 7.10 (m, 3H, H^1, H^4 and H^9), 6.86 (dd, J = 6.3, 3.4 Hz, 2H, H^2 and H^3), 6.75 (d, J = 3.8 Hz, 1H, H^{10}), 6.56 (d, J = 8.1 Hz, 1H, H^8), 3.82 (s, 2H, H^7), 3.41 (t, J = 6.2 Hz, 2H, H^5), 2.75 (t, J = 6.3 Hz, 2H, H^6). ^{13}C NMR (101 MHz, DMSO-d_6) δ 158.69, 156.00, 153.56, 148.42, 132.16, 130.42, 126.61, 124.19, 122.18, 119.48, 118.66, 115.54, 111.88, 49.59, 48.37, 42.29. HPLC-MS (ESI): Purity = 98%, t_R = 0.307 min, m/z $[M+H]^+$ = 317.1.

7.2.3.3 Procedure for the synthesis of intermediate 4c (Scheme 2.9)

A mixture of intermediate **4b**, N-boc glycinal and a catalytic amount of acetic acid in methanol was stirred at 25 °C for an hour. $NaBH_3CN$ was then added, and the resulting mixture was heated at 80 °C under reflux for 5 hours. When the reaction had completed, the methanol was removed *in vacuo* and the residue reconstituted in DCM. Saturated $NaHCO_3$ solution was then added to neutralize the acetic acid. The organic layer was washed with brine, dried over anhydrous Na_2SO_4 and concentrated *in vacuo*. The residue was purified via column chromatography to obtain intermediate **4c**.

***Tert*-butyl(2-((2-((1H-benzo[d]imidazol-2-yl)amino)ethyl)(4-chloro-2 hydroxybenzyl)amino)ethyl)carbamate (4c):**

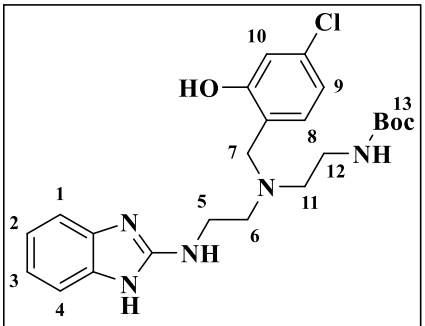

Chemical Formula: $C_{23}H_{30}ClN_5O_3$
Exact Mass: 459.20
Molecular Weight: 459.98

Obtained from intermediate **4b** (500 mg, 1.58 mmols) and N-boc glycinal (500 mg, 3.16 mmols) as an off-white solid (86%, 622.30 mg); R_f (DCM: MeOH, 9:1) 0.55; ^{1}H NMR (400 MHz, MeOH-d_4) δ 7.23 (dd, J = 5.8, 3.3 Hz, 2H, H^1 and H^4), 7.09 – 7.03 (m, 3H, H^2, H^3 and H^9), 6.75 – 6.67 (m, 2H, H^8 and H^{10}), 3.83 (s, 2H, H^7), 3.57 (t, J = 6.2 Hz, 2H, H^5), 3.25 (t, J = 6.1 Hz, 2H, H^6), 2.88 (t, J = 6.5 Hz, 2H, H^{11}), 2.72 (t, J = 6.5 Hz, 2H, H^{12}), 1.42 (s, 9H, H^{13}). ^{13}C NMR (101 MHz, MeOD) δ 157.72, 157.11, 154.30, 135.96, 133.50, 130.46, 122.81,

121.75, 120.67, 120.98, 118.88, 115.44, 111.33, 78.85, 60.64, 55.40, 53.26, 52.90, 40.06, 37.47, 27.33 (3C). HPLC-MS (ESI): Purity = 98%, t_R = 2.466 min, m/z $[M+H]^+$ = 460.2.

7.2.3.4 Procedure for the synthesis of target compound 1.3-NBD (Scheme 2.9)

(a) Boc-deprotection: Intermediate **4c** was dissolved in 4 M HCl/dioxane, and the mixture was stirred at 25 °C for 2 hours. When the reaction was complete, the solvent was removed *in vacuo,* and the residue was neutralized with Amberlyst A21 in a mixture of DCM and methanol. The Amberlyst was filtered off, the solvent was removed *in vacuo,* and the residue was used in the next reaction without further purification.

(b) Nucleophilic substitution: A mixture of the crude product from step (a) above, $NaHCO_3$ and NBD-Chloride in ethyl acetate, was stirred at 60 °C for 16 hours. The reaction was quenched with water and extracted with ethyl acetate. The organic layer was washed with brine, dried over anhydrous Na_2SO_4 and concentrated *in vacuo*. The residue was purified via column chromatography to obtain the fluorescent probe **1.3-NBD**.

2-(((2-((1H-benzo[d]imidazol-2-yl)amino)ethyl)(2-((7-nitrobenzo[c][1,2,5]oxadiazol-4-yl)amino)ethyl)amino)methyl)-5-chlorophenol (1.3-NBD):

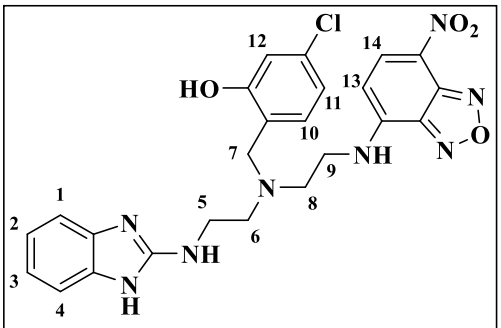

Chemical Formula: $C_{24}H_{23}ClN_8O_4$
Exact Mass: 522.15
Molecular Weight: 522.95

Obtained from intermediate **4c** (400 mg, 1.01 mmols) and N-boc glycinal (241 mg, 1.21 mmols) as a brick-red solid (60%, 316.8 mg); R_f (DCM: MeOH, 9:1) 0.56; ^{1}H NMR (400 MHz, DMSO-d_6) δ 8.36 (d, J = 8.9 Hz, 1H, H^{14}), 7.16 – 7.12 (m, 3H, H^1, H^4 and H^{13}), 6.93 – 6.88 (m, 2H, H^2 and H^3), 6.61 – 6.52 (m, 2H, H^{11} and H^{12}), 6.26 (d, J = 9.0 Hz, 1H, H^{10}), 3.73 (s, 2H, H^7), 3.58 (t, J = 6.3 Hz, 2H, H^5), 3.50 (t, J = 6.4 Hz, 2H, H^6), 2.87 – 2.82 (m, 4H, H^8 and H^9). ^{13}C NMR (101 MHz, DMSO) δ 157.46, 155.21, 151.93, 148.37, 145.40, 142.96, 138.04, 136.04, 132.22, 131.78, 129.12, 125.67, 123.75, 121.10, 120.15, 118.90, 115.33, 112.23, 99.52, 53.40, 51.23, 41.55, 29.48, 25.96. HPLC-MS (ESI): Purity = 98%, t_R = 2.352 min, m/z $[M+H]^+$ = 523.1.

7.2.4 Imidazopyridine Fluorescent Probe

7.2.4.1 Procedure for the synthesis of intermediate 5a (Scheme 2.10)

A mixture of p-methoxybenzyl amine and *N*,*N*-Diisopropylethylamine (DIPEA) in tetrahydrofuran (THF) was added dropwise to a 0 °C solution of 2,4-dichloro-5-nitropyridine in THF. The solution was then warmed up to 25 °C and stirred for an additional 30 min. Water was then added, and the resulting mixture was extracted with ethyl acetate. The combined organic layer was dried over anhydrous Na_2SO_4 and concentrated under reduced pressure to produce the desired intermediate as a yellow solid in 98% yield.

2-chloro-N-(4-methoxybenzyl)-5-nitropyridin-4-amine (5a):

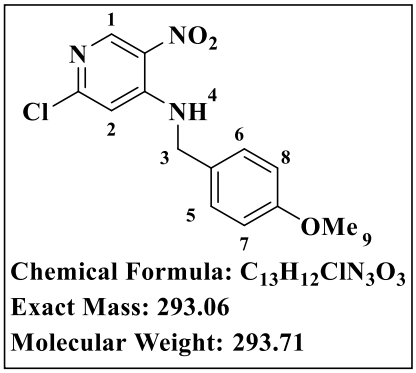

Chemical Formula: $C_{13}H_{12}ClN_3O_3$
Exact Mass: 293.06
Molecular Weight: 293.71

Obtained from 2,4-dichloro-5-nitropyridine (2.00 g, 10.36 mmol) and p-methoxybenzyl amine (2.56 g, 18.65 mmol) as a yellow solid (98%, 3.54 g); Rf (Hex: EtOAc, 1:1) 0.54; ^{1}H-NMR (600 MHz, DMSO-d_6) δ 8.96 (t, *J* = 6.1 Hz, 1H, H^4), 8.85 (s, 1H, H^1), 7.29 (d, *J* = 8.7 Hz, 2H, H^5 and H^6), 6.94 (s, 1H, H^2), 6.89 (d, *J* = 8.7 Hz, 2H, H^7 and H^8), 4.57 (d, *J* = 6.1 Hz, 2H, H^3), 3.71 (s, 3H, H^9). ^{13}C-NMR (151 MHz, DMSO) δ 159.91, 155.92, 150.57, 150.08, 130.29, 129.76 (2C), 115.42 (2C), 108.83, 56.41, 46.26. HPLC-MS (ESI): Purity = 98%, t_R = 2.457 min, *m/z* $[M-H]^+$ = 294.0.

7.2.4.2 Procedure for the synthesis of intermediate 5b (Scheme 2.10)

A mixture of 2-chloro-N-(4-methoxybenzyl)-5-nitropyridin-4-amine (**5a**), *N*-boc ethylenediamine, and triethylamine was made in *N*,*N*-dimethylformamide (DMF). The mixture was heated under microwave radiation at 100 °C for 1 hour. When the reaction had completed, water was added, and the mixture was extracted with ethyl acetate (4 × 30 mL). The combined organic layer was dried over anhydrous Na_2SO_4, concentrated under reduced pressure, and purified via column chromatography. A yellow solid was obtained as the product.

***Tert*-butyl (2-((4-((4-methoxybenzyl)amino)-5-nitropyridin-2-yl)amino)ethyl)carbamate (5b):**

Obtained from intermediate **5a** (3.50 g, 11.92 mmols) and *N*-boc ethylenediamine (2.26 mL, 14.30 mmols) as a yellow solid (96%, 4.78 g); R_f (DCM: MeOH, 9:1) 0.68; ^{1}H NMR (600

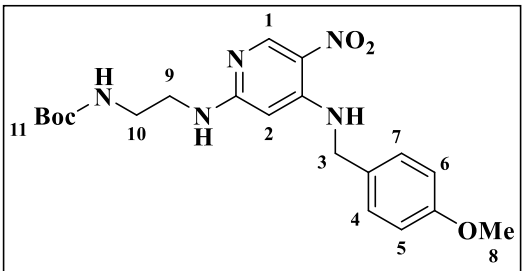

Chemical Formula: $C_{20}H_{27}N_5O_5$
Exact Mass: 417.20
Molecular Weight: 417.47

MHz, MeOH-d_4) δ 8.84 (s, 1H, H^1), 7.31 (d, J = 8.3 Hz, 2H, H^4 and H^7), 6.93 (d, J = 8.4 Hz, 2H, H^5 and H^6), 5.67 (s, 1H, H^2), 4.46 (s, 2H, H^3), 3.79 (s, 3H, H^8), 3.33 (t, J = 6.3 Hz, 2H, H^9), 3.20 (t, J = 6.3 Hz, 2H, H^{10}), 1.43 (s, 9H, H^{11}). ^{13}C NMR (151 MHz, MeOD) δ 161.46, 159.24, 157.20, 150.04, 149.55, 129.35, 128.20 (2C), 124.25, 113.86 (2C), 84.12, 78.77, 54.33, 45.37, 41.45, 39.31, 27.35 (3C). HPLC-MS (ESI): Purity = 97%, t_R = 2.598 min, m/z $[M+H]^+$ = 418.2.

7.2.4.3 Procedure for the synthesis of intermediate 5c (Scheme 2.10)

A mixture of *tert*-butyl (2-((4-((4-methoxybenzyl)amino)-5-nitropyridin-2-yl)amino)ethyl)carbamate (**5b**), Zinc and acetic acid in DCM was stirred for 30 minutes at 25 °C. After the reaction had been completed, the mixture was filtered through a pad of celite and concentrated *in vacuo* to obtain the product, which was used in the next reaction without any further purification.

***Tert*-butyl (2-((5-amino-4-((4-methoxybenzyl)amino)pyridin-2-yl)amino)ethyl)carbamate (5c):**

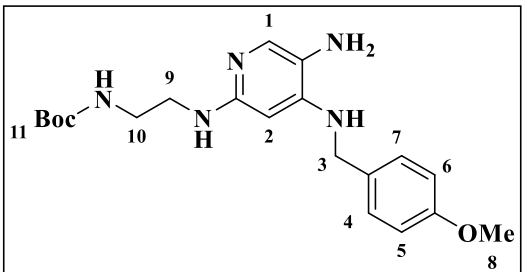

Chemical Formula: $C_{20}H_{29}N_5O_3$
Exact Mass: 387.23
Molecular Weight: 387.48

Obtained from intermediate **5b** (3.30 g, 7.90 mmols) as a wine-coloured solid (92%, 2.81 g); R_f (DCM: MeOH, 9:1) 0.40; ^{1}H NMR (600 MHz, MeOH-d_4) δ 7.32 (d, J = 8.2 Hz, 2H, H^4 and H^7), 7.24 (s, 1H, H^1), 6.90 (d, J = 8.3 Hz, 2H, H^5 and H^6), 5.75 (s, 1H, H^2), 4.41 (s, 2H, H^3), 3.78 (s, 3H, H^8), 3.16 – 3.13 (m, 4H, H^9 and H^{10}), 1.44 (s, 9H, H^{11}). ^{13}C NMR (151 MHz, MeOD) δ 159.12, 158.86, 157.13, 149.76, 129.81, 128.34 (2C), 128.06, 113.71 (2C), 113.42, 86.01, 78.84, 54.34, 45.61, 41.99, 39.20, 27.38 (3C). HPLC-MS (ESI): Purity = 97%, t_R = 2.246 min, m/z $[M+H]^+$ = 388.2.

7.2.4.4 Procedure for the synthesis of intermediates 5d and 5e (Scheme 2.10)

(a) Amide coupling (intermediate 5d): Intermediate **5c** (1 eq) was dissolved in DCM with 3-trifluoromethyl benzoic acid (1.3 eq) and 4-dimethylaminopyridine (DMAP, 0.1 eq). 1-Ethyl-3-(3-dimethylaminopropyl)carbodiimide hydrochloride (EDCI.HCl, 1.5 eq) was then added, and the reaction mixture was stirred at 25 °C for 16 hours. Water was added, and the solution was extracted with ethyl acetate, dried over anhydrous Na_2SO_4, and concentrated under reduced pressure. The residue was used in the subsequent reaction without any further purification.

(b) Cyclization (intermediate 5e): The amide intermediate **5d** was dissolved in ethanol (10 mL), and 2 M NaOH solution (10 mL) was added. The resulting mixture was heated at 80 °C for 16 hours. When the reaction had gone to completion, the solvent was removed *in vacuo,* and saturated citric acid was added to the residue. Extraction was done with DCM (2 × 20 mL), and the combined organic extract was dried over anhydrous Na_2SO_4, filtered, and concentrated *in vacuo*. The residue was purified via column chromatography (DCM/MeOH) to obtain the desired product.

***Tert*-butyl (2-((1-(4-methoxybenzyl)-2-(3-(trifluoromethyl)phenyl)-1H-imidazo[4,5-c]pyridin-6-yl)amino)ethyl)carbamate (5e):**

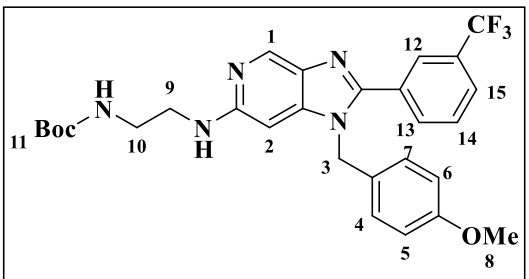

Obtained from intermediate **5c** (5.10 g, 13.16 mmols) and 3-trifluoromethyl benzoic acid (3.25 g, 17.11 mmols) as a wine-coloured sticky solid (65%, 4.63 g); R_f (DCM: MeOH, 9:1) 0.58; ^{1}H NMR (600 MHz, MeOH-d_4) δ 8.49 (s, 1H, H^1), 8.36 (ddd, J = 1.6, 1.5, 0.8 Hz, 1H, H^{12}), 8.27 (ddd, J = 7.8, 1.6, 1.3 Hz, 1H, H^{13}), 7.92 (s, 1H, H^2), 7.73 (d, J = 8.7 Hz, 2H, H^4 and H^7), 7.60 (ddd, J = 8.6, 1.5, 1.3 Hz, 1H, H^{15}), 7.53 (ddd, J = 8.6, 7.8, 0.8 Hz, 1H, H^{14}), 6.99 (d, J = 8.7 Hz, 2H, H^5 and H^6), 5.32 (s, 2H, H^3), 3.76 (s, 3H, H^8), 3.42–3.39 (m, 4H, H^9 and H^{10}), 1.40 (s, 9H, H^{11}). ^{13}C NMR (151 MHz, MeOD) δ 170.61, 159.53, 134.48, 134.06, 132.87, 132.28, 129.89, 129.53, 128.59 (2C), 128.23, 127.75, 127.24, 126.86, 126.65, 126.21, 114.56 (2C), 86.37, 79.61, 55.85, 48.06, 45.50, 44.34, 43.44, 28.37 (3C). HPLC-MS (ESI): Purity = 96%, t_R = 2.650 min, m/z $[M+H]^+$ = 542.2.

7.2.4.5 Procedure for the synthesis of intermediate 5f (Scheme 2.10)

(a) Boc-deprotection: Intermediate **5e** was dissolved in 4 M HCl/dioxane, and the mixture was stirred at 25 °C for 2 hours. When the reaction was complete, the solvent was removed *in vacuo,* and the residue was neutralized with Amberlyst A21 in a mixture of DCM and methanol. The Amberlyst was filtered off, the solvent was removed *in vacuo,* and the residue was used in the next reaction without further purification.

(b) Reductive amination: The crude product from step (a) above and 4-chloro-2-hydroxybenzaldehyde in methanol was stirred at 25 °C for 6 hours. The mixture was cooled at 0 °C, and sodium borohydride ($NaBH_4$) was added portion-wise. After the addition, the reaction was allowed to warm to room temperature (25 °C) for 3 hours. The solvent was removed *in vacuo,* and the residue was diluted with deionized water. The compound was extracted with DCM and dried over anhydrous sodium sulphate. The solvent was removed *in vacuo,* and the residue was purified via column chromatography to obtain the desired product.

5-chloro-2-(((2-((1-(4-methoxybenzyl)-2-(3-(trifluoromethyl)phenyl)-1H-imidazo[4,5-c]pyridin-6-yl)amino)ethyl)amino)methyl)phenol (5f):

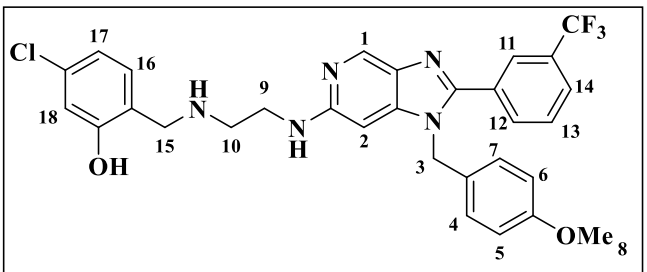

Chemical Formula: $C_{30}H_{27}ClF_3N_5O_2$
Exact Mass: 581.18
Molecular Weight: 582.02

Obtained from intermediate **5e** (1.50 g, 3.49 mmols) and 3-trifluoromethyl benzoic acid (800 mg, 5.10 mmols) as a wine-coloured sticky solid (65%, 1.32 g); R_f (DCM: MeOH, 9:1) 0.60; ^{1}H NMR (600 MHz, MeOH-d_4) δ 8.47 (d, J = 1.0 Hz, 1H, H^1), 7.92 – 7.88 (m, 2H, H^{11} and H^{14}), 7.85 (d, J = 2.3 Hz, 1H, H^{12}), 7.71 (t, J = 7.8 Hz, 1H, H^{13}), 7.06 (d, J = 8.1 Hz, 1H, H^{16}), 6.95 (d, J = 8.7 Hz, 2H, H^4 and H^7), 6.84 (d, J = 8.7 Hz, 2H, H^5 and H^6), 6.74 (d, J = 2.1 Hz, 1H, H^{18}), 6.71 (dd, J = 8.0, 2.1 Hz, 1H, H^{17}), 6.47 (d, J = 1.0 Hz, 1H, H^2), 5.32 (s, 2H, H^3), 3.96 (s, 2H, H^{15}), 3.74 (s, 3H, H^8), 3.50 (t, J = 5.8 Hz, 2H, H^9), 2.96 (t, J = 5.8 Hz, 2H, H^{10}). ^{13}C NMR (151 MHz, MeOD) δ 159.51, 158.83, 155.74, 153.11, 144.35, 138.64, 133.98, 133.57, 132.42, 130.44, 130.29, 129.58, 127.65, 127.30 (2C), 126.70, 125.68, 124.66, 122.86, 121.00, 118.16, 115.57, 114.10 (2C), 86.40, 62.94, 58.97, 54.36, 48.88, 40.93. HPLC-MS (ESI): Purity = 96%, t_R = 2.466 min, m/z $[M+H]^+$ = 582.1.

7.2.4.6 Procedure for the synthesis of intermediate 5g (Scheme 2.10)

The intermediate **5f** was stirred in neat TFA (10 mL) at 100 °C for 16 hours. Once the reaction was complete, TFA was removed under reduced pressure. The residue was dissolved in DCM/MeOH (9:1) and stirred with Amberlyst A21 for 1 hour. The resin was filtered off and the filtrate concentrated under reduced pressure. The residue was purified via column chromatography to obtain the product.

5-chloro-2-(((2-((2-(3-(trifluoromethyl)phenyl)-1H-imidazo[4,5-c]pyridin-6-yl)amino)ethyl)amino)methyl)phenol (5g):

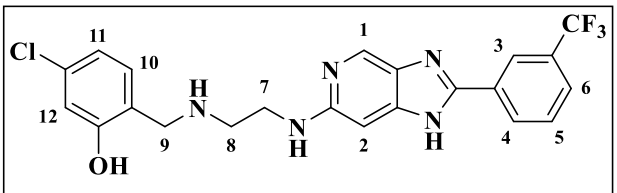

Obtained from intermediate **5f** (1.00 g, 1.72 mmols) as a wine-coloured solid (75%, 595.82 mg); R_f (DCM: MeOH, 9:1) 0.18; ^{1}H NMR (600 MHz, MeOH-d_4) δ 8.40 (s, 1H, H^1), 8.36 (dd, J = 2.8, 2.2 Hz, 1H, H^3), 8.31 (dd, J = 7.8, 2.2 Hz, 1H, H^{11}), 7.83 (d, J = 2.2 Hz, 1H, H^{12}), 7.75 (ddd, J = 7.8, 2.8, 2.3 Hz, 1H, H^6), 7.27 (d, J = 7.8 Hz, 1H, H^{10}), 6.90 – 6.85 (m, 2H, H^4 and H^5), 6.73 (s, 1H, H^2), 4.22 (s, 2H, H^9), 3.65 – 3.62 (m, 4H, H^7 and H^8). ^{13}C NMR (151 MHz, MeOD) δ 156.96, 154.42, 153.25, 136.07, 132.34, 131.19, 130.11, 129.89, 128.88, 127.06, 126.60, 124.81, 123.36, 123.01, 119.59, 116.81, 115.04, 113.98, 89.42, 48.65, 46.31, 39.63. HPLC-MS (ESI): Purity = 98%, t_R = 2.413 min, m/z $[M+H]^+$ = 462.1.

7.2.4.7 Procedure for the synthesis of intermediate 5h (Scheme 2.10)

A mixture of intermediate **5g**, N-boc glycinal and a catalytic amount of acetic acid in methanol was stirred at 25 °C for an hour. $NaBH_3CN$ was then added, and the resulting mixture was heated at 80 °C under reflux for 16 hours. When the reaction had completed, the methanol was removed *in vacuo* and the residue reconstituted in DCM. Saturated $NaHCO_3$ solution was then added to neutralize the acetic acid. The organic layer was washed with brine, dried over anhydrous Na_2SO_4 and concentrated *in vacuo*. The residue was purified via column chromatography to obtain intermediate **5h**.

***Tert*-butyl (2-((4-chloro-2-hydroxybenzyl)(2-((2-(3-(trifluoromethyl)phenyl)-1H-imidazo[4,5-c]pyridin-6-yl)amino)ethyl)amino)ethyl)carbamate (5h):**

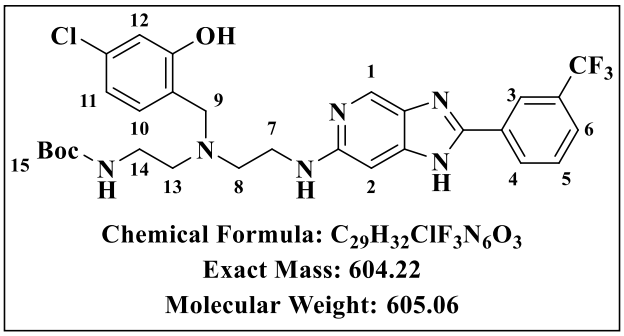

Obtained from intermediate **5g** (370 mg, 0.80 mmols) and N-boc glycinal (254 mg, 1.60 mmols) as an off-white solid (75%, 338.84 mg); R_f (DCM: MeOH, 9:1) 0.56; ^{1}H NMR (600 MHz, MeOH-d_4) δ 8.38 (s, 1H, H^1), 8.37 (dd, J = 2.8, 2.2 Hz, 1H, H^3), 8.29 (dd, J = 7.8, 2.2 Hz, 1H, H^{11}), 7.80 (d, J = 2.2 Hz, 1H, H^{12}), 7.73 (ddd, J = 7.8, 2.8, 2.3 Hz, 1H, H^6), 7.01 (d, J = 7.8 Hz, 1H, H^{10}), 6.69 – 6.63 (m, 2H, H^4 and H^5), 6.53 (s, 1H, H^2), 3.78 (s, 2H, H^9), 3.45 (t, J = 6.3 Hz, 2H, H^{14}), 3.21 (t, J = 6.2 Hz, 2H, H^7), 2.82 (t, J = 6.2 Hz, 2H, H^8), 2.68 (t, J = 6.3 Hz, 2H, H^{13}), 1.38 (s, 9H, H^{15}). ^{13}C NMR (151 MHz, MeOD) δ 159.47, 157.87, 157.09, 155.59, 147.18, 138.23, 133.37, 131.33, 131.12, 130.37, 129.77, 128.72, 127.86, 126.57, 126.04, 124.87, 123.15, 121.86, 118.78, 115.49, 113.84, 93.10, 78.77, 55.73, 53.44, 39.82, 27.35 (3C). HPLC-MS (ESI): Purity = 98%, t_R = 2.562 min, m/z $[M+H]^+$ = 605.2.

7.2.4.8 Procedure for the synthesis of target compound 3.14-NBD (Scheme 2.10)

(a) Boc-deprotection: Intermediate **5h** was dissolved in 4 M HCl/dioxane, and the mixture was stirred at 25 °C for 2 hours. When the reaction was complete, the solvent was removed *in vacuo,* and the residue was neutralized with Amberlyst A21 in a mixture of DCM and methanol. The Amberlyst was filtered off, the solvent was removed *in vacuo,* and the residue was used in the next reaction without further purification.

(b) Nucleophilic substitution: A mixture of the crude product from step (a) above, $NaHCO_3$ and NBD-Chloride in ethyl acetate, was stirred at 60 °C for 16 hours. The reaction was quenched with water and extracted with ethyl acetate. The organic layer was washed with brine, dried over anhydrous Na_2SO_4 and concentrated *in vacuo*. The residue was purified via column chromatography to obtain the fluorescent probe **3.14-NBD**.

5-chloro-2-(((2-((7-nitrobenzo[c][1,2,5]oxadiazol-4-yl)amino)ethyl)(2-((2-(3-(trifluoromethyl)phenyl)-1H-imidazo[4,5-c]pyridin-6-yl)amino)ethyl)amino)methyl)phenol (3.14-NBD):

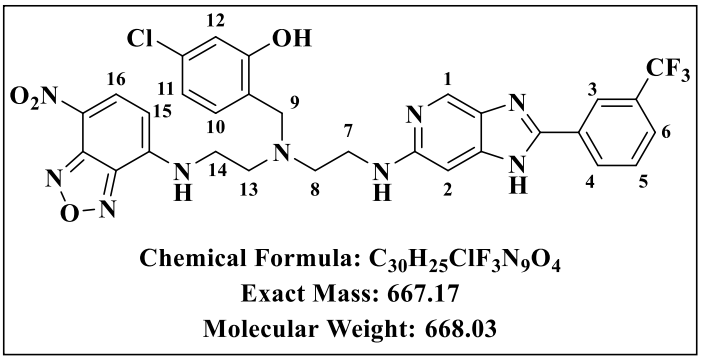

Obtained from intermediate **5g** (370 mg, 0.80 mmols) and N-boc glycinal (254 mg, 1.60 mmols) as an off-white solid (75%, 338.84 mg); R_f (DCM: MeOH, 9:1) 0.56; ^{1}H NMR (600 MHz, DMSO-d_6) δ 8.39 (s, 1H, H^1), 8.37 (d, J = 8.8 Hz, 1H, H^{16}), 8.35 (dd, J = 2.8, 2.2 Hz, 1H, H^3), 8.31 (d, J = 8.8 Hz, 1H, H^{15}), 7.82 (dd, J = 7.8, 2.2 Hz, 1H, H^{11}), 7.74 (ddd, J = 7.8, 2.8, 2.3 Hz, 1H, H^6), 7.13 (dd, J = 8.4, 7.8 Hz, 1H, H^5), 6.85 (d, J = 7.8 Hz, 1H, H^{10}), 6.59 (ddd, J = 8.4, 2.3 Hz, 1H, H^4), 6.19 (d, J = 2.2 Hz, 1H, H^{12}), 6.04 (s, 1H, H^2), 3.70 (s, 2H, H^9), 3.53 (t, J = 6.3 Hz, 2H, H^{14}), 3.39 (t, J = 6.0 Hz, 2H, H^7), 2.82 – 2.76 (m, 4H, H^8 and H^{13}). ^{13}C NMR (151 MHz, DMSO) δ 159.13, 158.92, 157.57, 155.85, 154.95, 149.82, 147.41, 143.12, 139.53, 138.17, 137.90, 135.58, 132.31, 131.80, 131.35, 129.01, 128.78, 126.30, 123.09, 118.92, 115.35, 99.50, 92.26, 86.51, 55.54, 53.70, 51.38, 44.39, 41.56, 36.89. HPLC-MS (ESI): Purity = 98%, t_R = 0.905 min, m/z $[M+H]^+$ = 668.2.

7.3 Biological Evaluation

7.3.1 *In vitro* Asexual Blood Stage Antiplasmodium Assay

7.3.1.1 Modified [^{3}H]-Hypoxanthine Incorporation Assay

The modified [^{3}H]-hypoxanthine incorporation assay[1] was used to screen compounds against both the chloroquine-sensitive (NF54) and multidrug-resistant (K1) strains of *Plasmodium falciparum* parasites. The parasites were cultivated in human red blood cells as previously described[2,3] but with some alterations to the medium, which contained RPMI 1640 supplemented with 0.5% ALBUMAX® II, 25 mM $NaHCO_3$ (pH 7.3), 25 mM Hepes, 0.36 mM hypoxanthine, and 100 microgram/ml neomycin. Parasite cultures were preserved in an atmosphere of 3% O_2, 4% CO_2 and 93% N_2 in humidified modular chambers at 37 °C.

10 mg/mL stock solutions of the test compounds were made by dissolving them in DMSO through sonication and diluted in a hypoxanthine-free culture medium. Infected erythrocytes (100 microliters per well with 2.5% hematocrit and 0.3% parasitaemia) were added to each

compound titrated in 100 microliter duplicates over a 64-fold range and incubated for 48 hours. 0.5 microCi of [^{3}H]-hypoxanthine in 50 microliter media was then added, and the culture plates were incubated for an extra 24 hours. Radioactivity was determined using a Betaplate liquid scintillation counter (Wallac, Zurich) from the parasites harvested onto glass-fiber filters at the end of the incubation period. The radioactivity results were recorded as counts per minute (cpm) per well at each compound concentration and furnished as a percentage of the untreated controls. Concentrations resulting in fifty percent inhibition (IC_{50}) were estimated by linear interpolation.[4]

7.3.1.2 Lactate Dehydrogenase (LDH) Assay

Both chloroquine-sensitive (NF54) and multidrug-resistant (K1) strains of *Plasmodium falciparum* were cultured according to the method previously described by Trager and Jensen[3] but with slight modifications. Antiplasmodium activity was determined by measuring the parasite's lactate dehydrogenase enzyme activity.

20 mg/mL stock solutions of the test compounds in DMSO were prepared and stored at -20 °C prior to the experiment. The stock solutions were subsequently diluted to 100 µg/mL concentration in the assay medium. Serial dilutions were performed to obtain ten different concentrations between the ranges of 0.2-100 µg/mL. A dose-response analysis was then carried out to establish the concentration at which 50% of the parasite growth is inhibited. Non-linear dose-response curves were generated using GraphPad Prism software.

7.3.2 *In vitro* Gametocytocidal Assay

The luciferase reporter assay was set up to enable quantifiable, reliable and accurate investigations of the stage-specific action of gametocytocidal compounds for the early and late gametocyte marker cell line NF54-PfS16-GFP-Luc. Gametocytes were produced according to the method previously described by Reader *et al.*[5] Compound analysis was set up on days 5 and 10 (representing >90% of either early stage II/III or mature stage IV/V gametocytes, respectively). In each instance, assays were set up using a 2 – 3% gametocytaemia, 1.5% haematocrit culture and 48 hours drug pressure in a gas chamber (90% N_2, 5% O_2, and 5% CO_2) at 37 ºC. Luciferase activity was determined in 30 µL parasite lysates by adding 30 µL luciferin substrate (Promega Luciferase Assay System) at room temperature. The resultant bioluminescence was determined at an integration constant of 10 s with the GloMax® Explorer

Detection System with Instinct® Software. Methylene blue (5 μM) and internal project-specific control (MMV390048, 5 μM) were used as controls.

7.3.3 *In vitro* Cytotoxicity Assay

In vitro cytotoxicity was performed on the Chinese Hamster Ovarian cell line by measuring cellular growth and survival calorimetrically through the 3-(4,5-dimethylthiazol-2-yl)-2,5-diphenyltetrazolium bromide (MTT) assay.[6,7] The formation of tetrazolium salt was used as a measure of chemosensitivity and growth.

2 mg/mL stock solutions of the test compounds were prepared in DMSO and stored at -20 °C until required. The stock solution was subsequently diluted with the assay medium to make up an initial concentration of 100 μg/mL. The initial 100 μg/mL solution is serially diluted 10-fold to attain six assay concentrations of 100-0.001 μg/mL. Emetine was used as the reference compound in this assay. The highest concentration of DMSO, which was used as the negative control, had no measurable effect on cell viability. After 44 hours of exposure of the cells to the test compounds, a solution of MTT was added. This was followed by an additional 4 hours of incubation at 37 °C. The assay plates were centrifuged, medium removed, and DMSO was added to the crystals. The amount of formazan was ascertained by measuring the absorbance at 540 nm. GraphPad Prism software was then used to generate IC_{50} values through a non-linear dose-response curve analysis.

7.3.4 *In vitro* hERG Inhibition Assay

The inhibition potency of the target compounds against the hERG potassium ion channel was performed by utilizing the QPatch hERG assay, which employs a four-point concentration-response format. This experiment was carried out by Metrion Biosciences Ltd, based in the United Kingdom. The hERG channel gene was stably expressed in a CHO cell line under standard culture conditions according to Metrion's in-house Working Practice Documents. 10 mM stock solutions of the test compounds were prepared in DMSO and serially diluted in a 0.5-log unit to obtain test concentrations of 0.3, 1, 3 and 10 μM. Recordings of hERG currents were obtained electrophysiologically following Metrion's in-house procedures.

Experiments were executed in three separate cells as technical replicates. The concentration-response curves were established by a progressive double sample addition of each test concentration to the same cell. The percentage inhibition was calculated as a reduction in the mean peak current relative to the peak current measured before the cells were exposed to the

test compounds. The percentage inhibition results from each cell were then used to construct concentration-response curves with the 4-parameter logistic fit, which helped calculate IC_{50} values. Test compounds that could not exhibit >40% inhibition at the highest test concentration were assigned an arbitrary IC_{50} value 0.5 log unit above the highest concentration tested. Verapamil was used as the reference compound in this assay and was treated the same as the test compounds.

7.3.5 Beta-Hematin Inhibition Assay

20 mM stock solutions of controls and test compounds were made in DMSO. A solution containing water, 305.5 μM NP-40 and DMSO at a v/v ratio of 70%:20%:10%, respectively, was added to every well in columns 1-11 of a 96-well plate. 140 μL of water and 40 μL of 305.5 μM NP-40 were added to column 12 to mediate the formation of beta-hematin. 20 μL of test compounds (20 mM) were added to column 12 and 100 μL of this solution serially diluted to column 2, leaving column 1 blank (0 μM of test compound). 178.8 μL aliquot of hematin stock was suspended in 20 ml of a 1 M acetate buffer at pH 4.9. 100 μL of this hematin suspension was then added into each well, and the plates were incubated for ±5 hrs at 37°C. Subsequently, 32 μL of pyridine solution (20% water, 20% acetone, 10% 2M HEPES buffer at pH 7.4 and 50% pyridine) and 60 μL of acetone were added to all wells. The absorbances of plate wells were recorded at 405 nm on a SpectraMax plate reader. Sigmoidal dose-response curves with variable slopes were fitted to the absorbance data using GraphPad Prism to obtain the IC_{50} values for each compound.

7.3.6 *In vitro* Metabolic Stability Assay

The one-time point assay[8] was used in conducting the metabolic stability experiment. The investigation was carried out in triplicate in a 96-well microtiter plate with test compounds at a concentration of 0.1 μM incubated in mouse, human and rat liver microsomes obtained from XenoTech. 1 mM NADPH in a 100 mM phosphate buffer solution at pH 7.4 was added to the microsomes and incubated for 30 minutes to initiate metabolic reactions. The reactions were quenched by adding 300 μL of ice-cold acetonitrile, which contained an internal standard (carbamazepine, 0.0236 μg/mL). The supernatant was centrifuged and then filtered off. The analysis was then performed by HPLC-MS/MS (Agilent Rapid Resolution HPLC, AB SCIEX 4500 MS). The differences in the concentration of the test compounds before and after incubation were determined. The results were recorded as the percentage of each test

compound remaining after 30 minutes of incubation. In this assay, no metabolite searches were performed.

7.3.7 Metabolite Identification Studies

Metabolite identification studies were performed in male mouse (CD1, Lot No.1510043 Xenotech) liver microsomes. Microsomes (1 mg/mL) were suspended in a solution containing $MgCl_2$ (5 mM) and phosphate buffer (100mM, pH 7.4). The test compound was spiked in a portion of this microsome mix to achieve a compound concentration of 10 μM. A buffer mixture was also prepared, containing only phosphate buffer and $MgCl_2$ (5 mM) without any microsomes. Two separate 96-well microtiter plates were used; one for T0 (0 minutes) and the other for T60 (60 minutes) incubations set up. Each plate was laid out to accommodate four sets of incubations in duplicates. In the first case, 90 μL of the microsomal mix containing the test compound (10 μM) was introduced into two separate sets of wells. In another set of wells, 90 μL from the pre-mix lacking microsomes (buffer mixture) was placed. A control was prepared in another set of wells by placing an aliquot of 90 μL from the microsomal mix that did not have the test compound. After that, NADPH (10 μL, 1 mM) was added to one of the two sets of wells containing microsomal mix that had been spiked with the test compound. To the other sets of wells, 10 μL of buffer was added such that all the wells held a total volume of 100 μL of samples. The above procedures were performed for both T0 and T60 plates. To one of the plates (T0 plate), 300 μL of acetonitrile was added to all the wells, and the plate was immediately stored at -20 °C, pending analysis. The other plate (T60 plate) was incubated for 60 minutes at 37 °C with gentle shaking before adding acetonitrile (300 μL) to all wells. Both T0 and T60 plates were centrifuged, and the supernatant was transferred to a clean microtiter plate for LC-MS/MS analysis following in-house procedures.

7.3.8 Fluorescence Live-cell Microscopy

7.3.8.1 General Methods

Nunc Lab-Tek II eight-well chamber slides (Thermo Fisher Scientific, Massachusetts, USA) with a cover glass of No. 1.5 thickness were coated with 150 μL of 0.01% (w/v) poly-L-lysine solution. After ten minutes, the solution was removed, and the plates were left to air-dry. Ringer's solution was prepared according to the compositions outlined in Table 7.1, as previously described.[9] The pH was adjusted to 7.4, after which the solution was filtered through a 0.22 μm nylon syringe filter.

Table 7.1: **Constituents of Ringer's solution for live-cell imaging of the *P. falciparum*.**

Component	Molecular weight	Final Concentration	Mass required for 100mL
NaCl	58.44	122.5 mM	715.9 mg
KCl	74.56	5.4 mM	40.3 mg
$CaCl_2$	147.02	1.2 mM	17.6 mg
$MgCl_2$	95.21	0.8 mM	7.6 mg
D-glucose	180.16	11 mM	198.2 mg
Hepes	238.30	25 mM	595.8 mg
NaH_2PO_4	119.98	1 mM	12.0 mg

Human erythrocytes infected with *P. falciparum* trophozoites (NF54 strain) were generously donated by colleagues at the Division of Pharmacology, Department of Medicine, University of Cape Town. After harvesting and centrifugation of the cells, 5 µL of the parasitized erythrocyte pellets were resuspended in 5 mL Ringer's solution and vortexed to reduce clumping of the erythrocytes. 150 µL aliquots of suspended cells were placed in each well of the chamber slide and incubated for at least 20 minutes to allow the erythrocytes to adhere to the cover glass. After this, the Ringer's solution was removed and replaced with a fresh aliquot of Ringer's solution (150 µL) to remove non-adhered cells. This solution was then removed again and replaced with Ringer's solution (150 µL) containing appropriate concentration(s) of the fluorescent dye(s) as listed in Table 7.2.

7.3.8.2 Live-cell Confocal Microscopy

Confocal microscopy was performed using a Zeiss Axiovert 200 M LSM 150-META confocal microscope at the Confocal and Light Microscope Imaging Facility at the University of Cape Town. A Plan-Apochromat 63x/1.40 Oil DIC M27 objective lens was used, and the cells were incubated at 37°C. Images were captured and processed with ZEN 2018 (Carl Zeiss MicroscopyGmbH). Laser transmission was kept as low as possible to minimize phototoxicity to the cells.[10] Dye concentrations with respective excitation and emission settings are listed in Table 7.2.

Table 7.2: Concentrations of fluorescent dyes used for confocal imaging of *P. falciparum* with respective excitation lasers and emission filter settings.

Dye	Concentration	Excitation Laser	Emission filter
DRAQ 5	500 nM	580 nm	600-630 nm
LysoTracker	100 nM	561 nm	575-630 nm
Nile Red	100 nM	561 nm	575-630 nm
ER-Tracker	100 nM	561 nm	575-630 nm
MitoTracker	100 nM	561 nm	650-710 nm
1.3-NBD	50 nM	420 nm	500-550 nm
3.14-NBD	75 nM	420 nm	500-550 nm

7.3.9 Heme Fractionation Assay

7.3.9.1 Preparation of Counting Plate and Cell Fixation

The heme fractionation assay was performed according to the methods previously described.[11] After the IC_{50} of the target compounds was determined, a counting plate was prepared by adding 10 µL of the isolated washed trophozoites to the corresponding wells of a flat-bottomed 96-well plate. The cells were fixed with 0.125 % (v/v) glutaraldehyde in PBS pH 7.5 to a final volume of 200 µL and refrigerated at 4 °C overnight.

7.3.9.2 Hemocytometer Counting

Hemocytometer counting was performed on the first row of each plate only, corresponding to six samples, each at a different concentration of the drug tested. The hemocytometer determined cell counts for these six samples were statistically compared to the cell counts determined by flow cytometry to test for agreement. 10 µL of cells from the counting plate were loaded onto a bright-lined hemocytometer, and five large squares were counted after 10 minutes of settling. The concentration of cells in each well of the plate was determined using equation 1:

CH ¼ N x F x DF x 10,000 **(1)**

Where: CH = concentration of cells per ml as determined with hemocytometer

N = number of cells counted in five fields

F = number of fields counted = 5

DF = dilution factor

7.3.9.3 Flow Cytometry Counting

Cell counts for all samples on the counting plate were determined using flow cytometry. Samples were analyzed on a Becton Dickinson FACSCalibur using SSC/$FL1_{530nm}$ with CellQuestPro software. Typically, 10,000 events were counted for each sample. Samples were prepared by diluting 100 µL of cells from the counting plate with 800 µL of 1 × SYBR® green I in PBS at pH 7.5 and incubated for 30 minutes in the dark at 37 °C. Next, each sample was spiked with 100 µL of Trucount™ beads (Becton Dickinson) such that each sample contained a known fixed amount of fluorescent beads in a final volume of 1 mL. The concentration of cells in the acquisition tube was calculated according to equation 2:

CF= (T/B) x CB **(2)**

Where:

CF = concentration of cells per ml as determined with flow cytometry

T = number of trophozoites gated

B = number of fluorescent beads gated

CB = concentration of fluorescent beads in the acquisition tube per ml (calibrated bead count per acquisition is unique to each lot of tubes obtained from the supplier).

7.3.9.4 Heme Fractionation

After thawing the stock plate, 50 µL of water was added, and the plate was sonicated for 5 min in an ultrasound bath (53 kHz, 320 W, Bandelin Sonerex). This was followed by adding 50 µL each of 0.2 M HEPES buffer at pH 7.5 and water. The plate was then centrifuged at 3600 rpm for 20 minutes. Very carefully, without disturbing the pellet, the supernatant was transferred to an adjacent set of wells on the same plate. The supernatant was processed further with 50 µL of 4% SDS, sonicated for 5 minutes and then incubated at 37 °C for 30 minutes. 50 µL of 0.3 M NaCl and 50 µL of 25% (v/v) pyridine in 0.2 M HEPES buffer at pH 7.5 were added, and 200 µL of the solution was transferred to a flat-bottomed UV-Star 96-well plate. This fraction corresponds to the hemoglobin fraction.

The pellet was treated with 50 µL water, 50 µL of 4% SDS and resuspended. The plate was sonicated for 5 minutes and incubated at 37 °C for 30 minutes to solubilize free heme. This was followed by adding 50 µL 0.2 M HEPES buffer at pH 7.5, 50 µL 0.3 M NaCl and 50 µL

of 25% pyridine. The plate was centrifuged at 3700 rpm for 20 minutes. Very carefully, without disturbing the pellet, the supernatant was transferred to an adjacent set of wells on the same plate. The supernatant was diluted to a final volume of 400 µL with water. This fraction corresponds to the free heme fraction. 200 µL of this solution was transferred to the flat-bottomed UV-Star 96-well plate, the same plate previously used for the hemoglobin fraction. The remaining pellet containing hemozoin was solubilized in 50 µL of water and 50 µL 0.3 M NaOH. The plate was sonicated for 15 minutes and incubated at 37 °C for 30 minutes. 50 µL each of 0.2 M HEPES buffer at pH 7.5, 0.3 M HCl and 25 % pyridine was added, followed by 150 µL of water. This fraction corresponds to the hemozoin fraction. 200 µL of this solution was transferred to vacant wells in the flat-bottomed UV-Star 96-well plate containing the hemoglobin and free heme fractions. The UV-visible spectra of heme as Fe(III)heme-pyridine complex were recorded using a multi-well plate reader (SpectraMax 340PC, Molecular Devices). The absorbance maxima of the Fe(III)heme-pyridine complex in each well was used to calculate the percentage of heme species in each sample as the final volume for each fraction was identical.

7.3.9.5 Heme Curve

The total amount of heme in each fraction was quantified using a standard heme curve prepared from a 100 µg/mL standard heme solution of hematin (porcine) in 0.3 M NaOH. Serial dilutions of the standard were carried out in a 96-well plate with 100 µL 0.3 M NaOH as a blank. 50 µL of each of the following solutions were added to 100 µL of hematin standard: 0.2 M HEPES buffer pH 7.5, 4% (w/v) SDS, 0.3 M NaCl, 0.3 M HCl, 25% pyridine in 0.2 M HEPES buffer pH 7.5 and water. The visible spectra of heme as Fe(III)heme-pyridine complex were recorded in a multi-well plate reader. The amount of heme Fe per cell was calculated by dividing the total heme Fe in each fraction by the number of cells determined in each fraction.

7.3.10 Docking Studies

Compounds were docked against the β-hematin surface using the previously published 3D crystal structure.[12] The Fe-O bonds were treated as zero-order bonds to constrain the input geometry. The receptor grid encompassed the (100) and (001) faces of the crystal. The protonation states of both the crystal and the ligands were generated at pH 4.8 ± 0.5 using Epik. The ligands were minimized using Schrodinger's OPLS3e force field. The output conformers were docked using Grid-based ligand docking with energetics (Glide extra

precision). Epik state penalties were added to the docking score, and intramolecular hydrogen bonds were rewarded. The planarity of conjugated π groups was also enhanced.

7.4 Solubility Determination

7.4.1 Kinetic Solubility via HPLC-based Method

The miniaturized shake-flask method[13] was employed in this solubility assay. 10 mM stock solutions of the test compounds were prepared in DMSO. Calibration standards (10-220 µM in DMSO) were also prepared. The stock solutions were used to spike (1:50) duplicate aqueous samples in phosphate buffered saline at pH 6.5. The DMSO was dried off in a Genevac (MiVac) for 90 minutes at 37 °C followed by incubation while shaking for 20 hours at 25 °C. The solutions were filtered off, and their absorbance was determined using HPLC-DAD (Agilent 1200 Rapid Resolution HPLC with a diode array detector) instrument. Calibration curves were plotted using the calibration standards, which were then used to determine the solubility of the test compounds.

7.4.2 Turbidimetric-based Kinetic Solubility[14]

10 mM stock solutions of the test compounds were prepared in DMSO. Predilution plates were prepared in 96-well plates from the stock solutions in triplicate to obtain a concentration range between 0.125 and 8mM. Secondary serial dilutions (5-200 µM) in DMSO and 0.01 M PBS buffer at pH 7.4 were also prepared in triplicate. Aliquots (4 µL) were pipetted from the predilution plate to respective wells in the secondary plate, which contained a mixture of DMSO and PBS buffer (196 µL), making a final volume of 200 µL in each well. Serial dilutions in only DMSO were used as controls. The plates were incubated at 25 °C for 2 hours, after which absorbance was measured at 620 nm by a SpectraMax 340PC microplate reader. The corrected concentration-absorbance curves were plotted in Microsoft Excel®. The concentration above which there was a sustained deviation of absorbance from the baseline was recorded as the solubility of the test compound. Reserpine and hydrocortisone were used as negative and positive controls, respectively, in this assay.

7.5 References

(1) Snyder, C.; Chollet, J.; Santo-Tomas, J.; Scheurer, C.; Wittlin, S. In Vitro and in Vivo Interaction of Synthetic Peroxide RBx11160 (OZ277) with Piperaquine in Plasmodium Models. *Exp. Parasitol.* **2007**, *115* (3), 296–300. https://doi.org/10.1016/j.exppara.2006.09.016.

(2) Dorn, A.; Stoffel, R.; Matile, H.; Bubendorf, A.; Ridley, R. G. Malarial Haemozoin/β-Haematin Supports Haem Polymerization in the Absence of Protein. *Nature* **1995**, *374* (6519), 269–271. https://doi.org/10.1038/374269a0.

(3) Trager, W.; Jensen, J. Human Malaria Parasites in Continuous Culture. *Science (80-.).* **1976**, *193* (4254), 673–675. https://doi.org/10.1126/science.781840.

(4) Huber, W.; Koella, J. C. A Comparison of Three Methods of Estimating EC50 in Studies of Drug Resistance of Malaria Parasites. *Acta Trop.* **1993**, *55* (4), 257–261.

(5) Reader, J.; Botha, M.; Theron, A.; Lauterbach, S. B.; Rossouw, C.; Engelbrecht, D.; Wepener, M.; Smit, A.; Leroy, D.; Mancama, D.; et al. Nowhere to Hide: Interrogating Different Metabolic Parameters of Plasmodium Falciparum Gametocytes in a Transmission Blocking Drug Discovery Pipeline towards Malaria Elimination. *Malar. J.* **2015**, *14* (1), 213. https://doi.org/10.1186/s12936-015-0718-z.

(6) Mosmann, T. Rapid Colorimetric Assay for Cellular Growth and Survival: Application to Proliferation and Cytotoxicity Assays. *J. Immunol. Methods* **1983**, *65* (1–2), 55–63. https://doi.org/10.1016/0022-1759(83)90303-4.

(7) van Meerloo, J.; Kaspers, G. J. L.; Cloos, J. Cell Sensitivity Assays: The MTT Assay. **2011**, 237–245. https://doi.org/10.1007/978-1-61779-080-5_20.

(8) Bertrand, M.; Jackson, P.; Walther, B. Rapid Assessment of Drug Metabolism in the Drug Discovery Process. *Eur. J. Pharm. Sci.* **2000**, *11*, S61–S72. https://doi.org/10.1016/S0928-0987(00)00165-2.

(9) Pisciotta, J. M.; Coppens, I.; Tripathi, A. K.; Scholl, P. F.; Shuman, J.; Bajad, S.; Shulaev, V.; Sullivan, D. J. The Role of Neutral Lipid Nanospheres in Plasmodium Falciparum Haem Crystallization. *Biochem. J.* **2007**, *402* (1), 197–204. https://doi.org/10.1042/BJ20060986.

(10) Wissing, F.; Sanchez, C. P.; Rohrbach, P.; Ricken, S.; Lanzer, M. Illumination of the Malaria Parasite Plasmodium Falciparum Alters Intracellular PH. *J. Biol. Chem.* **2002**, *277* (40), 37747–37755. https://doi.org/10.1074/jbc.M204845200.

(11) Combrinck, J. M.; Fong, K. Y.; Gibhard, L.; Smith, P. J.; Wright, D. W.; Egan, T. J. Optimization of a Multi-Well Colorimetric Assay to Determine Haem Species in

Plasmodium Falciparum in the Presence of Anti-Malarials. *Malar. J.* **2015**, *14* (1), 253. https://doi.org/10.1186/s12936-015-0729-9.

(12) Pagola, S.; Stephens, P. W.; Bohle, D. S.; Kosar, A. D.; Madsen, S. K. The Structure of Malaria Pigment β-Haematin. *Nature* **2000**, *404* (6775), 307–310. https://doi.org/10.1038/35005132.

(13) Hill, A. P.; Young, R. J. Getting Physical in Drug Discovery: A Contemporary Perspective on Solubility and Hydrophobicity. *Drug Discov. Today* **2010**, *15* (15–16), 648–655. https://doi.org/10.1016/j.drudis.2010.05.016.

(14) Bevan, C. D.; Lloyd, R. S. A High-Throughput Screening Method for the Determination of Aqueous Drug Solubility Using Laser Nephelometry in Microtiter Plates. *Anal. Chem.* **2000**, *72* (8), 1781–1787. https://doi.org/10.1021/ac9912247.